Sheffield Hallam University

A Sheffield Hallam University thesis

Enhancement of Breast Cancer Chemotherapy and Radiotherapy Responses by Modulation of Ferroptosis

Alaa Awad Alzufairi

A thesis submitted in partial fulfilment of the requirements of Sheffield Hallam University for the degree of Doctor of Philosophy

April 2024

Candidate declaration

I hereby declare that:

1. I have not been enrolled for another award of the University, or other academic or professional organisation, whilst undertaking my research degree.

2. None of the material contained in the thesis has been used in any other submission for an academic award.

3. I am aware of and understand the University's policy on plagiarism and certify that this thesis is my own work. The use of all published or other sources of material consulted have been properly and fully acknowledged.

4. The work undertaken towards the thesis has been conducted in accordance with the SHU Principles of Integrity in Research and the SHU Research Ethics Policy.

5. The word count of the thesis is 76661.

Name	Alaa Awad Alzufairi
Date	April 2024
Award	PhD
Research Institute	BMRC
Director(s) of Studies	Dr. Neil Cross Dr. Nicola Jordan-Mahy

Abstract

Breast cancer is the most common cancer in women in the UK. Surgery, radiotherapy, hormone therapy and chemotherapy are all current therapies. The success rate of chemotherapy and radiotherapy are affected by intrinsic insensitivity, and acquired resistance, and novel chemo-sensitisation and radio-sensitisation strategies are currently being researched. Ferroptosis is an iron-dependent program cell death pathway characterised by massive accumulation of reactive oxygen species. Reactive oxygen species accumulation and subsequent lipid peroxidation-mediated death is Fe^{2+}-dependent, leading to a form of cell death that is distinct from apoptosis. Since it is known that both chemotherapy and radiotherapy exert some ferroptosis-mediated effects, it was hypothesised that chemotherapy responses and radiotherapy responses would be enhanced by co-treatment with ferroptosis inducers. To test the co-treatment with ferroptosis inducers in a disease relevant model, both 2D standard cell culture and 3D tumour spheroids in two breast cancer cell lines were assessed. Ferroptosis inducers affected MDA-MB-231, but not MCF-7. Ferroptosis inducers did not have a robust enhancement of Doxorubicin responses, although more promising responses were observed with Cisplatin but only in MDA-MB-231 and only in 2D cell culture, not in spheroids. Since ferroptosis is controlled in-part by Nrf2, the Nrf2-inhibitor ML385 was tested, which partially enhanced chemotherapy responses, and also identified a specific drug combination vulnerability when combined with the ferroptosis inducer RSL3, whereby MDA-MB-231 cells did not respond potently to RSL3 plus Doxorubicin, but were sensitive when ML385 was added. This was not observed in MCF-7. In spheroids, responses to RSL3 were heterogeneous in that adjacent spheroids showed differential responses to RSL3, which is a novel finding and may identify a resistance mechanism. Radiotherapy responses were not robustly enhanced by ferroptosis inducers. Despite the being a strong theoretical case for combining ferroptosis inducers with chemotherapy or radiotherapy, responses in these two cell lines were promising at times, but data does not strongly support further study in pre-clinical models.

Acknowledgements

I would thank Allah the Almighty, the most merciful and sympathetic, for His countless blessings, and generosity.

My PhD journey was one of my unforgettable journeys in my lifetime, with many ups and downs, especially when it was my first time to leave my country and family back home, and with the COVID-19 pandemic situation, again thank Allah how He gave me the strength to manage my studies that time. It has been a very difficult time, but it has been an amazing and wonderful opportunity that has made my dream become true.

First and foremost, I would like to express my sincere thanks to my lovely country "Kuwait" for encouraging us as citizens to complete our high education and supporting us financially and emotionally, with the huge care that we get from all the workers in the country institutions.

A special thanks to my wonderful and amazing supervisor Dr. Neil Cross, how was very helpful and understandable and without his precious guidance and help I will never reach the level of knowledge that I reached, many thanks for your precious time that you always give it to me when I need it. A special thanks for my co-supervisor, Dr. Nicola Jordan-Mahy, and to Dr. Celine Souilhol, senior technical specialist in the BMRC labs, for their valuable advice during my PhD journey. They were incredibly kind with their support, direction, and excellent feedback, which helped me the entire time I was conducting my research.

My gratefulness also goes out to my friends, especially Hamza Alaswad and Aya Samir, lab mates and colleagues who helped me during this work.

From my heart I dedicate this thesis to my much-loved Mum, Dad, brothers, sisters, husband, children, mother- and sister-in-law who have all been affected by my journey in various ways. Thanks for taking care of my children while I'm studying. Thanks for all the surprise visits that fill my heart with happiness and tears just by seeing you.

Dissemination

Papers in Preparation

Alzufairi, A, Souihol, C, Jordan-Mahy, NJ, Cross, NA. Enhancement of radiotherapy responses in 2D and 3D cell culture models of breast cancer.

Alzufairi, A, Souihol, C, Jordan-Mahy, NJ, Cross, NA. Chemotherapy responses in 3D spheroids using ferroptosis inducers and Nrf2 inhibitors.

Conference Presentations

Winter Poster Event: 10th December (2021). Title of presented work: Enhancement of Ferroptosis to Overcome Chemo- and Radio-resistance in Breast Cancer. Sheffield, United Kingdom.

COVID-19 impact statement

The PhD started in February 2020, and after 6 weeks, lockdown resulted in complete lab closure, and only part-time limited access for much of the following year. Given that the project required extensive cell culture and long-term 3D cell culture experiments, the lack of access to facilities significantly limited the available lab access for the planned experiments. Cell culture was being completed for the first time, and so with a 6-month break, all training had to be re-started after lock-down. Almost all data generated in the first 6 weeks had to be repeated, and so, the PhD effectively had to start from scratch in Sept 2020. The period between lockdown and re-gaining lab access could not be used for data analysis as very little data had been generated in the first six weeks. Although Doxorubicin experiments were comprehensively completed, no extra lab time was possible, resulting in less comprehensive experimental coverage of Cisplatin combination experiments, and less comprehensive validation of RTx responses with respect to ferroptosis marker detection and drug combinations. Throughout 2020 and part of 2021, there was little or no access to radiotherapy facilities at University of

Sheffield, limiting initial optimisation experiments, and limiting the total number of experiments that could be completed in this arm of the study.

Table of Contents

List of Figures

List of tables

Abbreviations

2D	Two-dimensional
3'UTR	3' untranslated region
3D	Three-dimensional
AA	Arachidonic acid
ACC	Acetyl-CoA carboxylase
ACSL	Enzyme acyl-CoA synthetase long-chain
ACSL4	Acyl coenzyme A synthetase long chain family member 4
AdA	Adrenic acid
AJCC	American Joint Committee on Cancer
AMPK	AMP-activated protein kinase
ARF	ADP-ribosylation factor
ATF3	Activating transcription factor 3
ATM	Ataxia telangiectasia mutated
CDKi	Cyclin-dependent kinase inhibitors
cDNA	Complementary DNA
CMF	Cyclophosphamide, methotrexate, and fluorouracil
CoA	Coenzyme A
CoQ10	Coenzyme Q10
DAGs	Diacylglycerols
DCFH-DA	Dichlorofluorescein diacetate
DFO	Deferoxamine
DMEM	Dulbecco's Modified Eagle Medium
DMSO	Dimethyl sulfoxide
DR5	Death receptor 5
DSBs	Double strand breaks
ECM	Extracellular matrix
EDTA	Ethylenediaminetetraacetic acid
EGF	Epidermal growth factor
ER	Oestrogen receptor

EU	European Union
FAO	Fatty acid oxidation
FAT	Fatty acid translocase
FATP	Fatty acid transport protein
FBS	Foetal bovine serum
Fe^{2+}	Ferrous ion
Fe^{3+}	Ferric ion
FECH	Ferrochelatase
FGF	Fibroblast growth factors
FINs	Ferroptosis inducers
FISH	Fluorescent in situ hybridization
GCL	Glutamate-cysteine ligase
Glu	Glutamate
Gly	Glycine
GPX4	Glutathione peroxidase 4
GSR	Glutathione reductase
GSS	Glutathione synthetase
GST	Glutathione S-transferase
H_2O_2	Hydrogen peroxide
HCV	Hepatitis C viruses
HER2	Human epidermal growth factor receptor
HIF	Hypoxia-inducible factor
HMOX1	Heme-oxygenase 1
HPV	Human papillomavirus
HRT	Hormone replacement therapy
IC50	Half maximal inhibitory concentration
IDC	Invasive Ductal carcinoma
IFN	Interferon
IFN-α	Interferon alfa
IFN-β	Interferon-beta
IFN-γ	Interferon-gamma
IGF	Insulin-like growth factor

IHC	Immunohistochemistry
ILC	Invasive Lobular Carcinoma
KEAP1	Kelch-like ECH-associated protein 1
LDH	lactate dehydrogenase
LIP	Labile iron pool
LOXs	Lipoxygenases
L-PAM	L-phenylalanine mustard
LPCAT	Lysophosphatidylcholine acyltransferase
LysoPLs	Lysophospholipids
MBC	Metastatic breast cancer
MDM2	Mouse double minute 2
MDR	Multi drug resistance
MDR1	Multidrug resistance-associated protein 1
Met	Methionine
miRNA	MicroRNA
MTOC	Microtubule organising centres
mTOR	Mammalian target of rapamycin
NADPH	Nicotinamide adenine dinucleotide phosphate
NER	Nucleotide Excision Repair
NK	Natural killer
NQO1	NAD(P)H-quinone oxidoreductase 1
Nrf2	Nuclear factor erythroid 2-related factor 2
NSABP	National Surgical Adjuvant Breast and Bowel Project
NSCLC	Non-small cell lung cancer
PARA	Pro-apoptosis receptors agonists
PARP	Poly-ADP ribose polymerase
PEs	Phosphatidylethanolamines
PGRMC1	Progesterone receptor membrane component1
PI	Propidium Iodide
PLD	Pegylated liposomal doxorubicin
PMRT	Postmastectomy radiation
PPi	Pyrophosphate

PR	Progesterone receptor
pRb	Retinoblastoma protein
PUFA	Polyunsaturated fatty acid
RCD	Regulated cell death
RCPath	Royal College of Pathologists
RNA	Ribonucleic Acid
ROS	Reactive oxygen species
RSL	RAS-selective lethal
RT	Room temperature
RT-qPCR	Real time quantitative polymerase chain reaction
RTx	Radiotherapy
SASP	Senescence-associated secretory phenotype
SERMs	Selective oestrogen-receptor modulators
SLC7A11	Solute Carrier Family 7 Member 11
SMAC	Second mitochondria-derived activator of caspase
SQS	Squalene synthase
SSBs	Single strand breaks
tBid	Truncated active form of Bid
TBS	Tris-buffered saline
TFR	Transferrin receptor
TFRC	Transferrin receptor
TNBC	Triple negative breast cancer
TNF-α	Tumour necrosis factor alpha
VDAC2/3	Voltage dependent anion channels 2 and 3
VEGF	Vascular endothelial growth factor
WHI	Women's Health Institute
WHO	World Health Organisation

Chapter 1: Introduction

1.1 Cancer

Cancer is a group of diseases which have biological characteristics of uncontrolled cell growth during cell division, abnormal cell differentiation and have the capacity to invade nearby tissues (Sarkar *et al.*, 2013). Normally, mammalian cells divide and proliferate to maintain development and growth of the organism. The process of normal cell division is tightly regulated by a conserved cell cycle machinery which checks and repairs genetic alterations to obtain two genetically identical daughter cells (Diaz-Moralli *et al.*, 2013). On the other hand, the failure to repair the detected DNA damage during cell cycle drives cells to undergo apoptosis to eliminate it cancer formation (Pucci *et al.,* 2000). Perturbation in cell cycle progression mechanisms induced by genetic mutations through activation of oncogenes and/or inhibition of tumour suppressor genes is the key cause of uncontrolled cell growth (tumour) which can be malignant (cancerous) or benign (non-cancerous) (Sarkar *et al.*, 2013). Although both tumour types result from aberrant cell divisions, the cells in malignant type acquire the ability to invade surrounding tissue and migrate to distant parts of body in a process called metastasis (Patel, 2020). Cancer metastasis is described as the development of secondary tumours into a distant organ from an initial primary tumour site (Seyfried and Huysentruyt, 2013). Both benign and malignant tumours can be classified based on the type of cell and origin tissue. Carcinoma, sarcomas and leukaemias are the main categories of malignancies which are derived from epithelial cells, connective tissue and blood forming cells, respectively (Cooper, 2000).

Cancer is considered one of the primary causes of global morbidity and mortality. It is noteworthy that metastatic cancer is associated with about 90% of all cancer related mortality among cancer patients (Seyfried and Huysentruyt, 2013). According to international agency for research on cancer using GLOBOCAN 2020 database, nearly 19.3 million new cancer cases (10.1 million case in males and 9.2 in females) and approximately 10 million cancer deaths (5.5 million death in males and 4.4 million death in females) were estimated globally in 2020 (Sung *et al.*, 2021). The incidence rate is predicted to rise by 47% by 2040 compared to 2020 (Sung *et al.*, 2021). Although there are more than 200 different types of cancer, the top ten common cancers worldwide frequently newly diagnosed in 2020 are breast (11.7%), lung (11.4%), colorectal (10%),

prostate (7.3%), stomach (5.6%), liver (4.7%), oesophagus (3.1%) cervix and uterus (3.1%), thyroid (3%) and bladder (3%) (Sung *et al.*, 2021). Theses top ten common cancer types represent more than 60% of all cancer incidences. Regarding cancer-related death in 2020, lung cancer is the primary cause of cancer death (18%), followed by colorectal (9.4%), liver (8.3%), stomach (7.7%), and female breast (6.9%) cancers. In men, the highest percentage of all cancer types is lung cancer, responsible for 14.3% incidence and 21.5% mortality. This is followed by prostate and colorectum for incidence and liver and colorectal cancer for death. Whereas, breast cancer (24.5%) is the most commonly occurring cancer in women followed by colorectal (9.4%) and lung cancer (8.4%) (Sung *et al.*, 2021). In children, cancer prevalence is highest in blood followed by cancer types associated with the brain and sarcomas (Sung *et al.*, 2021).

In general, cancer is considered a genetic disease that occurs as a result from an accumulation of a series of genetic mutations, leading to a change in normal cell function (Hassanpour and Dehghani, 2017). Many risk factors are contributed to cancer-related genetic mutation includes: Internal factors (such as inherited mutations) and acquired factors (such as environmental and behavioural factors causing sporadic genetic mutation including chemicals, tobacco, unhealthy diets, obesity, UV radiation, alcohol consumption and infectious organisms. Only 10% of all cancer diagnosed cases are linked to inherited gene mutation and 90% are contributed to environmental and behaviour factors (Anand *et al.*, 2008). It is believed that exposure to chemicals with carcinogenic properties have a vital role in gene mutation and cancer induction (Kemp, 2015). In addition, life style-related factors such as tobacco smoking and alcohol consumption are responsible for 25–68% of different cancers (Irigaray *et al.*, 2007). An estimated 10% of total cancer incidences are attributable to radioactive substances and UV radiation (Belpomme *et al.*, 2007). Infectious organisms such as viruses, bacteria and parasites are others carcinogens that have been linked to about 17.8% of all cancers (Anand *et al.*, 2008). For instance, human papillomavirus (HPV) and hepatitis C viruses (HCV) are believed to associated with cervical and liver cancers, respectively. A bacterial infection with *Helicobacter pylori* is also increase the risk of the development of gastric cancers (Masrour-Roudsari and Ebrahimpour, 2017). Furthermore, an estimated 4-8% of all cancer cases are linked to obesity. Cancers induced by obesity include pancreas,

breast, colorectum, oesophagus, endometrium, kidney and gall bladder cancers (Pati *et al.*, 2023). Obesity is a contributor to high rates of cancer particularly in women, and in the UK in next 25 years, rising obesity levels may cause an extra 670,000 cases of cancer by 2035 (Richards *et al.,* 2018)

1.1.1 Hallmarks of cancer

The word neoplasm means a new abnormal growth that leads to a major division of cancers into malignant and benign. These changes include the interaction between tumours and normal cells by switch the signalling in pro- and anti-proliferative pathways to avoid the cell death, and altering normal cellular functions (Sarkar *et al.*, 2013). Primarily, there are six main hallmarks are shared among all cancers (Figure 1).

Continuous proliferative signalling: In normal cells, signalling function is tightly regulated to ensure cell growth and division cycle is in progress to ensure cellular homeostasis, and number of cells keep constant. In cancer cells, deregulation of signalling to stop dividing affects the growth factors by modification of tyrosine kinase receptors (Hanahan and Weinberg, 2011). These growth factor receptors are overexpressed in several cancers, leading to their activation by growth factors (such as epidermal growth factor (EGF) and HER2/neu receptor) in stomach and breast cancers (Hanahan and Weinberg, 2000).

Escaping from growth suppressors signalling: There are two primary ways that antigrowth signals prevent cell division. First, in response to these signals, cells can enter a quiescent (G_0) state, temporarily pausing their proliferative process until extracellular signals allow re-entry into the cell cycle. Second, cells have the ability to enter postmitotic states that are linked to particular differentiation features and permanently quit the proliferative cycle (Hanahan and Weinberg, 2000).

Cancer cells must avoid these antigrowth signals in order to proliferate. The cell cycle clock, in particular the elements controlling the G1 phase, plays a key role in how well normal cells respond to anti-growth signals (Hanahan and Weinberg, 2000). Cells monitor their environment during G1 and decide whether to proliferate, remain dormant, or reach a postmitotic stage based on signals they perceive. In this process,

the retinoblastoma protein (pRb) and its related proteins, p107 and p130, are essential. In their hypophosphorylated condition, pRb sequesters and alters the function of E2F transcription factors, which regulate the expression of genes necessary for passage from G1 to S phase (Hanahan and Weinberg, 2000). Cells can ignore anti-growth signals and continue to proliferate because anti-growth factors like TGFβ (transforming growth factor beta) impair the pRb pathway. This happens when TGF promotes the formation of p15^{INK4B} and p21 proteins, which inhibit the cyclin:CDK complexes in charge of phosphorylating pRb (Hannon and Beach, 1994).

Other mechanisms, which include p27 and cyclin-dependent kinase inhibitors (CDKi), is by inducing the cells to enter a post-mitotic states, usually correlated with gaining specific differentiation-associated traits (Hanahan and Weinberg, 2000). The ability of cancer cells to avoid anti-proliferative signalling can be via by the cell cycle components (Cyclins). These proteins bind CDKs to control the transit of the cell through the cell cycle phases, initially G1-S phase (Hanahan and Weinberg, 2000).

Avoiding apoptosis: Cancer cells have the potential to escape from the natural programmed cell death (apoptosis) (Fernald and Kurokawa, 2013). In the presence of abnormalities within the cell (e.g. DNA damage, hypoxia), the intracellular sensors maintain homeostasis (Hanahan and Weinberg, 2000). However, cancer cells do not response to these signals due to mutation in tumour suppressor gene TP53 and degradation of pro-apoptotic protein BAX (Fernald and Kurokawa, 2013).

Immortality: Cancer cells divide uncontrollably, due to their ability to protect the telomers at the ends of chromosomal DNA. These telomers have thousand repeats of a short 6 bp sequence element that protect the chromosome. In the normal situation at each cell cycle the chromosomal DNA loss a number of 50–100 bp (Hanahan and Weinberg, 2011). The chromosomal DNA loss is due to DNA polymerases to in completely replicating the 3′ ends of chromosomal DNA during each S phase. After depletion of telomeres the DNA is no longer protected and cells lose their ability to divide, due to the depletion of telomeres and cells die due to detection of exposed non-telomere DNA and activation of the DNA damage response (Hanahan and Weinberg, 2000).

Angiogenesis: The process of formation new blood vessels. The process is regulated by vascular endothelial growth factor (VEGF) and acidic and basic fibroblast growth factors (FGF1/2), which bind to tyrosine kinase receptors on endothelial cells (Veikkola and Alitalo, 1999). Thrombospondin-1 (TSP-1) is a classical angiogenesis inhibitor which play a critical role in homeostasis (Sheibani *et al.*, 2000). Cancer cells alter the balance between the angiogenesis inducers and inhibitors. For instance, VEGF is overexpressed in some types of malignancies due to activation of the Ras oncogene (Rak *et al.*, 1995) or hypoxic conditions which in turn induce the expression of hypoxia inducible factor-1 (HIF-1) (Okada *et al.*, 2005). Moreover, the endogenous level of thrombospondin-1 (angiogenic inhibitor) is downregulated, which is primarily associated with loss of p53 function in many cancers (Hanahan and Weinberg, 2000).

Metastasis: Tumours can spread to other parts of the body from their original site, causing 90% of human cancer deaths. The process is very complex including changes in the cellular microenvironment and activation of extracellular proteases (Hanahan and Weinberg, 2000). Several cellular proteins help in the invasion of cancer cells, involving the cell–cell adhesion molecules protein, which binds cells together. One of the famous cell-to-environment interactions is the E-cadherin, which acts as a bridge between epithelial cells in normal situations. In cancer, mutations or altered differentiation lead to loss of expression of E-cadherin leading to reduced ability to connect cells and this the significant of metastasis (Hanahan and Weinberg, 2000). Following their initial invasion of adjacent tissues, cancer cells can intravasate into nearby blood arteries or lymphatic vessels. They can then enter the circulation and move through the lymphatic or blood systems as a result (Stetler-Stevenson, 1999). As they travel through the circulation, cancer cells encounter a variety of obstacles, such as shear pressures and interactions with immune cells such as natural killer (NK) and CD8^{+} T cells (Teng *et al.*, 2015). Some cells can, however, withstand the immune system and reach distant organs (Teng *et al.*, 2015). In order to create secondary tumours, cancer cells must leave the bloodstream after travelling to a distant place. Cancer cells adhere to the inner walls of blood vessels or lymphatic vessels at the target organ and migrate through the vessel walls to infiltrate the surrounding tissue in this process, which is referred to as extravasation (Chiang *et al.,* 2016). Cancer cells require a blood supply to support their

proliferation once they have extravasated. They have the ability to stimulate angiogenesis, also known as neovascularization, which results in the growth of new blood vessels (Katayama *et al.*, 2019). The new blood vessels guarantees a constant flow of nutrients and oxygen, promoting the development of secondary tumours at the distant site (Carmeliet and Jain, 2000). Figure 1.2 shows the metastatic cascade.
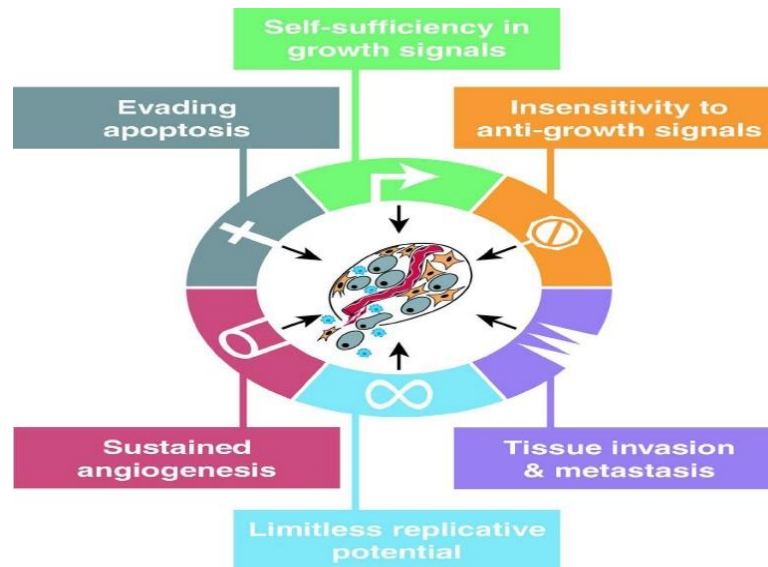
Figure 1.1: The six essential variations in cell physiology that communally cause malignant growth. Taken from Hanahan and Weinberg, (2000).
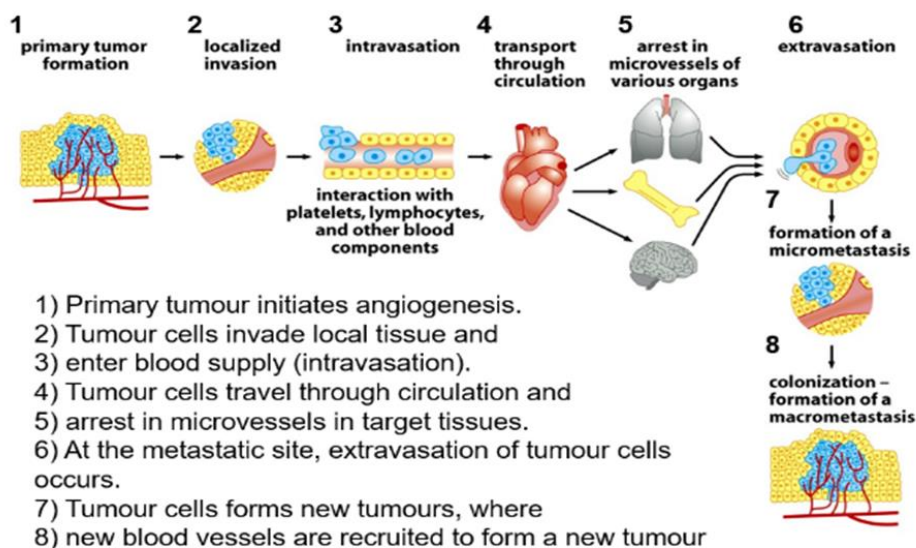
Figure 1.2: The diagram shows how cancer cells invade other sites in the body and form new tumours. Modified from Weinberg, (2013).

Since 2011 to 2022 a new hallmark of cancer has been identified (Figure 1.3). These include:

Inflammation: There were previously indications that the inflammatory response linked to tumours had the unexpected and paradoxical effect of promoting the growth and metastasis of tumours, hence assisting neoplastic development. Research on the connections between inflammation and cancer pathogenesis, has yeilded numerous and convincing examples of the functionally significant tumor-promoting effects immune cells—primarily those of the innate immune system—have on the development of neoplastic growth (Colotta *et al.*, 2009; DeNardo *et al.,* 2010; Grivennikov *et al.,* 2010; Qian and Pollard, 2010). By providing bioactive molecules to the tumour microenvironment, inflammation can support several hallmark capabilities. These include growth factors that maintain proliferative signalling, survival factors that prevent cell death, proangiogenic factors, extracellular matrix-modifying enzymes that promote angiogenesis, invasion, and metastasis (Karnoub and Weinberg, 2007; DeNardo *et al.,* 2010; Grivennikov *et al.,* 2010; Qian and Pollard, 2010).

Genomic instability and mutation: The remarkable capacity of genome maintenance mechanisms to identify and correct DNA defects that spontaneous mutation rates are typically extremely low throughout each cell generation. Cancer cells frequently increase the rates of mutation in order to accumulate sufficient mutated TSGs or oncogenes required for successful carcinogenesis (Negrini *et al.,* 2010; Salk *et al.,* 2010). This mutability can be brought about by an increase in sensitivity to mutagenic agents, a malfunction in one or more parts of the machinery that maintains genomic integrity, or by both. Moreover, the monitoring systems that typically oversee genomic integrity and drive genetically compromised cells into apoptosis or senescence can be compromised, which can hasten the accumulation of mutations (Hanahan and Weinberg, 2011).

Deregulating cellular metabolism: In normal cellular situation and under aerobic conditions, glucose is converted to pyruvate through glycolysis in the cytosol and then transported to the mitochondria for ATP production. In anaerobic conditions, cells undergo anaerobic glycolysis leading to lactate production (Zheng, 2012). In cancer cells, the rate of glucose uptake is increase and thereby glycolysis and LDH utilisation

even in the presence of oxygen in the phenomenon called the Warburg effect (Hanahan and Weinberg, 2011).

Evading immune destruction: Cancer cells can form a barrier against the immune system and escape from the T-helper cells and natural killer cells, this will lead cancerous cells to grow and form tumours (Hanahan and Weinberg, 2011). In the tumour microenvironment, programmed cell death-1 (PD-1)/PD-1 ligand 1 (PD-L1) is one of the most important key element of the underlying mechanism of cancer immune escape. PD-1 is mainly expressed on T-cells, natural killer cells, monocyte and macrophage, while PD-L1 is normally expressed on antigen presenting cells, bone marrow derived mast cells and mesenchymal stem cells (Zheng *et al.*, 2019). The (PD-1)/PD-1 ligand 1 (PD-L1) pathway regulates immune response and maintain immune tolerance under normal physiological condition by inhibition of T-cell activation, proliferation, and cytokine production. The binding of PD-L1 to PD-1 on T-cells promote inactivation of T-cells and in turn evading immune responses (Hamanishi *et al.*, 2016). Interestingly, PD-L1 is overexpressed by different cancers including breast, ovarian, melanoma, gastro-intestinal and lung cancers (Hamanishi *et al.*, 2016)**.**

Non-mutational epigenetic reprogramming: This term used to describe changes in the epigenetic marks and patterns of gene expression in cancer cells that do not involve changes to the underlying DNA sequence. DNA methylation, histone modifications, and non-coding RNA molecules are examples of epigenetic changes that play a significant role in controlling gene expression and cellular identity (Skinner, 2011; Olynik and Rastegar, 2012). DNA methylation modifications include the addition of a methyl group to particular DNA sequences resulting in DNA methylation, which frequently silences genes (Vandiver *et al.*, 2015). Genomic instability and the reactivation of usually silent genes can result from global hypomethylation (decrease in DNA methylation) in cancer. On the other side, excessive DNA methylation, or hypermethylation, can result in the silencing of tumour suppressor genes, which promotes unchecked cell proliferation and survival (Vandiver *et al.*, 2015).

DNA is wrapped around proteins called histones to form a structure called chromatin. Histones can undergo a number of chemical alterations, such as acetylation,

methylation, phosphorylation, and ubiquitination, which can affect how genes are expressed (Demetriadou *et al.,* 2020). Changes in histone modifications in cancer can lead to aberrant gene activation or repression, affecting crucial physiological functions and encouraging tumour growth (Demetriadou *et al.,* 2020). These epigenetic markers can undergo dysregulation in cancer, resulting in abnormal gene expression patterns and promoting carcinogenesis. (Hanahan, 2022).

Gene expression is controlled by non-coding RNAs, including long non-coding RNAs (lncRNAs) and microRNAs (miRNAs), these non-coding RNAs may exhibit abnormal expression and function in cancer (Costa *et al.*, 2023). For instance, some miRNAs can function as tumour-promoting oncogenes when their expression is overexpressed, whereas others can work as tumour-suppressors when their expression is lost or decreased (Costa *et al.*, 2023).

Polymorphic microbiomes: The human body is full of different microorganisms that can be located in different parts in the body such as colon or mucosa or either in tumours, which can alter their capabilities such as development and progress, eventually to their response to treatments. An example of microbe that promote tumours is the bacterial of the colon *E. coli* that produces toxins resulting in genomic mutations by the *PKS* locus causing colon cancer (Hanahan, 2022)**.**

Cellular senescence: is a type of proliferative pause that is usually irreversible and probably developed as a defence mechanism to preserve tissue homeostasis**.** When the cell division cycle is shut down, the senescence program induces changes in cellular morphology and metabolism, which is done by the initiation of a senescence-associated secretory phenotype (SASP) relating to the release of a plethora of bioactive proteins such as chemokines, cytokines, and proteases, whose uniqueness is reliant on the cell and tissue type from which a senescent cell comes from (Faget *et al.,* 2019; Gorgoulis *et al.*, 2019; Birch and Gil, 2020). Many factors can cause cells to go into senescence, including abnormalities in cellular signalling networks, damage to organelles and cellular machinery, and microenvironmental pressures such starvation and DNA damage (Faget *et al.,* 2019; Gorgoulis *et al.*, 2019; Birch and Gil, 2020).

The SASP has been suggested to be the main mechanism by which senescent cells promote tumour phenotypes. It has been shown to be capable of transmitting signalling

molecules and proteases that activate or excluded them to nearby viable cancer cells as well as to other cells in the tumour microenvironment to convey hallmark capabilities. Senescent cancer cells have therefore been demonstrated to play a variety of roles in proliferative signalling, evading apoptosis, promoting angiogenesis, inciting invasion and metastasis, and inhibiting tumour immunity in numerous experimental systems (He and Sharpless, 2017; Faget *et al.,* 2019; Lee and Schmitt, 2019; Wang *et al.,* 2020).

Unlocking Phenotypic Plasticity: The process of organogenesis involves the development, differentiation, and organisation of cells into tissues to perform homeostatic activities. This is accompanied by terminal differentiation, in which progenitor cells either grow or irreversibly stop growing (Yuan *et al.,* 2019). Therefore, the final product of cellular differentiation is typically antiproliferative, providing a significant obstacle to the ongoing proliferation required for neoplasia. The key element of cancer pathogenesis may involve restricted capacity for phenotypic plasticity in order to avoid or escape the condition of terminal differentiation (Yuan *et al.,* 2019). Dedifferentiation from mature to progenitor states, blocked differentiation from progenitor cell states, and trans-differentiation into distinct cell lineages are only a few of the modifications of cellular differentiation that can be facilitated by phenotypic plasticity, which is arguably an acquired hallmark capability (Hanahan, 2022)**.**
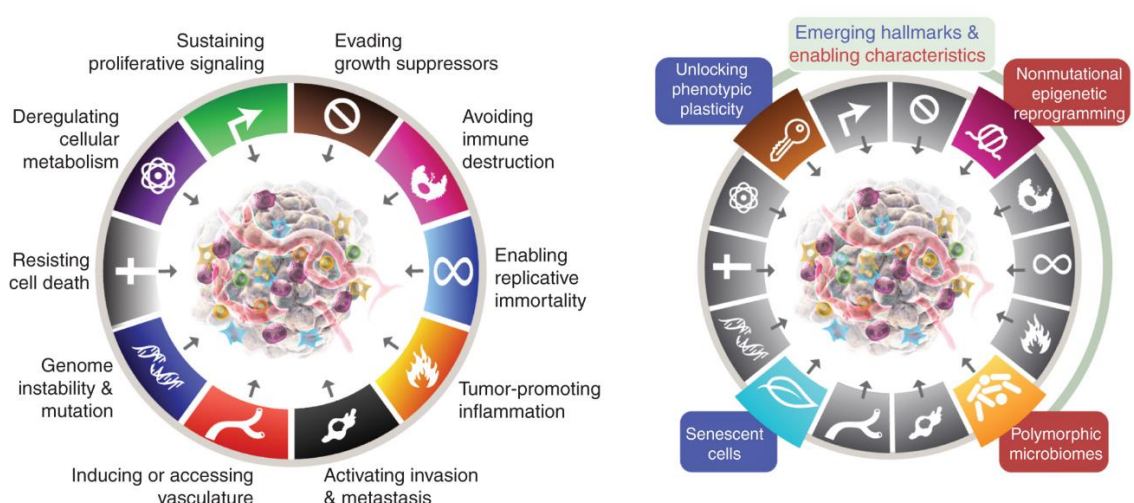
Figure 1.3: The latest hallmarks of cancer. Taken from Hanahan, (2022)**.**

1.2 Breast cancer

Breast is defined as milk-producing gland that made up of fatty connective tissue. Structurally, the ducts carry the milk from the glands to the nipple (Lyons *et al.*, 2020). Hormone changes can affect breast tissue development at different stages of life, for instance, breastfeeding, periods of pregnancy, and puberty (Osborne *et al.*, 2015). Breast cancer is the most common form of female cancer, for example in the UK around 1 in 8 women are diagnosed annually with this disease (Burgess *et al.*, 2005). It is also the most cause of death over 50 years; however, younger women also can get breast cancer (Burgess *et al.*, 2005). The incidence and mortality rates in UK (period of 2011-2014) for every 5 females newly identify with breast cancer, one death will occur with an overall death rate of 34% in UK females aged between 50-69 (period of 2010-2012) (Dubey *et al.,* 2015). In 2017 About 252,710 new cases of invasive breast cancer and 40,610 breast cancer deaths may occur among US women (DeSantis *et al.*, 2017). In 2018 newly breast cancer patients were 2 088 849 worldwide, representing 11.6% of the diagnosed cancers at the same year, with a number of 626 679 deaths (Bray *et al.*, 2018). Recently it is the tumour with the highest incidence rate globally (Duggan *et al.*, 2021) and the most common diagnosed cancer in women and replaces lung cancer as the primary cause of cancer death in 2020 (Bull *et al.*, 2020).

1.2.1 Aetiology

There are no exact causes of the development of sporadic breast cancer. Recent studies displayed several risk factors which might increase the tumour growth. An increasing age, particularly for women over 50 years, a family history of breast cancer, and the inheritance of mutated BRCA1, BRCA2, TP53, and CHEK2 genes (McPherson, 2000). Abnormal cell growth such as atypical ductal hyperplasia and lobular carcinoma could increase the risk of disease (McPherson, 2000). Similarly, use of the female contraceptive pill may slightly increase the risk of breast cancer. Additionally, the lifestyle is one of the problem that connected with it, such as drinking alcohol and smoking (McPherson, 2000). Increased level of oestrogen and other sex hormones such as; oestradiol, estrone, estrone sulphate, androstenedione, dehydroepiandrosterone, dehydroepiandrosterone sulphate and testosterone, have a significant role in increasing

the risk of the development of breast cancer (Kamińska *et al.*, 2015). According to Women's Health Institute (WHI) clinical studies in 2017, there was a similar death rate from breast cancer for women who received hormone replacement therapy (HRT) and vs those who underwent neither oestrogen-alone nor in combination with medroxyprogesterone acetate. In addition, HRT was recommended by the North American Menopause Society for women who under 60 or within ten years of menopause (Micha *et al.*, 2022). In 2019, WHI trials reported 23% reduction in breast cancer incidences for women who underwent oestrogen therapy, while the cancer mortality rate increased by 29% in the case of oestrogen/progestin usage. These trials suggested that oestrogen therapy-alone had mitigating effect on breast cancer incidence compared to oestrogen/progesterone therapy (Micha *et al.*, 2022). On the other hand, obese menopausal women have a twofold increase in the risk of developing breast cancer than premenopausal women (McPherson, 2000).

Furthermore, women with polycystic ovary syndrome have a high level of oestrogens, insulin, and serum insulin-like growth factor [IGF]-I, which may stimulate breast cancer development (Gadducci *et al.*, 2005). High level of lipids intake can induce breast cancer morbidity; there is a clear link between the adiposity and the risk of breast cancer (Blücher and Stadler, 2017). In the same vein, lipid oxidation also can significantly increase the frequency of breast cancer (Gratas-Delamarche *et al.*, 2014).

1.2.2 Type of breast cancer

1.2.2.1 Histological types are divided into four main types according to their site:

Ductal carcinoma in situ (DCIS): Also called intraductal carcinoma type of a non-invasive (or *in situ*) breast cancer. DCIS type begins in the lining of breast milk duct and has not spread into the surrounding breast tissues. Generally is treatable, and it may spread into the surrounding breast tissue if untreated (Feng *et al.*, 2018).

Invasive Ductal carcinoma (IDC): This is the most common type of breast cancer 70-80% of all breast cancer diagnosis. IDC is locally invasive within the breast, spread from the normal breast ducts and invading the surrounding breast tissues (Feng *et al.*, 2018).

This type has several subtypes of the breast carcinomas (tubular, medullary, mucinous, papillary, and cribriform) (Polyak, 2007).

Invasive Lobular Carcinoma (ILC): 10-15% of breast cancers are ILC, making it the second common type (Sharma *et al.*, 2010). It differs from invasive ductal carcinoma in that invasive cells from single-file lines of cells through the stroma, whereas in ductal carcinoma, cells remain predominantly associated with ducts (Barroso-Sousa and Metzger-Filho, 2016)

Metastatic breast cancer: Known to be the advanced breast cancer or stage IV, which have the ability to invade other organs in the body such as liver, lungs, bone and brain and initiate new tumours by entering the circulatory lymph system or migration through blood circulation (Al-Mahmood *et al.*, 2018).

1.2.2.2 Molecular Subtypes of breast cancer: Breast cancers are also divided into four main groups according to the expression of certain genes: Human epidermal growth factor receptor 2 (HER2), oestrogen receptor (ER), and progesterone receptor (PR) as follows: luminal A (ER+, PR±, HER2−), luminal B (ER+, PR±, HER2+), HER2 overexpressing (ER−, PR−, HER2+) and Triple negative breast cancer (TNBC) (ER−, PR−, HER2−) (Parise *et al.*, 2009). TNBC is found in 10-20 % of diagnosed breast cancers, an aggressive form of breast cancer as unlike other forms of breast cancer it will not respond to hormone therapy or Her-2-targeting therapies (Al-Mahmood *et al.*, 2018).

1.2.3 Nottingham grade

Pathologists classify breast tumours according to their histological type and grade. The World Health Organisation (WHO), the American Joint Committee on Cancer (AJCC), the European Union (EU), and the Royal College of Pathologists in the UK (RCPath) are just a few of the organisations that endorse the Nottingham Grading System (Rakha *et al.*, 2010; Provenzano *et al.*, 2015). The system of grading is based on the structure, morphology, and frequency of mitoses in the tumour. Grading specifically reflects the level of differentiation and is based on three factors: nuclear pleomorphism, tubule development, and mitotic count. Each variable receives a score between 1-3, with 3 denoting the least well-differentiated variable. A final grade is assigned, ranging from 1

(low grade, scoring less than 6) to 3 (high grade, scoring more than 7). Compared to grade 1 tumours, grade 3 tumours are more aggressive (Rakha *et al.*, 2010).

Numerous studies have demonstrated that histological grade is a reliable indicator of tumour behaviour and prognosis, particularly in smaller or early-stage tumours where the tumour has not yet had a chance to grow and express its other characteristics. Although there is a correlation between grade and some of the unique forms of breast cancer, such as the fact that tubular tumours are invariably grade 1, it has also been demonstrated to be an independent prognostic factor in several breast cancer subgroups (Rakha *et al.*, 2010). On the other hand, grading is a subjective evaluation that necessitates extensive training and is susceptible to inter-observer inconsistency even in situations that follow best practises (Robbins *et al.*, 1995; Chowdhury *et al.*, 2006).

1.2.4 Stages of breast cancer

The stages of breast cancer cells and its grading influences the prognosis. According to the American Joint Committee on Cancer (AJCC) breast cancer is classified into stages corresponding closely to the TNM staging system, which indicates the tumour size (T), lymph node status (N), and distant metastasis (M) of the malignancy (Brierley *et al.,* 2016). T1 cancers are <2cm, T2 are <5cm, and this relates to stage 1 disease (below). T3 are >5cm without lymph node involvement and this relates to stage 2A (with stage 2B being between 2 and 5cm but with local lymph nodes affected). T4 relates to any tumour attached to the chest well. N1 relates to any local/regional lymph node involvement and N2 relates to distant lymph node involvement. M1 refers to distant metastasis unrelated to N1 or N2 (above) and is referred to as stage 4 disease (below) (Brierley *et al.,* 2016).

Stage 0 or ductal carcinoma *in situ* means the cancer cells have not spread to any surrounding tissue or the lymph nodes. At this stage, the survival rate during the 5 years following diagnosis is usually 100% (Sharma *et al.*, 2010).

Stage 1 breast cancer means that the tumours have not spread to lymph nodes or other organs, and the tumour size is less than 2 cm (Maughan *et al*., 2010). The survival rate during of 5 years is usually 100% (Maughan *et al.,* 2010).

Stage 2A shows that the tumours are less than 2 cm and spread to no more than three local lymph nodes forming metastases around 2mm in diameter. At this stage, the survival rate during of 5 years is almost 95% (Sharma *et al.*, 2010).

Stage 2B is a 2-5 cm tumour that spread to the axillary lymph nodes, or greater than 5 cm in size but not spread to the axillary lymph nodes (Thomson, 2012).

IIIa, IIIb, IIIc (locally advanced) **and IV** (metastasis) stages of breast cancer, the tumour size starts to increase in diameter and spread to more than 10 lymph nodes and form a large size of metastases in bone, liver, or lungs (Maughan *et al.,* 2010) and the survival rate for 5 years is vary between 93% to 22% (Maughan *et al.,* 2010).

1.2.5 Molecular sub-typing of breast cancers

Pathologists also report the tumour hormone receptor and HER2 status, which are then used to further categorise individuals for treatment and prognosis (Thomas and Berner, 2000; Sopik *et al.,* 2017). Using immunohistochemistry (IHC), the ER and PR status is assessed based on the percentage of cancer cells that exhibit positivity and the strength of the stain. Response to endocrine therapy depends on the level of expression, and as few as 1% of cells that stain positively for ER suggest a potential benefit from the treatment with ER antagonists such as Tamoxifen (Campbell *et al.*, 2016). Since the HER2 gene is amplified when the HER2 protein is overexpressed, the HER2 receptor status is reported semi-quantitatively by IHC, and any borderline tumours are further evaluated using fluorescent in situ hybridization (FISH) prior to HER2 targeting therapies such as Herceptin (Gajria and Chandarlapaty, 2011).

1.3 Treatments

Many treatments can help treat breast cancer partially or completely. However, the grade and stage of cancer are usually detecting the type of treatment (Smoot *et al*., 2009). There are different types of treatments that are used separately or in combinations, such as surgical removal, chemotherapy, and local irradiation (Formenti and Demaria, 2009).

1.3.1 Surgery

Surgical options in breast cancer management include lumpectomy, segmentectomy, and quadrantectomy, which require tumour removed. The number of tumours within breast tissue, stage, and grade of cancer determine the need breast conservation surgery, or mastectomy, which includes the removal of the entire breast (Smoot *et al.,* 2009). Surgery is the best choice of treatment mostly for the early stages of the disease including stage 0 and 1 and 2A and mostly curable during these stages. At stage 2B (local lymph node involvement) surgery is combined with chemotherapy, as surgery is not curable alone. Sometimes radiotherapy can be an option of treatment with surgery at this stage (Maughan *et al.,* 2010).

1.3.2 Radiotherapy

The major difference between the radiation and chemotherapy treatments is the way to deliver the therapy. Since the chemotherapies have unspecific distribution of chemical drugs and the toxic nature, radiation therapy is targeted only the area of the body where the cancer is exist (Sharma *et al.*, 2019). Radiotherapy treatment requires exposing cancer cells to high-energy ionizing radiation, which damages DNA in the targets the cell and blocks their ability to divide and proliferate, finally causing cell death (Baskar *et al.*, 2012). It is also recommended for advanced tumour, axillary lymph nodes, and following mastectomy and could be used pre-surgery to reduce the tumour size and increase the effective of operation or after mastectomy (Lawrence, 2012).

To kill the cancerous cells, radiotherapy dose (known as a fraction) is given on alternate days for several weeks (Smoot *et al.,* 2009). The most commonly used worldwide is 50 Gy, delivered in 25 fractions of 2 Gy over 5 weeks (Overgaard *et al.*, 1987). Methods that are used for radiotherapy are external beam, internal radiation, and intraoperative radiation. The external beam (most frequent) uses radiation from linear accelerator to the tumours site.

1.3.3 Chemotherapy

The most conventional breast cancer treatment is chemotherapy. There are many different types of chemotherapy, and around 90% of breast cancer patients receive this treatment (Ogston *et al.*, 2003). The effect of chemotherapy on tumour cells is mainly by obstructing the cell cycle phases specifically or nonspecific. 5'- Fluorouracil (5-FU), Methotrexate, Docetaxel, Paclitaxel, and Vincristine are phase specific drugs that affect primarily DNA replication phase (S) and mitosis phase (M) (Smoot *et al.,* 2009).

Paclitaxel and Docetaxel, inhibits the normal breakdown of microtubules during M phase. Vincristine, alters the chromosomal microtubules separation during M phase. All the previous mentioned drugs affect DNA synthesis or replication, hopefully killing the tumour cells. Unfortunately, they spend long periods of time in the resting stage (G_0). Agents that affect DNA replication (S-phase) and mitosis (M-phase) do not have potent effect on G_0 cells (Smoot *et al.,* 2009). The development of phase nonspecific drugs such as Cyclophosphamide, Doxorubicin, Cisplatin, and Carboplatin improve responses. Cyclophosphamide is a DNA alkylating agent and Doxorubicin is a topoisomerase II inhibitor (Fischbach *et al.*, 2007). Cisplatin and Carboplatin, inhibit cellular DNA synthesis in S-phase (Smoot *et al.,* 2009).

Other targeted drugs are the selective oestrogen-receptor modulators (SERMs) includes Tamoxifen, which is given to ER+ breast cancer women to slow the growth and reproduction of tumour cells by binding to oestrogen receptors, having an anti-proliferative effect. Another targeted drug with a biological modifier is Herceptin, which prevents cellular division by binding to the HER2 protein on mutant cells (Jones, 2003).

However, there are several biological side effects of combined breast cancer treatments. In general chemotherapeutic drugs target all rapidly proliferating cells, which can cause osteoporosis, anaemia, fatigue, and it also targets immune cells, hair loss, and bone marrow cells which leads to reverse side effects (Baldo and Pham, 2013).

1.3.4 Mechanism of drug resistance

Cancer cells can resist anti-cancer therapy via different factors that involve drug resistance such as acquired mutations, the presence of apoptosis suppression, multi-drug resistance proteins that reduce drug uptake, DNA repair mechanisms and the amplification of genes (Assaraf *et al.*, 2019). Additionally, the oncogenes pathway is able to activate cellular metabolism to support the cell proliferation. Overall, 90% of breast cancer patients respond to therapy at the early stages of the disease and 50% of them during metastases, still some patients develop resistance to treatment during the progress of the disease and at a certain time they may develop a total drug resistance (Gonzalez-Angulo *et al.,* 2007).

The anti-cancer drug cisplatin and carboplatin becomes less sensitive due to the direct detoxification by glutathione S-transferases (GST), that have a major role in the drug detoxification (Pathania *et al.*, 2018). These enzymes catalyse sulfydryl group of glutathione to react with electrophilic sites to reduce the damage and lethality of anticancer drugs (Pathania *et al.*, 2018). Multi drug resistance (MDR) proteins reduce the drug accumulation via export the drugs outside the cells. For example in cell culture studies, the breast cancer resistance protein (BCRP/MRP1/ABCG2) is over-expressed in breast cancer cells (MCF-7) that have been selected for topoisomerase-inhibitor resistance (Topotecan, Doxorubicin), and resistance is mediated by BCRP/MRP1/ABCG2 pumping the chemotherapy drugs outside the cells (Zhu *et al.*, 2019).

1.4 Mechanisms of cell death

In multicellular organisms, cell death is an indispensable homeostatic mechanism to maintain tissue mechanism and morphology. Tumour-specific cell death is the main goal of cancer therapies, and malignant cell eradication (Sun and Peng, 2009). Cell death can be programmed or uncontrolled according to the condition of cells. The programmed cell death pathways exist endogenous mechanisms that is distinguished by morphological criteria such as nuclear fragmentation in apoptosis and vacuolation in autophagy. The uncontrolled cell death such as necrosis, is usually due to physical damage of the cells, resulting in cellular content leakage to the surrounding tissues that causes cellular damage (D'Arcy, 2019).

1.4.1 Apoptosis

Apoptosis is a regular programmed cell death in multicellular organisms. It causes DNA fragmentation, cell shrinking, the condensation of chromatin, and nuclear fragmentation that lead to cell death (Napoletano *et al.*, 2019). There are two pathways that initiated apoptosis extrinsic and intrinsic which are triggered by pro-apoptotic death receptors and intracellular BCL2 proteins, respectively (Figure 3).

The intrinsic apoptosis or mitochondrial, pathway signal is elicited inside the cell to damage the cytoskeleton and the DNA, initialised by many factors such as heat shock, toxins, ionising, and bacteria or viral infection (D'Arcy, 2019). Furthermore, the deprivation and decrease in concentration of growth factors in tissues enhances apoptosis. During the mitochondrial outer membrane permeabilization (MOMP) which is induced by Bax, the efflux of effector proteins are mainly regulated by BCL2 protein family, which are divided to many subclasses such as anti-apoptotic (e.g. A1, BCLW, BCL2, BCLXL, MCL1, and promote survival), pro-apoptotic (e.g. BAX, BAK, BCLXS, BOK), and BH3-only death proteins (D'Arcy, 2019). The BCL2 family members insert into the mitochondrial membrane to release apoptogenic factors such as cytochrome *c* and second mitochondria-derived activator of caspase (SMAC), which inhibits XIAP (X-linked inhibitor of apoptosis protein) (Kalkavan and Green, 2018).

An apoptotic protease activating factor (APAF1) binds to cytochrome *c* co-operates with caspase-9 as well as other cofactors, and activate cell death, by the initiation of caspase-9 (Bunz, 2001). Active caspase-9 activates the executioner caspase-3 and -7 (Kalkavan and Green, 2018).

Whereas **the extrinsic apoptosis (death receptor) pathway**, is activated by death ligands binding to cell surface Death receptors to form death inducing signalling complex (DISC) (Figure 1.4) (D'Arcy, 2019). These ligands with the targeted cell membrane receptors induce the pathway via the activation of procaspase-8 or -10 to caspase-8, followed by activation of caspase-3 and caspase-7 (Sun and Peng, 2009; D'Arcy, 2019), ultimately leading to apoptosis unless they are inhibited by XIAP (Kalkavan and Green, 2018).

The activation of caspase-8 can activate the extrinsic pathway directly or indirectly by activation the Bcl-2 family member Bid to release cytochrome *c* from mitochondria (Bunz, 2001). The p53 gene protein crossroads with apoptosis pathway and DNA repair. If DNA damage occurs, p53 orchestrates the repair of it and if not, apoptosis occurs. Caspase-9 and its cofactor Apaf-1 can be essential downstream effectors of p53 during apoptosis, such that inactivation of either Apaf-1 or caspase-9 can substitute for loss of p53 in the inactivation of apoptosis (Bunz, 2001).

In general, avoidance the apoptosis might enable and promote the metastasis (Roos *et al.*, 2013). Many cancer cells depend on the deregulation of proteins to survive; however, if the survival factors such as BCL2 are inactivated, for example by Bax or BH-3 only proteins such as tBid, the carcinogenic cells are more susceptible to apoptosis than normal cells. Currently, the intrinsic and extrinsic apoptosis pathways are possible options for potential targeted cancer therapies, in particular the pro-apoptosis receptors agonists (PARA) and BCL2 are in focus (Roos *et al.*,2013).

1.4.2 Autophagy

Autophagy is another type of programmed cell death where cellular components are degraded, that differ from apoptosis morphologically and mechanically. Morphological changes include the degradation of cellular proteins and cytoplasmic organelles (Rubinsztein *et al.*, 2007). Chromatin condensation or membrane blebbing may occur without any DNA fragmentation, or prominent vacuoles may form (Codogno and Meijer, 2005).

In autophagy type of programmed cell death, lysozymes are able to digest macroproteins or whole organelles as a substrate (D'Arcy, 2019). The component of which can either be recycled or processed and used as a source of energy. The autophagy process could be initiated by many factors such as nutrient deprivation, variety of stressors or signals present during cellular differentiation (D'Arcy, 2019). Three forms of autophagy have been distinguished: macroautography, microautography, and selective autography (D'Arcy, 2019).
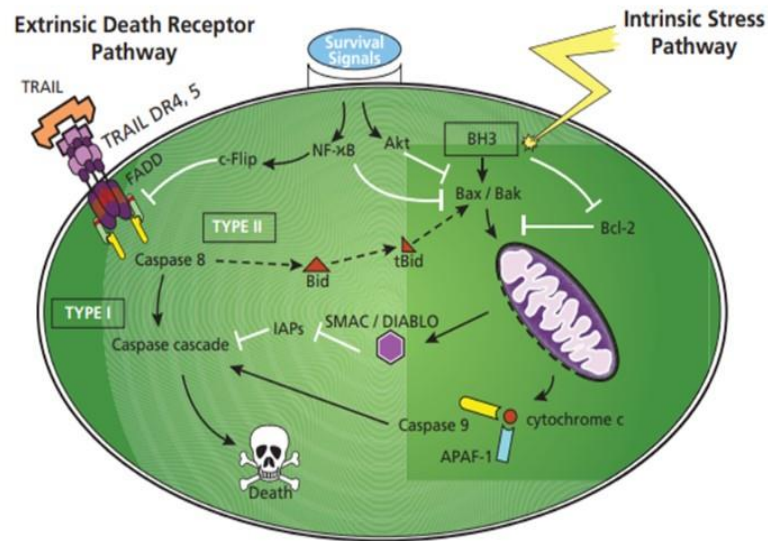
Figure 1.4: Apoptosis signalling pathway. When TRAIL binds to DR4/5 it recruits FADD, activating caspase-8, and triggers the executioner caspase in type I cells. The caspase-8-mediated cleavage and activation of the pro-apoptotic BH3 family member Bid in type II cells upon TRAIL signalling provides a link to the intrinsic apoptosis pathway. After being cleaved by caspase-8, the truncated active form of Bid (tBid) interacts with Bak or Bax to cause MOMP (mitochondrial outer membrane permeabilization). The second mitochondria-derived activator of caspases (SMAC)/DIABLO is then released from mitochondria, together with the pro-apoptotic protein cytochrome *c*. The protein complex formed by cytochrome c, APAF-1, and procaspase-9 enables the production of active caspase-9, which then cleaves the downstream effector caspases, convergently and enhancing death receptor-mediated caspase activation. Additionally, the caspase activation-restraining inhibitors of apoptosis (IAP) family members are antagonised by the release of SMAC/DIABLO from the mitochondria. The intrinsic pathway can be activated by cellular stress such as hypoxia, growth factor depletion, chemotherapy, and p53, a part of DR4/5. Moreover, a number of anti-apoptotic survival signals may block this pathway. Taken from Sayers and Cross, (2014).

Microautophagy are more specific than macroautophagy and can be detected by signalling molecules present on the surface of damaged organelles such as mitochondria resulting in specific fusion lysosomes with these organelles (D'Arcy, 2019). In normal cellular conditions, autophagy process to maintain biological functions, hemeostasis, controlling cell content, and removing old proteins and injured organelles (Yun and Lee, 2018). A series of proteins control autophagy. Mammalian target of rapamycin (mTOR) is related with cell proliferation, stress, and cancer progression. mTOR have two complexes, mTORC1 and mTORC2, each exhibit distinct functions and localization. Phosphorylation of autophagy-related protein (ATG) leads to the inhibition of autophagy, which is activated by mTORC1. Inhibition of mTORC1 during starvation or organelle damage enhances autophagy. mTORC1 is regulated by AMP-activated protein

kinase (AMPK), an increase in AMPK induces the autophagic process by the inhibition of mTORC1 (Yun and Lee, 2018).

In cancer, autophagy is a physiological mechanism that allows cells to survive, consequently by recycling macromolecules. By understanding the relationship between autophagy and cancer, several potential anti-cancer drugs have been developed, and an example is rapamycin, which targets mTORC1 in cancer cells (Rubinsztein *et al.*, 2007).

1.4.3 Necrosis

Necrosis is a process of uncontrolled cell death, which is stimulated external agents such as radiation, heat, chemicals, hypoxia (D'Arcy, 2019). The premature cell death is due to cell swelling followed by blebbing, shrinking of the nucleus, condensation of chromatin, and finally degradation of the nucleus into the cytoplasm (White-Gilbertson *et al.,* 2008). The process includes upregulation of several pro-inflammatory proteins, such as nuclear factor-κB, causing the cell membrane rupturing and spillage of the cell contents into nearby cellular tissues, causing in a cascade of inflammation and tissue damage (D'Arcy, 2019).

Another form of cell death is a **necroptosis**, which is a highly regulated process of cell death, it is mediated by death receptors commonly by TNFR-1, TRAIL and FAS receptors which can promote necroptosis. Whereas the term oncosis is a mechanism that switches between apoptosis, autophagy and necrosis. Oncosis can be induced by sudden cell death and causes a leakage of cellular debris into surrounding tissues, and damage surrounding cells (D'Arcy, 2019).

1.4.4 Anoikis

Anoikis, is a form of apoptotic form of cell death that occur due to the cellular loss of adherence to its extracellular matrix (ECM) (Taddei *et al.*, 2012). As being an apoptotic related form of cell death, it can be initiated by both intrinsic pathway by mitochondria cytochrome c release and/or extrinsic pathway by cell death receptors to start the activation of series of executioner caspases, which are both controlled by Bcl-2 family (Taddei *et al.*, 2012) as explained previously in the apoptotic section. Cancer cells have

the potential to avoid anoikis, allowing metastasis to other tissues due to the initial loss of adherence to ECM (Simpson *et al.,* 2008).

1.5 Ferroptosis

Ferroptosis is a newly discovered form of cell death established in 2012 by the work of Dixon and his colleagues (Dixon *et al.*, 2012). This form of death is an iron programmed cell death that is induced by lipid peroxidation. It is characterised by the massive accumulation of reactive oxygen species (ROS) to induce lipid peroxidation in the cell (Figure 1.5) (Dixon *et al.*, 2012). Morphological features differ from other forms of PCD and includes mitochondria that appear smaller than normal (Yagoda *et al.*, 2007; Dixon *et al.*, 2012). Due to the role of iron in mediating the production of reactive oxygen species and enzyme activity in lipid peroxidation, many aspects of iron metabolism, such as iron uptake storage and efflux, control it (Li *et al.*, 2020). Moreover, the sensitivity of ferroptosis is regulated by iron homeostasis (Liang *et al.*, 2019).

Many studies have found that glutathione peroxidase 4 (GPX4), lipid synthesis, iron metabolism and the Nrf2 pathway play a critical role to regulate the ferroptosis process (Li *et al.*, 2020).

1.5.1 Mechanism of ferroptosis

Iron plays an essential role in sensitising cells to ferroptosis (Cao and Dixon, 2016), as an important factor for the formation of ROS via enzymatic or non-enzymatic reactions. Intracellular iron maintains a delicate balance by iron transport systems (Lu *et al.*, 2018). Extracellular iron can be imported by its carrier protein transferrin receptor (TFR) and circulating glycoprotein transferrin (TF) (Lu *et al.*, 2018). Imported iron is stored and transported in the form of the iron-protein complex (mainly ferritin) (Trujillo-Alonso *et al.*, 2019). The only known iron exporter that controls iron efflux in mammal by ferroportin (FPN) (Trujillo-Alonso *et al.*, 2019). Either increased iron uptake or reduced iron export can sensitize cancer cells to oxidative damage and ferroptosis. Intra- cellular labile iron (redox-active Fe^{2+}) levels can be elevated by TF-mediated iron uptake or autophagic/lysosomal degradation of ferritin (ferritinophagy) (Stockwell *et al.*, 2017).
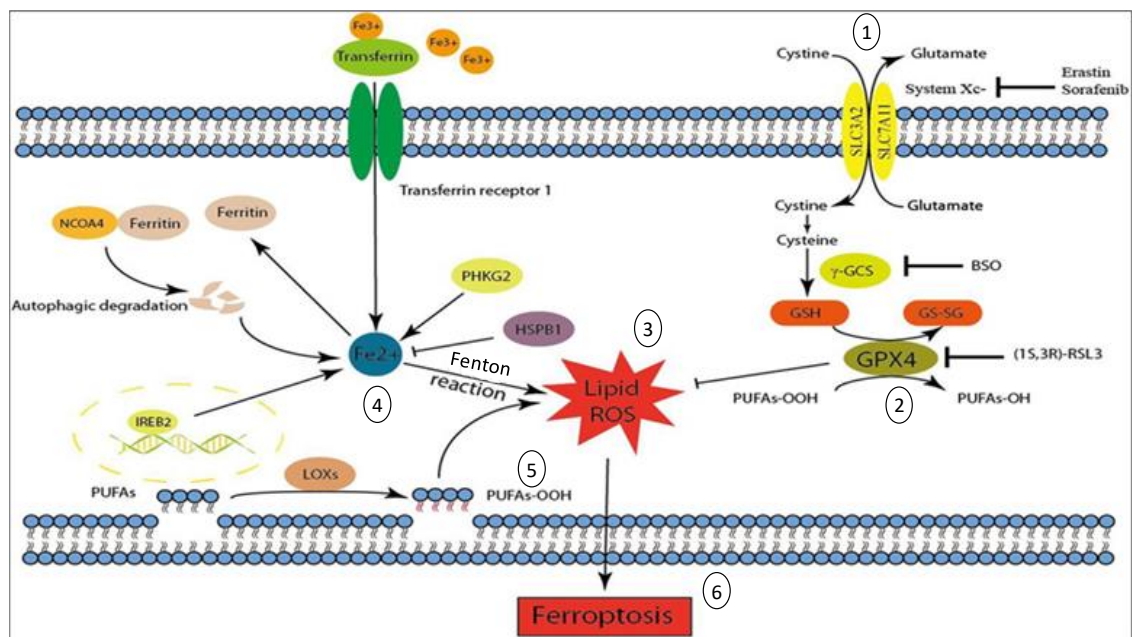
Figure 1.5: Ferroptosis pathway starts by the inhibition of system Xc– (1) or GPX4 activity (2) by ferroptosis inducers leading to the accumulation of ROS (3), excess cellular iron (4) and PUFAs all lead to Lipid ROS or Lipid Peroxidation (5) leading to ferroptosis (6). Modified from Lu *et al.*, (2018).

The uptake of Cystine (Cys), a precursor of cysteine, by system Xc– represents the upstream event of ferroptosis cascade under oxidative extracellular conditions. Under reducing conditions, cystine can be directly imported via the alanine/serine/cysteine transporter (system ASC). Glutathione (GSH) is an important intracellular antioxidant, which is generated from glutamate (Glu), cysteine, and glycine (Gly) in two steps under the catalysis of cytosolic enzymes glutamate-cysteine ligase (GCL) and glutathione synthetase (GSS), respectively (Liang *et al.*, 2019) (Figure 1.6). The transulfurylation pathway, converting methionine (Met) into cysteine, can sustain the intracellular cysteine level (Liang *et al.*, 2019). Phosphatidylethanolamines (PEs) containing arachidonoyl (AA) or adrenoyl (AdA) moieties (PE-AA/PE-AdA) are the predominant substrates that undergo oxidation and involve in ferroptosis. The fatty acid translocase (FAT) and fatty acid transport protein (FATP) are responsible for the uptake of AA/AdA. With the help of enzyme acyl-CoA synthetase long-chain family member 4 (ACSL4) and lysophosphatidylcholine acyltransferase 3 (LPCAT3), free polyunsaturated fatty acids (PUFAs) can be esterised and incorporated into membrane phospholipids (Liang *et al.*, 2019). Iron-catalyzed enzymatic (ALOXs) and non-enzymatic (Fenton chemistry) processes are involved in the production of phospholipid hydroperoxides (PE-AA-

OOH/PE-AdA-OOH) (Liang *et al.*, 2019) (Figure 1.6). The mevalonate pathway involved in ferroptosis can generate biomolecules with potential anti-ferroptotic activity. GPX4, an important protein for ferroptosis, competes with lipid peroxidation by transforming toxic PE-AA-OOH/ PE-AdA-OOH into non-toxic phospholipid alcohols (PE-AA-OH/PE-AdA-OH) (Liang *et al.*, 2019) (Figure 1.6). During this process, GSH acts as the electron donor. Oxidized GSH (GSSG) can be reduced to GSH by glutathione reductase (GSR) using reduced nicotinamide adenine dinucleotide phosphate (NADPH) (Liang *et al.*, 2019). In addition, the RAS–RAF–MEK pathway was found to play a decisive role in ferroptosis sensitivity in some cancer cell lines (Yagoda *et al.*, 2007) (Figure 1.6).
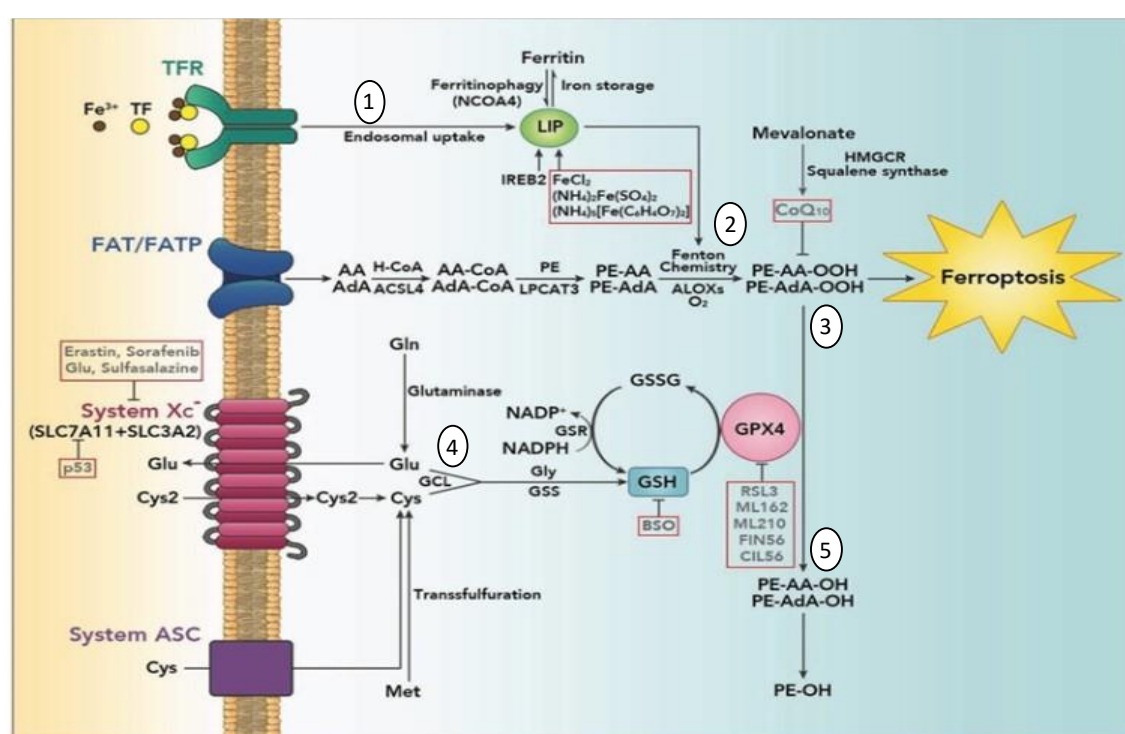
Figure 1.6: **Ferroptosis regulating components**. Intracellular iron contributes to the labile iron pool (LIP) and iron is provided from TFR-mediated endocytosis or ferritin ferritinophagy (1). Increased LIP leads labile iron ions to undergo Fenton-like reaction, leading to ferroptosis (2). PUFAs esterified and absorbed into membrane phospholipids. Iron catalyzed enzymatic (ALOXs) and non-enzymatic such fenton chemistry, processes are involved in the generation of phospholipid hydroperoxides (PE-AA-OOH/PE-AdA-OOH) (3). Cys and Glu uptake controlled by system Xc– allows the formation of GSH (4). GPX4, an important enzyme for ferroptosis, competes with lipid peroxidation by transforming toxic PE-AA-OOH/ PE-AdA-OOH into non-toxic phospholipid alcohols (5). Abbreviations: ALOXs, arachidonate lipoxygenases; BSO, buthionine sulfoxi- mine; CoQ10, coenzyme Q10; Gln, glutamine; HMGCR, 3-hydroxy-3-methylglutaryl-CoA reductase; IREB2, iron-responsive element binding protein 2; NCOA4, Nuclear receptor coactivator 4; NADP+, nicotinamide adenine dinucleotide phosphate; TF, transferrin receptor. Modified from Liang *et al.*, (2019).

One reason is that oncogenic RAS increases cellular iron by upregulating transferrin receptor (TFR) and downregulating ferritin. To sustain the fast proliferation, cancer cells have a higher demand for iron than their non-malignant counterparts. Down regulated FPN and upregulated TFR1 have been observed in many cancer cell lines (Yagoda *et al.*, 2007). The strong iron dependency (iron addiction) produces cancer cells that are more susceptible to iron overload and ROS accumulation than noncancerous cells, potentially enabling tumour microenvironment targeted, ferroptosis-mediated cancer therapy (Yagoda *et al.*, 2007).

1.5.2 Nuclear factor erythroid 2-related factor 2 (Nrf2)

The activity of Nrf2 is regulated by Kelch-like ECH-related protein1 (Keap1)(Choi and Jeon, 2020). The overexpression of Nrf2 is involved in preventing or correcting redox imbalances in the cell (Choi and Jeon, 2020). Nrf2 is a transcription factor that binds to and activates genes containing an antioxidant response element (ARE). Furthermore, it plays a critical role in mediating the metabolite pathways such as drug and apoptosis metabolism, with dysfunction of Nrf2 pathway with contributing to the development of a wide array of pathologies (Choi and Jeon, 2020). This infers that while electrophilic modification of Keap1 can activate Nrf2 to prevent lipid peroxidation and ferroptosis, several reactive lipid species can suppress the function of Nrf2 target genes, which could in turn play an important role in initiating the ferroptotic cascade (Y. Zhang *et al.*, 2020).

During oxidative stress, Nrf2 helps to promote the cell survival, and the inhibition of Nrf2 pathway or its downstream target genes could increase the rate of cell death (Schwarz *et al.*, 2019). Likewise, RLS3 (RAS-selective lethal) and Erastin are the two ferroptosis-inducing agents and downstream targets of Nrf2, also they initiate the ferroptosis cascade via the inhibition of GPX4 and the cysteine/glutamate transporter system Xc−, respectively (Shin *et al.*, 2018). The main role of Nrf2 target genes are anti-oxidant response genes, as well as ferroportin (SLC40A1), which is responsible for iron efflux out of the cell (Dodson *et al.,* 2019).

Furthermore, many enzymes, such as heme-oxygenase 1 (HMOX1), catalase, and ferrochelatase (FECH) are directly regulated by Nrf2 (Schwarz *et al.*, 2019). Apart from heme and iron, Nrf2 regulates a host metabolism process such as catabolism and

detoxification for regenerating NADH that plays a critical role in substrate oxidation (Chen *et al.*, 2020). Also, Nrf2 induces glutathione S-transferase. Also as Nrf2 is an integral indirect anti-ferroptotic reducer of lipid peroxides, the mitigation of both ferroptosis and lipid peroxidation and their associated diseases could be result by Nrf2 signalling (Chen *et al.*, 2020). The lipid peroxidation of Nrf2 signalling pathway components is involved in preventing the formation of lipids peroxides and progression of the ferroptosis cascade (Chen *et al.*, 2020). In summery Nrf2 is a key regulator of the antioxidant response that regulate the activity of numerous ferroptosis and lipid peroxidation-related proteins. Nrf2 proteins can be divided into three major classes, iron/metal metabolism, intermediate metabolism, and GSH synthesis/metabolism) (Dodson *et al.,* 2019).

1.5.3 Inducers of ferroptosis

Ferroptosis can be induced by blocking system Xc- with small molecules such as Erastin leading to decreased glutathione. Ferroptosis can also be induced by deletion of GPX4 encoded genes or inhibition of GPX4. Both causes disruption of lipid metabolism balance by increasing oxidizable polyunsaturated phospholipids or interfere iron homeostasis can also sensitize cells to ferroptosis (Doll *et al.*, 2017).

There are different types of ferroptosis inducers that have been reported. The survival and growth of cancer cells are strongly dependent on the transport activity of system Xc- (Hassannia *et al.,* 2019). System Xc- inhibitors such a Erastin can inhibit cystine uptake leading to glutathione depletion in cells dispossessed of cysteine. (Dixon *et al.*, 2014).

System Xc- also known as xCT is encoded by SLC7A11 (Solute Carrier Family 7 Member 11)*,* that functions as substrate-specific subunit of the cysteine-glutamate transporter. Inducing cells with ferroptosis inducers causes upregulation compensatory of SLC7A11 eventually causing anti-cancerous activity (Zhao *et al.*, 2020). These variations can be pharmacodynamic biomarkers for identification of system Xc- inhibition and ferroptosis (Dixon *et al.*, 2014).

1.5.3.1 Erastin

Erastin is a cell-permeable ferroptosis activator and an anti-tumour agent that is selective for cell expressing oncogenic RAS (Dixon *et al.*, 2012). Erastin can reduce GSH levels by inhibiting system Xc− directly by preventing cystine and glutamate uptake. Erastin is the prototype ferroptosis inducer, causing a novel type of cell death that differs from the traditional apoptotic cell death (mitochondrial cytochrome *c* release, caspase activation) (Dixon *et al.*, 2012, 2014). Recent studies showed that Erastin can hyperpolarize mitochondria membranes in cancer cells, resulting in mitochondrial damage eventually to cell death (Fang and Maldonado, 2018).

1.5.3.2 RSL3

Dolma *et al.*, (2003) identified two structurally unrelated small molecules, named Erastin and RSL3, that were selectively lethal to oncogenic RAS- mutant cell lines, and which are referred to together as RAS-selective lethal (RSL) compounds (Dolma *et al.*, 2003). Yang and Stockwell, 2008 identified voltage dependent anion channels 2 and 3 (VDAC2/3) as an additional direct target of Erastin (Yagoda *et al.*, 2007), but not RSL3. RSL3 induces ferroptosis by targeting GPX4 directly via its chloroacetamide moiety. RSL3 stops GPX4 activity directly throw its alkylation of the selenocysteine (Yang and Stockwell, 2008). Both Erastin and RSL3 inhibit the ferroptosis pathway in cancer cells by disturbing the redox homeostasis and allowing the iron-independent accumulation of lethal ROS (Dixon *et al.*, 2012)

1.5.3.3 FIN56

Recently Shimada and his colleagues discovered the novel mechanism by which FIN56 triggers cellular death and provides new insights on the regulation of ferroptosis (Shimada *et al.*, 2016). FIN56 was discovered by modulatory profiling of 56 caspase-independent lethal compounds. There are two distinct pathways that contribute to the ferroptosis inducing ability of FIN56. First, FIN56 binds to and activates the enzyme squalene synthase (SQS), an enzyme responsible to produce cholesterol, resulting in the depletion of endogenous antioxidant coenzyme Q10 (CoQ10). Second, FIN56 promotes the degradation of GPX4, which requires the enzymatic activity of acetyl-CoA

carboxylase (ACC) (Hassannia *et al.*, 2019; Liang *et al.*, 2019a). The cells that die by FIN56-induced ferroptosis are accompanied lipid ROS production and can be reversed by vitamin E or iron chelators, that mean they are potent inducers of ferroptosis (Shimada *et al.*, 2016).

1.5.4 Inhibitors of ferroptosis

1.5.4.1 Deferoxamine

Deferoxamine (DFO) is a classic ferroptosis inhibitor that can be used as a neutralizer to prevent ferroptosis and injury to normal cells and tissues. Iron chelating agent deferoxamine has been used as a ferroptosis inhibitor (Kose *et al.*, 2019). However, the short half-life of which limits its clinical application (Wu *et al.*, 2020).

1.5.4.2 Liproxstatin-1

Liproxstatin-1, a spiroquinoxalinamine derivative, is able to prevent cell death caused by ferroptosis inducers (Erastin and RSL3). However, it could not rescue cells dying by apoptosis or necroptosis, indicating that Liproxstatin-1 is a specific inducible loss of ferroptosis. Also, Liproxstatin-1 could significantly increase the protein levels of Nrf2 which helps to promote the cell survival (Feng *et al.*, 2019).

1.5.4.3 Ferrostatin-1

Ferrostatin-1 is an arylalkylamine lipid ROS scavenger, with N-cyclohexyl moiety serving as lipophilic anchor within biological membranes and eliminating free radicals (Li *et al.,* 2017). Ferrostatin-1 was identified as a selective inhibitor of ferroptosis, that prevents cellular accumulation of lipid ROS induced by Erastin (Dixon *et al.*, 2012).

1.5.5 Role of iron in ferroptosis

Execution of ferroptosis requires the existence of high levels of intracellular iron Ferroptotic death could be suppressed by iron chelators and promoted by transferrin and its receptor (Gao *et al.*, 2015). Owing the ability of iron to pass electrons by converting between ferric (Fe^{3+}) and ferrous (Fe^{2+}) oxidation states, and it has a critical

role in cellular energy producing and intermediate metabolism (Andrews, 2008).

1.5.6 Modulation of ferroptosis with chemotherapy

Cancer cells can experience numerous forms of regulated cell death during tumour development. Activation of regulated cell death is a primary and favourable strategy for cancer therapy (Lu *et al.*, 2018). Cancer cell resistance to chemotherapy is a main problem in cancer treatment, making cells resistance to cell death and is a common feature of most chemotherapy drugs. Due to the different molecular mechanism and features of ferroptosis, it is likely to become a promising treatment to overcome chemotherapy resistance in cancer cells (Xu *et al.*, 2019). Studies on epithelial mesenchymal transition state showed that ferroptosis inducers on GPX4 inhibition are specifically lethal in via ferroptotic cell death. These promising results lights the way to overcome drug resistance in many cancers (Xu *et al.*, 2019).

A promising study showed a sensitive effect of ferroptosis on triple-negative breast cancer than ER positive breast cancer (Doll *et al.*, 2017). Other study showed that the inhibition of GPX4 can be a potential treatment to overcome drug resistance in breast cancer using RSL3 (Chen *et al.*, 2017; Yu *et al.*, 2019). Li *et al.*, (2019) investigated the potential of combining ferroptosis-inducing agents with standard chemotherapy in lung cancer. They discovered that the combination of Erastin, a ferroptosis inducer, with cisplatin enhanced the therapeutic effect against lung cancer cells compared to chemotherapy alone (Y. Li *et al.*, 2019). The human pancreatic duct epithelial cell line H6C7 was targeted with ferroptosis to improve chemotherapy efficacy. The researchers demonstrated that the combination of gemcitabine, a commonly used chemotherapy drug, with a ferroptosis inducer RSL3, effectively enhanced the sensitivity of gemcitabine in pancreatic cancer (Z. Ye *et al.*, 2020). Combinations of NCX4040 (non-steroidal nitric oxide donor), a highly toxic anti-cancer compound, with Erastin or RSL3 enhanced the cytotoxic effects of NCX4040. Ferroptosis caused by NCX4040 may also be a dynamic type of cell death used to treat different malignancies such as ovarian cancer (Sinha *et al.*, 2023).

1.5.7 Potential role of ferroptosis in cancer radiotherapy

Radiotherapy treatment is used to treat the primary tumour as well as dissemination to secondary sites such as the lymph nodes (Wu *et al.*, 2020). The high energy ionizing radiation (IR) using X-rays targets the double stranded DNA and establishes ssDNA or dsDNA breaks. Ferroptosis inducers able to inhibit the both system Xc− and GPX4 and increase the effect of radiation against breast cancer and sarcoma in part via glutathione depletion (Wu *et al.*, 2020)

Additionally, the IR upregulates and induces ROS directly which can result in activation and release of Nrf2 from Keap-1. This can have two possible effects: Nrf2 induced anti-oxidant response genes to combat ROS, potentially preventing further IR-mediated cell death. Alternatively IR inactivates SLC7A11 and GPX4 pathway to increase the radiosensitivity of cancer cells to IR, which suggest the improvement of radiotherapy effect on resistance cancer cells (Figure 1.7) (Li *et al.*, 2020).
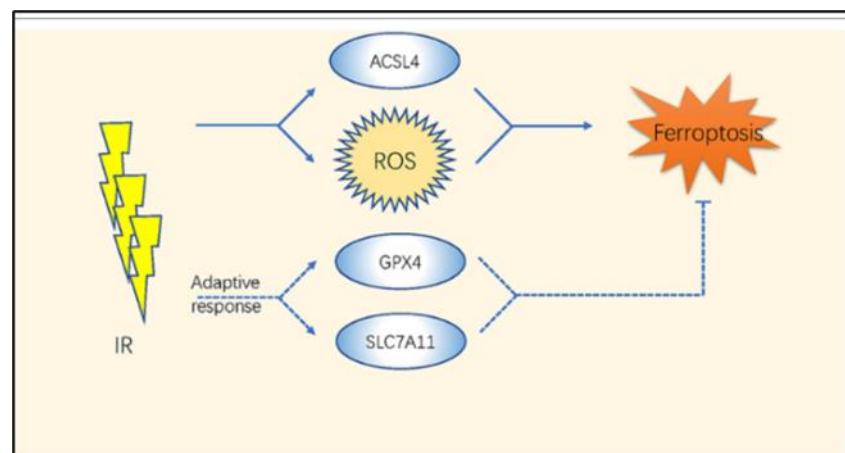
Figure 1.7: The mechanism of ferroptosis in cancer with radiotherapy. Taken from Wu *et al.,* (2020).

1.5.8 Ferroptosis as potential treatment in cancer therapy

In the recent years, many drugs have emerged as cancer therapy, and researchers have attempted to apply ferroptosis to overcome therapy resistance in breast cancer. For example, both of salinomycin and ironomycin can induce the iron accumulation in lysozymes and promote the ferroptosis significantly (Mai *et al.*, 2017). Furthermore, the

use of the tyrosine kinase inhibitor sorafenib increases the death rate of cancer cells with a positive effect on ferroptosis pathway (Sang *et al.*, 2019).

1.6 Cell culture

The term "cell culture" describes techniques used in laboratories to allow eukaryotic cells to grow under physiological circumstances. Its introduction to the study of tissue growth and maturation, virus biology and vaccine creation, the function of genes in health and illness, and the production of biopharmaceuticals using large-scale hybrid cell lines may be traced back to the early 20th century (Segeritz and Vallier, 2017). The varieties of cells that can be cultivated in vitro are as varied as the experimental uses for cultured cells. However, when used in a therapeutic setting, cell culture is most frequently associated with the development of model systems used to research fundamental cell biology, mimic illness processes, or test the toxicity of novel medication molecules (Segeritz and Vallier, 2017).

1.6.1 2D cultures

In two-dimensional (2D) cell culture, cells grow as a monolayer structure attached to a plastic surface, in flasks or in a flat petri dish. 2D cell culturing is very simple to perform and functional. It is also non expensive technique (Kapałczyńska *et al.*, 2016). 2D cell culture has many disadvantages, most important the grown cells in 2D do not mimic the microenvironment of tissues or tumours (Kapałczyńska *et al.*, 2016). Because cell-cell and cell-extracellular environment interactions are not embodied as they should be in the tumours, cell differentiation and proliferation, gene expression, drug metabolism, and other cellular functions are altered. Also, after isolating cells from tissues to 2D mode, morphological changes occur. These changes can affect cellular function as well as signalling pathways (Kapałczyńska *et al.*, 2016).

1.6.2 3D cultures

Hamburg and Salmon in the 1970s made the first three-dimensional (3D) cultures in a soft agar solution (Hamburger and Salmon, 1977). Since then, 3D cell culture modules are sharing similarities between the morphology and behaviour of cells growing in

tumours, allowing them to mimic the *in vivo* conditions of them. On the advantages of using 3D cell culture that it can provide an alternative to animal models (Kapałczyńska *et al.*, 2016).

1.6.2.1 Types of 3D cultures

There are many types of 3D cultures, one is the Harrison technique was modified to create 3D spheroid shapes using the hanging drop technique (Figure 1.8), which was adapted by Kelm and his colleagues (Kelm *et al.*, 2003). The method in general is simple, it is done by adding 20 μl of cell suspension into each well of a well plate. After cell seeding, the tray is turned upside down, and aliquots of the cell suspension become hanging droplets that are held in place by surface tension. At the liquid-air interface at the drop's tip, cells accumulate and have the ability to grow. Cells are incubated according to traditional cell culture techniques while moisture levels are maintained using bioassay dishes, which serve as moisture chambers (Kelm *et al.*, 2003). For several different cell lines, the hanging drop approach has been shown to produce one 3D spheroid per drop with nearly 100% repeatability (Kelm *et al.*, 2003). Instead of loose cell aggregates, firmly packed spheroids are created, and they exhibit minor size variation. This approach relies on cells innate tendency to adhere to one another rather than matrices or scaffolds, consequently there are no concern about how these materials might affect the 3D structures created. The amount of the liquid drop holding cells is a potential disadvantage of the hanging drop (Kelm *et al.*, 2003).

Another type is the low adherence plate method (Figure 1.9) (also called forced-floating method), is a relatively easy method for creating 3D spheroids, by preventing the cells from adhering to the vessel surface through altering the surface, so they can float. This encourages cell-cell interactions, which encourages the creation of multicellular spheres (Lin and Chang, 2008). Spheroid production with forced-floating has many advantages. As similar amounts of cells can be set in each well to produce consistent spheroids, it can be straightforward to do and typically reproducible (Ivascu and Kubbies, 2006).

A) Hanging drop in 96 well plate
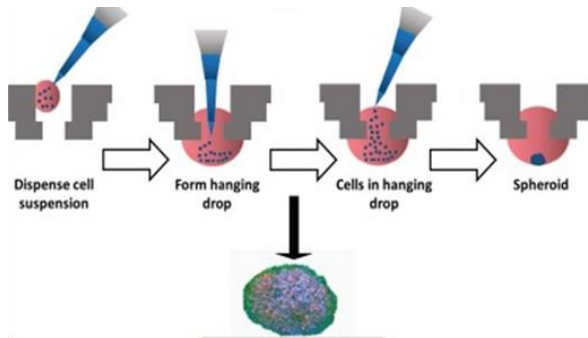
A) Hanging drop in 96 well plate   **B) Hanging drop in petri dish**
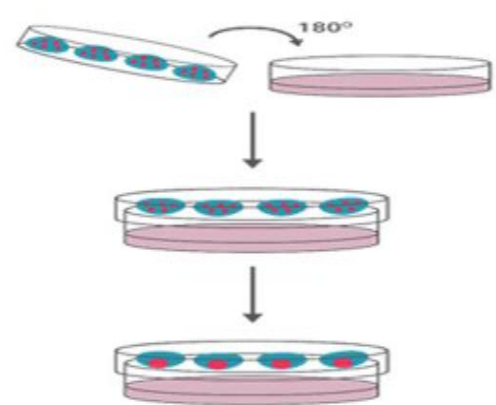
Figure 1.8: Hanging drop 3D culture technique. Taken from Palubeckaite, (2018); Creative Bioarray, (2023).

Spheroids can therefore be made in a variety of sizes, to make larger spheroids, simply seed them with more cells. Spheroids can be used for high-throughput drug testing since the created spheroids can be conveniently assessed for experimentation on individual spheroids when it is needed (Ivascu and Kubbies, 2006). It is simple to create a large number of morphologically homogenous 3D spheroids because they are normally produced in a 96-well plate. The efficacy vs toxicity of medications, gene expression in spheroids, and various other cellular and biochemical assays can all be studied in high-throughput using this method (Friedrich *et al.*, 2009). 3D cultures can be created using the same basic idea of inhibiting cell adhesion to the culture vessel, by applying a thin layer of 1.5% agarose in culture medium to the surface of the culture plate. The formation of 3D spheroids is the result of the agar's ability to hinder cell attachment to the surface (Friedrich *et al.*, 2009; Li *et al.*, 2011). The technique using agar is simple and affordable, and it is suggested to enable long-term cell culture at least 20 days (Friedrich *et al.*, 2009).
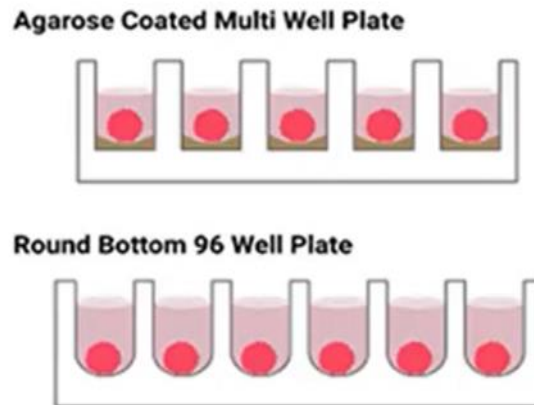
Figure 1.9: Low adherence plate method. Taken from Shoval *et al.*, (2017)**.**

One of the most common type of 3D cell culture for cancer studies is the scaffolds (Figure 1.10) (or spheroids) (Arhoma *et al.*, 2017; Lucy E. Flint *et al.*, 2020), which allow cells to be seeded and allow the cells to move between the scaffold's fibres and adhere to them. Cells fill the interstitial space between fibres as they multiply and expand, creating three-dimensional (3D) cellular structures (Sourla *et al.,* 1996). For this aim, biodegradable compounds including collagen, laminin, alginate are frequently utilised. (Glicklis *et al.*, 2000). These components can be addressed to create hydrogels that can be used as scaffolding for 3D cell culture. Extracellular matrix (ECM)-containing gels appear to be able to relay *in vivo*-like stimuli to cells, enabling *in vivo*-like cell behaviour (Justice *et al.,* 2009).

3D spheroids of malignant cells has been generated using sodium alginate, a naturally occurring polymer taken from algae, after it has been chelated with Ca^{2+} and created crosslinks to create a scaffold (Palubeckaitė *et al.,* 2020). This method has the benefit of having a clonal developed model that is dependent on cancer cells' capacity to form colonies, which is a crucial trait of cancer stem cells or tumour-initiating cells. (Liu *et al.*, 2015). Few spheres in this model grow to be larger than 400 μm in diameter. (Palubeckaitė *et al.*, 2020).

Based on the regional distribution of a range of endogenous chemicals in a 3D spheroid, regions of tumour heterogeneity and the hypoxic microenvironment can be identified.

The aggregoid models metabolic signalling was described by protein markers of proliferation (Ki-67) and hypoxia (GLUT1), which identify the cellular environments within 3D spheroid with Ki-67 proliferation cells around the outer edge, and GLUT1 expressed only in the hypoxic core (Lucy E. Flint *et al.*, 2020).
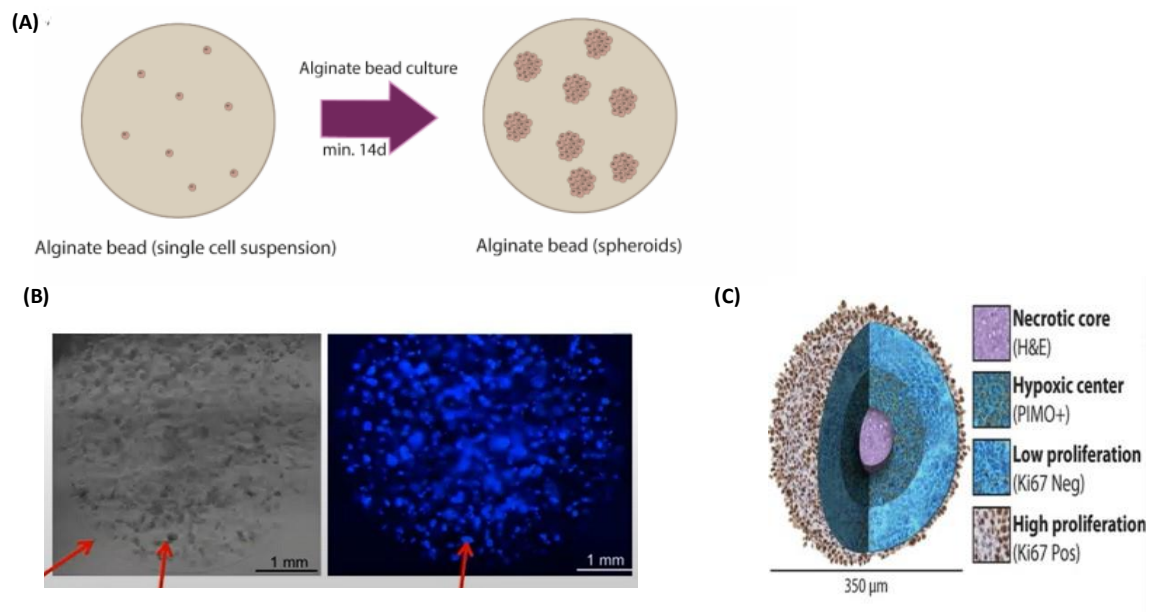
Figure 1.10: 3D Alginate Spheroids. (A) Alginate bead from single cell suspension. **(B)** A spheroid imaged under bright field and fluorescent microscope. **(C)** A spheroid microtumour model. The necrotic core is depicted in a composite of immunohistochemical images as having extensive lacunae of necrosis (haematoxylin and eosin stained), hypoxic region (pimonidazole duct staining), and zones of low and high proliferation (Ki67 low and Ki67 high respectively). Taken from Horman, (2016); Palubeckaite, (2018).

1.6.3 Comparison between 2D and 3D cell cultures with ferroptosis

Adherent cultures normally grow as monolayers that allow the study of only one cell type of cells (Fischbach *et al.*, 2007), resulting in a lack of tumour microenvironment (Jose, 1998). Due to the many disadvantages of 2D systems, an alternative model such as 3D culture was established to mimic the natural microenvironment of the tumours (Kapałczyńska *et al.*, 2016).

A study showed that 90% of cells cultured in 2D cell culture are sensitive to ferroptosis whereas in 3D spheroids using the same cell lines, the sensitivity of these cells to ferroptosis decreased from 90% to 30%. (Demuynck *et al.*, 2020). 3D spheroid survival and resistance to ferroptosis inducers was explained in a resect study in 2020, suggesting that Nrf2 hyperactivation and its role in regulating selenoprotein expression such as

GPX4, prevents ferroptotic death of the inner spheroid cells. At the same study Takahashi and his colleagues found that blocking of Nrf2 and GPX4 can induce ferroptotic death within spheroids (Takahashi *et al.*, 2020).

1.7 Aims and hypothesis

Hypothesis:

In this thesis, the aim is to test the general hypothesis that inducers of Ferroptosis enhance chemo- and radio-sensitivity in both 2D and 3D cell culture.

To achieve this, we aim to:
1. Assess the sensitivity of ferroptosis inducers and inhibitors and Nrf2 inhibitors in 2D vs 3D cell cultures (Chapter 3).
2. Assess changes in ferroptosis-related gene expression in 2D vs 3D cell culture (Chapter 3).
3. Assess the effects of sub-lethal doses of ferroptosis inducers on chemotherapy sensitivity in 2D vs 3D cell culture (Chapter 4).
4. Assess the effects of sub-lethal doses of ferroptosis inducers on radiotherapy sensitivity in 2D vs 3D cell culture (Chapter 5).

Chapter 2: Materials and Methods

2.1 Materials and Methods

2.1.1 Cell culture

MDA-MB-231 cells (ECACC, USA) are a triple negative breast cancer (TNBC) cell line taken from a 51-year-old Caucasian woman, characterised by the absence of expression of oestrogen receptor (ER), progesterone receptor (PR) and a human epidermal growth factor receptor 2 (HER2) (Cailleau *et al.*, 1974). It represents approximately 15–20% of all breast cancer cases and is commonly considered as the most severe subgroup of breast cancer with a high relapse rate (Maria *et al.*, 2015). The MCF-7 (ECACC, USA) is an ER+, PR+, and Her-2 negative breast tumour isolated in 1970 from a 69-year-old Caucasian woman (Soule *et al.*, 1973).

MCF-7 and MDA-MB-231 were cultured in Dulbecco's Modified Eagle Medium (DMEM) (Lonza, Manchester, UK), supplemented with 10% (v/v) heat-inactivated foetal bovine serum (FBS) (Lonza) and 1% of 100 IU penicillin and 100 µg/ml streptomycin (ThermoFisher Scientific, Altrincham, UK). Both cell lines were cultured in T75 flasks (ThermoFisher Scientific) incubated at 37°C under 5% CO_2 Cell viability of trypan blue stained cells was determined prior to all studies and percentage of viability was measured using the Countess™ automated cell counter (ThermoFisher Scientific).

Cells were washed with PBS and 2.5mL trypsin-EDTA (ThermoFisher Scientific) added to detach to each culture flask for 3 minutes at 37°C in 5% CO_2, to detach the cell from the bottom of the flask. Next, 3 mL of complete medium was then added to the cell suspension to deactivate the trypsin prior to centrifugation (5 min/400g). In order to check viability, cell pellet was resuspended in 1mL of appropriate medium, 50 µl of cell suspension was mixed with 50 µl of 0.4% of trypan blue solution (Invitrogen) and loaded into the Countess chamber and the percentage of viable cell was determined by the countess automatic cell counter. Cells were routinely passaged 1:4 twice per week or when 80-90% confluency was reached. MCF-7 and MDA-MB-231 cells were below passage 30 from receipt from ECACC for all experiments.

MCF-7 and MDA-MB-231 cells were regularly examined for mycoplasma testing using the EZ-PCR™ Mycoplasma Detection Kit (Biological Industries) and the MycoAlert™ Mycoplasma Detection Kit (Lonza) to confirm to be mycoplasma free.

2.1.1.1 Plating of cells

After cell counting, 100 μl of 1×10^5 cells/ml were seeded in 96-well plates (ThermoFisher, Altrincham, UK). Cells were left to adhere for 24 hours at 37°C under 5% CO_2 condition.

2.1.1.2 Treatment of cells with ferroptosis inducers and inhibitors

Cells were treated with either RSL3 (Sigma, Poole, UK), Erastin (Selleck Chem, Ely, UK) or FIN56 (Sigma) at 0, 1.25, 2.5, 5 or 10 μM in the presence or absence of the ferroptosis inhibitors Deferoxamine (Selleck Chemical company Ely, UK) at 10 μM, Liproxstatin-1 (Sigma) at 1 μM or Ferrostatin-1 (Sigma) at 1 μM. All treatments and controls contained a final concentration of 0.2% Dimethyl sulfoxide (DMSO) as a vehicle control. All treatments were carried out in triplicate in at least three technical repeats.

All ferroptosis inducers RSL3, Erastin and FIN56 were prepared in DMSO at a concentration 5mM and as follows:

To dissolve RSL3, 5mg of RSL3 was dissolved in 2.277 ml of DMSO, giving a stock concentration of 5mM and stored as 10 μl aliquots at -20°C. For Erastin, 2 mg of Erastin was dissolved in 0.365 ml of DMSO, giving a stock concentration of 5mM and stored as 10 μl aliquots at -20°C. For FIN56, 5mg of FIN56 was dissolved in 3.87 ml of DMSO, giving a stock concentration of 5 mM and stored as 10 μl aliquots at -20°C.

For Ferroptosis inhibitors 25 mg Deferoxamine was diluted in 3.8 ml of DMSO giving a final concentration of 10 mM and stored as 10 μl aliquots at -20°C. 5 mg Ferrostatin-1 was diluted in 1.91 ml DMSO, and 5 mg Liproxstatin-1 was diluted 1.47 ml DMSO to give final concentrations of 10 mM. A 10 μl aliquots of all treatments were stored at -20°C.

To treat the cells, 10 μl of Erastin, RSL3 or FIN56 (5mM stock) was diluted in 490 μl of medium giving a stock of 100 μM. 10 μl of this was added per 100 μl well to give a final concentration of 10 μM. Serial dilutions were prepared in medium containing 1 in 50

DMSO to give a range of 10, 5, 2.5, 1.25 and 0.6 µM. For Ferroptosis inhibitors (Ferrostatin-1, Liproxstatin-1 and Deferoxamine), 10 µl of inhibitor (10 mM) was diluted in 10 ml of medium to give a stock of 10 µM and 10 µl was added per 100 µl well to give a final concentration of 1 µM.

2.1.1.3 Treatment of cells with chemotherapy agents

A 7.5 mM Paclitaxel solution (Sigma) was prepared by diluting 5 mg of Paclitaxel in 0.76 ml DMSO and stored in 10 µl aliquots stored at -20°C. Cells were treated by diluting 10 µl of 7.5 mM Paclitaxel in 90 µl of medium to give 750 µM. 10ul of Paclitaxel was serially diluted to give a range of 5, 2.5, 0.6, 0.15 and 0.075 µM. Likewise, a 20 mM Cisplatin solution (Sigma) was prepared in DMSO in 10 µl aliquots stored at -20°C. 10 µl was added to 490 µl of medium to give 400 µM stock. Cisplatin was serially diluted to give 40, 10, 5, 2.5 and 0.6 µM. A 1mM stock solution of Doxorubicin (Sigma) was supplied already diluted in PBS. Doxorubicin was serially diluted to give and range of 10, 5, 2.5 and 0.6 µM. All treatments were compared against a control with 0.1% or 0.2% *w/v* DMSO.

2.1.1.4 Treatment of cells with ML385 (Nfr2 inhibitor)

A 5mM Nrf2 inhibitor ML385 (Sigma) solution was prepared in DMSO and stored as 10 µl aliquots at -20°C. 10 µl of stock was diluted with 490 µl of medium to give 200 µl. 10 µl of ML385 was used per 100 µl well in a 96-well plate to give 10 µM final concentration. All treatments were compared against a control with 0.1% or 0.2% w/v DMSO.

2.1.1.5 Radiotherapy

Cells were either plated in 96 well plates at a cell density of $1x10^5$ cells/ml (Section 2.1.1) or prepared at $1x10^5$ cells/ml of medium in a falcon tube and transported to University of Sheffield for irradiation. In other experiments, cells were transported to University of Sheffield in solution in 50 ml Falcon tubes seeded as $1x10^5$ cells/ml of medium and irradiated. Cells were irradiated in ^{137}Cs irradiator at University of Sheffield (CIS Bio international). The source (62.9 TBq (May 1993)) delivering 1 Gy per 28 seconds, decreasing annually based on half-life to 29.72 seconds per Gy in 2022 was used. After irradiation, cells were transported to SHU plated out for colony formation assays and treated within the 96 well plates with ferroptosis inducers (Section 2.1.1.2) and/or the

Nfr2 inhibitor ML385 (Section 2.1.1.4). In all experiment, a control plate or tube of cells was mock-irradiated, including travel to University of Sheffield to account for time outside of the incubator. All treatments were compared against a control with 0.1% or 0.2% *w/v* DMSO.

2.1.1.5.1 Colony Formation Assay

A colony assay is an *in vitro* cell survival test, based on the capacity of a single cells to multiply and form a colony. This is described as a clonogenic assay or colony formation assay. At least 50 cells are required to constitute a colony (Puck and Marcus, 1956).

Radiation exposure of MDA-MB-231 and MCF-7 cells at doses of 0, 0.3, 0.6, 1.25, 2.5, 5, 10, 20 Gy, was followed by a colony formation assay. Cells were seeded at a density of 1000 and 2000 cells/ml in 6-well plates (ThermoFisher) and grown in complete medium for 15 days. After 15 days excess medium was removed and cells were fixed with 5 mL 10% neutral buffered formalin solution for 15 minutes, allowed to dry then been stained with 2 mL 0.5% (w/v) crystal violet in dH_2O for 30 minutes. Then excess crystal violet was washed form the cells using dH_2O and plates were allowed to dry. Colonies containing more than 50 individual cells are counted as an individual colony.

Colony assay was used to detect the surviving percentage of cells after exposure to radiation and measured as the following formula:

$$\% \, Surviving \, Fraction = \frac{\text{\# of colonies formed}}{\text{\# of colonies in control}} \times 100$$

2.1.2 3D Alginate sphere cell culture

MDA-MB-231 and MCF-7 cultured cells were trypsinized (Section 2.1.1), washed with PBS (1X) (Lonza), and resuspend in 3mL of 0.15M NaCl (Saline, prepared by adding 4.383g of NaCl in 500 ml of dH_2O)) to the number of viable cells were counted (Section 2.1.1). The cell suspension was centrifuged for 5 minutes at 400 g and the Saline discarded. After centrifugation, the cell pellet was resuspended in 1mL of a sterile 1.2%

(w/v in Saline) sodium alginate (1 million cells/ml) and dropped into 15-20 ml of sterile 0.2M $CaCl_2$ (prepared by adding 11.98g of $CaCl_2$ in 500 ml dH_2O) in a 50ml falcon tube using a 21G needle (Sigma-Aldrich). This solution was then incubated at 37°C for 5 minutes. Beads were then washed twice in 15ml sterile 0.15M NaCl, for 5 minutes. Finally, 20ml of medium was added to the alginate beads and cultured in an upright T25 flask at 37°C under 5% CO_2, for up to 14 days prior to treatment.

2.1.2.1 Irradiation of 3D alginate beads

After forming the alginate beads (Section 2.1.2), alginate beads were moved in 50ml Falcon tubes with medium. Cells were irradiated in ^{137}Cs irradiator at University of Sheffield (CIS Bio international). The source (62.9 TBq (May 1993)) delivering 1 Gy per 28 seconds, decreasing annually based on half-life to 29.72 seconds per Gy in 2022 was used. After irradiation, cells were transported back to the laboratory and treated either plated out for treatment with ferroptosis inducers (Section 2.1.1.2) or and Nfr2 inhibitor (Section 2.1.1.4).

2.1.2.2 Dissolving of alginate beads for flow cytometry or qRT-PCR analysis

Following treatment, MDA-MB-231 and MCF-7 cells were dissociated from their alginate beads for either flow cytometry or qRT-PCR analysis. Alginate hydrogel beads were placed in sterile alginate dissolving buffer (55 mM sodium citrate, 30 mM EDTA, and 0.15 M sodium chloride) for 10 minutes at 37°C to release the spheroid colonies. These colonies were then centrifuged at 400g for 5 minutes, washed with PBS ready for a subsequent analysis.

2.1.3 CellTiter-Glo® Luminescent Cell Viability Assay (2D)

The CellTiter-Glo® Luminescent Cell Viability Assay measures the level of ATP precent in living cells, an indicator of metabolic activity within the cells. The ATP present in directly proportion to the luminescent signal, which is directly proportional to the live cells present. The assay depends on the thermostable luciferase (Ultra-Glo™ Recombinant Luciferase) that gives a stable luminescent signal, resulting in the improvement of the function with broad range of assay requirements (Figure 2.1) (Promega, 2002).

For ATP measurement, cells were seeded in white 96-well plates (Fisher Scientific) at 1 x 10^4 cell per well and treated with each ferroptosis inducer (RSL3, Erastin, FIN56) at concentration of 10, 5, 2.5, 1.25 µM, alongside a 0.2% (v/v) DMSO vehicle control. To reverse the effects of the ferroptosis inducer, cells were co-treated with a ferroptosis inhibitors (Deferoxamine 10 µM, Liproxstatin-1 1 µM or Ferrostatin-1 1µM). Treated cells were incubated at 37°C with 5% CO_2, for 24 hours. After treatments, 25 µl of CellTiter-Glo® Reagent from CellTiter-Glo® Luminescent Cell Viability Assay Kit (Promega, Southampton, UK) was added to each well and mixed for 2 minutes on a plate shaker and incubated at room temperature (RT) for 10 minutes to stabilize the luminescent signal. The luminescent signal was measured by a luminometer detector using CLARIOstar plate reader (BMG Labtech, Ortenberg, Germany). The luminescence is proportional to the total ATP present within each well. The average from three luminescence measurements was calculated and all treated cells were normalized to the vehicle controls, which was assigned a 100% ATP activity. All treatments were performed in triplicate, in three independent experiments.
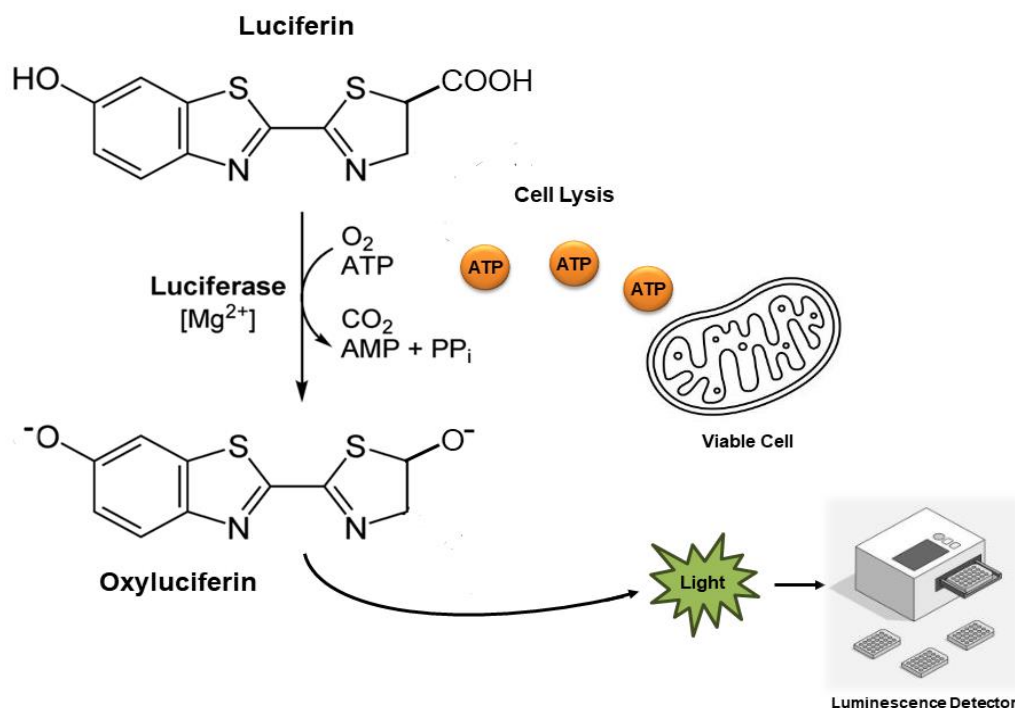
Figure 2.1: CellTiter-Glo® Luminescent Assay chemistry. The cells were treated with CellTiter-Glo® Reagent, which led to cell lysis and the release of ATP. The ATP is hydrolyzed into AMP and pyrophosphate (PPi) in the presence of the cofactors ATP and magnesium (Mg^{2+}), and luciferase oxidises luciferin to oxyluciferin, producing a luminescence signal that can be detected by the CLARIOstar luminescence detector (BMG Labtech).

2.1.4 CellTiter-Glo® 3D cell viability assay

The CellTiter-Glo® 3D Cell Viability Assay measures the living cells in 3D cell culture models, by quantitating the ATP levels present within the cells. The ATP present in directly proportion to the luminescent signal, which is directly proportional to the live cells present. The assay relies on the thermostable luciferase (Ultra-Glo™ Recombinant Luciferase), that produces a stable glow-type luminescent signal and adjusts the performance with a across a wide-ranging assay conditions (Figure 2.2) (Baarsma *et al.,* 2013).

For ATP measurement, alginate spheres were seeded in white 96-well plates (Fisher Scientific) with one alginate bead per well and treated with each ferroptosis inducer (RSL3, Erastin, FIN56) at concentration of 10, 5, 2.5, 1.25 μM, alongside a 0.2% (v/v) DMSO vehicle control. Treated cells were incubated at 37°C with 5% CO_2, for 48 hours. After treatments, 100 μl of CellTiter-Glo® Reagent from CellTiter-Glo® 3D Cell Viability Assay Kit (Promega-UK) was added to each well and mixed for 5 minutes on a plate shaker and incubated at room temperature (RT) for 25 minutes to stabilize the luminescent signal. The luminescent signal was measured by a luminometer detector using CLARIOstar plate reader. The luminescence is proportional to the total ATP present within each well. The average from at least 4 luminescence measurements was calculated and all treated cells were normalized to the controls.
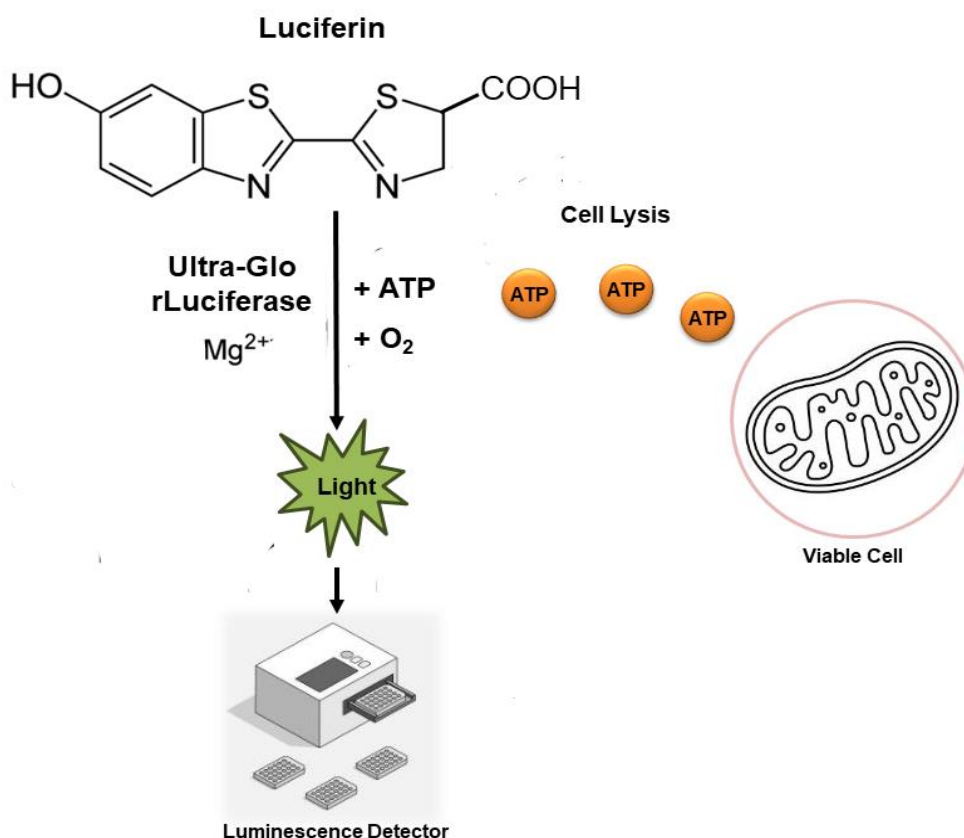
Figure 2.2: CellTiter-Glo® 3D Cell Viability Assay. The cells were treated with CellTiter-Glo® 3D reagent, which led to cell lysis and the release of ATP. The ATP is hydrolyzed in the presence of the cofactor ATP, Ultra glo rLuciferase, Mg^{+2} and O_2 to produce a luminescence signal that can be detected by the CLARIOstar luminescence detector (BMG Labtech).

2.1.5 Assessment of cell death using Hoechst 33342 and propidium iodide staining

Hoechst 33342 and propidium iodide (PI) staining was used to assess cell death. Hoechst 33342 is a bisbenzimidazole dye that penetrates the plasma membrane and stains the DNA within cells. It does not need permeabilization to stain the DNA, giving a blue fluorescence color that can be observed for both living cells and apoptotic cells (stains all nuclei), a condensed nucleus and brighter staining for apoptotic cells. Conversely, PI stains necrotic cells with cell membrane damage and apoptotic cells in late stages (stains nuclei of cells with a interrupted plasma membrane), giving the necrotic cells a red color under fluorescent microscope (Huang *et al.*, 2013).

For analysis of cell death and morphological changes of apoptosis in MDA-MB-231 and MCF-7 cells. 100 µl of 1×10^5 cells/ml of cells were seeded in 96 well plates and treated with the ferroptosis inducers: RSL3, Erastin, or FIN56 (Section 2.1.1.2) for 24 to 72 hours,

and then stained with Hoechst 33342 (Sigma) and PI (Sigma). 10 µl of 100 µg/ml Hoechst 33342 and PI, was added to each well, giving a final concentration 10 µg/ml Hoechst 33342 and 10 µg/ml PI and incubated for 30 minutes at 37°C. Cells were examined using an IX81 or IX70 fluorescence microscope (Olympus) and images captured using Cell-F software (Olympus). Live cells and apoptotic cells are stained blue with Hoechst 33342 (excitation/ emission maxima ~350/461 nm when bound to DNA), dead cells are stained red with PI (excitation/emission maxima ~535/617 nm when bound to DNA). Apoptotic cells were counted manually, and the percentage of apoptosis was calculated based on duplicate representative fields of view each containing at least 100 cells.

All cells were counted, and cell viability was calculated using the following formula:

$$\% \, dead \, cells = \frac{\text{dead cells}}{\text{total cells}} \times 100$$

2.1.6 Caspase inhibition

Apoptosis is a regular cell death that is initiated by a series of cysteine aspartic acid proteases called caspases (Lawen, 2003). Caspase-8 or -10 initiate the external pathway and caspase-9 initiate the internal or intrinsic pathway, and both can initiate apoptosis and activate caspase-3 and -7 (Kalkavan and Green, 2018).

Caspase inhibitors prevent apoptotic cell death and can be used to exclude apoptotic cell death in ferroptosis studies. The irreversible Pan-caspase inhibitor Z-VAD-FMK, caspase-8 inhibitor Z-IETD-FMK, caspase-9 inhibitor Z-LEHD-FMK, and caspase-3 inhibitor Z-DEVD-FMK were obtained from R&D Systems (Abingdon, UK). 100 µl of 1x10^5 cells/ml MDA-MB-231 cells were seeded in 96 well plate. Cells were left to adhere for 24 hours at 37°C under 5% CO_2 condition. MDA-MB-231 cell line was treated with the ferroptosis inducers (RSL3, Erastin, or FIN56) at a concentration of 10 µM, alongside a 0.2% (v/v) DMSO vehicle control. The caspase inhibitors were used at a final concentration of 10 µM, and were added 1 hour prior to ferroptosis inducer treatment (Ozoren *et al.*, 2000), to exclude all apoptotic cell death. Treated MDA-MB-231 cells were assessed at 24 hr and were stained with 10 µg/ml Hoechst 33342 and 10 µg/ml PI for 30 minutes at 37°C

and examined using an IX81 and IX70 fluorescence microscope (Olympus). The study was undertaken in triplicates wells in three individual technical repeats (n = 3).

2.1.7 Effect of ferroptosis inducers on markers of ferroptosis (Mito-FerroGreen)

Free iron is a very high interest of researchers, due to its reactive action within cells and resulting in cellular abnormalities or death (Manual, 2020). Free iron present in its stable redox states, ferrous ion (Fe^{2+}) and ferric ion (Fe^{3+}). Studying the Fe^{2+} is more vital for the intracellular reductive environment than Fe^{3+}. Mito-FerroGreen is fluorescent dye that detection intracellular Fe^{2+} in the mitochondria of living cells (Manual, 2020).

Mito-FerroGreen dye (Dojindo, Munich, Germany) was used for Staining MDA-MB-231 and MCF-7 cells after treatment with ferroptosis inducers as well as ferroptosis inhibitors**:**

A total count 1 x 10^4 cells/ 100 µM medium of MCF-7 and MDA-MB-231 cells were seeded in a 96-well plate (ThermoFisher). Cells were left to adhere for 24 hours at 37°C under 5% CO_2 condition. MCF-7 and MDA-MB-231 cell lines were treated with the ferroptosis inducers (RSL3, Erastin, and FIN56) at a concentration of 10 µM, with control (0.2% (v/v) DMSO) +/- ferroptosis inhibitors (Deferoxamine 10 µM, Liproxstatin-1 1 µM and Ferrostatin-1 1µM). After 1 hour, 6 and 24 hours of treating both MDA-MB-231 and MCF-7 cells with ferroptosis inducers and 24 hours with treating both MCF-7 and MDA-MB-231 with ferroptosis inducers combined with ferroptosis inhibitors, Mito-FerroGreen working solution (5 µM, in 100 µl phenol red free medium) was added to the cells, and cells were incubated at 37°C for 30 minutes in a 5% CO_2 incubator, washed with phenol red free medium (100 µl). Cells were stained with 10 µg/ml Hoechst 33342 and 10 µg/ml PI for 30 minutes at 37°C and imaged using IX81 fluorescence microscope (Olympus) and images captured using Cell-F software (Olympus). Ferrous iron was stained green, live cells and apoptotic cells are stained blue with Hoechst 33342, dead cells are stained red with PI.

2.1.8 Lipid peroxidation measurements

Ferroptosis is an iron-dependent oxidative form of cell death associated with increased lipid peroxidation and inadequate capacity to eliminate lipid peroxides (Dixon *et al.*,

2012). Lipid peroxidation was assessed using a fluorogenic lipid peroxidation sensor BODIPY™ 581/591 C11 (Cat: D3861, ThermoFisher), which is a lipophilic and selectively reacts with peroxyl radicals, providing an assessment of membrane lipid peroxidation in living cells in the absence and presence of 200 µM H_2O_2 as a positive control.

MCF-7 cells were plated at $2x10^5$ cells/ml and seeded in a 12 well plate (ThermoFisher). Cells were left to adhere for 24 hours at 37°C under 5% CO_2 condition. MCF-7 cells were treated with Doxorubicin (0.6 µM) and the ferroptosis inducers RSL3, Erastin or FIN56 (at 10 µM) for 48 hours.

MCF-7 cells were also grown in 3D alginate bead culture (Section 2.1.2) and 10 beads were place in each well of a 24 well plates (ThermoFisher). Alginate spheres were treated with Doxorubicin (10 µM) and the ferroptosis inducer RSL3 (10 µM) for 48 hours. After 48 hours (the day of measurement) a positive control 3D MCF-7 cells culture was prepared, by exposing cultures to 200 µM H_2O_2, for 30 minutes.

Following treatments, triplicate samples of ten beads per sample were dissolved using alginate dissolving buffer (55 mM Sodium Citrate, 30 mM ethylenediaminetetraacetic acid (EDTA) and 0.15 m Sodium Chloride (NaCl) in 500 ml H_2O) at 37°C for 15 minutes and cells were pelleted at 400g for 5 minutes.

After treatment the lipid peroxidase dye was added to treated cells and incubated for 30 minutes at 37°C with 5% CO_2 incubator. Excess dye was removed by washing the cells twice with PBS. Labelled cells were then resuspended in PBS and transferred to a 5 mL flow cytometry tube. Cells were then excited using CytoFLEX Flow Cytometry (Beckman Coulter, Indiana, United States) at two wavelengths: Ex/Em 488/530 nm (FITC filter set (green channel)) and 572 nm (PE filter set (red channel)). Lipid peroxidation was characterised with an increase of green fluorescence. Gating was performed for the -ve control with no dye, and any cells more intense than the -ve cells were classed as positive. Flowjo software 10.6.2 has been used to do all the flow cytometry analysis. For each data point, a minimum of 10000 cells have been acquired for analysis.

2.1.9 Quantification of intracellular reactive oxygen species

Intracellular reactive oxygen species (ROS) were detected by ROS Assay Kit "Highly Sensitive 2',7'-dichlorofluorescein diacetate" (DCFH-DA-) (Dojindo, Munich, Germany).

MCF-7 cells were seeded at a cell density of 2×10^5 per ml in a 12 well plates (ThermoFisher). Cells were left to adhere for 24 hours at 37°C under 5% CO_2 condition. Cells were treated with Doxorubicin (0.6 µM) or Cisplatin (5 µM) in the presence and absence of the ferroptosis inducer RSL3 (10 µM) for 48 hours.

For 3D alginate cultures, MCF-7 alginate beads were grown for 14 days, with 10 beads per well in a 24 well plate (ThermoFisher). Beads were treated with Doxorubicin (10 µM) or Cisplatin (5 µM) alone or in combination with the ferroptosis inducer RSL3 (10 µM) for 48 hours. After 48 hours (the day of measurement) a positive control was created by exposing MCF-7 alginate beads to 200 µM H_2O_2, for 30 minutes as well.

Likewise, MDA-MB-231 cells were treated with ML385 (10 µM) or Cisplatin (5 µM) and ferroptosis inducers RSL3 (0.0375 µM) for 48 hours. 3D MDA-MB-231 alginate cultures were treated with ML385 (10 µM) or Cisplatin (5 µM) and the ferroptosis inducer RSL3 (0.075 µM) for 48 hours.

After treatment the DCFH-DA fluorescent probe and serum-free culture medium were diluted at a ratio of 1:1,000 and incubated with cells for 30 minutes at 37°C with 5% CO_2 incubator. Excess dye was removed by washing the cells twice with PBS. Labelled cells were then resuspended in PBS and transferred to a 5 mL flow cytometry tube. Cells were then analysed using a CytoFLEX Flow Cytometry (Beckman Coulter) detected using FITC channel. Gating was performed for the -ve control with no dye, and any cells more intense than the -ve cells were classed as positive. Flowjo software 10.6.2 has been used to do all the flow cytometry analysis. For each data point, a minimum of 10000 cells have been acquired for analysis.

2.1.10 Measurement of glutathione (GSH) / glutathione disulfide (GSSG) ratio

The GSH/GSSG-Glo™ Assay is used to measure total glutathione (GSH +GSSG), of both oxidized (GSSG) and reduced (GSH) in living cells, the GSH/GSSG ratios then will be

detected by a luminescence signal that is directly proportion to the amount of GSH/GSSG within the samples. This is done by the GSH-dependent transfer of a GSH probe (Luciferin-NT) to luciferin by a glutathione S-transferase enzyme that combined to a firefly luciferase reaction. Light from luciferase varies on the amount of luciferin formed, that represent the amount of GSH that occur (Promega, 2011).

MCF-7 cells were seeded in white 96-well plates (Fisher Scientific) at a cell density of 1×10^4 cell per well. Cells were left to adhere for 24 hours at 37°C under 5% CO_2 condition. 2D MCF-7 cells were treated with Doxorubicin (0.6 µM) or Cisplatin (5 µM) and the ferroptosis inducers RSL3 (10 µM) for 48 hours.

For 3D MCF-7 alginate cultures, one alginate bead was placed in each well of a white 96-well plates (Fisher Scientific). These 3D MCF-7 alginate spheres were treated with Doxorubicin (10 µM) or Cisplatin (5 µM) and the ferroptosis inducer RSL3 (10 µM) for 48 hours. After 48 hours (the day of measurement) a positive control was created by exposing MCF-7 cells to 200 µM H_2O_2, for 30 minutes.

Likewise, MDA-MB-231 cells were treated with ML385 (10 µM) or Cisplatin (5 µM) and ferroptosis inducers RSL3 (0.0375 µM) for 48 hours. 3D MDA-MB-231 alginate cultures were treated with ML385 (10 µM) or Cisplatin (5 µM) and the ferroptosis inducer RSL3 (0.075 µM) for 48 hours.

The intracellular total glutathione (GSH) and glutathione disulphide (GSSG) levels were detected by GSH Kit (Promega) according to the manufacturers' protocols. The relative levels were analysed by a luminometer detector using CLARIOstare plate reader.

For 3D alginate cells following treatments, alginate beads were dissolved using alginate dissolving buffer as described previously (Section 2.1.2.2), then measured for the GSH/GSSG ratio.

Glutathione levels were calculated as GSH/GSSG ratio as the following formula:

$$\text{Ratio GSH/GSSG} = \frac{\text{total GSH} - (\text{GSSG} \times 2)}{\text{GSSG}}$$

2.1.11 Immunocytochemistry to detect Nrf2

Untreated 2D MCF-7 and MDA-MB-231 cells were seeded at 2×10^4 cell per well on 8-well glass chamber slides (™ Nunc™ Lab-Tek™ II Chamber Slide™, Thermo Scientific). Cells were left to adhere for 24 hours in a 5% CO_2 incubator at 37°C. Untreated 3D MCF-7 and MDA-MB-231 alginate cells (3 beads per sample) were dissolved using alginate dissolving buffer and cell suspension cytospin onto glass slides using a Cytospin for Centrifuge (Thermo Scientific).

Cells were fixed in 50:50 acetone/methanol in a Coplin jar in the fume hood for 10-15 min, washed in Tris-buffered saline (TBS) for 5 minutes, followed by blocking for 15 minutes with goat serum (25 % in TBS), then wash with TBS for 5 minutes. Cells were incubated with a 1:200 dilution of primary Nrf2 antibodies (Nrf2 (D1Z9C) XP® Rabbit mAb, Cell Signalling Technology, Danvers, USA). Then incubate for 2 hours in a humid atmosphere in the dark. After incubation cells were washed three times in TBS and dried, incubated with secondary antibody (Anti-rabbit IgG (H+L), F(ab')2 Fragment (Alexa Fluor® 488 Conjugate) (Cell Signalling Technology) in a 1:500 dilution in TBS for 2 hours at room temperature in the dark. After incubation cells were washed three times with TBS, then the nuclei were stained with a mounted 4,6-diamidino-2-phenyindole (DAPI, Sigma) and imaged using confocal microscope (ZEISS LMS 800).

2.1.12 Detection of ferroptosis-related gene expression by qRT-PCR

2.1.12.1 RNA extraction

Total RNA was isolated from both MDA-MB-231 and MCF-7 2D cultured cells and 3D alginate (after dissolving with alginate dissolving buffer) using the Reliprep RNA mini system (Promega). Briefly, the ReliaPrepTM RNA Miniprep System (Promega) was used to extract total RNA from monolayer cells that were collected and lysed from cell culture T25 flasks at 90% confluency using 500 µL BL-TG buffer (4M Guanidine thiocyanate, 0.01M Tris, 1% 1-Thioglycerol, Promega), then 170 µl of isopropanol was added and mixed by vortex for 5 seconds. The lysate was then transported to a ReliaPrep™ Minicolumn and centrifuged at 12,000–14,000 × g for 1 minute at 20–25°C. Then the liquid was discarded from the collection tube. After that 500µl of RNA wash solution was added to the ReliaPrep™ Minicolumn and centrifuged at 12,000–14,000 × g for 30

seconds and discard the liquid in the collection tube. 30 µl of DNase was added to the core of the ReliaPrep™ Minicolumn and incubate for 15 minutes at room temperature. 200µl of Column Wash Solution was added to the ReliaPrep™ Minicolumn and centrifuged at 12,000–14,000 × g for 15 seconds. Then 500 µl of RNA wash solution (with ethanol added) and centrifuged at 12,000–14,000 × g for 30 seconds. The ReliaPrep™ Minicolumn was placed into a new Collection Tube and 300 µl of RNA Wash Solution was added and centrifuged at 14,000 × g for 2 minutes. Finally, the ReliaPrep™ Minicolumn was transferred from the collection tube to the elution tube, and 30 µl of Nuclease-Free Water was added to the elution tube and centrifuged at 14,000 × g for 1 minute. The elution tube contained the purified RNA and stored at −80°C.

A NanoDrop 1000 (ThermoFisher Scientific) was used to measure the quantity and purity of RNA.

2.1.12.2 cDNA synthesis

cDNA was reverse transcribed using High-Capacity RNA-to-cDNA Kit (Thermo Fisher Scientific). For cDNA synthesis, each reaction contained 10 µl of 2x RT (reverse transcriptase) buffer mix, 1 µl of 20x RT enzyme mix, and RNA (1 µg) + Nuclease free water up to a final volume of 20 µl. The no-RT reactions were prepared by omitting the 20x RT enzyme mix. Samples were incubated at 37°C. for 1 hour, then 95°C for 5 minutes using a PCR cycler.

2.1.12.3 RT-qPCR

cDNA samples were interrogated by qRT-PCR for the expression of genes of interest (Table 2.1) Real-time quantitative polymerase chain reaction (RT-qPCR) was performed using TaqMan® Assays in 10 µL reaction mixtures. TaqMan Assay reaction mixtures contained: 5 µL of TaqMan® Fast Advance (Applied Biosystems), 2.5 µL nuclease-free H_2O, 0.5 µL primer-probe (TaqMan Gene Expression Assays, FAM, ThermoFisher Scientific) (Table 2.1) and 2 µL cDNA or water for a no template control. Beta-2 microglobulin was used as a housekeeping gene (HKG). the primer-probes were purchased from Life Technologies Limited (ThermoFisher Scientific) and the MicroAmp™ Optical 96-Well Reaction Plates were used for all RT-qPCR experiments (ThermoFisher Scientific). TaqMan qPCR thermal profile was consisted of an initial activation step of 10

minutes at 95°C, then by 40 cycles of 30 seconds denaturation at 95°C and 1 minute annealing at 60°C. Plates were run on The QuantStudio 3 Detection System (QuantStudio Design and Analysis Software, Applied Biosystems) to perform the RT-qPCR. Relative gene expression levels were calculated using the $2^{-\Delta\Delta CT}$ method and normalized against the housekeeping gene.

Gene expression calculation was done using the $2^{-\Delta\Delta CT}$ method as the following formula where:

$\Delta CT = CT \text{ (gene)} - CT \text{ (HKG)}$

and $\Delta\Delta CT = \Delta CT \text{ (gene)} - \Delta CT \text{ (HKG)}$

Finally, $2^{-\Delta\Delta CT}$ calculated the fold change of the gene expression in cells relative to the housekeeping gene (Beta-2 microglobulin).

Table 2.1: TaqMan primer-probes for RT-qPCR

Gene of Interest	Assay ID
HMOX1	Hs01110250_m1
SLC7a11	Hs00921938_m1
GSTP1	Hs00168310_m1
Keap-1	Hs00202227_m1
NQ01	Hs01045994_m1
GPX4	Hs00157812_m1
Nrf2	Hs00975960_m1
TFRS	Hs00951087_m1
Beta-2 microglobulin	Hs99999907_m1

Table 2.1 TaqMan primer-probes for RT-qPCR. The genes detected using TaqMan Gene Expression primer-probes include (*Homo sapiens*): HMOX1, SLC7a11, GSTP1, Keap-1, NQ01, GPX4, Nrf2, TFRS, and Beta-2 microglobulin.

2.1.13 Statistical analysis

The Stats Direct software (Stats Direct Ltd, England) was used to test for normality using a Shapiro-Wilks test. The data was predominantly non-parametric; and a Kruskal-Wallis test with a Dunn's *post-hoc* test was used to determine statistical significance. Results were considered statistically significant when $P \leq 0.05$. All graphs are expressed as median and range, or interquartile range, using Graph Pad Prism, normalized to vehicle control. Synergistic effects were defined as those where the combination treatment is statistically significantly greater (or less) than the sum of individual treatments. Additive effects were defined as changes that were less than the sum of the effects from individual treatments.

Chapter 3: Optimisation of ferroptosis inducers on cell death in breast cancer cell lines

3.1 Introduction

Ferroptosis is a more recently discovered form of cell death established in 2012 by the work of Dixon and his colleagues. This form of death is an iron dependent programme of cell death that is induced by lipid peroxidation, It is characterised by the massive accumulation of reactive oxygen species (ROS) which induces lipid peroxidation in the cell (Dixon *et al.*, 2012), causing morphological features differently from other forms of PCD (Yagoda *et al.*, 2007; Dixon *et al.*, 2012). Due to the role of iron in mediating the production of reactive oxygen species and enzyme activity in lipid peroxidation, aspects of iron metabolism, such as iron uptake storage and efflux, control ferroptosis (Li *et al.*, 2020). Moreover, the sensitivity of ferroptosis is regulated by the transcriptional of iron homeostasis (Liang *et al.*, 2019). Intracellular iron is the only source of metal that is used to activate the ferroptosis pathway (Liang *et al.*, 2019). Many studies have found that glutathione peroxidase 4 (GPX4), lipid synthesis, iron metabolism, Nrf2 pathway also play a critical role to regulate the ferroptosis process (Li *et al.*, 2020).

Ferroptosis can be induced by blocking system Xc- with small molecule ferroptosis inhibitors such as Erastin. Ferroptosis can also be induced by inhibition of GPX4 stability or activity using FIN56 or RSL3 respectively (Dixon *et al.*, 2014). All cause disruption of lipid metabolism balance by increasing oxidizable polyunsaturated phospholipids or interfere iron homeostasis and can sensitize cells to ferroptosis (Doll *et al.*, 2017). The survival and growth of cancer cells is strongly dependent on the transport activity of system Xc- (Hassannia *et al.,* 2019).

There are different types of ferroptosis inducers that have been reported. Dolma *et al.,* (2003) identified two structurally unrelated small molecules, named Erastin and RSL3, that were selectively lethal to oncogenic Ras mutant cell lines, and which are referred to together as RAS-selective lethal (RSL) compounds (Dolma *et al.*, 2003). Erastin is one of the ferroptosis inducers and an anti-tumour agent that is selective for cell expressing RAS (Dixon *et al.*, 2012). Erastin can reduce cellular GSH level by inhibiting system Xc– directly, reducing cystine and glutamate uptake which are crucial for glutathione production. Loss of glutathione renders cells very susceptible to lipid peroxidation. RSL3 induces ferroptosis by targeting GPX4 directly. The chloroacetamide moiety in RSL3

structure is essential for its activity, according to affinity-based chemoproteomics. The RSL3 inactivates GPX4 directly via alkylation of the selenocysteine, and also targets enzymes with nucleophilic site (e.g., serine, cysteine, selenocysteine, etc.) (Yang and Stockwell, 2008). Both Erastin and RSL3 inhibit the ferroptosis pathway in cancer cells by disturbing the redox homeostasis and allowing the iron-independent accumulation of lethal ROS (Dixon *et al.*, 2012).

Recently Shimada and his colleagues (2016) discovered the novel mechanism of action of two more ferroptosis inducers, FIN56 and FINO2. FINO2 promotes lipid peroxidation by inducing iron oxide and indirectly inactivating GPX4 (Hassannia *et al.*, 2019). The cells that are killed by FIN56-induced ferroptosis have an accumulation of lipid ROS which can be reversed by iron chelators, which suggested that FIN56 is a inducer of ferroptosis (Shimada *et al.*, 2016).

Ferroptosis can be prevented by ferroptosis inhibitors, such as Ferrostatin-1, which is an iron dependent selective inhibitor of ferroptosis, that prevents cellular accumulation of lipid ROS induced by Erastin (Dixon *et al.*, 2012). Another ferroptosis inhibitor is Liproxstatin-1. This is a spiroquinoxalinamine derivative, able to prevent ferroptosis cell death induced by GPX4 knockdown, or induced by Erastin and RSL3, by directly preventing lipid peroxidation. However, Liproxstatin-1, could not rescue cells dying by apoptosis or necroptosis, indicating that it is a specific inhibitor of ferroptosis (Feng *et al.*, 2019). Liproxstatin-1 also has been shown to significantly increase the protein levels of Nrf2 which helps to promote the cell survival (Feng *et al.*, 2019). The Iron chelating agent Deferoxamine has also been used as a ferroptosis inhibitor (Kose *et al.*, 2019). Deferoxamine is a classic iron-chelating ferroptosis inhibitor that can be used to prevent ferroptosis and damage to normal cells and tissues (Wu *et al.*, 2020). However, Deferoxamine has a short half-life, which limits its clinical application (Wu *et al.*, 2020).

Free iron is a very high interest of researchers, due to its reactive action within cells and resulting in cellular abnormalities or death (Manual, 2020). Free iron present in its stable redox states, ferrous ion (Fe^{2+}) and ferric ion (Fe^{3+}). Studying the Fe^{2+} is more vital for the intracellular reductive environment than Fe^{3+}. Mito-Ferro-Green is fluorescent dye that

detects intracellular Fe^{2+} in the mitochondria of living cells and can be used an indicator or ongoing ferroptosis in *in vitro* studies (Manual, 2020).

3.1.1 Aims and hypothesis

It is hypothesised that:

Ferroptosis inducers cause death in both 2D and 3D breast cancer cell culture models, and that this is reversed by ferroptotic inhibitors.

Here we aim to:

1. Optimise ferroptosis inducer doses for combination studies with chemotherapy and radiotherapy.
2. Develop a 3D breast cancer cell culture model to test the effects of ferroptosis modulators in a more representative *in vitro* model that standard cell culture.
3. Confirm the occurrence of ferroptosis in breast cancer cells by applying ferroptosis inhibitors, and use caspase inhibitors to exclude apoptotic cell death, use MitoFerro-Green dye to detect the present of iron within cells.

3.2 Results

3.2.1 Assessment of cell death in response to low doses of ferroptosis inducers using Hoechst 33342 and propidium iodide in breast cancer cells

The effects of ferroptosis inducers on cell death of MB-MDA-231 cells and MCF-7 cells was detected using fluorescent microscopic images after staining with Hoechst 33342 and propidium iodide. Live cells and apoptotic cells are stained blue with Hoechst 33342, dead cells are stained red with PI staining. The percentage of cell death was counted after 24 hours treatment for three independent experiments. Any cell with evidence of PI positivity was classed as dead, as these cells have permeabilised membranes. Due to co-staining with Hoechst 33342, dead cells appear pink, or red, on images.

To establish a suitable dose for later studies in combination with chemotherapy and radiotherapy, and in experiments with ferroptosis inhibitors, caspase inhibitors and measurements of ROS, free iron and lipid peroxidation, a dose response curve was established for each ferroptosis inducer across the range of 1.25, 0.6, 0.3, 0.15, and 0.075 µM, for Erastin, RSL3 and FIN56 in MB-MDA-231 cells. MB-MDA-231 cells were sensitive to all ferroptosis inducers, whereas MCF-7 cells were generally resistant.

3.2.1.1 Optimisation of the ferroptosis inducer Erastin in MDA-MB-231 cells

MDA-MB-231 cells were highly sensitive to Erastin, showing significant cells death at all doses above 0.15 µM. Therefore 0.15 µM was considered a suitable dose for combination studies, whereas 10 µM was considered a suitable positive control dose for studies with ferroptosis inhibitors to establish that cell death was indeed ferroptotic. Propidium iodide-positive cells did not appear to be apoptotic in morphology with absence of pycnotic and condensed nuclei, although this was not formally quantified. (Figure 3.1).

3.2.1.2 Optimisation of the ferroptosis inducer RSL3 in MDA-MB-231 cells

The ferroptosis inducer RSL3 induced significant cell death at all doses tested from 0.075 µM in MDA-MB-231 cells with >50% cell death at 0.075 µM (Figure 3.2). For subsequent combination studies in Chapter 4 and 5, the optimum dose for combination studies was determined to be 0.0375 µM, because as can be seen from Figure 3.2A that 0.075 µM causes over 50% death. Whereas 0.0375 induces significant death but only approximately 25%, allowing potential synergy to be observed in combination studies. As with RSL3, cell death was observed by propidium iodide positivity. Although nuclear morphology was not formally scored for apoptotic morphology, most dead cells did not appear to have characteristic apoptotic condensed and pycnotic nuclei, suggestive of ferroptotic cell death.

Figure 3.1: Effect of the ferroptosis inducer Erastin in MDA-MB-231 cells

(A)
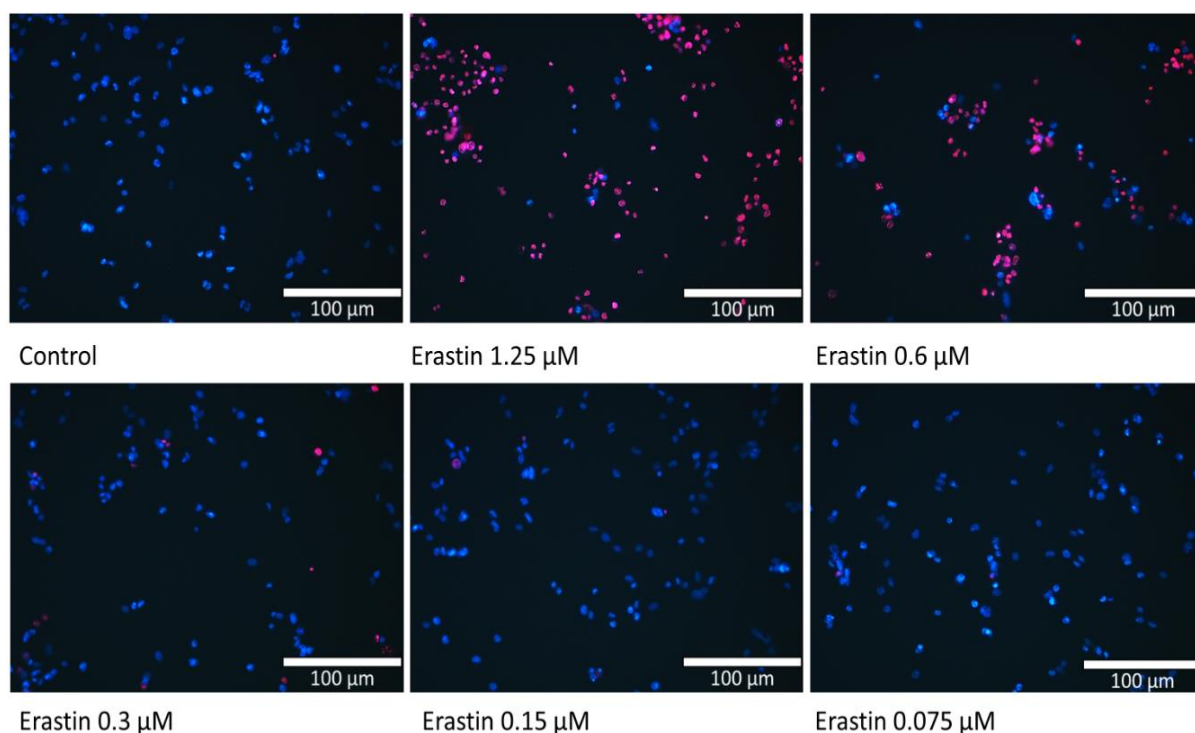
(B)
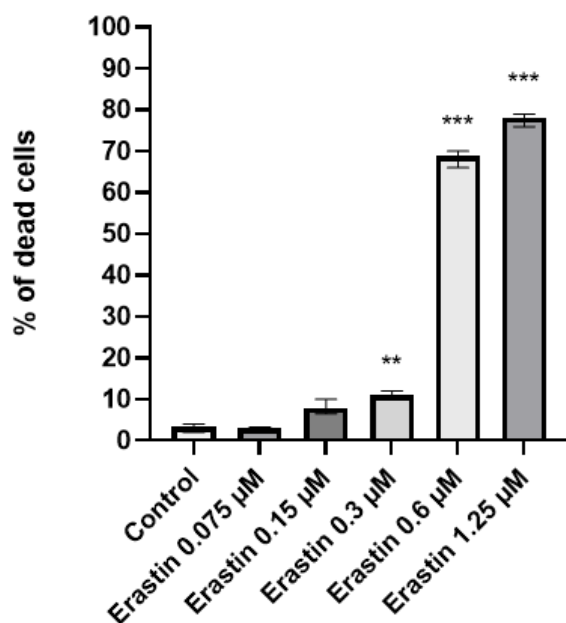
Figure 3.1: Effect of Erastin on MDA-MB-231 cells after 24 hours of treatment. (A) Fluorescence microscopy analysis of cell death by Hoechst 33342/PI staining after treatment with the ferroptosis inducer Erastin at concentration of 1.25, 0.6, 0.3, 0.15, and 0.075 μM. **(B)** Percentage of cells death calculated from n=3 independent experiments each analysing triplicate wells. Data is presented as median ± range. The statistical significance was determined by comparison with the control (0.2% (v/v) DMSO), analysed by a Kruskal-Wallis followed by Dunn's multiple comparisons test (*=P≤0.05, **=P≤0.01, and ***=P≤0.001).

Figure 3.2: Effect of the ferroptosis inducer RSL3 in MDA-MB-231 cells

(A)

Control

RSL3 1.25 µM
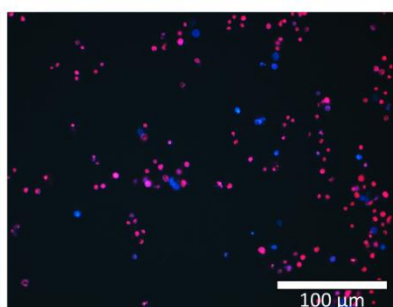
RSL3 0.6 µM
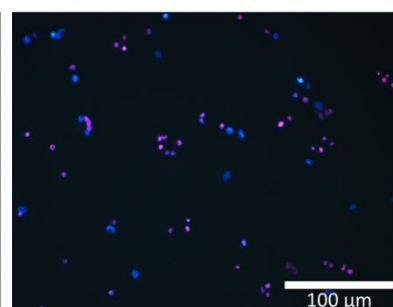
RSL3 0.3 µM
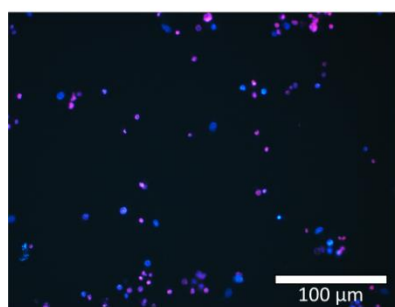
RSL3 0.15 µM
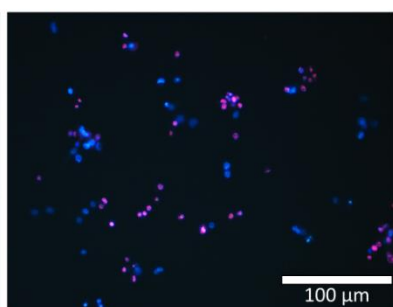
RSL3 0.075 µM
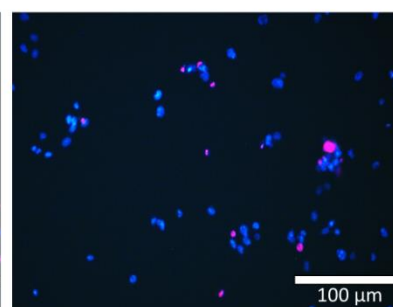
RSL3 0.0375 µM

(B)
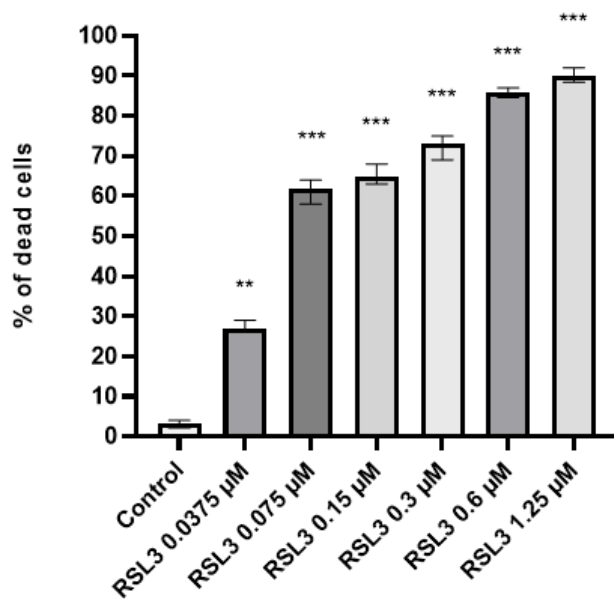
Figure 3.2: Effect of low doses of RSL3 on MDA-MB-231 cells after 24 hours of treatment. (A) Fluorescence microscopy analysis of cell death by Hoechst 33342/PI staining after treatment with the ferroptosis inducer RSL3 at concentration of 1.25, 0.6, 0.3, 0.15, 0.075 and 0.0375 µM. **(B)** Percentage of cells death calculated from n=3 independent experiments each analysing triplicate wells. Data is presented as median ± range. The statistical significance was determined by comparison with the control (0.2% (v/v) DMSO), analysed by a Kruskal-Wallis followed by Dunn's multiple comparisons test (*=P≤0.05, **=P≤0.01, and ***=P≤0.001).

3.2.1.3 Optimisation of the ferroptosis inducer FIN56 in MDA-MB-231 cells

The ferroptosis inducer FIN56 induced significant cell death at all doses tested from 0.15 µM, (Figure 3.3). Since this dose induced a small but significant amount of cell death (15%), this was appropriate for use in combination studies with chemotherapy and radiotherapy in Chapters 4 and 5 respectively. As with RSL3 and Erastin, dead cells did not appear to be apoptotic in morphology.

3.2.2 Effect of ferroptosis inducers and inhibitors on MDA-MB-231 cell culture

3.2.2.1 The effect of Erastin is reversed by ferroptosis inhibitors in MDA-MB-231 cells

Erastin (10 µM) significantly and potently induced cell death in MDA-MB-231 cells. To establish whether this cell death was likely to be ferroptotic, co-incubation with three ferroptotic inhibitors with differing mechanisms of action was tested against a range of doses of Erastin. The cell death induced by RSL3, Erastin and FIN56 was completely or partially reversed by ferroptosis inhibitor Deferoxamine, Liproxstatin-1, Ferrostatin-1, as determined by Hoechst 33342 and PI staining. The finding is also consistent with the results obtained for cell viability measurements using CellTiter-Glo® Luminescent Cell Viability Assay (Figure 3.4A and B). Erastin alone produced a significant decrease on ATP level in the MDA-MB-231 cell line (Figure 3.4C). The effect of ferroptosis inducers were almost fully reversed by all ferroptosis inhibitors.

Erastin potently decreased ATP levels at all doses (1.25-10 µM) in the MDA-MB-231 cell line in a dose-dependent manner. The effect of ferroptosis inducer Erastin was almost fully reversed by all ferroptosis inhibitors (Deferoxamine 10 µM, Liproxstatin-1 1µM and Ferrostatin-1 1µM) ($P \leq 0.001$).

3.2.2.2 The effect of RSL3 is reversed by ferroptosis inhibitors in MDA-MB-231 cells

Similar to the observations with Erastin, RSL3 significantly (10 µM) potently induced cell death in MDA-MB-231 cells, and the majority of this response was reversed by ferroptosis inhibitors (Deferoxamine, Liproxstatin-1, Ferrostatin-1). This finding is also consistent with the results obtained for cell viability using ATP levels measured using CellTiter-Glo® Luminescent Cell Viability Assay (Figure 3.5A and B). RSL3 alone produced

a significant decrease on ATP level in the MDA-MB-231 cell line (Figure 3.5C). The effect of ferroptosis inducers were almost fully reversed by all ferroptosis inhibitors.

RSL3 potently decreased ATP levels at all doses (1.25-10 µM) in the MDA-MB-231 cell line. The effect of ferroptosis inducer RSL3 was almost fully reversed by all ferroptosis inhibitors (Deferoxamine 10 µM, Liproxstatin-1 1µM and Ferrostatin-1 1µM) (P≤0.001).

3.2.2.3 The effect of FIN56 is reversed by ferroptosis inhibitors in MDA-MB-231 cells

FIN56 significantly induced cell death in MDA-MB-231 cells, and the majority of this response was reversed by ferroptosis inhibitors (Deferoxamine, Liproxstatin-1, Ferrostatin-1) (Figure 3.6A and B). The finding is consistent with the results obtained for % of ATP measured using CellTiter-Glo® Luminescent Cell Viability Assay. FIN56 alone produced a significant decrease on ATP level in the MDA-MB-231 cell line (Figure 3.6C). The effect of ferroptosis inducers were almost fully reversed by all ferroptosis inhibitors.

FIN56 potently decreased ATP levels at all doses (1.25-10µM) in the MDA-MB-231 cell line in a dose-dependent manner. The effect of ferroptosis inducer FIN56 was almost fully reversed by all ferroptosis inhibitors (Deferoxamine 10 µM, Liproxstatin-1 1µM and Ferrostatin-1 1µM) (P≤0.001).

Figure 3.3: Effect of the ferroptosis inducer FIN56 in MDA-MB-231 cells

(A)

Control   FIN56 1.25 µM   FIN56 0.6 µM

FIN56 0.3 µM   FIN56 0.15 µM   FIN56 0.075 µM
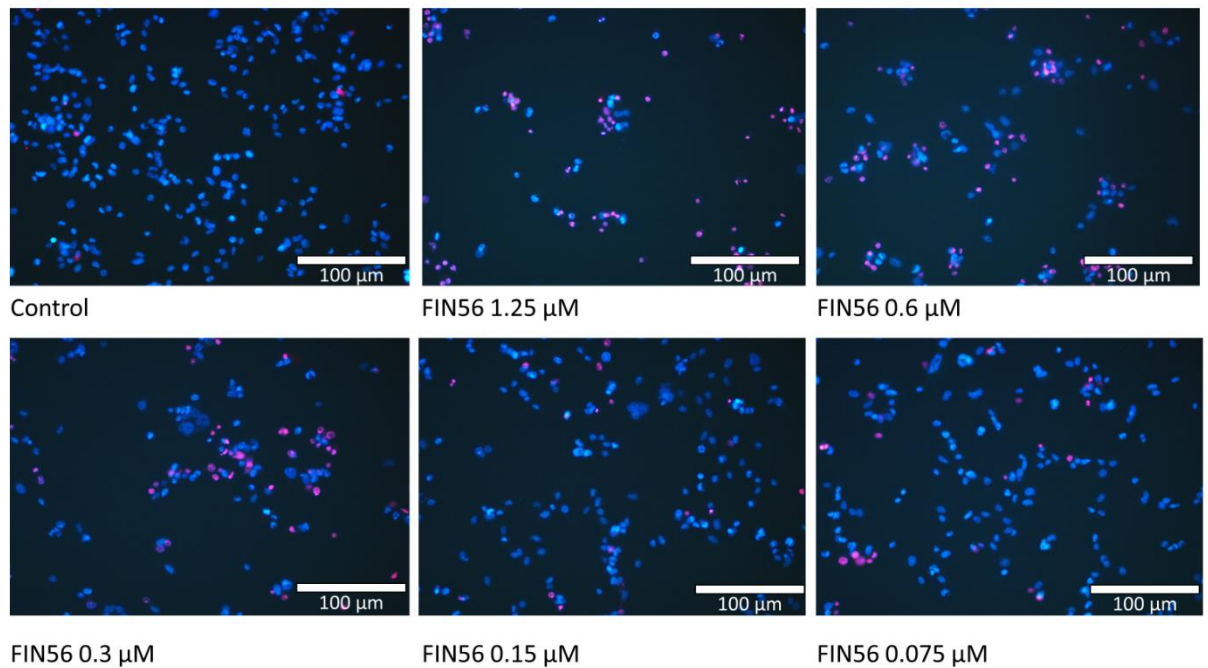
(B)
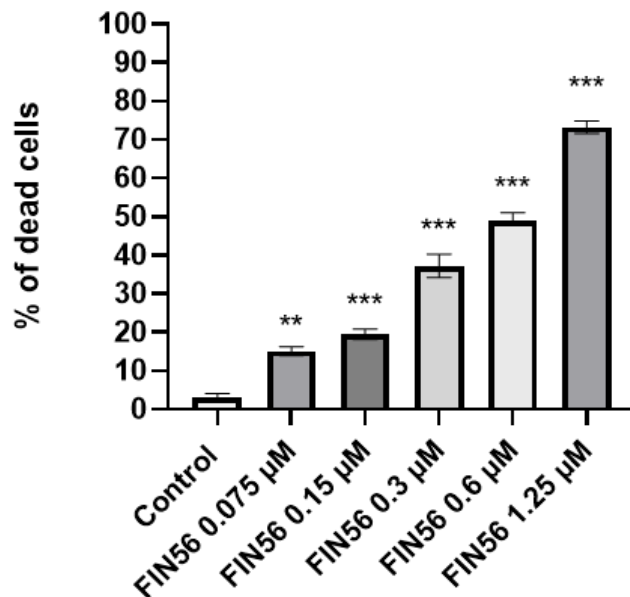
Figure 3.3: Effect of low doses of FIN56 on MDA-MB-231 cells after 24 hours of treatment. (A) Fluorescence microscopy analysis of cell death by Hoechst 33342/PI staining after treatment with the ferroptosis inducer FIN56 at concentration of 1.25, 0.6, 0.3, 0.15, and 0.075 µM. **(B)** Percentage of cells death calculated from n=3 independent experiments each analysing triplicate wells. Data is presented as median ± range. The statistical significance was determined by comparison with the control (0.2% (v/v) DMSO), analysed by a Kruskal-Wallis followed by Dunn's multiple comparisons test (*=P≤0.05, **=P≤0.01, and ***=P≤0.001).

Figure 3.4: Effect of ferroptosis inhibitors on Erastin responses in MDA-MB-231 cells

(A)

Control

Erastin 10 µM

Erastin + Deferoxamine 10 µM

Erastin + Liproxstatin-1 1 µM

Erastin + Ferrostatin-1 1 µM

Deferoxamine 10 µM

Liproxstatin-1 1 µM

Ferrostatin-1 1 µM
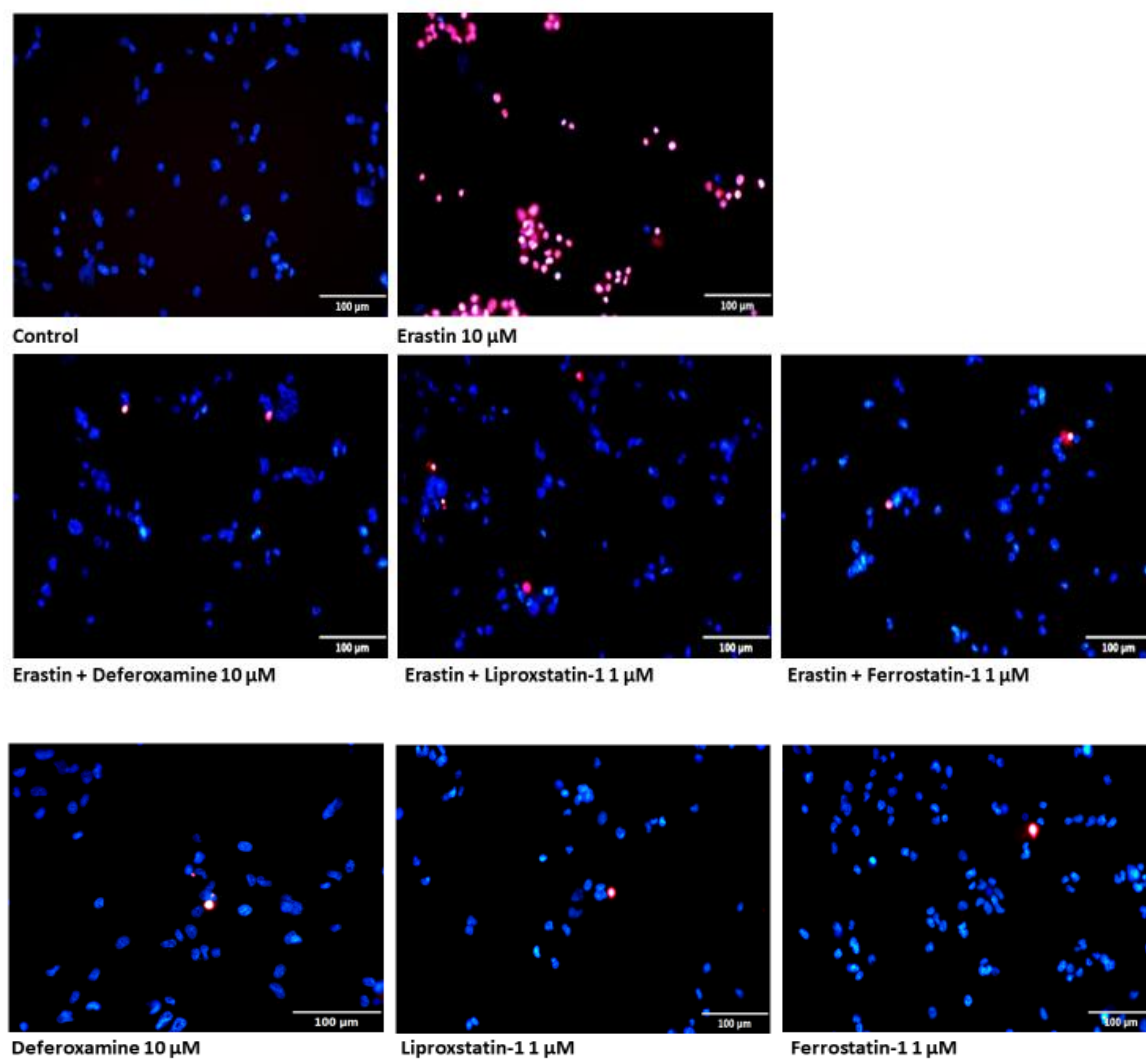
(B)
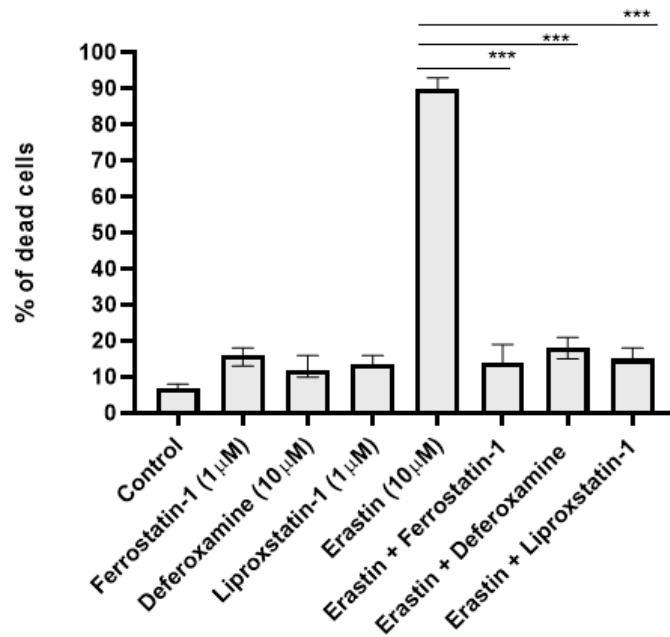
(C)
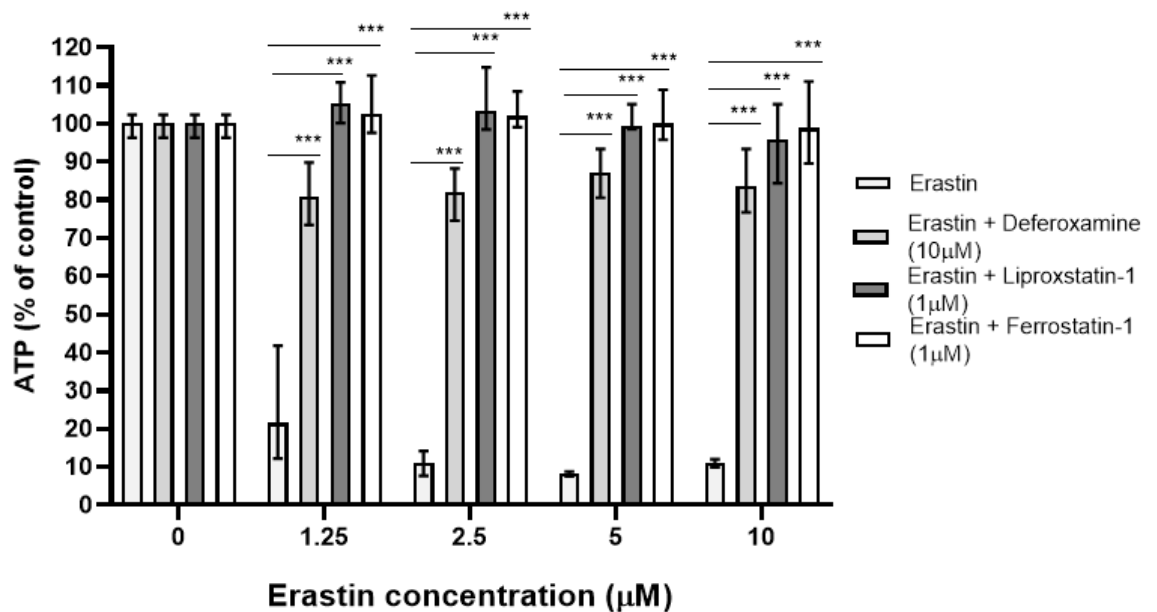
Figure 3.4: Effect of Erastin on MDA-MB-231 cells after 24 hours of treatment. (A) Fluorescence microscopy analysis of cell death by Hoechst 33342/PI staining after treatment with the ferroptosis inducer Erastin (10 μM) +/- ferroptosis inhibitors (Deferoxamine 10 μM, Liproxstatin-1 1μM and Ferrostatin-1 1μM). **(B)** Percentage of cell death calculated from n=3 independent experiments each analysing triplicate wells. Data is presented as median ± range. **(C)** ATP level (% of control) assessed by CellTiter-Glo® Luminescent Cell Viability Assay after treatment with ferroptosis inducer Erastin +/- ferroptosis inhibitors. Data is presented as median ± range from n=3 independent experiments each with 3 technical repeats. The statistical significance was determined by comparison with the Erastin alone, analysed by a Kruskal-Wallis followed by Dunn's multiple comparisons test (*=P≤0.05, **=P≤0.01, and ***=P≤0.001).

Figure 3.5: Effect of ferroptosis inhibitors on RSL3 responses in MDA-MB-231 cells

(A)
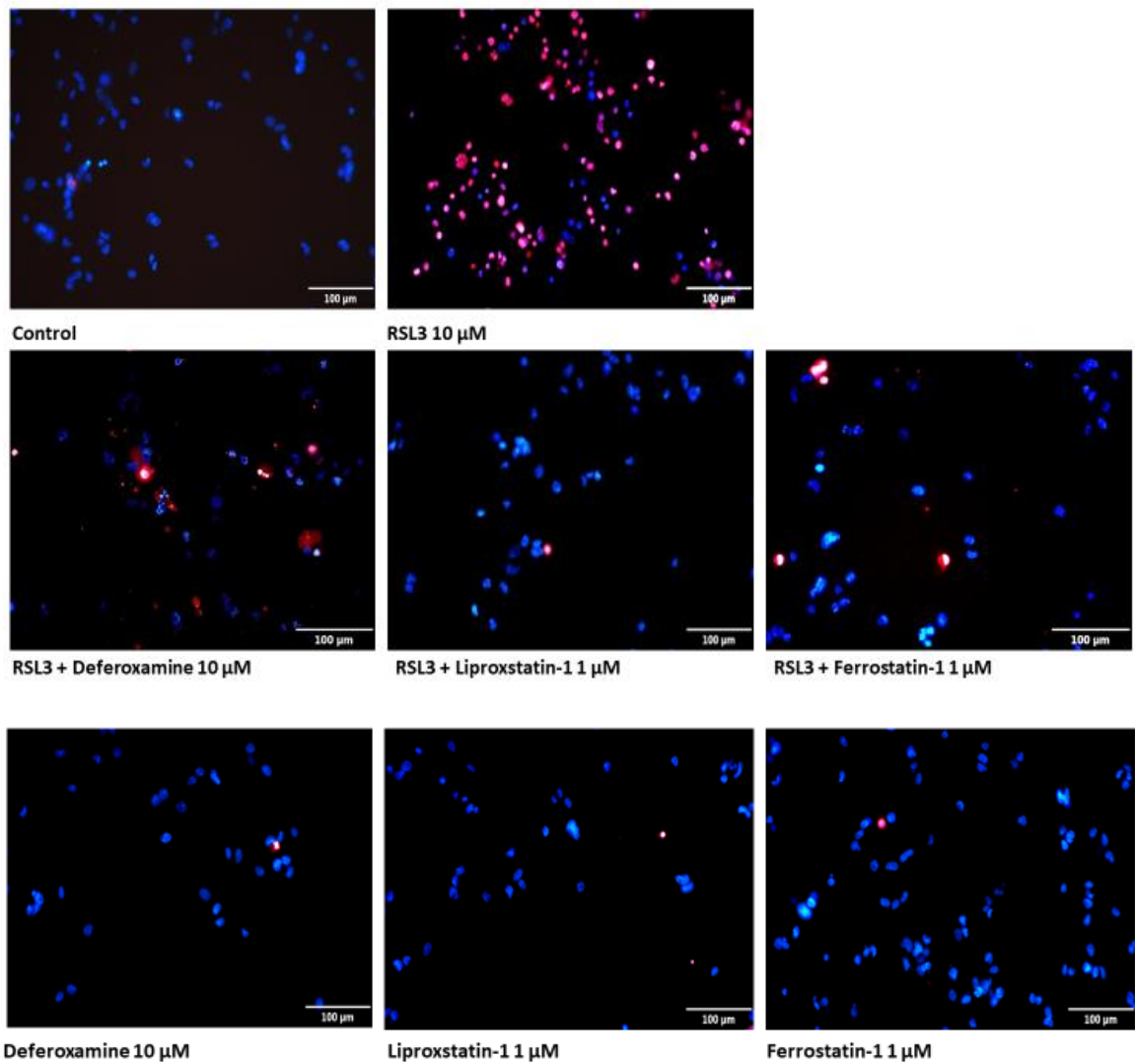
(B)
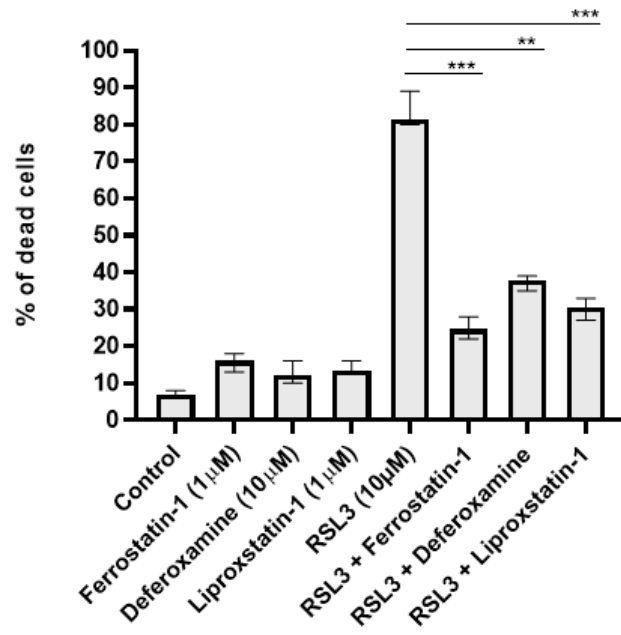
(C)
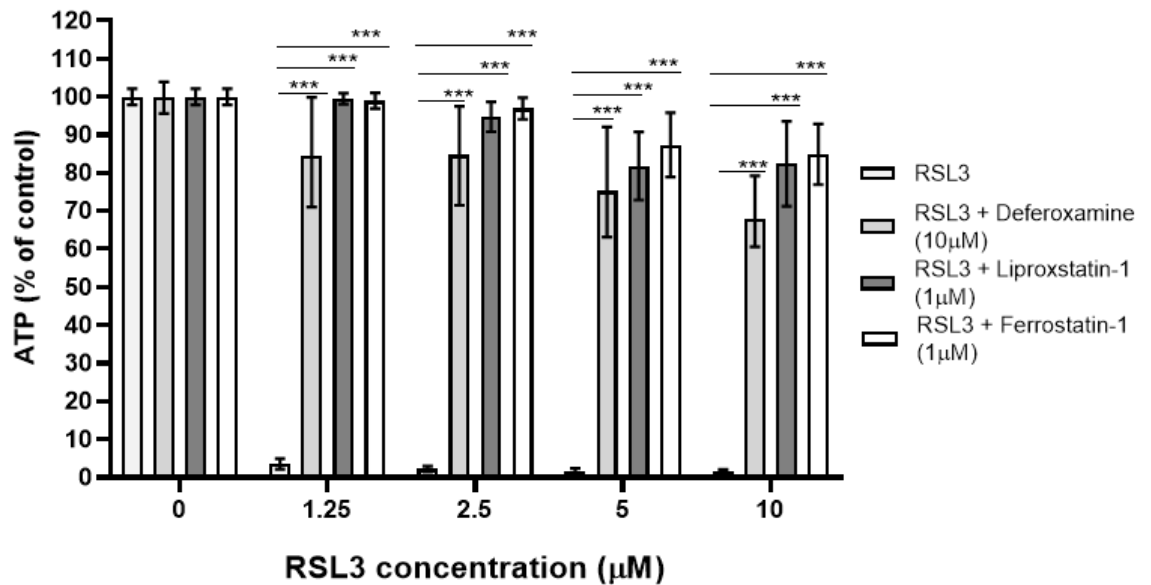
Figure 3.5: Effect of RSL3 on MDA-MB-231 cells after 24 hours of treatment. (A) Fluorescence microscopy analysis of cell death by Hoechst 33342/PI staining after treatment with the ferroptosis inducer RSL3 (10 μM) +/- ferroptosis inhibitors (Deferoxamine 10 μM, Liproxstatin-1 1μM and Ferrostatin-1 1μM). **(B)** Percentage of cell death calculated from n=3 independent experiments each analysing triplicate wells. Data is presented as median ± range. **(C)** ATP level (% of control) assessed by CellTiter-Glo® Luminescent Cell Viability Assay after treatment with ferroptosis inducer RSL3 +/- ferroptosis inhibitors. Data is presented as median ± range from n=3 independent experiments each with 3 technical repeats. The statistical significance was determined by comparison with the RSL3 alone, analysed by a Kruskal-Wallis followed by Dunn's multiple comparisons test (*=P≤0.05, **=P≤0.01, and ***=P≤0.001).

Figure 3.6: Effect of ferroptosis inhibitors on FIN56 responses in MDA-MB-231 cells

(A)

Control

FIN56 10 µM

FIN56 + Deferoxamine 10 µM

FIN56 + Liproxstatin-1 1 µM

FIN56 + Ferrostatin-1 1 µM

Deferoxamine 10 µM

Liproxstatin-1 1 µM

Ferrostatin-1 1 µM
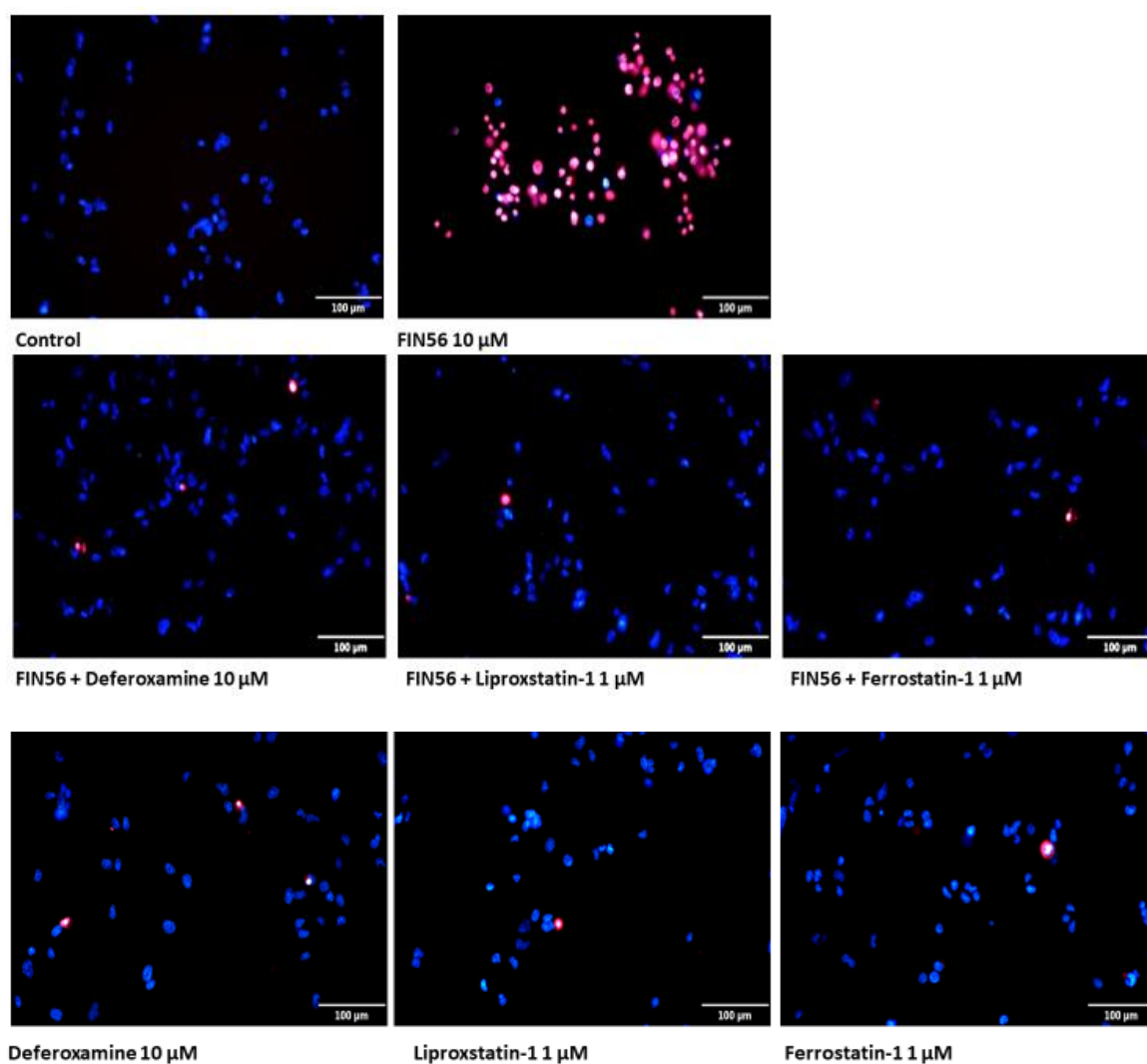
(B)
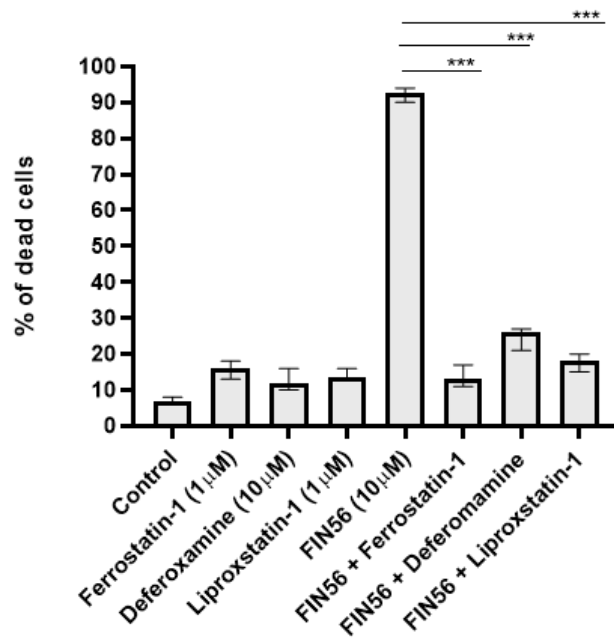
(C)
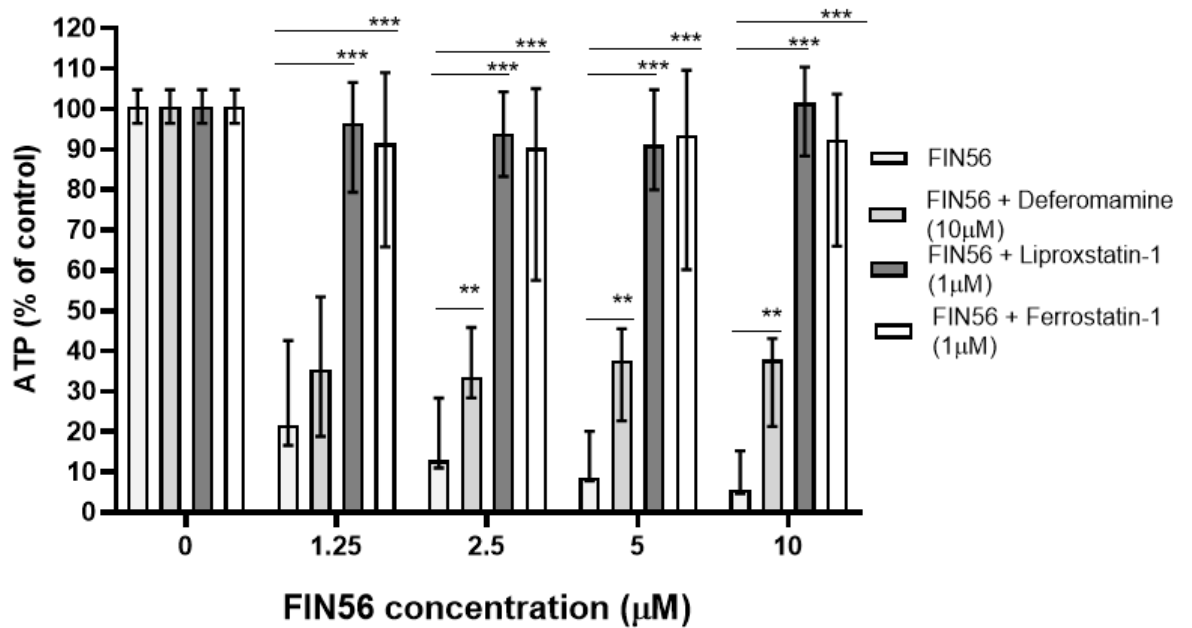
Figure 3.6: Effect of FIN56 on MDA-MB-231 cells after 24 hours of treatment. (A) Fluorescence microscopy analysis of cell death by Hoechst 33342/PI staining after treatment with the ferroptosis inducer FIN56 (10 μM) +/- ferroptosis inhibitors (Deferoxamine 10 μM, Liproxstatin-1 1μM and Ferrostatin-1 1μM). **(B)** Percentage of cell death calculated from n=3 independent experiments each analysing triplicate wells. Data is presented as median ± range. **(C)** ATP level (% of control) assessed by CellTiter-Glo® Luminescent Cell Viability Assay after treatment with ferroptosis inducer FIN56 +/- ferroptosis inhibitors. Data is presented as median ± range from n=3 independent experiments each with 3 technical repeats. The statistical significance was determined by comparison with the FIN56 alone, analysed by a Kruskal-Wallis followed by Dunn's multiple comparisons test (*=P≤0.05, **=P≤0.01, and ***=P≤0.001).

3.2.3 Effect of ferroptosis inducers and inhibitors on MCF-7 cell culture

3.2.3.1 The effect of Erastin and ferroptotic inhibitors on MCF-7 cells

The ferroptosis inducer Erastin showed no potent ferroptotic effect on MCF-7 cell death when compared to control cells at 10 µM. 10 µM is the highest dose that can reasonably be added to cells due its solubility in DMSO and the potential cytotoxic effects of DMSO on cultured cells. This dose also killed almost all MDA-MD-231 cells so 10 µM was used for all further experiments with MCF-7 (Figure 3.7A and B). Therefore, a dose response curve was not performed, and the maximal achievable dose used. The finding is consistent with the results obtained for % of ATP measured using CellTiter-Glo® Luminescent Cell Viability Assay (Figure 3.7C).

The ferroptosis inducer Erastin had a modest effect on ATP levels but did not show the potent effect seen in MDA-MB-231 cells. Ferroptosis inhibitors did not reverse this response, and conversely, Deferoxamine decreased increased cell death (P≤0.01, Figure 3.7A and B) and decreased ATP levels (P≤0.001, Figure 3.7C) when combined with the ferroptosis inducer Erastin at all doses with Erastin (1.25-10 µM) in the MCF-7 cell line.

3.2.3.2 The effect of RSL3 is reversed by ferroptosis inhibitors in MCF-7 cells

The ferroptosis inducer RSL3 showed no potent ferroptotic effect on MCF-7 cell death when compared to control cells, while the ferroptosis inhibitor Deferoxamine slightly induced ferroptosis when combined with the ferroptosis inducer RSL3 (P≤0.01) (Figure 3.8A and B) Deferoxamine co-treatment decreased ATP levels at all doses of RSL3 (1.25-10µM) in the MCF-7 cell line. (P≤0.001). The finding is consistent with the results obtained for Hoechst 33342 and PI staining (Figure 3.8A and B).

Figure 3.7: Effect of ferroptosis inhibitors on Erastin responses in MCF-7 cells

(A)

Control   Erastin 10 µM

Erastin + Deferoxamine 10 µM   Erastin + Liproxstatin-1 1 µM   Erastin + Ferrostatin-1 1 µM

Deferoxamine 10 µM   Liproxstatin-1 1 µM   Ferrostatin-1 1 µM
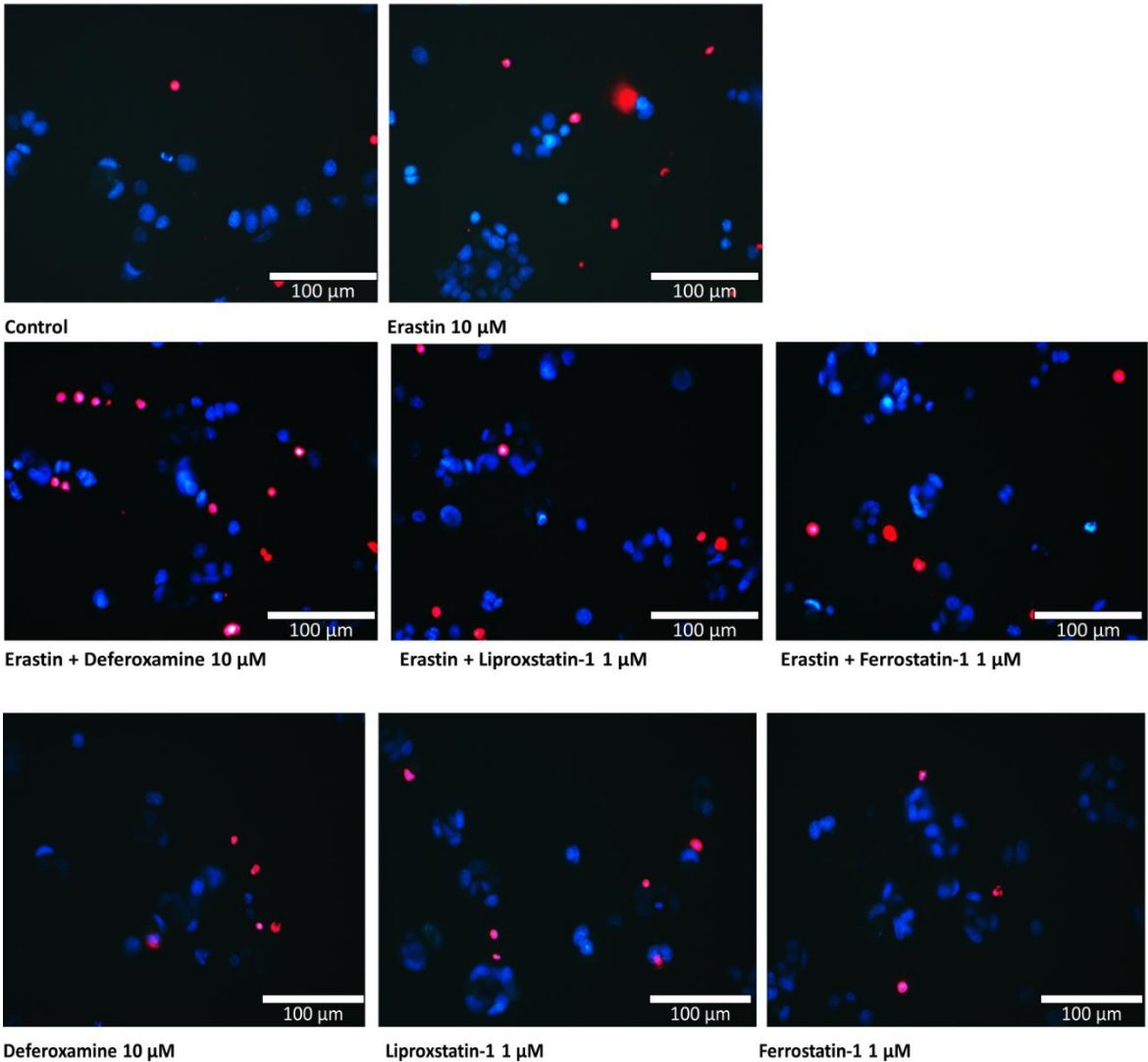
(B)
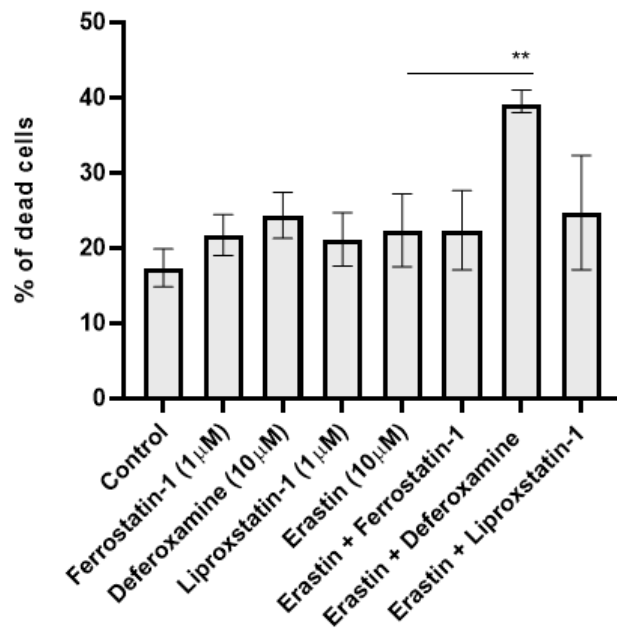
(C)
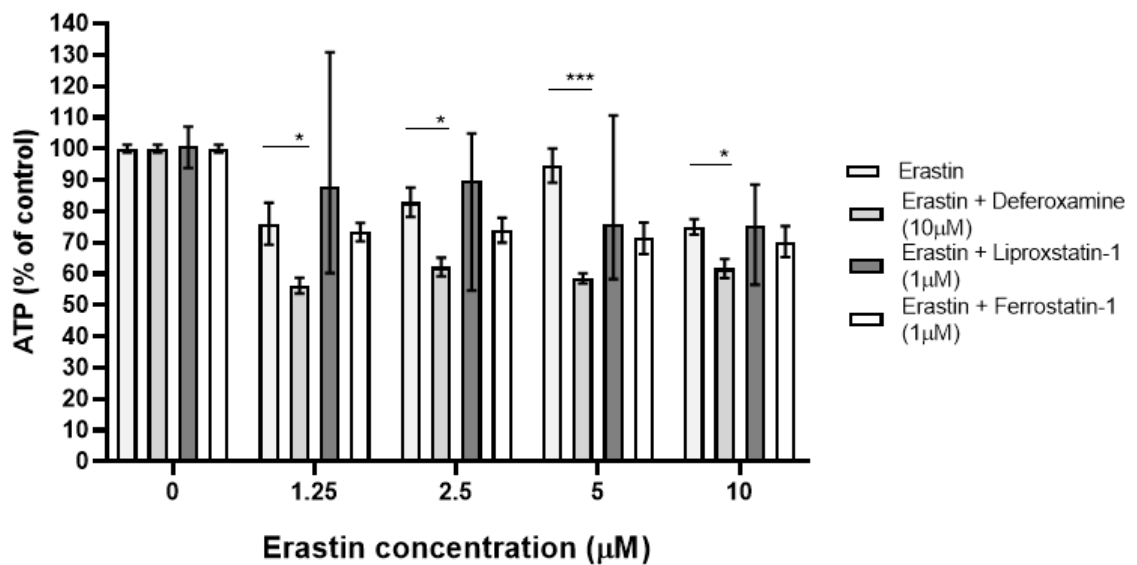
Figure 3.7: Effect of Erastin on MCF-7 cells after 24 hours of treatment. (A) Fluorescence microscopy analysis of cell death by Hoechst 33342/PI staining after treatment with the ferroptosis inducer Erastin (10 µM) +/- ferroptosis inhibitors (Deferoxamine 10 µM, Liproxstatin-1 1µM and Ferrostatin-1 1µM). **(B)** Percentage of cell death calculated from n=3 independent experiments each analysing triplicate wells. Data is presented as median ± range. **(C)** ATP level (% of control) assessed by CellTiter-Glo® Luminescent Cell Viability Assay after treatment with ferroptosis inducer Erastin +/- ferroptosis inhibitors. Data is presented as median ± range from n=3 independent experiments each with 3 technical repeats. The statistical significance was determined by comparison with the Erastin alone, analysed by a Kruskal-Wallis followed by Dunn's multiple comparisons test (*=P≤0.05, **=P≤0.01, and ***=P≤0.001).

Figure 3.8: Effect of ferroptosis inhibitors on RSL3 responses in MCF-7 cells

(A)

Control

RSL3 10 µM

RSL3 + Deferoxamine 10µM

RSL3 + Liproxstatin-1 1 µM

RSL3 + Ferrostatin-1 1 µM

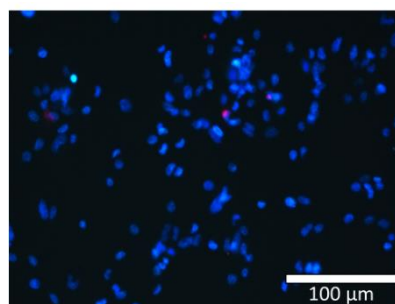Deferoxamine 10µM

Liproxstatin-1 1 µM

Ferrostatin-1 1 µM
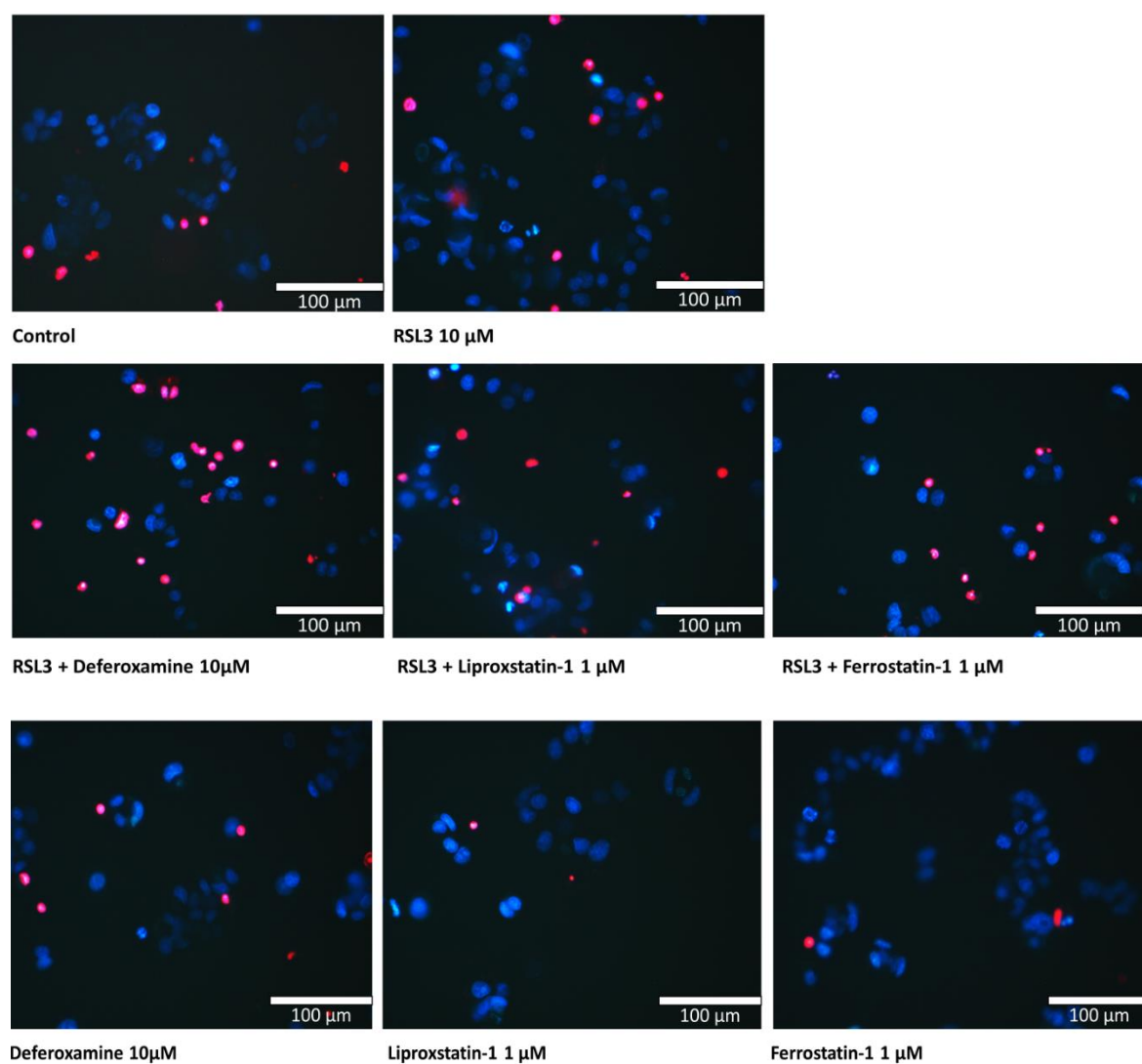
(B)
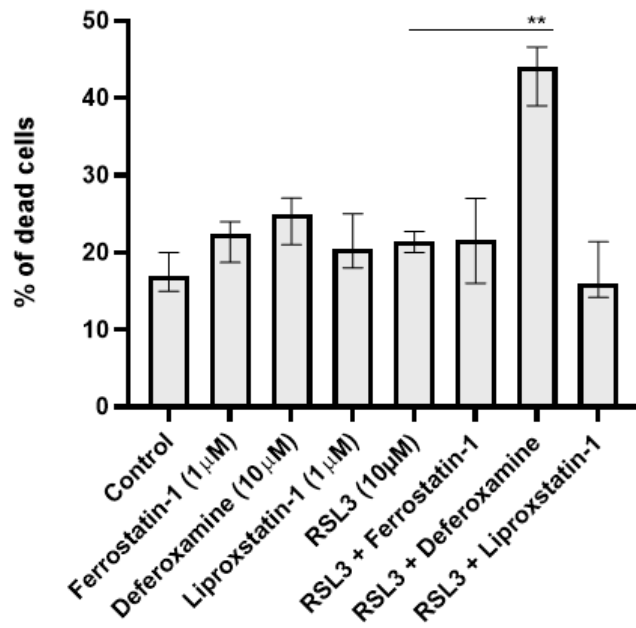
(C)

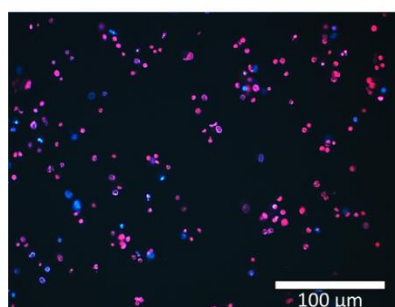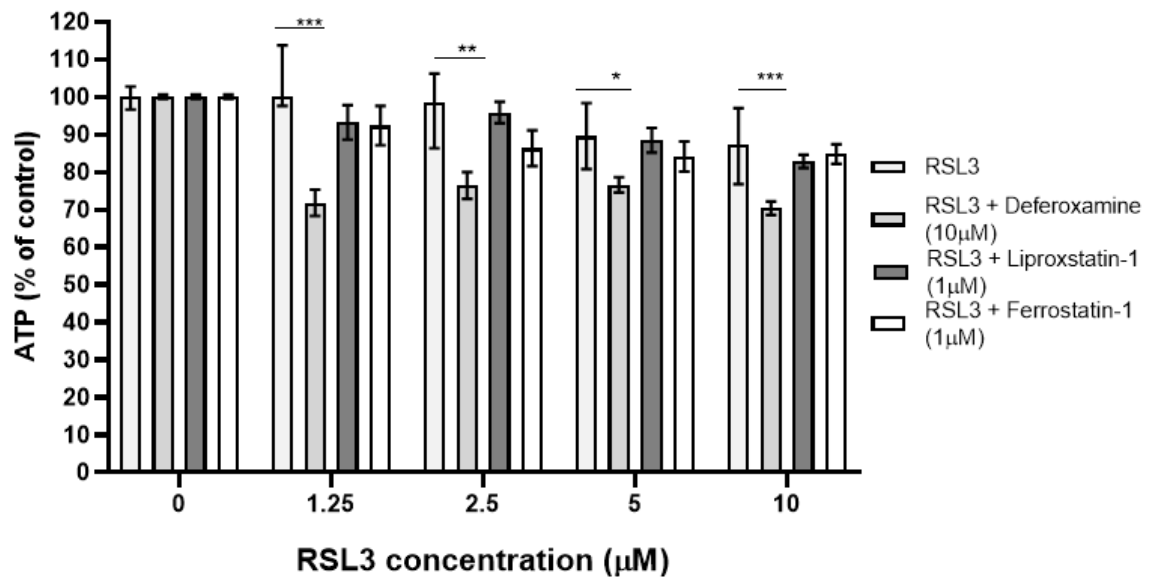
Figure 3.8: Effect of RSL3 on MCF-7 cells after 24 hours of treatment. (A) Fluorescence microscopy analysis of cell death by Hoechst 33342/PI staining after treatment with the ferroptosis inducer RSL3 (10 µM) +/- ferroptosis inhibitors (Deferoxamine 10 µM, Liproxstatin-1 1µM and Ferrostatin-1 1µM). **(B)** Percentage of cell death calculated from n=3 independent experiments each analysing triplicate wells. Data is presented as median ± range. **(C)** ATP level (% of control) assessed by CellTiter-Glo® Luminescent Cell Viability Assay after treatment with ferroptosis inducer RSL3 +/- ferroptosis inhibitors. Data is presented as median ± range from n=3 independent experiments each with 3 technical repeats. The statistical significance was determined by comparison with the RSL3 alone, analysed by a Kruskal-Wallis followed by Dunn's multiple comparisons test (*=P≤0.05, **=P≤0.01, and ***=P≤0.001).

3.2.3.3 The effect of FIN56 is reversed by ferroptosis inhibitors in MCF-7 cells

The ferroptosis inducer FIN56 showed no potent ferroptotic effect on MCF-7 cell death by Hoechst 33342/PI staining. As with Erastin and RSL3 observations, only when combined with Deferoxamine a significant increase in cell death was noticed ($P \leq 0.05$) (Figure 3.9A and B). On the other hand, ATP levels show no difference when the ferroptosis inducer FIN56 was combined with the ferroptosis inhibitors, including Deferoxamine (Figure 3.9C).

3.2.4 Effect of caspase-inhibitors on ferroptosis-inducer-mediated cell death

To exclude the possibility of apoptosis-mediated cell death, a Pan-caspase inhibitor and inhibitors to specific caspases was used in combination with ferroptosis inducers. The ferroptosis inducers (Erastin, RSL3, and FIN56) significantly induced cell death in MDA-MB-231 cells according to the cell viability assay and Hoechst 33342/PI staining as shown previously (Figure 3.1, 3.2, and 3.3). Unlike with observations using ferroptosis inhibitors, the Pan-caspase inhibitor Z-VAD-FMK, caspase-8 inhibitor Z-IETD-FMK, caspase-9 inhibitor Z-LEHD-FMK, and caspase-3 inhibitor Z-DEVD-FMK did not prevent Erastin, RSL3 or FIN56-mediated cell death. Cell death induced by ferroptosis inducers was not inhibited by any caspase inhibitors (Figure 3.10, 3.11, and 3.12). Since MCF-7 did not show potent responses to ferroptosis-inducing agents, MCF-7 cells were not tested with caspase inhibitors in the presence of ferroptosis inducers.

Figure 3.9: Effect of ferroptosis inhibitors on FIN56 responses in MCF-7 cells

(A)
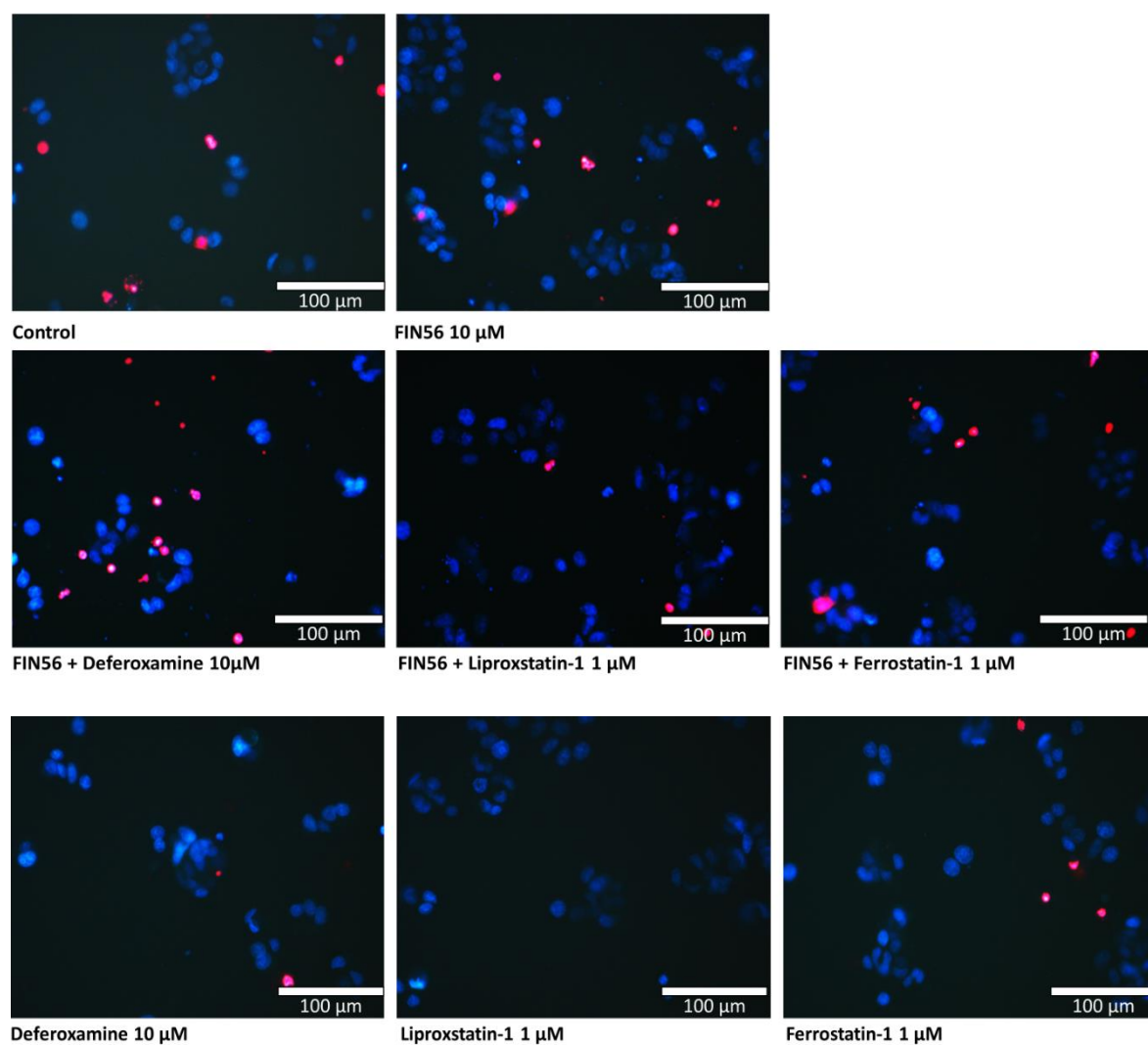
(B)
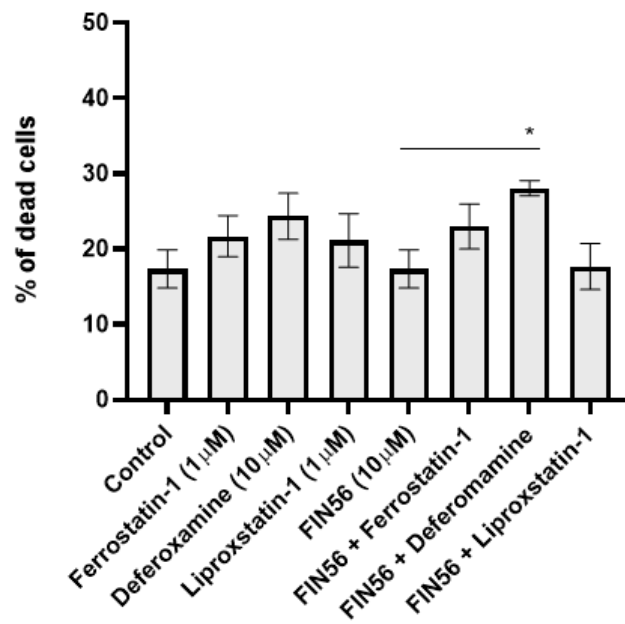
(C)
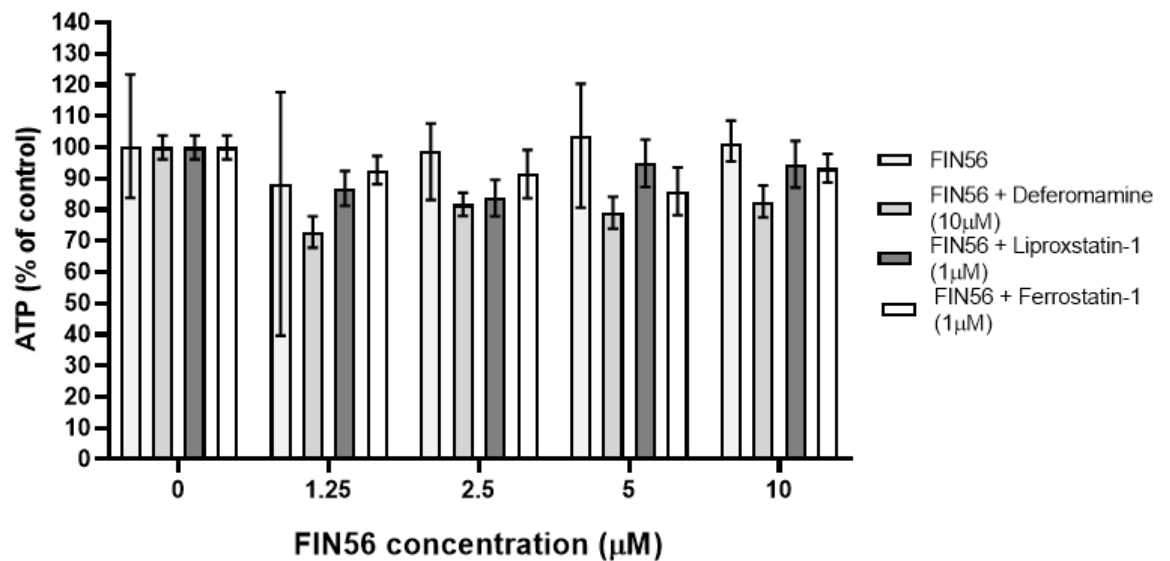
Figure 3.9: Effect of FIN56 on MCF-7 cells after 24 hours of treatment. (A) Fluorescence microscopy analysis of cell death by Hoechst 33342/PI staining after treatment with the ferroptosis inducer FIN56 (10 µM) +/- ferroptosis inhibitors (Deferoxamine 10 µM, Liproxstatin-1 1µM and Ferrostatin-1 1µM). **(B)** Percentage of cell death calculated from n=3 independent experiments each analysing triplicate wells. Data is presented as median ± range. **(C)** ATP level (% of control) assessed by CellTiter-Glo® Luminescent Cell Viability Assay after treatment with ferroptosis inducer FIN56 +/- ferroptosis inhibitors. Data is presented as median ± range from n=3 independent experiments each with 3 technical repeats. The statistical significance was determined by comparison with the FIN56 alone, analysed by a Kruskal-Wallis followed by Dunn's multiple comparisons test (*=P≤0.05, **=P≤0.01, and ***=P≤0.001).

Figure 3.10: Effect of caspase-inhibitors on Erastin-mediated cell death in MDA-MB-231

(A)

Control | Erastin 10uM | Erastin 10 µM & PanCI 10 µM

Erastin 10 µM & C3I 10 µM | Erastin 10 µM & C8I 10 µM | Erastin 10 µM & C9I 10 µM
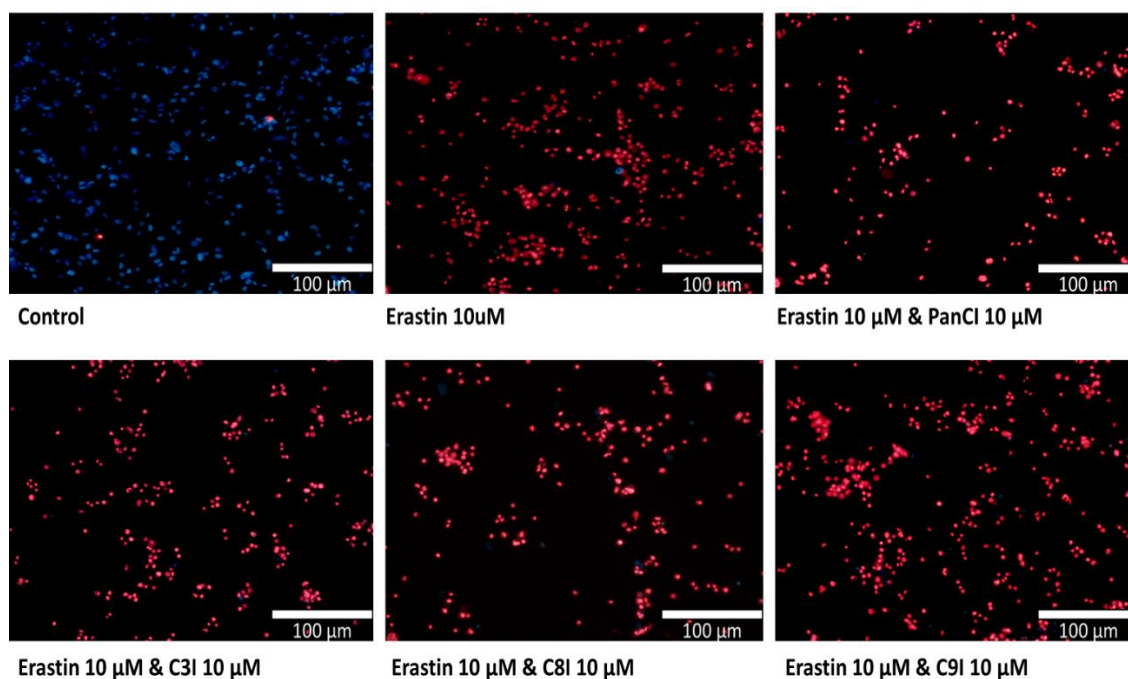
(B)
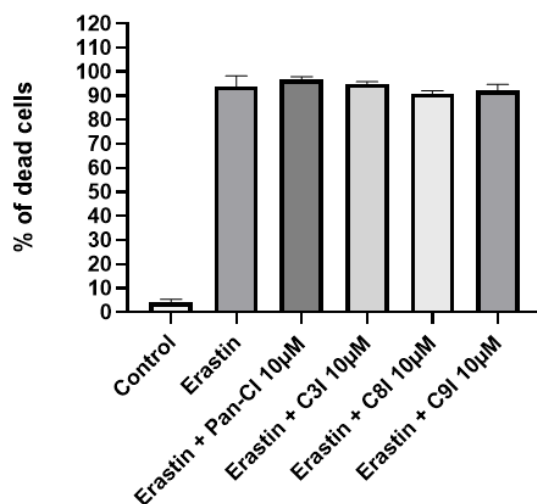
Figure 3.10: **(A) MDA-MB-231 cells were preincubated with caspase inhibitors at concentration of 10 µM for 1 hour prior to treatment with ferroptosis inducer Erastin at concentration of 10 µM, with control (0.2% (v/v) DMSO) for 24 hours. Cell death was determined by Hoechst 33342/PI staining. (B)** Cell death count as determined by Hoechst 33342/PI staining after treating MDA-MB-231 cell line with ferroptosis inducer Erastin at concentration of 10 µM, with control (0.2% (v/v) DMSO) for 24 hours preincubated with caspase inhibitors for 1 hour prior to treatment. n=3 independent experiments each with 3 technical repeats. The statistical significance was determined by comparison with the ferroptosis inducer Erastin, analysed by a Kruskal-Wallis followed by Dunn's multiple comparisons test (*=P≤0.05, **=P≤0.01, and ***=P≤0.001).

Figure 3.11: Effect of caspase-inhibitors on RSL3-mediated cell death in MDA-MB-231

(A)
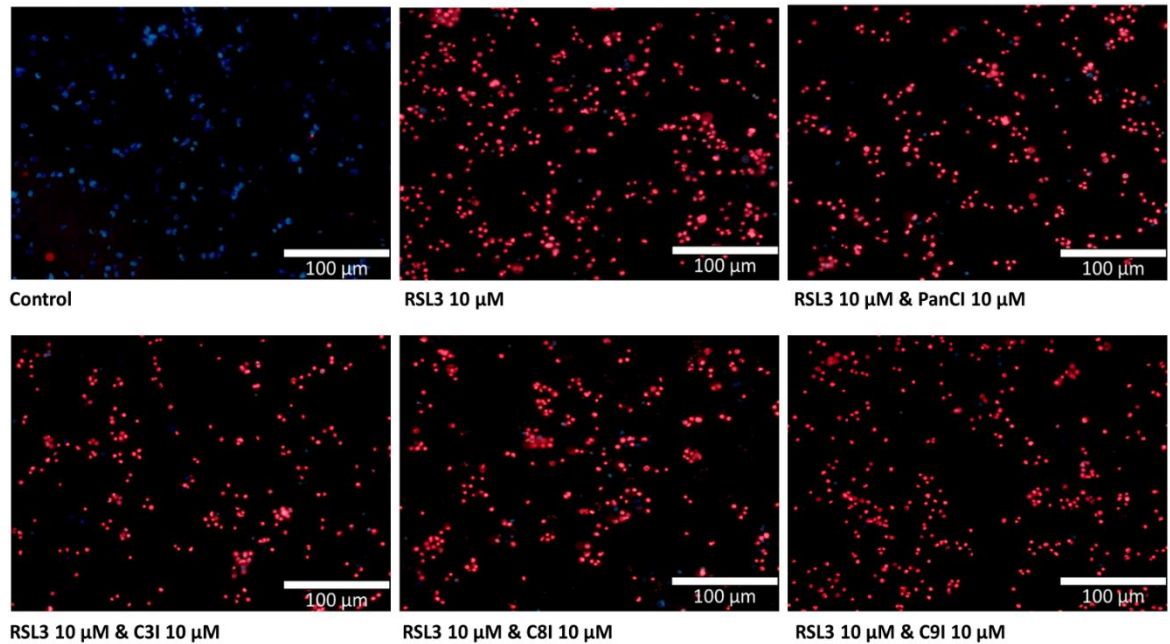
(B)
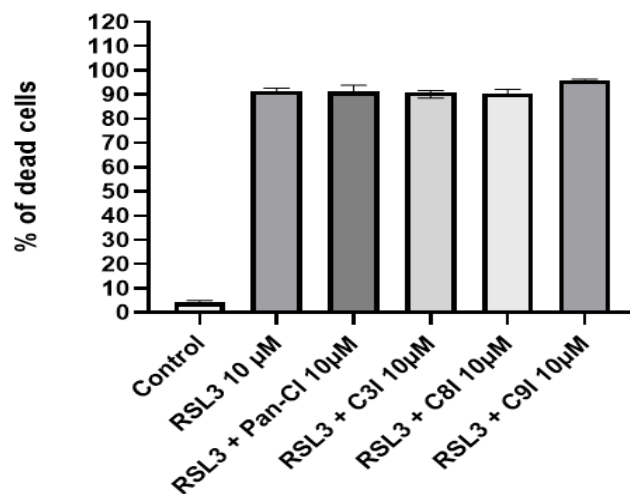
Figure 3.11: **(A) MDA-MB-231 cells were preincubated with caspase inhibitors at concentration of 10 μM for 1 hour prior to treatment with ferroptosis inducer RSL3 at concentration of 10 μM, with control (0.2% (v/v) DMSO) for 24 hours. Cell death was determined by Hoechst 33342/PI staining. (B)** Cell death count as determined by Hoechst 33342/PI staining after treating MDA-MB-231 cell line with ferroptosis inducer RSL3 at concentration of 10 μM, with control (0.2% (v/v) DMSO) for 24 hours preincubated with caspase inhibitors for 1 hour prior to treatment. n=3 independent experiments each with 3 technical repeats. The statistical significance was determined by comparison with the ferroptosis inducer RSL3, analysed by a Kruskal-Wallis followed by Dunn's multiple comparisons test (*=P≤0.05, **=P≤0.01, and ***=P≤0.001).

Figure 3.12: Effect of caspase-inhibitors on FIN56-mediated cell death in MDA-MB-231

(A)

Control   FIN56 10 µM   FIN56 10 µM & PanCI 10 µM

FIN56 10 µM & C3I 10 µM   FIN56 10 µM & C8I 10 µM   FIN56 10 µM & C9I 10 µM
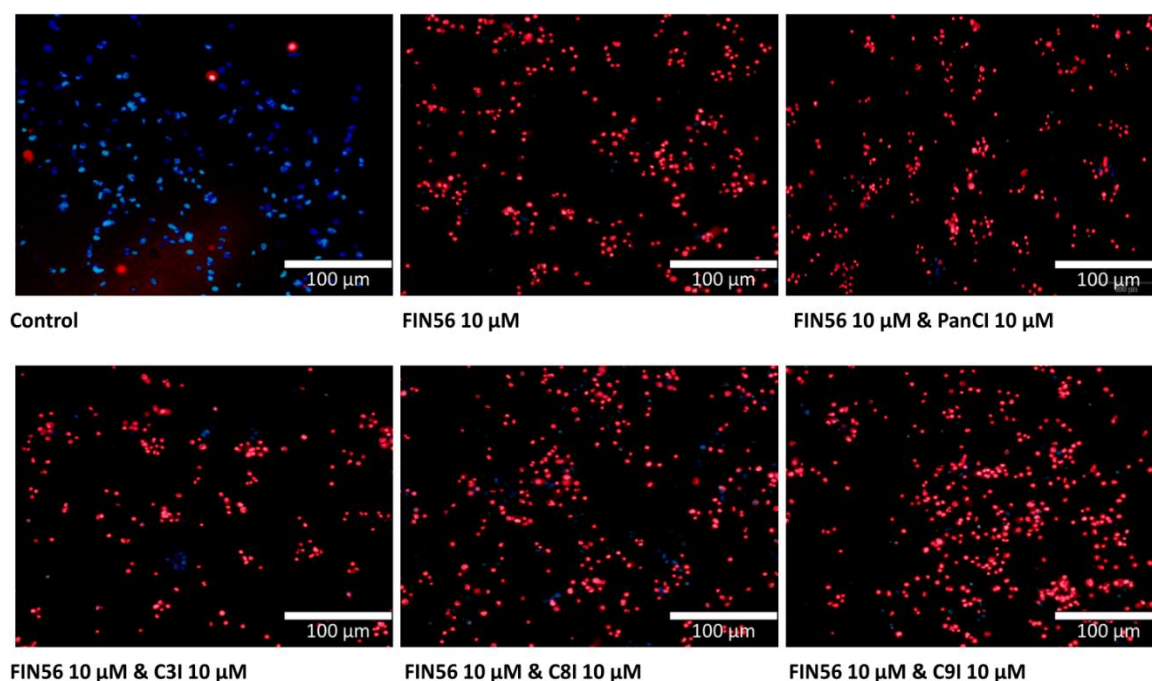
(B)
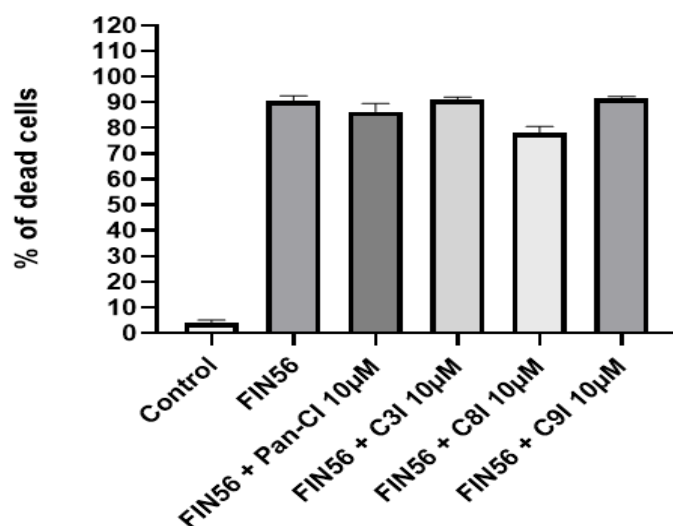
Figure 3.12: **(A) MDA-MB-231 cells were preincubated with caspase inhibitors at concentration of 10 µM for 1 hour prior to treatment with ferroptosis inducer FIN56 at concentration of 10 µM, with control (0.2% (v/v) DMSO) for 24 hours. Cell death was determined by Hoechst 33342/PI. (B)** Cell death count as determined by Hoechst 33342/PI staining after treating MDA-MB-231 cell line with ferroptosis inducer FIN56 at concentration of 10 µM, with control (0.2% (v/v) DMSO) for 24 hours preincubated with caspase inhibitors for 1 hour prior to treatment. n=3 independent experiments each with 3 technical repeats. The statistical significance was determined by comparison with the ferroptosis inducer FIN56, analysed by a Kruskal-Wallis followed by Dunn's multiple comparisons test (*=P≤0.05, **=P≤0.01, and ***=P≤0.001).

3.2.5 Effect of ferroptosis inducers on Fe^{2+} levels

Mito-FerroGreen is a fluorescent probe that allows for live cell fluorescence imaging of intracellular Fe^{2+} and allows for the detection of ferrous ions (Fe^{2+}) in mitochondria where soluble iron accumulates and heme proteins are produced (Dojindo, 2023). Detection of Fe^{2+} is strongly suggestive of iron-mediated cell death, specifically ferroptosis. The Mito-FerroGreen reagent dye was applied after treating MDA-MB-231 and MCF-7 cells with ferroptosis inducers and with the presence and absence of ferroptosis inhibitors at different time points (1, 6, and 24 hours). This experiment was a qualitative analysis that was done once to determine the present of iron within treated cells with ferroptosis inducers, and the absence of iron within cells confirm the reverse action of ferroptosis inhibitors in MDA-MB-231 cells treated with ferroptosis inducers (Figure 3.4, 3.5, and 3.6). No overt effect was observed in MCF-7 cells consistent with the lack of ferroptosis observed in these cells (Figure 3.7, 3.8, and 3.9).

3.2.5.1 Detection of ferroptosis markers (Fe^{2+}) after induction of ferroptosis in MDA-MB-231 cells

The ferroptosis inducer Erastin, induced mitochondrial labile Fe^{2+} consistent with ferroptosis cell death. Mito-FerroGreen detected mitochondrial ferrous iron. Mito-FerroGreen dye showed Fe^{2+} in cells treated with Ferroptosis inducers, confirming that it is ferroptotic cell death (Figure 3.13). After 1 hour and 6 hours of Erastin treatment, a small number of Mito-FerroGreen cells are visible, however at this timepoint, very few cells were dead as determined by Hoechst 33342/PI staining. However, at 24 hour treatment with Erastin, most cells were dead and also the majority were Mito-FerroGreen/Fe^{2+} positive (Figure 3.13). Similar observations were seen for RSL3 and FIN56 whereby free iron was detected after 24 hours of treatment with the ferroptosis inducer (Figure 3.14 and 3.15).

Figure 3.13: Induction of labile Fe^{2+} after Erastin treatment at different time points in MDA-MB-231 cells
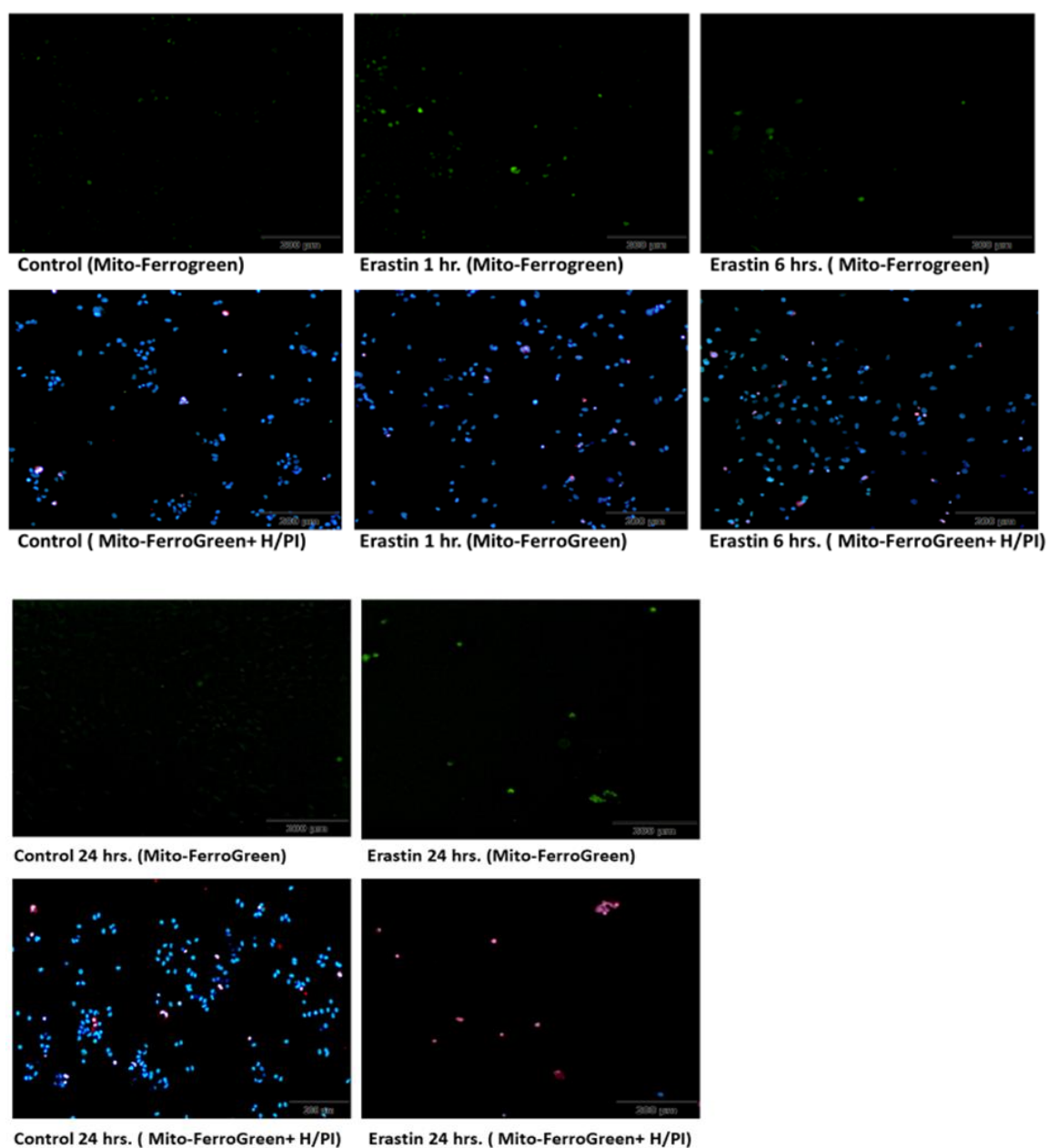
Figure 3.13: Mitochondrial labile Fe^{2+} and death detection under fluorescent microscope after treating MDA-MB-231 cell line for 1 hour, 6 and 24 hours with ferroptosis inducer Erastin at concentration of 10 µM, with control (0.2% (v/v) DMSO), determined by Hoechst 33342/PI staining and Mito-FerroGreen dye staining. Live cells are stained blue with Hoechst 33342, dead cells are stained red with PI staining, and Fe^{2+} stained green with Mito-FerroGreen (Scale bars = 200 µm).

Figure 3.14 Induction of labile Fe^{2+} after RSL3 treatment at different time points in MDA-MB-231 cells
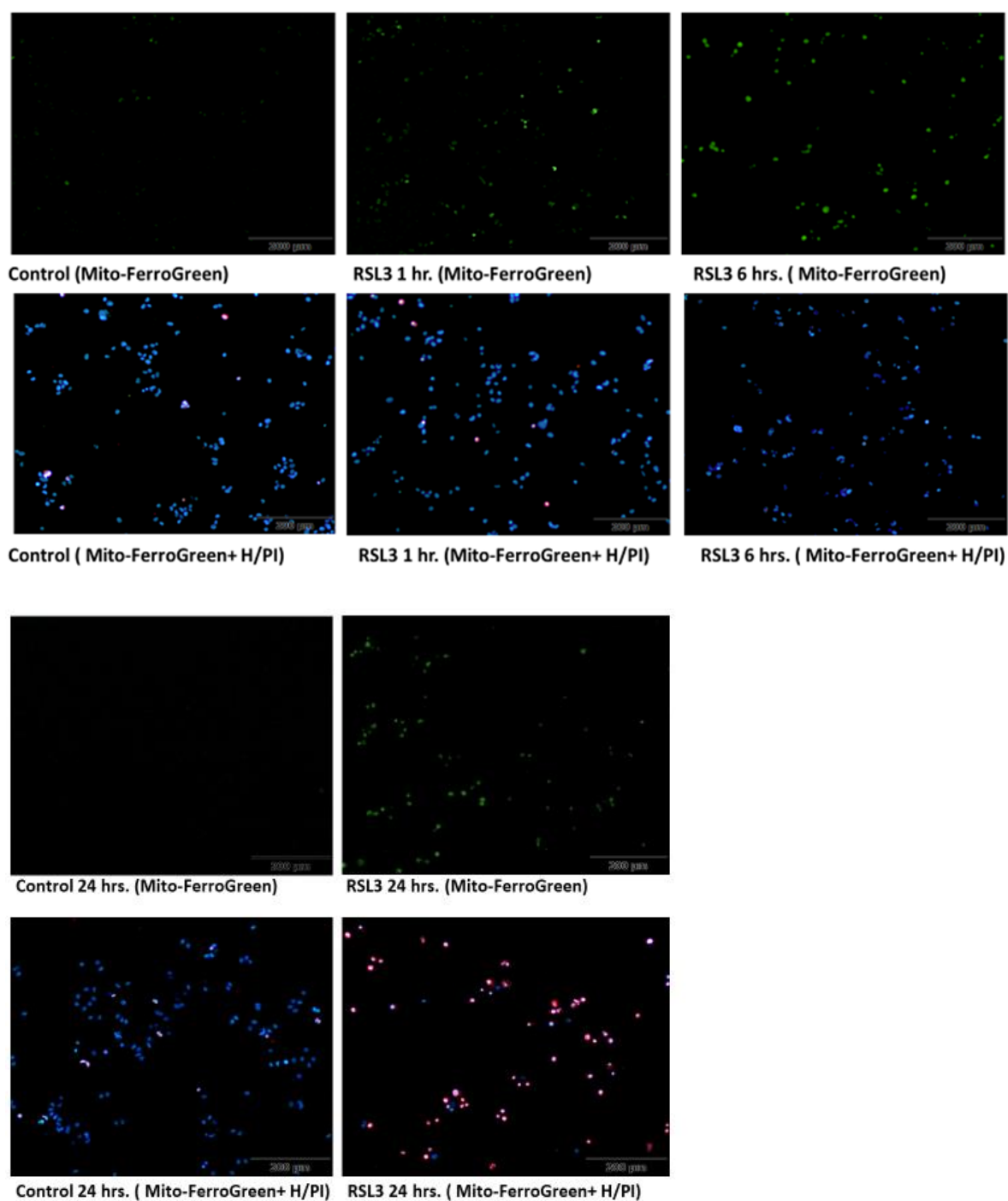
Figure 3.14: Mitochondrial labile Fe^{2+} and death detection under fluorescent microscope after treating MDA-MB-231 cell line for 1 hour, 6 and 24 hours with ferroptosis inducer RSL3 at concentration of 10 µM, with control (0.2% (v/v) DMSO), determined by Hoechst 33342/PI staining and Mito-FerroGreen dye staining. Live cells are stained blue with Hoechst 33342, dead cells are stained red with PI staining, and Fe^{2+} stained green with Mito-FerroGreen (Scale bars = 200 µm).

Figure 3.15 Induction of labile Fe²⁺ after FIN56 treatment at different time points in MDA-MB-231 cells
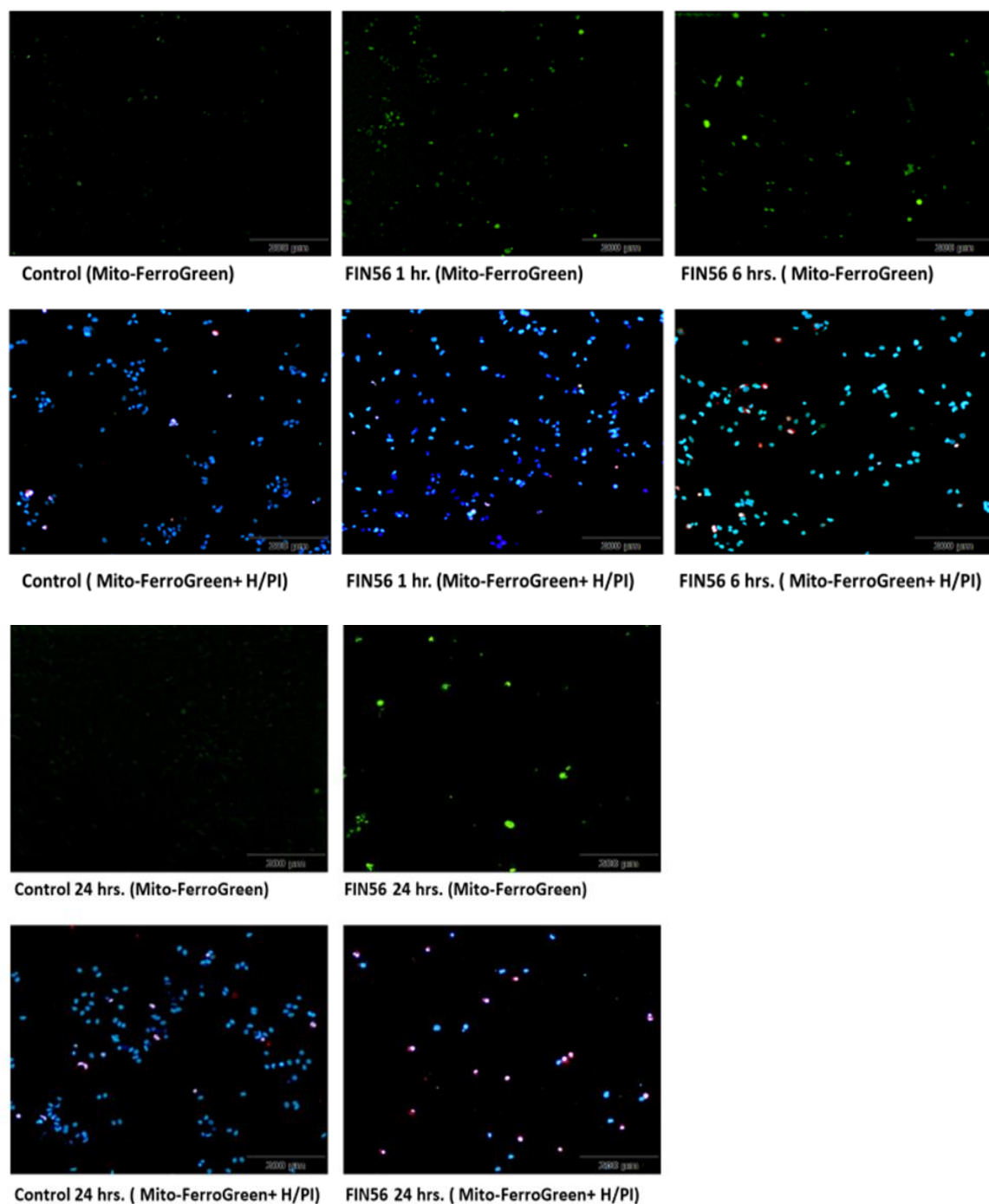
Figure 3.15: Mitochondrial labile Fe^{2+} and death detection under fluorescent microscope after treating MDA-MB-231 cell line for 1 hour, 6 and 24 hours with ferroptosis inducer FIN56 at concentration of 10 µM, with control (0.2% (v/v) DMSO), determined by Hoechst 33342/PI staining and Mito-FerroGreen dye staining. Live cells are stained blue with Hoechst 33342, dead cells are stained red with PI staining, and Fe^{2+} stained green with Mito-FerroGreen (Scale bars = 200 µm).

3.2.5.2 Ferroptosis inhibitors reverse the effects of ferroptosis inducers on free iron (Fe^{2+}) in MDA-MB-231 cells

To assess whether ferroptosis inhibitors affected free iron, cells were treated with ferroptosis inducing agents and co-treated with ferroptosis inhibitors and free iron assessed using Mito-FerroGreeen staining. Consistent with previous cell death and ATP measurements, ferroptosis inhibitors Liproxstatin-1 and Ferrostatin-1 prevented the detection of free iron in cell treated with Erastin. The absence of iron within cells confirms the reverse action of ferroptosis inhibitors to death (Figure 3.16). Similar observations were seen in cells treated with RSL3 or FIN56, whereby ferroptosis inhibitors prevented the detection of free iron after 24 hours of treatment with ferroptosis inducers (Figure 3.17 and 3.18). However, Deferoxamine did not prevent the detection of free iron after Erastin treatment, however these cells containing free iron were not killed by Erastin (Figure 3.16).

Figure 3.16: Induction of labile Fe^{2+} after Erastin treatment is reversed by ferroptosis inhibitors in MDA-MB-231 cells

Erastin Liproxstatin-1 (Mito-FerroGreen)   Erastin + Ferrostatin-1 (Mito-FerroGreen)   Erastin + Deferoxamine (Mito-FerroGreen)

Erastin + Liproxstatin-1 (Mito-FerroGreen+ H/PI)   Erastin + Ferrostatin-1 (Mito-FerroGreen+ H/PI)   Erastin + Deferoxamine (Mito-FerroGreen+ H/PI)
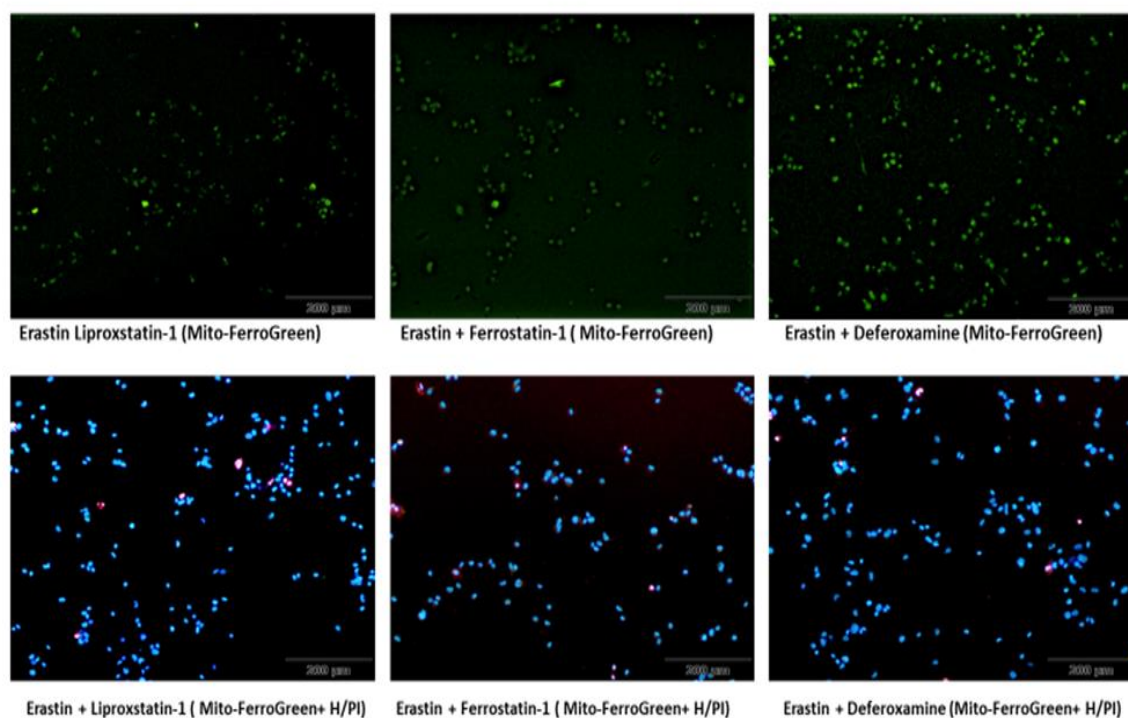
Figure 3.16: Mitochondrial labile Fe^{2+} and death detection under fluorescent microscope after treating MDA-MB-231 cell line for 24 hours with ferroptosis inducer Erastin at concentration of 10 µM and ferroptosis inhibitors (Deferoxamine 10 µM, Liproxstatin-1 1 µM and Ferrostatin-1 1µM), with control (0.2% (v/v) DMSO). Determined by Hoechst 33342/PI staining and Mito-FerroGreen dye. Live cells are stained blue with Hoechst 33342, dead cells are stained red with PI staining, and Fe^{2+} stained green with Mito-FerroGreen (Scale bars = 200 µm).

Figure 3.17: Induction of labile Fe^{2+} after RSL3 treatment is reversed by ferroptosis inhibitors in MDA-MB-231 cells
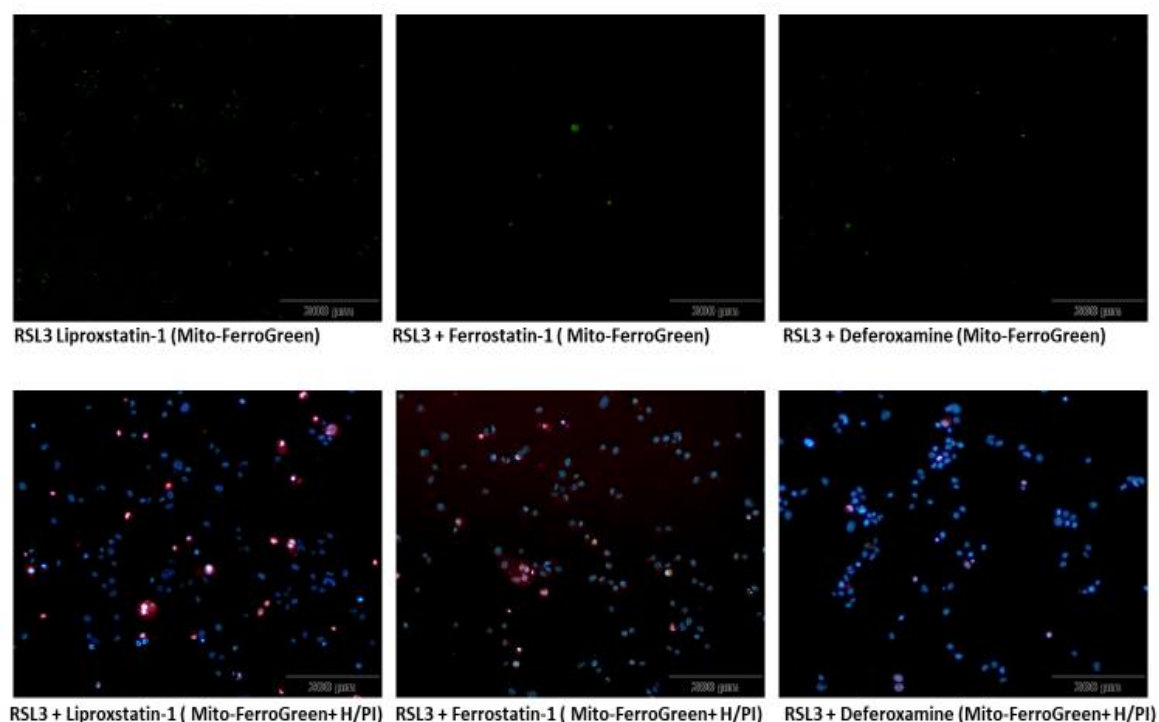
Figure 3.17: Mitochondrial labile Fe^{2+} and death detection under fluorescent microscope after treating MDA-MB-231 cell line for 24 hours with ferroptosis inducer RSL3 at concentration of 10 μM and ferroptosis inhibitors (Deferoxamine 10 μM, Liproxstatin-1 1 μM and Ferrostatin-1 1μM), with control (0.2% (v/v) DMSO). Determined by Hoechst 33342/PI staining and Mito-FerroGreen dye. Live cells are stained blue with Hoechst 33342, dead cells are stained red with PI staining, and Fe^{2+} stained green with Mito-FerroGreen (Scale bars = 200 μm).

Figure 3.18 Induction of labile Fe^{2+} after FIN56 treatment is reversed by ferroptosis inhibitors in MDA-MB-231 cells
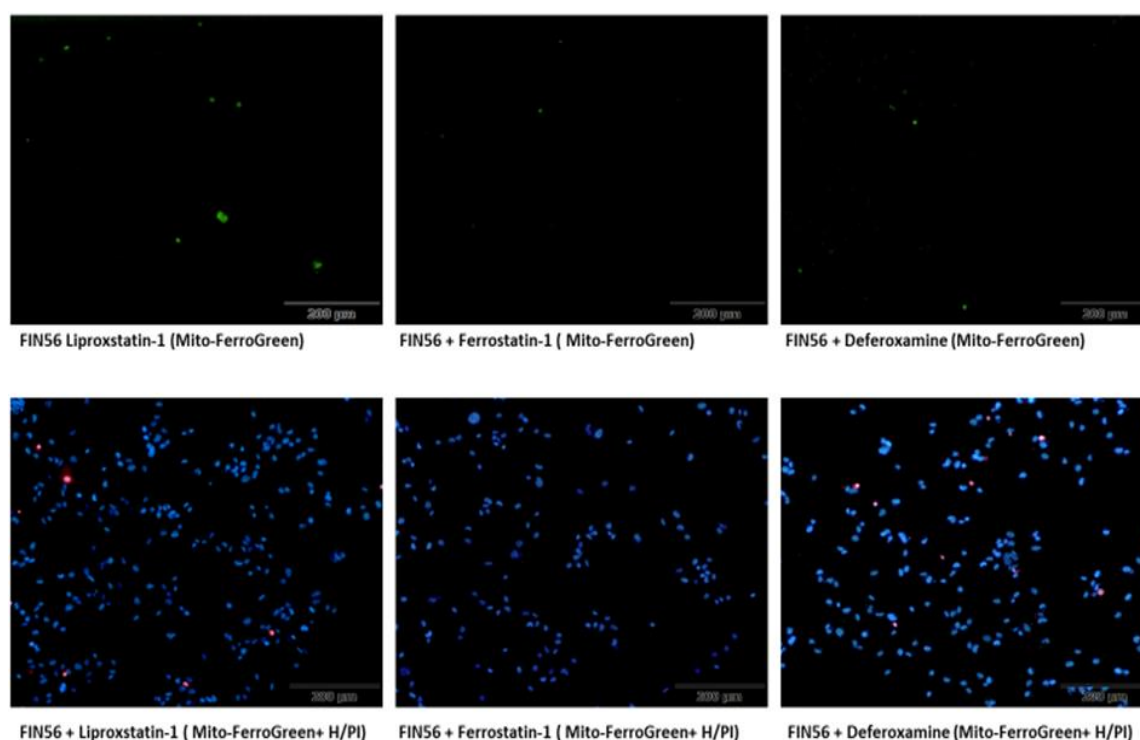
Figure 3.18: Mitochondrial labile Fe^{2+} and death detection under fluorescent microscope after treating MDA-MB-231 cell line for 24 hours with ferroptosis inducer FIN56 at concentration of 10 µM and ferroptosis inhibitors (Deferoxamine 10 µM, Liproxstatin-1 1 µM and Ferrostatin-1 1µM), with control (0.2% (v/v) DMSO). Determined by Hoechst 33342/PI staining and Mito-FerroGreen dye. Live cells are stained blue with Hoechst 33342, dead cells are stained red with PI staining, and Fe^{2+} stained green with Mito-FerroGreen (Scale bars = 200 µm).

3.2.5.3 Detection of Ferroptosis markers (Fe^{2+}) after treatment with ferroptosis inducers +/- ferroptosis inhibitors in MCF-7 cells

To assess the effect of ferroptotic inducers on the production of free iron in MCF-7 cells that are not responsive to ferroptosis, cells were treated with Erastin (Figure 3.19), RSL3 (Figure 3.20) or FIN56 (Figure 3.21) as before, in the presence of ferroptosis inhibitors. Data shows that a few cells had Fe^{2+} induction in response to ferroptotic inducers, and that the ferroptosis inhibitors had minimal effect (Figure 3.22, 3.23 and 3.24).

Figure 3.19: Induction of labile Fe^{2+} after Erastin treatment at different time points in MCF-7 cells

Control (Mito-FerroGreen)   Erastin 1 hr. (Mito-FerroGreen)   Erastin 6 hrs. (Mito-FerroGreen)

Control (Mito-FerroGreen+ H/PI)   Erastin 1 hr. (Mito Ferrogreen)   Erastin 6 hrs. (Mito-FerroGreen+ H/PI)

Control 24 hrs. (Mito-FerroGreen)   Erastin 24 hrs. (Mito-FerroGreen)

Control 24 hrs. (Mito-FerroGreen+ H/PI)   Erastin 24 hrs. (Mito-FerroGreen+ H/PI)
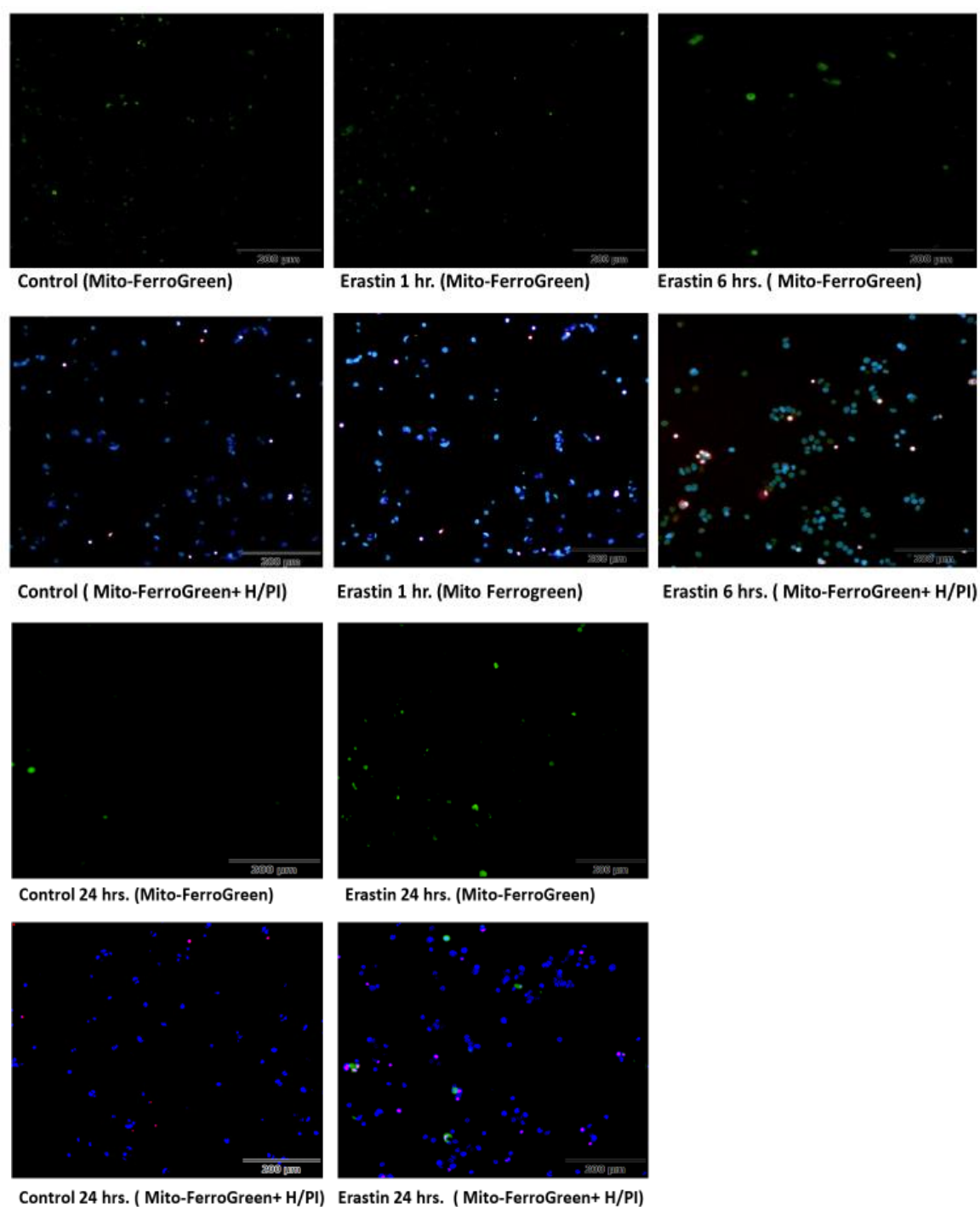
Figure 3.19: Mitochondrial labile Fe^{2+} and death detection under fluorescent microscope after treating MCF-7 cell line for 1 hour, 6 and 24 hours with ferroptosis inducer Erastin at concentration of 10 µM, with control (0.2% (v/v) DMSO), determined by Hoechst 33342/PI staining and Mito-FerroGreen dye staining. Live cells are stained blue with Hoechst 33342, dead cells are stained red with PI staining, and Fe^{2+} stained green with Mito-FerroGreen (Scale bars = 200 µm).

Figure 3.20: Induction of labile Fe²⁺ after RSL3 treatment at different time points in MCF-7 cells

Control (Mito-FerroGreen)   RSL3 1 hr. (Mito-FerroGreen)   RSL3 6 hrs. (Mito-FerroGreen)

Control (Mito-FerroGreen+ H/PI)   RSL3 1 hr. (Mito-FerroGreen+ H/PI)   RSL3 6 hrs. (Mito-FerroGreen+ H/PI)

Control 24 hrs. (Mito-FerroGreen)   RSL3 24 hrs. (Mito-FerroGreen)

Control 24 hrs. (Mito-FerroGreen+ H/PI)   RSL3 24 hrs. (Mito-FerroGreen+ H/PI)
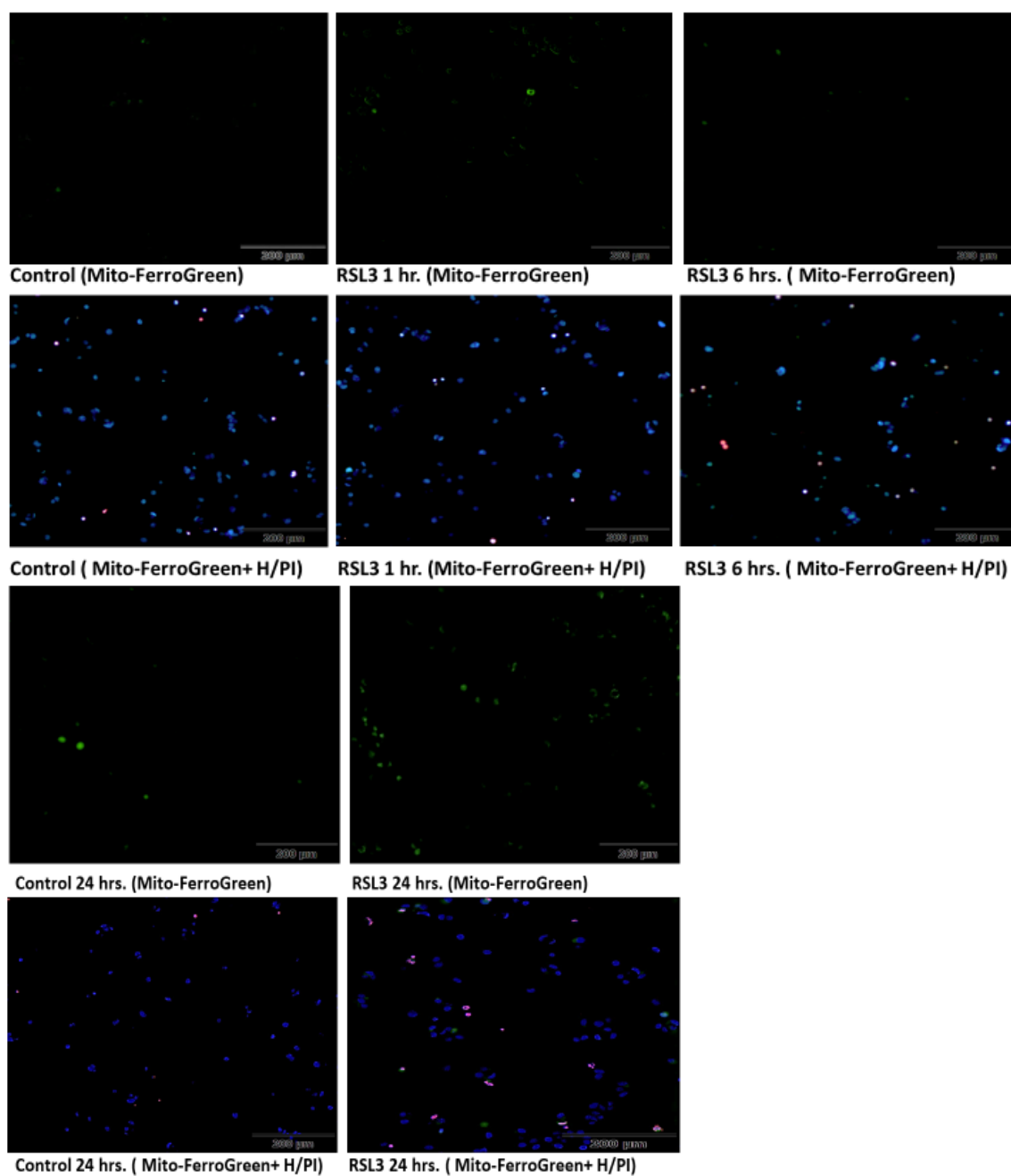
Figure 3.20: Mitochondrial labile Fe²⁺ and death detection under fluorescent microscope after treating MCF-7 cell line for 1 hour, 6 and 24 hours with ferroptosis inducer RSL3 at concentration of 10 µM, with control (0.2% (v/v) DMSO), determined by Hoechst 33342/PI staining and Mito-FerroGreen dye staining. Live cells are stained blue with Hoechst 33342, dead cells are stained red with PI staining, and Fe²⁺ stained green with Mito-FerroGreen (Scale bars = 200 µm).

Figure 3.21: Induction of labile Fe^{2+} after FIN56 treatment at different time points in MCF-7 cells
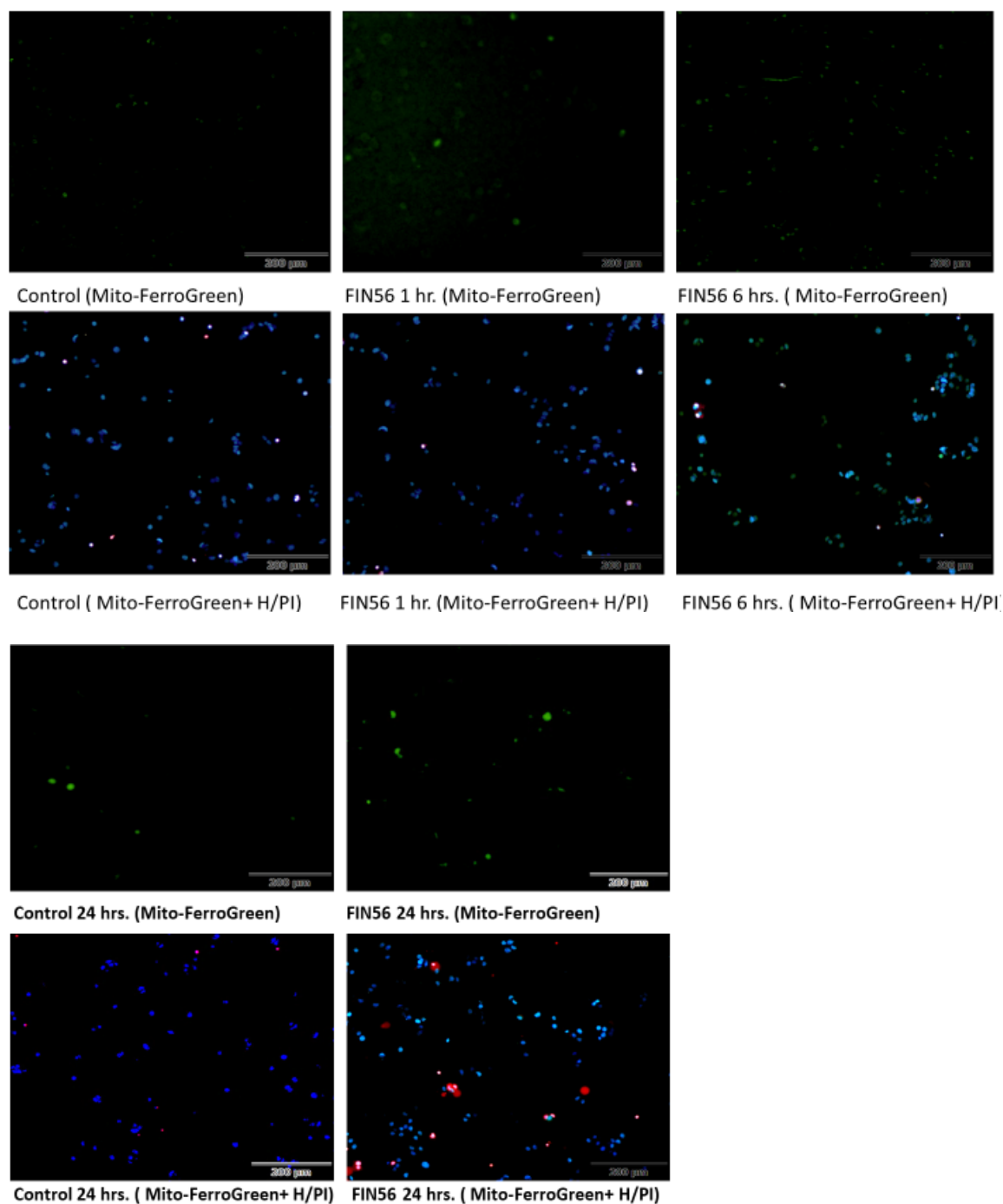
Figure 3.21: Mitochondrial labile Fe^{2+} and death detection under fluorescent microscope after treating MCF-7 cell line for 1 hour, 6 and 24 hours with ferroptosis inducer FIN56 at concentration of 10 μM, with control (0.2% (v/v) DMSO), determined by Hoechst 33342/PI staining and Mito-FerroGreen dye staining. Live cells are stained blue with Hoechst 33342, dead cells are stained red with PI staining, and Fe^{2+} stained green with Mito-FerroGreen (Scale bars = 200 μm).

Figure 3.22: Induction of labile Fe^{2+} after Erastin treatment with ferroptosis inhibitors in MCF-7 cells
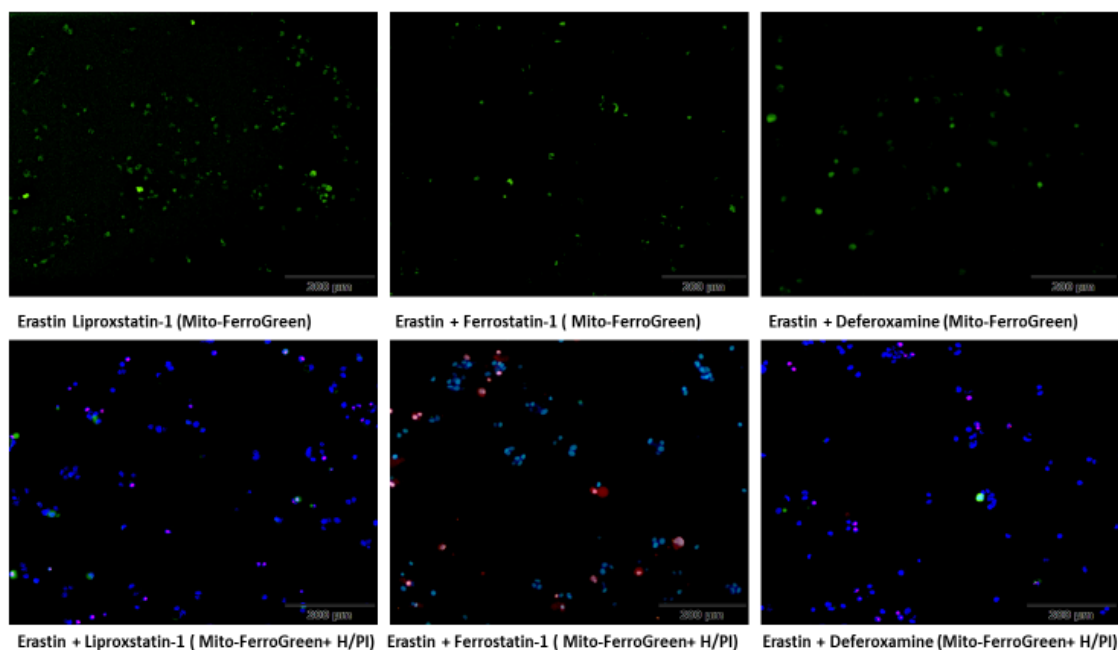
Figure 3.22: Mitochondrial labile Fe^{2+} and death detection under fluorescent microscope after treating MCF-7 cell line for 24 hours with ferroptosis inducer Erastin at concentration of 10 µM and ferroptosis inhibitors (Deferoxamine 10 µM, Liproxstatin-1 1 µM and Ferrostatin-1 1µM), with control (0.2% (v/v) DMSO). Determined by Hoechst 33342/PI staining and Mito-FerroGreen dye. Live cells are stained blue with Hoechst 33342, dead cells are stained red with PI staining, and Fe^{2+} stained green with Mito-FerroGreen (Scale bars = 200 µm).

Figure 3.23: Detection of labile Fe²⁺ after RSL3 treatment with ferroptosis inhibitors in MCF-7 cells
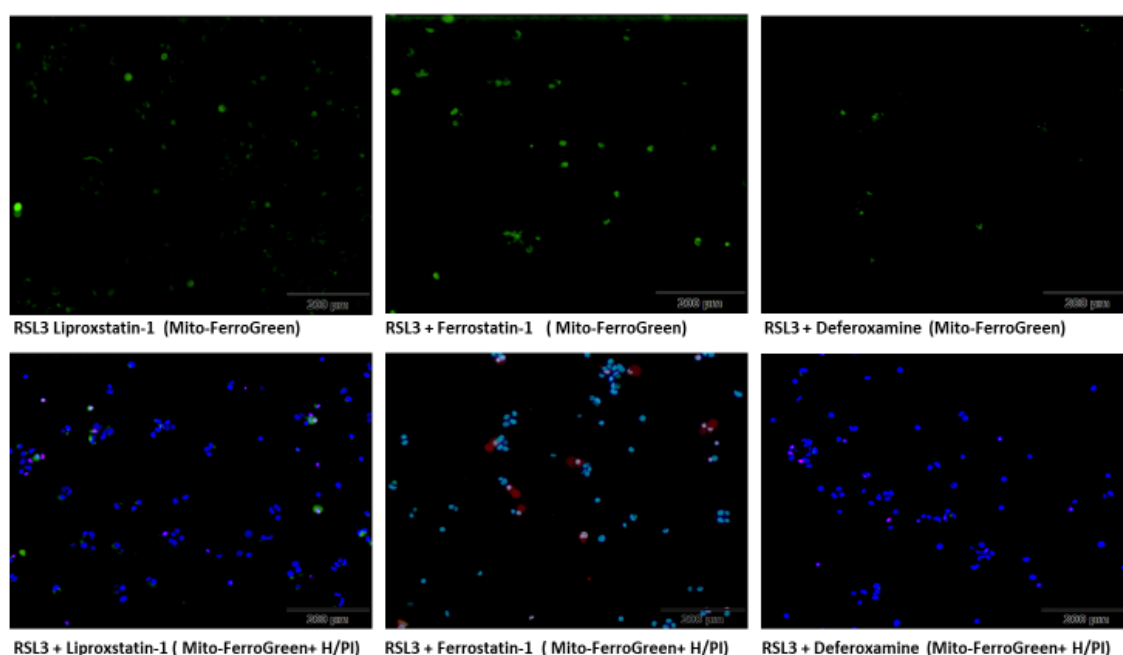
Figure 3.23: Mitochondrial labile Fe^{2+} and death detection under fluorescent microscope after treating MCF-7 cell line for 24 hours with ferroptosis inducer RSL3 at concentration of 10 µM and ferroptosis inhibitors (Deferoxamine 10 µM, Liproxstatin-1 1 µM and Ferrostatin-1 1µM), with control (0.2% (v/v) DMSO). Determined by Hoechst 33342/PI staining and Mito-FerroGreen dye. Live cells are stained blue with Hoechst 33342, dead cells are stained red with PI staining, and Fe^{2+} stained green with Mito-FerroGreen (Scale bars = 200 µm).

Figure 3.24: Detection of labile Fe^{2+} after FIN56 treatment with ferroptosis inhibitors in MCF-7 cells

FIN56 Liproxstatin-1 (Mito-FerroGreen)   FIN56 + Ferrostatin-1 (Mito-FerroGreen   FIN56 + Deferoxamine (Mito-FerroGreen)

FIN56 + Liproxstatin-1 (Mito-FerroGreen+ H/PI)   FIN56 + Ferrostatin-1 (Mito-FerroGreen+ H/PI)   FIN56 + Deferoxamine (Mito-FerroGreen+ H/PI)
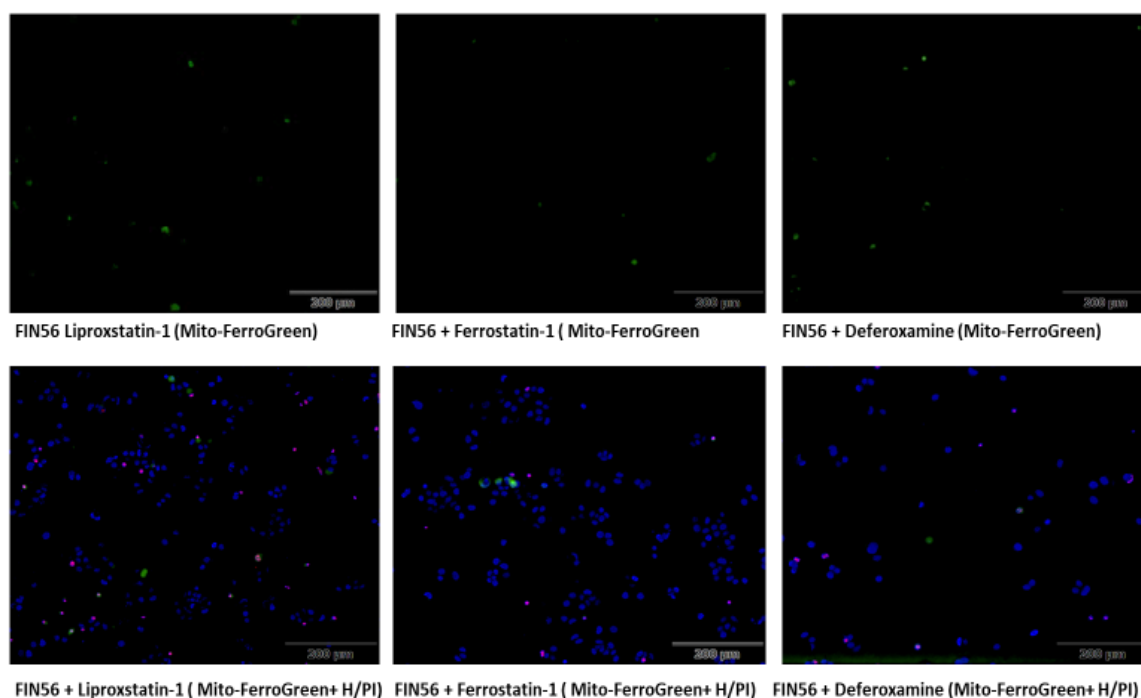
Figure 3.24: Mitochondrial labile Fe^{2+} and death detection under fluorescent microscope after treating MCF-7 cell line for 24 hours with ferroptosis inducer FIN56 at concentration of 10 µM and ferroptosis inhibitors (Deferoxamine 10 µM, Liproxstatin-1 1 µM and Ferrostatin-1 1µM), with control (0.2% (v/v) DMSO). Determined by Hoechst 33342/PI staining and Mito-FerroGreen dye. Live cells are stained blue with Hoechst 33342, dead cells are stained red with PI staining, and Fe^{2+} stained green with Mito-FerroGreen (Scale bars = 200 µm).

3.2.6 Effect of ferroptosis inducers and inhibitors in the breast cancer 3D alginate spheroid model

MDA-MB-231 and MCF-7 were cultured in 3D cell culture using the alginate sphere assay. Cells were grown for 12-14 days until colonies were at approximately 100-200 µm in diameter or spheroid colonies were approximately 10 cells in diameter. The effects of ferroptosis inducers and inhibitors on cell death was assessed by measuring ATP levels after treating MDA-MB-231 and MCF-7 spheroids with ferroptosis inducers and inhibitors for 48 hours. Cell viability was assessed by measurement of ATP levels using Cell Titer-Glo® 3D Cell Viability Assay in all investigations.

3.2.6.1 The effect of Erastin +/- ferroptosis inhibitors in MDA-MB-231 3D alginate spheroids

Initial experiments showed that MDA-MB-231 cells grown in alginate-based 3D cell culture did not respond to ferroptosis inducers. Therefore, all subsequent experiments were conducted using 10 µM of Erastin, RSL3 or FIN56 for MDA-MB 231 and MCF-7 cells. Erastin significantly decreased ATP levels at 10 µM dose in the MDA-MB-231 cell line when compared to vehicle control (Figure 3.25) (P≤0.01). However, responses were much weaker than observed at this dose in 2D cell culture. In contrast to 2D cell culture studies, the effect of ferroptosis inducer Erastin was not reversed by all ferroptosis inhibitors (Deferoxamine 10 µM, Liproxstatin-1 1µM and Ferrostatin-1 1µM) (Figure 3.25), in that there was no statistical difference between Erastin and Erastin + ferroptosis inhibitors.

3.2.6.2 The effect of RSL3 +/- ferroptosis inhibitors in MDA-MB-231 3D alginate spheroids

RSL3 potently decreased ATP levels at 10 µM in the MDA-MB-231 cell line (P≤0.001) in alginate spheroids. The effect of ferroptosis inducer RSL3 was significantly and partially reversed by all ferroptosis inhibitors (Deferoxamine 10 µM, Liproxstatin-1 1µM and Ferrostatin-1 1µM) (P≤0.001) (Figure 3.26).

Figure 3.25: Effect of ferroptosis inhibitors on Erastin responses in MDA-MB-231 3D alginate spheroids
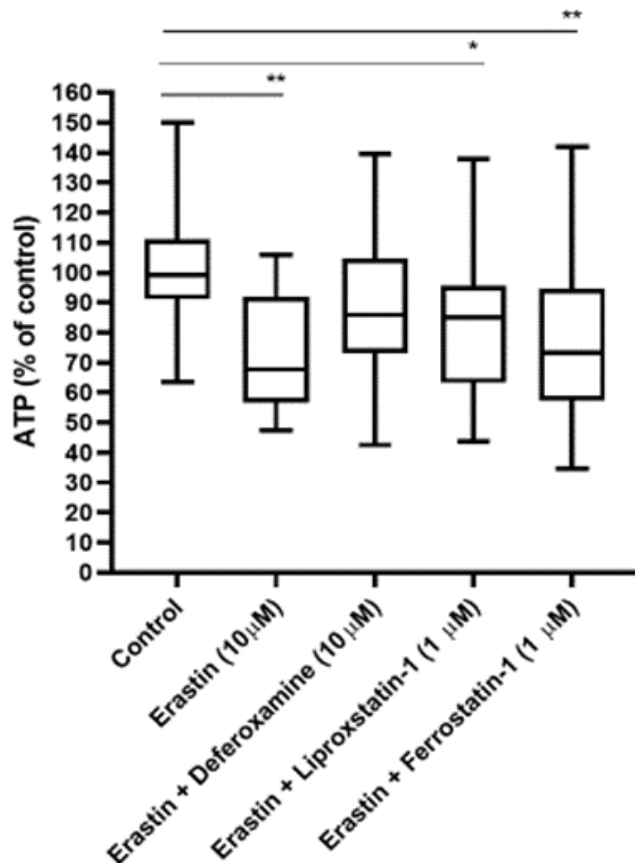
Figure 3.25: ATP level (% of control) via Cell Titer-Glo® 3D Cell Viability Assay after treating MDA-MB-231 spheroids for 48 hours with the ferroptosis inducer Erastin at concentration of 10 µM, vs. control (0.2% (v/v) DMSO) +/- ferroptosis inhibitors (Deferoxamine 10 µM, Liproxstatin-1 1µM and Ferrostatin-1 1µM). Data is presented as median ± interquartile range from n=3 independent experiments each with 6 technical repeats, analysed by a Kruskal-Wallis followed by Dunn's multiple comparisons test (*=P≤0.05, **=P≤0.01, and ***=P≤0.001).

Figure 3.26: Effect of ferroptosis inhibitors on RSL3 responses in MDA-MB-231 3D alginate spheroids
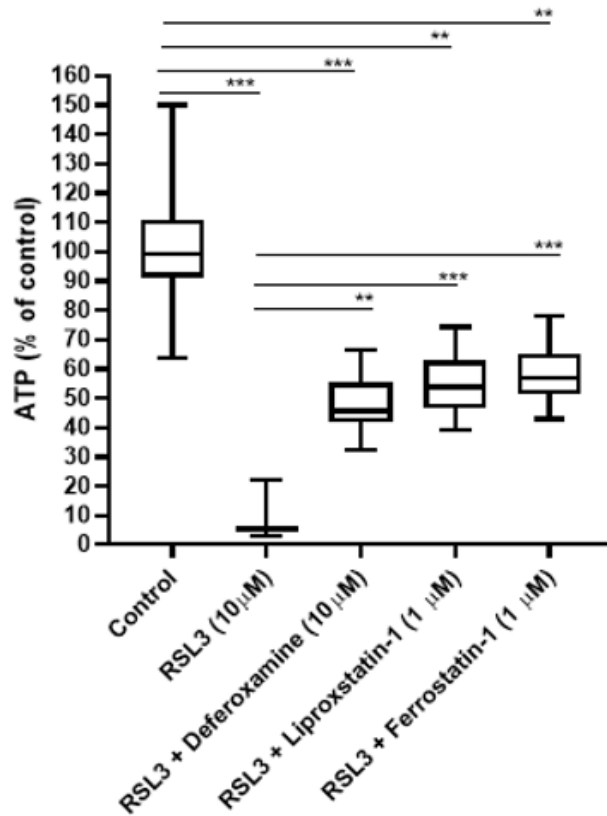
Figure 3.26: ATP level (% of control) via Cell Titer-Glo® 3D Cell Viability Assay after treating MDA-MB-231 spheroids for 48 hours with the ferroptosis inducer RSL3 at concentration of 10 μM, vs. control (0.2% (v/v) DMSO) +/- ferroptosis inhibitors (Deferoxamine 10 μM, Liproxstatin-1 1μM and Ferrostatin-1 1μM). Data is presented as median ± interquartile range from n=3 independent experiments each with 6 technical repeats, analysed by a Kruskal-Wallis followed by Dunn's multiple comparisons test (*=P≤0.05, **=P≤0.01, and ***=P≤0.001).

3.2.6.2.1 Optimized dosage of the ferroptosis inducer RSL3 in MDA-MB-231 3D alginate spheroids

Because RSL3 at 10 µM dose caused a significant reduction in ATP levels when compared to control in MDA-MB-231 spheroid cells (Figure 3.26), it needed further optimization to select an optimal dose when using in the further combination studies in Chapters 4 and 5. The effects of ferroptosis inducer RSL3 on cell death was assessed by measuring ATP levels after treating MDA-MB-231 spheroids for 48 hours over a much lower concentration range. As previously, ATP levels were measured using Cell Titer-Glo® 3D Cell Viability Assay. From the following graph (Figure 3.27) ATP levels shows significant reduction with the concentration of RSL3 at 0.075 µM and since 0.0375 µM had no effect on ATP levels, this shows that the optimal dosage of RSL3 that can be used in combination studies in 3D alginate spheroids of MDA-MB-231 cells is 0.075 µM, which displays approximately 35% reduction of ATP activity.

3.2.6.3 The effect of FIN56 +/- ferroptosis inhibitors in MDA-MB-231 3D alginate spheroids

FIN56 decreased ATP levels at 10 µM dose in the MDA-MB-231 cell line ($P \leq 0.001$), but not as potently as seen in 2D cell culture at this dose. The effect of ferroptosis inducer FIN56 was significantly and almost fully reversed by all ferroptosis inhibitors (Deferoxamine 10 µM, Liproxstatin-1 1µM and Ferrostatin-1 1µM) ($P \leq 0.001$). FIN56 with 10 µM Deferoxamine, 1µM Liproxstatin-1, and 1µM of Ferrostatin-1 ATP levels show a significant difference to FIN56 alone in MDA-MB-231 cell line (Figure 3.28).

Figure 3.27: RSL3 optimization in MDA-MB-231 3D alginate spheroids
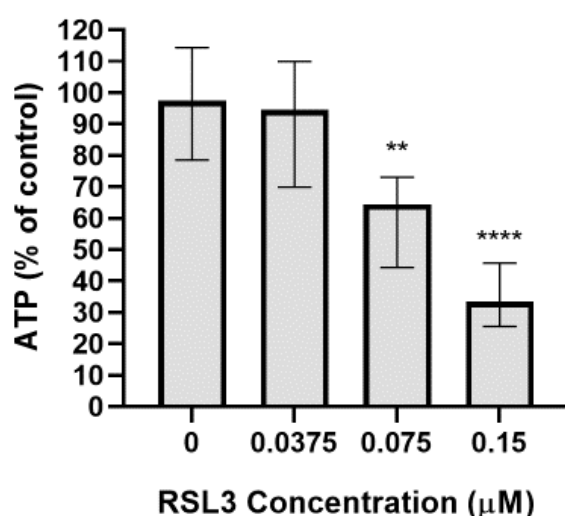
Figure 3.27: ATP level (% of control) via Cell Titer-Glo® 3D Cell Viability Assay after treating MDA-MB-231 spheroids for 48 hours with the ferroptosis inducer RSL3 at concentration of 0.15, 0.075, 0.0375 µM, with control (0.2% (v/v) DMSO), analysed by a Kruskal-Wallis followed by Dunn's multiple comparisons test (*=P≤0.05, **=P≤0.01, and ***=P≤0.001).

Figure 3.28: Effect of ferroptosis inhibitors on FIN56 responses in MDA-MB-231 3D alginate spheroids
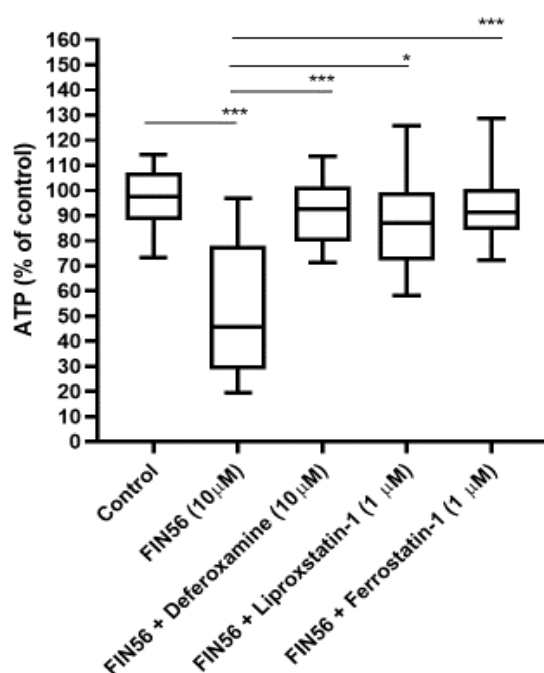
Figure 3.28: ATP level (% of control) via Cell Titer-Glo® 3D Cell Viability Assay after treating MDA-MB-231 spheroids for 48 hours with the ferroptosis inducer FIN56 at concentration of 10 µM, vs. control (0.2% (v/v) DMSO) +/- ferroptosis inhibitors (Deferoxamine 10 µM, Liproxstatin-1 1µM and Ferrostatin-1 1µM). Data is presented as median ± interquartile range from n=3 independent experiments each with 6 technical repeats, analysed by a Kruskal-Wallis followed by Dunn's multiple comparisons test (*=P≤0.05, **=P≤0.01, and ***=P≤0.001).

3.2.6.4 The effect of Erastin +/- ferroptosis inhibitors in MCF-7 3D alginate spheroids

Consistent with 2D cell culture data, Erastin at 10 µM produced no effect on the ATP level in MCF-7 cultured as alginate spheroid cultures (Figure 3.29). Erastin when combined with 1 µM Liproxstatin-1 or 1µM Ferrostatin-1 show slight reduction in ATP level in MCF-7 spheroids, but this was not significantly different to ATP levels in cell treated with Erastin alone.

Figure 3.29: Effect of ferroptosis inhibitors on Erastin responses in MCF-7 3D alginate spheroids
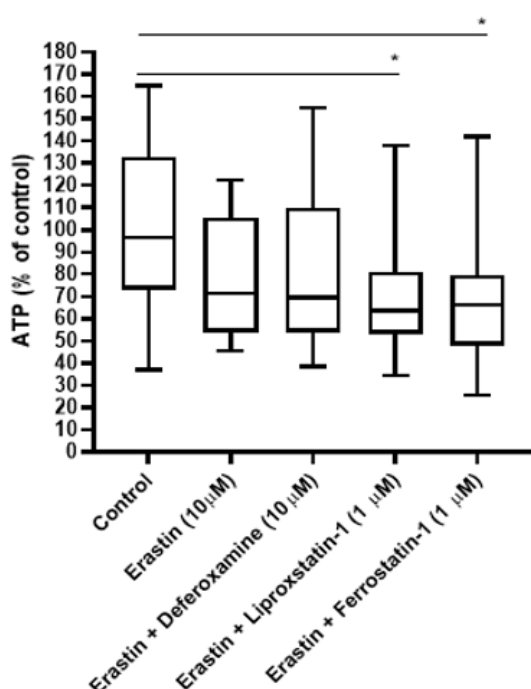
Figure 3.29: ATP level (% of control) via Cell Titer-Glo® 3D Cell Viability Assay after treating MCF-7 spheroids for 48 hours with the ferroptosis inducer Erastin at concentration of 10 µM, vs. control (0.2% (v/v) DMSO) +/- ferroptosis inhibitors (Deferoxamine 10 µM, Liproxstatin-1 1µM and Ferrostatin-1 1µM). Data is presented as median ± interquartile range from n=3 independent experiments each with 6 technical repeats, analysed by a Kruskal-Wallis followed by Dunn's multiple comparisons test (*=P≤0.05, **=P≤0.01, and ***=P≤0.001).

3.2.6.5 The effect of RSL3 +/- ferroptosis inhibitors in MCF-7 3D alginate spheroids

In contrast to observations in 2D cell culture, RSL3 when used alone produced a significant effect at 10 µM in MCF-7 spheroid cells ($P \leq 0.01$). Only Ferrostatin-1 significantly reversed the effects of RSL3 ($P \leq 0.05$). Although ATP levels for RSL3 and Liproxstatin-1 or Deferoxamine were reduced, they were not significantly different to RSL3 alone (Figure 3.30).

3.2.6.6 The effect of FIN56 +/- ferroptosis inhibitors in MCF-7 3D alginate spheroids

FIN56 at 10 µM produced no effect on the ATP level in MCF-7 spheroids, and the addition of all three ferroptosis inhibitors had no effect on ATP levels (Figure 3.31).

Figure 3.30: Effect of ferroptosis inhibitors on RSL3 responses in MCF-7 3D alginate spheroids
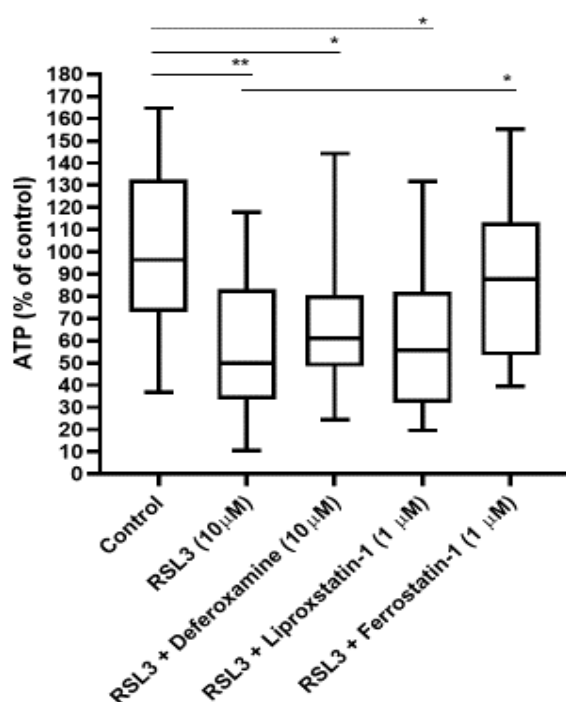
Figure 3.30: ATP level (% of control) via Cell Titer-Glo® 3D Cell Viability Assay after treating MCF-7 spheroids for 48 hours with the ferroptosis inducer RSL3 at concentration of 10 µM, vs. control (0.2% (v/v) DMSO) +/- ferroptosis inhibitors (Deferoxamine 10 µM, Liproxstatin-1 1µM and Ferrostatin-1 1µM). Data is presented as median ± interquartile range from n=3 independent experiments each with 6 technical repeats, analysed by a Kruskal-Wallis followed by Dunn's multiple comparisons test (*=$P \leq 0.05$, **=$P \leq 0.01$, and ***=$P \leq 0.001$).

Figure 3.31: Effect of ferroptosis inhibitors on FIN56 responses in MCF-7 3D alginate spheroids
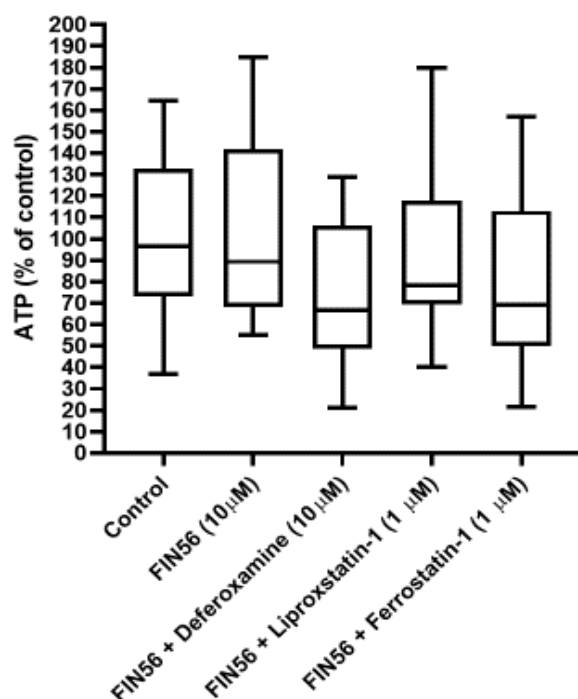
Figure 3.31: ATP level (% of control) via Cell Titer-Glo® 3D Cell Viability Assay after treating MCF-7 spheroids for 48 hours. With the ferroptosis inducer FIN56 at concentration of 10 µM, vs. control (0.2% (v/v) DMSO) +/- ferroptosis inhibitors (Deferoxamine 10 µM, Liproxstatin-1 1µM and Ferrostatin-1 1µM). Data is presented as median ± interquartile range from n=3 independent experiments each with 6 technical repeats, analysed by a Kruskal-Wallis followed by Dunn's multiple comparisons test (*=P≤0.05, **=P≤0.01, and ***=P≤0.001).

3.3 Discussion

3.3.1 The effect of ferroptosis inducers and inhibitors on breast cancer cells

In the recent years, many drugs have emerged as cancer therapy, and the researchers attempted to apply ferroptosis to overcome therapy resistance in breast cancer (Mai *et al.*, 2017). According to the data obtained from CellTiter-Glo® Luminescent Cell Viability Assay (2D) using ferroptosis inducers (RSL3, Erastin, and FIN56) triple-negative breast cancer (MDA-MB-231) cell line was far more sensitive to ferroptosis inducers than ER positive breast cancer (MCF-7) cells. This finding matches what is found in the literature studies (Doll *et al.*, 2017). The reasons for this are unclear, however this data highlights that, similar to apoptosis, MDA-MB-231 are highly susceptible to ferroptotic cell death, whereas others are resistant and sensitivity to apoptosis correlates with sensitivity to ferroptosis (Neville-Webbe *et al.*, 2004). This correlation of hormone sensitive cells being generally ferroptosis and apoptosis-resistant also extends to prostate cancer, another major hormone-dependent malignancy whereby PC-3 and Du145 hormone independent cell lines are highly apoptosis and ferroptosis-sensitive, whereas hormone dependent LNCap and 22Rv1 are highly apoptosis and ferroptosis resistant (Holen *et al.*, 2002; Ghoochani *et al.*, 2021). Potential mechanistic differences relating to ferroptosis sensitivity are addressed in Chapter 4 of this thesis. MDA-MB-231 are more dependent on glutamine, which is also crucial for glutathione biosynthesis, than MCF-7 cells. Glutamine is transported through cell membrane transport, which is controlled by alanine, serine, a cysteine-preferring transporter 2 (ASCT2), and is overexpressed in basal cells, as well as system Xc-, making them more dependent on glutamine uptake for tumour growth and survival. Since MDA-MB-231 are dependent on glutamine, targeting glutamine uptake and glutathione synthesis causes increased cellular damage in MDA-MB-231 vs MCF-7 with ferroptosis inducers that affect glutathione levels (van Geldermalsen *et al.*, 2016; Dilshara *et al.*, 2017; Vogg *et al.*, 2018)

In the ferroptosis-sensitive cell line MDA-MB-2321, the potent pro-ferroptotic effects of Erastin, RSL3 and FIN56 were all potently reversed by the ferroptosis inhibitors Deferoxamine, Liproxstatin-1 and Ferrostatin-1. This data strongly suggests that cell death observed using Hoechst 33342 and propidium iodide staining, with PI+ve cells being classed as dead, are indeed ferroptotic cells. This is also consistent with the

observation of lack of characteristic apoptotic morphology seen. Since propidium iodide positivity inversely correlated with ATP measurements, and ferroptosis inhibitors reversed the decrease in ATP levels in response to ferroptosis inducers Erastin, RSL3 and FIN56, it can be concluded that the observed cell death is largely due to ferroptosis.

MCF-7 showed a counter-intuitive action of Deferoxamine, which is an iron chelator agent considered as a ferroptotic inhibitor (Kose *et al.*, 2019). Deferoxamine induced cell death and decreased ATP levels so rather than being a ferroptosis inhibitor, it appears to enhance the weak effects of all ferroptosis-inducers. A reasonable explanation is that the MCF-7 cancer cells exhibit excess cellular iron. Additionally the excess iron supports the theory behind cancer cell drug resistance (Whitnall *et al.*, 2006). This is further supported by observations of differential sensitivity of MCF-7 and MDA-MB-231 cells to Deferoxamine, with MCF-7 cells undergoing cell death albeit at higher doses (100 µM) than used in the present study (Chen *et al.,* 2019). This suggests that the failure to reverse the weak ferroptosis-induced cells death in MCF-7 was in-part due to ferroptosis resistance, and in-part a cell-line specific sensitivity to Deferoxamine. The initial finding of responses in 2D cell culture of MDA-MB-231 and MCF-7 cells are encouraging to conclude that these two cell lines display extreme opposite responses to ferroptosis inducers and are suitable for the study of combination therapies to either a) enhance existing ferroptosis sensitivity or b) overcome cell death resistance that might be in-part, ferroptosis-mediated.

3.3.2 Caspase inhibitors do not reverse the effect of ferroptosis inducers

Ferroptosis inducers (Erastin, RSL3, and FIN56) cause death in MDA-MB-231, although not much death can be noticed in MCF-7 cells in both 2D and 3D culture. To exclude apoptotic death, caspase inhibitors were applied during treating the MDA-MB-231 cells, because they were more sensitive to the ferroptosis inducers than the MCF-7. Research shows that for Erastin-induced cell death, some of this is apoptotic but only in hypoxic environments, and this apoptotic cells death was reversed by the Pan-caspase inhibitor Z-VAD-FMK (Owada *et al.*, 2021). Furthermore, studies combining ferroptosis inducers with chemotherapy show that the resulting cell death can be reversed with Ferrostatin-1, but not inhibitors of caspases (Yu *et al.*, 2015). Specifically in the Acute Myeloid Leukaemia cell line HL-60, cells were sensitive to ferroptosis inducer Erastin when

combined with the chemotherapy cytarabine and doxorubicin. Therefore, we assessed whether Erastin, FIN56 and RSL3-induced cell death could be in-part, due to apoptosis. Caspases are a group of cysteine aspartic acid proteases that start the process of apoptosis, which is a typical form of cell death (Lawen, 2003). The external pathway is initiated by caspase-8 or -10, while the internal pathway is initiated by caspase-9, and both can begin apoptosis by activating caspase-3 and-7 (Kalkavan and Green, 2018). The irreversible Pan-caspase inhibitor Z-VAD-FMK, which is a is a broad-spectrum caspase inhibitor that can prevent apoptosis due to its cell permeability and irreversibility features (Zhou *et al.*, 2004). The effect of Erastin was reversed when using the ferroptosis inhibitor Ferrostatin-1 for 24 hours, but not Z-VAD-FMK or necrostatin-1 (a caspase inhibitor and necroptosis inhibitor, respectively) (Yu *et al.*, 2015). The result of the study demonstrates that ferroptosis enhances the chemotherapy effect in HL-60 cells via enhanced ferroptotic cells death (Yu *et al.*, 2015). The caspase-8 inhibitor Z-IETD-FMK, caspase-9 inhibitor Z-LEHD-FMK, and caspase-3 inhibitor Z-DEVD-FMK all failed to prevent death while treating MDA-MB-231 cells in this study. This indicate that the form of death was not an apoptotic cell death, consistent with nuclear morphological analysis. This finding has relevance to data in Chapter 4 whereby chemotherapy responses were tested in the presence of ferroptosis inducers, and Chapter 5 where radiotherapy undergo apoptosis.

3.3.3 Ferroptosis inducers show reduced activity in 3D cell culture

To assess the effects of ferroptosis inducers in 3D cell culture vs 2D cell culture, cells were cultured in the alginate 3D spheroid assay. As it had previously been shown that ferroptosis might be induced more readily in hypoxia, and that 3D cell cultures better represent human tumours, findings of responses in 3D might be more representative of the likely in vivo responses of these agents. The results of CellTiter-Glo® 3D, which measures ATP levels in alginate spheres showed a significant reduction in activity in 3D cell culture vs. 2D cell culture with Erastin and FIN56 in MDA-MB-231, whereas RSL3 showed similar toxicity in 3D and 2D cell culture. Despite the similarity in action for both RSL3 and FIN56, RSL3 induced ferroptosis in both models for MDA-MB-231 cells. This finding may contribute to the specific mode of action of each compound: FIN56 triggers GPX4 degradation by an unknown mechanism (Cotto-Rios and Gavathiotis, 2016) while

RSL3 inhibit GPX4 function directly (Dixon, 2017). Overall, both MCF-7 and MDA-MB-231 cell lines are resistant to Erastin- and FIN56-mediated ferroptosis in 3D cell culture. Interestingly, MCF-7 was also sensitive to RSL3 in 3D cell culture, but not in 2D cell culture, potentially highlighting some hypoxia-mediated vulnerability (Zheng *et al.,* 2023). Although hypoxia is generally associated with reduced ferroptosis in normal cells, in cancer cells, there reverse has been reported, and this is mediated by HIF2a but not HIF1a. Specifically, HIF2a activates HILPDA, which is known to promote lipid peroxidation in response to RSL3 (Zou *et al.*, 2019). In glioblastoma, HIF2a was shown to enhance ferroptosis-regulatory genes such as ACSL4 to enhance lipid peroxidation (Su *et al.*, 2022). Furthermore, HIF2a upregulated iron and lipid peroxidation-related genes, resulting in enhanced ferroptosis in colorectal cancer cells (Singhal *et al.*, 2021). Taken together, the observation of generally decreased ferroptosis responses in 3D vs. 2D cell cultures in a novel finding which may have a hypoxia-mediated explanation, however it is clear that RSL3 responses are not attenuated in 3D cell culture vs. 2D cell culture. This may make RSL3 (or GPX4 inhibition) a more promising mechanism for therapeutic applications of ferroptosis modulation.

Another reason for 3D drug resistance is due to the excessive cell adhesion and matrix elements, making drug penetration process less effective to enter the spheroids (Niero *et al.*, 2014). Also, downregulation of caspase-3 and -8 in hypoxic environments may cause drug resistance (IMAMURA *et al.*, 2015). Another cause of resistance in 3D cell culture, is because cancer cells develop several mechanisms to resist anoikis to survive in the absence of cell-cell contact, in the early phase or the alginate assay, cells are in isolation, so the assay may select for an anoikis-resistance phenotype (Gudipaty *et al.*, 2018).

Analysis of cell death in 3D cell cultures using the CellTitre-Glo 3D assay proved problematic due to the nature of the assay, leading to a large spread of data leading to large error bars and the requirement for increased numbers of technical repeats. This is in part due to the number of cells present in each spheroid that vary during preparation of alginate beads.

Glutathione system is enhanced in response to tumour hypoxia leading to increased reactive oxygen species (ROS), which is controlled by Keap1-Nrf2, whereby with ROS, Nrf2 is released switching on GSH synthesis and glutathione-S-transferase, and other antioxidant genes, in the core of cancer spheroids (the hypoxia region)(Kennedy *et al.*, 2020). In a study done on 3D cancer cell spheroids, Nrf2 levels were overexpressed in the hypoxic regions, leading to the idea that it plays a crucial role in responding to the increased ROS in tumor hypoxia and developing resistance to stress inducing treatments (Kipp *et al.*, 2017). This finding contributes to ferroptosis resistance seen in 3D MDA-MB-231 and MCF-7 cells, which is characterised by excess ROS, and during hypoxia the Nrf2 levels may play as a safeguard in protecting the cells and making them more resistance to ferroptosis treatments, leading to the idea of targeting Nrf2 in 3D modules may enhance the ferroptotic effect on them.

In an interesting study done by Takahashi and his colleagues on measuring the Nrf2 levels and their effect on ferroptosis, they found that Nrf2 protecting matrix-deprived cells from ferroptosis and blocking Nrf2 and GPX4 promote death in spheroids (Takahashi *et al.*, 2020). The finding from this study is lightening us to concentrate on the role of Nrf2 with ferroptosis in 3D cultured breast cancer cells.

3.3.4 The role of free iron in ferroptosis induction

Ferroptosis is characterised by the excess accumulation of intracellular iron, which is the fundamental metal for activating the ferroptosis process (Liang *et al.*, 2019). Through the Fenton reaction, iron may directly produce an excessive amount of ROS, leading to oxidative damage (Dixon *et al.*, 2012). Several studies used Mito-FerroGreen dye with ferroptosis to confirm the present of iron (Mei *et al.*, 2020b; Zheng *et al.*, 2020; P. Zhang *et al.*, 2022), and this supports the notion that ferroptosis is being observed in MDA-MB-231 and MCF-7 cells in this study. Mito-FerroGreen dye was used to for staining MDA-MB-231 and MCF-7 Cells after treatment with ferroptosis inducers as well as ferroptosis inhibitors to detect iron within cells. The experiment was done once to observe the present of iron. Results confirm the present of intracellular iron, which is the hallmark of ferroptosis death. The iron present was less while using the ferroptosis inhibitors, which also confirm the reverse effect of ferroptosis inducers. The present of iron in general was noticed to be higher in MCF-7 cells (control) without ferroptosis treatment than MDA-

MB-231 cells. The ferroptosis inhibitors when combined with ferroptosis inducers also show iron within both cell lines, except the ferroptosis inhibitor Deferoxamine with MCF-7 cells that show less iron, and may be because of its mode of action that chelate iron (Kose *et al.*, 2019). However, Erastin + Deferoxamine resulted in considerable Fe^{2+} detection in MDA-MB-231 cells, showing that although Mito-FerroGreen could detect abundant free iron, it may be bound up with Deferoxamine, allowing cell survival. A major caveat is that this was an n=1 experiment.

3.3.5 MCF-7 cells may be insensitive to ferroptosis although of having excess iron

Intracellular iron participates in Fenton chemistry and increases the oxidative stress of cells, and this overloaded iron may cause Ferroptosis (Dixon and Stockwell, 2014). MDA-MB-231 cells contain lower iron than MCF-7 cells in general. When labile iron-$FeCl_3$ is added to MDA-MB-231 and MCF-7 cells, ROS production increased in both, but only MDA-MB-231 cells observed an inhibition of cell viability (Zhang *et al.*, 2021). MDA-MD-231 cells may be more susceptible to iron overload than MCF-7 cells due to differences in how iron homeostasis is regulated. A higher percentage of MDA-MB-231 cells died after being exposed to different Erastin doses, demonstrating the improved ability of MCF-7 cells to maintain a redox balance as compared to MDA-MB-231 cells. This explain in part why MDA-MB-231 cells were more sensitive to ferroptosis than MCF-7 cells (Zhang *et al.*, 2021). Deferoxamine, an iron chelator, was found to considerably enhance mitochondrial iron accumulation and iron metabolism in MDA-MB-231 cells while significantly decreasing mitochondrial iron accumulation and iron metabolism in MCF-7 cells. Deferoxamine caused MCF-7 cells to undergo apoptosis, but it also caused cellular and mitochondrial ROS to be produced in MDA-MB-231 and MCF-7 cells (Chen, Wang and Liu, 2019). Deferoxamine decreases iron levels in MCF-7 cells, in contrast it increases iron in MDA-MB-231 cells. This is due to the increasing the expression of TFR (Transferrin receptor) and DMT1 (Divalent metal transporter 1, a protein that is responsible for ferrous iron uptake) (Liu *et al.*, 2016). The majority of intracellular iron distribution occurs in mitochondria. Iron from mitochondria is largely used for heme synthesis, iron-sulfur cluster biogenesis, mitochondrial ferritin storage, and chelatable labile iron (Paul *et al.*, 2017). Deferoxamine is thought to increase mitochondrial iron levels in MDA-MB-231 cells, by enhancing mitochondrial heme levels and chelatable iron in MDA-MB-231

cells. This revealed that Deferoxamine induced accumulation of mitochondrial iron may be crucial for promoting cell proliferation in MDA-MB-231 cells (Chen *et al.,* 2019). The more chelatable iron catalyses more Fenton reactions, which increases the amount of ROS produced (Dixon and Stockwell, 2014; Urrutia *et al.,* 2014). Studies confirmed that Deferoxamine is also a hypoxia mimic compound, that causes the increase of ROS accumulation in cells (Liu *et al.*, 2014; Zhang *et al.*, 2014). In MCF-7 and MDA-MB-231 cells, Deferoxamine increases the formation of cellular and mitochondrial ROS (Chen *et al.,* 2019). A mild rise in ROS may encourage cell growth and survival. However, when the level of ROS rises above a particular point (the hazardous threshold), it may be too much for the cell's antioxidant defences to handle, leading to cell death (Gupta *et al.,* 2012). MCF-7 cells and MDA-MB-231 cells respond differently to Deferoxamine-induced ROS and mitochondrial ROS in terms of cell survival and death. Chen *et al.,* (2019) showed that scavenging intercellular and mitochondrial ROS revealed that Deferoxamine-induced ROS led to cell death in MCF-7 cells however maintained cell survival in MDA-MB-231 cells, indicating that Deferoxamine-induced ROS levels were above the tolerance threshold in MCF-7 cells but below it in MDA-MB-231 cells (Chen *et al.,* 2019).

Summary

In summary, these optimisation studies demonstrate the optimal doses to be used for combination studies with chemotherapy (Chapter 4) and Radiotherapy (Chapter 5), by identification of doses of Erastin, RLS3 and FIN56 that induces modest levels of ferroptosis in both 2D and 3D cell culture. Furthermore, we show that assessment of cell death after treatment is a good measure of ferroptosis, based on the use of three different ferroptosis inhibitors that all completely reversed ferroptosis in MDA-MB-231. Furthermore, we show that observed responses are not apoptotic, and are associated with increased free iron, characteristic of ferroptosis. We therefore conclude that ferroptosis is occurring in these cells and in both 2D and 3D cell culture and have optimised conditions to interrogate interactions with chemotherapy and radiotherapy. The optimized doses for both modules will be used in the following studies to enhance the chemotherapy and radiotherapy effect on breast cancer cells.

Chapter 4: Enhancement of chemotherapy response using ferroptosis inducers in 2D and 3D breast cancer cell models

4.1 Introduction

4.1.1 Chemotherapy

Chemotherapy is used to treat cancer, and its major objective is to expose tumour cells to anticancer drugs, causing them to undergo apoptosis (Roubalová *et al.*, 2010, Köberle *et al.*, 2010). During the 1950s and 1960s, alkylating agents and antimetabolites were occasionally used in single-agent chemotherapy, which led to the discovery of several groups of cytotoxic agents that were effective against metastatic breast carcinoma and the conclusion that metastatic breast carcinoma was moderately sensitive to chemotherapy (Carter, 1972). The National Surgical Adjuvant Breast and Bowel Project (NSABP) B-04 study, which began in 1971, was one of the landmark studies that impacted the use of adjuvant therapy in breast cancer (Fisher, 1971). In the NSABP B-05 experiment, 380 women with node-positive breast cancer were randomly assigned to receive L-phenylalanine mustard (L-PAM) or a placebo after primary breast cancer surgery between 1972 and 1974. Results showed that postoperative adjuvant therapy could affect breast cancer natural history and lower the probability of recurrence (Fisher *et al.*, 1975). In 1975 one of the first studies was started with a follow up time of 20 years for women with node-positive breast cancer with adjuvant chemotherapy (cyclophosphamide, methotrexate, and fluorouracil (CMF)). The long-term outcomes demonstrate a significant overall benefit for adjuvant treatment, which confirm the benefit of receiving early systemic treatment for patients who are at high risk for metastases (Bonadonna *et al.*, 1995).

Cytotoxic chemotherapy is routinely used in the metastatic scenario for patients with malignancies that lack hormone receptors as well as those who have hormone receptor-positive cancer that is resistant to hormonal therapy and is progressing quickly (Beslija *et al.*, 2007). Cytotoxic chemotherapy is also used in primary breast cancer, particularly in TNBC and Her-2 positive cases, but also in ER+ positive early-stage breast cancer where features suggest aggressive behaviour (Sparano *et al.*, 2018), such as high Nottingham grade, and/or high Ki-67. To assess patients suitability for chemotherapy, the Nottingham prognostic index may be used to calculate likely relapse based on grade and stage, or Oncotype-Dx test may be used to predict which cases might benefit from chemotherapy, and which cases would not (Cuzick *et al.*, 2011). The patient's condition and preceding

(adjuvant) chemotherapeutic treatments will determine which chemotherapy drug is used. The most popular current treatment agents for first-line chemotherapy are anthracyline and/or taxane-based regimens (Beslija *et al.*, 2007; Jones, 2008; Cardoso *et al.*, 2017). An antimetabolite cytotoxic drug (capecitabine) is typically employed as a second-line chemotherapeutic agent in cases of resistance to anthracyclines or taxanes (Karachaliou *et al.*, 2012).

Surgery alone can cure a patient with early-stage breast cancer, and subsequently adjuvant chemotherapeutic drugs are intended to treat micro-metastatic phases. (Shafei *et al.*, 2017). To target the areas affected by the disease, systemic approaches were used for cases of metastatic breast cancer (MBC) and recurrent cases. Chemotherapy and hormone therapy are the two main systemic therapies with some also receiving Herceptin (Vogel *et al.*, 2001; Shafei *et al.*, 2017). Patients with disease that is oestrogen- and/or progesterone-positive and do not have a life-threatening metastasis would normally receive hormonal therapy in addition to surgery and/or radiotherapy. Cytotoxic chemotherapy is an option for patients who become hormone resistant and also those with high-grade tumours and local lymph node involvement (Shafei *et al.*, 2017).

4.1.1.1 Paclitaxel

Microtubules are the target of the Taxane group of anticancer medications, including Paclitaxel. Tubulin polymers in dynamic equilibrium with tubulin heterodimers form the cylindrical hollow structures that make up microtubules, which have a diameter of roughly 25–30 nm (consisting of alpha and beta protein subunits). The creation of the mitotic spindle during cell division is one of the main purposes of microtubules (Parness and Horwitz, 1981; Rowinsky and Donehower, 1995). They are also necessary for the preservation of cell motility, structure, and cytoplasmic movement. During the G2 phase and the prophase of mitosis, tubulin dimers form microtubules. With their alpha and beta subunits, tubulins are arranged in a head-to-tail pattern with preferentially quicker growth (plus ends) at one end and slower growth (minus ends) at the other end, and are in a state of dynamic equilibrium. Since the net tubulin assembly rate equals the net disintegration rate under steady-state conditions, the microtubule length remains constant. As opposed to the plus ends, which explore the cytoplasm and engage with

cellular structures, the minus ends of microtubules are often anchored mostly in the centrosome (Dammermann, Desai and Oegema, 2003).

Rather than affecting how tubulin dimers combine to create microtubules, as in the case of other tubulin-binding chemotherapies such as Vinca alkaloids, Paclitaxel binds exclusively and irreversibly to the beta-tubulin subunit in the microtubules, affecting tubulin dynamics (Rao *et al.*, 1995; Dong *et al.*, 2014) and stabilises them (Sackett and Fojo, 1997; Weaver, 2014). Taxanes shorten the tubulin polymer by decreasing the critical concentration of tubulin needed for its assembly (Schiff *et al.* , 1979). Cell division therefore comes to a halt at the G2 or M phase as a result of the cell's inability to divide. Only free microtubules that are not linked to or already present in the microtubule organising centres (MTOC) are bound by Paclitaxel (De Brabander *et al.*, 1981). Microtubules that are attached vanish when Paclitaxel is present, causing failure in chromosomal segregation and interfering with the dynamics of microtubules and microtubule polymerization. Paclitaxel slows the process of mitosis and ultimately causes apoptosis and mitotic arrest (Jordan *et al.*, 1993; Long and Fairchild, 1994; Jordan and Wilson, 1998). Taxane resistance is mostly via altered expression of different tubulin subunits that Taxanes cannot bind to, or via P-glycoprotein expression leading to drug efflux (Weaver, 2014).

4.1.1.2 Doxorubicin

One of the principal therapies for both early-stage and advanced breast cancer is Doxorubicin. Anthracycline antibiotic Doxorubicin is derived from *Streptomyces peucetius var. caesius*. It is a topoisomerase II inhibitor that functions by intercalating DNA, preventing DNA unwinding during DNA replication and transcription, and also topoisomerase-II-mediated DNA repair. While being used to treat a wide range of malignancies, its use is limited by cardiotoxic side effects that can eventually lead to heart failure. (Thorn *et al.*, 2011). With BC cells, the cause of Doxorubicin resistance is due to efflux by P-glycoprotein/multidrug resistance-associated protein 1 (MDR1) that reduces intracellular accumulation in of the drug (Bao *et al.*, 2011). In BC and MBC, Doxorubicin is administration is constrained by the aforementioned cardiotoxicity (Chang *et al.*, 2018). To lessen Doxorubicin toxicity, pegylated liposomal Doxorubicin (PLD) was created along with other nanoparticle-based formulations (Shafei *et al.*, 2017).

However cardiotoxicity is thought to involve ferroptosis, highlighting that a) Doxorubicin actions might synergise with ferroptosis inducers and b) if synergy occurs, this might also be reflected in enhanced side effects (Abe *et al.*, 2022).

4.1.1.3 Cisplatin

Cisplatin is also utilised as the first-line drug for BC treatment, just like it is for other malignancies (DeSantis *et al.*, 2011). BC may be treated using radiotherapy, surgery, chemotherapy, or any combination of these methods (LI *et al.*, 2016). The interaction of Cisplatin with DNA to form DNA adducts mediates the mechanism of action of Cisplatin (Aldossary, 2019). According to the theory of action, Cisplatin kills cancer cells by forming DNA adducts, such as mono-, inter-, and intra-strand Cisplatin DNA cross-links, which stop the cell cycle at S, G1, or G2-M and cause apoptosis. As a result Cisplatin causes cell cycle arrest at the G2, S, or G1 phases as cells attempt to repair the damage (Aldossary, 2019). This leads to a failure of sufficient repair, which may cause the cells to undergo abnormal mitosis before dying. The intra-strand crosslink adducts are the main DNA adducts that activate apoptosis via activation of the DNA damage repair pathways (Aldossary, 2019). The death of the most rapidly proliferating cancerous cells is caused by the consequent impairment of their DNA replication (Aldossary, 2019).

However, the side effects of Cisplatin, such as nephrotoxicity, neurotoxicity, hepatotoxicity, and myelosuppression all occur (Cohen *et al.*, 2011). Cisplatin is known to cause undesirable side effects and drug resistance, either by reduced uptake or efflux mechanisms is common, particularly after prolonged use (Jemal *et al.*, 2011). Additionally, improving the susceptibility of cancer cells to Cisplatin in low doses is still a goal for chemotherapeutic success (Scagliotti, 2005). Although Cisplatin is known to be effective in treating a wider variety of cancer types, research has shown that many patients with these tumours eventually relapse and develop chemotherapeutic resistance (Go and Adjei, 1999). The usefulness of Cisplatin in treating some common malignancies, including advanced hormone-refractory prostate cancer and colorectal and pancreatic cancer, has also been criticised by other researchers (Amable, 2016). Cross-resistance of Cisplatin-resistant cancer cells greatly increases the complexity and difficulty of treatment (Dunn *et al.*, 1997). Resistance may develop over time from repeated drug exposure for example by over-expression of P-

glycoprotein/MDR1/ABCB2, cells increase drug efflux pumps and become resistant (Fang *et al.*, 2017). Related to this copper transporters such as CTR1 which uptake Cisplatin, can be downregulated in cancer resulting in reduced Cisplatin uptake, and hence Cisplatin-resistance (Katano *et al.*, 2002). Reduced drug accumulation is a crucial mechanism that leads to resistance, and reductions in drug accumulation can lead to drug resistance (Hartmann *et al.*, 2018).

The enhanced repair of the damaged DNA is the other mechanism that might keep tumour cells resistant to Cisplatin (Sarin *et al.*, 2018). This mechanism of resistance has been corroborated by evidence from earlier investigations, found that a higher rate of repair is associated with the suppression of drug-induced cytotoxicity in a number of tumour cells (Nikounezhad *et al.*, 2017). Platinum adduct elimination and DNA repair are thought to primarily occur via Nucleotide Excision Repair (NER). The relevance of NER is demonstrated by study results indicating that Cisplatin hypersensitivity is caused by a cellular malfunction, and that sensitivity to Cisplatin is restored to normal levels when NER integrity is restored (Nikounezhad *et al.*, 2017).

Cytosolic inactivation of Cisplatin is the third Cisplatin resistance mechanism. Cisplatin's effectiveness is impacted by inactivation because it loses its capacity to interact with DNA due to sequestration within the cytoplasm by glutathione and other molecules aimed at detoxification (Kartalou and Essigmann, 2001). This results in less DNA damage, which increases cancer cell survival by reducing DNA adduct formation. The main or primary method of Cisplatin inactivation is when it is conjugated with glutathione and then exported from the cell via multidrug resistance transporters (Borst *et al.*, 2000; Dmitriev, 2011). Their capacity to transport a variety of anticancer medications out of cells and their presence in many tumours make them strong causes of drug resistance (Borst *et al.*, 2000). Recent research has started to define the role of the multidrug resistance transporters family members. Multidrug resistance transporters are organic anion transporters that move both neutral pharmaceuticals and medicines that have been conjugated to acidic ligands, such as glutathione (GSH). Methotrexate is an example of an anionic medication that they transport (Borst *et al.*, 2000). Thiol-containing compounds lead to greater inactivation. One such process is the conjugation of GSH to Cisplatin, which is catalysed by glutathione-S-transferases (GSTs) (Sarin *et al.*,

2018). As a result, when Cisplatin solubility is improved, the medication is rendered inactive by the creation of platinum-glutathione conjugates (Sarin *et al.*, 2018). Higher drug excretion rates from cells are the outcome of this. According to Brozovic et al. (2010), intracellular glutathione serves as an antioxidant and preserves reduced sulfhydryl groups, which helps to maintain the redox environment. This process causes the GSH levels in Cisplatin-resistant cells to drop, which increases the drug's toxicity (Brozovic *et al.,* 2010). A study that looked at ovarian cancer cells found that the platinum resistant cell lines had higher levels of GSH. Metallothionein binding proteins are a further component of the Cisplatin activation process (Brozovic *et al.,* 2010).

4.1.2 Combination of chemotherapy with ferroptosis inducers

The primary way that Cisplatin may enhance ferroptosis is by directly depleting intracellular GSH, which limits GPX4 activity as a consequence (Guo *et al.*, 2018). In addition, when ferritinophagy raises free iron levels, Cisplatin can potentially cause ferroptosis (X. Zhang *et al.*, 2020). Because of this, while treating several cancer types, including lung, colorectal, ovarian, and pancreatic ductal adenocarcinoma tumours, ferroptosis inducers like Erastin or RSL3 invariably boost the anticancer effects of Cisplatin synergistically by inhibiting system Xc or GPX4 respectively (Guo *et al.*, 2018; Sato *et al.*, 2018; Daher *et al.*, 2019; X. Zhang *et al.*, 2020).

In non-small cell lung cancer (NSCLC) cell lines A549, human colorectal cancer cell line HCT116, Cisplatin was thought to trigger both ferroptosis and apoptosis (Guo *et al.*, 2018). Further investigation revealed that the inactivation of GPXs including GPX4 and the depletion of reduced GSH were key factors in the overall process of Cisplatin-induced ferroptosis. Additionally, Cisplatin and Erastin were used in combination therapy on A549/HCT116 cells, and the outcomes showed a notable synergistic effect on their anti-tumour activity. All of these data suggested that ferroptosis has a significant potential to open up new therapeutic avenues for the treatment of cancer (Guo *et al.*, 2018). In head and neck squamous cell carcinoma cell lines, Progesterone receptor membrane component 1 (PGRMC1) is a protein that binds to heme and causes dimerization with cytochrome P450, causing chemoresistance. PGRMC1 expression is elevated in a variety of resistant tumours (You *et al.*, 2021). From *in vivo* mouse trials, PGRMC1 expression elevated fatty acid oxidation (FAO) and ferroptosis sensitivity. The

finding imply that PGRMC1 stimulates ferroptosis in Paclitaxel-tolerant persister cancer cells by inhibiting xCT, albeit in head and neck squamous cell cancer cells, rather than breast cancer cells (You *et al.,* 2021). In a study done on 2015 showed that Acute myeloid leukaemia cells (HL-60), were sensitive to ferroptosis inducer Erastin when combined with the chemotherapy Cytarabine and Doxorubicin. The effect of Erastin was reversed when using the ferroptosis inhibitor Ferrostatin-1 for 24 hours, but not Z-VAD-FMK or necrostatin-1 (a caspase inhibitor and necroptosis inhibitor, respectively). The result of the study demonstrates that ferroptosis enhances the chemotherapy-mediated effect in HL-60 cells (Yu *et al.*, 2015).

4.1.3 Role of Nrf2 in mediating chemoresistance

Nrf2 is a key protein that mediates the anti-oxidant response, by binding to the promoter of genes with an anti-oxidant response element and inducing their expression. Previous studies have shown that Nrf2 is over-expressed in many tumour types either via Nrf2 over-expression, or via loss of Keap-1, which prevents Nrf2 activity (No *et al.,* 2014). Specifically, Keap-1 binds Nrf2 and acts as a ubiquitin ligase resulting in Nrf2 degradation. Therefore Nrf2 over-expression or loss of Keap-1 by mutation can result in an enhanced anti-oxidant response allowing tumour to survive in conditions that would cause normal cells to undergo stress due to reactive oxygen species (Abdalkader *et al.*, 2018). In the present of reactive oxygen species, Nrf2 is displaces from Keap-1, leading to the anti-oxidant response being activated. Small molecule inhibitors of Nrf2 such as ML385 have been shown to prevent chemoresistance in other tumour models such as lung cancers (Singh *et al.*, 2016) and this may be in part due to modulating p-glycoprotein (Sargazi *et al.*, 2023). However, to date little is known about whether targeting Nrf2 with ML385 might overcome chemoresistance in breast cancer, and to date, no work has been done on this in 3D cell culture.

4.1.4 Aims and hypothesis

Hypothesis:

Ferroptosis inducers enhance chemotherapy responses in both 2D and 3D breast cancer cell culture models.

To achieve this, we aim to:

1. Assess chemotherapy responses in breast cancer 2D cell culture.
2. Combine chemotherapy (Doxorubicin, Cisplatin, and Paclitaxel) with ferroptosis inducers in breast cancer 2D cell culture.
3. Assess chemotherapy response in cells treated with the Nrf2 inhibitor ML385.
4. Assess chemotherapy responses in breast cancer 3D cell culture.
5. Combine chemotherapy with ferroptosis inducers and Nrf2 inhibitors in breast cancer 3D cell culture.

4.2 Results

4.2.1 Determination of the IC50 of Doxorubicin in breast cancer cells

To assess the effects of Doxorubicin treatment on cell survival, total ATP measurements using CellTitre-Glo® were performed as a proxy marker for cell numbers and/or total cellular metabolism in response to drug treatments. Cells were treated with Doxorubicin at different concentration (10, 5, 2.5, 1.25, 0.6, 0.3 and 0.15 µM) with control (0.2% (v/v) DMSO for 48 hours. After treatments, ATP level was assessed using CellTiter-Glo® Luminescent Cell Viability Assay. All treatments were performed in triplicate, in three independent experiments. Half maximal inhibitory concentration (IC50), which measures the effectiveness of Doxorubicin IC50 was determined by using non-linear regression of GraphPad Prism software version 8.

IC50 was used to compare between different chemotherapies, and between 2D and 3D cell cultures. For combination studies with ferroptosis inducers, the lowest dose that significantly induced cell death or reduced ATP measurements was used subsequently in combination studies with ferroptosis inducers.

4.2.1.1 Effect of Doxorubicin on cell viability in MDA-MB-231 cells

Cells were treated with increasing doses of Doxorubicin for 48 hours to assess its cytotoxicity and identify the IC50 and identify the lowest dose to induce significant cytotoxicity for combination studies with ferroptosis inducers. The IC50 of Doxorubicin after measuring ATP activity of MDA-MB-231 cells was estimated to be 0.8 µM (Figure 4.1). Based on the observed effects of Doxorubicin, 0.6 µM was chosen as the ideal dose for combination experiments.

4.2.1.2 Effect of Doxorubicin on cell viability in MCF-7 cells

Cells were treated with increasing doses of Doxorubicin for 48 hours to assess its cytotoxicity and identify the IC$_{50}$, and identify the lowest dose to induce significant cytotoxicity for combination studies with ferroptosis inducers. The IC50 of Doxorubicin after measuring ATP activity of MCF-7 cells was initially estimated to be 0.45 µM (Figure 4.2). However, based on the observed effects of Doxorubicin in subsequent combination studies, 0.6 µM was chosen as the ideal dose for combination experiments.

Figure 4.1: Effect of Doxorubicin on ATP levels in MDA-MB-231 cells
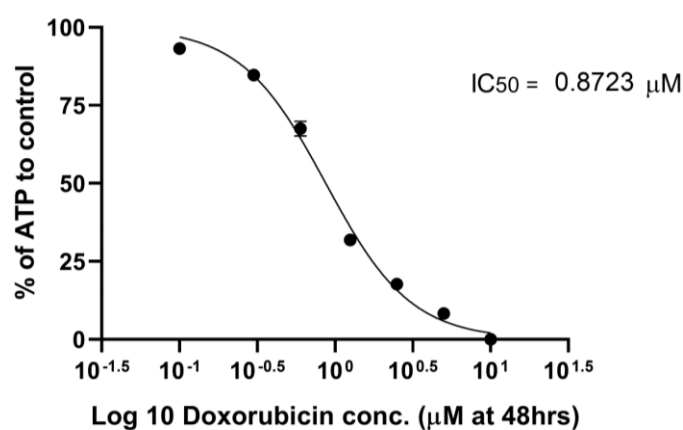
Figure 4.1: ATP level (% of control) was assessed by CellTiter-Glo® Luminescent cell viability assay after treating MDA-MB-231 cells for 48 hours with Doxorubicin (10, 5, 2.5, 1.25, 0.6, 0.3, and 0.15 µM). Data is expressed as ATP levels normalised to control based on 3 replicate wells from n=3 independent experiments. IC50 was determined by using non-linear regression of GraphPad Prism software version 8. Data are presented as the mean ± SEM.

Figure 4.2: Effect of Doxorubicin on ATP levels in MCF-7 cells
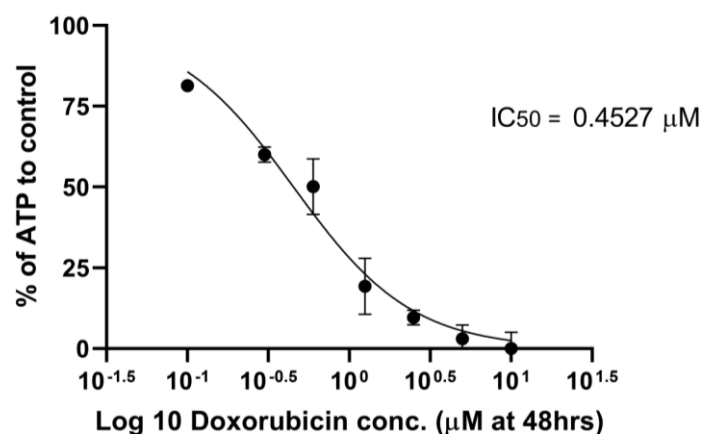
Figure 4.2: ATP level (% of control) was assessed by CellTiter-Glo® Luminescent cell viability assay after treating MCF-7 cells for 48 hours with Doxorubicin (10, 5, 2.5, 1.25, 0.6 0.3 and 0.15 µM). Data is expressed as ATP levels normalised to control based on 3 replicate wells from n=3 independent experiments. IC50 was determined by using non-linear regression of GraphPad Prism software version 8. Data are presented as the mean ± SEM.

4.2.2 Determination of the IC50 of Doxorubicin in breast cancer 3D alginate spheroids

To assess the effects of Doxorubicin treatment on cell survival in 3D alginate spheroids, total ATP measurements using CellTitre-Glo® 3D cell viability assay were performed as a proxy marker for cell numbers and/or total cellular metabolism in response to drug treatments. For 3D alginate treatment with Doxorubicin, cells were seeded (1 million cells/1 ml alginic acid) in white 96-well plates (Fisher Scientific) as one alginate bead per well and treated with Doxorubicin at different concentration (40, 10, 2.5, and 0.6 µM) with control (0.2% (v/v) DMSO). A higher dose range was used for 3D studies as initial experiments showed limited activity at the doses used for 2D cell culture studies. DMSO was included in this optimization as combination treatments would be performed with drugs dissolved in DMSO, so was included to assess the effects of the vehicle carrier in optimizing doses for future combination studies. Tumour cells were seeded into alginate and spheroids allowed to develop for 12-14 days or until the spheroid diameters reached 50-200 µm approximately. Treated cells were incubated at 37°C with CO_2, for 48 hours and 72 hours after treatments, the CellTiter-Glo® 3D Cell Viability Assay Kit (Promega-UK) was used to assess ATP levels. Luminescence is proportional to the total ATP present within each well. The average from three luminescence measurements was calculated and all treated cells were normalized to the controls. Half maximal inhibitory concentration (IC_{50}), which measures the effectiveness of Doxorubicin was then calculated.

4.2.2.1 Effect of Doxorubicin on MDA-MB-231 3D alginate spheroids using CellTiter-Glo® 3D Cell Viability Assay (3D)

The IC_{50} of Doxorubicin after measuring ATP activity of 3D MDA-MB-231 alginate spheres were estimated to be 4.8 µM after 48 hours and 3.0 µM after 72 hours. (Figure 4.3). Based on these observations, 2.5 µM was chosen as the optimal dose for combination studies with ferroptosis inducers.

4.2.2.2 Effect of Doxorubicin on MCF-7 3D alginate spheroids using CellTiter-Glo® 3D Cell Viability Assay (3D)

The IC_{50} of Doxorubicin after measuring ATP activity of 3D MCF-7 alginate spheres were estimated to be 11.8 µM after 48 hours and 6.2 µM after 72 hours (Figure 4.4). Based in

these observations, 10 µM was chosen as a suitable dose for combination studies with ferroptosis inducers, in that it showed sufficient cell death at 48 hours, and levels of cell death that were not too excessive at 72 hours.

Figure 4.3: Effect of Doxorubicin on ATP level of 3D alginate MDA-MB-231 cells
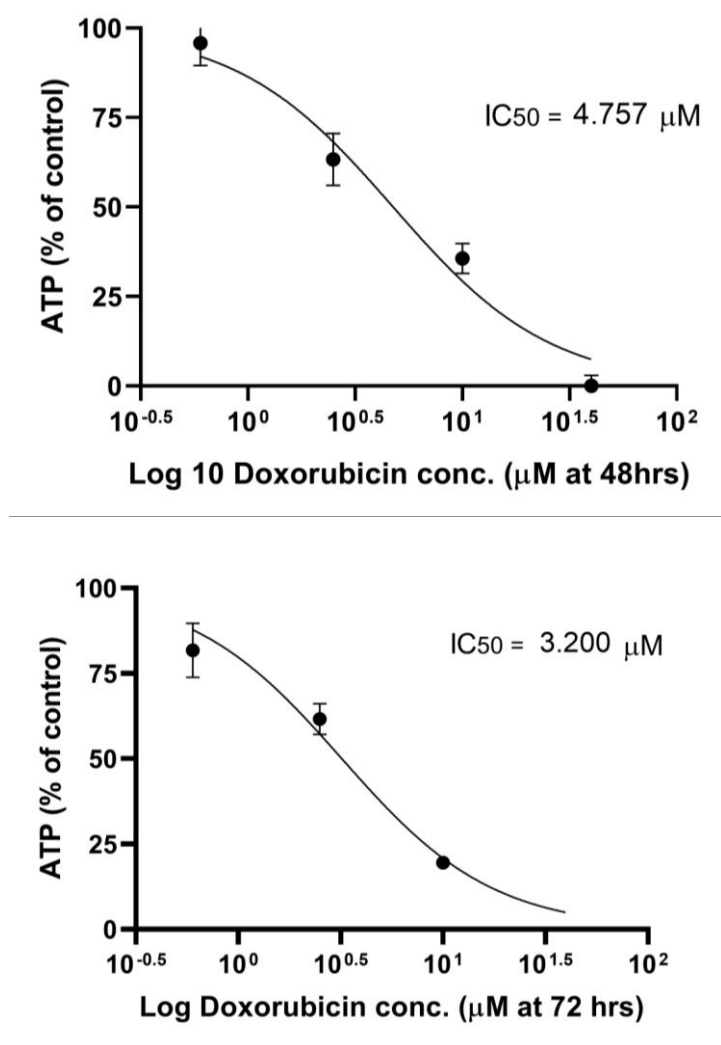
Figure 4.3: Effect of Doxorubicin on ATP level (% of control) using Cell Titer-Glo® 3D Cell Viability after treating 3D MDA-MB-231 alginate spheroids (1 alginate sphere/well, 4 replicate spheroids) for 48 and 72 hours with Doxorubicin (40, 10, 2.5, and 0.6 µM). Data is expressed as ATP levels normalised to control from n=3 independent experiments. IC50 was determined by using non-linear regression of GraphPad Prism software version 8. Data are presented as the mean ± SEM.

Figure 4.4: Effect of Doxorubicin on ATP level of 3D alginate MCF-7 cells
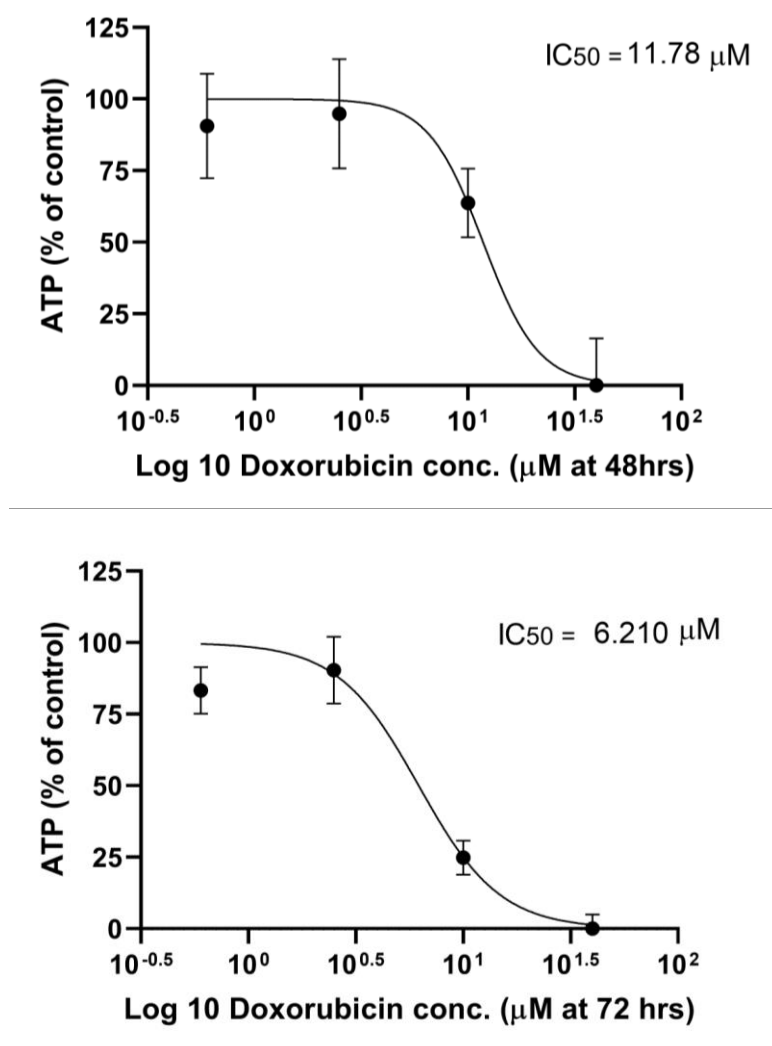
Figure 4.4: Effect of Doxorubicin on ATP level (% of control) using Cell Titer-Glo® 3D Cell Viability after treating 3D MCF-7 alginate spheroids (1 alginate sphere/well, 4 replicate spheroids) for 48 and 72 hours with Doxorubicin (40, 10, 2.5, and 0.6 μM). Data is expressed as ATP levels normalised to control from n=3 independent experiments. IC50 was determined by using non-linear regression of GraphPad Prism software version 8. Data are presented as the mean ± SEM.

4.2.3 The effect of MDA-MB-231 and MCF-7 cells treated with Doxorubicin and ferroptosis inducers

To assess the effects of combination treatment, cells were treated with Doxorubicin at the doses identified in optimisation studies with the ferroptosis inducers Erastin, RSL3 and FIN56. For ATP measurement, MDA-MB-231 cells were treated with Doxorubicin at concentration of 0.6 µM with ferroptosis inducers (RSL3 (0.0375 µM), Erastin (0.15 µM), FIN56 (0.15 µM)), with control (0.2% (v/v) DMSO). MCF-7 cells were treated with Doxorubicin at concentration of 0.6 µM with ferroptosis inducers (RSL3, Erastin, FIN56) at concentration of 10 µM, with control (0.2% (v/v) DMSO) for 24 and 48 hours after treatments, ATP measurements were performed using the CellTiter-Glo® Luminescent Cell Viability Assay. All treatments were performed in triplicate, in three independent experiments.

4.2.3.1 Effect of Doxorubicin in the presence of ferroptosis inducers in MDA-MB-231 on ATP levels

Consistent with optimization studies, 0.6 µM Doxorubicin significantly reduced ATP levels after 24 hours and to determine whether effects required a longer time point, experiments were repeated after 48 hours treatment. Erastin reduced cell viability also, but combination with Doxorubicin did not show any synergistic interaction. Combination treatment was significantly lower than control (P≤0.001), but not significantly different to Doxorubicin alone, showing that the majority of the cell death observed was due to Doxorubicin and no enhancement of effects seen with Erastin (Figure 4.5).

RSL3 reduced cell viability also, but combination with Doxorubicin did not show any synergistic interaction with Doxorubicin. Combination treatment was significantly lower than control (P≤0.001), but not significantly different to Doxorubicin alone, showing that the majority of the cell death observed was due to Doxorubicin and no enhancement of effects seen with RSL3 (Figure 4.6).

Again, Doxorubicin significantly and potently reduced ATP levels when compared to control (P≤0.001), and FIN56 alone also significantly reduced ATP levels, however combination treatment as almost identical to Doxorubicin-alone, again suggesting no interaction (Figure 4.7).

From obtained results, ferroptosis inducers (Erastin, RSL3, FIN56) treated MDA-MB-231 cells with Doxorubicin show no synergistic effect. This means that that the ferroptosis inducers do not enhance the chemotherapy effect of Doxorubicin in 2D cell culture.

Figure 4.5: Effect of Doxorubicin and Erastin on MDA-MB-231 cells

(A)   **(B)**
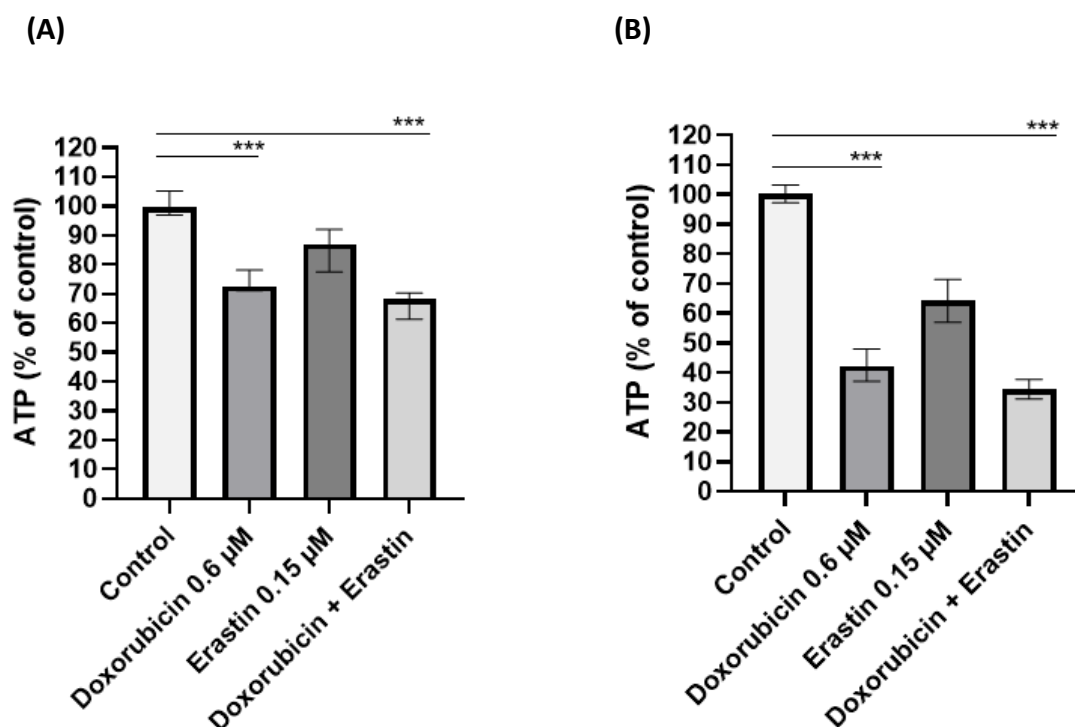
Figure 4.5: ATP level (% of control) assessed by CellTiter-Glo® Luminescent Cell Viability Assay after treating MDA-MB-231 cells for **(A)** 24 and **(B)** 48 hours with ferroptosis inducer Erastin (0.15 µM) and Doxorubicin (0.6 µM), with control (0.2% (v/v) DMSO). Data is presented as median ± range from n=3 independent experiments each with 3 technical repeats. The statistical significance was determined by comparison with the control and Doxorubicin, analysed by a Kruskal-Wallis followed by Dunn's multiple comparisons test (*=P≤0.05, **=P≤0.01, and ***=P≤0.001).

Figure 4.6: Effect of Doxorubicin and RSL3 on MDA-MB-231 cells

(A)   **(B)**

Figure 4.6: ATP level (% of control) assessed by CellTiter-Glo® Luminescent Cell Viability Assay after treating MDA-MB-231 cells for **(A)** 24 and **(B)** 48 hours with ferroptosis inducer RSL3 (0.0375 μM) and Doxorubicin (0.6 μM), with control (0.2% (v/v) DMSO). Data is presented as median ± range from n=3 independent experiments each with 3 technical repeats. The statistical significance was determined by comparison with the control and Doxorubicin, analysed by a Kruskal-Wallis followed by Dunn's multiple comparisons test (*=P≤0.05, **=P≤0.01, and ***=P≤0.001).

Figure 4.7: Effect of Doxorubicin and FIN56 on MDA-MB-231 cells

(A)   **(B)**

Figure 4.7: ATP level (% of control) assessed by CellTiter-Glo® Luminescent Cell Viability Assay after treating MDA-MB-231 cells for **(A)** 24 and **(B)** 48 hours with ferroptosis inducer FIN56 (0.15 µM) and Doxorubicin (0.6 µM), with control (0.2% (v/v) DMSO). Data is presented as median ± range from n=3 independent experiments each with 3 technical repeats. The statistical significance was determined by comparison with the control and Doxorubicin, analysed by a Kruskal-Wallis followed by Dunn's multiple comparisons test (*=P≤0.05, **=P≤0.01, and ***=P≤0.001).

4.2.3.2 Effect of Doxorubicin in the presence of ferroptosis inducers on ATP levels in MCF-7

Consistent with optimization studies, 0.6 µM Doxorubicin significantly reduced ATP levels after 24 hours and to determine whether effects required a longer time point, experiments were repeated after 48 hours treatment. Erastin reduced cell viability, but combination with Doxorubicin did not show any synergistic interaction with Doxorubicin although there was a significant difference from Doxorubicin alone ($P \leq 0.05$) but not a level that is synergistic effect, showing that the majority of the cell death observed was due to Doxorubicin and no enhancement of effects seen with Erastin (Figure 4.8).

RSL3 reduced cell viability also, and when combined with Doxorubicin showed a synergistic interaction ($P \leq 0.01$). Combination treatment was significantly lower than the expected levels of death based on the sum of RSL3 + Doxorubicin effects after 24 hours. ATP levels therefore shows enhancement of cell death effects seen with RSL3 when combined with Doxorubicin (Figure 4.9).

Again, Doxorubicin significantly and potently reduced ATP levels when compared to control ($P \leq 0.001$), and FIN56 has no effect on ATP levels, however combination treatment as almost identical to Doxorubicin-alone, again suggesting no interaction (Figure 4.10).

From obtained results, ferroptosis inducers Erastin and FIN56 treated MCF-7 cells with Doxorubicin show no synergistic effect. The only ferroptosis inducer to have a synergistic effect with Doxorubicin is RSL3, this means that the ferroptosis inducer RSL3 enhances the chemotherapy effect of Doxorubicin.

Figure 4.8: Effect of Doxorubicin and Erastin on MCF-7 cells

(A)

(B)
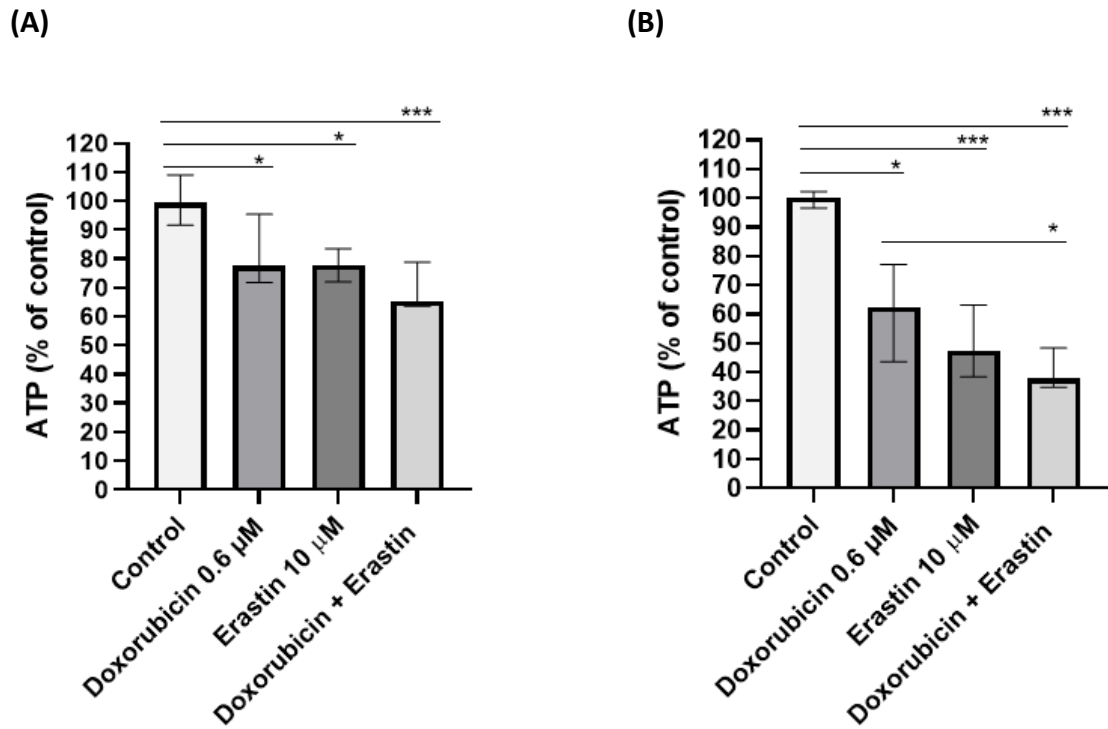
Figure 4.8: ATP level (% of control) assessed by CellTiter-Glo® Luminescent Cell Viability Assay after treating MCF-7 cells for **(A)** 24 and **(B)** 48 hours with ferroptosis inducer Erastin (10 µM) and Doxorubicin (0.6 µM), with control (0.2% (v/v) DMSO). Data is presented as median ± range from n=3 independent experiments each with 3 technical repeats. The statistical significance was determined by comparison with the control and Doxorubicin, analysed by a Kruskal-Wallis followed by Dunn's multiple comparisons test (*=P≤0.05, **=P≤0.01, and ***=P≤0.001).

Figure 4.9: Effect of Doxorubicin and RSL3 on MCF-7 cells

(A)   **(B)**
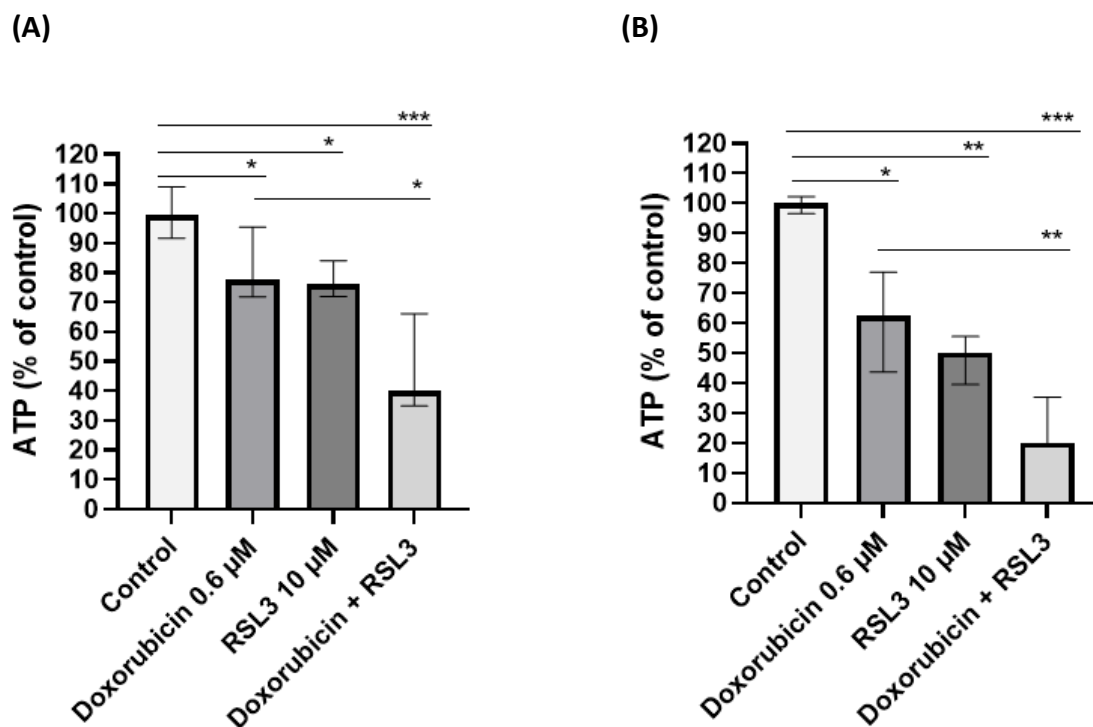
Figure 4.9: ATP level (% of control) assessed by CellTiter-Glo® Luminescent Cell Viability Assay after treating MCF-7 cells for **(A)** 24 and **(B)** 48 hours with ferroptosis inducer RSL3 (10 µM) and Doxorubicin (0.6 µM), with control (0.2% (v/v) DMSO). Data is presented as median ± range from n=3 independent experiments each with 3 technical repeats. The statistical significance was determined by comparison with the control and Doxorubicin, analysed by a Kruskal-Wallis followed by Dunn's multiple comparisons test (*=P≤0.05, **=P≤0.01, and ***=P≤0.001).

Figure 4.10: Effect of Doxorubicin and FIN56 on MCF-7 cells

(A)   **(B)**
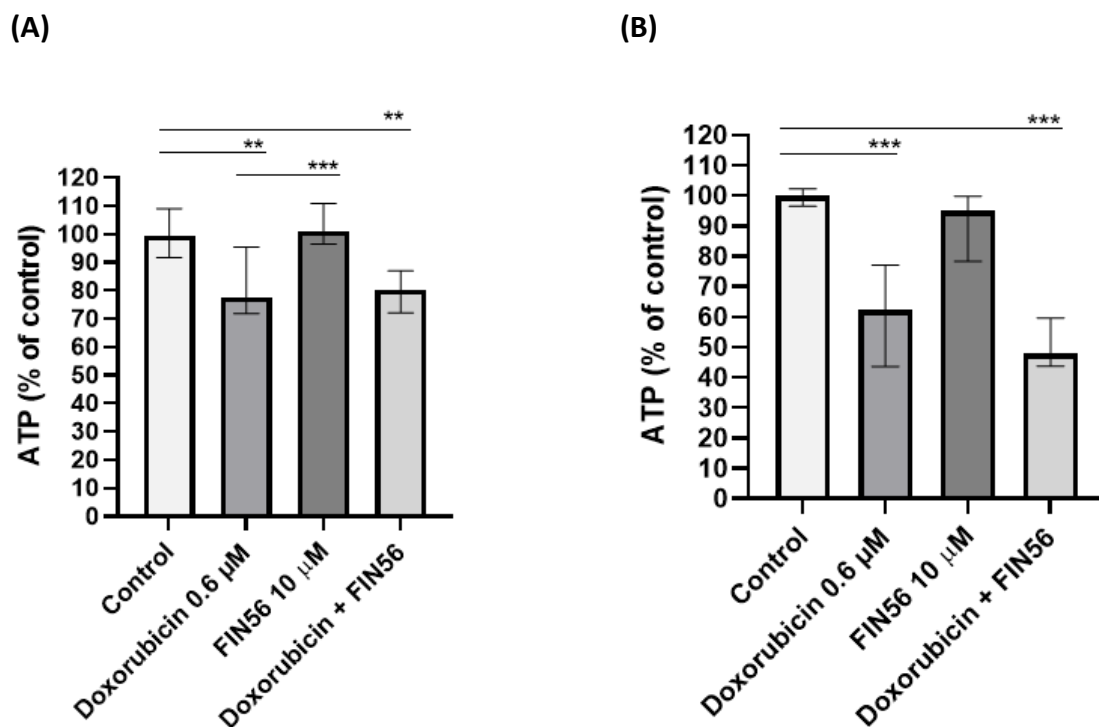
Figure 4.10: ATP level (% of control) assessed by CellTiter-Glo® Luminescent Cell Viability Assay after treating MCF-7 cells for **(A)** 24 and **(B)** 48 hours with ferroptosis inducer FIN56 (10 µM) and Doxorubicin (0.6 µM), with control (0.2% (v/v) DMSO). Data is presented as median ± range from n=3 independent experiments each with 3 technical repeats. The statistical significance was determined by comparison with the control and Doxorubicin, analysed by a Kruskal-Wallis followed by Dunn's multiple comparisons test (*=P≤0.05, **=P≤0.01, and ***=P≤0.001).

4.2.4 MDA-MB-231 and MCF-7 3D alginate spheroids treated with Doxorubicin and ferroptosis inducers

To assess the effects of combination treatment, cells were treated with Doxorubicin at the doses identified in optimisation studies with the ferroptosis inducers Erastin, RSL3 and FIN56. For ATP measurement MDA-MB-231 cells were treated with Doxorubicin at concentration of 2.5 µM with ferroptosis inducers (RSL3 (0.075 µM), Erastin (10 µM), FIN56 (10 µM)), with control (0.2% (v/v) DMSO). MCF-7 cells were treated with Doxorubicin at concentration of 10 µM with ferroptosis inducers (RSL3, Erastin, FIN56) at concentration of 10 µM, with control (0.2% (v/v) DMSO) for 48 hours After treatments, ATP measurements were performed using the CellTiter-Glo® 3D Cell Viability Assay. All treatments were performed in triplicate, in three independent experiments.

4.2.4.1 Effect of Doxorubicin in the presence of ferroptosis inducers in MDA-MB-231 3D alginate spheroids on ATP levels

Consistent with optimization studies, 2.5 µM Doxorubicin significantly reduced ATP levels in MDA-MB-231 cells after 48 hours. Erastin reduced cell viability also, but combination with Doxorubicin did not show any synergistic interaction with Erastin. Combination treatment was significantly lower than control ($P \leq 0.001$), and significantly different to Doxorubicin alone, showing that there is at least an additive response. However due to the approximately 60% reduction in ATP by Doxorubicin alone, it is difficult to determine whether this is synergistic (Figure 4.11).

RSL3 reduced cell viability also, but combination with Doxorubicin did not show any synergistic interaction with Doxorubicin. Combination treatment was significantly lower than control ($P \leq 0.001$), but not significantly different to Doxorubicin alone, showing that the majority of the cell death observed was due to Doxorubicin and no enhancement of effects seen with RSL3 (Figure 4.12).

Again, Doxorubicin significantly and potently reduced ATP levels when compared to control ($P \leq 0.001$), and FIN56 alone also significantly reduced ATP levels, however combination treatment of FIN56 with Doxorubicin showed high levels of death, potentially synergistic and worthy of further study ($P \leq 0.001$) (Figure 4.13).

From obtained results, ferroptosis inducers Erastin and RSL3 treated MDA-MB-231 cells with Doxorubicin show no synergistic effect. The only ferroptosis inducer that has a synergistic effect with Doxorubicin is FIN56, this means that the ferroptosis inducer FIN56 enhance the chemotherapy effect of Doxorubicin in 3D alginate spheroids.

Figure 4.11: Effect of Doxorubicin and Erastin on MDA-MB-231 spheroids
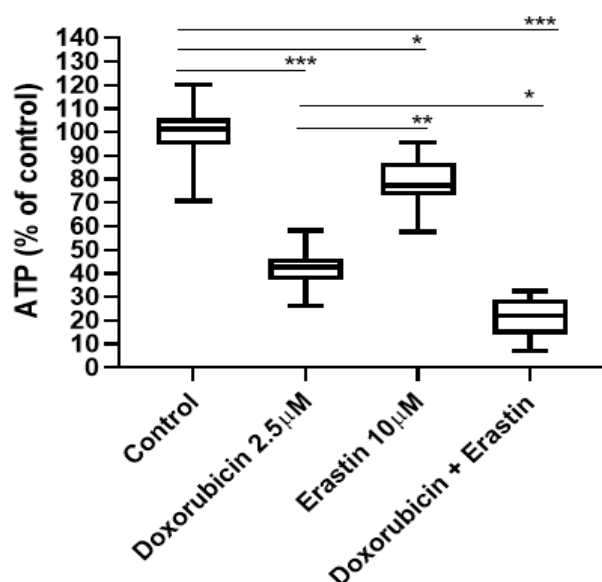
Figure 4.11: ATP level (% of control) assessed by CellTiter-Glo® Luminescent Cell Viability Assay after treating MDA-MB-231 spheroids for 48 hours with ferroptosis inducer Erastin (10 µM) and Doxorubicin (2.5 µM), with control (0.2% (v/v) DMSO). Data is presented as median ± interquartile range from n=3 independent experiments each with ≥4 technical repeats. The statistical significance was determined by comparison with the control and Doxorubicin, analysed by a Kruskal-Wallis followed by Dunn's multiple comparisons test (*=P≤0.05, **=P≤0.01, and ***=P≤0.001).

Figure 4.12: Effect of Doxorubicin and RSL3 on MDA-MB-231 spheroids
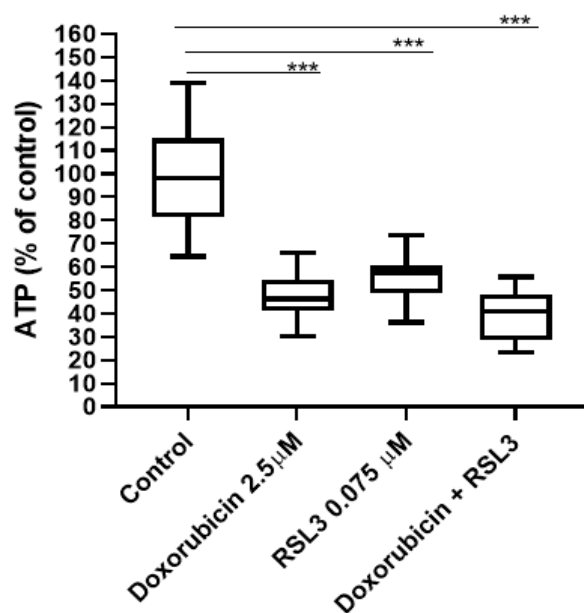
Figure 4.12: ATP level (% of control) assessed by CellTiter-Glo® Luminescent Cell Viability Assay after treating MDA-MB-231 spheroids for 48 hours with ferroptosis inducer RSL3 (0.075µM) and Doxorubicin (2.5 µM), with control (0.2% (v/v) DMSO). Data is presented as median ± interquartile range from n=3 independent experiments each with ≥4 technical repeats. The statistical significance was determined by comparison with the control and Doxorubicin, analysed by a Kruskal-Wallis followed by Dunn's multiple comparisons test (*=P≤0.05, **=P≤0.01, and ***=P≤0.001).

Figure 4.13: Effect of Doxorubicin and FIN56 on MDA-MB-231 spheroids
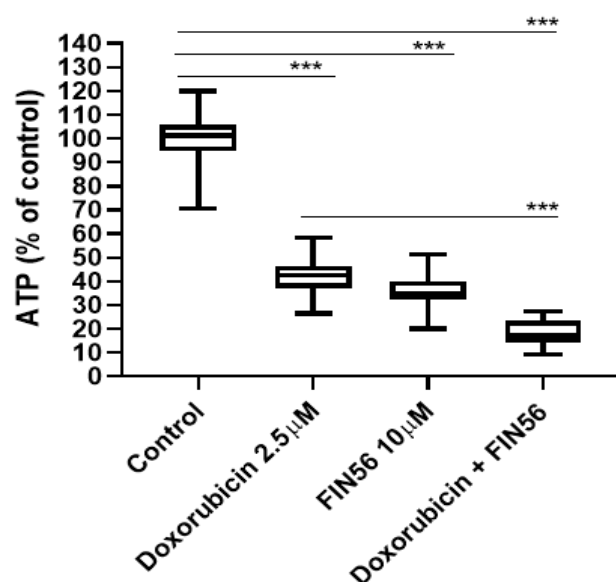
Figure 4.13: ATP level (% of control) assessed by CellTiter-Glo® Luminescent Cell Viability Assay after treating MDA-MB-231 spheroids for 48 hours with ferroptosis inducer FIN56 (10µM) and Doxorubicin (2.5 µM), with control (0.2% (v/v) DMSO). Data is presented as median ± interquartile range from n=3 independent experiments each with ≥4 technical repeats. The statistical significance was determined by comparison with the control and Doxorubicin, analysed by a Kruskal-Wallis followed by Dunn's multiple comparisons test (*=P≤0.05, **=P≤0.01, and ***=P≤0.001).

140

4.2.4.2 Effect of Doxorubicin in the presence of ferroptosis inducers in MCF-7 3D alginate spheroids on ATP levels

Consistent with optimization studies, 10 µM Doxorubicin significantly reduced ATP levels after 48 hours. Erastin reduced cell viability also, but combination with Doxorubicin did not show any synergistic interaction with Erastin. Combination treatment was significantly lower than control ($P \leq 0.001$), but not significantly different to Doxorubicin alone, showing that the majority of the cell death observed was due to Doxorubicin and no enhancement of effects seen with Erastin (Figure 4.14).

RSL3 reduced cell viability also, and when combination with Doxorubicin show a potentially synergistic interaction with Doxorubicin which was worthy of future study ($P \leq 0.01$). Combination treatment was significantly lower than control ($P \leq 0.001$), ATP levels shows enhancement of cell death effects seen with RSL3 when combined with Doxorubicin (Figure 4.15).

Again, Doxorubicin significantly and potently reduced ATP levels when compared to control ($P \leq 0.001$), and FIN56 has no effect on ATP levels, however combination treatment as almost identical to Doxorubicin-alone, suggesting no interaction (Figure 4.16).

From obtained results, ferroptosis inducers Erastin and FIN56 treated MCF-7 cells with Doxorubicin show no synergistic effect. The only ferroptosis inducer to have a potentially synergistic effect with Doxorubicin is RSL3 in 3D spheroid alginate, this means that the ferroptosis inducer RSL3 enhances the chemotherapy effect of Doxorubicin.
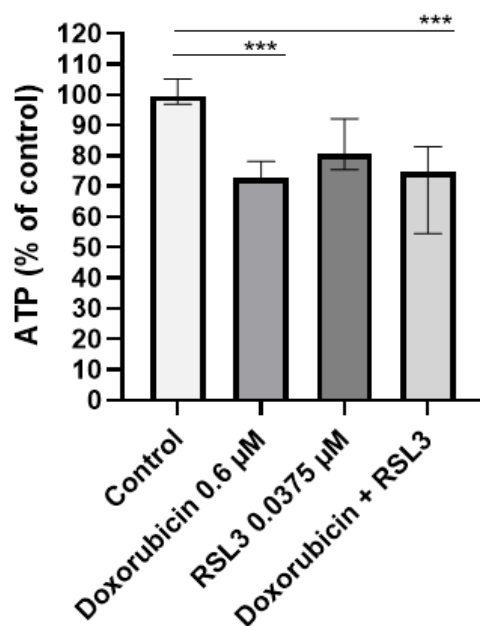
Figure 4.14: Effect of Doxorubicin and Erastin on MCF-7 spheroids
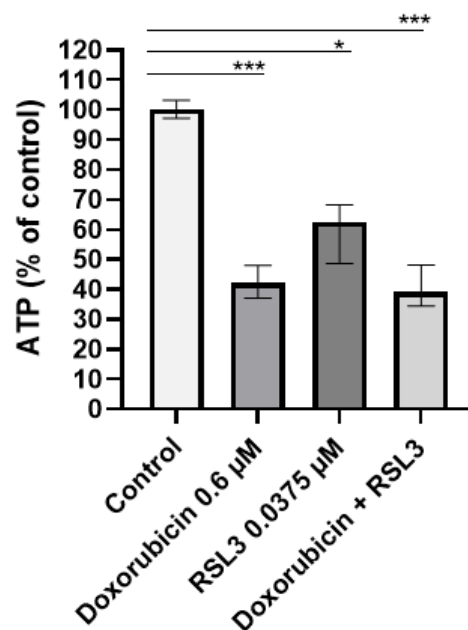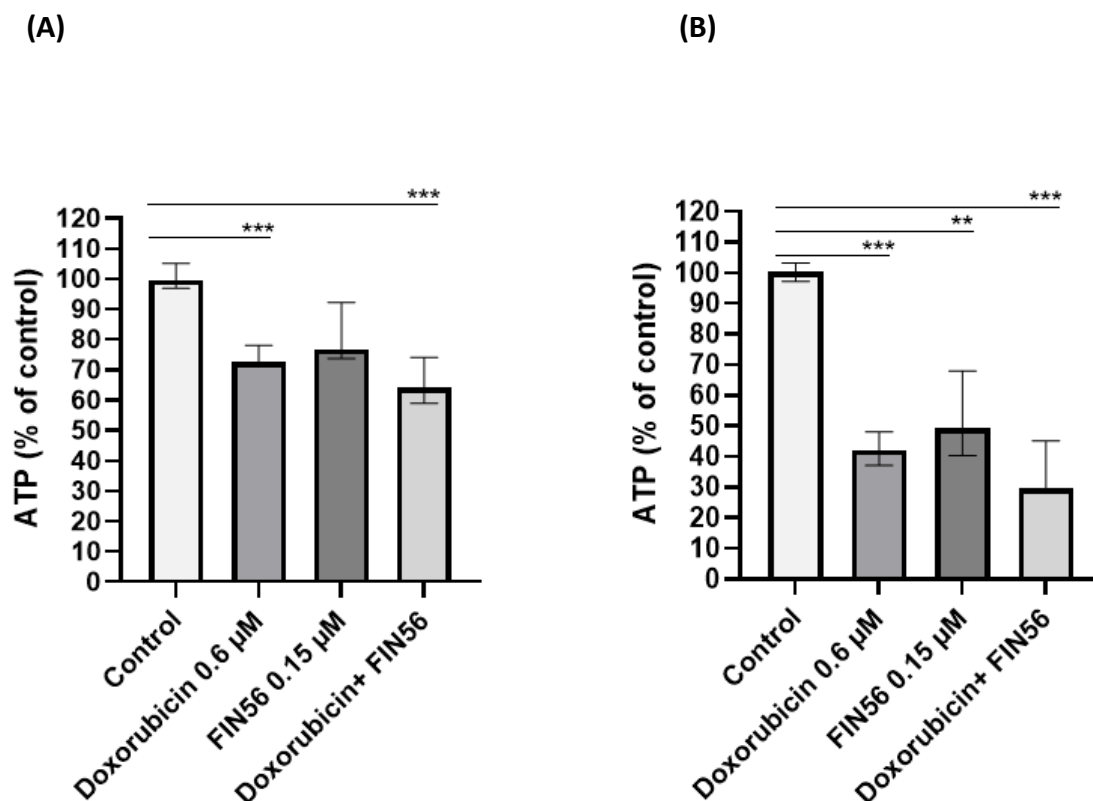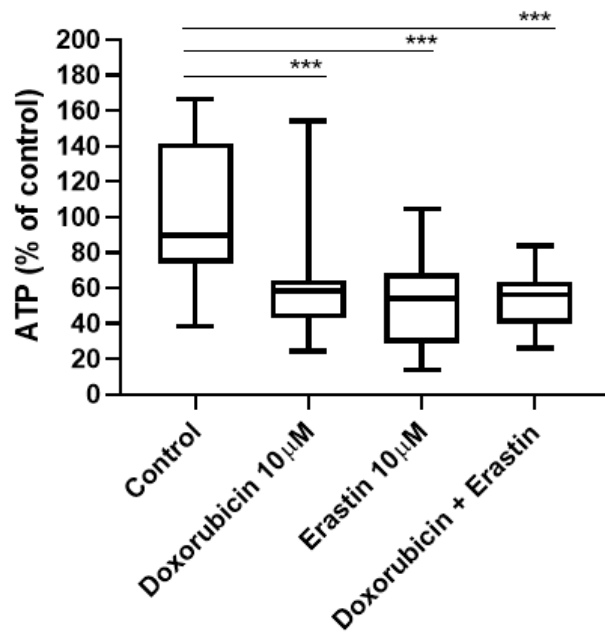

Figure 4.14: ATP level (% of control) assessed by CellTiter-Glo® Luminescent Cell Viability Assay after treating MCF-7 spheroids for 48 hours with ferroptosis inducer Erastin (10 µM) and Doxorubicin (10 µM), with control (0.2% (v/v) DMSO). Data is presented as median ± interquartile range from n=3 independent experiments each with ≥4 technical repeats. The statistical significance was determined by comparison with the control and Doxorubicin, analysed by a Kruskal-Wallis followed by Dunn's multiple comparisons test (*=P≤0.05, **=P≤0.01, and ***=P≤0.001).

Figure 4.15: Effect of Doxorubicin and RSL3 on MCF-7 spheroids
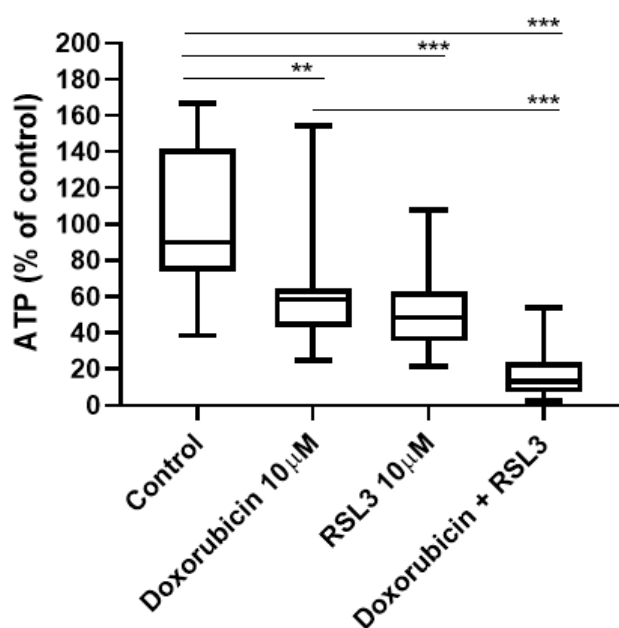
Figure 4.15: ATP level (% of control) assessed by CellTiter-Glo® Luminescent Cell Viability Assay after treating MCF-7 spheroids for 48 hours with ferroptosis inducer RSL3 (10 µM) and Doxorubicin (10 µM), with control (0.2% (v/v) DMSO). Data is presented as median ± interquartile range from n=3 independent experiments each with ≥4 technical repeats. The statistical significance was determined by comparison with the control and Doxorubicin, analysed by a Kruskal-Wallis followed by Dunn's multiple comparisons test (*=P≤0.05, **=P≤0.01, and ***=P≤0.001).

Figure 4.16: Effect of Doxorubicin and FIN56 on MCF-7 spheroids

Figure 4.16: ATP level (% of control) assessed by CellTiter-Glo® Luminescent Cell Viability Assay after treating MCF-7 spheroids for 48 hours with ferroptosis inducer FIN56 (10 μM) and Doxorubicin (10 μM), with control (0.2% (v/v) DMSO). Data is presented as median ± interquartile range from n=3 independent experiments each with ≥4 technical repeats. The statistical significance was determined by comparison with the control and Doxorubicin, analysed by a Kruskal-Wallis followed by Dunn's multiple comparisons test (*=P≤0.05, **=P≤0.01, and ***=P≤0.001).

4.2.5 Effect of caspase inhibitor and ferroptosis inhibitor on Doxorubicin-mediated cell death in breast cancer cells

To distinguish between apoptotic cell death and ferroptotic cell death, a caspase inhibitor and a ferroptosis inhibitor (Pan-caspase inhibitor Z-VAD-FMK and Ferrostatin-1 respectively) were used in combination with Doxorubicin. Doxorubicin significantly induced cell death in both MDA-MB-231 and MCF-7 cells according to the ATP levels, measurements were performed using the CellTiter-Glo® Luminescent Cell Viability Assay The Pan-caspase inhibitor Z-VAD-FMK do not prevent cell death when combined with Doxorubicin, and similarly, neither did Ferropststin-1 in both MBA-MB-231 cells (Figure 4.17) and MCF-7 (Figure 4.18).

Figure 4.17: Effect of caspase inhibitor and ferroptosis inhibitor on Doxorubicin-mediated cell death in MDA-MB-23
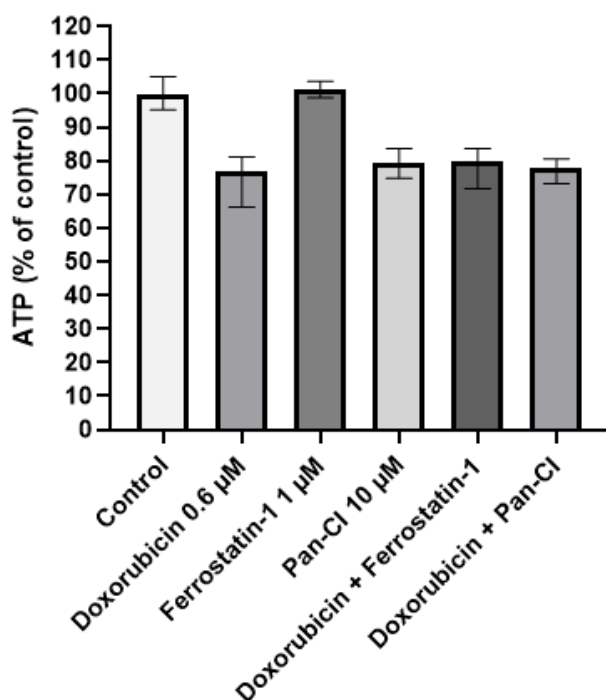
Figure 4.17: ATP level (% of control) assessed by CellTiter-Glo® Luminescent Cell Viability Assay after MDA-MD-231 cells were preincubated with caspase inhibitor Pan-caspase inhibitor Z-VAD-FMK at concentration of 10 µM and ferroptosis inhibitor Ferrostatin-1 at concentration of 1 µM for 1 hour prior to treatment with Doxorubicin at concentration of 0.6 µM, with control (0.2% (v/v) DMSO) for 48 hours n=3 independent experiments each with 3 technical repeats. The statistical significance was determined by comparison with Doxorubicin, analysed by a Kruskal-Wallis followed by Dunn's multiple comparisons test (*=P≤0.05, **=P≤0.01, and ***=P≤0.001).

Figure 4.18: Effect of caspase inhibitors and ferroptosis inhibitors on Doxorubicin-mediated cell death in MCF-7
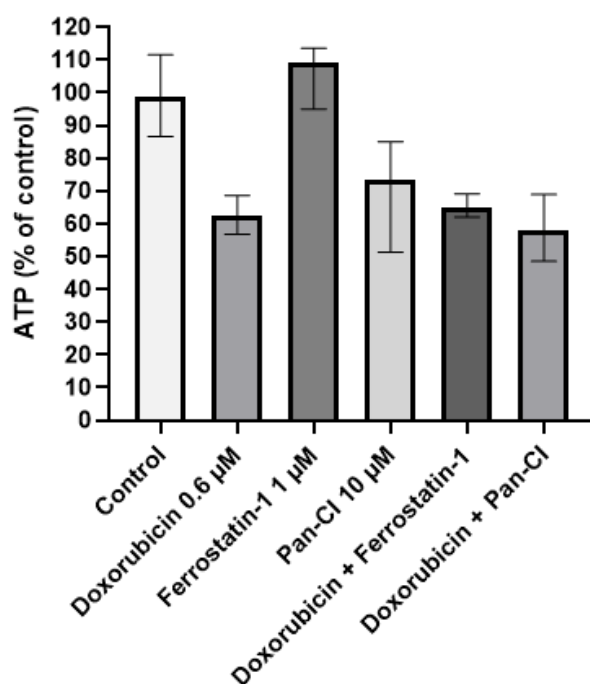
Figure 4.18: ATP level (% of control) assessed by CellTiter-Glo® Luminescent Cell Viability Assay after MCF-7 cells were preincubated with caspase inhibitor Pan-caspase inhibitor Z-VAD-FMK at concentration of 10 µM and ferroptosis inhibitor Ferrostatin-1 at concentration of 1 µM for 1 hour prior to treatment with Doxorubicin at concentration of 0.6 µM, with control (0.2% (v/v) DMSO) for 48 hours n=3 independent experiments each with 3 technical repeats. The statistical significance was determined by comparison with Doxorubicin, analysed by a Kruskal-Wallis followed by Dunn's multiple comparisons test (*=P≤0.05, **=P≤0.01, and ***=P≤0.001).

4.2.6 Immunocytochemistry to detect Nrf2 in breast cancer cells

Ferroptosis is controlled in part by the antioxidant response pathway, with is largely regulated by Nrf-2, a transcription factor that binds to the promoter and induces transcription of many genes responsible for preventing ROS-induced cell stress, such as those resulting in glutathione synthesis. Prior to treatment with Nrf2 inhibitor ML385, the levels of Nrf2 protein were assessed. Untreated 2D MDA-MB-231 and MCF-7 cells were stained with immunocytochemistry stain to localize the present of Nrf2 within cells. In MDA-MB-231 cells the distribution of Nrf2 was noticed in the nucleus, but signal was quite weak and uniformly distributed (Figure 4.19B), while for MCF-7 cells the distribution of Nrf2 was seen strongly in the nucleus (Figure 4.20B).

Figure 4.19: Nrf2 detection in MDA-MB-231 cells

(A)

| Nrf2 | Combined | DAPI |

(B)

| Nrf2 | Combined | DAPI |
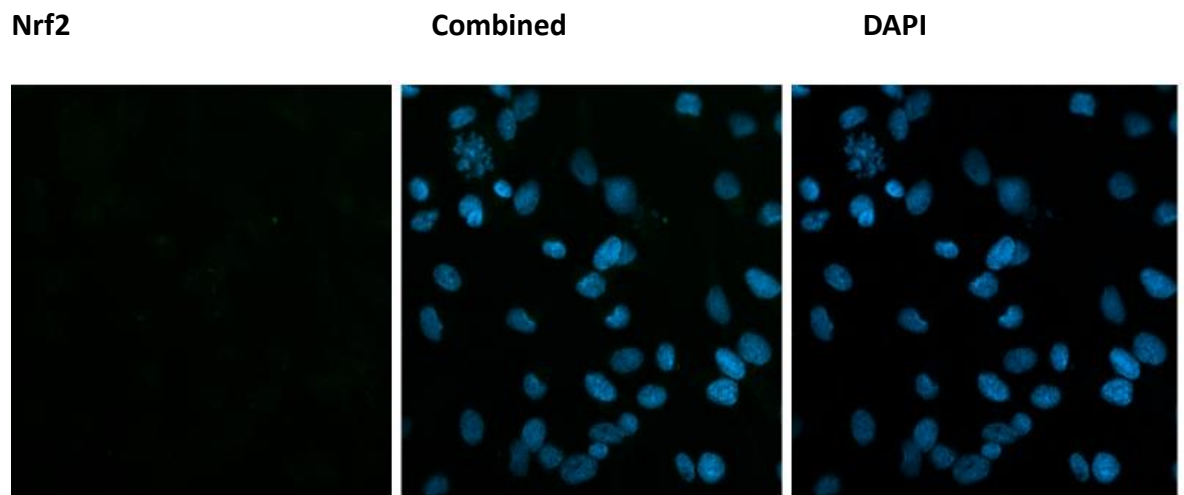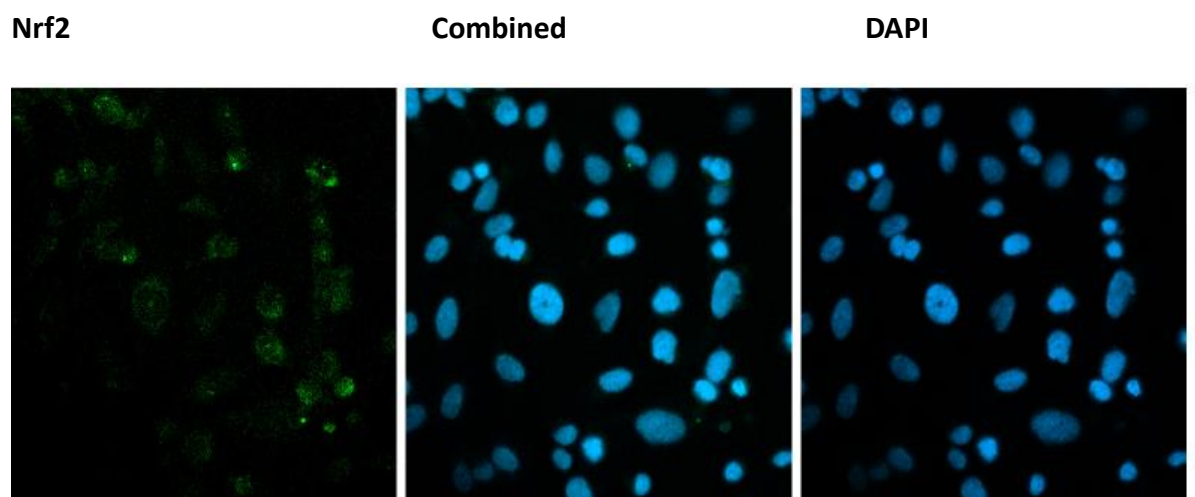
Figure 4.19: MDA-MB-231 cells were stained with Nrf2 stain probed with a primary anti-NRF2 antibody diluted 1:800 **(B)** and visualized with a goat anti-Rabbit Alexa Fluor 488-conjugated secondary antibody. Nuclei were stained with DAPI. **(A)** cells without Nrf2 antibody (control). Images were photographed using confocal fluorescence microscopy using a 40x objective lens.

Figure 4.20: Nrf2 detection in MCF-7 cells

(A)

Nrf2   **Combined**   **DAPI**

(B)

Nrf2   **Combined**   **DAPI**
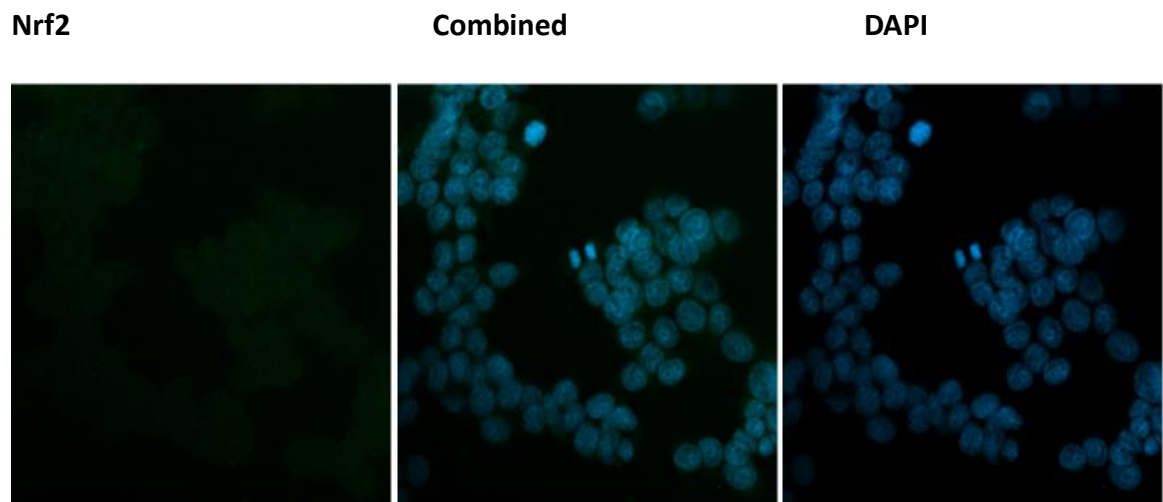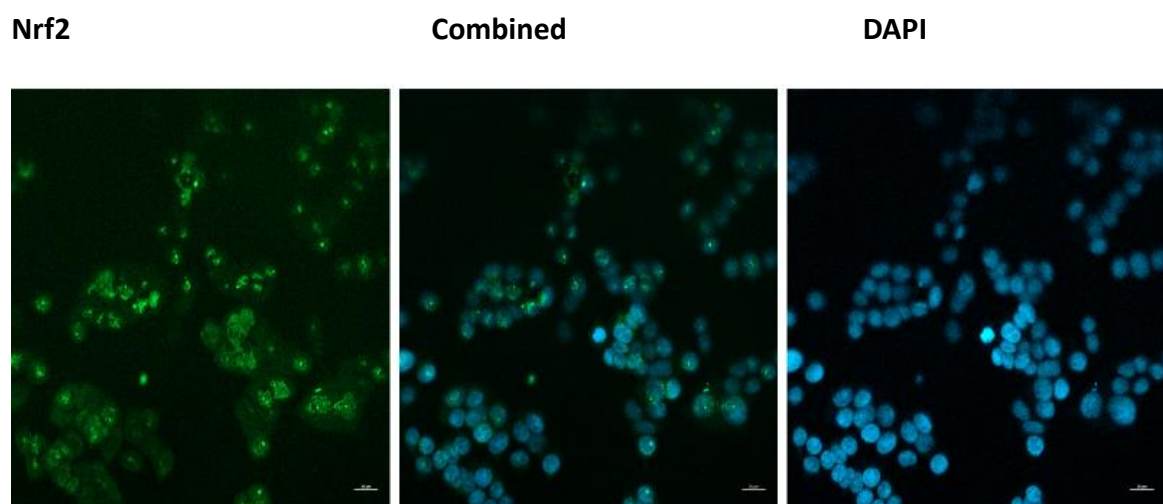
Figure 4.20: MCF-7 cells were stained with Nrf2 stain probed with a primary anti-NRF2 antibody diluted 1:800 **(B)** and visualized with a goat anti-Rabbit Alexa Fluor 488-conjugated secondary antibody. Nuclei were stained with DAPI. **(A)** cells without Nrf2 antibody (control). Images were photographed using confocal fluorescence microscopy using a 40x objective lens.

.

4.2.7 Detection of ferroptosis-related gene expression by qRT-PCR

To assess expression profiles of genes associated with ferroptosis, or the antioxidant response that is mediated by Nrf2, a panel of genes was selected for qRT-PCR analysis of mRNA levels. The genes detected using TaqMan Gene Expression primer-probes include: HMOX1, SLC7a11, GSTP1, Keap-1, NQO1, GPX4, Nrf2, TFRS, and Beta-2 microglobulin as a housekeeping gene.

4.2.7.1 Genes expression in 2D and 3D MDA-MB-231 cell line

In MDA-MB-231, gene expression was detected for all Taqman gene expression assays, with highest expression observed for GSTP1. There was significantly higher GSTP1 and TFRC mRNA expression level in the 2D model compared to the 3D model in MDA-MB-231 cells (Figure 4.21) ($P \leq 0.05$). However, no differences in the expression levels of HMOX1, SLC7A11, KEAP1, NQO1, GPX4 and NFR2 mRNA were seen in the 2D and 3D models in MDA-MB-231 cells (Figure 4.21).

4.2.7.2 Genes expression in 2D and 3D MCF-7 cell line

In contrast to MDA-MB-231, where GSTP1 was the most highly expressed, in MCF-7, GSTP1 was transcriptionally silent in both 2D and 3D cell culture. No significant changes in the expression levels of HMOX1, SLC7A11, KEAP1, NQO1, GPX4, NFR2 and TFRC mRNA were seen between 2D and 3D cultures of MCF-7 cells (Figure 4.22).

4.2.7.3 Gene expression comparison between MDA-MB-231 and MCF-7 cells

The mRNA expression of GSTP1 was significantly higher in the 2D model of MDA-MB-231 cells compared to the 2D model of MCF-7 cells ($P \leq 0.05$), being absent in the latter (Figure 4.23). However, no significant changes were seen in the expression of HMOX1, SLC7A11, KEAP1, NQO1, GPX4, NFR2 and TFRC genes in the 2D model of MDA-MB-231 and MCF-7 cells (Figure 4.23).

4.2.7.4 Genes expression comparison between MDA-MB-231 and MCF-7 3D alginate spheroids

There was significantly higher mRNA expression of NQO1 and of the 3D model of MCF-7 cells compared to the 3D model of MDA-MB-231 cells ($P \leq 0.05$) (Figure 4.24). Also, the

expression of GSTP1 was significantly higher in the 3D model of MDA-MB-231 cells compared to the 3D model of MCF-7 cells where GTSP1 was absent (P≤0.05).

The expression of HMOX1, SLC7A11, GSTP1, KEAP1, GPX4, NFR2 and TFRC genes were however similar in the MCF-7 and MDA-MB-231 cells (Figure 4.24).

Figure 4.21: Ferroptosis gene expression in 2D and 3D MDA-MB-231 cells
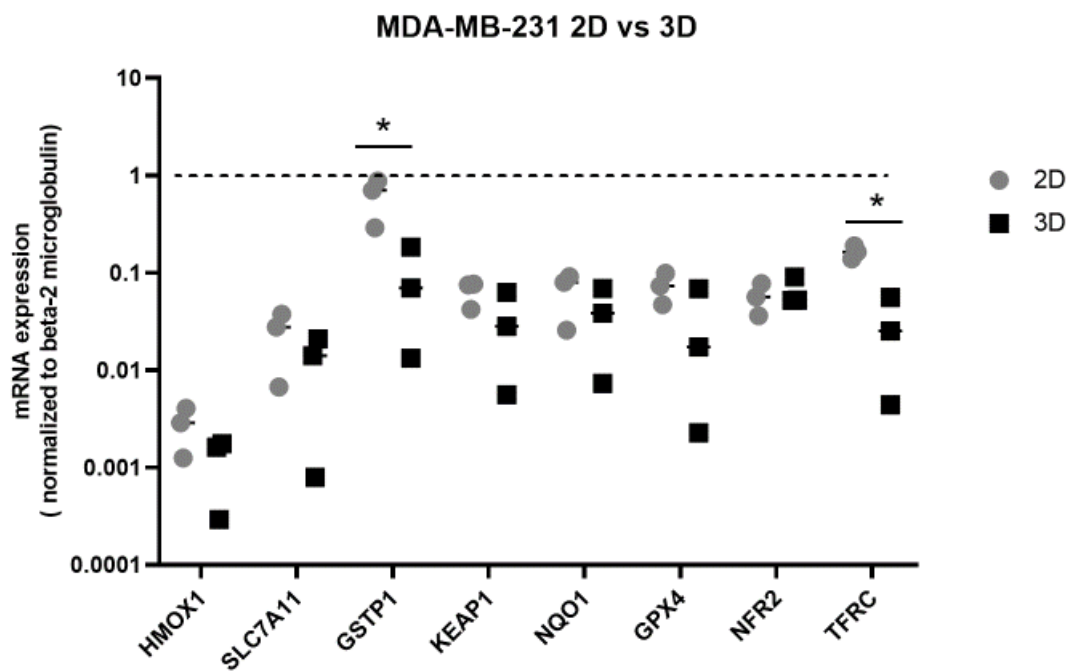
Figure 4.21: HMOX1, SLC7A11, GSTP1, KEAP1, NQO1, GPX4, NFR2 and TFRC gene expression in 2D (Grey) and 3D (Black) of MDA-MB-231 cells. Gene expression was measured by qRT-PCR. Data is expressed was normalized to the housekeeping gene (Beta-2 microglobulin) and Ct values were used to determine relative expression. The data is shown as median (-) and ranges, and significance was determined using a Kruskal-Wallis with a Dunn's post-hoc test and significance (*) and set at P≤0.05.

Figure 4.22: Ferroptosis gene expression in 2D and 3D MCF-7 cells
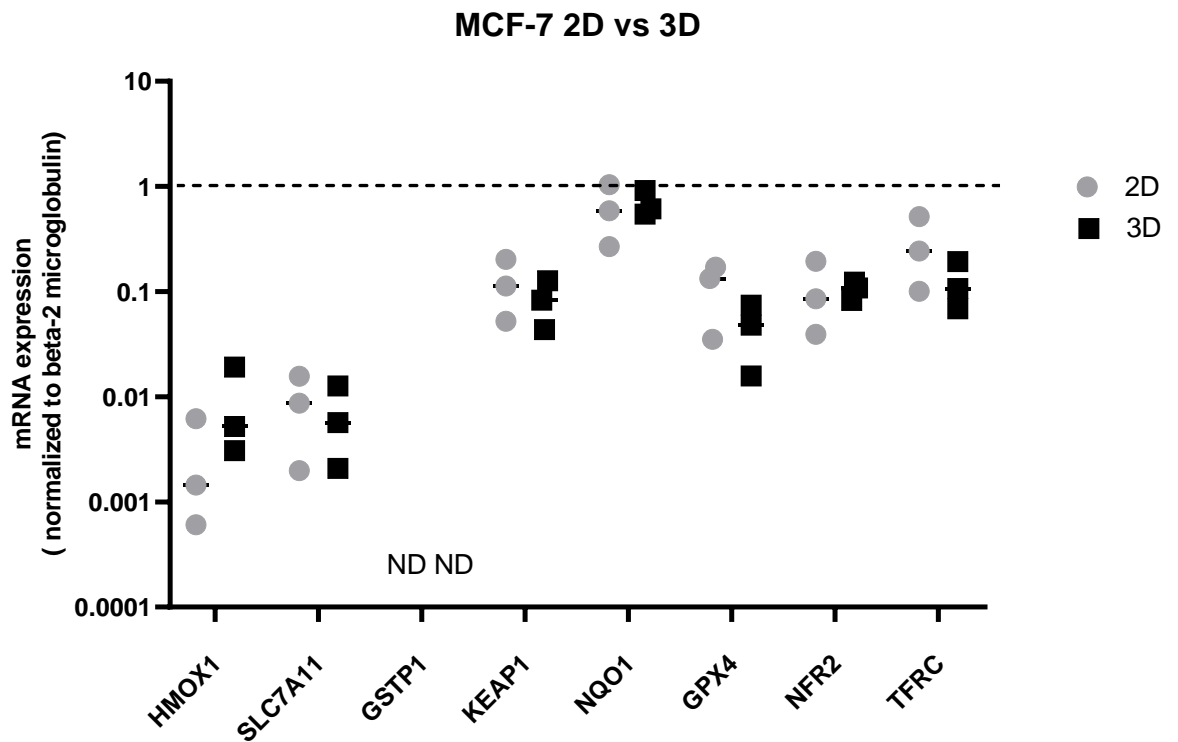
Figure 4.22: HMOX1, SLC7A11, GSTP1, KEAP1, NQO1, GPX4, NFR2 and TFRC gene expression in 2D (Grey) and 3D (Black) of MCF-7 cells. Gene expression was measured by qRT-PCR. Data is expressed was normalized to the housekeeping gene (Beta-2 microglobulin) and Ct values were used to determine relative expression. The data is shown as median (-) and ranges, and significance was determined using a Kruskal-Wallis with a Dunn's post-hoc test and significance (*) and set at P≤0.05. ND = not detected.

Figure 4.23: Ferroptosis gene expression comparison in MDA-MB-231 and MCF-7 cells

2D MCF-7 vs MDA-MB-231
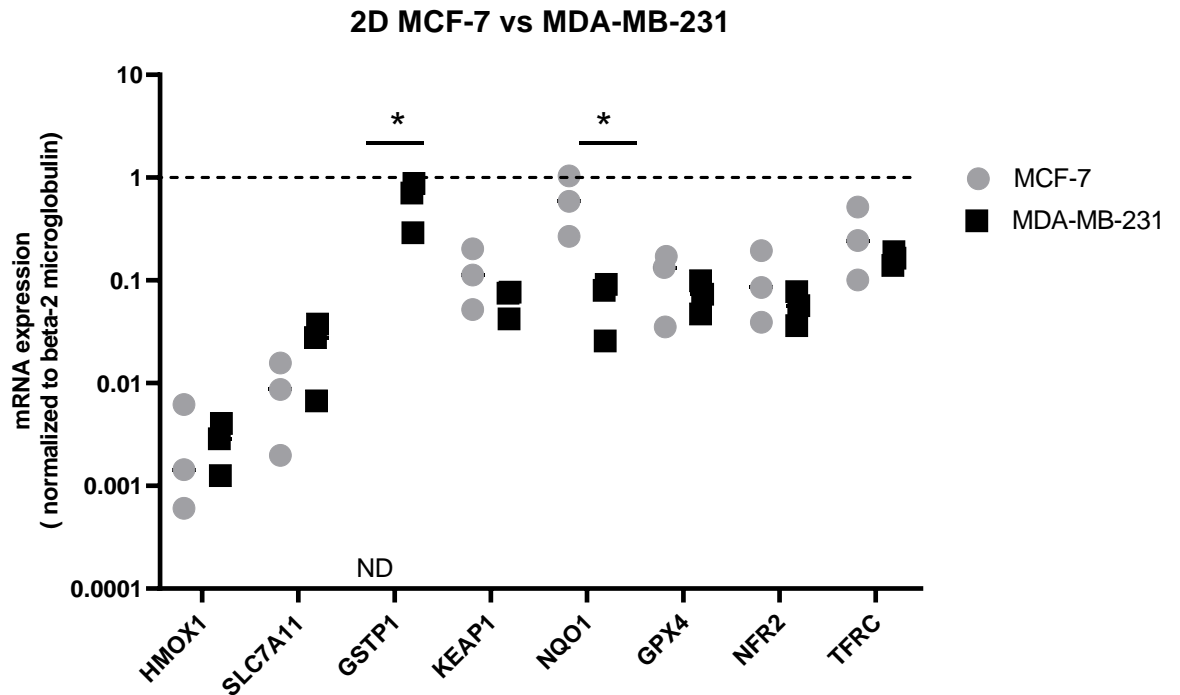
Figure 4.23: HMOX1, SLC7A11, GSTP1, KEAP1, NQO1, GPX4, NFR2 and TFRC gene expression in 2D of MCF-7 (Grey) and MDA-MB-231 (Black) cells. Gene expression was measured by qRT-PCR periodically throughout the study period. Data is expressed was normalized to the housekeeping gene (Beta-2 microglobulin) and Ct values were used to determine relative expression. The data is shown as median (-) and ranges, and significance was determined using a Kruskal-Wallis with a Dunn's post hoc test and significance (*) and set at P≤0.05. ND = not detected.

Figure 4.24: Ferroptosis gene expression comparison in MDA-MB-231 and MCF-7 3D alginate spheroids

3D MCF-7 vs MDA-MB-231
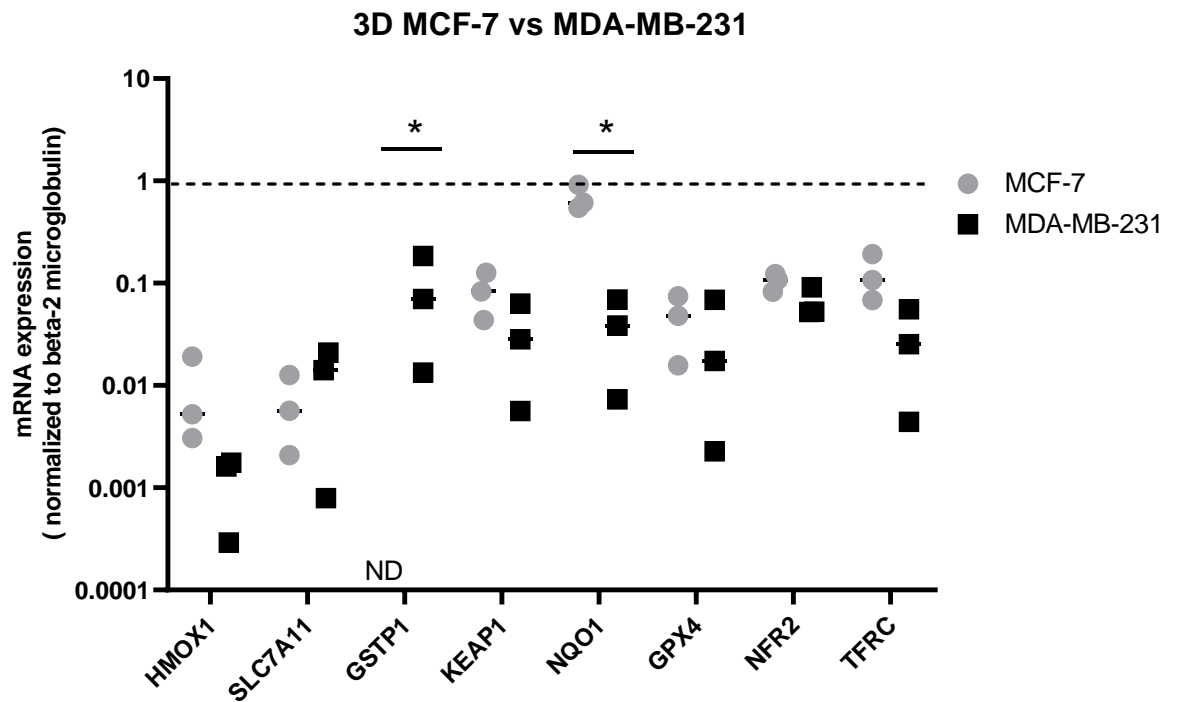
Figure 4.24: HMOX1, SLC7A11, GSTP1, KEAP1, NQO1, GPX4, NFR2 and TFRC gene expression in 3D of MCF-7 (Grey) and MDA-MB-231 (Black) cells. Gene expression was measured by qRT-PCR. Data is expressed was normalized to the housekeeping gene (Beta-2 microglobulin) and Ct values were used to determine relative expression. The data is shown as median (-) and ranges, and significance was determined using a Kruskal-Wallis with a Dunn's post hoc test and significance (*) and set at P≤0.05. ND = not detected.

4.2.8 Effect of the Nrf2 inhibitor on chemotherapy responses in breast cancer 2D cell culture

Since both breast cancer cell lines expressed the NRF2 gene and Nrf2 protein, and Nrf2 is known to control the antioxidant response driving expression of many of the genes assessed by qRT-PCR, cells were treated with ML385, a specific Nrf2 inhibitor. To assess ML385-inhibitor effects, cells were treated with ML385 (10 µM) with the ferroptosis inducer RSL3 in the presence and absence of chemotherapy. The rationale for this is two-fold: firstly, RSL3 was the only ferroptosis inducer that showed a pro-ferroptotic effect with both 2D and 3D cell culture modules (Chapter 3), and secondly it was the most promising agent when combined with chemotherapy, particularly in the ferroptosis-resistant MCF-7 cell line. Again, cells were treated with Doxorubicin alone, RSL3 alone, then ML385 effect was assessed with the combination of both Doxorubicin and RSL3 combination. This was done for both MDA-MB-231 and MCF-7 cell lines.

4.2.8.1 Effect of combination treatment of Nrf2 inhibitor ML385 +/- RSL3 in MDA-MB-231 cells

To assess the effects of ML385, cells were treated with ML385 (10 µM) with ferroptosis inducer RSL3 (0.0375 µM) for 48 hours. To assess cell activity, ATP levels were measured using CellTiter-Glo® Luminescent Cell Viability Assay (2D).

For ATP activity, combined treatments were significantly different to control ($P \leq 0.001$), but ML385 alone when compared to control was significant ($P \leq 0.01$). Combined treatment of ML385 with RSL3 ($P \leq 0.001$) when compared to ML385 alone showed a potent synergistic effect (Figure 4.25).

4.2.8.2 Effect of combination treatment of Nrf2 inhibitor ML385 +/- RSL3 in MCF-7 cells

To assess the effects of ML385, MCF-7 cells were treated with ML385 (10 µM) with ferroptosis inducer RSL3 (10 µM) for 48 hours. To assess cell activity, ATP levels were measured using CellTiter-Glo® Luminescent Cell Viability Assay (2D).

For ATP activity, ML385 alone when compared to control was significantly lower than control, and combined treatments were significantly different to control ($P \leq 0.001$). Combined treatment of ML385 with RSL3 when compared to ML385 alone were not

significantly different to each other so majority of cell death in combination is due to ML385, and there was no enhancement in the ferroptotic effect (Figure 4.26).

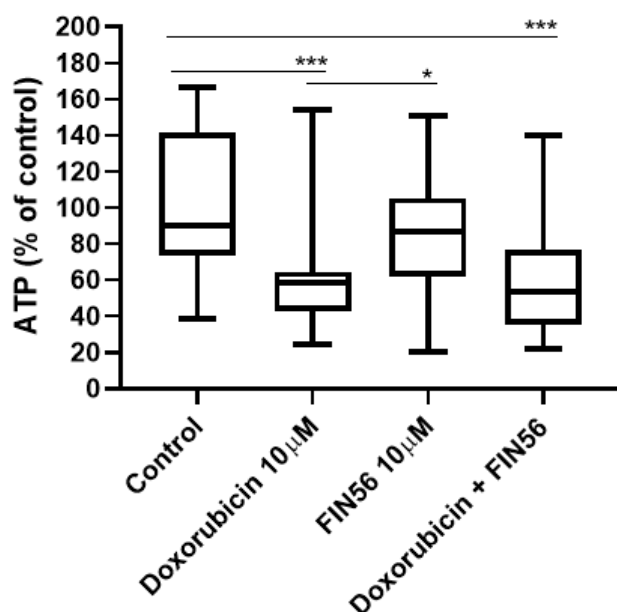**Figure 4.25: Combination treatment of ML385 +/- RSL3 in MDA-MB-231 cells**
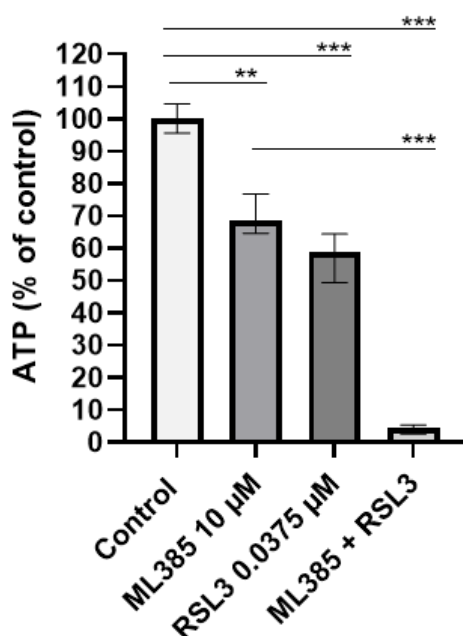
Figure 4.25: ATP level (% of control) assessed by CellTiter-Glo® Luminescent Cell Viability Assay after treating MDA-MB-231 cells for 48 hours with ML385 (10 µM) with control (0.2% (v/v) DMSO) +/- RSL3 (0.0375 µM). Data is presented as median ± range from n=3 independent experiments each with 3 technical repeats. The statistical significance was determined by comparison with the control and ML385, analysed by a Kruskal-Wallis followed by Dunn's multiple comparisons test (*=P≤0.05, **=P≤0.01, and ***=P≤0.001).

Figure 4.26: Combination treatment of ML385 +/- RSL3 in MCF-7 cells
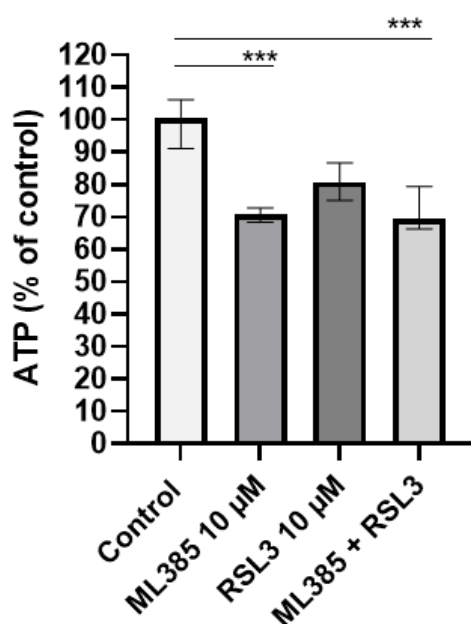
Figure 4.26: ATP level (% of control) assessed by CellTiter-Glo® Luminescent Cell Viability Assay after treating MCF-7 cells for 48 hours with ML385 (10 µM) with control (0.2% (v/v) DMSO) +/- RSL3 (10 µM). Data is presented as median ± range from n=3 independent experiments each with 3 technical repeats. The statistical significance was determined by comparison with the control and ML385, analysed by a Kruskal-Wallis followed by Dunn's multiple comparisons test (*=P≤0.05, **=P≤0.01, and ***=P≤0.001).

4.2.8.3 Effect of combination treatment of Nrf2 inhibitor ML385 +/- Doxorubicin in MDA-MB-231 cells

To assess ML385 effects in combination with chemotherapy, cells were treated with ML385 (10 µM) with ferroptosis inducer Doxorubicin (0.6 µM) for 48 hours. To assess cell activity, ATP levels were measured using CellTiter-Glo® Luminescent Cell Viability Assay (2D). For ATP activity, combined treatments were significantly different to control ($P \leq 0.001$). Combined treatment of ML385 with Doxorubicin ($P \leq 0.001$) when compared to ML385 alone was significant, but the majority of effect is due to Doxorubicin (Figure 4.27). This confirms that there is no interaction between ML385 and Doxorubicin in MDA-MB-231 cells.

Figure 4.27: Combination treatment of ML385 +/- Doxorubicin in MDA-MB-231 cells

Figure 4.27: ATP level (% of control) assessed by CellTiter-Glo® Luminescent Cell Viability Assay after treating MDA-MB-231 cells for 48 hours with ML385 (10 µM) with control (0.2% (v/v) DMSO) +/- Doxorubicin (0.6 µM). Data is presented as median ± range from n=3 independent experiments each with 3 technical repeats. The statistical significance was determined by comparison with the control and ML385, analysed by a Kruskal-Wallis followed by Dunn's multiple comparisons test (*=$P \leq 0.05$, **=$P \leq 0.01$, and ***=$P \leq 0.001$).

4.2.8.4 Effect of combination treatment of Nrf2 inhibitor ML385 +/- Doxorubicin in MCF-7 cells

To assess ML385 effects on MCF-7, cells were treated with ML385 (10 µM) with ferroptosis inducer Doxorubicin (0.6 µM) for 48 hours. To assess cell activity, ATP levels were measured using CellTiter-Glo® Luminescent Cell Viability Assay (2D). For ATP activity, combined treatments were significantly different to control (P≤0.001), but ML385 alone when compared to control was also significantly different (P≤0.001). Combined treatment of ML385 with Doxorubicin when compared to ML385 alone were not significantly different to each other so majority of cell death in combination is due to ML385, and there was no enhancement in the chemotherapy effect (Figure 4.28).

4.2.8.5 Effect of combination treatment of Nrf2 inhibitor ML385 +/- Doxorubicin with combination of RSL3 in MDA-MB-231 cells

To assess ML385 effects in the presence of RSL3 and chemotherapy, cells were treated with ML385 (10 µM) with Doxorubicin (0.6 µM) combined with ferroptosis inducer RSL3 (0.0375 µM) for 48 hours. To assess cell activity, ATP levels were measured using CellTiter-Glo® Luminescent Cell Viability Assay (2D). For ATP activity, combined treatments were significantly different to control (P≤0.001). Combined treatment of ML385 with Doxorubicin and RSL3 (P≤0.001) when compared to ML385 alone show a potent effect however since the combination of RSL3 and Doxorubicin proved toxic (Figure 4.9), this may be a potent additive effect (Figure 4.29).

Figure 4.28: Combination treatment of ML385 +/- Doxorubicin in MCF-7 cells
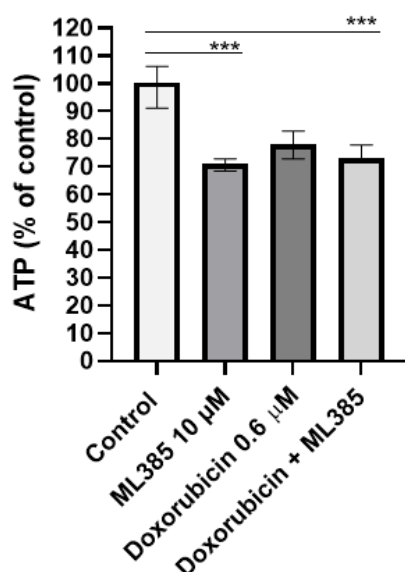
Figure 4.28: ATP level (% of control) assessed by CellTiter-Glo® Luminescent Cell Viability Assay after treating MCF-7 cells for 48 hours with ML385 (10 μM) with control (0.2% (v/v) DMSO) +/- Doxorubicin (0.6 μM). Data is presented as median ± range from n=3 independent experiments each with 3 technical repeats. The statistical significance was determined by comparison with the control and ML385, analysed by a Kruskal-Wallis followed by Dunn's multiple comparisons test (*=P≤0.05, **=P≤0.01, and ***=P≤0.001).

Figure 4.29: Combination treatment of ML385 +/- Doxorubicin combined with RSL3 in MDA-MB-231 cells
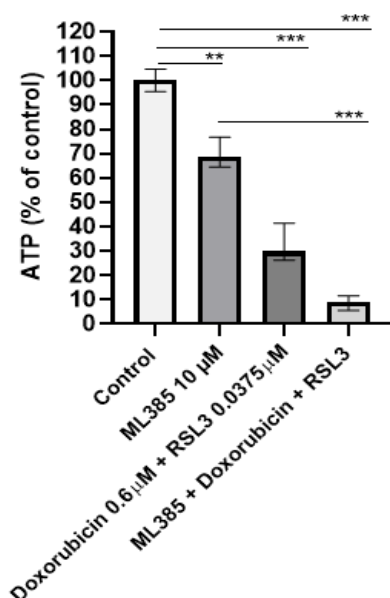
Figure 4.29: ATP level (% of control) assessed by CellTiter-Glo® Luminescent Cell Viability Assay after treating MDA-MB-231 cells for 48 hours with ML385 (10 μM) with control (0.2% (v/v) DMSO) +/- (Doxorubicin (0.6 μM) + RSL3 (0.0375 μM)). Data is presented as median ± range from n=3 independent experiments each with 3 technical repeats. The statistical significance was determined by comparison with the control and ML385, analysed by a Kruskal-Wallis followed by Dunn's multiple comparisons test (*=P≤0.05, **=P≤0.01, and ***=P≤0.001).

4.2.8.6 Effect of combination treatment of Nrf2 inhibitor ML385 +/- Doxorubicin with combination of RSL3 in MCF-7 cells

To assess the effects of ML385, cells were treated with ML385 (10 µM) with Doxorubicin (0.6 µM) combined with ferroptosis inducer RSL3 (10 µM) for 48 hours. To assess cell activity, ATP levels were measured using CellTiter-Glo® Luminescent Cell Viability Assay (2D).

For ATP activity, combined treatments were significantly different to control (P≤0.001). Combined treatment of ML385 with Doxorubicin and RSL3 (P≤0.01) when compared to ML385 show a significant difference but majority of the effect is due to the combined treatment of Doxorubicin and RSL3 and no additional effect is observed by the addition of ML385 (Figure 4.30).

4.2.9 Effect of the Nrf2 inhibitor on chemotherapy responses in breast cancer 3D spheroid alginate cells

To assess the effects of ML385, cells were treated with ML385 (10 µM) with ferroptosis inducer RSL3 only, because it was the only ferroptosis inducer that shows an effect with both 2D and 3D cell culture modules (Chapter 3). Again, cells were treated with Doxorubicin alone, then ML385 effect was assessed with the combination of both Doxorubicin and RSL3 combination. This was done for both MDA-MB-231 and MCF-7 3D alginate spheroids.

4.2.9.1 Effect of combination treatment of Nrf2 inhibitor ML385 +/- RSL3 in MDA-MB-231 3D alginate spheroids

To assess the ML385 effect on MDA-MB-231, cells were treated with ML385 (10 µM) with ferroptosis inducer RSL3 (0.075 µM) for 48 hours. To assess cell activity, ATP levels were measured using Cell Titer-Glo® 3D Cell Viability Assay.

For ATP activity, combined treatments were significantly different to control (P≤0.001), but ML385 alone when compared to control was not significant. Combined treatment of ML385 with RSL3 (P≤0.001) when compared to ML385 alone show a synergistic effect (Figure 4.31) in that ML385 alone showed no activity, whereas it enhanced the effects of RSL3.

Figure 4.30: Combination treatment of ML385 +/- Doxorubicin combined with RSL3 in MCF-7 cells
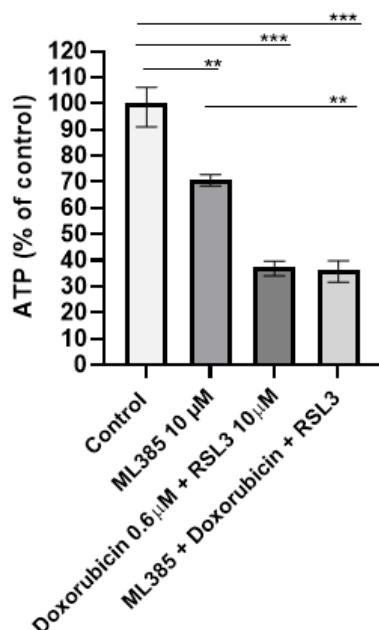
Figure 4.30: ATP level (% of control) assessed by CellTiter-Glo® Luminescent Cell Viability Assay after treating MCF-7 cells for 48 hours with ML385 (10 μM) with control (0.2% (v/v) DMSO) +/- (Doxorubicin (0.6 μM) + RSL3 (10 μM)). Data is presented as median ± range from n=3 independent experiments each with 3 technical repeats. The statistical significance was determined by comparison with the control and ML385, analysed by a Kruskal-Wallis followed by Dunn's multiple comparisons test (*=P≤0.05, **=P≤0.01, and ***=P≤0.001).

Figure 4.31: Combination treatment of ML385 +/- RSL3 in MDA-MB-231 3D spheroid alginate
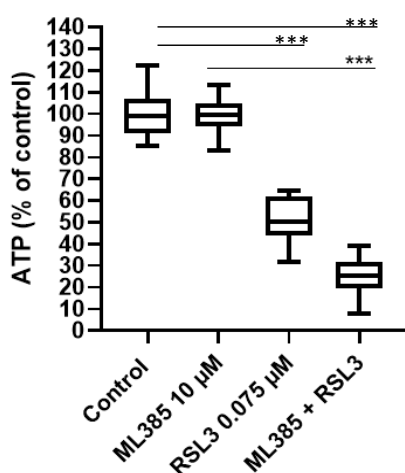
Figure 4.31: ATP level (% of control) assessed by Cell Titer-Glo® 3D Cell Viability Assay after treating MDA-MB-231 spheroids for 48 hours with ML385 (10 μM) with control (0.2% (v/v) DMSO) +/- RSL3 (0.075 μM). Data is presented as median ± interquartile range from n=3 independent experiments each with ≥4 technical repeats. The statistical significance was determined by comparison with control and ML385, analysed by a Kruskal-Wallis followed by Dunn's multiple comparisons test (*=P≤0.05, **=P≤0.01, and ***=P≤0.001).

4.2.9.2 Effect of combination treatment of Nrf2 inhibitor ML385 +/- RSL3 in MCF-7 3D spheroid alginate

To assess ML385 effects, cells were treated with ML385 (10 µM) with ferroptosis inducer RSL3 (10 µM) for 48 hours. To assess cell activity, ATP levels were measured using Cell Titer-Glo® 3D Cell Viability Assay. For ATP activity, combined treatments were significantly different to control ($P \leq 0.001$). Combined treatment of ML385 with RSL3 when compared to RSL3 alone were not significantly different to each other so majority of cell death in combination is due to RSL3, and there was no enhancement in the ferroptotic effect (Figure 4.32).

4.2.9.3 Effect of combination treatment of Nrf2 inhibitor ML385 +/- Doxorubicin in MDA-MB-231 3D spheroid alginate

To assess the ML385 effect on chemotherapy responses, cells were treated with ML385 (10 µM) with ferroptosis inducer Doxorubicin (2.5 µM) for 48 hours. To assess cell activity, ATP levels were measured using Cell Titer-Glo® 3D Cell Viability Assay. For ATP activity, combined treatments were significantly different to control ($P \leq 0.001$), but ML385 alone when compared to control was not significant. Combined treatment of ML385 with Doxorubicin ($P \leq 0.001$) when compared to ML385 alone was significant, but the majority of effect is due to Doxorubicin (Figure 4.33), and combination treatment was no different to Doxorubicin alone.

Figure 4.32: Combination treatment of ML385 +/- RSL3 in MCF-7 3D spheroid alginate
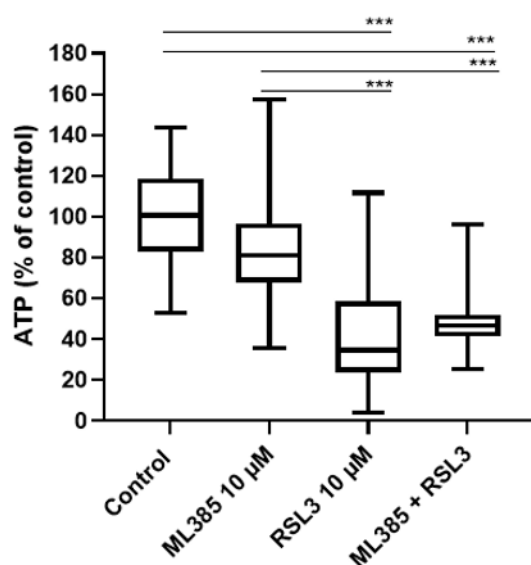
Figure 4.32: ATP level (% of control) assessed by Cell Titer-Glo® 3D Cell Viability Assay after treating MCF-7 spheroids for 48 hours with ML385 (10 µM) with control (0.2% (v/v) DMSO) +/- RSL3 (10 µM). Data is presented as median ± interquartile range from n=3 independent experiments each with ≥4 technical repeats. The statistical significance was determined by comparison with control and ML385, analysed by a Kruskal-Wallis followed by Dunn's multiple comparisons test (*=P≤0.05, **=P≤0.01, and ***=P≤0.001).

Figure 4.33: Combination treatment of ML385 +/- Doxorubicin in MDA-MB-231 3D spheroid alginate
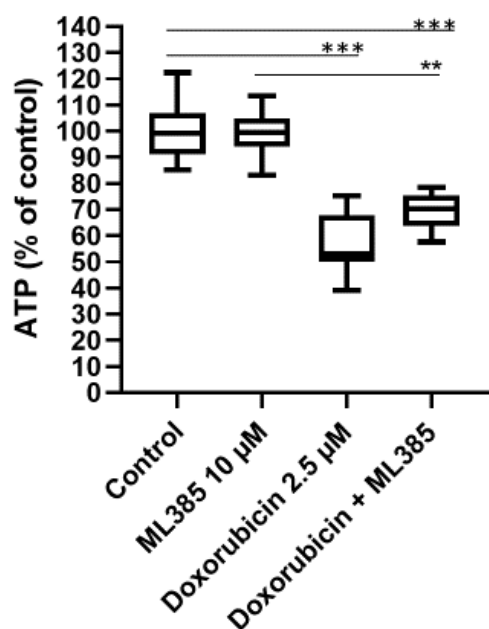
Figure 4.33: ATP level (% of control) assessed by Cell Titer-Glo® 3D Cell Viability Assay after treating MDA-MB-231 spheroids for 48 hours with ML385 (10 µM) with control (0.2% (v/v) DMSO) +/- Doxorubicin (2.5 µM). Data is presented as median ± interquartile range from n=3 independent experiments each with ≥4 technical repeats. The statistical significance was determined by comparison with the control and ML385, analysed by a Kruskal-Wallis followed by Dunn's multiple comparisons test (*=P≤0.05, **=P≤0.01, and ***=P≤0.001).

4.2.9.4 Effect of combination treatment of Nrf2 inhibitor ML385 +/- Doxorubicin in MCF-7 3D spheroid alginate

To assess ML385 effects on chemotherapy responses in MCF-7, cells were treated with ML385 (10 µM) with ferroptosis inducer Doxorubicin (10 µM) for 48 hours. To assess cell activity, ATP levels were measured using Cell Titer-Glo® 3D Cell Viability Assay. For ATP activity, combined treatments were significantly different to control ($P \leq 0.001$). Combined treatment of ML385 with Doxorubicin when compared to Doxorubicin alone were not significantly different to each other so majority of cell death in combination is due to Doxorubicin, and there was no enhancement in the chemotherapy effect (Figure 4.34).

4.2.9.5 Effect of combination treatment of Nrf2 inhibitor ML385 +/- Doxorubicin with combination of RSL3 in MDA-MB-231 in the 3D spheroid alginate model

To assess ML385 effects on RSL3 combined with Doxorubicin and to determine whether Nrf2 specifically might mimic the observed effects in 3D cell culture, cells were treated with ML385 (10 µM) with Doxorubicin (2.5 µM) combined with ferroptosis inducer RSL3 (0.075 µM) for 48 hours. To assess cell activity ATP levels were measured using Cell Titer-Glo® 3D Cell Viability Assay. For ATP activity, combined treatments were significantly different to control ($P \leq 0.001$). However, ML385 alone when compared to control was not significant and unchanged. Combined treatment of ML385 with Doxorubicin and RSL3 ($P \leq 0.001$) when compared Doxorubicin and RSL3 show a synergistic effect, in that ML385 had no effect alone, but enhanced the effects of RSL3 combined with Doxorubicin (Figure 4.35).

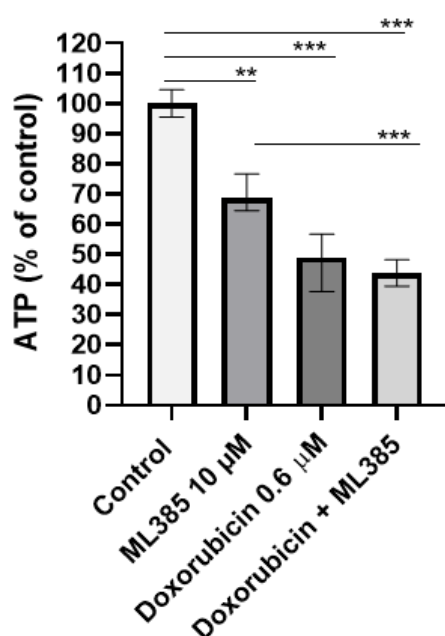**Figure 4.34: Combination treatment of ML385 +/- Doxorubicin in MCF-7 3D spheroid alginate**
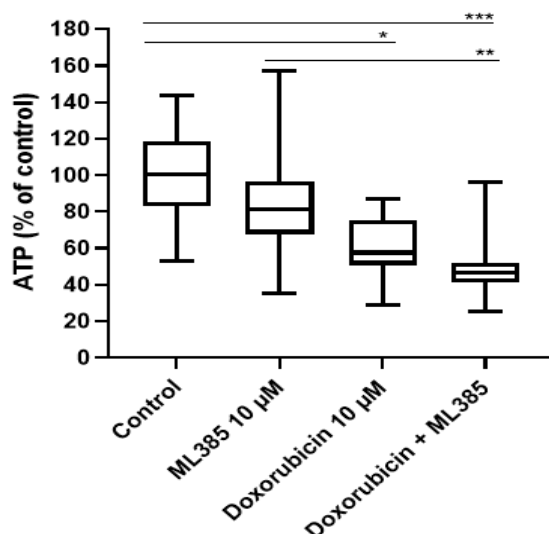
Figure 4.34: ATP level (% of control) assessed by Cell Titer-Glo® 3D Cell Viability Assay after treating MCF-7 spheroids for 48 hours with ML385 (10 µM) with control (0.2% (v/v) DMSO) +/- Doxorubicin (10 µM). Data is presented as median ± interquartile range from n=3 independent experiments each with ≥4 technical repeats. The statistical significance was determined by comparison with the control and ML385, analysed by a Kruskal-Wallis followed by Dunn's multiple comparisons test (*=P≤0.05, **=P≤0.01, and ***=P≤0.001).

Figure 4.35: Combination treatment of ML385 +/- Doxorubicin combined with RSL3 in MDA-MB-231 3D spheroid alginate
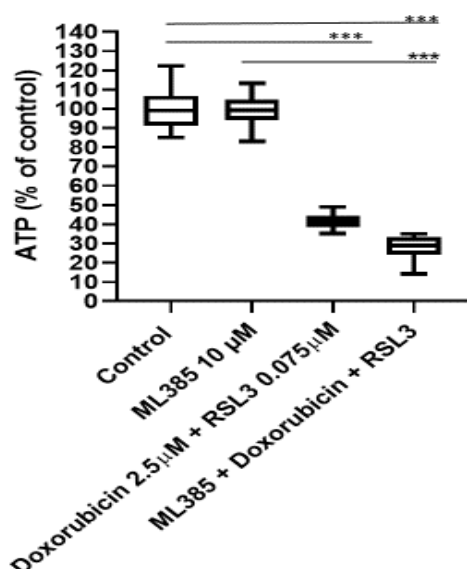
Figure 4.35: ATP level (% of control) assessed by Cell Titer-Glo® 3D Cell Viability Assay after treating MDA-MB-231 spheroids for 48 hours with ML385 (10 µM) with control (0.2% (v/v) DMSO) +/- (Doxorubicin (2.5 µM) + RSL3 (0.075 µM)). Data is presented as median ± interquartile range from n=3 independent experiments each with ≥4 technical repeats. The statistical significance was determined by comparison with the control and ML385, analysed by a Kruskal-Wallis followed by Dunn's multiple comparisons test (*=P≤0.05, **=P≤0.01, and ***=P≤0.001).

4.2.9.6 Effect of combination treatment of Nrf2 inhibitor ML385 +/- Doxorubicin with combination of RSL3 in MCF-7 3D spheroid alginate

To assess ML385 effect on RSL3 + Doxorubicin and to determine whether Nrf2 specifically might mimic the observed effects in 3D cell culture, cells were treated with ML385 (10 μM) with Doxorubicin (10 μM) combined with ferroptosis inducer RSL3 (10 μM) for 48 hours. To assess cell activity ATP levels were measured using Cell Titer-Glo® 3D Cell Viability Assay. For ATP activity, combined treatments were significantly different to control ($P \leq 0.001$), but ML385 alone when compared to control was not significant. Combined treatment of ML385 with Doxorubicin and RSL3 ($P \leq 0.01$) when compared to ML385 show a significant difference but majority of the effect is due to the combined treatment of Doxorubicin and RSL3, with triple-treatment being identical to RSL3 + Doxorubicin (Figure 4.36).

Figure 4.36: Combination treatment of ML385 +/- Doxorubicin combined with RSL3 in MCF-7 3D spheroid alginate
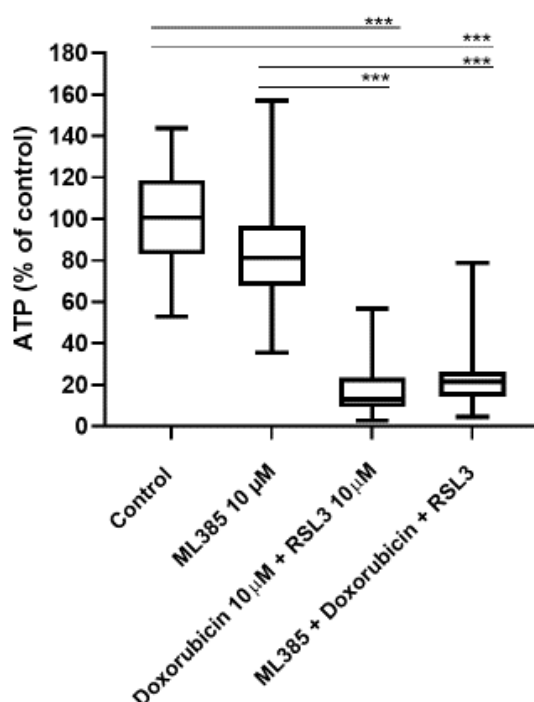
Figure 4.36: ATP level (% of control) assessed by Cell Titer-Glo® 3D Cell Viability Assay after treating MCF-7 spheroids for 48 hours with ML385 (10 μM) with control (0.2% (v/v) DMSO) +/- (Doxorubicin (10 μM) + RSL3 (10 μM)). Data is presented as median ± interquartile range from n=3 independent experiments each with ≥4 technical repeats. The statistical significance was determined by comparison with the control and ML385, analysed by a Kruskal-Wallis followed by Dunn's multiple comparisons test (*=$P \leq 0.05$, **=$P \leq 0.01$, and ***=$P \leq 0.001$).

### 4.2.10 Determination of the IC50 of Cisplatin in breast cancer cells

To assess the effects of Cisplatin treatment on cell survival, total ATP measurements using CellTitre-Glo® were performed as a proxy marker for cell numbers and/or total cellular metabolism in response to drug treatments at different concentration (40, 10, 5, 2.5, and 0.6 µM) with control (0.2% (v/v) DMSO). All treatments were performed in triplicate, in three independent experiments. Half maximal inhibitory concentration (IC50), which measures the effectiveness of Cisplatin, was determined by using non-linear regression of GraphPad Prism software version 8.

4.2.10.1 Effect of Cisplatin on cell viability in MDA-MB-231 cells

Cells were treated with increasing doses of Cisplatin for 48 hours assess its cytotoxicity and identify the IC50, and to identify the lowest dose to induce significant cytotoxicity for combination studies with ferroptosis inducer RSL3 only because it showed the maximum effect in both 2D and 3D cell culture (Chapter 3). The IC50 of Cisplatin after measuring ATP activity of MDA-MB-231 cells was estimated to be 5.2 µM (Figure 4.37). Based on the observed effects of Cisplatin, 5 µM was chosen as the ideal dose for combination experiments, as no effect was observed at 2.5 µM.

4.2.10.2 Effect of Cisplatin on cell viability in MCF-7 cells

Cells were treated with increasing doses of Cisplatin for 48 hours to assess its cytotoxicity and identify the IC50, and identify the lowest dose to induce significant cytotoxicity for combination studies with ferroptosis inducer RSL3 only because it show the maximum effect in both 2D and 3D cell culture (Chapter 3). The IC50 of Cisplatin after measuring ATP activity of MCF-7 cells was estimated to be 3.6 µM (Figure 4.38). Based on the observed effects of Cisplatin, 2.5 µM was chosen as the ideal dose for combination experiments.

Figure 4.37: Effect of Cisplatin on ATP levels in MDA-MB-231 cells
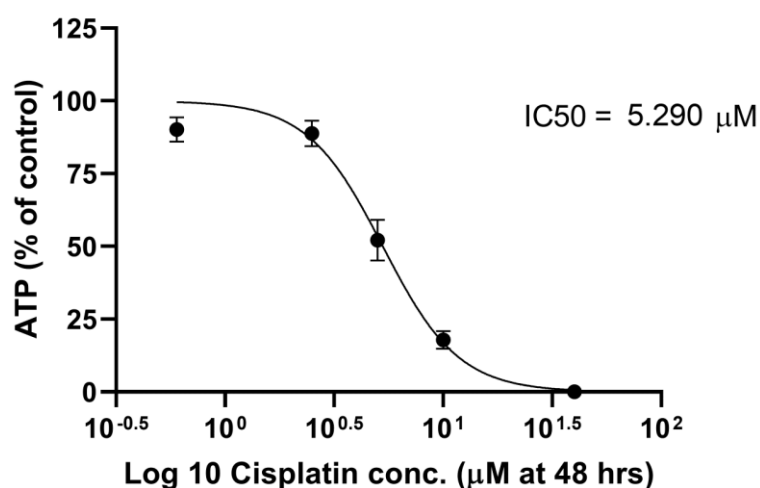
Figure 4.37: ATP level (% of control) was assessed by CellTiter-Glo® Luminescent cell viability assay after treating MDA-MB-231 cells for 48 hours with Cisplatin (40, 10, 5, 2.5, and 0.6 µM). Data is expressed as ATP levels normalised to control based on 3 replicate wells from n=3 independent experiments. IC50 was determined by using non-linear regression of GraphPad Prism software version 8. Data are presented as the mean ± SEM.

Figure 4.38: Effect of Cisplatin on ATP levels in MCF-7 cells
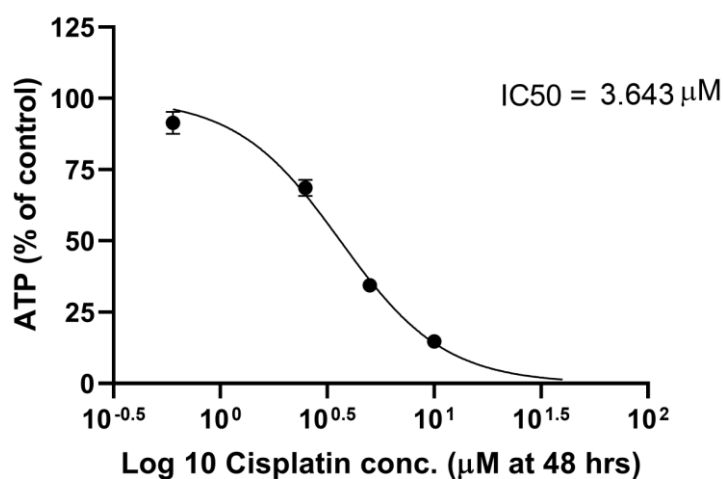
Figure 4.38: ATP level (% of control) was assessed by CellTiter-Glo® Luminescent cell viability assay after treating MCF-7 cells for 48 hours with Cisplatin (40, 10, 5, 2.5, and 0.6 µM). Data is expressed as ATP levels normalised to control based on 3 replicate wells from n=3 independent experiments. IC50 was determined by using non-linear regression of GraphPad Prism software version 8. Data are presented as the mean ± SEM.

4.2.11 Determination of the IC50 of Cisplatin in breast cancer 3D alginate spheroids

To assess the effects of Cisplatin treatment on cell survival in 3D alginate spheroids, total ATP measurements using CellTitre-Glo® 3D cell viability assay were performed as a proxy marker for cell numbers and/or total cellular metabolism in response to drug treatment at different concentration (40, 10, 2.5, and 0.6 µM) with control (0.2% (v/v) DMSO) for 48 hours and 72 hours. All treatments were performed in triplicate, in three independent experiments. Half maximal inhibitory concentration (IC50), which measures the effectiveness of Cisplatin, was determined by using non-linear regression of GraphPad Prism software version 8.

4.2.11.1 Effect of Cisplatin on MDA-MB-231 3D alginate spheroids using CellTiter-Glo® 3D Cell Viability Assay (3D)

The IC50 of Cisplatin after measuring ATP activity of MDA-MB-231 3D alginate spheres were estimated to be 7.0 µM after 48 hours and 8.0 µM after 72 hours. (Figure 4.39). Based on these observations, 5 µM was chosen as the optimal dose for combination studies with the ferroptosis inducer RSL3.

4.2.11.2 Effect of Cisplatin on MCF-7 3D alginate spheroids using CellTiter-Glo® 3D Cell Viability Assay (3D)

The IC50 of Cisplatin after measuring ATP activity of MCF-7 3D alginate spheres were estimated to be 9.9 µM after 48 hours and 5.9 µM after 72 hours. (Figure 4.4). Based in these observations, 5 µM was chosen as the optimal dose for combination studies with the ferroptosis inducer RSL3.

4.2.12 MDA-MB-231 and MCF-7 cells treated with Cisplatin and ferroptosis inducer RSL3

To assess the effects of combination treatment, cells were treated with Cisplatin at the doses identified in optimisation studies with the ferroptosis inducer RSL3. MDA-MB-231 cells were treated with Cisplatin at concentration of 5 µM with ferroptosis inducer RSL3 at concentration 0.0375 µM, with control (0.2% (v/v) DMSO). MCF-7 cells were treated with Cisplatin at concentration of 2.5 µM with ferroptosis inducer RSL3 at concentration of 10 µM, with control (0.2% (v/v) DMSO) for 48 hours. After treatments, ATP

measurements were performed using the CellTiter-Glo® Luminescent Cell Viability Assay. All treatments were performed in triplicate, in three independent experiments.

4.2.12.1 Effect of Cisplatin in the presence of ferroptosis inducer RSL3 in MDA-MB231 cells on ATP levels

Consistent with optimization studies, 5 µM Cisplatin significantly reduced ATP levels after 48 hours as well as RSL3 when compared to control (P≤0.001). RSL3 combination with Cisplatin shows a potential synergistic interaction with Cisplatin (P≤0.001). Combination treatment was significantly lower than control (P≤0.001), and significantly different to Cisplatin alone, (Figure 4.41).

Figure 4.39: Effect of Cisplatin on ATP level of 3D alginate MDA-MB-231 cells
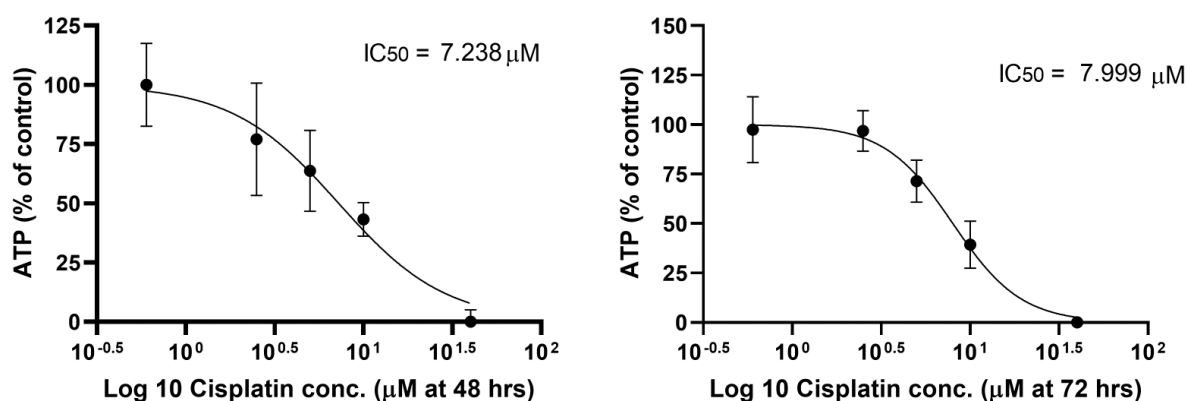
Figure 4.39: Effect of Cisplatin on ATP level (% of control) using Cell Titer-Glo® 3D Cell Viability after treating 3D MDA-MB-231 alginate spheroids (1 alginate sphere/well, 4 replicate spheroids) for 48 and 72 hours with Cisplatin (40, 10, 2.5, and 0.6 µM). Data is expressed as ATP levels normalised to control from n=3 independent experiments. IC50 was determined by using non-linear regression of GraphPad Prism software version 8. Data are presented as the mean ± SEM.

Figure 4.40: Effect of Cisplatin on ATP level of 3D alginate MCF-7 cells
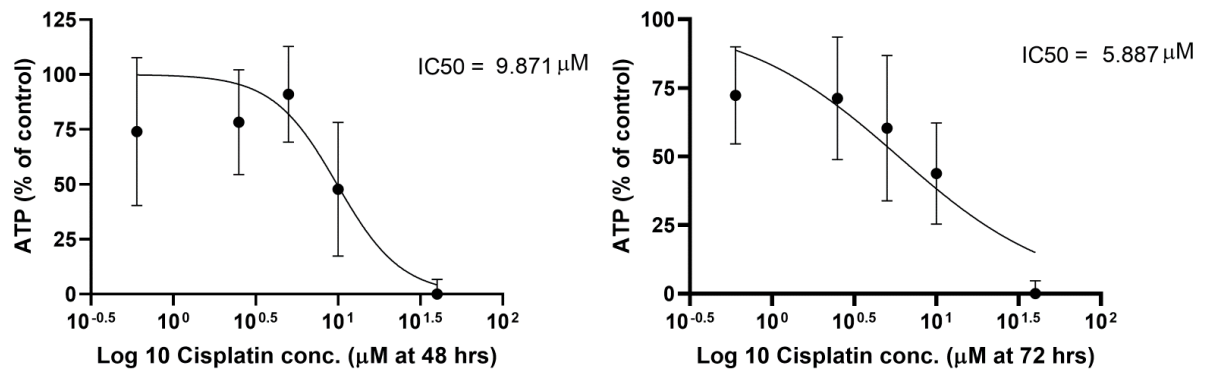
Figure 4.40: Effect of Cisplatin on ATP level (% of control) using Cell Titer-Glo® 3D Cell Viability after treating 3D MCF-7 alginate spheroids (1 alginate sphere/well, 4 replicate spheroids) for 48 and 72 hours with Cisplatin (40, 10, 2.5, and 0.6 µM) Data is expressed as ATP levels normalised to control from n=3 independent experiments. IC50 was determined by using non-linear regression of GraphPad Prism software version 8. Data are presented as the mean ± SEM.

Figure 4.41: Effect of Cisplatin and RSL3 on MDA-MB-231 cells
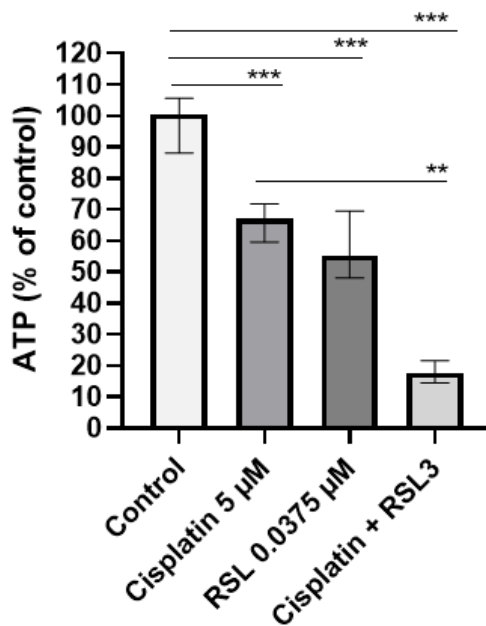
Figure 4.41: ATP level (% of control) assessed by CellTiter-Glo® Luminescent Cell Viability Assay after treating MDA-MB-231 cells for 48 hours with ferroptosis inducer RSL3 (0.0375 µM) and Cisplatin (5 µM), with control (0.2% (v/v) DMSO). Data is presented as median ± range from n=3 independent experiments each with 3 technical repeats. The statistical significance was determined by comparison with the control and Cisplatin, analysed by a Kruskal-Wallis followed by Dunn's multiple comparisons test (*=P≤0.05, **=P≤0.01, and ***=P≤0.001).

4.2.12.2 Effect of Cisplatin in the presence of ferroptosis inducer RSL3 in MCF-7 cells on ATP levels

Consistent with optimization studies, 2,5 μM Cisplatin significantly reduced ATP levels after 48 hours. RSL3 reduced cell viability, but combination with Cisplatin did not show any synergistic interaction with Cisplatin although there was a significant difference from Cisplatin ($P \leq 0.05$) but not a level that is synergistic effect, showing an additive effect is seen and no enhancement of Cisplatin-mediated effects seen with RSL3 (Figure 4.42).

4.2.13 MDA-MB-231 and MCF-7 3D alginate spheroids treated with Cisplatin and ferroptosis inducer RSL3

To assess the effects of combination treatment, MDA-MB-231 spheroid cells were treated with Cisplatin at concentration of 5 μM with ferroptosis inducer RSL3 0.075 μM, with control (0.2% (v/v) DMSO). MCF-7 spheroid cells were treated with Cisplatin at concentration of 5 μM with ferroptosis inducers RSL3 at concentration of 10 μM, with control (0.2% (v/v) DMSO) for 48 hours. After treatments, ATP measurements were performed using the CellTiter-Glo® 3D Cell Viability Assay. All treatments were performed in triplicate, in three independent experiments.

4.2.13.1 Effect of Cisplatin in the presence of ferroptosis inducer RSL3 in MDA-MB231 3D alginate spheroids on ATP levels

Consistent with optimization studies, 5 μM Cisplatin do not reduced ATP levels after 48 hours in 3D alginate spheroids, RSL3 significantly reduced ATP levels when compared to control ($P \leq 0.001$), combined treatment when compared to Cisplatin alone significantly reduce ATP levels ($P \leq 0.001$), but the majority of effect is due to RSL3. Since RSL3 and RSL3 + Cisplatin effects are identical, this means that the ferroptosis inducer RSL3 does not enhance the chemotherapy effect of Cisplatin in MDA-MB-231 3D alginate spheroids (Figure 4.43).

Figure 4.42: Effect of Cisplatin and RSL3 on MCF-7 cells
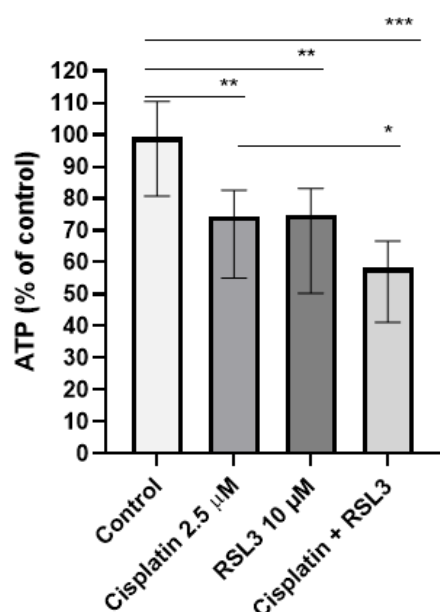
Figure 4.42: ATP level (% of control) assessed by CellTiter-Glo® Luminescent Cell Viability Assay after treating MCF-7 cells for 48 hours with ferroptosis inducer RSL3 (10 µM) and Cisplatin (2.5 µM), with control (0.2% (v/v) DMSO). Data is presented as median ± range from n=3 independent experiments each with 3 technical repeats. The statistical significance was determined by comparison with the control and Cisplatin, analysed by a Kruskal-Wallis followed by Dunn's multiple comparisons test (*=P≤0.05, **=P≤0.01, and ***=P≤0.001).

## Figure 4.43: Effect of Cisplatin and RSL3 on MDA-MB-231 spheroids
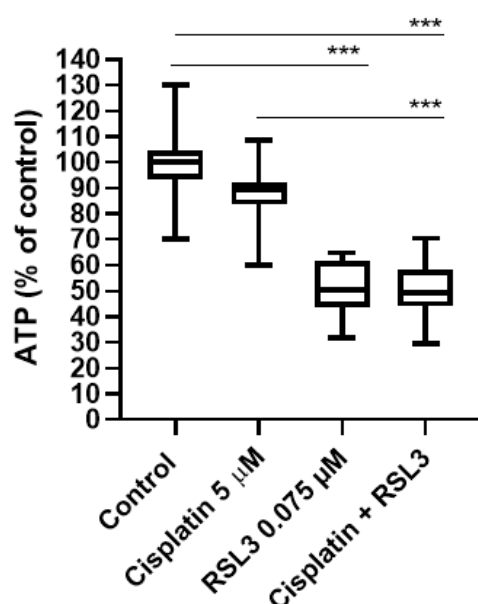
Figure 4.43: ATP level (% of control) assessed by CellTiter-Glo® Luminescent Cell Viability Assay after treating MDA-MB-231 spheroids for 48 hours with ferroptosis inducer RSL3 (0.075 µM) and Cisplatin (5 µM), with control (0.2% (v/v) DMSO). Data is presented as median ± interquartile range from n=3 independent experiments each with ≥4 technical repeats. The statistical significance was determined by comparison with the control and Cisplatin, analysed by a Kruskal-Wallis followed by Dunn's multiple comparisons test (*=P≤0.05, **=P≤0.01, and ***=P≤0.001).

4.2.13.2 Effect of Cisplatin in the presence of ferroptosis inducer RSL3 in MCF-7 3D alginate spheroids on ATP levels

Cisplatin did not reduce ATP levels after 48 hours in MCF-7 3D alginate spheroids, RSL3 significantly reduced ATP levels when compared to control ($P \leq 0.001$), combined treatment when compared to Cisplatin alone show no significant difference in the ATP level. This means that the ferroptosis inducer RSL3 does not enhance the chemotherapy effect of Cisplatin in MCF-7 3D alginate spheroids (Figure 4.44).

4.2.14 Determination of the IC50 of Paclitaxel in breast cancer cells

To assess the effects of Paclitaxel treatment on cell survival, total ATP measurements using CellTitre-Glo® were performed as a proxy marker for cell numbers and/or total cellular metabolism in response to drug treatments at different concentration (5, 2.5, 0.6, 0.15 and 0.075 μM) with control (0.2% (v/v) DMSO). All treatments were performed in triplicate, in three independent experiments.

4.2.14.1 Effect of Paclitaxel on cell viability in MDA-MB-231 cells

Cells were treated with increasing doses of Paclitaxel for 48 hours to assess its cytotoxicity and identify the IC50 and detect the lowest dose to induce significant cytotoxicity for combination studies. The IC50 of Paclitaxel after measuring ATP activity of MDA-MB-231 cells cannot be detected (Figure 4.45). Due to a lack of response and also time constraints, no further work was completed using Paclitaxel in MDA-MB-231 cells.

4.2.14.2 Effect of Paclitaxel on cell viability in MCF-7 cells

Cells were treated with increasing doses of Paclitaxel for 48 hours to assess its cytotoxicity and identify the IC50 and detect the lowest dose to induce significant cytotoxicity for combination studies. The IC50 of Paclitaxel after measuring ATP activity of MCF-7 cells cannot be calculated as ATP levels remained > 50 % of control at all doses (Figure 4.46). Due to a lack of response and also time constraints, no further work was completed using Paclitaxel in MCF-7 cells.

Figure 4.44: Effect of Cisplatin and RSL3 on MCF-7 spheroids
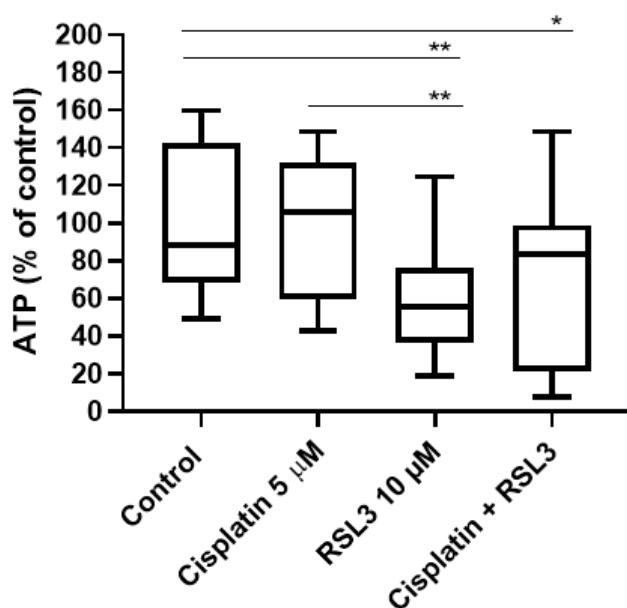
Figure 4.44: ATP level (% of control) assessed by CellTiter-Glo® Luminescent Cell Viability Assay after treating MCF-7 spheroids for 48 hours with ferroptosis inducer RSL3 (10 µM) and Cisplatin (5 µM), with control (0.2% (v/v) DMSO). Data is presented as median ± interquartile range from n=3 independent experiments each with ≥4 technical repeats. The statistical significance was determined by comparison with the control and Cisplatin, analysed by a Kruskal-Wallis followed by Dunn's multiple comparisons test (*=P≤0.05, **=P≤0.01, and ***=P≤0.001).

Figure 4.45: Effect of Paclitaxel on ATP levels in MDA-MB-231 cells
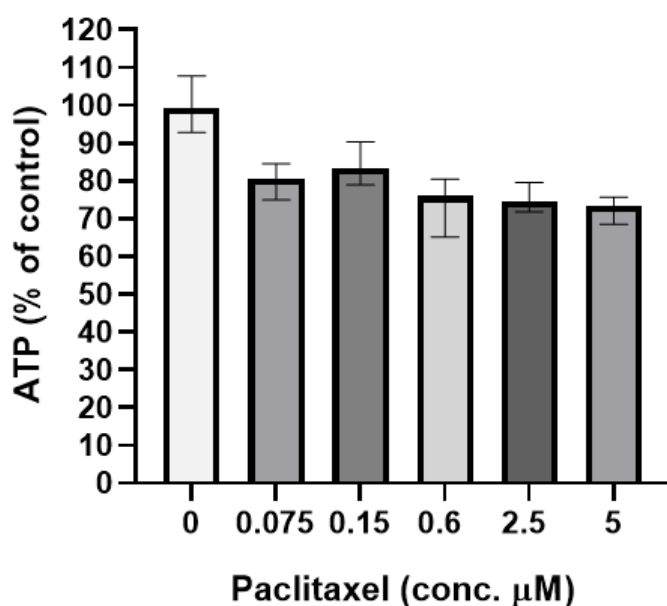
Figure 4.45: ATP level (% of control) was assessed by CellTiter-Glo® Luminescent cell viability assay after treating MDA-MB-231 cells for 48 hours with Paclitaxel (5, 2.5, 0.6, 0.15 and 0.075 µM). Data is expressed as ATP levels normalised to control based on 3 replicate wells from n=3 independent experiments.

Figure 4.46: Effect of Paclitaxel on ATP levels in MCF-7 cells
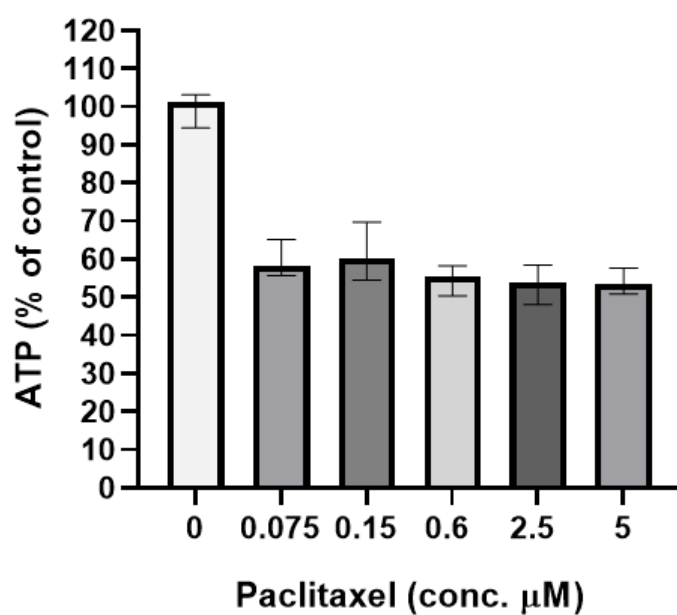
Figure 4.46: ATP level (% of control) was assessed by CellTiter-Glo® Luminescent cell viability assay after treating MCF-7 cells for 48 hours with Paclitaxel (5, 2.5, 0.6, 0.15 and 0.075 µM). Data is expressed as ATP levels normalised to control based on 3 replicate wells from n=3 independent experiments.

4.2.15 Determination of GSH (Glutathione) /GSSG (Glutathione disulfide) ratio in breast cancer cells with combination treatments of chemotherapy, RSL3 and ML385

The GSH/GSSG-Glo™ Assay was used to measure total glutathione (GSH+GSSG), and both oxidized (GSSG) and reduced (GSH) in living cells, after finding the synergistic effect between the effective doses of treatments of chemotherapies Doxorubicin and Cisplatin as well as the Nrf2 inhibitor ML385 with ferroptosis inducer RSL3. MDA-MB-231 cells were treated with ML385 (10 µM), Cisplatin (5 µM) and Ferroptosis inducer RSL3 (0.0375 µM) for 48 hours. 2D MCF-7 cells were treated with Doxorubicin (0.6 µM) and Ferroptosis inducer RSL3 (10 µM) for 48 hours.

4.2.15.1 Determination of GSH (Glutathione) /GSSG (Glutathione disulfide) ratio in MDA-MB-231 cells with combined studies

The GSH/GSSG ratio in untreated cells was approximately 27, reducing significantly with Cisplatin, consistent with glutathione depletion by Cisplatin. Although RSL3 reduced the ratio, combination of Cisplatin and RSL3 were no different to Cisplatin alone suggesting no enhancement of GSH depletion with RSL3 in MDA-MB-231 cells (Figure 4.47).

Combination of RSL3 with ML385 showed an additive effect in terms of decrease in the GSH/GSSG ratio, although individual treatments significantly reduced the ratio (P≤0.001) (Figure 4.48).

4.2.15.2 Determination of GSH (Glutathione) /GSSG (Glutathione disulfide) ratio in MCF-7 cells with combined studies

In contrast to observations in MDA-MB-231 cells, the GSH/GSSG ratio was much higher in MCF-7 cells, suggestive of higher free Glutathione. In response to treatment with RSL3 or Cisplatin, the GSH/GSSG ratio inexplicably increased further, showing an additive effect (P≤0.001) (Figure 4.49). It was anticipated that GSH levels would decrease, thus decreasing the GSH/GSSG ratio.

Figure 4.47: GSH (Glutathione) /GSSG (Glutathione disulfide) ratio in MDA-MB-231 cells after treatment with Cisplatin and RSL3
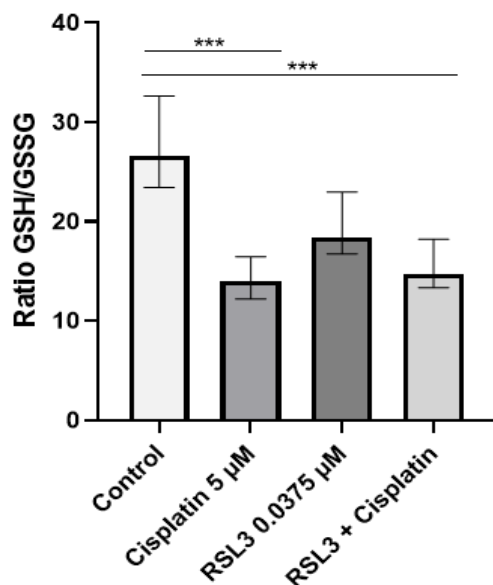
Figure 4.47: The reduced glutathione (GSH)/oxidized glutathione (GSSG) ratio was measured after treating MDA-MB-231 cells for 48 hours with Cisplatin (5 µM) and Ferroptosis inducer RSL3 (0.0375 µM). Data is presented as median ± range from n=3 independent experiments each with 4 technical repeats. The statistical significance was determined by comparison with the control, analysed by a Kruskal-Wallis followed by Dunn's multiple comparisons test (*=P≤0.05, **=P≤0.01, and ***=P≤0.001).

Figure 4.48: GSH (Glutathione) /GSSG (Glutathione disulfide) ratio in MDA-MB-231 cells after treatment with ML385 and RSL3
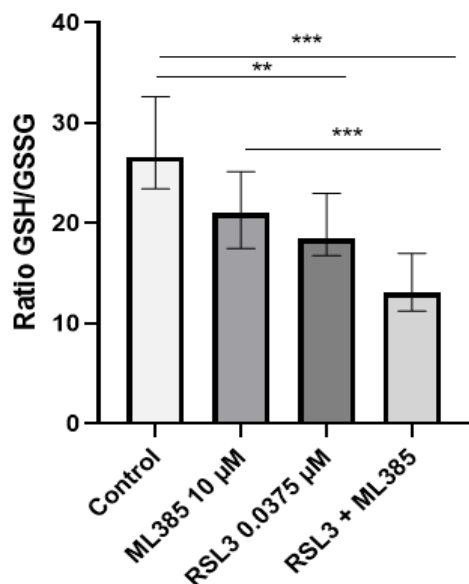
Figure 4.48: The reduced glutathione (GSH)/oxidized glutathione (GSSG) ratio was measured after treating MDA-MB-231 cells for 48 hours with ML385 (10 µM) and Ferroptosis inducer RSL3 (0.0375 µM). Data is presented as median ± range from n=3 independent experiments each with 4 technical repeats. The statistical significance was determined by comparison with the control, analysed by a Kruskal-Wallis followed by Dunn's multiple comparisons test (*=P≤0.05, **=P≤0.01, and ***=P≤0.001).

Figure 4.49: GSH (Glutathione) /GSSG (Glutathione disulfide) ratio in MCF-7 cells after treatment with Doxorubicin and RSL3
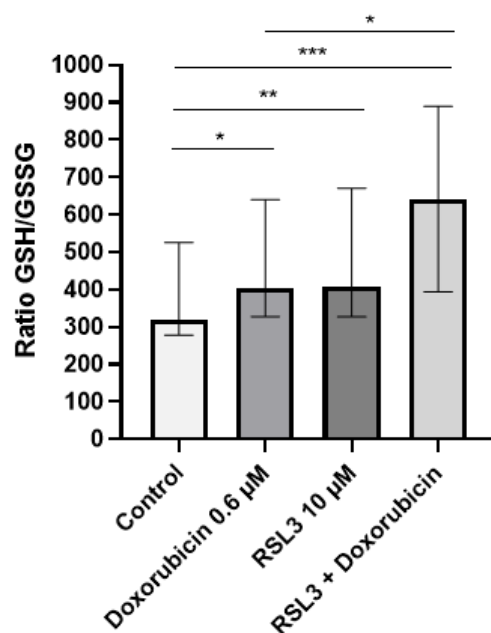
Figure 4.49: The reduced glutathione (GSH)/oxidized glutathione (GSSG) ratio was measured after treating MCF-7 cells for 48 hours with Doxorubicin (0.6 µM) and Ferroptosis inducer RSL3 (10 µM). Data is presented as median ± range from n=3 independent experiments each with 4 technical repeats. The statistical significance was determined by comparison with the control, analysed by a Kruskal-Wallis followed by Dunn's multiple comparisons test (*=P≤0.05, **=P≤0.01, and ***=P≤0.001).

4.2.16 Determination of GSH (Glutathione) /GSSG (Glutathione disulfide) ratio in breast cancer 3D spheroid alginates cells with combined studies

The GSH/GSSG-Glo™ Assay was used to measure total glutathione (GSH + GSSG), and both oxidized (GSSG) and reduced (GSH) in living cells after finding the synergistic effect between the effective doses of treatments of chemotherapies Doxorubicin and Cisplatin as well as the Nrf2 inhibitor ML385 with ferroptosis inducer RSL3. Because there was a variation in GSH/GSSG ratio in 3D alginate spheroids, and the assay was only designed for 2D cell culture, the assay was to measure the total GSH levels alone to compare results to GSH/GSSG ratio. 3D MDA-MB-231 alginate cultures were treated with ML385 (10 µM) Cisplatin (5 µM) and ferroptosis inducer RSL3 (0.075 µM) for 48 hours with control (0.2% (v/v) DMSO). For 3D MCF-7 alginate spheres were treated with Doxorubicin (10 µM), and ferroptosis inducer RSL3 (10 µM).

4.2.16.1 Determination of Total GSH in MDA-MB-231 3D spheroid alginate cells with combined studies

The level of total GSH was not significantly altered by RSL3, but was decreased by Cisplatin, however there was no significant difference between Cisplatin and Cisplatin + RSL3, confirming no interaction or synergy with respect to total GSH levels (Figure 4.50).

The addition of ML385 to RSL3 did significantly and potently decrease GSH levels, however ML385 treatment showed highly variable results. These were not significantly different to control, but some spheres showed almost complete loss of GSH whereas others were unaffected. In dual-treated, all spheroids showed potent loss of GSH (Figure 4.51).

4.2.16.2 Determination of total GSH in MCF-7 3D spheroid alginate cells with combined studies

The level of glutathione was significantly decreased by Doxorubicin alone, whereas RSL3 had a variable response, however combination treatment of RSL3 and Doxorubicin showed a potent decrease in GSH levels ($P \leq 0.001$) (Figure 4.52).

Figure 4.50: Total GSH in MDA-MB-231 3D spheroids after treatment with Cisplatin and RSL3
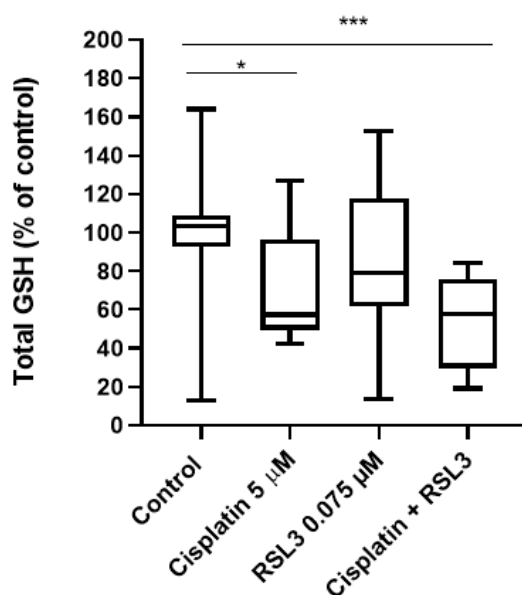
Figure 4.50: Total GSH was measured after treating MDA-MB-231 spheroids for 48 hours with Cisplatin (5 µM) and Ferroptosis inducer RSL3 (0.075 µM). Data is presented as median ± interquartile range from n=3 independent experiments each with 4 technical repeats. The statistical significance was determined by comparison with the control, analysed by a Kruskal-Wallis followed by Dunn's multiple comparisons test (*=P≤0.05, **=P≤0.01, and ***=P≤0.001).

Figure 4.51: Total GSH in MDA-MB-231 3D spheroids after treatment with ML385 and RSL3
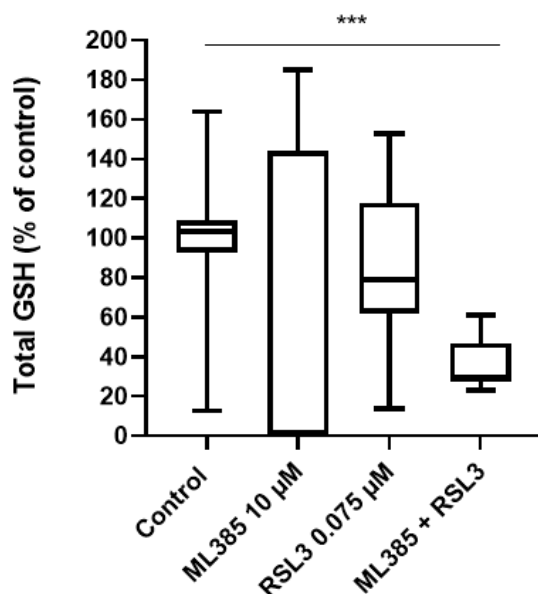
Figure 4.51: Total GSH was measured after treating MDA-MB-231 spheroid for 48 hours with ML385 (10 µM) and Ferroptosis inducer RSL3 (0.075 µM). Data is presented as median ± interquartile range from n=3 independent experiments each with 4 technical repeats. The statistical significance was determined by comparison with the control, analysed by a Kruskal-Wallis followed by Dunn's multiple comparisons test (*=P≤0.05, **=P≤0.01, and ***=P≤0.001).

Figure 4.52: Total GSH in MCF-7 3D spheroids after treatment with Doxorubicin and RSL3
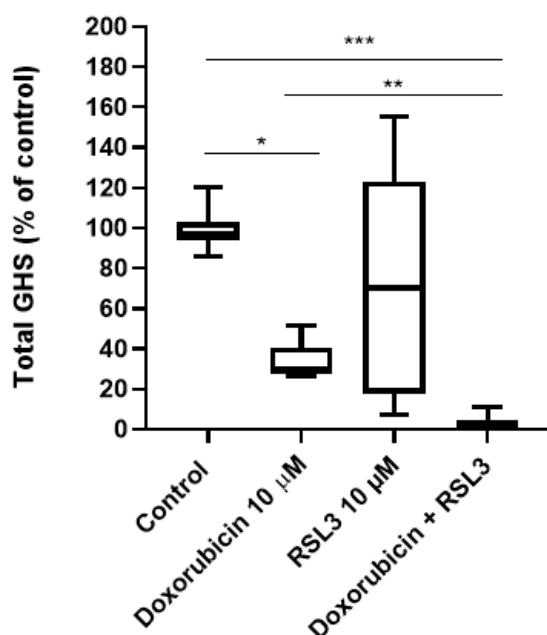
Figure 4.52: Total GSH was measured after treating MCF-7 cells for 48 hours with Doxorubicin (10 µM) and Ferroptosis inducer RSL3 (10 µM). Data is presented as median ± interquartile range from n=3 independent experiments each with 4 technical repeats. The statistical significance was determined by comparison with the control, analysed by a Kruskal-Wallis followed by Dunn's multiple comparisons test (*=P≤0.05, **=P≤0.01, and ***=P≤0.001).

4.2.17 Determination of Intracellular Reactive Oxygen Species in breast cancer cells with combined studies

Since chemotherapy and ferroptosis inducers result in enhanced ROS production, intracellular ROS was detected after drug treatments. Intracellular reactive oxygen species (ROS) were detected by ROS Assay Kit "-Highly Sensitive 2',7'-dichlorofluorescein diacetate (DCFH-DA-)" and assessed by flow cytometry and assessed using drug combinations of Chemotherapy and/or RSL3 and/or ML385 shown to be effective in cytotoxicity assays. For MDA-MB-231, cells were treated with ML385 (10 µM), Cisplatin (5 µM) and Ferroptosis inducer RSL3 (0.0375 µM) for 48 hours. For MCF-7, cells were treated with Doxorubicin (0.6 µM) and Ferroptosis inducer RSL3 (10 µM) for 48 hours.

4.2.17.1 Determination of ROS in MDA-MB-231 cells with combined treatments

ROS production was defined as detection of signal above negative control cells (no DCFH-DA dye added) as defined by the manufacturer's instructions. Compared to untreated cells, Cisplatin and RSL3 both increased ROS production in terms of % positive cells (Figure 4.53 A) with a clear increase in intensity vs control cells visible in representative data (Figure 4.53 A). Although Cisplatin significantly increased ROS detection (P≤0.001), as did RSL3 (P≤0.05) in terms of % of cells positive for ROS, combination of Cisplatin and RSL3 did not further enhance ROS production and the level of ROS was not significant difference between Cisplatin and during combination with RSL3 (Figure 4.53 Ci).

ML385 alone did not significantly increase ROS production in terms of % positivity and neither did combination treatment with RSL3, whereas RSL3 alone significantly increased ROS production (Figure 4.53 Cii), confirming lack of synergistic response.

4.2.17.2 Determination of ROS in MCF-7 cells with combined studies

The level of ROS in control cells (expressed as % positive cells) showed that similarly to MDA-MB-231, the majority of MCF-7 were positive however there was a distinct bimodal population, with a proportion showing very high staining, and another population with low or negative staining. This pattern was observed in all treatment groups, of which only Doxorubicin-alone showed significantly increased ROS (P≤0.01) however Doxorubicin plus RSL3 were indistinguishable from the control. RSL3 alone had no effect on ROS in MCF-7 cells (Figure 4.54 C).

Figure 4.53: ROS level in MDA-MB-231 cells after treatment with Cisplatin and ML385 +/- RSL3

(A)
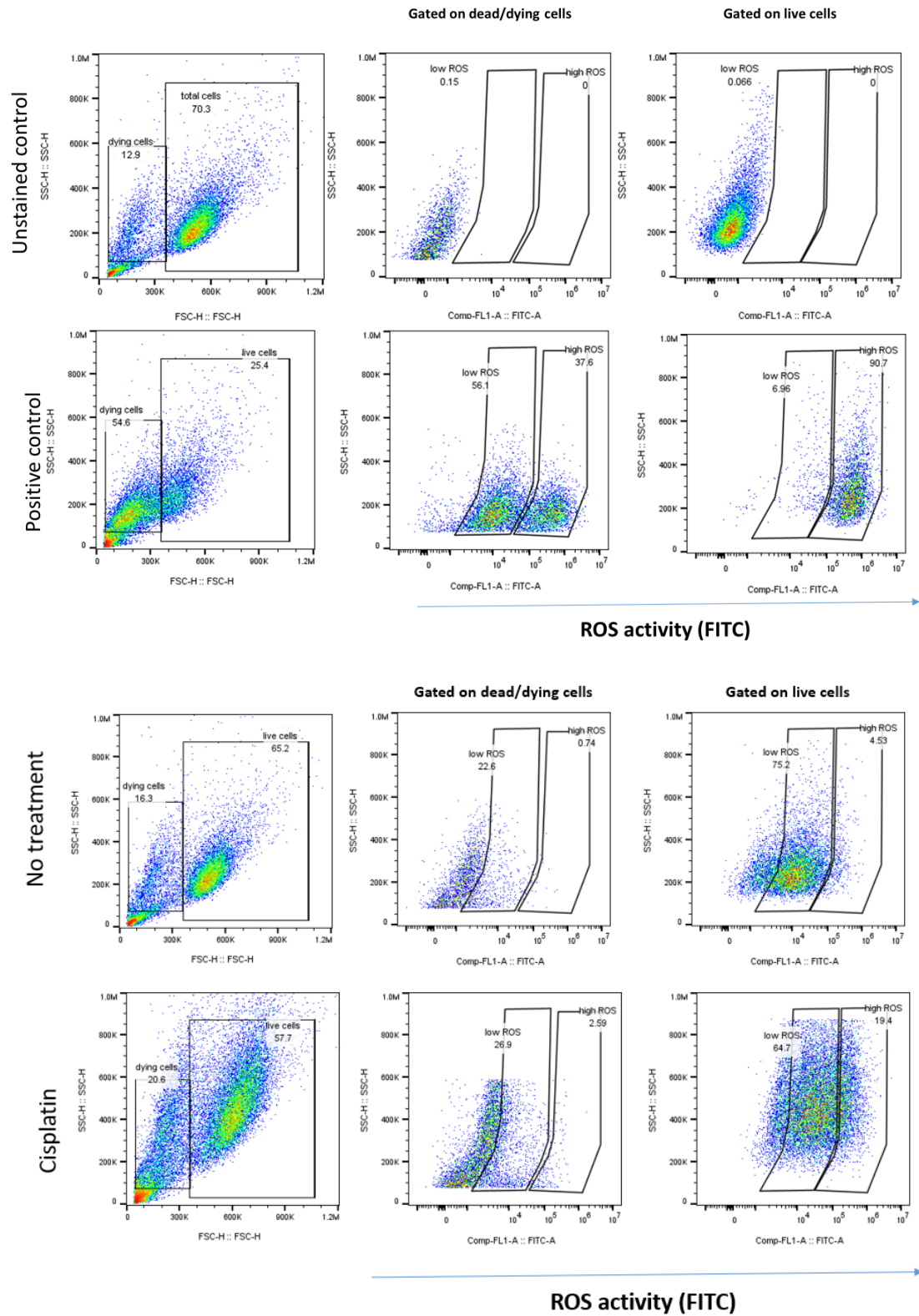
RSL3
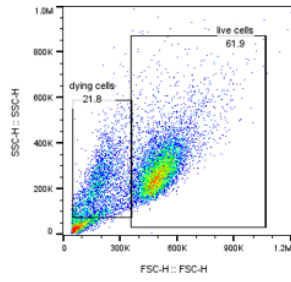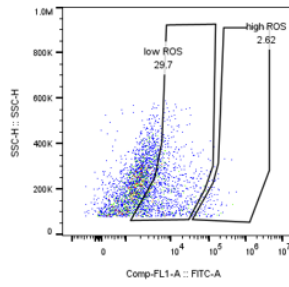
Gated on dead/dying cells   **Gated on live cells**
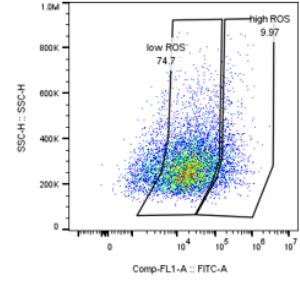
RSL3 + Cisplatin
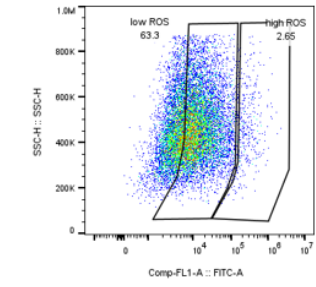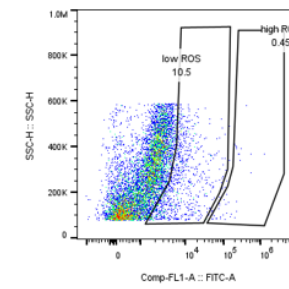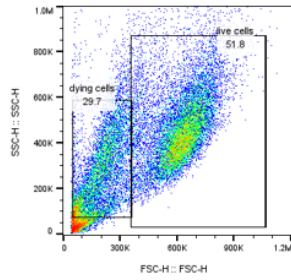
ROS activity (FITC)

ML385
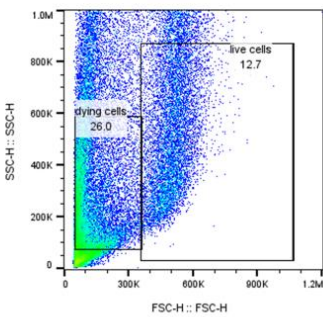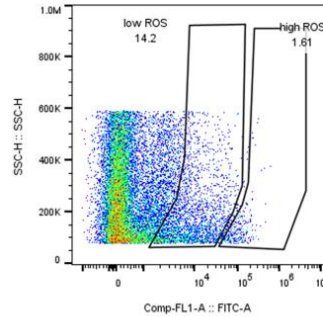
Gated on dead/dying cells   **Gated on live cells**
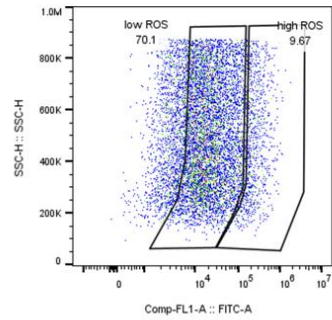
RSL3 + ML385
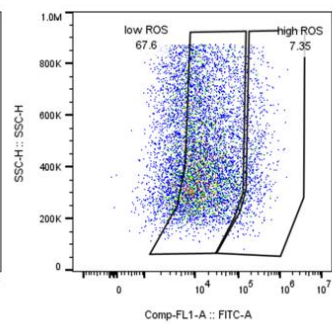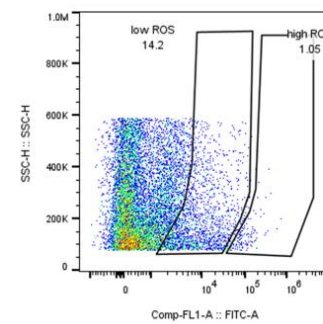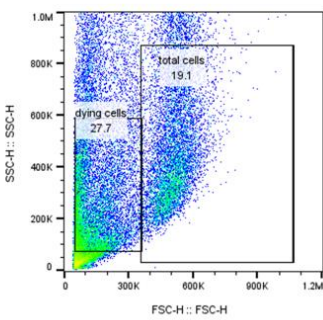
ROS activity (FITC)

(Bi)

(Bii)

(Ci)

(Cii)

188
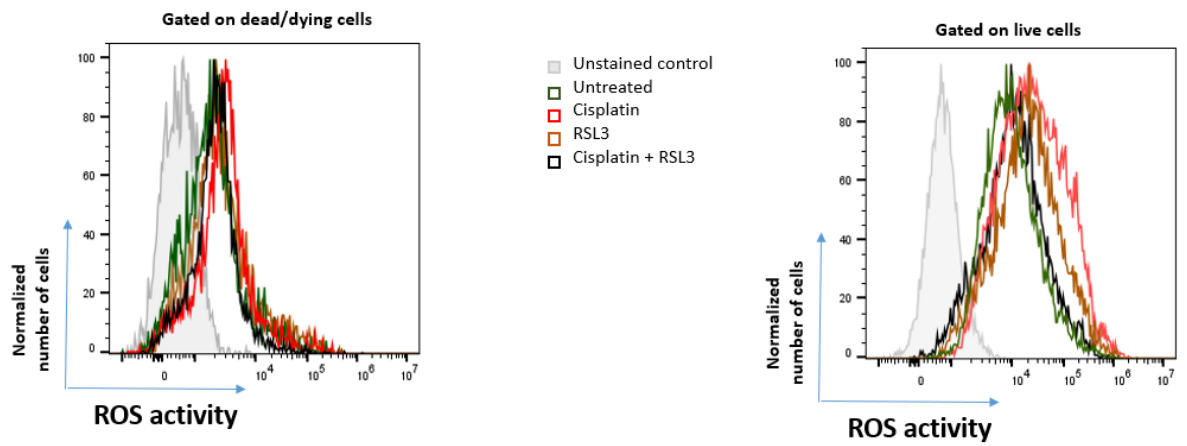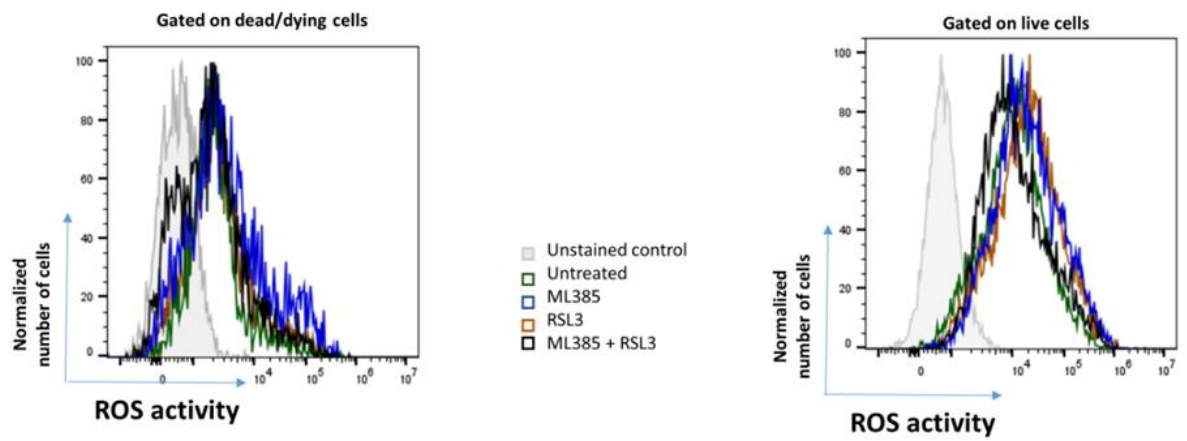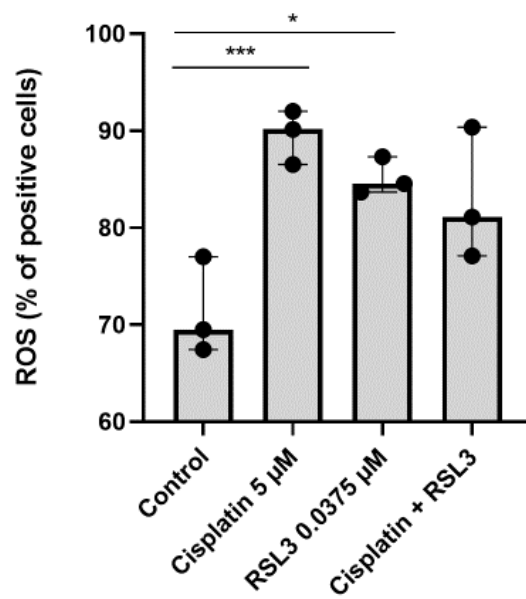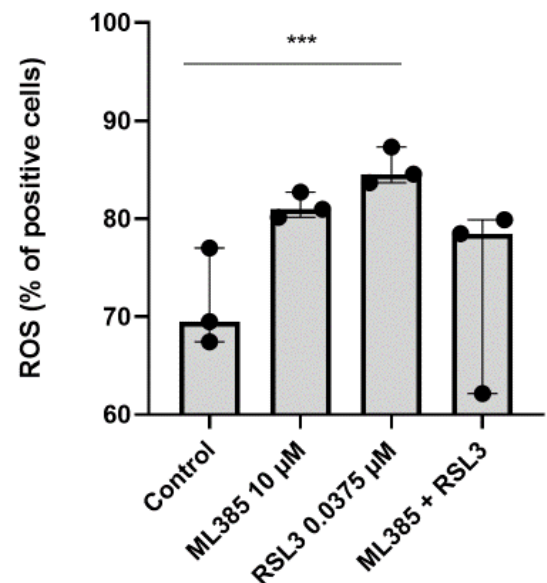
Figure 4.53: ROS level was detected by ROS Assay Kit -Highly Sensitive 2',7'-dichlorofluorescein diacetate (DCFH-DA-) after treating MDA-MB-231 cells for 48 hours with Cisplatin (5 µM), ML385 (10 µM) and Ferroptosis inducer RSL3 (0.0375 µM). **(A)** Example flow cytometry plot showing gating strategy of live and dead cells, and analysis of ROS levels separated into Low ROS and High ROS based on negative and positive controls. **(B)** Data is presented as normalised number of positive cells based on dead cells or live cells for all treatment groups. **(C)** ROS as a percent of positive cells from live cells is presented. The statistical significance was determined by comparison with the control, analysed by a Kruskal-Wallis followed by Dunn's multiple comparisons test (*=P≤0.05, **=P≤0.01, and ***=P≤0.001) from n=3 independent experiments each with 3 technical repeats.

Figure 4.54: ROS level in MCF-7 cells after treatment with Doxorubicin and RSL3

(A)

ROS activity (FITC)
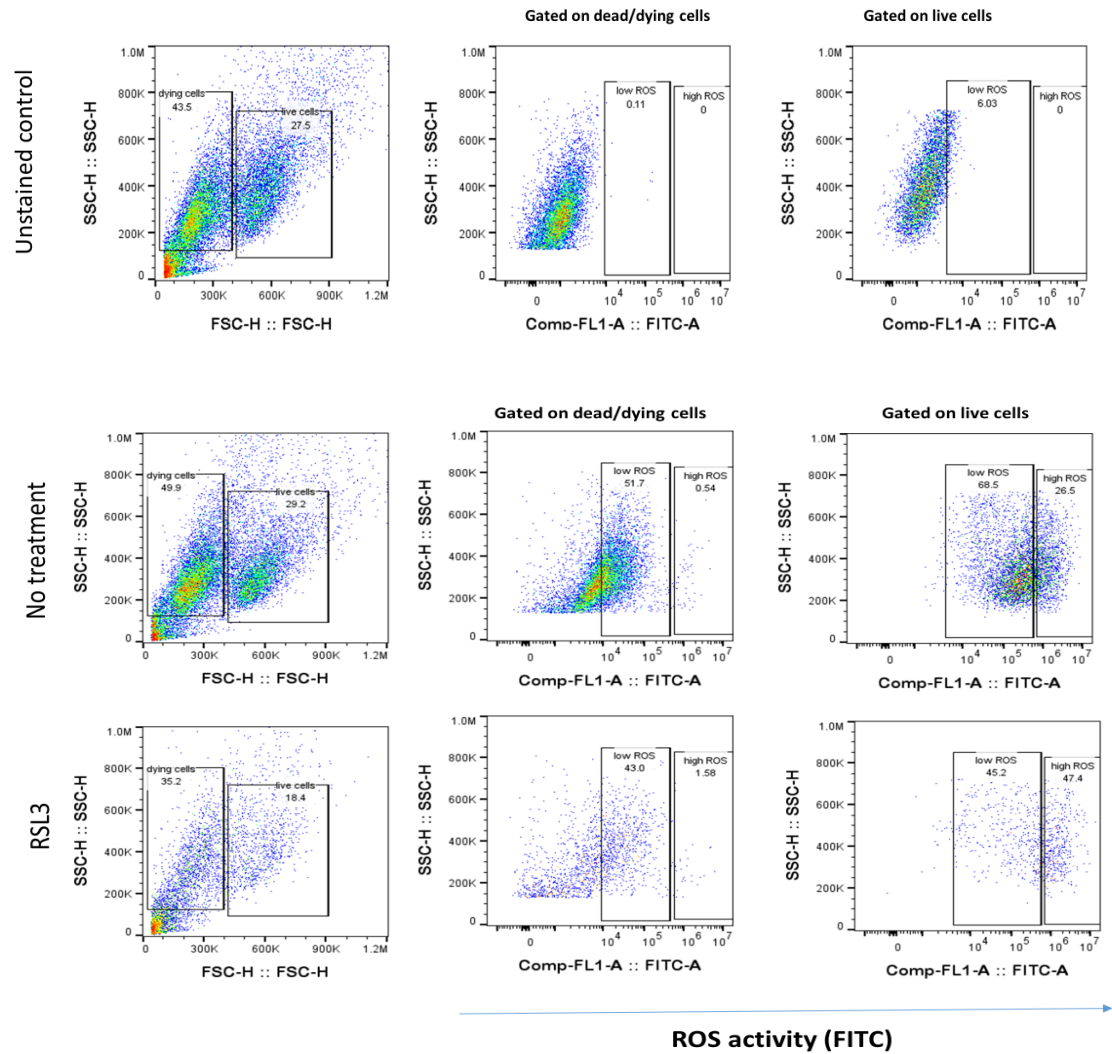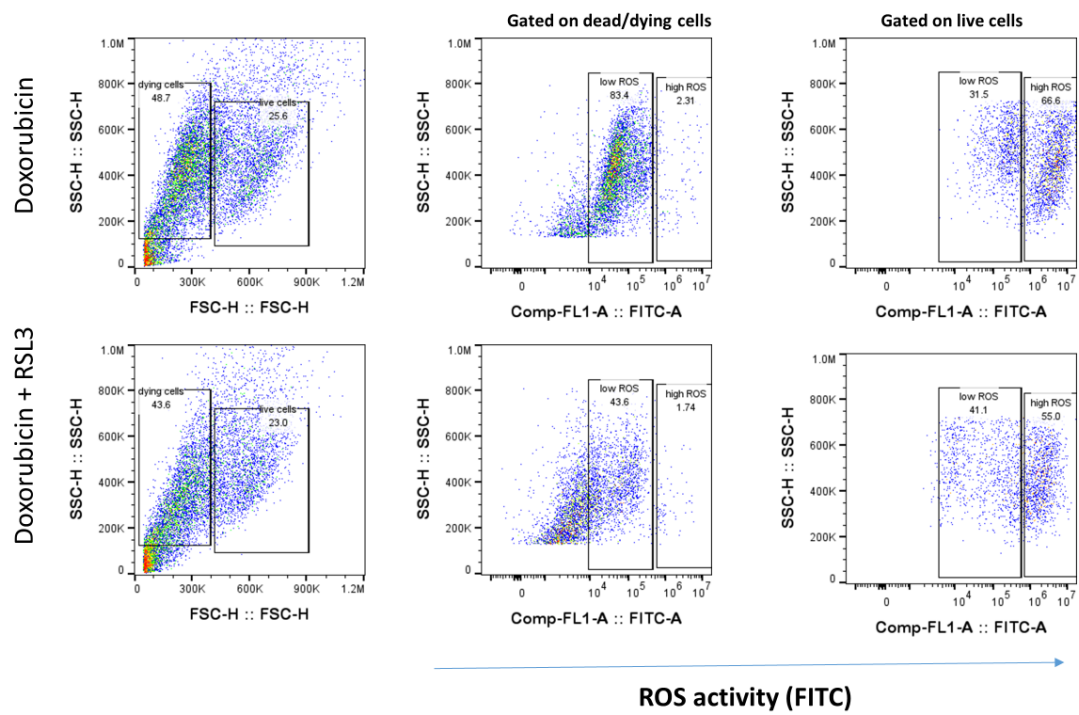
(B)
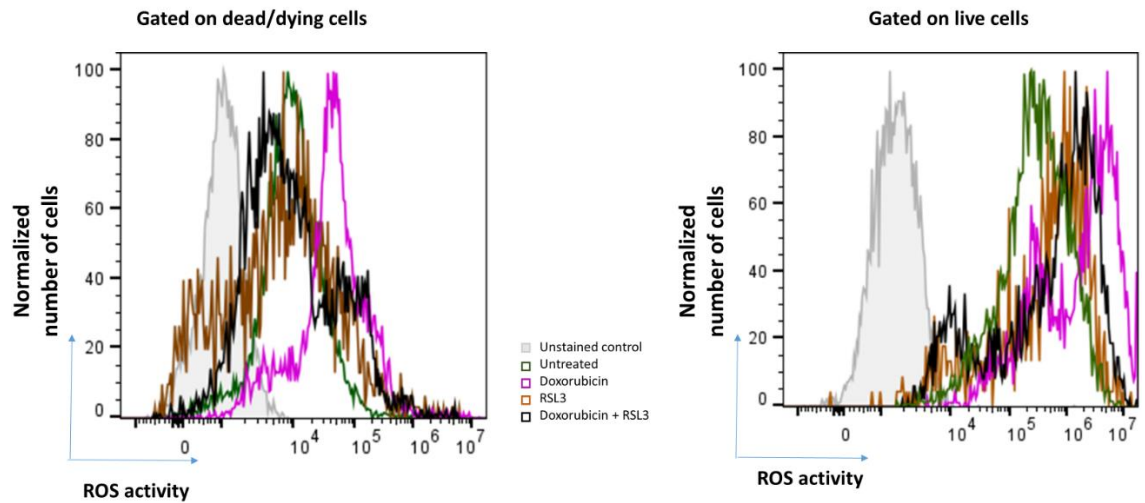
(C)
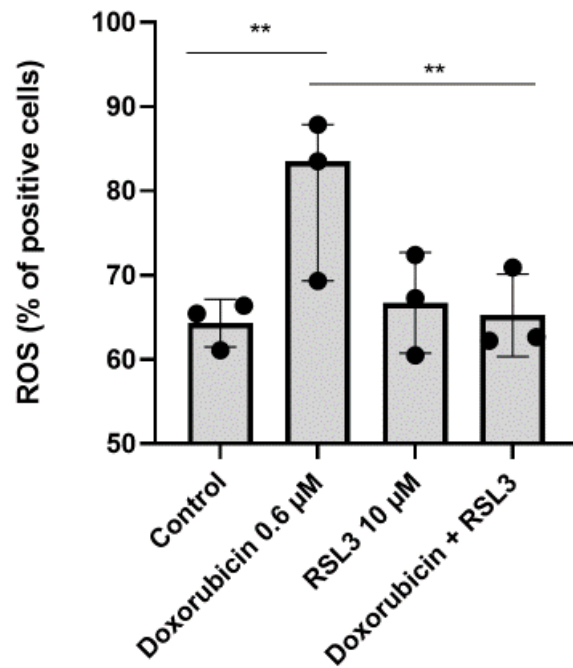
Figure 4.54: ROS level was detected by ROS Assay Kit -Highly Sensitive 2',7'-dichlorofluorescein diacetate (DCFH-DA-) after treating MCF-7 cells for 48 hours with Doxorubicin (0.6 μM) and ferroptosis inducer RSL3 (0.0375 μM). **(A)** Example flow cytometry plot showing gating strategy of live and dead cells, and analysis of ROS levels separated into Low ROS and High ROS based on negative and positive controls. **(B)** Data is presented as normalised number of positive cells based on dead cells or live cells for all treatment groups. **(C)** ROS as a percent of positive cells from live cells is presented. The statistical significance was determined by comparison with the control, analysed by a Kruskal-Wallis followed by Dunn's multiple comparisons test (*=P≤0.05, **=P≤0.01, and ***=P≤0.001) from n=3 independent experiments each with 3 technical repeats.

4.2.18 Determination of ROS in breast cancer 3D spheroid alginates cells with combined studies

Intracellular reactive oxygen species (ROS) were detected by ROS Assay Kit "-Highly Sensitive 2',7'-dichlorofluorescein diacetate (DCFH-DA-)", after finding the synergistic cytotoxic effect between the effective doses of treatments of chemotherapies Doxorubicin and Cisplatin as well as the Nrf2 inhibitor ML385 with ferroptosis inducer RSL3 in MDA-MB-231 cells.

3D MDA-MB-231 alginate cultures were treated with ML385 (10 μM) Cisplatin (5 μM) and Ferroptosis inducer RSL3 (0.075 μM) for 48 hours with control (0.2% (v/v) DMSO).

For 3D MCF-7 alginate spheres were treated with Doxorubicin (10 μM), and Ferroptosis inducer RSL3 (10 μM).

4.2.18.1 ROS level in MDA-MB-231 3D spheroid alginate cells with combined treatments

In contrast to findings in 2D cell culture, 3D cell cultures showed a lower % positivity of ROS. Furthermore, in situations where cytotoxic responses were observed in 2D cell culture, opposite effects were observed in 3D cell culture. Control cells showed a clear bimodal population, unlike in 2D cell culture. Furthermore, treatment with RSL3 alone and RSL3 plus Cisplatin resulted in a reduced % positivity for ROS (P≤0.01), whereas Cisplatin alone had no significant effect (Figure 4.55 Ci).

Treatment of 3D cell cultures of MDA-MD-231 with ML385 had no effect, whereas combination treatment with RSL3 significantly and potently decreased the % ROS positivity (P≤0.001) (Figure 4.55 Cii).

4.2.18.2 Determination of ROS in MCF-7 3D spheroid alginate cells with combined studies

In contrast to 2D cell cultures which showed a bimodal population, control MCF-7 cells showed a single population of cells with respect to ROS, albeit with a wide range of intensities. The level of ROS was significantly increased after RSL3 treatment but decreased during combination treatment with Doxorubicin (P≤0.05) (Figure 4.56).

Figure 4.55: ROS level in MDA-MB-231 3D spheroids after treatment with Cisplatin and ML385 +/- RSL3

(A)

(Bi)

Gated on dead/dying cells

Normalized number of cells

ROS activity

- Unstained control
- Untreated
- Cisplatin
- RSL3
- Cisplatin + RSL3

Gated on live cells

Normalized number of cells

ROS activity

(Bii)

Gated on dead/dying cells

Normalized number of cells

ROS activity

- Unstained control
- Untreated
- ML385
- RSL3
- ML385 + RSL3

Gated on live cells

Normalized number of cells

ROS activity
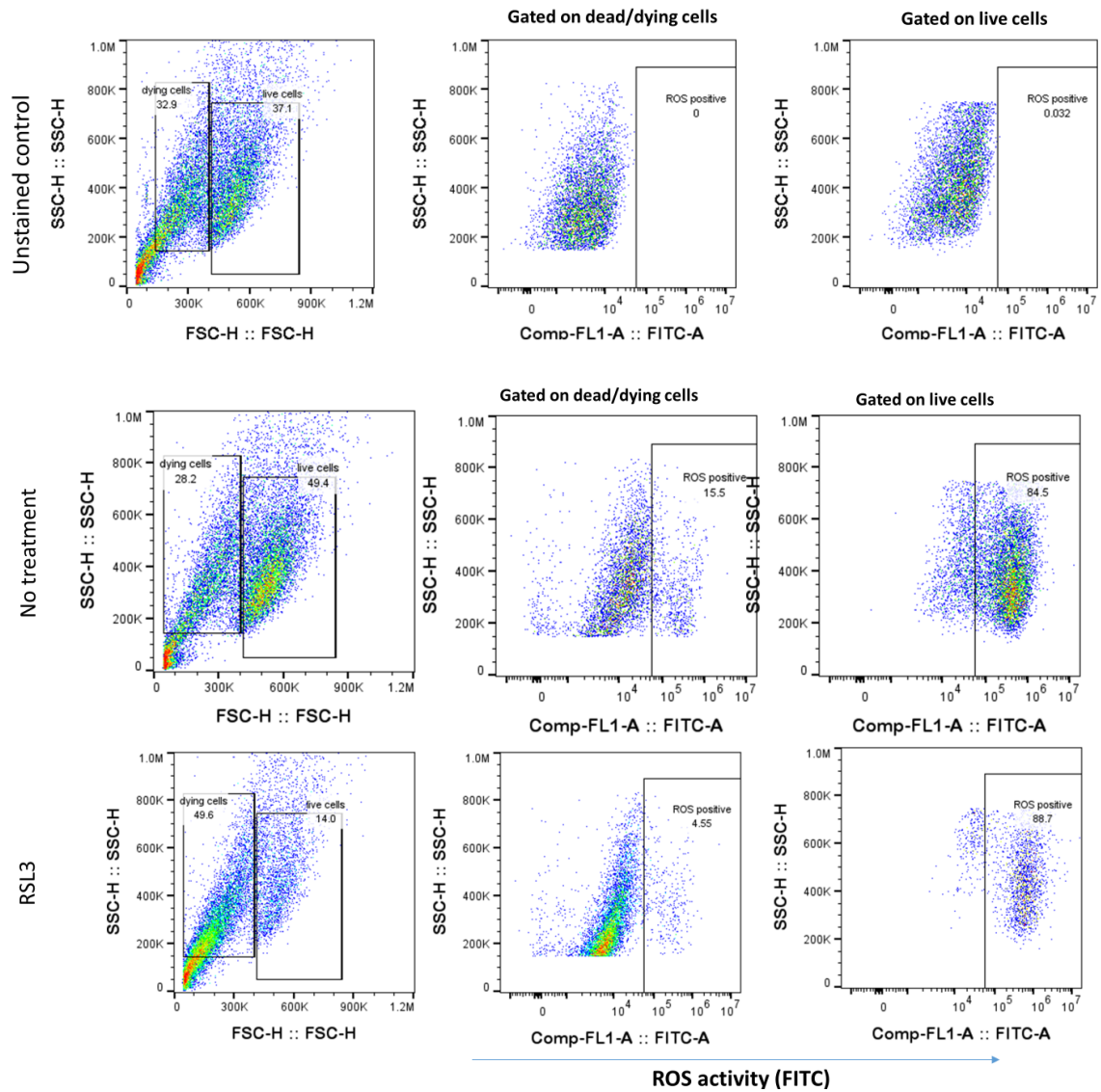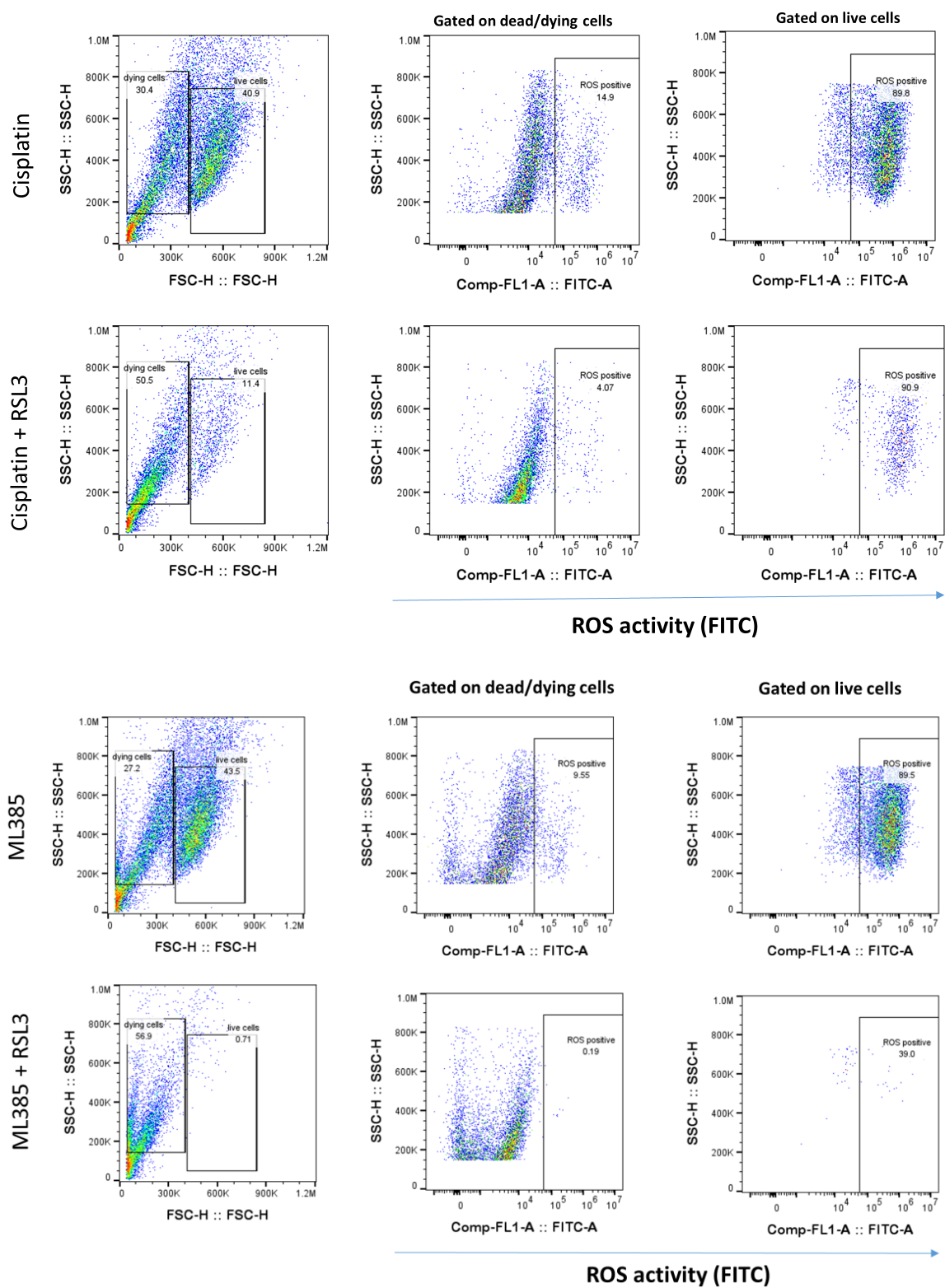
(Ci)
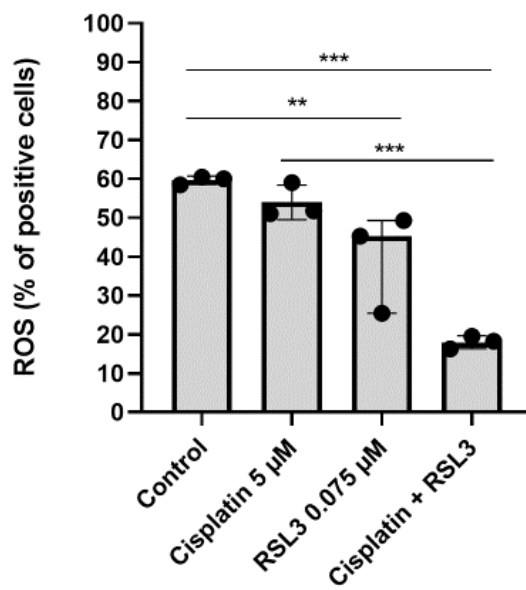
(Cii)
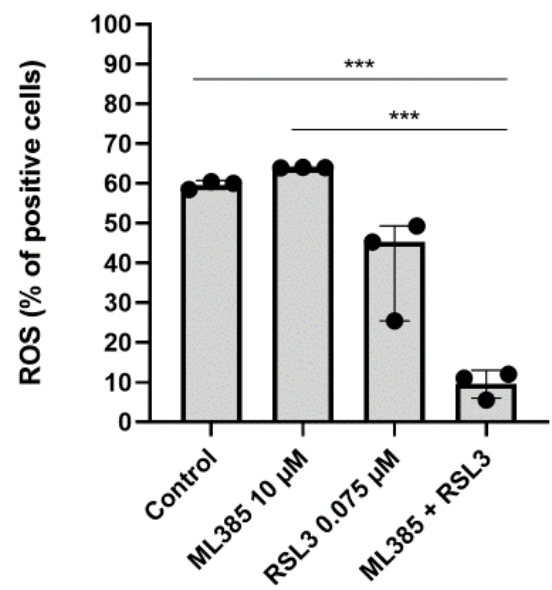
Figure 4.55: ROS level was detected by ROS Assay Kit -Highly Sensitive 2',7'-dichlorofluorescein diacetate (DCFH-DA-) after treating MDA-MB-231 spheroids for 48 hours with Cisplatin (5 µM), ML385 (10 µM) and Ferroptosis inducer RSL3 (0.075 µM). **(A)** Example flow cytometry plot showing gating strategy of live and dead cells, and analysis of ROS levels separated into Low ROS and High ROS based on negative and positive controls. **(B)** Data is presented as normalised number of positive cells based on dead cells or live cells for all treatment groups. **(C)** ROS as a percent of positive cells from live cells is presented. The statistical significance was determined by comparison with the control, analysed by a Kruskal-Wallis followed by Dunn's multiple comparisons test (*=P≤0.05, **=P≤0.01, and ***=P≤0.001) from n=3 independent experiments each with 3 technical repeats.

Figure 4.56: ROS level in MCF-7 3D spheroids after treatment with Doxorubicin and RSL3

(A)
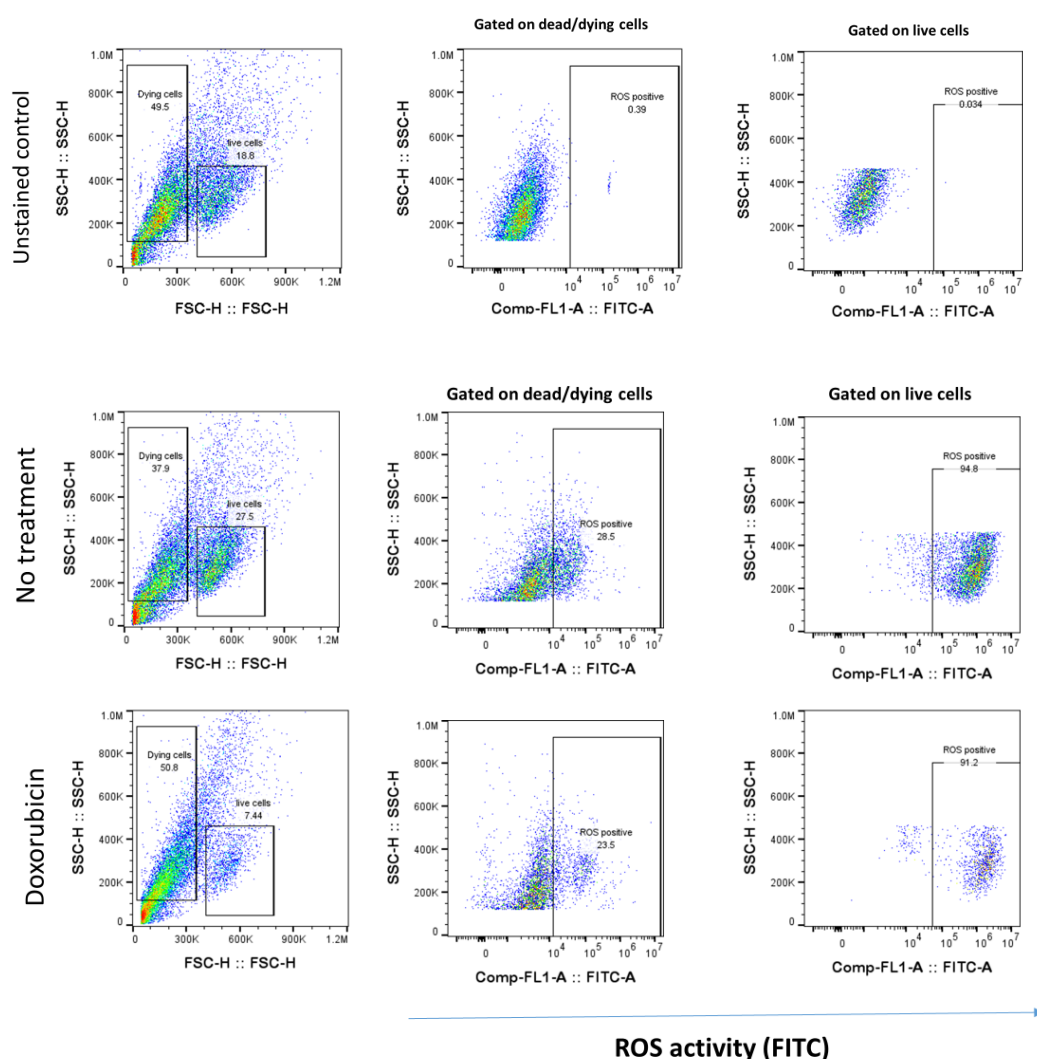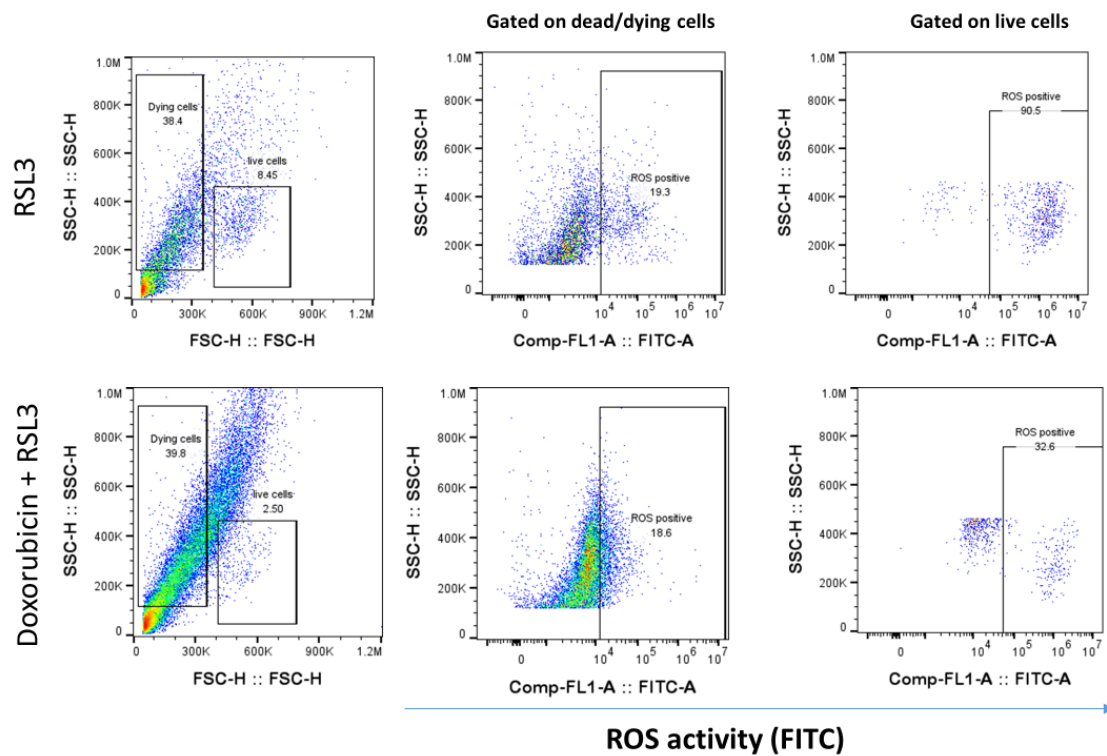
(B)
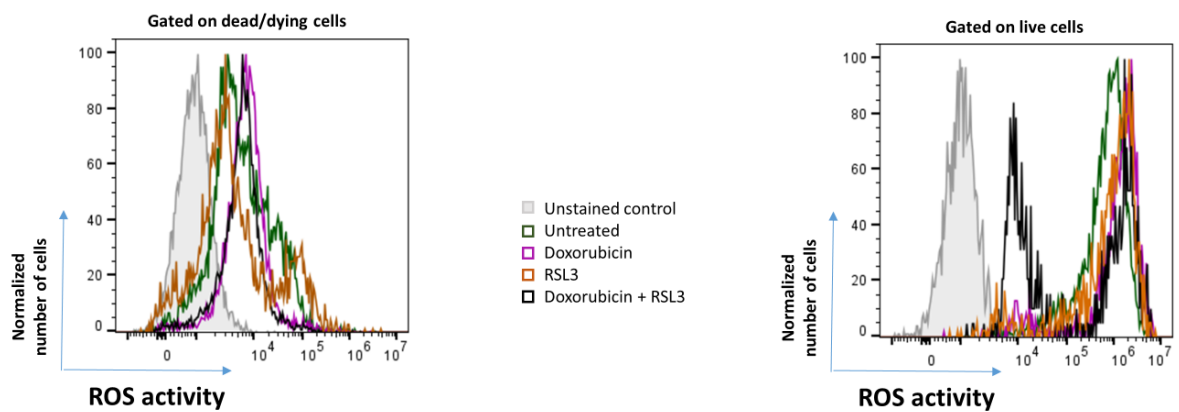
(C)
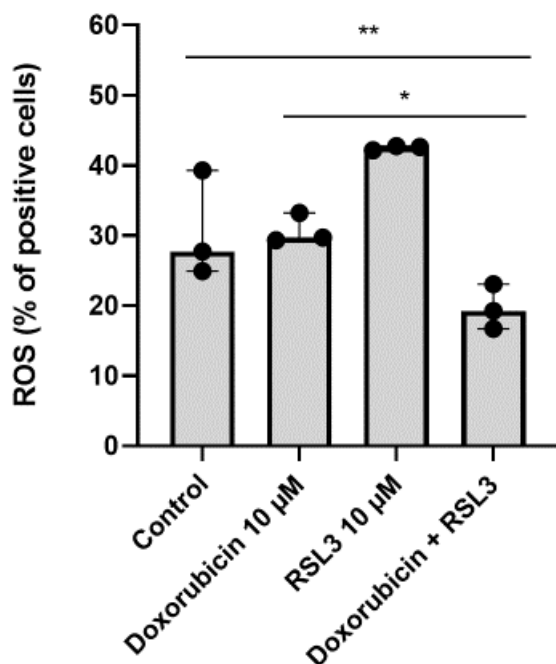
Figure 4.56: ROS level was detected by ROS Assay Kit -Highly Sensitive 2',7'-dichlorofluorescein diacetate (DCFH-DA-) after treating MCF-7 spheroids for 48 hours with Doxorubicin (10 µM) and Ferroptosis inducer RSL3 (10 µM). **(A)** Example flow cytometry plot showing gating strategy of live and dead cells, and analysis of ROS levels separated into Low ROS and High ROS based on negative and positive controls. **(B)** Data is presented as normalised number of positive cells based on dead cells or live cells for all treatment groups. **(C)** ROS as a percent of positive cells from live cells is presented. The statistical significance was determined by comparison with the control, analysed by a Kruskal-Wallis followed by Dunn's multiple comparisons test (*=P≤0.05, **=P≤0.01, and ***=P≤0.001) from n=3 independent experiments each with 3 technical repeats.

4.2.19 Assessment of free iron (Fe^{2+}) as a marker of ferroptosis

Mito-FerroGreen dye was used for staining for the presence of free iron in MDA-MB-231 and MCF-7 cells in combination treatments (Doxorubicin, Cisplatin, RSL3, ML385) previously found to induce enhanced cytotoxic effects. After staining, cells were assessed by fluorescent microscopy and percentage of positive cells determined. This experiment was done once as a confirmatory experiment to further support the evidence for ferroptotic cell death. MDA-MB-231 cells were treated with Cisplatin (5 µM) with and without the ferroptosis inducer RSL3 (0.0375 µM) for 48 hours, or RSL3 with and without ML385. MCF-7 cells were treated with Doxorubicin (0.6 µM) and Ferroptosis inducer RSL3 (10 µM) for 48 hours.

4.2.19.1 Assessment of free Iron (Fe^{2+}) in MDA-MB-231 cells with combined treatment

After treatment of MDA-MB-231 cells with Cisplatin or RSL3, no increase in free iron was observed, however after combination treatment, a potent induction of free iron was observed consistent with the synergistic cytotoxic response seen previously (Figure 4.57 and 4.59). Only Cisplatin with RSL3 shows convincing staining in the majority of cells. After treatment with RSL3 in the presence and absence of ML385, no convincing staining was observed (Figure 4.58 and 4.59).

Figure 4.59 show the MDA-MB-231 cells stained with Mito-FerroGreen, Hoechst and PI dyes to detect Iron existence using Fluorescent Microscope IX81.

Figure 4.57: Assessment of Fe^{2+} in MDA-MB-231 cells after treatment with Cisplatin and RSL3
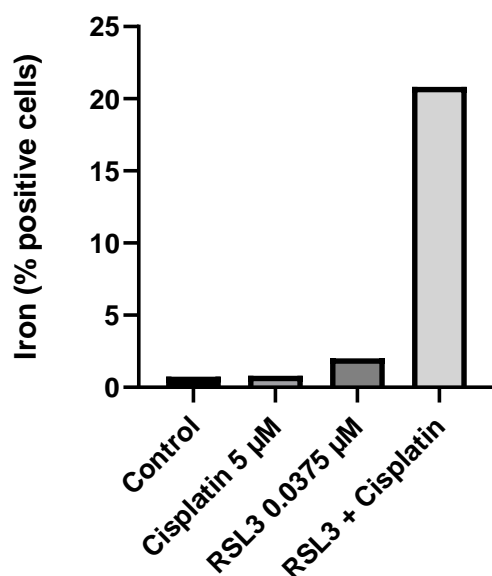
Figure 4.57: Mitochondrial labile Fe^{2+} detection (% positivity) using Mito-FerroGreen dye under fluorescent microscope after treating MDA-MB-231 cells for 48 hours with Cisplatin (5 µM) and Ferroptosis inducer RSL3 (0.0375 µM) from n=1 independent experiment.

Figure 4.58: Assessment of Fe^{2+}in MDA-MB-231 cells after treatment with ML385 and RSL3
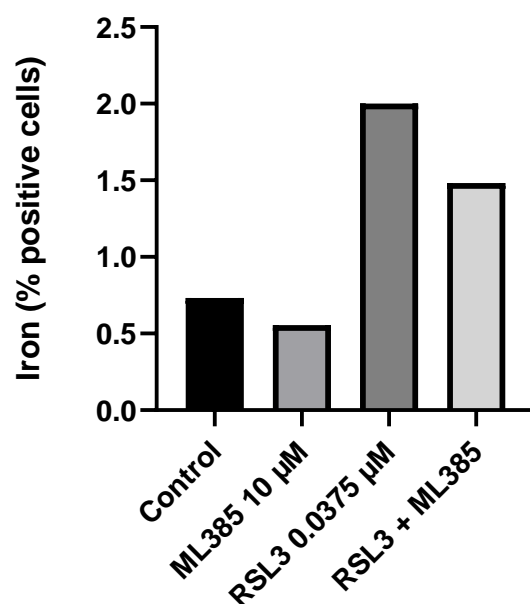
Figure 4.58: Mitochondrial labile Fe^{2+} detection (% positivity) using Mito-FerroGreen dye under fluorescent microscope after treating MDA-MB-231 cells for 48 hours with ML385 (10 µM) and Ferroptosis inducer RSL3 (0.0375 µM) from n=1 independent experiment.

Figure 4.59: MDA-MB-231 cells stained with Mito-FerroGreen and Hoechst 33342 in combined studies

Control (Hoechest)

RSL3 0.0375 µM (Hoechest)

Control (Mito-FerroGreen)

RSL3 0.0375 µM (Mito-FerroGreen)

Cisplatin 5 µM (Hoechest)

Cisplatin + RSL3 (Hoechest)

Cisplatin 5 µM (Mito-FerroGreen)

Cisplatin + RSL3 (Mito-FerroGreen)

ML385 10 µM (Hoechest)

ML385 + RSL3 (Hoechest)

ML385 10 µM (Mito-FerroGreen)

ML385 + RSL3 (Mito-FerroGreen)
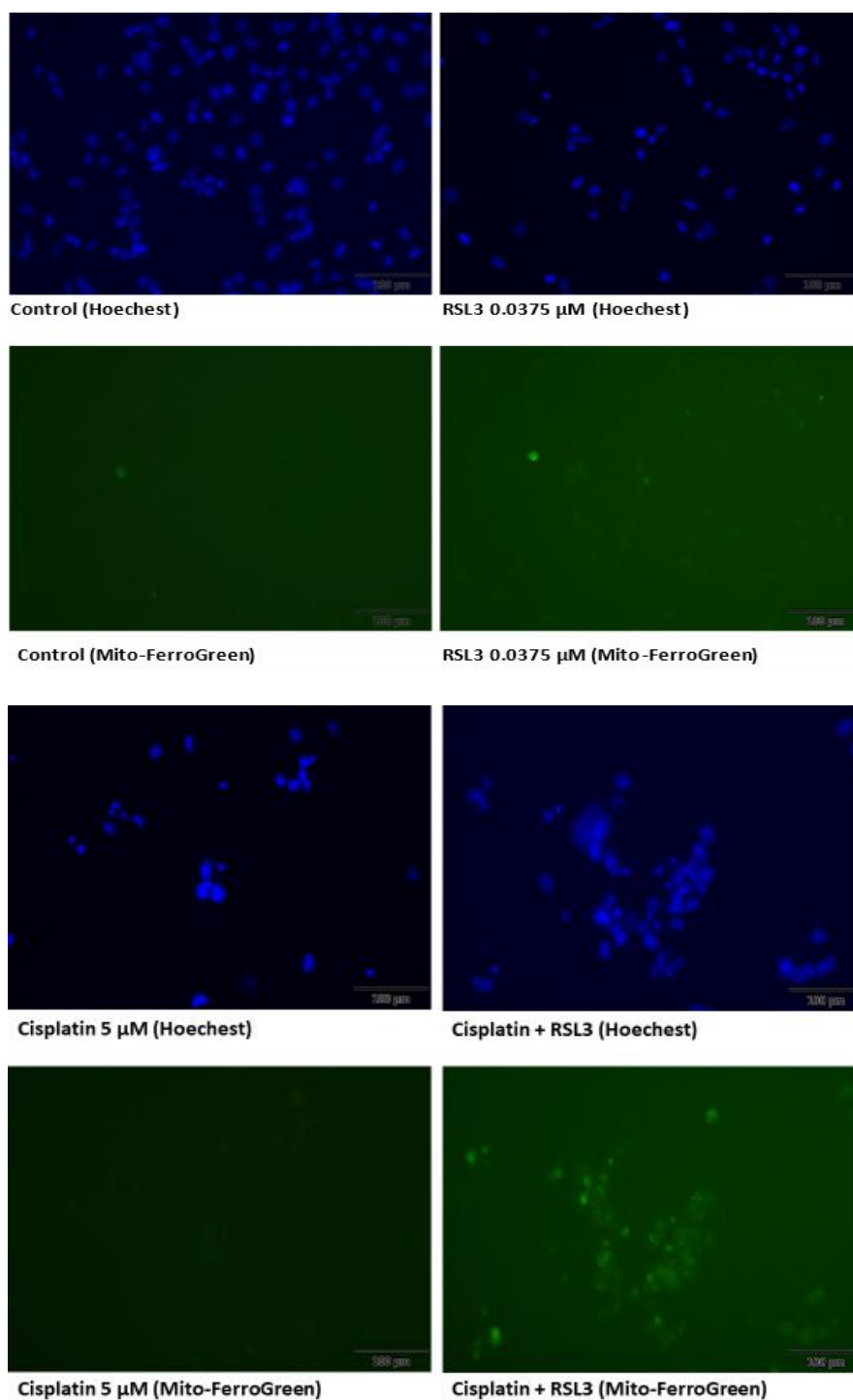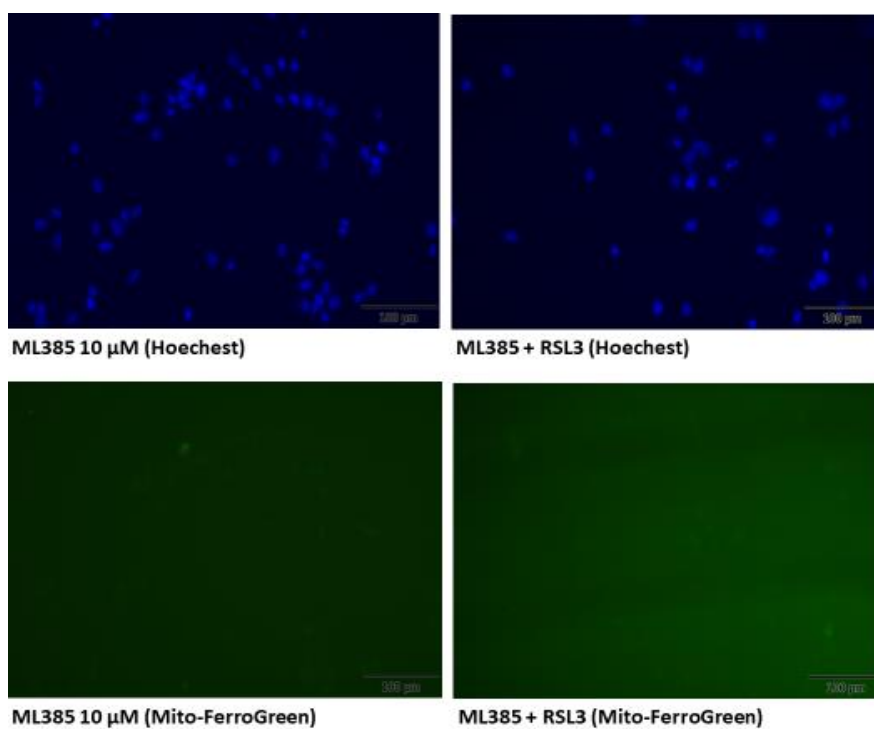
Figure 4.59: Mitochondrial labile Fe^{2+} under fluorescent microscope after treating MDA-MB-231 cells for 48 hours with Cisplatin (5 µM), ML385 (10 µM) and Ferroptosis inducer RSL3 (0.0375 µM), with control (0.2% (v/v) DMSO), determined by Hoechst 33342 staining and Mito-FerroGreen dye staining. Cells are stained blue with Hoechst 33342, and Fe^{2+} stained green with Mito-FerroGreen (Scale bars = 100 µm).

4.2.19.2 Assessment of free Iron (Fe^{2+}) in MCF-7 cells with combined studies

Iron levels were assessed after treatment with RSL3, and combination treatment with Doxorubicin, although not in response to Doxorubicin-alone (Figure 4.60 and 4.61). RSL3 alone increased Iron-positive cells, whereas Doxorubicin did not. Combination treatment resulted in similar levels as RSL3 alone suggesting that RSL3 in combination with Doxorubicin, although increasing cell death, does not achieve this by increasing free iron and enhanced ferroptosis.

Figure 4.60: Assessment of Fe^{2+} in MCF-7 cells after treatment with Doxorubicin and RSL3
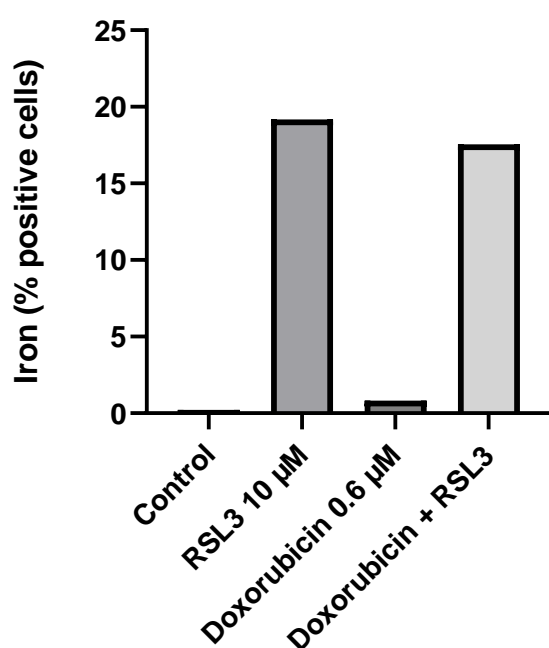
Figure 4.60: Mitochondrial labile Fe^{2+} detection (% positivity) using Mito-FerroGreen dye under fluorescent microscope after treating MCF-7 cells for 48 hours with Doxorubicin (0.6 μM) and Ferroptosis inducer RSL3 (10 μM) from n=1 independent experiment.

Figure 4.61: MCF-7 cells stained with Mito-FerroGreen and Hoechst 33342 in combined studies

Control (Hoechest) RSL3 10 µM (Hoechest)

Control (Mito-FerroGreen) RSL3 10 µM (Mito-FerroGreen)

Doxorubicin 0.6 µM (Hoechest) Doxorubicin + RSL3 (Hoechest)

Doxorubicin 0.6 µM (Mito-FerroGreen) Doxorubicin + RSL3 (Mito-FerroGreen)
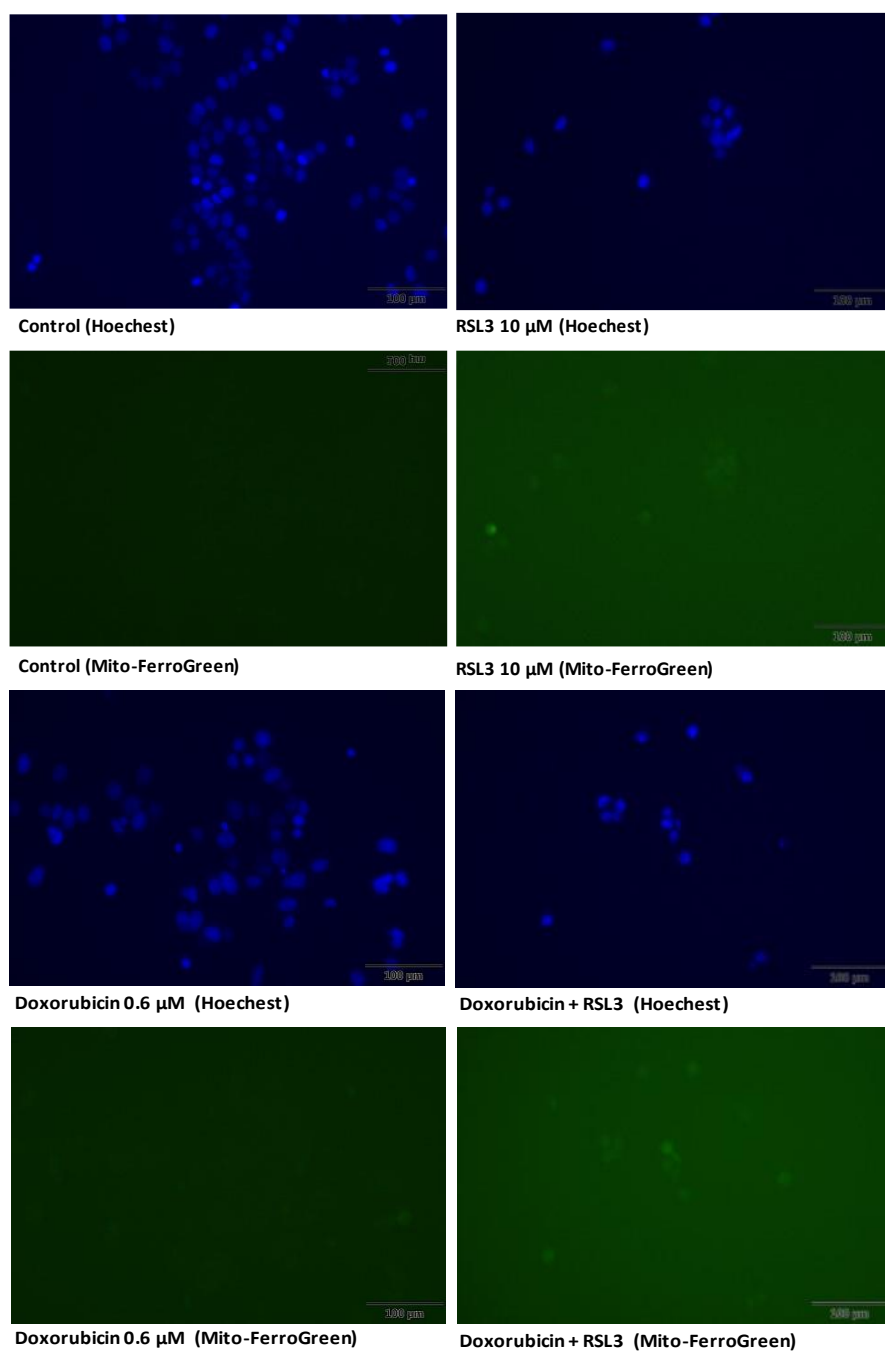
Figure 4.61: Mitochondrial labile Fe^{2+} and death detection under fluorescent microscope after treating MCF-7 cells for 48 hours with Doxorubicin (0.6 µM) and Ferroptosis inducer RSL3 (10 µM), with control (0.2% (v/v) DMSO), determined by Hoechst 33342 staining and Mito-FerroGreen dye staining. Cells are stained blue with Hoechst 33342, and Fe^{2+} stained green with Mito-FerroGreen (Scale bars = 100 µm).

4.2.20 Determination of Lipid peroxidation in MCF-7 cells and spheroids with combined studies

Lipid peroxidation was assessed using a fluorogenic lipid peroxidation sensor BODIPY™ 581/591 C11. In this experiment, cells were stained and assessed by flow cytometry. Two fluorophores were detected: Green on the Y axis which relates to lipid peroxidation, and red on the X axis which relates to lipids without peroxidation. The C11 (Undecanoic acid)-linked BODIPY dye interacts with phospholipids and emits at 581/591 in a reduced state, but emits at 510nm in an oxidised state after interaction with oxidised lipids and is therefore used to monitor lipid peroxidation. The 4 quadrants on the flow cytometry plot reflect the following: Bottom left, no detection of lipid peroxidation, as defined by fluorescent levels detected in the 'no dye' negative control. Botton right: Positive for lipid detection (non-peroxidation). Top right (Q2): Positive detection of lipid peroxidation. Top left (Q1) quadrant should contain no cells as cells should not be positive for lipid peroxidation, but negative for lipid. Therefore, to quantify data, the percent of cells in the top right quadrant (Q2) was calculated as this represents % of cells with lipid peroxidation. Control cells show some lipid peroxidation, therefore on flow cytometry plots, induction of high level lipid peroxidation is seen as a shift in the population from partially in bottom right and top right quadrant, to mainly in top right quadrant. Doxorubicin showed a clear induction of lipid peroxidation, with similar levels observed with RSL3, Erastin and FIN56 (Figure 4.62). Combination studies with Doxorubicin plus ferroptosis inducers showed similar levels, but no further increase.

In 3D cell culture, Doxorubicin showed a similar induction in lipid peroxidation. RSL3 induced lipid peroxidation to a lesser extent, and combination treatment was no different to Doxorubicin alone (Figure 4.63).

Figure 4.62: Lipid peroxidation levels in MCF-7 cells after treatment with Doxorubicin and Ferroptosis inducers
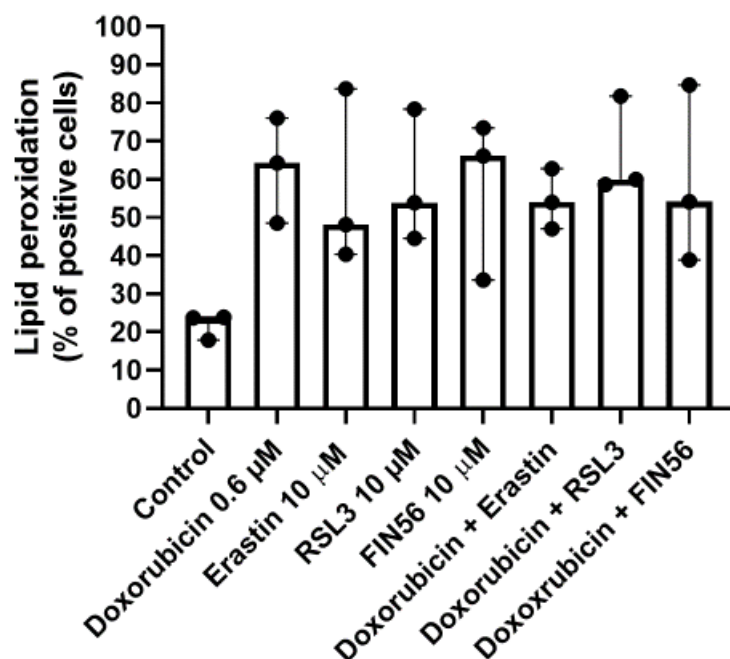
(A)

(B)

Figure 4.62: Lipid peroxidation level was detected by Lipid Peroxidation Assay Kit (Cell-based) (ab243377), fluorescence from red to green upon peroxidation by ROS in cells after treating MCF-7 cells for 48 hours with Doxorubicin (10 µM) and Ferroptosis inducers (Erastin, RSL3, FIN56) at concentration of 10 µM with control (0.2% (v/v) DMSO). **(A)** example flow cytometry plot showing intensity distribution. **(B)** Data is presented as median ± range from n=3 independent experiments each with 3 technical repeats. The statistical significance was determined by comparison with the control, analysed by a Kruskal-Wallis followed by Dunn's multiple comparisons test (*=P≤0.05, **=P≤0.01, and ***=P≤0.001).

Figure 4.63: Lipid peroxidation level in MCF-7 3D spheroids after treatment with Doxorubicin and RSL3

(A)

(B)

Figure 4.63: Lipid peroxidation level was detected by Lipid Peroxidation Assay Kit (Cell-based) (ab243377), fluorescence from red to green upon peroxidation by ROS in cells after treating MCF-7 spheroids for 48 hours with Doxorubicin (10 µM) and Ferroptosis inducer RSL3 (10 µM). **(A)** example flow cytometry plot showing intensity distribution. **(B)** Data is presented as median ± range from n=3 independent experiments each with 3 technical repeats. The statistical significance was determined by comparison with the control, analysed by a Kruskal-Wallis followed by Dunn's multiple comparisons test (*=P≤0.05, **=P≤0.01, and ***=P≤0.001).

4.3 Discussion

4.3.1 Comparison of chemotherapy responses in 2D and 3D cell culture

To assess whether there were differences in responses to chemotherapy in 2D vs 3D cell culture, MDA-MB-231 and MCF-7 were challenged with Doxorubicin or Cisplatin to identify the IC50 and identify a suitable dose for future combination studies with ferroptosis inducers and/or ML385. It is clear that in 2D cell culture, both cell lines were susceptible to Doxorubicin whereas in 3D cell culture, sensitivity was substantially reduced, with at least a 4-fold (MDA-MB-231) and over 10-fold (MCF7) decrease in sensitivity in alginate spheroids. In contrast for Cisplatin, there was little or no difference in sensitivity between 2D and 3D cell culture. There have been many reports of increased sensitivity in 2D cell culture vs 3D cell culture. For example, Palubeckaite *et al.,* (2020) showed that osteosarcoma cells were Doxorubicin-resistant in 3D cell culture, yet sensitive in the low µM range in 2D cell culture. This previous study also confirmed by mass spectrometry imaging, and by fluorescence imaging that doxorubicin is able to enter the centre of spheroids, including in much larger (approximately 1mm) aggregoid spheroids, which are up to 5x larger than those used in the current study. This strongly suggests that the decreased activity is not due to drug access, a point back up by observations using fluorescent microscopy: Doxorubicin stains cells red, preventing the use of propidium iodide use as a live/dead assay, and Doxorubicin-stained red cells are visible throughout spheroids. Therefore, the decreased activity is likely to reflect the 3D tumour microenvironment. Doxorubicin is highly dependent on cellular proliferation for some of its activity: It inhibits topoisomerase activity which results in stalled replication forks, as topoisomerase relieves tension in DNA during replication (Marinello *et al.,* 2018). Furthermore, spheroids exhibit a reduced Ki-67 positivity in the centre of spheroids and expressed Ki-67 primarily around the periphery in both osteosarcoma and lung adenocarcinoma spheroids (Lucy E Flint *et al.*, 2020; Flint *et al.*, 2021). The action of Doxorubicin is not limited to DNA replication, as topoisomerase II is crucial for DNA unwinding during transcription also, therefore Doxorubicin can have actions on cells not in the cell cycle (F. Yang *et al.*, 2014). In summary, the decreased Doxorubicin response in 3D cell culture is consistent with previous studies and may be in-part due to decreased cell cycling but is unlikely to be due to reduced drug access to tumour cells. The

observations of Cisplatin exhibiting similar responses in 2D and 3D cell culture is mixed in the literature, with ovarian carcinoma cell lines exhibiting over 10-fold lower sensitivity in 3D cell culture (Nowacka *et al.*, 2021), oral squamous cell carcinoma cells exhibiting moderately lower sensitivity to Cisplatin (Ono *et al.*, 2022b), whereas in breast cancer cells, specifically MDA-MB-231, responses appear highly dependent on cellular location, with cells in the spheroid core being completely resistant to Cisplatin, whereas cells at the periphery were sensitive. It is therefore likely that differences in spheroid formation affect drug responses, with larger spheroids with a larger core exhibiting Cisplatin resistance. It is noteworthy that the 'embedded spheroid model' of (Reynolds *et al.*, 2017) used spheroids much larger than in this current study (800 µM vs <250 µM). Similarly, (Muguruma *et al.*, 2020) used a different model (low-adhesion plates) and found MDA-MB-231 cells more resistant to Cisplatin and several other chemotherapy drugs in 3D cell culture vs 2D cell culture. In support of data in the current study, (Muguruma *et al.*, 2020) showed that only Cisplatin responses were similar in 2D and 3D cell culture using smaller spheroids (2000 cells/well, low adhesion plates), whereas Doxorubicin and Methotrexate were significantly less potent in 3D cell culture using MDA-MB-231. Therefore, the model employed may have a significant effect on the drug responses observed, as does the mechanism of action of the chemotherapy agent used.

4.3.2 Enhancement of Doxorubicin responses using ferroptosis inducers in 2D and 3D cell culture

Combination treatment with ferroptosis inducers showed no convincing evidence of synergistic, or even additive responses in MDA-MB-231 cells, despite extending incubation times from 24 hours to 48 hours. However, in 3D cell culture, Erastin and FIN56 appeared to enhance Doxorubicin activity, in that combination treatment resulted in greater cell death than either treatment alone, whereas in 2D cell culture, there was no difference. Doxorubicin is known to induce some ferroptotic activities, particularly in relation to adverse cardiac events after Doxorubicin treatment in cancer patients (Christidi and Brunham, 2021), yet direct pro-ferroptosis responses in tumour cells are less well studied, with no studies to date addressing this interaction in breast cancer cells, although previous studies have assessed RSL3-alone in breast cancer cells,

confirming our observations of MDA-MB-231 being sensitive, and MCF-7 being resistant (Park *et al.*, 2023).

RSL3 showed evidence of increased activity in MCF-7 cells when combined with Doxorubicin and was considered an interesting observation to warrant further study to assess ROS, glutathione depletion, Fe^{2+} levels and lipid peroxidation. RSL3 was also the only ferroptosis inducer to enhance cell death in MCF-7 3D spheroids. Therefore, the combination of RSL3 and Doxorubicin was examined in mechanistic studies, in particular with the potential ferroptosis inducer and Nrf2 inhibitor ML385. There is very little literature on the role of ferroptosis inducers in 3D cell culture models, however one intriguing study showed that RSL3 was able to eradicate tumour cells in the inner luminal space of spheroids in colon cancer spheroids, and that ferroptosis inhibitors could reverse this activity (Takahashi *et al.*, 2020). Furthermore, this study showed that Nrf2 was a pre-requisite for spheroid formation, and that blocking Nrf2 could limit spheroid formation. Therefore, Nrf2 inhibition was used in the present study. Unfortunately (Takahashi *et al.*, 2020) did not use Erastin or FIN56, so it is not clear the finding of RSL3 being the only ferroptosis inducer capable of enhancing Doxoribicin responses in 3D cell culture is related to RSL3's mechanism of action. RSL3 inhibits GPX4 directly, whereas FIN-56 increases GPX4 degradation (Cotto-Rios and Gavathiotis, 2016; Dixon, 2017). In contrast, Erastin inhibits system Xc- and prevent cystine uptake for glutathione formation (Dixon *et al.*, 2014). Since RSL3 appeared to be the only reliable ferroptosis inducer in MCF-7 and in particular the only inducer to enhance cell death in 3D cell culture, RSL3 was chosen for combination studies with Cisplatin. However, Erastin and FIN56 did appear to have some activity to enhanced Doxorubicin responses in MDA-MB-231 3D cell culture.

4.3.3 Enhancement of Cisplatin responses with ferroptosis inducers in 2D and 3D cell culture

Since RSL3 showed more promising responses in the 3D cell culture in the ferroptosis-resistant cell line MCF-7, and also appeared to show enhanced activity in 3D cell culture vs Erastin or FIN56. For time constraints, only RSL3 was taken forward for combination studies with Cisplatin. In MDA-MB-231, combination of RSL3 and Cisplatin resulted in promising data, with significant reduction in cell death vs either treatment alone,

although a much weaker response was seen in MCF-7. There is some literature on Cisplatin combined with ferroptosis inducers, suggesting potential interaction in several tumour types, however most studies focussed on targeting the Nrf2 pathway directly, rather than using Erastin, RSL3, or FIN56 (Fu *et al.*, 2021; Z. Zhang *et al.*, 2022). In prostate cancer cells, Cisplatin-induced cell death was increased by RSL3 (Li *et al.*, 2021). Furthermore, Erastin remarkably enhanced cisplatin sensitivity and overcame resistance in osteosarcoma (Liu and Wang, 2019). In breast cancer, a single study has shown that knockout of Lipocalin-2 (Lcn2), an anti-oxidant protein, results in enhanced Cisplatin sensitivity and enhanced Erastin-sensitivity, consistent with observations in the present study, and highlight that many additional resistance mechanisms to ferroptosis-induced cell death exist (Valashedi *et al.*, 2022). In MDA-MB-231 spheroids, RSL3 did not further enhance anti-tumour responses, and consistent with 2D studies, no enhanced activity was observed in MCF-7 spheroids. The current study highlights that there are cell line dependencies, and cell culture model dependencies which dictate whether cells respond to ferroptosis inducers and/or chemotherapy. Although the tumour microenvironment is likely key to elucidating what controls ferroptosis sensitivity, recent work has shown that increased cell density can have profound effects on ferroptosis in that low cell densities confer ferroptosis-sensitivity, and high cell densities confer ferroptosis resistance, potentially explaining some of the differences between 2D and 3D cell culture (Panzilius *et al.*, 2019).

4.3.4 Gene expression profiling of ferroptosis-response genes of breast cancer cells in 2D and 3D cell culture

To potentially elucidate the mechanisms of ferroptosis insensitivity between MCF-7 and MDA-MB-231 cells, and to identify and differences between 2D and 3D cell culture, qRT-PCR analysis of key ferroptosis-related genes was performed. Key finding are that MCF-7 does not express GSTP1, whereas MDA-MB-231 expresses high levels, and in particular GSTP1 is significantly higher in 2D vs 3D cell culture. Furthermore, Transferrin receptor is decreased in MDA-MB-231 spheroids, and MCF-7 expresses significantly higher levels of NQO1 than MDA-MB-231 (Figure 4.21-24). GSTP1 is one of the key enzymes that conjugates reduced glutathione to many hydrophobic and hydrophilic compounds, including chemotherapy agents, and increased expression has been linked to chemo-

resistance (Ruzza *et al.*, 2009). GSTP1 has been proposed as a target to enhance radiation-induced ferroptosis (Tan *et al.*, 2022) and the gene is known to be epigenetically silenced in MCF-7, and gene expression induced by Doxorubicin treatment (Hamadneh *et al.*, 2021). Epigenetic silencing is associated with cancer susceptibility, presumably due to its role in detoxification leading to neoplastic transformation, and typically highly expressed in cancers as a mechanism of chemo-resistance (Schnekenburger *et al.,* 2014). In MDA-MB-231, decreased chemosensitivity is consistent with reduced GSTP1 gene expression levels, however studies on protein activity would need to be performed to determine whether this was mechanistic for the reduced chemosensitivity observed for Doxorubicin in this cell line. The presence of chemotherapy sensitivity in MCF-7 confirms that other mechanisms are responsible., although it is known that GSTP1 is induced in response to Doxorubicin (Hamadneh *et al.*, 2021). NQO1 is another anti-oxidant protein, which was expressed at significantly higher levels in MCF-7 vs MDA-MD-231 in both 2D and 3D cell culture (Figure 4.21-24). NQO1 is induced by Nrf2, resulting in detoxification of a range of electrophilic compounds (Satoh *et al.,* 2013). The only other transcriptional change was transferrin receptor, which was decreased in 3D cell culture in MDA-MB-231 vs 2D cell culture but expressed at similar levels in MCF-7 in both models. Transferrin receptor allows increased iron uptake, and is a specific ferroptosis marker (Satoh *et al.,* 2013).

4.3.5 Targeting of Nrf2 to enhance ferroptosis and chemotherapy-induced cell death

Both MCF-7 and MDA-MB-231 cell lines expressed high levels of NRF2 mRNA and Nrf2 protein (Figure 4.19-20), although MCF-7 cells showed more nuclear staining whereas MDA-MB-231 showed predominantly cytoplasmic staining. Since both cell lines were Nrf2-positive and Nrf2 is known to mediate chemotherapy and ferroptosis responses, the specific Nrf2-ihibitor ML385 was used in chemotherapy/drug combinations that showed promising combination anti-tumour responses. To assess ML385-inhibitor effects, cells were treated with ML385 (10 μM) with the ferroptosis inducer RSL3 in the presence and absence of chemotherapy. The rationale for this is that RSL3 was the only ferroptosis inducer that showed a pro-ferroptotic effect with both 2D and 3D cell culture modules (Chapter 3), and it was the most promising agent when combined with chemotherapy, particularly in the ferroptosis-resistant MCF-7 cell line. ML385 showed a

potent response when combined with RSL3 in MDA-MB-231, but no effect in MCF-7. In other cell types, this combination has proven highly toxic, for example in Acute Myeloid Leukaemia (X. Liu *et al.*, 2023) and lung (Taufani *et al.*, 2023). ML385 did not enhance Doxorubicin responses in MDA-MB-231 or MCF-7, confirming that Nrf2-alone is not responsible for ferroptosis-related Doxorubicin or insensitivity. However, combination of Doxorubicin + RSL3, which was previously shown to result in significant cell death, was resulted in further enhanced cell death by ML385 in MDA-MB-231, but interestingly, not with MCF-7. This is unexpected since MCF-7 appeared to exhibit higher Nrf2 protein levels, consistent with a dependency on Nrf2. Similar responses were seen in spheroids, with MDA-MB-231 responding to ML385 with more potent response than with Doxorubicin + RSL3 alone, and no enhancement to Doxorubicin + RSL3 responses in MCF-7 spheroids. In contrast, ML385 did not affect Doxorubicin-alone-treated MDA-MB-231 spheroids confirming a specific vulnerability when treated with RSL3, but not necessarily Doxorubicin.

4.3.6 Assessment of markers of ferroptosis

To determine whether glutathione (GSH) levels correlate with drug responses, total and reduced GSH was determined following treatment. Cisplatin reduced GSH levels, consistent with its activity, as did RSL3 and combined RSL3 + ML385 in MDA-MB-231 whereas no effect was seen in MCF-7. In 3D cell culture, combination of Cisplatin and RSL3 decreased GSH in MDA-MB-231, and similar reductions seen in MCF7 treated with RSL3 + ML385. MCF-7 spheroids treated with Doxorubicin + RSL3 showed a potent decrease in GSH. These studies are consistent with the notion of chemotherapy, RSL3 and ML385 all contribution to decreased GSH and/or reduced GSH ratio. Previous studies have investigated the distribution of GSH in 3D spheroids. Flint et al. (2020) showed that in osteosarcoma cells, GSH is predominantly present in the outer cells of large spheroids, and completely absent in the hypoxic core. This is consistent with ROS-induced stress, and this correlated with high levels of background cell death, albeit in 1mm diameter spheroids. Similar observations were reported in control and Doxorubicin-treated large spheroids, again in osteosarcoma, with increased GSH metabolites present in Doxorubicin-treated spheroids, and peripheral GSH in control spheroids (Palubeckaitė *et al.*, 2020). Cisplatin induced ROS-detection, as did Doxorubicin, however combination

treatments that would be expected to further increase ROS did not result in significantly increased ROS detection. Counter-intuitively, ROS was not increased in 3D cell culture in response to cisplatin or RSL3 and was significantly decreased in dual treatment. Previous unpublished observation (Cross, NA, personal communication) showed that using a ROS and Hypoxia-specific sensor, spheroids generated in alginate exhibited constitutively high levels of ROS in all spheroids above 50 μM (Cross, NA, unpublished observations). Therefore, detection of increased ROS on a very high background of ROS might miss chemotherapy-induced changes, depending on the dynamic range of the assay. It is also likely that some of these decreases in ROS observed for some treatments relate to treatments with high levels of dead cells, as the ROS assay was not compatible with PI as a vital dye, and is really designed for treatments that induce stress but not cell death. This is a potential caveat to any data sets that result in reduced ROS in response to chemotherapy, ML385 and RSL3 combinations in MDA-MB-231.

ROS is known to result in mitochondrial free iron overload, leading to depletion of GSH (Y. Chen *et al.*, 2023). Therefore, free iron was monitored in response to ferroptosis inducers and chemotherapy treatments using the Mito-FerroGreen assay. This assay binds free iron, resulting in a green fluorescence readout in live cells. Interestingly, Cisplatin alone, and RSL3 alone did not induce significant free iron, whereas combination resulted in a highly potent and synergistic induction of free iron in MDA-MB-231 cells (Figure 4.59) consistent with ATP levels (Figure 4.41). The overwhelming majority of cells treated with Cisplatin + RSL3 were positive for mitochondrial free iron, whereas individual treatments, which resulted in 30-40% cell death did not induce Mito-FerroGreen. Previous work on breast cancer cells confirms that RSL3 can induce free iron in both MCF-7 and MDA-MB-231, although much higher doses were used (0.6 μM vs 0.0375 μM in the present study) (Park *et al.*, 2023), but no previous studies have assessed this drug combination in breast cancer cells using Mito-FerroGreen. Previous work in non-cancer cell models have shown that Cisplatin and RSL3 synergise to induce cell death in human ear cochlear cells (Mei *et al.*, 2020a), leading to increased free iron as detected by Mito-FerroGreen, and in this study, Ferrostatin-1 reversed the effects of Cisplatin + RSL3. Due to time constraints, the effects of Cisplatin + RSL3 were not reversed with Ferrostatin-1, but it would be interesting to see whether Ferrostatin-1 could reverse

low-level death induced by Cisplatin and in particular, RSL3, since low levels of each of these drugs caused low-level death without overt iron overload. From the images in Figure 4.61, RSL3 did appear to induce low levels of iron in almost all cells, but this was below the threshold taken for positivity (at least twice the background as a limit of detection), which was made difficult by the very high background of the Mito-FerroGreen stain. The assay requires washing excess dye from the cells, but this risked washing away dead cells also. A limited wash step was used whereby cells were stained, centrifuged in 96-well plates, and washed in PBS, and re-centrifuged to limit dead cell loss, but background stain levels remained a problem. We have shown that Ferrostatin-1 reversed the effects of high dose RSL3 in Chapter 3 (doses of RSL3 1.25-10 µM). What was not tested was whether Ferrostatin-1 could reverse low levels of cells death at the doses of RSL3 (0.0375 µM) used for combination treatments in MDA-MB-231. Consistent with cell death studies, RSL3 induced Mito-FerroGreen detection of free iron in MCF-7, whereas Doxorubicin did not. Combination treatment did not further enhance free iron, whereas in cell death assays, Doxorubicin and RSL3 exhibited an additive effect (Figure 4.9). Although due to the staining issues outlined earlier Mito-FerroGreen results may well be an underestimate, the enhanced cell death induced by Doxorubicin + RSL3 might not be due to ferroptosis.

Assessment of lipid peroxidation was performed to support observations of cytotoxicity and attempt to confirm that lipid peroxidation was occurring in response to chemotherapy in the presence and absence of ferroptosis-inducing agents. All treatments appeared to increase lipid peroxidation supporting this idea, however in all cases, the magnitude of increase did not reach statistical significance (Figure 4.64 and 4.65). The assay proved rather variable, with minute variation in the placing of the gate outlining the negative population greatly affecting the resulting % positivity. Each individual experiment showed convincing increases, but with large variation in % positivity caused by one outlier leading to overall no significant difference. Due to time constraints, the additional repeats of these experiments that would be needed to achieve significance, given the level of variability between technical repeats, was not possible. Previous studies have used the assay using in this study to successfully assess

RSL3-mediated cell death in MCF-7 and MDA-MB-231, albeit at higher doses that used in the present study (Park *et al.*, 2023).

Summary

In summary, this chapter shows that MDA-MB-231 and MCF-7 are sensitive to Doxorubicin and Cisplatin, although 3D cell cultures are highly resistant to Doxorubicin, and not Cisplatin. Of the ferroptosis inducers, RSL3 resulted in convincing cell death in both 2D and 2D cell cultures. Where enhanced cell death was observed in response to Doxorubicin or Cisplatin in combination with ferroptosis inducers, ROS induction, glutathione depletion, free iron overload and lipid peroxidation were generally observed, supporting the notion of ferroptosis induction by combination treatment. Combination of chemotherapy with RSL3 in the presence of the specific Nrf2 inhibitor ML385 proved highly effective at enhancing RSL3 effects in MDA-MB-231, but not MCF-7, and in MDA-MB-231, ML385 further enhanced combination treatment with RSL3 and Doxorubicin, but not Doxorubicin alone. Therefore, Nrf2 targeting strategies appear more effective at enhancing ferroptosis signalling in combination with ferroptosis inducers, rather than ferroptosis in combination with chemotherapy, which showed modest effects. Given that some of the potential side effects cardiotoxicity and ototoxicity can be linked to ferroptosis, this means that ferroptosis inducers combined with chemotherapy could be a double-edged sword: Enhanced side effects coupled with (modest) enhancement of tumour cell death, and with quite modest enhancement of cell death observed, this might limit the use of ferroptosis inducers as specific chemosensitizers, at least in breast cancer cells.

Chapter 5: Enhancement of radiotherapy response using ferroptosis inducers in 2D and 3D breast cancer cell model

5.1 Introduction

5.1.1 Radiotherapy

Radiotherapy (RTx) can be used to both limit cancer cell proliferation, and cause cell death (Huang and Zhou, 2020). It acts on cancer cells and causes DNA damage, which either directly results in cell death or prevents normal cell proliferation (Huang and Zhou, 2020). Radiation damages DNA by causing single-strand breaks, double-strand breaks, base or sugar damage, and/or crosslinking (Huang and Zhou, 2020). One of the main targets of RTx is DNA double-strand breaks, which are the most destructive to cells, and can result in chromosomal rearrangements and the loss of genetic information during DNA repair. (Kim *et al.*, 2019; Huang and Zhou, 2020). Simple double-strand breaks can be quickly repaired, but complex double-strand breaks, which often contain various types of DNA damage, cause genomic instability and cell death (Huang and Zhou, 2020). Radiation damages the DNA sugar backbone with high energy radiation, resulting in double-strand breaks (Srinivas *et al.*, 2019). Likewise, RTx can cause oxidation of DNA bases, via production of ROS, that are eliminated through base excision repair. This repair system becomes overwhelmed, leading to lack of repair of double-strand breaks (Kim *et al.*, 2019). Double-strand breaks are normally repaired by non-homologous end joining, or homologous repair, resulting in cells resuming normal function. However, DNA damage accumulated from radiation can causes cell death via apoptosis and necrosis; and/or cellular senescence which inhibits cellular replication (Kim *et al.*, 2019).

Additionally, RTx works in an indirect manner by triggering anti-tumour immune responses and immunogenic cell death. (Spiotto *et al.,* 2016). Pro-inflammatory cytokines such as tumour necrosis factor alpha (TNF-α), Interferon alpha (IFN-α), Interferon-beta (IFN-β), and Interferon-gamma (IFN-γ) are released when NFkB transcription factor or interferon (IFN) response pathway is activated by RTx (Spiotto *et al.,* 2016). The inflammatory reaction may result in immune cell maturation, and the identification, and elimination of the cancer cells (Spiotto *et al.,* 2016). Additionally, radiation-induced apoptosis and necrosis of cancer cells results in an increase in antigen release and the priming of immune cells for anti-tumour response, and generates DNA mutations leading to generation of neo-epitopes that are recognised as foreign by the immune system (Spiotto *et al.,* 2016).

5.1.2 Radiotherapy and Reaction Oxygen Species

RTx can also cause the production of reactive oxygen species (ROS) in cells (Srinivas *et al.*, 2019). ROS from RTx is predominantly produced endogenously in the mitochondria and radiolysis of water (Srinivas *et al.*, 2019). The generated ROS can stress cells and damage DNA, as well as other organelles, by interfering with the electron transport chain and interacting with biological substances (Srinivas *et al.*, 2019). ROS also causes lipid peroxidation in the plasma membrane, which lead to membrane damage and cell death (Kim *et al.*, 2019). Also, ROS can damage the mitochondria, causing the release of cytochrome *c* and the activation of the intrinsic apoptotic pathways (Kim *et al.*, 2019). Cellular stress brought on by ROS and RTx itself can also cause an accumulation of improperly folded proteins, via the unfolded protein response cell stress pathway, and trigger cell death via apoptosis or autophagy (Kim *et al.*, 2019). Furthermore, there is evidence that RTx can cause vascular damage and endothelial cell death, predominantly in regions of vascular remodelling such as around tumours. This can lead to a damage to the vascularisation of cancerous tumours, slow down growth of tumours and cause cancer cell death (Brown, Carlson and Brenner, 2014; Castle and Kirsch, 2019). Finally, high quantities of ROS from RTx mutates DNA, stabilising p53, which then drives the signalling pathways that promote apoptosis, typically via p53-mediated BAX expression and intrinsic apoptosis (Srinivas *et al.*, 2019).

5.1.3 Radiotherapy and breast cancer

Radiotherapy (RTx) is a common cancer treatment method, to target and destroy cancer cells by inducing DNA damage (Jaffray, 2012). The tumour area is penetrated by ionizing radiation, which has both direct and indirect cellular effects. Base damage, single strand breaks (SSBs), and double strand breaks (DSBs) are only a few of the types of DNA damage it directly causes *(*Baidoo *et al.,* 2013).

RTx involvement in the management of early breast cancer is evolving. Since the 1980s, an increasing number of patients with early-stage illness have undergone breast-conserving therapy (Joshi *et al.*, 2007). The use of post-mastectomy irradiation was on the decline, because it was believed that it did not increase patient survival, whilst

breast-conserving surgery therapy, where a portion of the mammary tissue was retained, lowering the frequency of total mastectomies (Joshi *et al.*, 2007). Recently, the use of RTx to the breast in the treatment of early-stage breast cancer has come under scrutiny since conventional radiotherapy following conservative surgery in early-stage breast cancer may be confounded by both treatment-related morbidity, and a lack of radiotherapy resources (Joshi *et al.*, 2007).

Research indicates that radiation used after mastectomy and/or breast-conserving surgery improves survival (Vinh-Hung and Verschraegen, 2004). Clinical studies of postmastectomy radiotherapy have revealed a 9–10% improvement in overall survival at 10 years for individuals who received radiotherapy, compared to those who did not receive radiotherapy (Joshi *et al.*, 2007). Determining which patients with breast cancer treated with conventional adjuvant chemotherapy followed by mastectomy, may benefit from postmastectomy radiation (PMRT) therapy is one of the most difficult issues facing breast cancer radiation oncologists. Regarding the indications for PMRT in the context of neoadjuvant chemotherapy, this has given rise to discussion by the Early Breast Cancer Trialists' Collaborative Group (2014). A meta-analysis of individual patient data for 10,801 women in 17 randomised trials of RTx versus no RTx after breast-conserving surgery; 8337 patients whom had pathologically proven node-negative or node-positive cancer, found that RTx lowers recurrence and breast cancer death (Darby *et al.,* 2011).

The involvement of the axillary lymph nodes in patients with early-stage breast cancer is the most important prognostic factor (Cianfrocca and Goldstein, 2004). Small local tumours may just be treated with surgery alone, whereas larger tumours or tumours with a higher grade would be more likely to be treated with additional therapies, one of which is RTx (Cianfrocca and Goldstein, 2004). The presence of lymph node metastasis means that surgery alone is not curative, and additional therapies, such as post-operative radiotherapy, and/or chemotherapy is required.

It is well recognised that there are many different types of breast cancer, each with unique histopathology and gene expression profiles. The categorization of breast tumours into subgroups that were not obvious using more standard histological criteria

has been made possible by gene expression profiles (Perou *et al.*, 2000). The clinical strategy for classifying subtypes still uses older histological techniques to evaluate the expression of three common molecular markers: oestrogen receptor (ER), progesterone receptor (PR), and human epidermal growth factor receptor 2 (HER2), with the hormone receptor (ER and PR) positive breast tumours falling under the luminal sub-types (luminal A and luminal B) (Sørlie *et al.*, 2001, 2003; Sotiriou *et al.*, 2003; Brenton *et al.*, 2005). Breast cancers with high levels of HER2, but low amounts of hormone receptors are classified as the HER2 subtype. Due to very low or negligible levels of ER, PR, and HER2 expression, whilst the basal-like subtype is often classified as triple negative breast cancer by standard immunohistochemistry and has none of the ER, PR or HER2 receptors and is described as a TNBC (Sørlie *et al.*, 2001, 2003; Sotiriou *et al.*, 2003; Brenton *et al.*, 2005).

Triple-negative breast cancer (TNBC) is more difficult to treat than ER/PR-positive or Her-2-positive cancer in that there is no specific targeted therapy available. Furthermore some TNBC patients have tumours that are intrinsically resistant to RTx, although combination of RTx with other treatment regimes, primarily cytotoxic chemotherapy, can help the control of TNBC control (Adams *et al.*, 2014). Age, tumour size, lymph node metastases, surgical margins, lymph vascular invasion, and histological grade are all thought to be important factors affecting locoregional recurrence (LRR) in TNBC (Adams *et al.*, 2014). One key factor that contributes to the poor radiation effects reported for TNBC is local recurrence following surgery and RTx treatment, indicating that if RTx is unsuccessful, the resulting tumour will be even more difficult to treat.

Different outcomes for women diagnosed with breast cancer can be attributed to the disease's heterogeneity. For instance, luminal subtypes have a better prognosis, whereas HER2 and basal-like subtypes have much higher recurrence rates and lower overall rate of survival (Sørlie *et al.*, 2001, 2003; Sotiriou *et al.*, 2003; Brenton *et al.*, 2005; Carey *et al.*, 2006). This has been supported by work by Wang and colleagues, who performed a retrospective analysis of 2118 patients with primary operable breast cancer. They discovered that molecular subtype could reliably predict the risk of recurrence, with luminal A tumours having the lowest rate of relapse (12.7%) and luminal B, HER2, and basal-like subtypes being associated with higher rates of relapse

(15.7%, 19.1%, and 20.1%) (Wang *et al.*, 2011). It is also clear that such heterogeneity accounts for variations in response to therapy. However, the question remains as to whether these breast cancer subtypes may be used to predict response to RTx, or whether specific subtypes may benefit from radio-sensitising agents to enhance the efficacy of this treatment. Data from *in vitro* experiments have demonstrated that breast cancer cell lines representing the various subtypes exhibit varying inherent sensitivity to ionising radiation (Smith *et al.*, 2009).

Postmastectomy RTx in a large trial done in women with breast cancer resulted in a substantial improvement in disease-free survival, and a reduction in the local recurrence irrespective of tumour size, number of involved nodes, histopathology grade (Rutqvist *et al.*, 2003). Another study shows in low grade localised Stage 1 breast cancer, when treated with either tamoxifen and RTx, both worked equally well, with comparable survival rates a good prognosis, and RTx alone was as beneficial as Tamoxifen (Blamey *et al.*, 2013).

Despite being a frequent treatment for many cancer types, including TNBC, patients may not react well to RTx, or indeed the response to RTx may fade as a result of the development of radio-resistance (Kyndi *et al.*, 2008). Furthermore, TNBC is more radioresistant than other breast cancer subtypes, thus reducing the effectiveness of RTx as a treatment (Zhou *et al.*, 2020). There are numerous hypotheses why radio-resistance can occur: (1) Non-coding RNAs that impact signalling pathways involved in cellular functions, (2) cell cycle regulation, or (3) cellular hypoxia (Aranza-Martínez *et al.*, 2021).

Numerous strategies have been developed to counteract the emergence and persistence of this resistance to radiotherapy, despite the fact that the mechanisms underlying radio-resistance may vary among patients, and still not fully elucidated (Wang *et al.*, 2018). The effective application of combination therapy regimens with RTx, in which chemotherapy, immunotherapy, or targeted medicines act to radio-sensitize cancer, or operate synergistically with RTx to enhance effects, is one such strategy that has been shown to hold promise (Bhat *et al.*, 2022).

5.1.4 Radiation combination therapies in breast cancer

Many cancers, including breast cancer, are treated with multimodality treatment strategies, which show great promise for the disease. In addition to RTx, various therapeutic drugs have been developed for the treatment of breast cancer. In a Phase I clinical trial, poly-ADP ribose polymerase (PARP) inhibitors, which inhibit the base-excision repair mechanism in cells, were studied in conjunction with RTx in TNBC (Loap *et al.*, 2021). The results showed no dose-limiting toxicities, but still need further studies for the efficacy of the therapy (Loap *et al.*, 2021).

Likewise, the combination of RTx with immunotherapies, is quite intriguing because it is known that the immune response plays a role in RTx-mediated cancer responses *(Nguyen et al.,* 2021). A Phase I clinical study using RTx in combination with the immune checkpoint inhibitor pembrolizumab, which prevents tumour-derived PD-L1 from inactivating T-cells, showed an overall response rate of 13.2% in a variety of metastatic malignancies, including 6 patients with metastatic breast cancer, and triggered more research on this combination therapy and its response on a number of cancer biomarkers (Luke *et al.*, 2018). This is likely a combination of RTx-induced neo-epitopes being produced, combined with re-awakening of T-cell responses to existing neo-epitopes.

5.1.5 Radiotherapy-induced breast cancer cell death mechanisms

Radiation can induce apoptosis this is mediated by p53 (Abuetabh *et al.*, 2022). In response to radiation, ataxia telangiectasia mutated (ATM) kinase, phosphorylates p53, stabilising it and preventing its destruction by mouse double minute 2 homolog (MDM2) protein (also known as E3 ubiquitin-protein ligase). Once stabilised, p53 acts as a transcription factor, driving expression of the pro-apoptotic BAX and PUMA as well as NOXA, all of which enhance mitochondrial-mediated apoptotic signalling (Abuetabh *et al.*, 2022). This now releases cytochrome *c* and activates the caspase-9, -3 and -7 pathways, leading to intrinsic apoptosis, including via caspase-3-mediated cleavage of Inhibitor of Caspase activated DNAse (I^{CAD}) leading to classic DNA fragmentation seen in apoptotic cells (Aubrey *et al.*, 2018). Alternately, p53 activates caspase-8 and its

downstream effectors to cause extrinsic apoptosis via inducing the death receptors FAS (also known as CD95), death receptor 5 (DR5), and FAS ligands (Sheikh and Fornace, 2000). Caspase-8 activates executioner caspases such as caspase-3, gain leading to DNA fragmentation. Upon resolution of DNA damage, ataxia telangiectasia mutated (ATM) kinase ceases to phosphorylate p53, and newly produced p53 is unphosphorylated, eventually leading to lowered BAX, NOXA, and PUMA levels (Abuetabh *et al.*, 2022). If this occurs before apoptosis occurs, the cells will survive, and decreasing p53 levels will also lead to decreased p21, a cyclin-dependent inhibitor, allowing continuation of the cell cycle (Abuetabh *et al.*, 2022).

5.1.6 Radiotherapy and ferroptosis

Recent research has revealed a new type of regulated cell death (RCD) called ferroptosis, which differs in morphology and processes from other RCD mechanisms such as apoptosis, autophagy, and necroptosis, as this is dependent on iron and lipid peroxidation (Cao and Dixon, 2016; Yuan *et al.*, 2016). Despite the fact that ferroptosis is occasionally referred to as an instance of autophagy-dependent cell death, inhibitors for these other RCDs typically are unsuccessful in preventing ferroptosis (Cao and Dixon, 2016; Gao *et al.*, 2016).

Ferroptosis is thought to be a crucial component of RTx-mediated tumour suppression and that RTx can cause strong ferroptosis induction (Lang *et al.*, 2019; Lei *et al.*, 2020a). According to one theory, (1) ionising radiation triggers ferroptosis and lipid peroxidation through at least three parallel mechanisms (Lang *et al.*, 2019; L. F. Ye *et al.*, 2020; Lei *et al.*, 2020a) (Figure 5.1): Phospholipids acylated with Polyunsaturated fatty acids (PL-PUFAs) are induced by (2) RTx-induced ROS in conjunction with RTx-induced ACSL4 expression, (3) decreased GSH levels, (4) weakening the GPX4-mediated ferroptosis defence, (5) and finally RTx can upregulate SLC7A11 expression. (6) In addition, by producing an excessive amount of ROS, immune responses can cause lipid peroxidation. In particular, polyunsaturated fatty acid (PUFA) radicals can be formed when immune response-generated ROS remove electrons from PUFAs. These unstable carbon-centred radicals which quickly combine with oxygen molecules to form lipid peroxyl radicals

which then use the Fenton reaction to remove hydrogen from other molecules to create lipid hydroperoxides (PUFA-OOH) (Shadyro *et al.,* 2002; Azzam *et al.,* 2012). Moreover immune cells increase the production of long-chain-fatty-acid CoA via increased Acyl-CoA synthetase long-chain family member 4 (ACSL4) to support the production of PL-PUFAs, however the specific method by which immune cells increases ACSL4 levels is still unknown (Lei *et al.*, 2020a). Ionizing radiation consistently has a major impact on the lipid metabolism linked to ferroptosis, with numerous lysophospholipids (LysoPLs) and diacylglycerols (DAGs) shown to be greatly elevated after irradiation (L. F. Ye *et al.*, 2020). Increased levels of LysoPLs and DAGs have also been seen after treatment with ferroptosis inducers (Colles and Chisolm, 2000; Dixon *et al.*, 2015; Yang *et al.*, 2016), indicating that ionizing radiation and ferroptosis inducers, which induce comparable lipidomic signatures, consistently with their shared effects to drive ferroptosis (Zhang *et al.*, 2019). Finally, ionizing radiation also causes GSH depletion, which impairs the GPX4-mediated ferroptosis defence and encourages ferroptosis (L. F. Ye *et al.*, 2020).
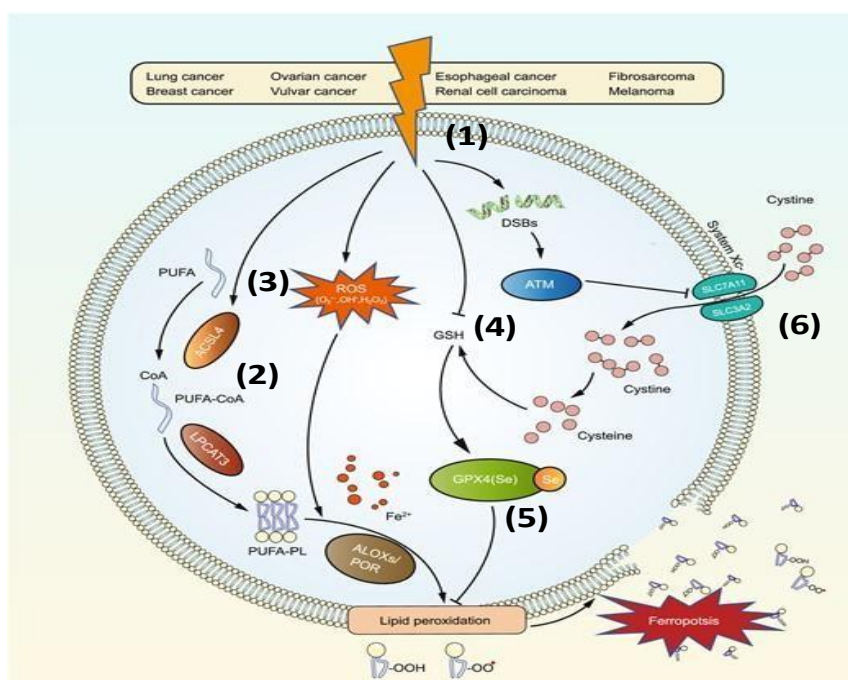
Figure 5.1: Radiotherapy (RTx) (1), through several mechanisms, causes ferroptosis in tumours. Ferroptosis and PL-PUFA peroxidation are induced by RTx-induced ROS (2) in conjunction with RTx-induced ACSL4 expression (3). Furthermore, RTx decreases GSH levels (4), weakens the GPX4-mediated ferroptosis defence (5), and hence promotes ferroptosis. Moreover, RTx can upregulate SLC7A11 expression as an adaptive response to prevent ferroptosis or repress SLC7A11 expression in an ATM-dependent manner to further promote ferroptosis (6). Modified from Lei *et al.*, (2021).

Cancer cells may be protected from RTx by pharmacological ferroptosis inhibition, and RTx also caused less potent lipid peroxidation and ferroptosis inducer-resistant cancer cells, which also seem to be radioresistant (Lang *et al.*, 2019; Lei *et al.*, 2020a). During RTx, the NRF2 gene is highly expressed, and as a results the Nrf2-driven antioxidant proteins being produced such as SLC7A11, a key importer of precursors of glutathione. The production of this cysteine-glutamate antiporters, inhibit ferroptosis by delivering cystine to promote glutathione (GSH) synthesis (Xie *et al.*, 2020). Another protein that is produced during the activation of Nrf2 is GPX4, which also inhibits ferroptosis by promoting the production of GSH and reduces ROS levels and prevents ferroptosis (Xie *et al.*, 2020). The expression of SLC7A11 and GPX4 is increased by ionizing radiation as an adaptive response to prevent cells from undergoing ferroptosis, which contributes to radio-resistance. Therefore, depletion or inhibition of SLC7A11 and/or GPX4 promotes ionizing radiation-induced ferroptosis, which increases radio-sensitisation (Xie *et al.*, 2011; Lei *et al.*, 2020a). Different tumour types, susceptibilities to ferroptosis does not necessarily correspond with the number of tumours that are sensitive to RTx. For instance, radioresistant tumours such as renal cell carcinoma and ovarian cancer, as well as tumour types for which RTx is a significant therapeutic option, such as hepatocellular carcinoma, pancreatic cancer, diffuse large B cell lymphoma, and triple-negative breast cancer, are all moderately vulnerable to ferroptosis (Zou and Schreiber, 2020).

Here using cell culture models, an investigation is made of the potential of the use of ferroptosis inducers and inhibitors of Nrf2 to enhance radiotherapy in breast cancer cells in both standard 2D cell culture, and 3D cell culture.

5.1.7 Aims and hypothesis

Hypothesis:

Ferroptosis inducers enhance radiotherapy responses in both 2D and 3D cell culture models.

To achieve this, we aim to:

1. Assess radiotherapy responses in breast cancer 2D cell culture.
2. Combine radiotherapy with ferroptosis inducers in breast cancer 2D cell culture.
3. Assess radiotherapy response in cells treated with the Nrf2 inhibitor ML385.
4. Assess radiotherapy responses in breast cancer 3D cell culture.
5. Combine radiotherapy with ferroptosis inducers and Nrf2 inhibitors in breast cancer 3D cell culture.

5.2 Results

5.2.1 Colony formation assay results

5.2.1.1 The effect of radiotherapy on colony formation in 2D breast cancer cells colonies

In initial experiments to determine the optimal doses of radiotherapy, cell suspensions of MDA-MB-231 and MCF-7 cells were irradiated at 0 to 20 Gy in a colony formation assay at cell density of either 1000 cells/wells or 2000 cells/wells (Figure 5.2 and 5.3). The data shows colony formation over a range of ionising radiation doses, at both cell densities. In this preliminary study colony formation was almost abolished at 10 and 20 Gy, hence all subsequent investigations used a 0 to 5 Gy irradiation doses. MCF-7 appeared slightly more radiosensitive than MDA-MB-231 (Figure 5.2 and 5.3).

5.2.1.2 Effect of low doses of radiotherapy on colony formation in 2D breast cancer cell colonies

Low dose of irradiation between 0 to 2.5 Gy were subsequently performed on the colony formation of MDA-MB-231 and MCF-7 cells grown in 2D (at a cell density of 1000 cells/wells) the percentage of cell survival was determined (Figure 5.4 and 5.5) in three technical repeats. For both cell lines, responded to these lower irradiation treatments with 1.25 Gy causing a 60% reduction in cell survival. This irradiation dose was then used in all subsequent combination treatment regimes, with the ferroptosis inducers (Erastin, RSL3, FIN56) and the Nrf2 inhibitor ML385 in 2D cell culture following further optimization using CellTiter-Glo® luminescent cell viability assay to assess cytotoxicity over shorter time periods.

Figure 5.2: Colony formation assay of MDA-MB-231 cell line following irradiation

(A) 1000 cells/wells
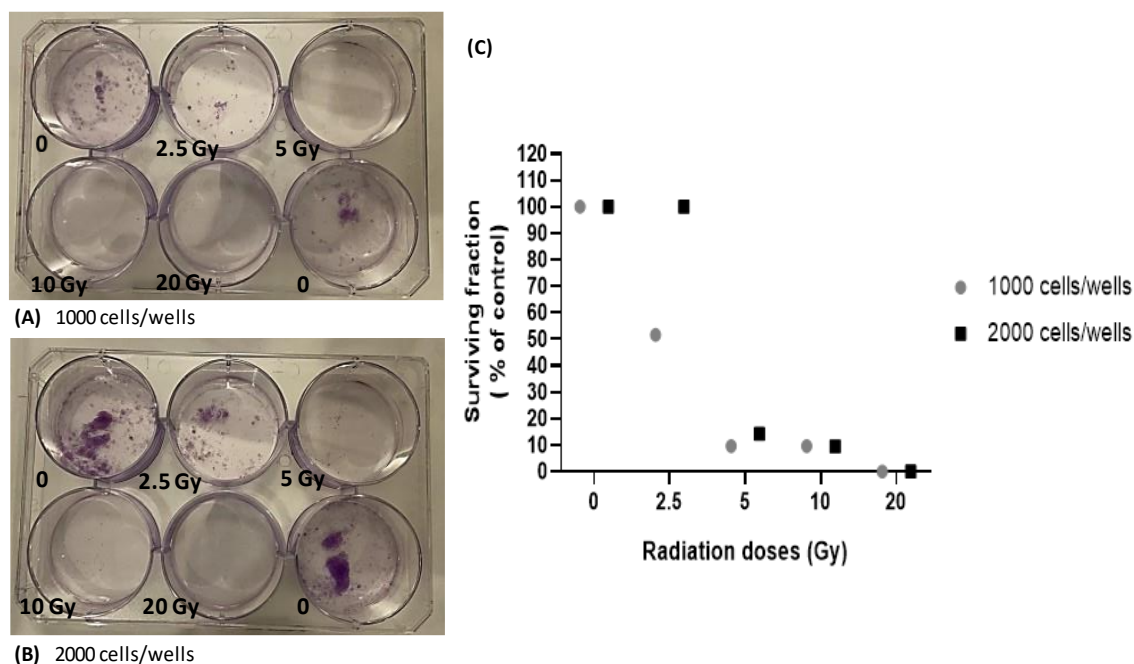
(B) 2000 cells/wells

Figure 5.2: Cell survival of MDA-MB-231 breast cancer cells was assessed in cells grown in 2D cell culture, at cell densities of 1000 and 2000 cell/well. Following irradiation cells were staining with crystal violet and the number of colonies formed were counted following irradiation at 0 to 20 Gy (n=1) in cells seeded a density of: **(A)** 1000 cells/wells and **(B)** 2000 cells/wells. **(C)** The cell survival was plotted against radiation dose (Gy) and was expressed as a percentage of non-irradiated control cells which was assigned 100% survival.

Figure 5.3: Colony formation assay of MCF-7 cell line following irradiation

(A) 1000 cells/wells
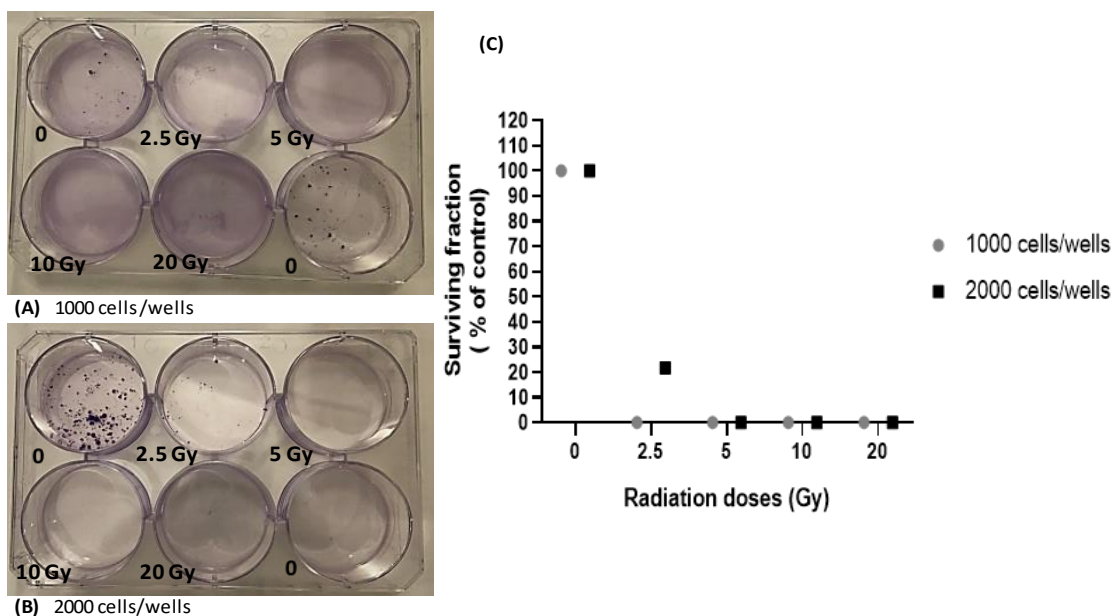
(B) 2000 cells/wells

Figure 5.3: Cell survival of MCF-7 breast cancer cells was assessed in cells grown in 2D, at cell densities of 1000 and 2000 cell/well. Following irradiation cells were staining with crystal violet. The number of colonies formed were counted following irradiation at 0 to 20 Gy (n=1) in cells seeded a density of: **(A)** 1000 cells/wells and **(B)** 2000 cells/wells. **(C)** The cell survival was plotted against radiation dose (Gy) and was expressed as a percentage of non-irradiated control cells which was assigned 100% survival.

231

Figure 5.4: Colony formation assay of MDA-MB-231 cell line following low doses of radiation
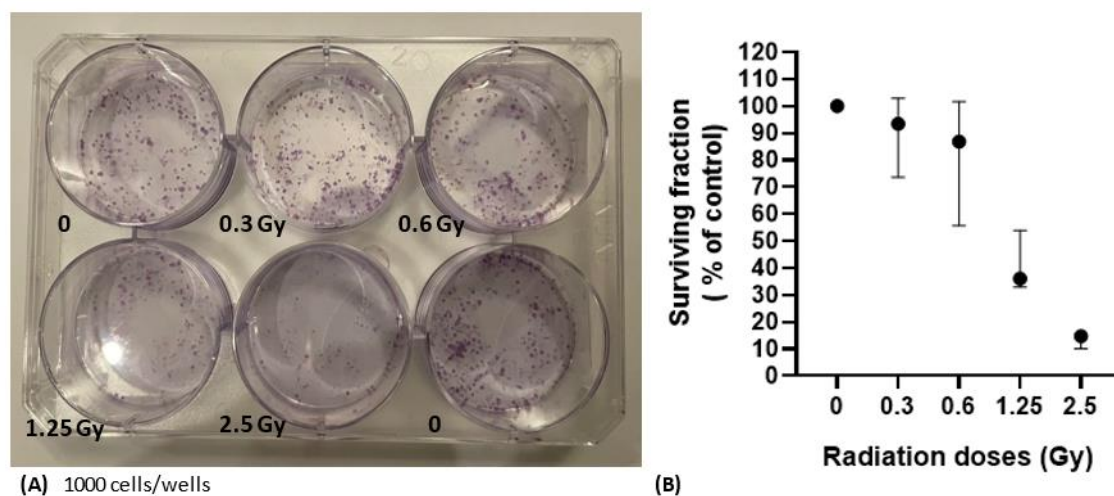
Figure 5.4: Cell survival of MDA-MB-231 breast cancer cells was assessed in cells grown in 2D, at a cell density of 1000 cells/wells. Following irradiation cells were staining with crystal violet. **(A)** The number of colonies formed were counted following irradiation at 0 to 2.5 Gy (n=3) 1000 cells/wells, and **(B)** the cell survival was plotted against radiation dose (Gy) and was expressed as a percentage of non-irradiated control cells which was assigned 100% survival.

Figure 5.5: **Colony formation assay of MCF-7 cell line following low doses of radiation**
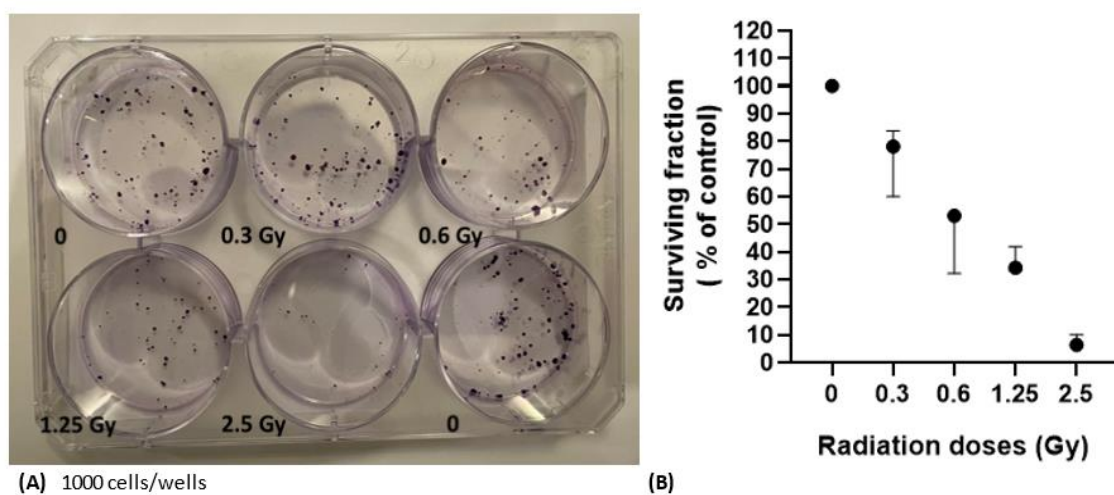
Figure 5.5: Cell survival of MCF-7 breast cancer cells was assessed in cells grown in 2D, at a cell density of 1000 cells/wells. Following irradiation cells were staining with crystal violet. **(A)** The number of colonies formed were counted following irradiation at 0 to 2.5 Gy (n=3) 1000 cells/wells, and **(B)** the cell survival was plotted against radiation dose (Gy) and was expressed as a percentage of non-irradiated control cells which was assigned 100% survival.

5.2.2 The effect of ferroptosis inducers on radiotherapy responses in MDA-MB-231 in 2D cell culture

5.2.2.1 The effect of combination treatment of Erastin +/- radiotherapy in MDA-MB-231 cells

Subsequent optimization of RTx sensitivity showed that 1.25 Gy induced low level of cell death in 72 hours (Figure 5.6). To assess Erastin-induced radiosensitivity, cells were treated with Erastin for 72 hours immediately after irradiation with x 1.25 Gy and stained with Hoechst 33342 and PI to assess cell death and apoptosis (Figure 5.6A and B). Although colony formation showed potent effects at 1.25 Gy after 10-14 days, at shorter timepoints used for Hoechst 33342/PI staining, 1.25 Gy had only very modest effects. Since we knew that this dose must be having profound effects on the cells long-term, we used this dose for short term treatments. Individual treatments did not significantly increase apoptosis or necrosis, but combined treatment did significantly increased cell death when compared to untreated control cells (P≤0.05), causing an additive effect.

The data for cell death analysis was consistent with the results obtained for ATP levels measured using 2D CellTiter-Glo® luminescent cell viability assay (Figure 5.6C), which showed a significant decrease in cell ATP levels after irradiation and Erastin combination treatment. However almost all of this effect was due to Erastin-alone. Erastin alone causes a significant decrease in ATP levels when compared to control cells (P≤0.001), Likewise, following Erastin and irritation combination treatment there was a significant decrease in ATP levels when compared to untreated control cells (P≤0.001), and radiotherapy alone (P≤0.001). Importantly the Erastin/irradiation combined treatment was not significant different from Erastin treatment alone (P≤0.05). This suggests that the majority of reduction in cell ATP levels in combination treatment was due to Erastin, and there was not enhancement by radiotherapy (Figure 5.6C). This was confirmed by the fact that there was no significance in ATP in irradiated and untreated control (P≤0.05).

Figure 5.6 The effect of radiotherapy and Erastin combination treatment of 2D MDA-MB-231 cells

(A)
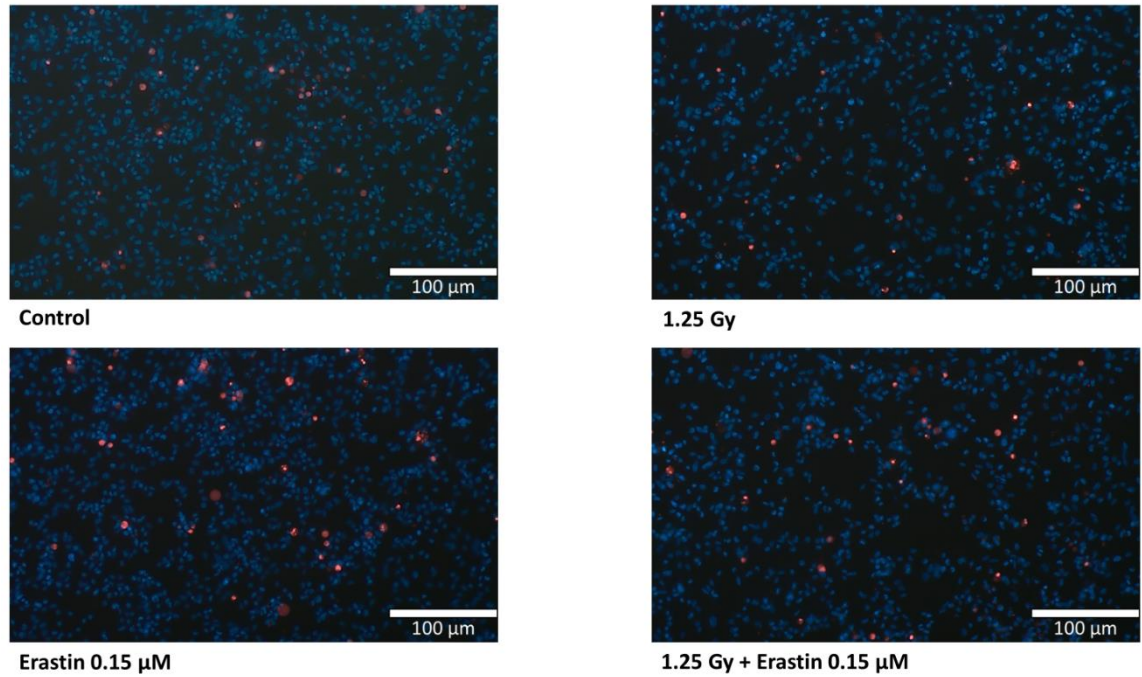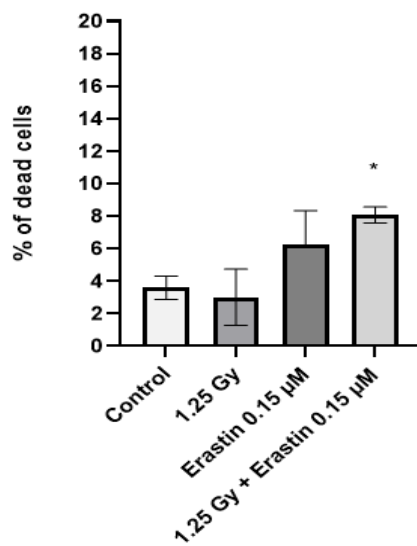
(B)   **(C)**
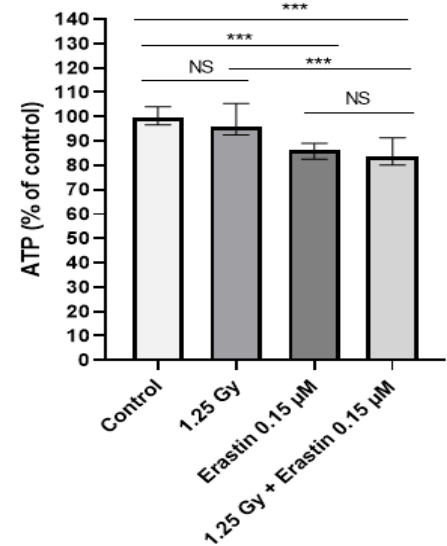
Figure 5.6: MDA-MB-231 cell line were treated with 1.25 Gy of radiation and the ferroptosis inducer Erastin (0.15 µM) for 72 hours. **(A)** Assessment of cell death following Hoechst 33342/PI staining. Live cells and apoptotic cells are stained blue with Hoechst 33342, and dead cells are stained red with PI staining. **(B)** The percentage of cell death was calculated from the by Hoechst 33342/PI-stained cells, when compared to the Erastin (0.15 µM) vehicle control (0.2% (v/v) DMSO) treated cells. **(C)** Assessment was made of cell ATP levels using the CellTiter-Glo® luminescent cell viability assay of MDA-MB-231 cell line treated with radiation (1.25 Gy), and Erastin (0.15 µM) alone and in combination. All data was compared to the vehicle control which was assigned 100% ATP levels. Data is presented as median ± range. n=3 independent experiments each with 3 technical repeats. Statistical significance was determined by the Kruskal-Wallis test with a Dunn's post hoc test. Comparison with the vehicle control and single and combined treatments. Statistical significance was set at *=P≤0.05, **=P≤0.01, and ***=P≤0.001.

5.2.2.2 The effect of combination treatment of RSL3 +/- radiotherapy in MDA-MB-231 cells

To assess RSL3-induced radiosensitivity, MDA-MB-231 cells were treated with RSL3 for 72 hours immediately after irradiation and stained with Hoechst 33342 and PI to assess cell death and apoptosis (Figure 5.7A and B). Individual and combination treatments of RLS3 and/or irradiation (1.25 Gy) treatments did not significantly increase apoptosis or necrosis in MDA-MB-31 cells, when compared to control cells.

The data for cell death analysis is generally consistent with the results obtained for ATP levels measured using the 2D CellTiter-Glo® luminescent cell viability assay (Figure 5.7C). The ATP levels were following RSL3/irradiation combined treatments were significantly reduced compared to the vehicle control ($P \le 0.001$) and the irradiation treatment alone ($P \le 0.001$). RSL3 also caused a significant decrease in ATP levels compared to the vehicle control ($P \le 0.001$). There was however, no significant difference in ATP levels between irradiation and the vehicle control and RSL3-alone ($P \le 0.001$) and when combination with radiation ($P \le 0.001$). Hence the action of RSL3, was not enhanced by radiotherapy (Figure 5.7C).

5.2.2.3 The effect of combination treatment of FIN56 +/- radiotherapy in MDA-MB-231 cells

To assess FIN56-induced radiosensitivity, MDA-MB-231 cells were treated with FIN56 for 72 hours immediately after irradiation at 1.25 Gy and stained with Hoechst 33342 and PI to assess cell death and apoptosis (Figure 5.8A and B). Individual treatments did not significantly increase apoptosis or necrosis, but FIN56/irradiation combined treatment significantly increased cell death compared to the vehicle control ($P \le 0.05$). Neither radiotherapy alone nor FIN56 alone significantly affected cell death (Figure 5.8A).

The cell death data is generally consistent with the results obtained for ATP levels measured using CellTiter-Glo® luminescent cell viability assay (Figure 5.8). In MDA-MB-231 cells, the FIN56/irradiation combination treatments significantly decreased ATP levels when compared to the vehicle control ($P \le 0.001$), and irradiation alone ($P \le 0.001$). Likewise, FIN56 alone also caused a significant decrease in ATP levels compared to the

vehicle control (P≤0.001). Importantly there was no significant differences in ATP levels when comparing FIN56/irradiation combination treatment and FIN56 treatment alone, and irradiation and the vehicle control. Hence, the majority of cell death and decrease in cell ATP levels here are due to FIN56 and are not enhanced by radiotherapy (Figure 5.8C).

Figure 5.7: The effect of radiotherapy and RSL3 combination treatment of 2D MDA-MB-231 cells

(A)
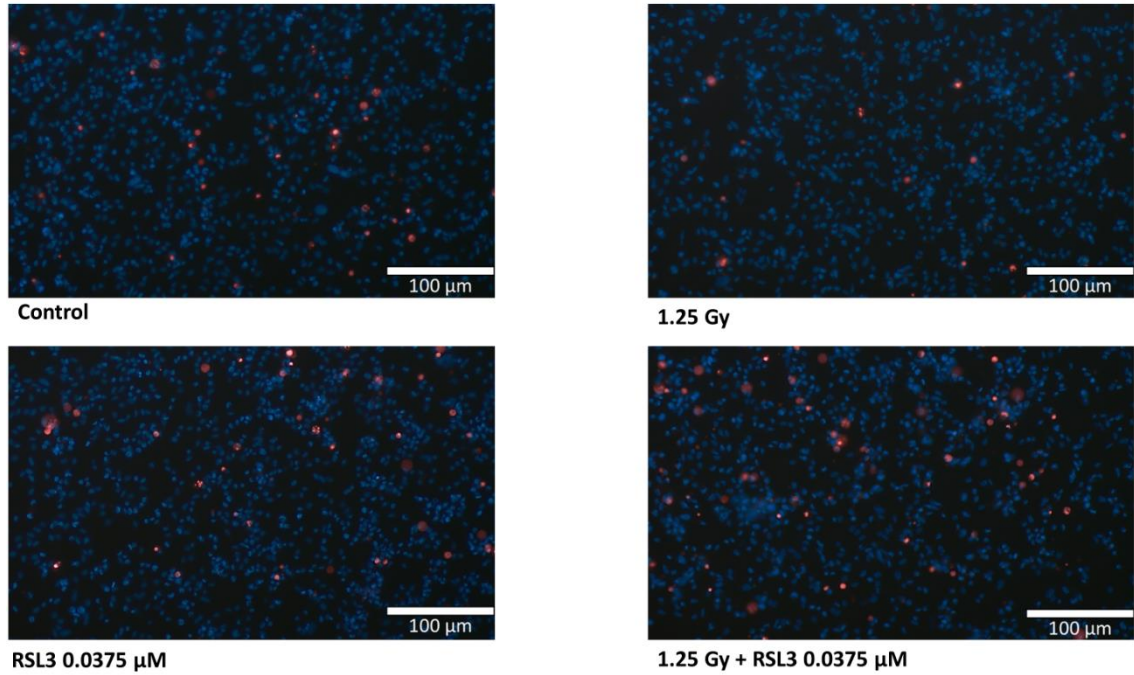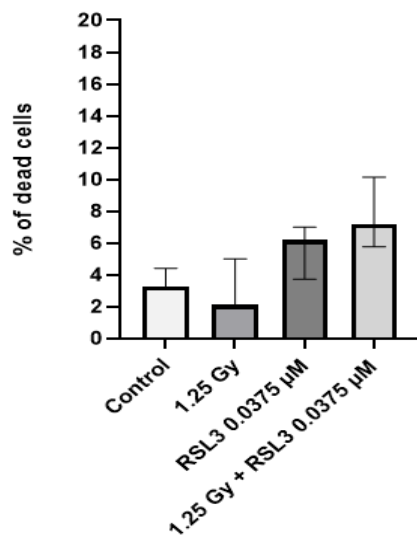
(B) **(C)**
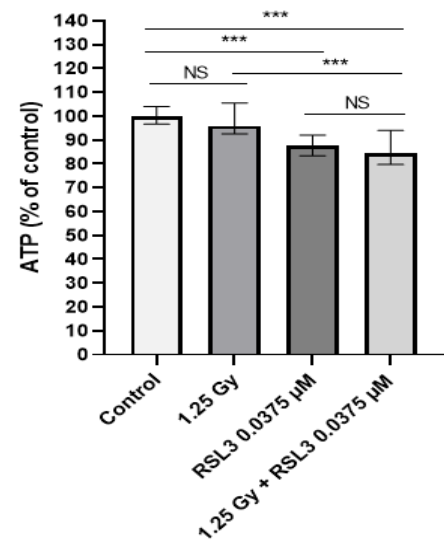
Figure 5.7: MDA-MB-231 cell line were treated with 1.25 Gy of radiation and the ferroptosis inducer RSL3 (0.0375 µM) for 72 hours. **(A)** Assessment of cell death following Hoechst 33342/PI staining. Live cells and apoptotic cells are stained blue with Hoechst 33342, and dead cells are stained red with PI staining. **(B)** The percentage of cell death was calculated from the by Hoechst 33342/PI-stained cells, when compared to the RSL3 (0.0375 µM) vehicle control (0.2% (v/v) DMSO) treated cells. **(C)** Assessment was made of cell ATP levels using the CellTiter-Glo® luminescent cell viability assay of MDA-MB-231 cell line treated with radiation (1.25 Gy), and RSL3 (0.0375 µM) alone and in combination. All data was compared to the vehicle control which was assigned 100% ATP levels. Data is presented as median ± range. n=3 independent experiments each with 3 technical repeats. Statistical significance was determined by the Kruskal-Wallis test with a Dunn's post hoc test. Comparison with the vehicle control and single and combined treatments. Statistical significance was set at *=P≤0.05, **=P≤0.01, and ***=P≤0.001.

Figure 5.8: The effect of radiotherapy and FIN56 combination treatment of 2D MDA-MB-231 cells

(A)

Control

1.25 Gy

FIN56 0.15 µM

1.25 Gy + FIN56 0.15 µM
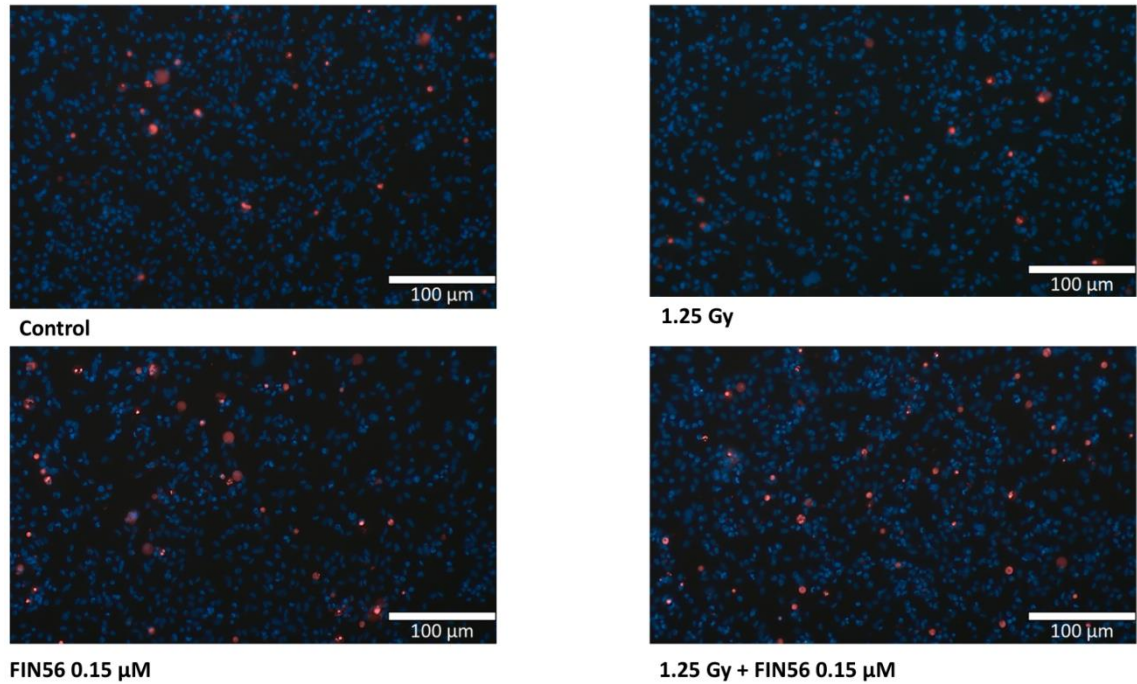
(B)
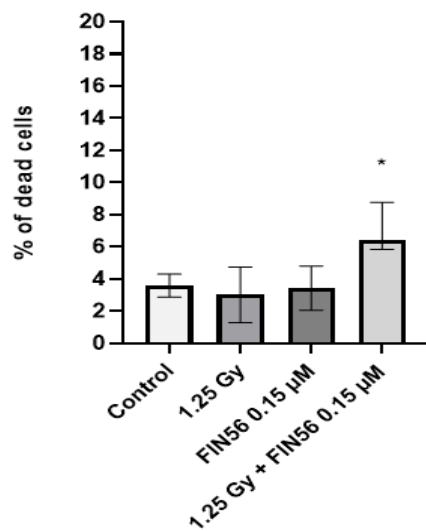
(C)
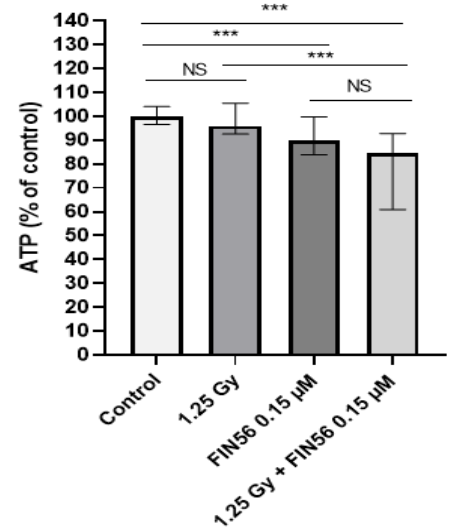
Figure 5.8: MDA-MB-231 cell line were treated with 1.25 Gy of radiation and the ferroptosis inducer FIN56 (0.15 µM) for 72 hours. **(A)** Assessment of cell death following Hoechst 33342/PI staining. Live cells and apoptotic cells are stained blue with Hoechst 33342, and dead cells are stained red with PI staining. **(B)** The percentage of cell death was calculated from the by Hoechst 33342/PI-stained cells, when compared to the FIN56 (0.15 µM) vehicle control (0.2% (v/v) DMSO) treated cells. **(C)** Assessment was made of cell ATP levels using the CellTiter-Glo® luminescent cell viability assay of MDA-MB-231 cell line treated with radiation (1.25 Gy), and FIN56 (0.15 µM) alone and in combination. All data was compared to the vehicle control which was assigned 100% ATP levels. Data is presented as median ± range. n=3 independent experiments each with 3 technical repeats. Statistical significance was determined by the Kruskal-Wallis test with a Dunn's post hoc test. Comparison with the vehicle control and single and combined treatments. Statistical significance was set at *=P≤0.05, **=P≤0.01, and ***=P≤0.001.

5.2.3 The effect of ferroptosis inducers on radiotherapy responses in MCF-7 cells

5.2.3.1 The effect of combination treatment of Erastin +/- radiotherapy in MCF-7 cells

To assess Erastin-induced radiosensitivity. MCF-7 cells were treated with Erastin for 72 hours immediately after irradiation and stained with Hoechst 33342 and PI to assess the percentage of cell death and apoptosis (Figure 5.9A and B). Individual treatments did not significantly increase apoptosis or necrosis, but Erastin/irradiation combined treatment significantly increased cell death when compared to the vehicle control, and an additive effect was observed ($P \leq 0.05$). Erastin-alone was not significant to control, most likely due to experimental variation.

The MCF-7 cell ATP levels following Erastin and radiotherapy combination treatment were significantly reduced compared to the vehicle control ($P \leq 0.001$) (Figure 5.9C). However, the use of radiotherapy alone compared to the vehicle control, and Erastin alone ($P \leq 0.001$) compared to the combined treatment of Erastin with radiotherapy ($P \leq 0.001$) were not significantly different. Likewise, in MCF-7 cells there was no significant difference between the ATP levels of cells treated with Erastin treatment alone, or in combination with radiotherapy, this suggested that the effect of the combination treatment on ATP levels was due to Erastin alone, and there was no further reduction in ATP levels attributed to radiotherapy (Figure 5.9C).

5.2.3.2 The effects of combination treatment of RSL3 +/- radiotherapy in MCF-7 cells

To assess RSL3-induced radiosensitivity, cells were treated with RSL3 for 72 hours immediately after irradiation and stained with Hoechst 33342 and PI to assess cell death and apoptosis (Figure 5.10A and B). RSL3 treatment alone ($P \leq 0.05$), and combined with radiotherapy significantly increased cell death compared to the vehicle control ($P \leq 0.05$). However, the dramatic increase in cell death seen with RSL3 alone compared to that shown by the RSL3/irradiation combination treatment shows that the major cause of cell death can be contributed to RSL3. The cell death data is generally consistent with the results obtained for ATP levels measured using CellTiter-Glo® luminescent cell viability assay (2D) (Figure 5.10C).

In MCF-7 cells the RSL3/irradiation combined treatments caused a significant reduction in ATP levels compared to the vehicle control ($P \leq 0.001$) and irradiation alone ($P \leq 0.001$). RSL3 alone causes a significant decrease in ATP levels compared to the vehicle control ($P \leq 0.001$). Importantly there was no significant deference between the RSL3/radiotherapy combination treatment and RSL3 alone, and radiotherapy compared to the vehicle control, suggesting that the majority of effect of the combination treatment on ATP levels was attributed to RSL3, and was not enhanced by radiotherapy (Figure 5.10C). Since RSL3 caused approximately a 90% reduction in cell ATP levels in MCF-7 cells, this was subsequently re-assessed using a lower doses (0.6, 1.25, 2.5, and 5 µM) (Section 5.2.4).

Figure 5.9: The effect of radiotherapy and Erastin combination treatment of 2D MCF-7 cells

(A)
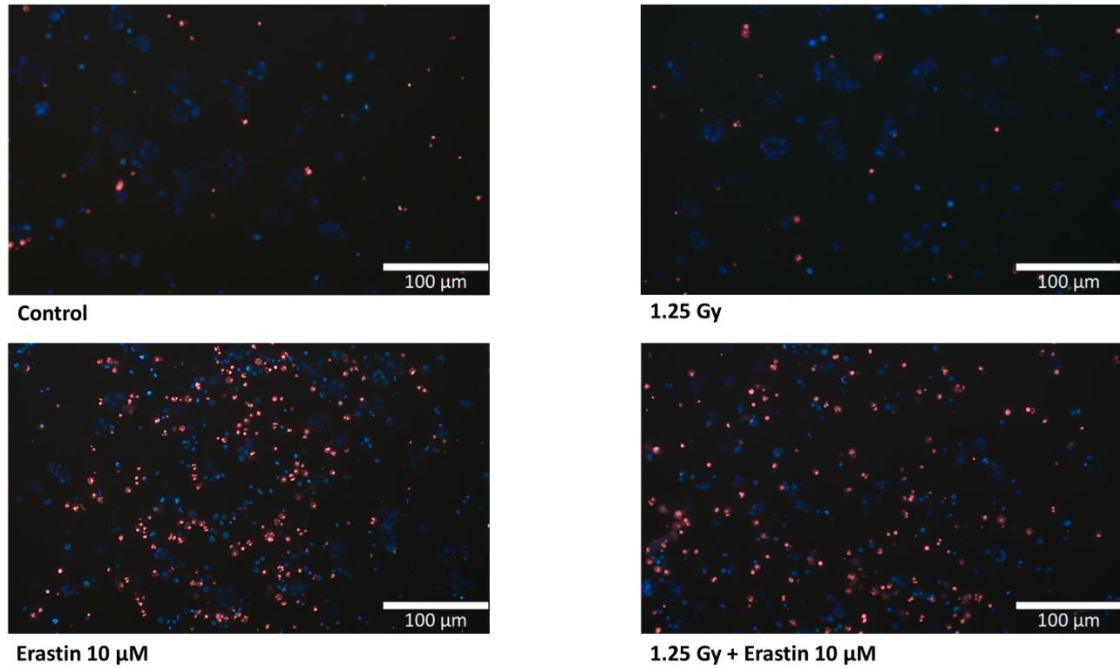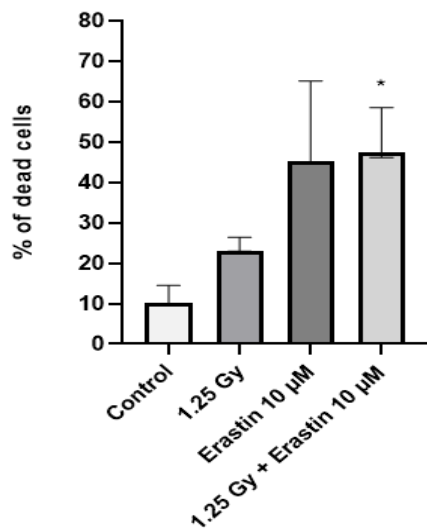
(B) **(C)**
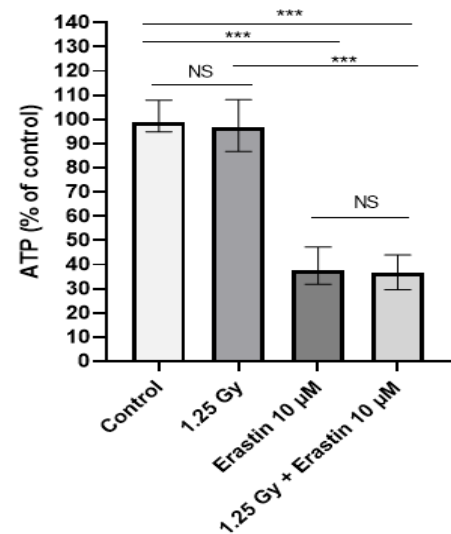
Figure 5.9: MCF-7 cell line were treated with 1.25 Gy of radiation and the ferroptosis inducer Erastin (10 µM) for 72 hours. **(A)** Assessment of cell death following Hoechst 33342/PI staining. Live cells and apoptotic cells are stained blue with Hoechst 33342, and dead cells are stained red with PI staining. **(B)** The percentage of cell death was calculated from the by Hoechst 33342/PI-stained cells, when compared to the Erastin (10 µM) vehicle control (0.2% (v/v) DMSO) treated cells. **(C)** Assessment was made of cell ATP levels using the CellTiter-Glo® luminescent cell viability assay of MCF-7 cell line treated with radiation (1.25 Gy), and Erastin (10 µM) alone and in combination. All data was compared to the vehicle control which was assigned 100% ATP levels. Data is presented as median ± range. n=3 independent experiments each with 3 technical repeats. Statistical significance was determined by the Kruskal-Wallis test with a Dunn's post hoc test. Comparison with the vehicle control and single and combined treatments. Statistical significance was set at *=P≤0.05, **=P≤0.01, and ***=P≤0.001.

Figure 5.10: The effect of radiotherapy and RSL3 combination treatment of 2D MCF-7 cells

(A)

Control

1.25 Gy

RSL3 10 µM

1.25 Gy + RSL3 10 µM

(B)

(C)
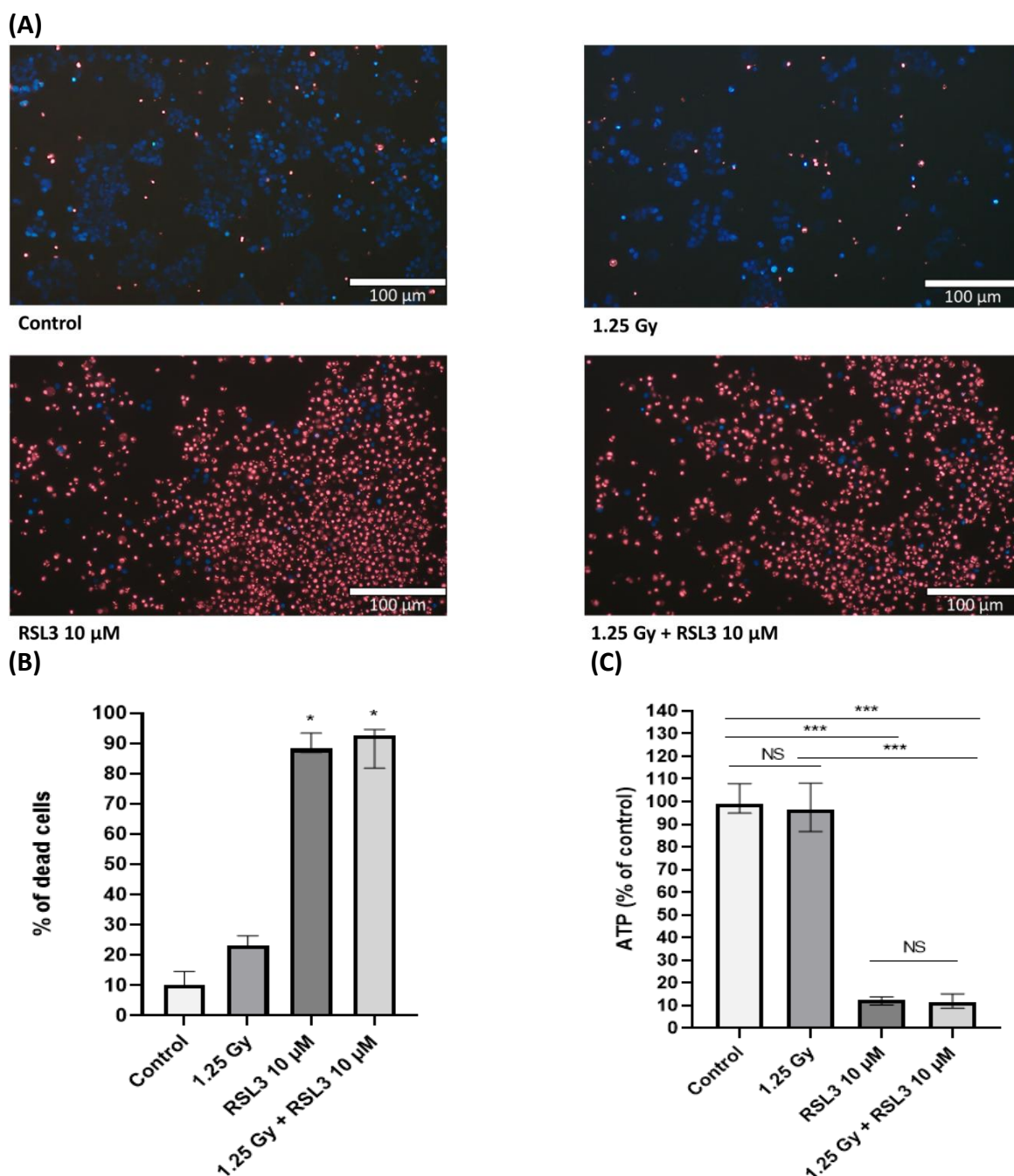
Figure 5.10: MCF-7 cell line were treated with 1.25 Gy of radiation and the ferroptosis inducer RSL3 (10 µM) for 72 hours. **(A)** Assessment of cell death following Hoechst 33342/PI staining. Live cells and apoptotic cells are stained blue with Hoechst 33342, and dead cells are stained red with PI staining. **(B)** The percentage of cell death was calculated from the by Hoechst 33342/PI-stained cells, when compared to the RSL3 (10 µM) vehicle control (0.2% (v/v) DMSO) treated cells. **(C)** Assessment was made of cell ATP levels using the CellTiter-Glo® luminescent cell viability assay of MCF-7 cell line treated with radiation (1.25 Gy), and RSL3 (10 µM) alone and in combination. All data was compared to the vehicle control which was assigned 100% ATP levels. Data is presented as median ± range. n=3 independent experiments each with 3 technical repeats. Statistical significance was determined by the Kruskal-Wallis test with a Dunn's post hoc test. Comparison with the vehicle control and single and combined treatments. Statistical significance was set at *=P≤0.05, **=P≤0.01, and ***=P≤0.001.

5.2.3.3 The effect of combination treatment of FIN56 +/- radiotherapy in MCF-7 cells

To assess FIN56-induced radiosensitivity, cells were treated with FIN56 for 72 hours immediately after irradiation and stained with Hoechst 33342 and PI to assess cell death and apoptosis (Figure 5.11A and B). Individual FIN56 and irradiation treatments and combined treatments did not significantly increase apoptosis or necrosis when compared to the vehicle control.

The cell death data is generally consistent with the results obtained for ATP levels measured using the 2D CellTiter-Glo® luminescent cell viability assay (Figure 5.11C). The FIN56/irradiation combined treatments significantly deceased cell ATP levels compared to the vehicle control (P ≤0.001) and irradiation alone (P≤0.001). FIN56 alone also caused a significant decrease in ATP levels compared to the vehicle control (P≤0.001). Importantly there were no significant differences in ATP levels when comparing the FIN56/irradiation combined treatment and FIN56 alone and when comparing irradiation treatment alone with the vehicle control. This suggested that majority of the reduction in cells ATP levels of the combination treatment was due to FIN56, and this was not enhanced by radiotherapy (Figure 5.11C).

Figure 5.11: The effect of radiotherapy and FIN56 combination treatment of 2D MCF-7 cells

(A)

Control

1.25 Gy

FIN56 10 µM

1.25 Gy + FIN56 10 µM
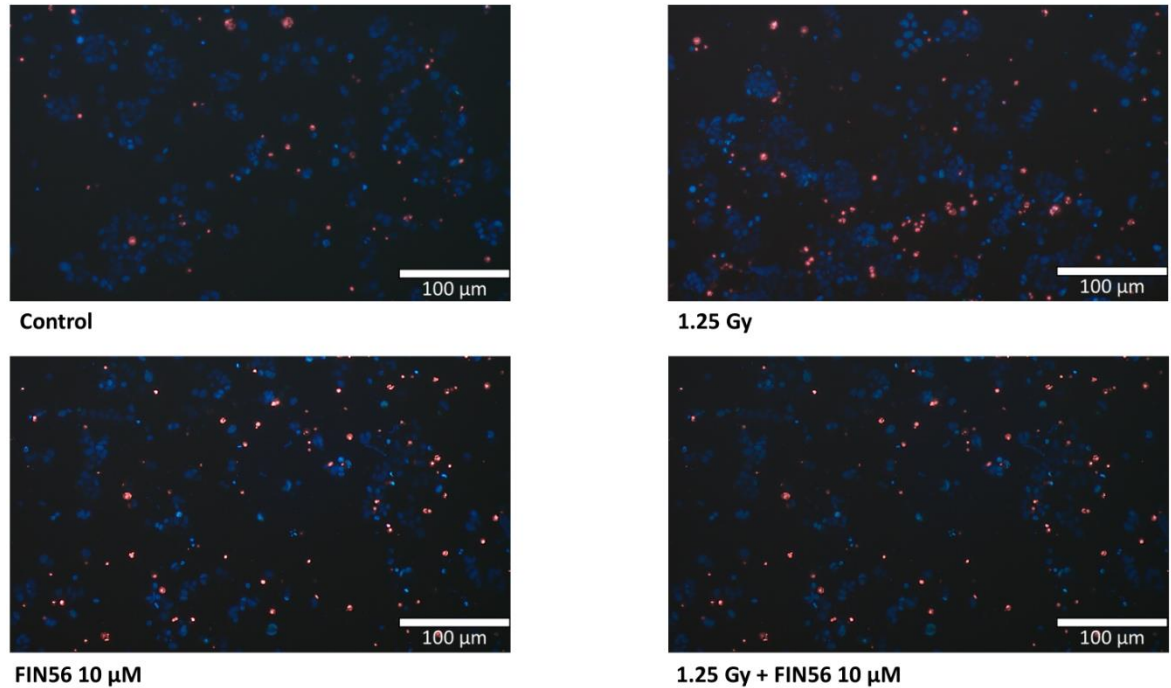
(B)
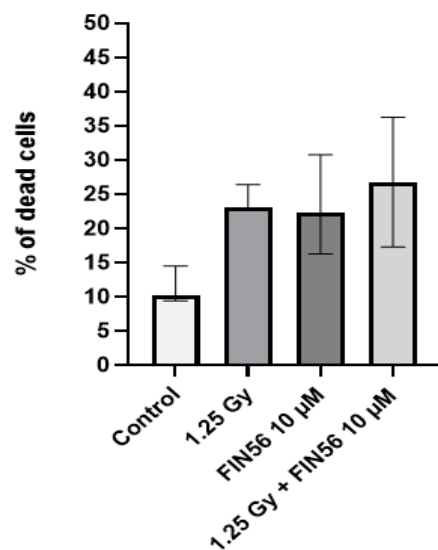
(C)
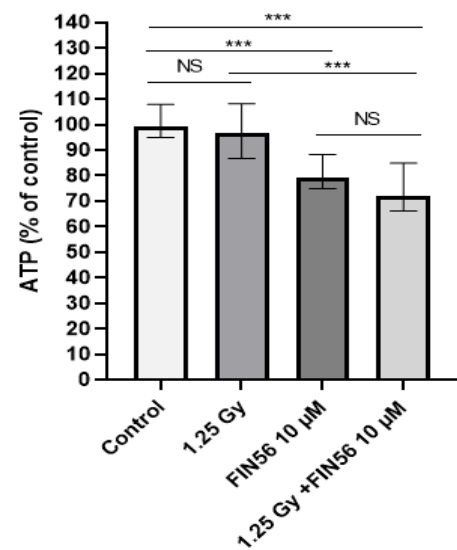
Figure 5.11: MCF-7 cell line were treated with 1.25 Gy of radiation and the ferroptosis inducer FIN56 (10 µM) for 72 hours. **(A)** Assessment of cell death following Hoechst 33342/PI staining. Live cells and apoptotic cells are stained blue with Hoechst 33342, and dead cells are stained red with PI staining. **(B)** The percentage of cell death was calculated from the by Hoechst 33342/PI-stained cells, when compared to the FIN56 (10 µM) vehicle control (0.2% (v/v) DMSO) treated cells. **(C)** Assessment was made of cell ATP levels using the CellTiter-Glo® luminescent cell viability assay of MCF-7 cell line treated with radiation (1.25 Gy), and FIN56 (10 µM) alone and in combination. All data was compared to the vehicle control which was assigned 100% ATP levels. Data is presented as median ± range. n=3 independent experiments each with 3 technical repeats. Statistical significance was determined by the Kruskal-Wallis test with a Dunn's post hoc test. Comparison with the vehicle control and single and combined treatments. Statistical significance was set at *=P≤0.05, **=P≤0.01, and ***=P≤0.001.

5.2.4 The optimisation of 72 hours RSL3 treatment dose, for use in combination with radiotherapy sensitisation in MCF-7 cells

The previously used 10 µM RSL3 dose, which was used in combination with radiotherapy in MCF-7 cell was original optimized for a 24 hours treatment period (Chapter 3) (Section 3.2.3.2). Here we used the same dose in combination with irradiation but for 72 hours. However, after 72 hours majority of the cells were dead, hence it was important to re-optimised the RSL3 treatment dose for 72 hours. The treatment doses selected were 0.6, 1.25, 2.5, and 5 µM, and this was validated using Hoechst 33342/PI staining to assess cellular death and reductions in ATP activity using the CellTiter-Glo® luminescent cell viability assay (Figure 5.12A and B). In MCF-7 cells there was a dose dependent increase in cell death and decrease in cell ATP as the concentration of RSL3 was increased (Figure 5.12A and B).

A 1.25 µM dose of RSL3 was the optimal dose for treating the MCF-7 cells after 72 hours, when compared to control ($P \leq 0.001$) and this was consistent with the percentage of cell death obtained from Hoechst 33342 / PI staining (Figure 5.12A-C). Although 2.5 µM was the optimal dose for RSL3 after optimization in 72 hours, all other concentrations of RSL3 (0.6, 1.25, and 5 µM) were also used in combination studies with radiotherapy.

5.2.5 Effect of the lower doses of ferroptosis inducer RSL3 on radiotherapy responses in MCF-7 in 2D cell culture

5.2.5.1 The effect of radiotherapy and 0.6 µM RSL3 combination treatment on 2D MCF-7 cell cultures

To assess RSL3-induced radiosensitivity at a concentration of 0.6 µM, cells were treated with RSL3 for 72 hours immediately after irradiation and stained with Hoechst 33342 and PI to assess cell death (Figure 5.13A and B). RSL3 alone and in combination with radiation significantly increase cell death compared to the vehicle control ($P \leq 0.001$ for both). However, this was clearly due to the RSL3 effect, which caused death to the majority of cells (Figure 5.13 A).

The cell death data is generally consistent with the results obtained for ATP levels measured using the 2D CellTitre-Glo® luminescent cell viability assay (2D) (Figure 5.13B).

The RSL3/irradiation combined treatment significantly decreased cell ATP in MCF-7 cells when compared to the vehicle control (P≤ 0.001) and irradiation alone (P≤0.001). However, RSL3 and irradiation alone was not significantly different form the vehicle control. Combined treatment of RSL3 with radiotherapy when compared to RSL3 alone were not significantly different (P≤0.001) suggesting the majority the effect on cell ATP levels caused by the combination treatment was due to RSL3, and there was no enhancement in the radiotherapy effect (Figure 5.13C).

Figure 5.12: Effect of the different doses of the ferroptosis inducer RSL3 on MCF-7 cells after 72 hours of treatment

(A)
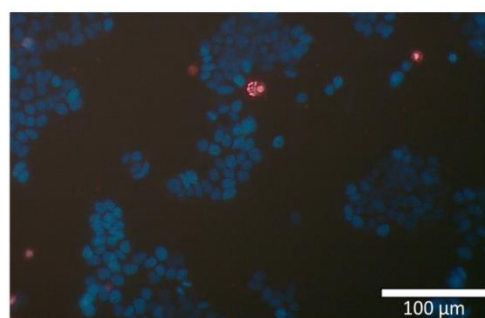
Control
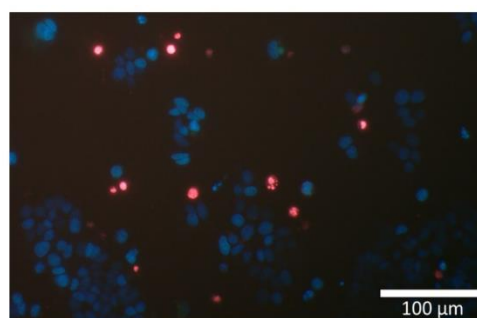
RSL3 0.6 µM
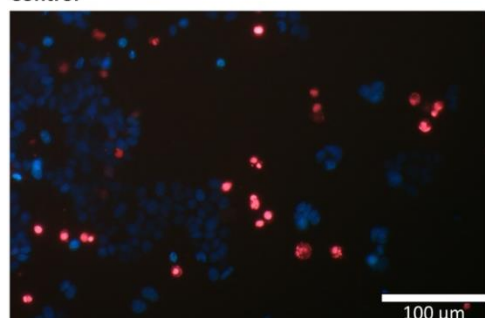
RSL3 1.25 µM
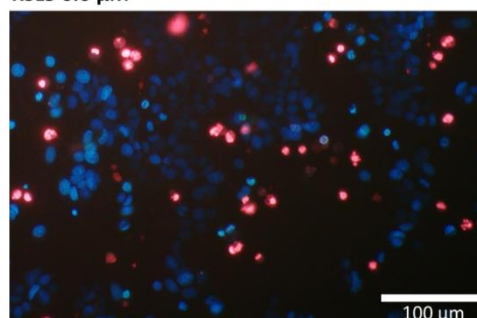
RSL3 2.5 µM
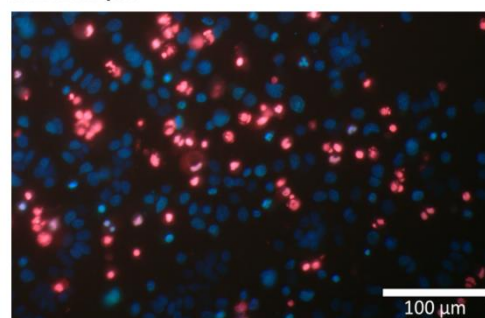
RSL3 5 µM

(B)
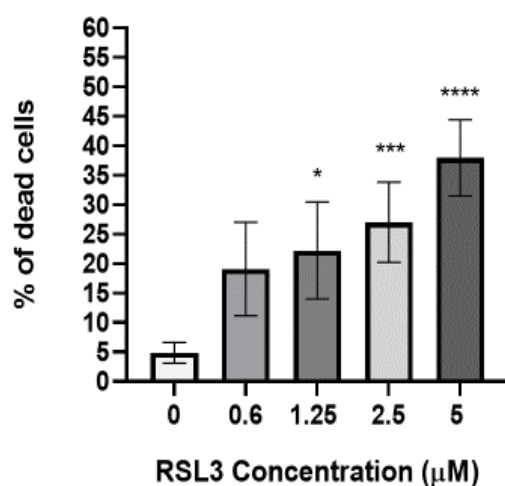
(C)
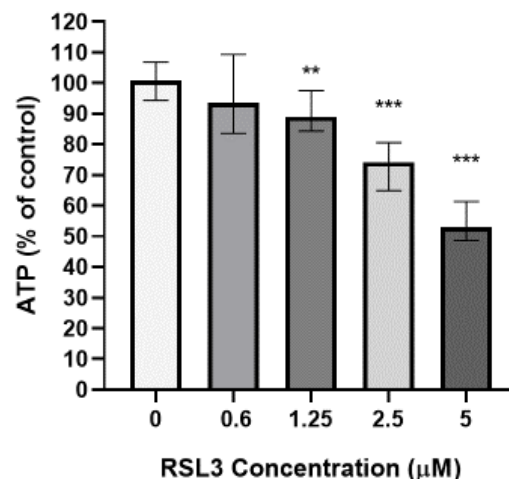
Figure 5.12: MCF-7 cells were treated for 72 hours with different doses of RSL3 **(A)** Cell death detection under fluorescent microscope after treating MCF-7 cell line with RSL3 (0.6, 1.25, 2.5, and 5 μM), with control (0.2% (v/v) DMSO), determined by Hoechst 33342/PI staining. Live cells and apoptotic cells are stained blue with Hoechst 33342, dead cells are stained red with PI staining. **(B)** Cell death count determined by Hoechst 33342/PI staining after treating MCF-7 cell line with RSL3 (0.6, 1.25, 2.5, and 5 μM), with control (0.2% (v/v) DMSO). **(C)** ATP level (% of control) assessed by CellTiter-Glo® Luminescent Cell Viability Assay after treating MCF-7 cell line with RSL3 (0.6, 1.25, 2.5, and 5 μM), with control (0.2% (v/v) DMSO). Data is presented as median ± range. n=3 independent experiments each with 3 technical repeats. Statistical significance was determined by the Kruskal-Wallis test with a Dunn's post hoc test. Comparison with the vehicle control and single and combined treatments. Statistical significance was set at *=P≤0.05, **=P≤0.01, and ***=P≤0.001.

Figure 5.13 Combination treatment of RSL3 (0.6 µM) +/- Radiotherapy in MCF-7 cells

(A)
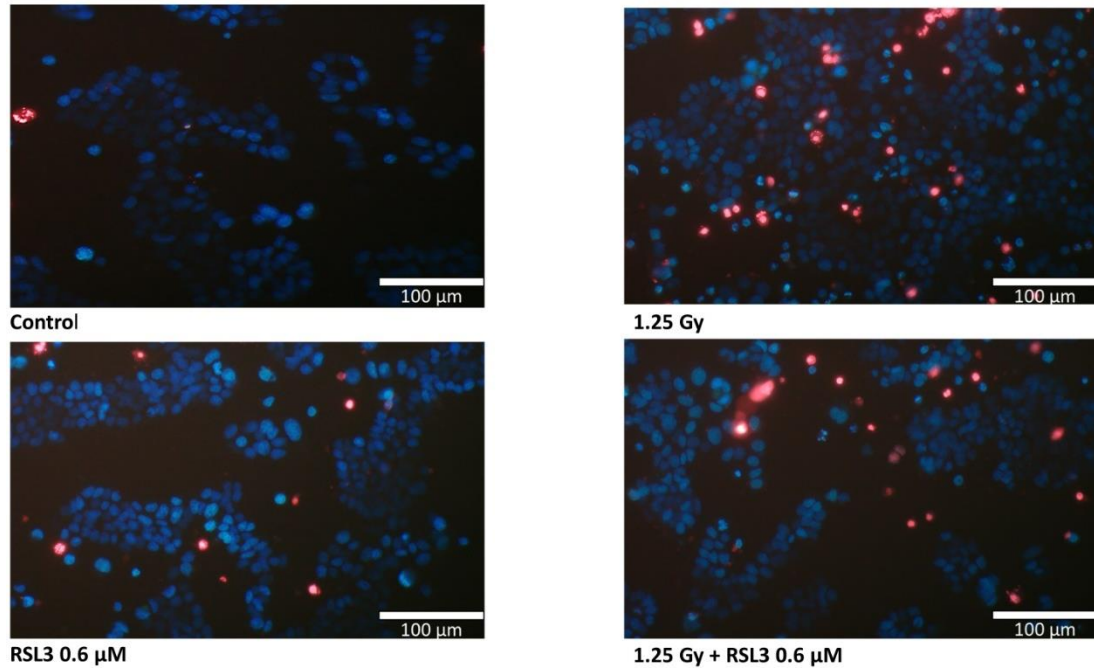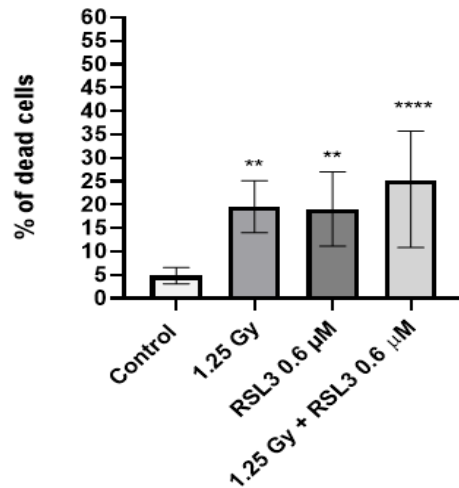
(B)   **(C)**
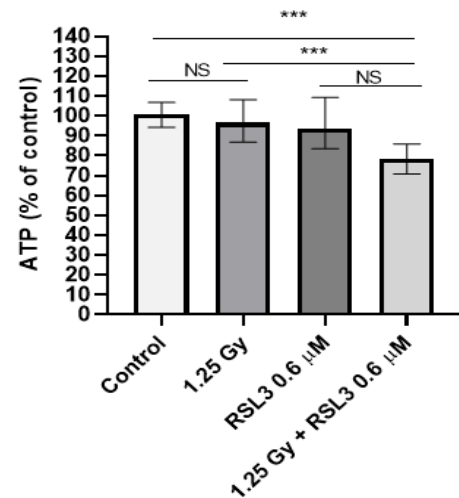
Figure 5.13: Effect of radiation and RSL3 on MCF-7 cells after 72 hours of treatment (A) Cell death detection under fluorescent microscope after treating MCF-7 cell line with 1.25 Gy radiation, with control (0.2% (v/v) DMSO) +/- ferroptosis inducer RSL3 (0.6 µM), determined by Hoechst 33342/PI staining. Live cells and apoptotic cells are stained blue with Hoechst 33342, dead cells are stained red with PI staining. **(B)** Cell death count determined by Hoechst 33342/PI staining after treating MCF-7 cell line with radiation (1.25 Gy) and ferroptosis inducer RSL3 (0.6 µM), with control (0.2% (v/v) DMSO). **(C)** ATP level (% of control) assessed by CellTiter-Glo® Luminescent Cell Viability Assay after treating MCF-7 cell line with radiation (1.25 Gy) and ferroptosis inducer RSL3 (0.6 µM), with control (0.2% (v/v) DMSO). Data is presented as median ± range. n=3 independent experiments each with 3 technical repeats. Statistical significance was determined by the Kruskal-Wallis test with a Dunn's post hoc test. Comparison with the vehicle control and single and combined treatments. Statistical significance was set at *=P≤0.05, **=P≤0.01, and ***=P≤0.001.

5.2.5.2 The effect of radiotherapy and 1.25 µM RSL3 combination treatment on 2D MCF-7 cell cultures

To assess RSL3-induced radiosensitivity at a concentration of 1.25 µM, cells were treated with RSL3 for 72 hours immediately after irradiation and stained with Hoechst and PI to assess cell death (Figure 5.14A and B). A 1.25 µM treatment dose of RSL3 alone, irradiation alone and the combination of both treatments caused significantly increase cell death when compared with the vehicle control (P≤0.001 for all). The greatest effect was seen when treatments were combined were an additive effect was observed (Figure 5.14 B).

The irradiation/RSL3 combination treatments caused a significant decrease in ATP levels compared to the vehicle control and irradiation alone (P≤0.001). Similarly, RSL3 alone causes a significant decrease in cell ATP compared to the vehicle control (P ≤ 0.001). Combined treatment of RSL3 with radiotherapy when compared to RSL3 alone were not significantly different, suggesting once again that majority cause of the reduction of ATP levels was to RSL3, and there was no enhanced effect by radiotherapy (Figure 5.14C).

5.2.5.3 The effect of radiotherapy and 2.5 µM RSL3 combination treatment on 2D MCF-7 cell cultures

To assess RSL3-induced radiosensitivity at a concentration of 2.5 µM, MCF-7 cells were treated with RSL3 for 72 hours immediately after irradiation and stained with Hoechst and PI to assess cell death (Figure 5.15A and B). RSL3 alone significantly increased cell death (P≤0.001), and combined treatment significantly increased cell death compared to the vehicle control (P≤0.001), with RSL3 causing an additive effect.

Likewise, following irradiation and RSL3 treatment the cell ATP levels of MCF-7 cells were significantly decrease compared to the vehicle control (P≤ 0.001), and irradiation alone (P≤ 0.001). However, the combination treatment was not significant compared to RSL3 alone when compared to control was significant (P≤ 0.001). Combined treatment of RSL3 with radiotherapy (P≤ 0.001) when compared to RSL3 alone were not significantly, and irradiation was not significantly different to the vehicle control. Once again, the majority of the deduction in cell ATP levels was attributed to RSL3, and there was no enhancement in the radiotherapy effect (Figure 5.15C).

Figure 5.14 Combination treatment of RSL3 (1.25 µM) +/- Radiotherapy in MCF-7 cells

(A)

(B)

(C)
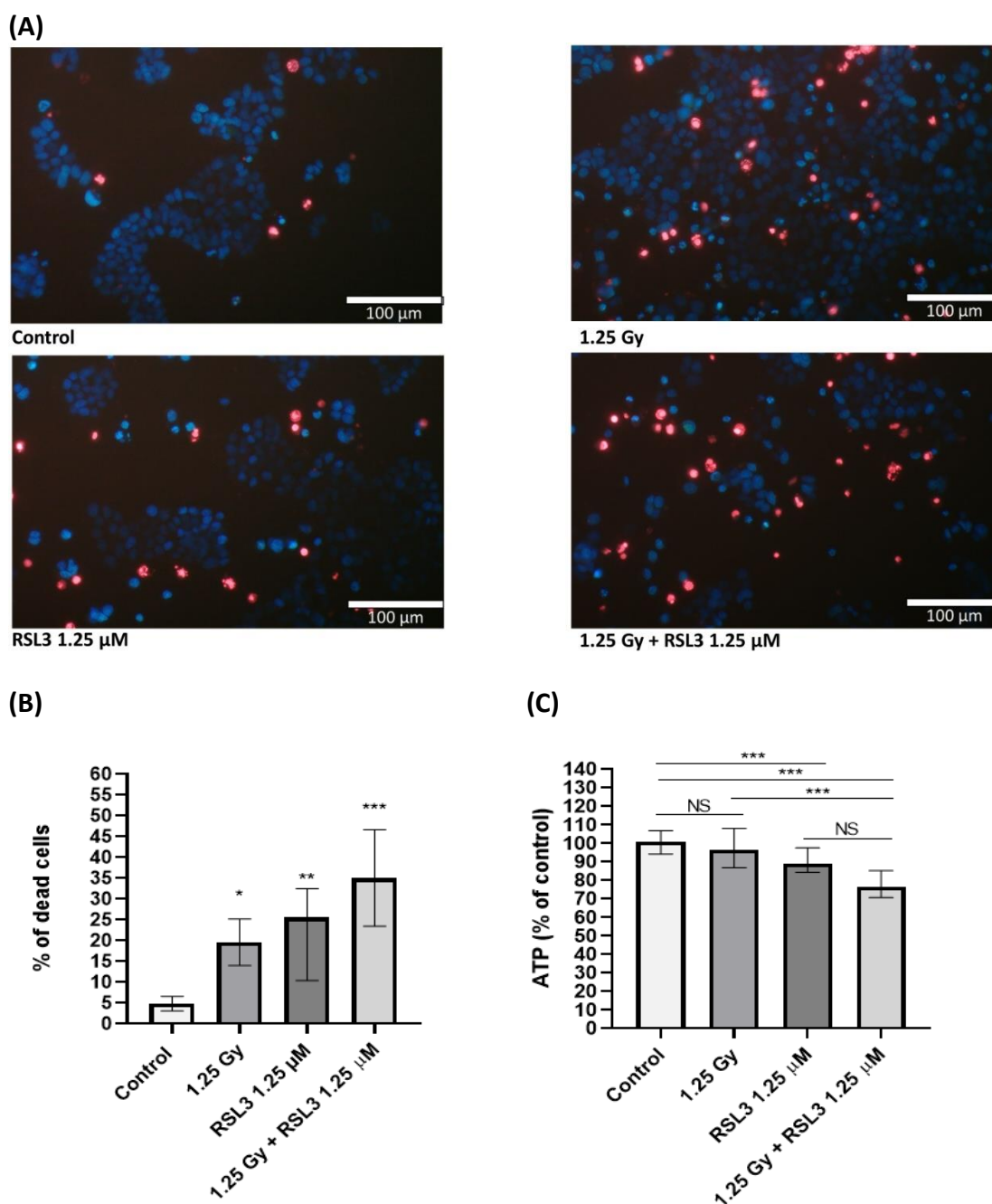
Figure 5.14: Effect of radiation and RSL3 on MCF-7 cells after 72 hours of treatment (A) Cell death detection under fluorescent microscope after treating MCF-7 cell line with 1.25 Gy radiation, with control (0.2% (v/v) DMSO) +/- ferroptosis inducer RSL3 (1.25 µM), determined by Hoechst 33342/PI staining. Live cells and apoptotic cells are stained blue with Hoechst 33342, dead cells are stained red with PI staining. **(B)** Cell death count determined by Hoechst 33342/PI staining after treating MCF-7 cell line with radiation (1.25 Gy) and ferroptosis inducer RSL3 (1.25 µM), with control (0.2% (v/v) DMSO). **(C)** ATP level (% of control) assessed by CellTiter-Glo® Luminescent Cell Viability Assay after treating MCF-7 cell line with radiation (1.25 Gy) and ferroptosis inducer RSL3 (1.25 µM), with control (0.2% (v/v) DMSO). Data is presented as median ± range. n=3 independent experiments each with 3 technical repeats. Statistical significance was determined by the Kruskal-Wallis test with a Dunn's post hoc test. Comparison with the vehicle control and single and combined treatments. Statistical significance was set at *=P≤0.05, **=P≤0.01, and ***=P≤0.001.

**Figure 5.15 Combination treatment of RSL3 (2.5 µM) +/- Radiotherapy in MCF-7 cells**

(A)

Control

RSL3 0.6 µM

RSL3 1.25 µM

RSL3 2.5 µM

(B)

(C)
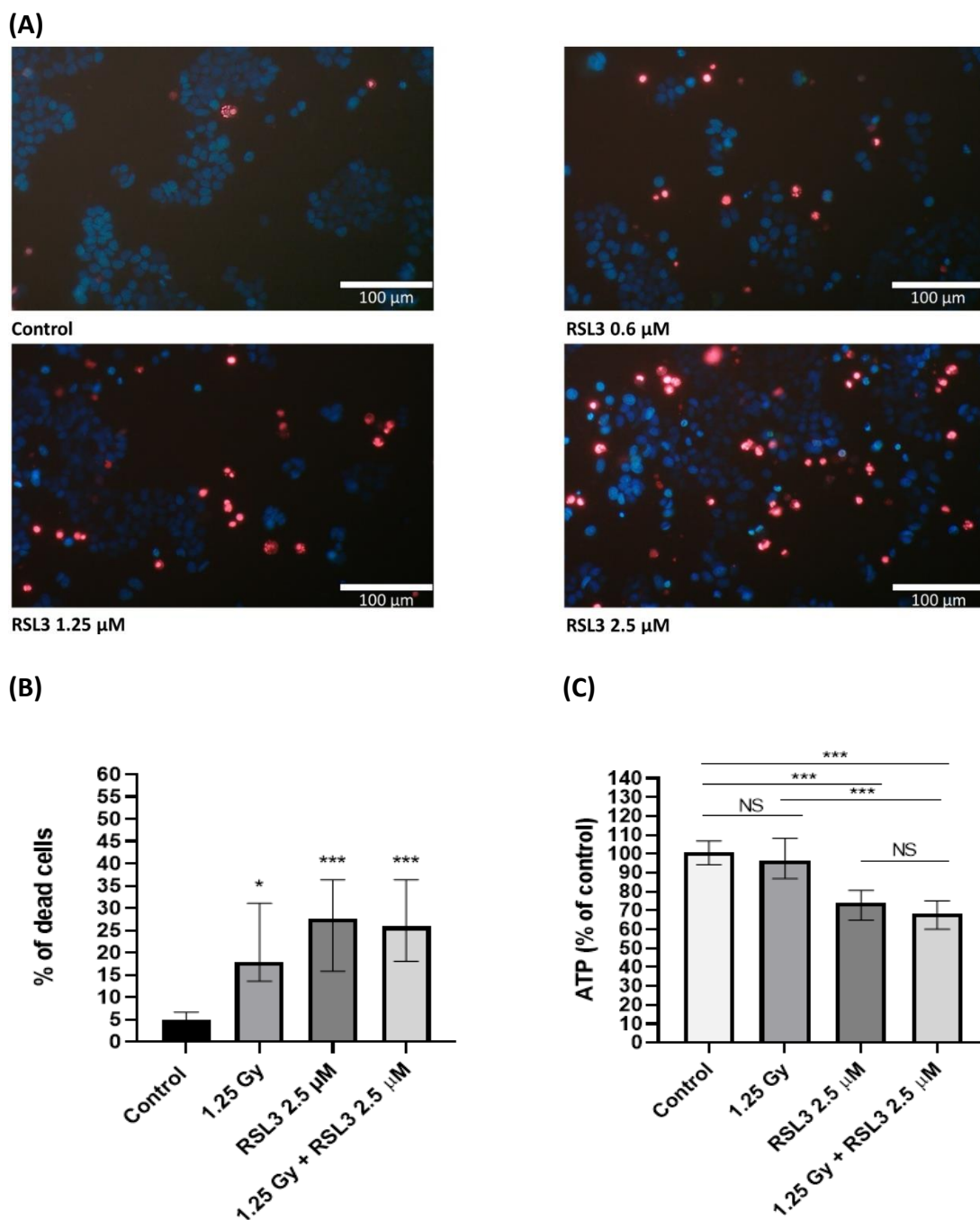
Figure 5.15: Effect of radiation and RSL3 on MCF-7 cells after 72 hours of treatment (A) Cell death detection under fluorescent microscope after treating MCF-7 cell line with 1.25 Gy radiation, with control (0.2% (v/v) DMSO) +/- ferroptosis inducer RSL3 (2.5 µM), determined by Hoechst 33342/PI staining. Live cells and apoptotic cells are stained blue with Hoechst 33342, dead cells are stained red with PI staining. **(B)** Cell death count determined by Hoechst 33342/PI staining after treating MCF-7 cell line with radiation (1.25 Gy) and ferroptosis inducer RSL3 (2.5 µM), with control (0.2% (v/v) DMSO). **(C)** ATP level (% of control) assessed by CellTiter-Glo® Luminescent Cell Viability Assay after treating MCF-7 cell line with radiation (2.5 Gy) and ferroptosis inducer RSL3 (2.5 µM), with control (0.2% (v/v) DMSO). Data is presented as median ± range. n=3 independent experiments each with 3 technical repeats. Statistical significance was determined by the Kruskal-Wallis test with a Dunn's post hoc test. Comparison with the vehicle control and single and combined treatments. Statistical significance was set at *=P≤0.05, **=P≤0.01, and ***=P≤0.001.

5.2.5.4 The effect of radiotherapy and 5 µM RSL3 combination treatment on 2D MCF-7 cell cultures

To assess RSL3-induced radiosensitivity at a concentration of 5 µM, MCF-7 cells were treated with RSL3 for 72 hours immediately after irradiation and stained with Hoechst and PI to assess cell death (Figure 5.16A and B). RSL3 alone significantly increase cell death ($P \leq 0.001$), and combined treatment significantly increased cell death vs. control ($P \leq 0.001$). This effect was clearly due to RSL3, and caused an additive effect. The cell death data was generally consistent with the results obtained for ATP levels measured using CellTiter-Glo® Luminescent Cell Viability Assay (2D) (Figure 5.16C).

Following irradiation/RSL3 combination and RSL3 treatment alone in MCF-7 cells there was a significantly decrease in cell ATP levels compared to the vehicle control ($P \leq 0.001$ for both). The irradiation/RSL3 combination also significant decreased cell ATP levels when compared to radiation alone ($P \leq 0.001$). However, there was however no significant decrease in cell ATP levels in MCF-7 cells receiving the combination treatment compared to the RSL3 alone, suggesting that the reduction in ATP observed with the combination treatment was caused by RSL3, and this was not enhanced by earlier irradiation. This was supported by the fact that there was no significant difference in ATP level in MCF-7 cells which were irradiated and the vehicle control.

Figure 5.16 Combination treatment of RSL3 (5 µM) +/- Radiotherapy in MCF-7 cells

(A)

(B)   **(C)**
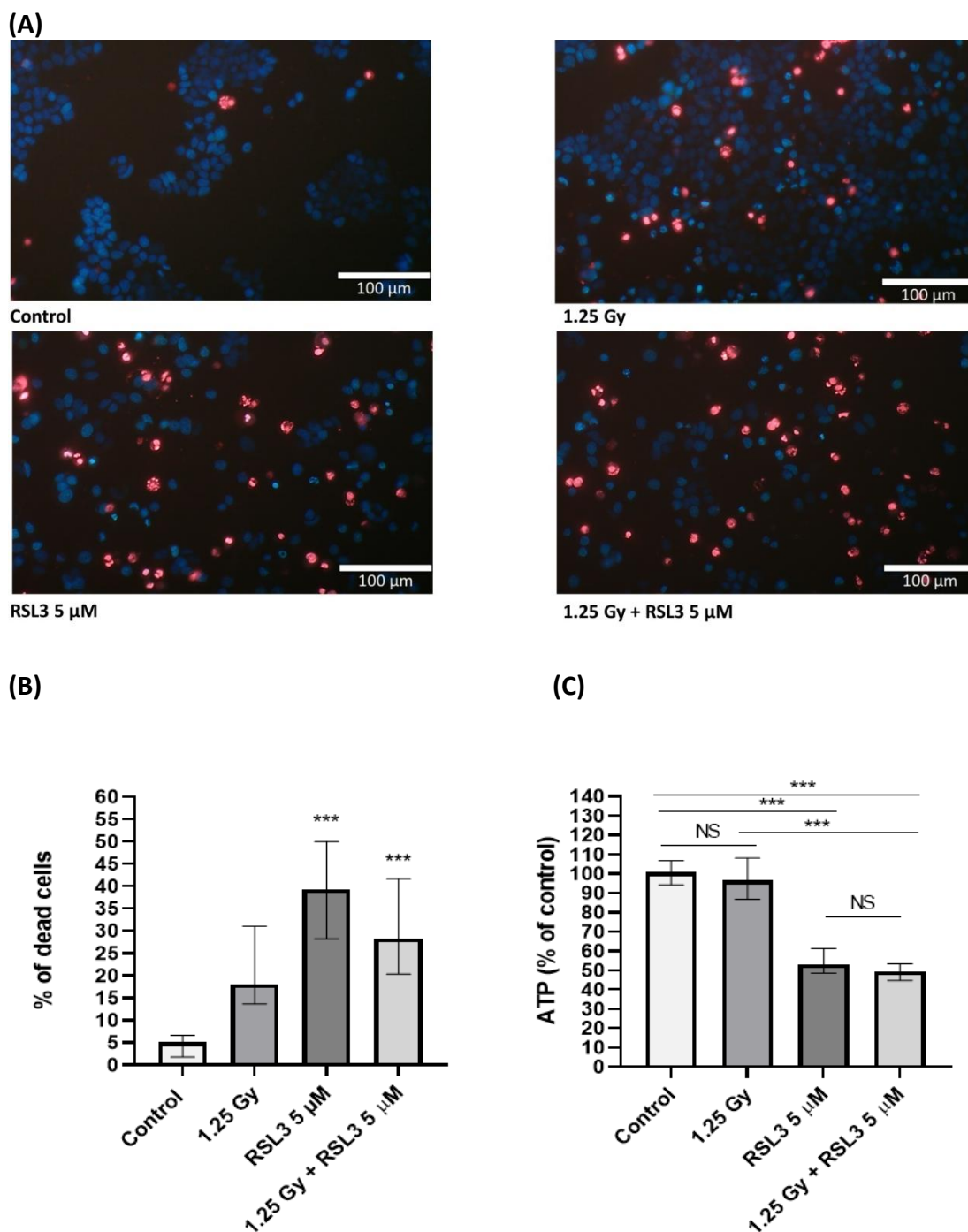
Figure 5.16: Effect of radiation and RSL3 on MCF-7 cells after 72 hours of treatment (A) Cell death detection under fluorescent microscope after treating MCF-7 cell line with 1.25 Gy radiation, with control (0.2% (v/v) DMSO) +/- ferroptosis inducer RSL3 (5 µM), determined by Hoechst 33342/PI staining. Live cells and apoptotic cells are stained blue with Hoechst 33342, dead cells are stained red with PI staining. **(B)** Cell death count determined by Hoechst 33342/PI staining after treating MCF-7 cell line with radiation (1.25 Gy) and ferroptosis inducer RSL3 (5 µM), with control (0.2% (v/v) DMSO). **(C)** ATP level (% of control) assessed by CellTiter-Glo® Luminescent Cell Viability Assay after treating MCF-7 cell line with radiation (2.5 Gy) and ferroptosis inducer RSL3 (5 µM with control (0.2% (v/v) DMSO). Data is presented as median ± range. n=3 independent experiments each with 3 technical repeats. Statistical significance was determined by the Kruskal-Wallis test with a Dunn's post hoc test. Comparison with the vehicle control and single and combined treatments. Statistical significance was set at *=P≤0.05, **=P≤0.01, and ***=P≤0.001.

5.2.6 The effect of the Nrf2 inhibitor on radiotherapy responses in breast cancer 2D cell culture

5.2.6.1 The effect of combination treatment of Nrf2 inhibitor ML385 +/- radiotherapy in MDA-MB-231 cells

To assess ML385-inhibitor radiosensitivity, cells were treated with ML385 for 72 hours immediately after irradiation and stained with Hoechst 33342 and PI to assess cell death and apoptosis (Figure 5.17 A and B). ML385 alone significantly increase apoptosis or necrosis (P≤0.05), and combined treatment significantly increased cell death vs. control (P≤0.05), however this was clearly due to the ML385 effect which causing an additive effect rather than synergistic effect. ML385 doses used were optimized for 24 and 48 hours, hence the higher response observed was at 72 hours.

For ATP activity, combined treatments were significantly different to control (p ≤ 0.001), but ML385 alone when compared to control was significant (P≤0.001). Combined treatment of ML385 with radiotherapy (P≤0.001) when compared to ML385 alone were not significantly different to each other so majority of cell death in combination is due to ML385, and there was no enhancement in the radiotherapy effect (Figure 5.17C). The data is generally consistent with the results obtained for ATP levels measured using CellTiter-Glo® Luminescent Cell Viability Assay (2D) (Figure 5.17).

5.2.6.2 Effect of combination treatment of Nfr2 inhibitor ML385 +/- radiotherapy in MCF-7 cells

To assess ML385-inhibitor radiosensitivity, cells were treated with ML385 for 72 hours immediately after irradiation and stained with Hoechst 33342 and PI to assess cell death and apoptosis (Figure 5.18 A and B). ML385 alone significantly increase apoptosis or necrosis (P≤0.05), and combined treatment significantly increased cell death vs. control (P≤0.05), however this was clearly due to the ML385 effect which causing an additive effect rather than synergistic effect.

For ATP activity, combined treatments were significantly decreased compared to control (P≤0.001), but ML385 alone when compared to control was significant decreased also (P≤0.001). Combined treatment of ML385 with radiotherapy (P≤0.001) when compared to ML385 alone were not significantly different to each other so majority of cell death in combination is due to ML385, and there was no enhancement in the radiotherapy effect (Figure 5.18 C).

The data is generally consistent with the results obtained for ATP levels measured using CellTiter-Glo® Luminescent Cell Viability Assay (2D) (Figure 5.18).

Figure 5.17 Combination treatment of ML385 +/- Radiotherapy in MDA-MB-231 cells

(A)
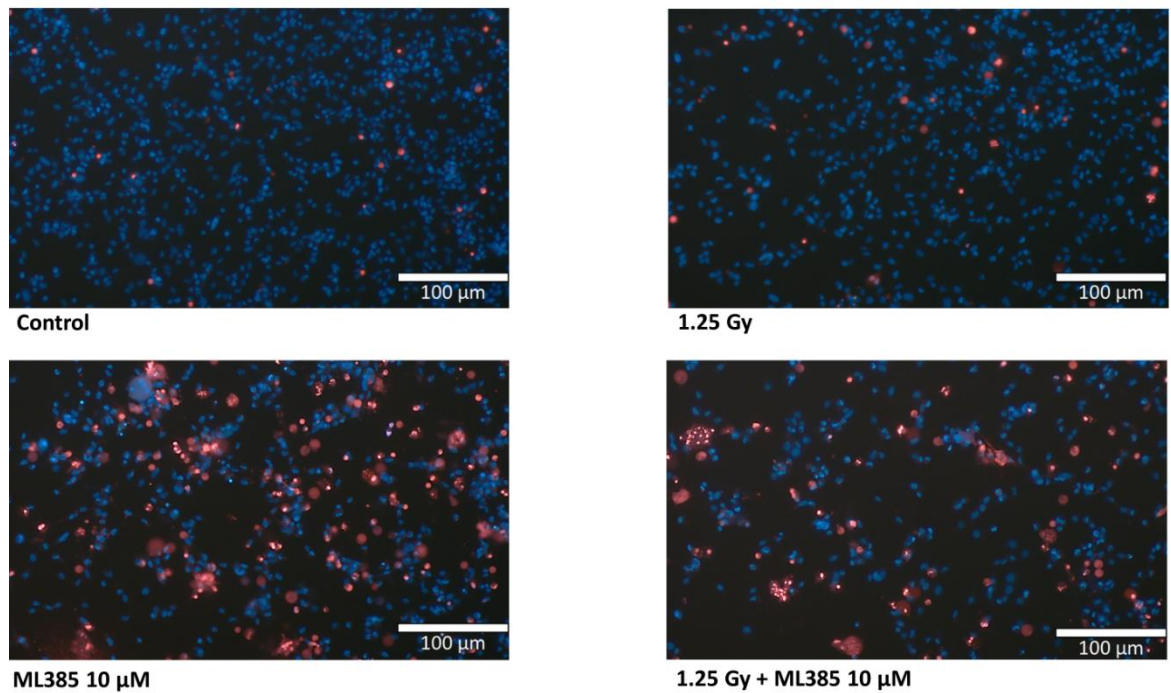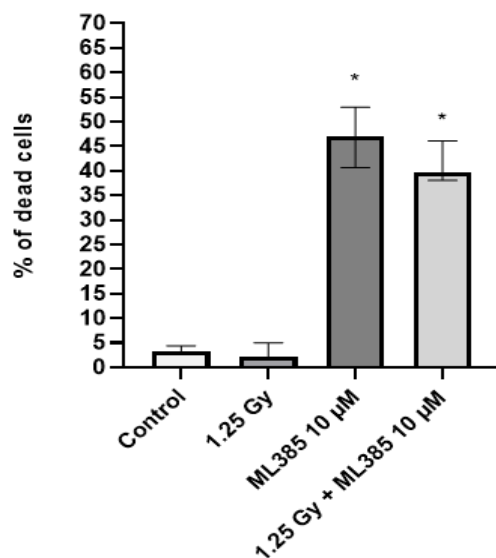
(B) **(C)**
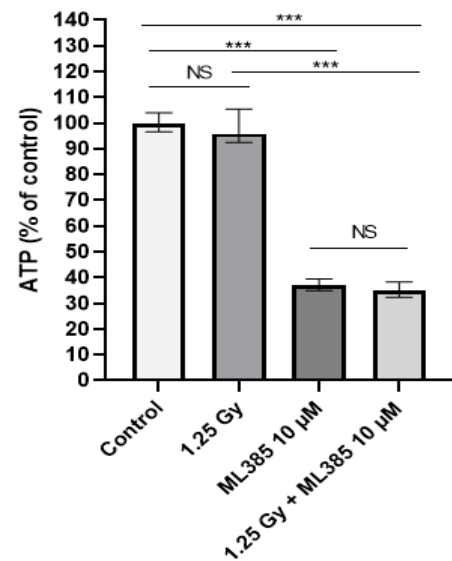
Figure 5.17: The effect of radiation and Nrf2 inhibitor ML385 on MDA-MB-231 cells after 72 hours of treatment (A) Cell death detection under fluorescent microscope after treating MDA-MB-231 cell line with 1.25 Gy radiation, with control (0.2% (v/v) DMSO) +/- ML385 (10 µM), determined by Hoechst 33342/PI staining. Live cells and apoptotic cells are stained blue with Hoechst 33342, dead cells are stained red with PI staining. **(B)** Cell death count determined by Hoechst 33342/PI staining after treating MDA-MB-231 cell line with radiation (1.25 Gy) and ML385 (10 µM), with control (0.2% (v/v) DMSO). **(C)** ATP level (% of control) assessed by CellTiter-Glo® Luminescent Cell Viability Assay after treating MDA-MB-231 cell line with radiation (1.25 Gy) and ML385 (10 µM), with control (0.2% (v/v) DMSO). Data is presented as median ± range. n=3 independent experiments each with 3 technical repeats. Statistical significance was determined by the Kruskal-Wallis test with a Dunn's post hoc test. Comparison with the vehicle control and single and combined treatments. Statistical significance was set at *=P≤0.05, **=P≤0.01, and ***=P≤0.001.

**Figure 5.18 Combination treatment of ML385 +/- Radiotherapy in MCF-7 cells**

(A)

Control

1.25 Gy

ML385 10 µM
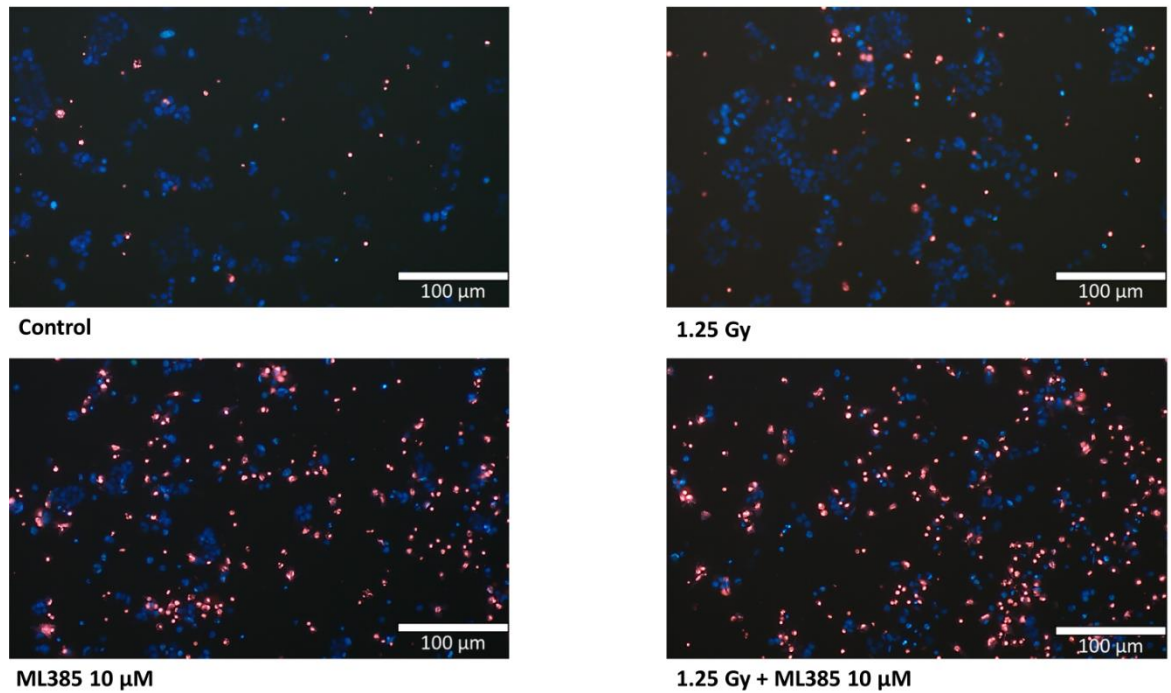
1.25 Gy + ML385 10 µM

(B)
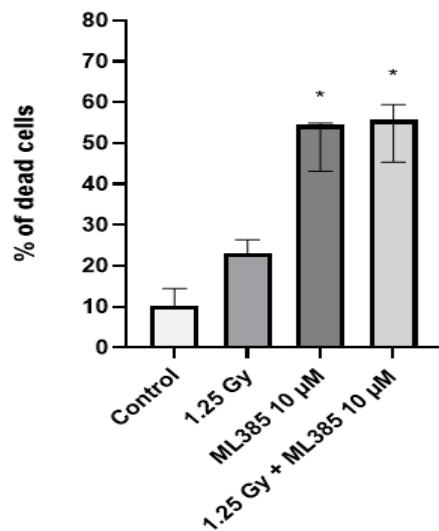
(C)
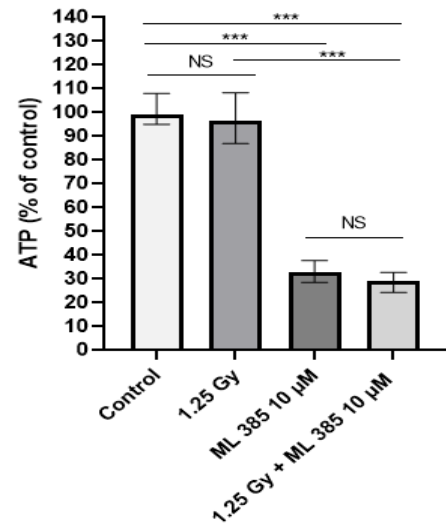
Figure 5.18: Effect of radiation and Nrf2 inhibitor ML385 on MCF-7 cells after 72 hours of treatment (A) Cell death detection under fluorescent microscope after treating MCF-7 cell line with 1.25 Gy radiation, with control (0.2% (v/v) DMSO) +/- ML385 (10 µM), determined by Hoechst 33342/PI staining. Live cells and apoptotic cells are stained blue with Hoechst 33342, dead cells are stained red with PI staining. **(B)** Cell death count determined by Hoechst 33342/PI staining after treating MCF-7 cell line with radiation (1.25 Gy) and ML385 (10 µM), with control (0.2% (v/v) DMSO). **(C)** ATP level (% of control) assessed by CellTiter-Glo® Luminescent Cell Viability Assay after treating MCF-7 cell line with radiation (1.25 Gy) and ML385 (10 µM), with control (0.2% (v/v) DMSO). Data is presented as median ± range. n=3 independent experiments each with 3 technical repeats. Statistical significance was determined by the Kruskal-Wallis test with a Dunn's post hoc test. Comparison with the vehicle control and single and combined treatments. Statistical significance was set at *=P≤0.05, **=P≤0.01, and ***=P≤0.001.

5.2.7 Effect of ferroptosis inducer RSL3 on radiotherapy responses in breast cancer 3D alginate spheroid cells

5.2.7.1 Effect of combination treatment of ferroptosis inducer RSL3 +/- radiotherapy in MDA-MB-231 3D alginate spheroids

To assess RSL3-induced radiosensitivity, 3D alginate spheroids were treated with RSL3 for 72 hours immediately after irradiation and stained with Hoechst 33342 and PI to assess cell death and apoptosis (Figure 5.19A and B). Individual treatments and combined treatments did not significantly increase apoptosis or necrosis when compared to control. The Hoechst 33342 and PI staining shows the different responses of treatment within the 3D spheroids, which clearly show the heterogeneity of responses within populations in that some spheroids were dead but others unaffected (Figure 5.19A).

For ATP activity, combined treatments were significantly different to control (P≤0.001), but RSL3 alone when compared to control was significant (P≤0.01). Combined treatment of RSL3 with radiotherapy (P≤0.001) when compared to RSL3 alone were not significantly different to each other so majority of cell death in combination is due to RSL3, and there was no enhancement in the radiotherapy effect (Figure 5.19C). The data is generally consistent with the results obtained for ATP levels measured using Cell Titer-Glo® 3D Cell Viability Assay (Figure 5.19).

5.2.7.2 Effect of combination treatment of ferroptosis inducer RSL3 +/- radiotherapy in MCF-7 3D alginate spheroids

To assess RSL3-induced radiosensitivity, 3D alginate spheroids were treated with RSL3 for 72 hours immediately after irradiation and stained with Hoechst 33342 and PI to assess cell death and apoptosis (Figure 5.20A and B). RSL3 alone and when combined with radiotherapy treatment significantly increased cell death vs. control (P≤0.05), however this was additive rather than synergistic. The Hoechst 33342 and PI staining shows the different responses of treatment within the 3D spheroids, which clearly show the heterogeneity of responses within populations in responses to RSL3 and RSL3 + RTx (Figure 5.20A).

For ATP activity, combined treatments were not significantly different to control, but that RSL3 when combined with radiotherapy was significantly different when compared to radiotherapy alone (P≤0.05). but there was no different between combined treatments to RSL3 alone, so majority of cell death in combination is due to RSL3, and there was no enhancement in the radiotherapy effect (Figure 5.20C). The data is generally consistent with the results obtained for ATP levels measured using Cell Titer-Glo® 3D Cell Viability Assay (Figure 5.20).

Figure 5.19 Combination treatment of RSL3 +/- radiotherapy in MDA-MB-231 3D alginate spheroids

(A)
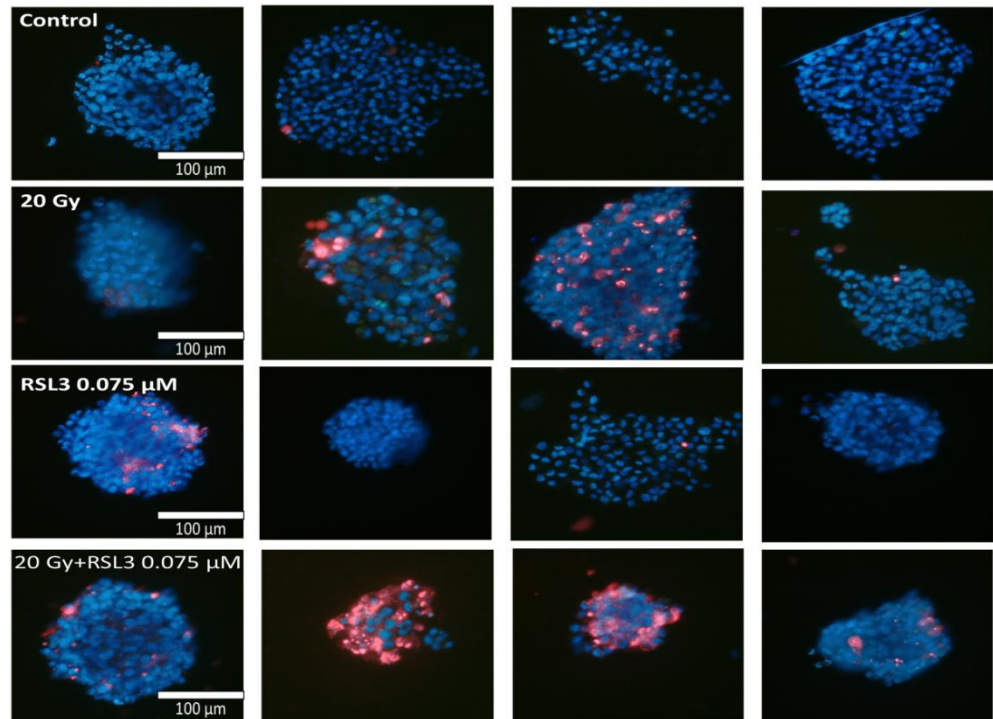
(B)
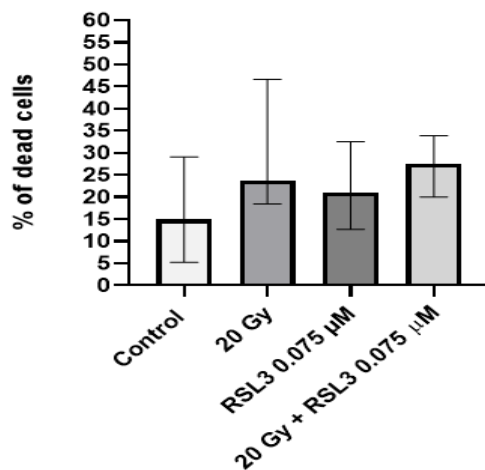
(C)
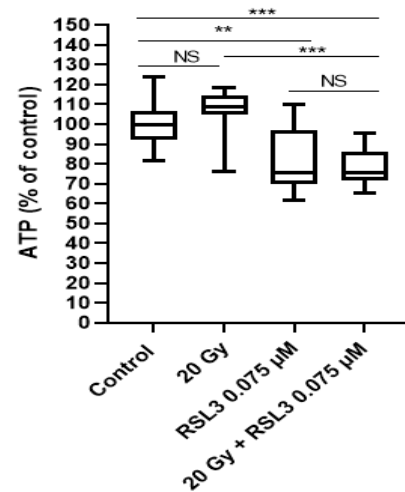
Figure 5.19: Effect of radiation and RSL3 on MDA-MB-231 3D alginate spheroids after 72 hours of treatment (A) Cell death detection after treating MDA-MB-231 spheroids with 20 Gy radiation, with control (0.2% (v/v) DMSO) +/- ferroptosis inducer RSL3 (0.075 μM), determined by Hoechst 33342/PI staining. **(B)** Cell death count determined by Hoechst 33342/PI staining after treating MDA-MB-231 spheroids with radiation (20 Gy) and ferroptosis inducer RSL3 (0.075 μM), with control (0.2% (v/v) DMSO). Data expressed as median ± range. **(C)** ATP level (% of control) assessed by Cell Titer-Glo® 3D Cell Viability Assay after treating MDA-MB-231 spheroids with radiation (20 Gy) and ferroptosis inducer RSL3 (0.075 μM), with control (0.2% (v/v) DMSO). Data expressed as median ± interquartile range from n=3 independent experiments each with ≥4 technical repeats. Statistical significance was determined by the Kruskal-Wallis test with a Dunn's post hoc test. Comparison with the vehicle control and single and combined treatments. Statistical significance was set at *=P≤0.05, **=P≤0.01, and ***=P≤0.001.

Figure 5.20 Combination treatment of RSL3 +/- radiotherapy in MCF-7 3D alginate cells

(A)
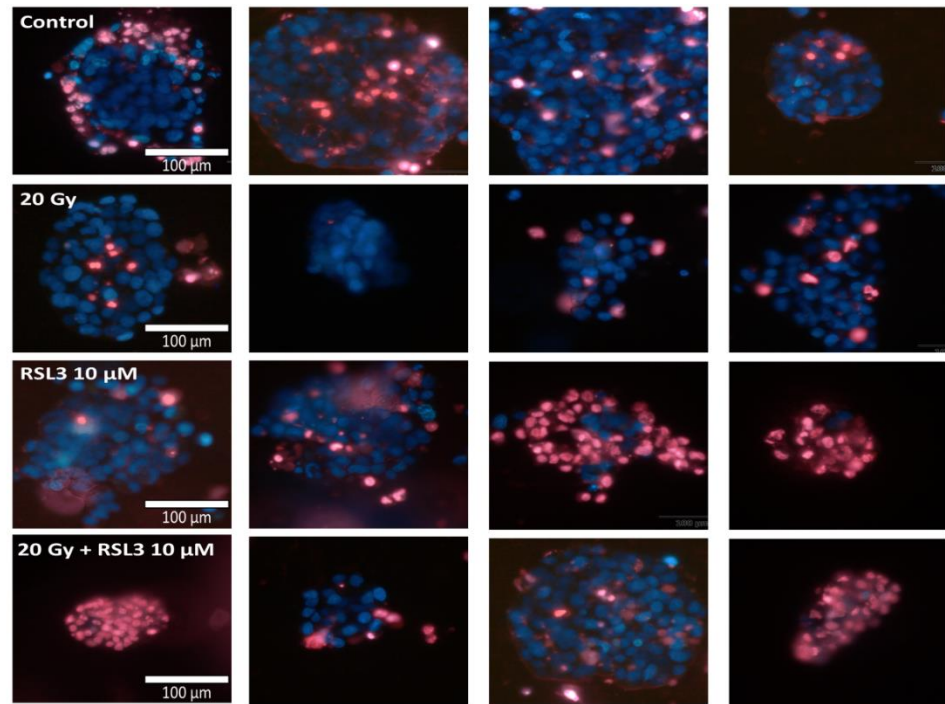
(B)
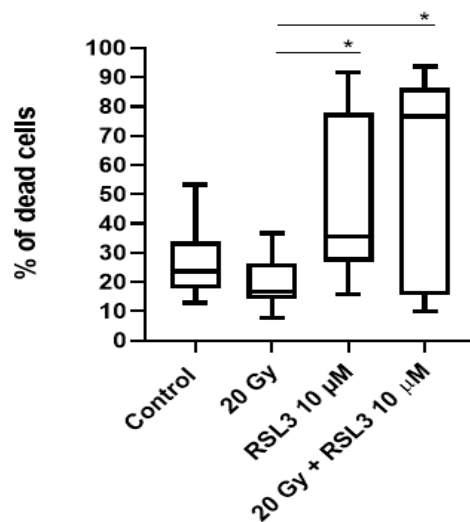
(C)
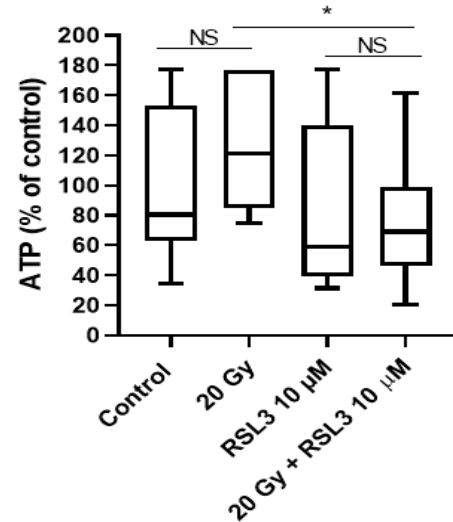
Figure 5.20: Effect of radiation and RSL3 on MCF-7 3D alginate spheroids after 72 hours of treatment
(A) Cell death detection under fluorescent microscope after treating MCF-7 spheroids with 20 Gy radiation, with control (0.2% (v/v) DMSO) +/- ferroptosis inducer RSL3 (10 μM), determined by Hoechst 33342/PI staining. **(B)** Cell death count determined by Hoechst 33342/PI staining after treating MCF-7 spheroids with radiation (20 Gy) and ferroptosis inducer RSL3 (10 μM), with control (0.2% (v/v) DMSO). **(C)** ATP level (% of control) assessed by Cell Titer-Glo® 3D Cell Viability Assay after treating MCF-7 spheroids with radiation (20 Gy) and ferroptosis inducer RSL3 (10 μM), with control (0.2% (v/v) DMSO). Data expressed as median ± interquartile range from n=3 independent experiments each with ≥4 technical repeats. Statistical significance was determined by the Kruskal-Wallis test with a Dunn's post hoc test. Comparison with the vehicle control and single and combined treatments. Statistical significance was set at *=P≤0.05, **=P≤0.01, and ***=P≤0.001.

**5.2.8 Effect of Nrf2 inhibitor on radiotherapy responses in breast cancer 3D alginate spheroid cells**

5.2.8.1 Effect of combination treatment of Nrf2 inhibitor ML385 +/- radiotherapy in MDA-MB-231 3D alginate spheroids

To assess ML385-inhibitor radiosensitivity, 3D alginate spheroids were treated with ML385 for 72 hours immediately after irradiation and stained with Hoechst 33342 and PI to assess cell death (Figure 5.21A and B). Individual treatments did not significantly cell death, but ML385 treatment alone significantly increased cell death vs. control ($P \leq 0.05$) and no difference was noticed between radiation and combined treatment.

For ATP activity, combined treatments were significantly different to control ($P \leq 0.01$), but ML385 alone when compared to control was significant ($P \leq 0.001$). Combined treatment of ML385 with radiotherapy ($P \leq 0.001$) when compared to ML385 alone were not significantly different to each other so majority of cell death in combination is due to ML385, and there was no enhancement in the radiotherapy effect (Figure 5.21C). The data is generally consistent with the results obtained for ATP levels measured using Cell Titer-Glo® 3D Cell Viability Assay (Figure 5.21). Due to time constraints, ML385 was only assessed in MDA-MB-231 and in the optimising chapter (Chapter 3) and since ML385 had no activity against MCF-7, it was not assessed in 3D cell culture.

Figure 5.21 Combination treatment of ML385 +/- radiotherapy in MDA-MB-231 3D alginate spheroids

(A)
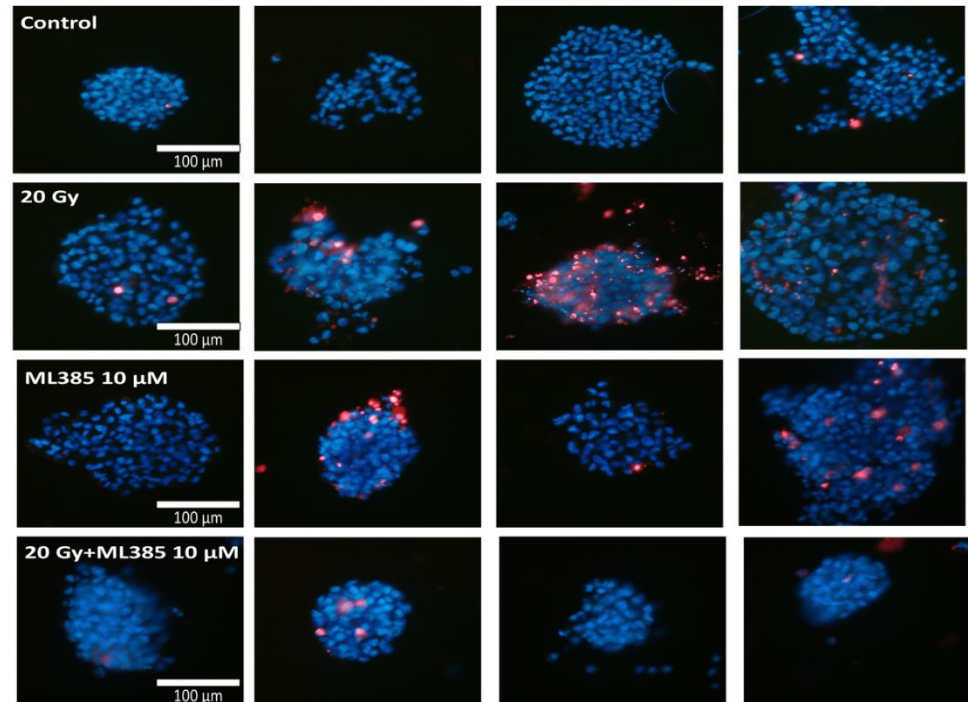
(B)
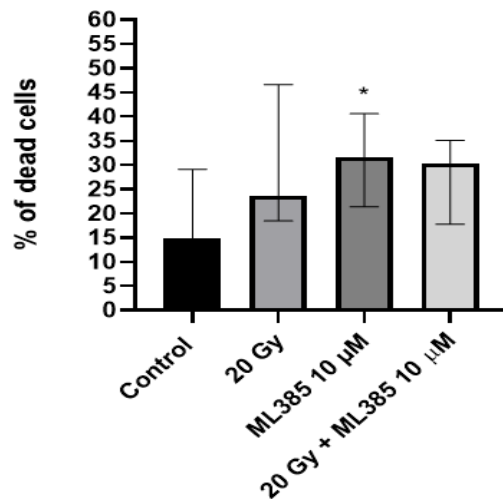
(C)
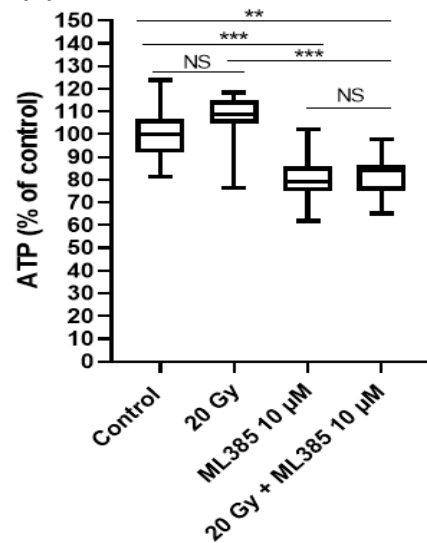
Figure 5.21: Effect of radiation and Nrf2 inhibitor ML385 on MDA-MB-231 3D alginate spheroids after 72 hours of treatment (A) Cell death detection after treating MDA-MB-231 spheroids with 20 Gy radiation, with control (0.2% (v/v) DMSO) +/- Nrf2 inhibitor ML385 (10 μM), determined by Hoechst 33342/PI staining **(B)** Cell death count determined by Hoechst 33342/PI staining after treating MDA-MB-231 spheroids with radiation (20 Gy) and ML385 (10 μM), with control (0.2% (v/v) DMSO). Data expressed as median ± range. **(C)** ATP level (% of control) assessed by Cell Titer-Glo® 3D Cell Viability Assay after treating MDA-MB-231 spheroids with radiation (20 Gy) and ML385 (10 μM), with control (0.2% (v/v) DMSO). Data expressed as median ± interquartile range from n=3 independent experiments each with ≥4 technical repeats. Statistical significance was determined by the Kruskal-Wallis test with a Dunn's post hoc test. Comparison with the vehicle control and single and combined treatments. Statistical significance was set at *=P≤0.05, **=P≤0.01, and ***=P≤0.001.

5.3 Discussion

The aim of this chapter was to assess whether radiotherapy responses could be enhanced in 2D cell cultures and 3D cell cultures of breast cancer cells. To assess this, MDA-MB-231 and MCF-7 cells were treated with ferroptosis inducers and Nrf2 inhibitors after radiotherapy and assessed by direct assessment of cell death, by colony formation assay and by measurements of ATP as a marker of cell viability. In summary, in these studies, MCF-7 and MDA-MB-231 breast cancer cells do not show enhanced radiosensitivity when treated with either ferroptosis inducer, or Nrf2 inhibitors and although weak synergistic effects were seen with RSL3 when assessing cell death, all other treatments resulted in no observed synergy.

5.3.1 Optimisation of radiotherapy doses

Colony assay was performed on breast cancer MDA-MB-231 and MCF-7 cells to initially optimize the doses of radiation, starting with higher doses 20 Gy to minimum dose of 0.6 Gy. Figure 5.2 and 5.3 show that at high doses, almost all cells were killed and very few colonies formed. Reduced doses below 2.5 Gy showed a dose-dependent relationship between radiation dose and colony numbers which was used to optimise doses for combination treatments. The optimal radiation dose for colony assay for 2D cells was 1.25 Gy. For 3D alginate assay was 20 Gy as determined by parallel studies in our group (Matos *et al.*, 2023). Doses of radiation that caused a significant reduction in colonies but did not kill the majority of cells were seen as ideal doses for combination studies, and Hoechst 33342 and PI staining confirmed that radiotherapy killed a minority of cells, ideal for combination studies. It is known that a single treatment of 1.25 Gy could significantly reduce colony growth long-term, so must be inducing DNA damage, hence 1.25 Gy was taken forward for cell death experiments despite 1.25 Gy not inducing significant cell death as a single treatment. Although subsequent experiments were performed using alternate cytotoxicity assays, these studies confirm the doses at which MDA-MB-231 and MCF-7 cells are affected by RTx long-term.

5.3.1 Ferroptosis inducers did not enhance radiotherapy effects in 2D cell culture

Both MCF-7 and MDA-MB-231 were irradiated and then immediately treated with doses of RSL3, Erastin or FIN56 at doses that were known to induce cell death in a minority of

cells, but not induce significant or high levels of cell death. These doses were based on optimisation experiments performed at 24 hours post-treatment, and for most situations, these worked well at 72 hours also without excessive cell death, the exception being RSL3 in MCF-7, which required further optimisation (Figure 5.12). In all cases, there was no consistent synergistic response in combination treatment. In only FIN56 treatment of MDA-MB-231 showed evidence of a synergistic effect, albeit rather weak (Figure 5.8). In all cases, ATP levels generally followed cell death observations with no strong synergistic responses seen.

Our study results was performed only at a time point of 72 hours for all ferroptosis inducers with the optimized levels of radiation of 1.25 Gy for 2D and 20 Gy for 3D and the result of ATP levels and cell death using Hoechst 33342/PI staining show more response of radiation with the ferroptosis inducer RSL3 in MCF-7 cells, but not in a way were it could be synergistic, while RSL3 and radiation in MDA-MB-231 do not show any enhancement of the radiation treatment. Neither ferroptosis inducers FIN56 and Erastin did not enhance the radiotherapy treatment in both breast cancer cell lines MCF-7 and MDA-MB-231. This can be due to the limitation of the study by using the optimized doses of ferroptosis inducers in 24 hrs but not optimized for 72 hours, another reason is that the cells were first irradiated then treated with the ferroptosis inducers and the time difference was about 2 hours because they were irradiated at Sheffield University not in BMRC at Sheffield Hallam University, or simply cancer cells are not responding to treatments.

5.3.3 Ferroptosis pathways leading to altered radiosensitivity

According to studies, ferroptosis can improve radio-resistance in breast cancer cells, as a promising approach for the treatment of cancer (Wu *et al.*, 2020). There is data that suggests ferroptosis may increase the radiation sensitivity of cancer cells. For instance, studies have demonstrated that the use of specific ferroptosis-inducing drugs, such as Erastin, can make cancer cells more susceptible to radiation therapy by reducing the activity of the cystine/glutamate antiporter, leading to decreased glutathione (L. F. Ye *et al.*, 2020). Ferroptosis may also affect the radiosensitivity of cancer stem cells, which are believed to be the cause of cancer recurrence and radiotherapy resistance, according to some research (Cosialls *et al.*, 2021; R. Liu *et al.*, 2022). Cancer stem cells may undergo

ferroptosis, which might also increase the effectiveness of radiation (Cosialls *et al.*, 2021; R. Liu *et al.*, 2022). Although researchers show that inducing ferroptosis by radiotherapy can provide enhanced radiosensitivity in cancer cells both in vitro and in vivo (Lang *et al.*, 2019) on the other hand cancer cells after radiation can evade ferroptosis by several mechanisms. It has been proposed that inducing ferroptosis in cancer cells may be counter-intuitive in that it may lead to enhanced radio-resistance depending on pre-existing vulnerabilities (Wu *et al.*, 2020; Lei, Mao, *et al.*, 2021). There is evidence to suggest that ferroptosis inducers such as Erastin may enhance the sensitivity of cancer cells to radiotherapy (L. F. Ye *et al.*, 2020). Erastin inhibits system Xc- reducing cysteine import and hence decreased glutathione, meaning there is less glutathione to respond to RTx-induced ROS. In addition, some studies have suggested that ferroptosis may play a role in the radiosensitivity of cancer stem cells (Cosialls *et al.*, 2021; R. Liu *et al.*, 2022), which are thought to be responsible for cancer recurrence and resistance to radiotherapy. By inducing ferroptosis in cancer stem cells, it may be possible to improve the efficacy of radiotherapy. On the other hand, cancer cells after radiation may evade cell death via modulation of ferroptosis by several mechanisms. In the presence of a Keap-1 mutation, Nrf2 is high, leading to an enhanced antioxidant response. RTx-mediated ROS may have little effect in this situation. Similarly, ACLS4 is low in some breast cancers. Acyl coenzyme A synthetase long chain family member 4 (ACSL4) is primarily responsible for catalysing the conversion of free PUFAs such arachidonic acids (AAs) and adrenic acids (AdAs) to their acyl coenzyme A (CoA) derivatives, such as AA/AdA-CoA. These PUFA-CoAs are then converted into lysophospholipids (LysoPLs), which are then further incorporated into PLs (such AA-PE and AdA-PE) by lysophosphatidylcholine acyltransferase 3 (LPCAT3) and other enzymes. Hence, PUFA-PL synthesis is suppressed and ferroptosis resistance is markedly increased when ACSL4 or LPCAT3 are suppressed (Dixon *et al.*, 2015; Doll, Proneth, Yulia Y Tyurina, *et al.*, 2017). This is further evidenced by studies on radioresistant sublines of MCF-7. Cells repeated irradiated are highly resistant to radiation and gene expression profiling shows that loss of ACSL4 is the primary mechanism for this (Kwon *et al.*, 2021). Furthermore, ASCL4 is essential for mediating radiation-induced damage in normal tissues, and specific ASCL4 inhibitors are being trialled as inhibitors of ferroptosis-induced radiation damage (Ji *et al.*, 2022).

The major ferroptosis defence system is thought to be the solute carrier family 7 member 11-glutathione-GPX4 (SLC7A11-GSH-GPX4) signalling axis; in fact, ferroptosis was first discovered due to experiments on this signalling axis (Dixon *et al.*, 2012; W. S. Yang *et al.*, 2014). A crucial part of the cystine/glutamate antiporter system Xc⁻, SLC7A11, sometimes referred to as xCT, facilitates the antiporter action of system Xc⁻ by bringing in extracellular cystine and releasing intracellular glutamate (Koppula *et al.*, 2018). Irradiation is known to increase SLC7A11 expression, leading to increased cystine uptake and increased GSH production, resulting in an reduced response to radiation (Koppula *et al.*, 2021) and therefore SLC11A7 overexpression leads to radio-resistance (Xie *et al.*, 2011; Lei *et al.*, 2020a), whereas decreased SLC11A7 leads to radiosensitivity (Cobler *et al.*, 2018; Nagane *et al.*, 2018; Lei *et al.*, 2020a). According to Koppula et al. (2018), after extracellular cystine is taken up by SLC7A11, it is immediately reduced to cysteine in the cytosol through a reduction mechanism that consumes NADPH. Next, as a key cofactor for GPX4 to detoxify lipid peroxides, cysteine acts as the rate-limiting precursor for the manufacture of GSH (Koppula *et al.*, 2021). Many cancer cells undergo significant ferroptosis when SLC7A11 transporter activity is blocked or when cystine is not present in culture media (Koppula *et al.*, 2021). Importantly, some tumour suppressors, including p53, BAP1, ADP-ribosylation factor (ARF), and Kelch-like ECH-associated protein 1 (KEAP1), induce ferroptosis by inhibiting the production or function of SLC7A11 (Jiang *et al.*, 2015; Zhang *et al.*, 2018). Similarly, by binding to the SLC7A11 promoter, activating transcription factor 3 (ATF3) suppresses SLC7A11 expression and increases the vulnerability of cancer cells to ferroptosis (Wang *et al.*, 2020). Nrf2 and activating transcription factor 4 (ATF4) are examples of stress-responsive transcription factors that can promote SLC7A11 under a variety of stress circumstances, including oxidative stress and amino acid deficiency, protecting cells from ferroptosis (Habib *et al.*, 2015). Therefore, SLC7A11 is an endogenous protective protein against radiation induced damage in normal cells, which can be exploited immediately after radiotherapy by tumour cells, and can be over-expressed in tumour cells to generate an intrinsically radioresistant phenotype.

In HT1080 human fibrosarcoma cells in vitro, radiotherapy directly causes tumour ferroptosis, a clonogenic survival assay after radiotherapy. During irradiation, it was

found that the iron chelator Deferoxamine (DFO), Liproxstatin-1, and Ferrostatin-1 enhanced clonogenic cell survival (Lang *et al.*, 2019). Additional research that targets SLC7A11, such as Erastin that targets GPX4 and RSL3 and FIN56 that depletes GPX4, could make non-small cell lung cancer cells more susceptible to RTx in vitro (Lei *et al.*, 2020a).

5.3.4 Nrf2 inhibitor did not enhance radiotherapy effects

The Nrf2 inhibitor, ML385 was combined with the optimized levels of radiation of 1.25 Gy for 2D and 20 Gy for 3D only at a time point of 72 hours and the result of ATP levels and cell death using Hoechst 33342/PI staining show no enhancement of radiation responses in both MDA-MB-231 and MCF-7 breast cancer cell lines. This can be due to the limitation of the study by using the optimized doses of ML385 in 24 hours but not optimized for 72 hours, another reason is that the cells were first irradiated then treated with ML385 and the time difference was about 2 hours because they were radiated at Sheffield University not in BMRC at Sheffield Hallam University, or simply cancer cells are not responding to treatments to many biological reasons.

The formation of ROS and DNA damage are two factors that affect radiotherapy effectiveness. Excessive ROS production can cause cell death or activate defence mechanisms like the Keap1/Nrf2 pathway, which controls intracellular cysteine availability by upregulating SLC7A11, a subunit of the system Xc$^-$ transporter, and subsequently glutathione synthesis, enhancing antioxidative defence (Bader *et al.*, 2021). In various cancer cell lines, Nrf2, a transcription factor that promotes the expression of genes containing antioxidant response elements (ARE), has been linked to providing resistance to chemotherapy and presumably radiotherapy also as both are associated with cell death mechanisms that are ROS-dependent (Roh *et al.*, 2017). Since ML385 is a direct inhibitor of Nrf2, it was hypothesised that ML385 would attenuate the Nrf2-mediated antioxidant response which becomes activated after radiotherapy, and increases cell death. Despite Nrf2 expression being much higher in MCF-7 cells than MDA-MB-231 cells at both mRNA level and protein level, with increased nuclear Nrf2 in MCF-7 (Chapter 4), both cell lines responded similarly to ML385 alone suggesting that in standard growth conditions, cells are dependent on Nrf2-mediated antioxidant response to survive. In both cases, combination of ML385 and ML385 + radiotherapy

resulted in essentially no difference in cell death, either by ATP measurements or Hoechst 33342/PI staining. The reason for this is unclear. Cells were treated within 2 hours of irradiation which may be a factor. Further experiments with either pre-treatment, or post-treatment are required. It is also possible that all radio-sensitive cells at the irradiation doses used killed all cells that are also Nrf2-dependent, and that for enhanced radio-responses, targeting the Nrf2-non-dependent cells is required. It is unclear why ML385 does not improve radiation in breast cancer cells. It is possible that the Nrf2 pathway does not play a significant role in the radiation response in breast cancer cells or that ML385 causes the activation of alternative compensatory mechanisms. However it is important to note that ML385 may have the ability to make other cancer cells more susceptible to radiation therapy in other tumour models, such as lung cancer (Singh *et al.*, 2020).

5.3.5 Cells grown in as 3D alginate spheres are intrinsically radio-resistant

Cells grown in 3D alginate spheres showed limited radiosensitivity at 20 Gy, whereas at this dose, almost all cells were killed in 2D colony formation assays. The reasons for this are unclear but observations supported by other researchers and results mirror chemotherapy responses. The radio-resistance of breast cancer cells could be due the capability of cancer cells to protect them self from excess ROS. It is known that cells in 3D cell culture experience increased ROS, and induce Nrf2 in the hypoxic core, and that Nrf2 expression is a pre-requisite for sphere formation (Takahashi *et al.*, 2020). Ionizing radiation (IR), which is frequently used in radiotherapy, damages DNA directly or indirectly by radiolyzing water, producing ROS and causing additional oxidative stress-related damage to biomolecules. Tumour cells evolve defence systems to prevent cell death due to repeated ROS exposure, and gain of Nrf2, or in the case of some breast cancers loss of Keap-1, allows clonal evolution of surviving Nrf2-high cells (Takahashi *et al.*, 2020). These Nrf2-dependent mechanisms enhance DNA repair and boost anti-oxidation defence, neutralising ROS, reducing oxidative stress, and limiting ROS-induced damage. So, in order to increase the effectiveness of radiation, new tactics must be developed (Bader *et al.*, 2021).

Another reason of radioresistant according to the "oxygen fixation hypothesis" and the activation of hypoxia-inducible factors (HIFs), the hypoxic tumour microenvironment is

a significant radio-resistance mechanism (Wang *et al.*, 2019). And usually this occurs in 3D cell culture as a mimic of in vivo responses rather than 2D monolayer cells, because they mimic the tumour microenvironment (DelNero *et al.*, 2015). On the other hand, hypoxia increases the production of ROS; as a result, hypoxic tumour cells heavily rely on antioxidant systems to maintain redox equilibrium, and GSH inhibition was demonstrated to overcome hypoxia-mediated radio-resistance (Wang *et al.*, 2019). It is intriguing to learn that HIFs (HIF-1 and -2) have been linked to ferroptosis susceptibility Renal cancer cells are also more vulnerable to ferroptosis when HIF-1 is activated (Zou *et al.*, 2019).

5.3.6 Cells growth in 3D cell culture show heterogeneous ferroptosis responses

From the data that was obtained it can notice that treating cells grown in 3D cell culture with ferroptosis inducer RSL3 (Figures 5.19, and 5.20) and ML385 (Figure 5.21) showed that some colonies response to treatment and die, while other colonies survives and this heterogeneity between the same population of tumour cells. Interestingly a parallel phenomenon has very recently been described in TNBC whereby cancers show marked heterogeneity with respect to ferroptosis markers (Yang *et al.*, 2023). Similarly, ferroptotic heterogeneity has also been reported in melanoma (Lin *et al.*, 2022) which mirrors observations for heterogeneity of apoptosis inducers in breast cancer cells and other tumour cell types (Cross *et al.*, 2008a; Sabrina L Spencer *et al.*, 2009).

Further research is necessary to determine the possibility and precise processes by which ferroptosis activation and Nrf2 inhibition can decrease the radio-resistance of hypoxic cancer cells in various cancer situations, and to identify metabolic signatures of ferroptosis-sensitive vs resistant populations.

Summary

MDA-MB-231 and MCF-7 cells were sensitive to RTx in 2D cell culture but resistant to RTx in 3D cell culture. After induction of cell death with ferroptosis inducers, there was no robust enhancement to radiation effect to the breast cancer cells either in 2D or 3D cell culture. The Nrf2 inhibitor ML385 showed no further effect on radiotherapy. These studies suggest targeting ferroptosis is not likely to be effective radio-sensitising strategy.

Chapter 6: Final discussion

6.1 General discussion

The assessment of ferroptosis as chemo- and radiosensitisers in breast cancer cells requires a) optimisation of optimal doses at initiate some death, but not extensive death, b) confirmation that ferroptotic death is occurring using ferroptosis inhibitors, c) exclusion of apoptotic cell death using nuclear morphology and/or caspase inhibitors, d) detection of glutathione depletion in ferroptotic cells, e) detection of ROS in ferroptotic cells, f) detection of free iron in ferroptotic cells and finally g) detection of lipid peroxidation in ferroptotic cells (Chapter 3 and 4). Furthermore, optimal doses of chemo-and radiotherapy doses need to be optimised (Chapters 4 and 5).

In Chapter 3, optimal doses of ferroptosis inducers were established for MDA-MB-231 and MCF-7 cells, in both 2D and 3D cell culture. Using these doses, combination studies with ferroptosis inducers were comprehensively completed with Doxorubicin, and combination studies also completed for Cisplatin, and radiotherapy. No further work was completed using Paclitaxel due to time constraints and lack of drug response and time limitations. It was shown that MCF-7 were highly resistant to all ferroptosis inducers, whereas MDA-MB-231 were highly sensitive. This supports existing data in the literature, and reasons for this difference are discussed in Chapter 3, although MCF-7 expression of oestrogen receptor (Liu *et al.*, 2022) and loss of p53 in MDA-MB-231 are implicated (Zhang, *et al.*, 2021).

Ferroptosis was confirmed with the use of three ferroptosis inhibitors, all of which reversed or partially reversed ferroptosis in MDA-MB-231, whereas apoptosis inhibition using caspase inhibitors did not. In all cases where cell death was observed with ferroptosis inducers, including both 2D and 3D cell cultures, ferroptotic inhibitors Deferoxamine, Liproxstatin-1 and Ferrostatin-1 all reversed the effects. In MCF-7, results were not so clear in that ferroptosis was not reliably induced, and in some cases ferroptosis inhibitors, particularly deferoxamine led to cell death. As a further confirmation of ferroptosis, cells treated with ferroptosis inducers alone, and with inhibitors were assessed, showing induction of free iron in ferroptosis induction, which was partially reversed with ferroptosis inhibitors. Ferroptosis inducers also generated a

lipid peroxidation signal, increased ROS and showed depletion of Glutathione, all consistent with ferroptosis being induced (Chapters 3 and 4).

In 3D cell culture, MDA-MB-231 cells were significantly more resistant to ferroptosis, although cells did show sensitivity to RSL3, but not Erastin or FIN56. Even in the ferroptosis-resistant cell line MCF-7, 3D spheroids were affected by RSL3, but not Erastin of FIN56. This is a highly interesting observation that across both ferroptosis-sensitive and resistant cell lines, RSL3 appears to have activity. In light of this observation, RSL3 was taken forward for the majority of combination studies with chemotherapy and radiotherapy in Chapters 4 and 5.

Prior to combination studies with chemotherapy, dose response of 2D and 3D cultured cells was performed with Doxorubicin and Cisplatin. Consistent with previous studies in other tumour models, 3D cultured cells were highly resistant to Doxorubicin in spheroids, with IC50 values 5-10 fold higher in 3D cell culture (Palubeckaite *et al.,* 2020). In contrast for Cisplatin, IC50 values were comparable to 2D cell culture, being less than 2-fold higher in 3D cell culture vs 2D cell culture, consistent with previous studies (Tanenbaum *et al.*, 2017; Gupta *et al.*, 2022; Ono *et al.*, 2022a). In combination studies, key findings are that ferroptosis inducers do not enhance Doxorubicin responses in MDA-MB-231, and only RSL3 induces robust reposes in combination with Doxorubicin in 2D cell culture, however Erastin and FIN56 showed some additional activity when combined with Doxorubicin in MDA-MB-231 spheroids, and RSL3 enhanced Doxorubicin-mediated death in MCF-7 spheroids. These promising drug combinations were followed-up with studies on free iron, ROS, glutathione and lipid peroxidase which generally supported the notion of ferroptosis-induced cell death in individual treatments, but no synergistic enhancement by combination treatment (Chapter 4). Cisplatin showed evidence of synergy with RSL3 in MDA-MB-231, although these observations did not replicate in 3D cell culture, and in MCF-7, modest effects in 2D cell culture were not replicated in 3D cell culture (Chapter 4). Some of the most promising drug combinations came from studies of Nrf2-modulation. Nrf2, the master regulator of the anti-oxidant response is expressed by both cell lines at mRNA and protein levels (Chapter 4). Specific Nrf2 inhibition did not further enhance Doxorubicin responses in either cell line, but did further enhance RSL3 responses specifically in MDA-MB-231, with

a very potent and synergistic interaction in both 2D and 3D cultured cells. This highlights a specific vulnerability in MDA-MB-231 cells, and is consistent with observations in acute myeloid leukaemia, where this specific vulnerability was also observed with FIN56 as well as RSL3 (X. Liu *et al.*, 2023). Furthermore, in normal transformed lung cells, RSL3 responses are enhanced by ML385 (Taufani *et al.*, 2023). Combinations treatments of RSL3 + ML385 were further enhanced by the addition of Doxorubicin in both 2D and 3D cell culture, however the majority of benefit appears to be via the combination of ML385 and RSL3. RLS3 inhibits GPX4 directly, whereas Erastin inhibits System Xc-. Inhibiting System Xc-, leading to depleted glutathione does not appear to be sufficient to bypass all resistance mechanisms, whereas directly blocking GPX4 with RSL3, appears a more robust mechanism of ferroptosis induction. Why FIN56 does not mirror RSL3 responses is unclear, however FIN56's mechanism of degradation of GPX4 is still unclear, and may involve other additional mechanisms including autophagy-related signalling (Sun *et al.*, 2021).

Very recent studies have highlighted that Nrf2, or ferroptosis suppressor protein-1 (FSP1) can independently mediate ferroptosis (Kim *et al.*, 2023) in Keap-1 mutant cells. Although MCF-7 and MDA-MB-231 are not known to be Keap-1 mutant, they both express high levels of Nrf2, analogous the keap-1 mutant situation, and high Nrf2 has been reported to mediate ferroptosis resistance in MCF-7, albeit only in hypoxia (Syu *et al.,* 2016). It would therefore be expected that MCF-7 cells would respond to ML385 in spheroids, but this was not the case. In summary, RSL3 is the most robust enhancer of chemotherapy responses in both 2D and 3D cell cultures, and is worthy of further study, but cell line-dependent insensitivities exist. Combination treatment of RSL3 with ML385 is a highly cytotoxic combination and certainly worthy of further study.

Studies in 3D cell culture highlighted a novel observation in that a heterogeneous response was observed: within individual alginate beads, spheroids either responded to ferroptosis inducers with the majority of cells dying, or the whole spheroid failed to respond. This occurred in adjacent spheroids, and so was not due to drug access, but was a genuine heterogeneous response. This is highly interesting in that it shows that the breast cancer cells are undergoing phenotypic plasticity, or that the cell line population contains a mixed population of ferroptosis-sensitive and ferroptosis-

resistant cells. Avery recent publication has reported similar observations on glioma (C. Wang *et al.*, 2023), whereby phenotypic plasticity occurs leading to the heterogeneous response. Future studies are planned to address this using clonal cell populations from each cell line in colony formation and sensitivity assays, and clonal populations in 3D spheroids. It is noteworthy that each individual spheroid in alginate originates from an individual cell, in the same manner as individual colonies in the colony formation assay. It is interesting that MDA-MD-231 and many other cell lines is known to exhibit phenotypic plasticity with respect to apoptotic signalling, with some cells from isogenic populations being sensitive, and others resistant (Cross *et al.*, 2008b; Sabrina L. Spencer *et al.*, 2009; Flusberg *et al.*, 2013). It would be intriguing to see if ferroptosis is similarly under the control of phenotypic plasticity and whether similar control mechanisms exist.

The role of ferroptosis in enhancing RTx is a widely discussed topic, leading to many commentaries and revies, but based on quite limited laboratory data from cell culture, spheroids or in vivo models of cancer. Ferroptosis has been proposed as a mechanism for enhancing RTx in cancer patients (Beretta and Zaffaroni, 2023; Z. Chen *et al.*, 2023). In addition, Lu et al. (2023) surveyed many pathways that in theory should enhance RTx, and identified a modest number of studies that have actually applied this combination therapy (Lu *et al.*, 2023). For example, a novel GPX4 inhibitor enhanced RTx in MDA-MB-231 and MCF-7 (Liu *et al.*, 2023). Interestingly, this study also showed enhanced RTx responses in Nrf2 knockdown cells, suggesting that Nrf2 inhibition could also, in theory enhance radio-sensitivity (Liu *et al.*, 2023). An inhibitor of SLC7A11 induced ferroptosis-mediated radio-sensitivity in organoids and patient-derived xenografts, specifically in those cells that lack p53 (Lei, Zhang, *et al.*, 2021). MCF-7 has wildtype TP53, whereas MDA-MB-231 has mutant TP53 (Zaza *et al.*, 2023), however in the present study, although ferroptosis responses differed considerably, no enhancement of RTx with ferroptosis inducers was observed. Another potential mediator of ferroptosis is Prostaglandin-endoperoxide synthase 2 (PTGS2) (Stockwell *et al.*, 2017), which is induced in a wide range of cancer cell lines tested in response to ferroptosis inducers, however MCF-7 was in a minority of cell lines tested MCF-7 in which PTGS2 not raised (Lei *et al.*, 2020b). Furthermore, MDA-MB-231 has been reported to be further sensitised to Erastin by DKK1 depletion (Wu *et al.*, 2022). DKK1 is a mediator of the Wnt

signaling pathway and specifically over-expressed in MDA-MB-231. These studies highlight that responses to ferroptosis inducers can be altered in individual cell lines in widely differing ways.

RTx-mediated radiosensitivity was not widely detected in the present study. Using a dose that initiated limited cell death in 72 hours but was known to induce highly significant reduction in colony formation at 14 days yielded limited data suggestive of a synergistic interaction, with low levels of additional death with FIN56 in MDA-MB-231 and an additive response of RSL3 in MCF-7 at doses up to 1.25 µM only in MCF-7 cells. Combination with Nrf2 also failed to initiate any synergistic interaction with RTx, either in 2D or 3D cell culture. Therefore, the conclusion from this study is that in MCF-7 and MDA-MB-231 cell, there is no reliable and robust radio-sensitising effect of ferroptosis inducers, or Nrf2 inhibitors. It may be that reported radio-sensitising effects are cell line-dependent, or cell model dependent. Of the few studies reporting reliable ferroptosis-mediated radio-sensitisation, colony formation assay was the chosen method, and doses typically over 2 Gy used to show a reliable effect (L. F. Ye *et al.*, 2020; Lei *et al.*, 2020b). Colony formation was attempted as part of the present study in some experiments with RSL3 and ML385 (data not shown) and due to time constraints not comprehensively completed, however preliminary experiments failed to show a synergistic interaction with either agent, however doses of RSL3 were most likely too high and needed optimising further. ML385 did not robustly enhance RTx responses in colony formation assays in either cell line (Appendix 1).

Lu et al. (2023) highlighted studies that suggest radiation-induced pulmonary fibrosis and radiation-induced lung injury can be exacerbated by ferroptosis inducers and/or alleviated by ferroptosis inhibitors (Li *et al.*, 2019; Zhuang and Qiao, 2019) highlighting that any enhancement of ferroptosis as a therapy needs to be carefully balanced against enhanced side effects of the treatment, in the same manner as ferroptosis-induced cardiotoxicity via chemotherapy (Sahebkar *et al.*, 2023). However as shown by Sahebkar et al, (2023), deleterious effects of ferroptosis induced by chemotherapy might be reversed by statins (Sahebkar *et al.*, 2023). Statins are known to increase anti-oxidant enzymes, in part via the induction of Nrf2 (Mansouri *et al.*, 2022). Similarly, ferroptosis-mediated RTx intestinal injury is via the ASCL4 pathway and can be alleviated by

inhibition of the Nrf2 axis (Kong *et al.*, 2023) or by ferrostatin-1 (Wang *et al.*, 2023). Therefore, as with chemotherapy-induced ferroptosis, enhancement of RTx-induced cancer cell death has to be balanced with normal tissue injury. As stated above, a small number of very recent studies are starting to investigate this emerging field.

6.2 Final conclusions

Ferroptosis induction, primarily with RSL3 can enhance Doxorubicin and Cisplatin responses, some of which are also observed in 3D cell culture, but radiotherapy responses are not reliably enhanced by ferroptosis inducers. More potent cell death is induced by the combination of RSL3 with the Nrf2 inhibitor ML385, and this will be the focus of future mechanistic studies. Spheroids respond heterogeneously to ferroptotic stimuli, and future studies are aimed at addressing whether this is a phenotypic plasticity-dependent mechanism, or mixed cell phenotypes in breast cancer cell lines.

6.3 Future work

At the beginning of the study, all ferroptosis inducers were optimized for 24 hours for 2D cell culture experiments and later in the study, for 48 hours for 3D alginates experiments (Chapter 3) due to lack of responses at 24 hours. Further optimization of the ferroptosis inducers at different time points (48 hours or even longer durations) would make these data sets more comparable, and also identify any effects that might have been missed. This is notable for MCF-7 which was more much sensitive to RSL3 at 48 hours than 24 hours.

In the combination studies with chemotherapy agents (Chapter 4), only Doxorubicin was used with all ferroptosis inducers, and due to time constraints only the ferroptosis inducer RSL3 was used with Cisplatin. Cisplatin gave some promising observations with RSL3, and therefore testing the ferroptosis inducers Erastin and FIN56 could be done to assess whether this is an RSL3-specific effect, or a ferroptosis-specific effect.

For the radiotherapy combination studies with ferroptosis inducers (Chapter 5), cells were treated with ferroptosis inducers after irradiation. Since irradiation may initiate a burst of ROS, this may prime the cell to be protected from subsequent ferroptosis. Therefore, to complement the data in chapter 5, the plan is to repeat these studies by

first treating the cells with ferroptosis inducers for 24 hours and then irradiating the cells to assess enhancement of the treatments. This data is being generated by a research student.

The effects of ferroptosis inducers on chemo- and radio-therapy using colony formation assay, which assesses the long-term effects of irradiation and chemotherapy responses, rather than short-term cell death assays could be completed. The rationale for assessing cell death over short time periods is that ferroptosis, like apoptosis, is a short-duration form of cell death. The aims of the studies were to assess specifically whether cell death was occurring immediately after treatment, rather than assessing the percentage of colony forming cells surviving after 2 weeks. However irradiation responses are often assessed using colony formation assay, and this data would benefit publication of the irradiation work.

Heterogeneity of ferroptosis responses was observed in 3D cell culture in isogenic spheroids, i.e. spheroids that are generated from a single cell. Theoretically all cells should be equally sensitive to ferroptosis inducers however this was not the case. Furthermore, there are clearly ferroptic sensitive and resistant populations in bath cell lines. Therefore, to assess whether this phenomenon occurs in 2D cell cultures also, cells could be cloned by serial dilution, and then cells from a single colony trypsinised to form more colonies and ferroptosis responses assessed in these isogenic colonies. If ferroptosis responses differ between colonies, that would confirm that ferroptosis sensitivity exhibits phenotypic plasticity. The MDA-MD-231 cell line has previously been shown to exhibit phenotypic plasticity for apoptosis responses.

7. References

Abdalkader, M. *et al.* (2018) 'Targeting Nrf2 to suppress ferroptosis and mitochondrial dysfunction in neurodegeneration', *Frontiers in Neuroscience*, 12(JUL), pp. 1–9. doi: 10.3389/fnins.2018.00466.

Abe, K. *et al.* (2022) 'Doxorubicin causes ferroptosis and cardiotoxicity by intercalating into mitochondrial DNA and disrupting Alas1-dependent heme synthesis', *Science Signaling*, 15(758). doi: 10.1126/scisignal.abn8017.

Abuetabh, Y. *et al.* (2022) 'DNA damage response revisited: the p53 family and its regulators provide endless cancer therapy opportunities', *Experimental & Molecular Medicine*, 54(10), pp. 1658–1669. doi: 10.1038/s12276-022-00863-4.

Adams, S. *et al.* (2014) 'Prognostic Value of Tumor-Infiltrating Lymphocytes in Triple-Negative Breast Cancers From Two Phase III Randomized Adjuvant Breast Cancer Trials: ECOG 2197 and ECOG 1199', *Journal of Clinical Oncology*, 32(27), pp. 2959–2966. doi: 10.1200/JCO.2013.55.0491.

Al-Mahmood, S. *et al.* (2018) 'Metastatic and triple-negative breast cancer: challenges and treatment options', *Drug Delivery and Translational Research*, 8(5), pp. 1483–1507. doi: 10.1007/s13346-018-0551-3.

Aldossary, S. A. (2019) 'Review on Pharmacology of Cisplatin: Clinical Use, Toxicity and Mechanism of Resistance of Cisplatin', *Biomedical and Pharmacology Journal*, 12(1), pp. 07–15. doi: 10.13005/bpj/1608.

Amable, L. (2016) 'Cisplatin resistance and opportunities for precision medicine', *Pharmacological Research*, 106, pp. 27–36. doi: 10.1016/j.phrs.2016.01.001.

Anand, P. *et al.* (2008) 'Cancer is a Preventable Disease that Requires Major Lifestyle Changes', *Pharmaceutical Research*, 25(9), pp. 2097–2116. doi: 10.1007/s11095-008-9661-9.

Andrews, N. C. (2008) 'Forging a field: the golden age of iron biology', *Blood*, 112(2), pp. 219–230. doi: 10.1182/blood-2007-12-077388.

Aranza-Martínez, A. *et al.* (2021) 'Non-Coding RNAs Associated With Radioresistance in Triple-Negative Breast Cancer', *Frontiers in Oncology*, 11. doi: 10.3389/fonc.2021.752270.

Arhoma, A. *et al.* (2017) 'SAHA-induced TRAIL-sensitisation of Multiple Myeloma cells is enhanced in 3D cell culture', *Experimental Cell Research*, 360(2), pp. 226–235. doi: 10.1016/j.yexcr.2017.09.012.

Assaraf, Y. G. *et al.* (2019) 'The multi-factorial nature of clinical multidrug resistance in cancer', *Drug Resistance Updates*, 46, p. 100645. doi: 10.1016/j.drup.2019.100645.

Aubrey, B. J. *et al.* (2018) 'How does p53 induce apoptosis and how does this relate to p53-mediated tumour suppression?', *Cell Death & Differentiation*, 25(1), pp. 104–113. doi: 10.1038/cdd.2017.169.

Azzam, E. I., Jay-Gerin, J.-P. and Pain, D. (2012) 'Ionizing radiation-induced metabolic oxidative stress and prolonged cell injury', *Cancer Letters*, 327(1–2), pp. 48–60. doi: 10.1016/j.canlet.2011.12.012.

Baarsma, H. A., Königshoff, M. and Gosens, R. (2013) 'The WNT signaling pathway from ligand secretion to gene transcription: Molecular mechanisms and pharmacological targets', *Pharmacology and Therapeutics*, 138(1), pp. 66–83. doi: 10.1016/j.pharmthera.2013.01.002.

Bader, S. *et al.* (2021) 'Activation of anti-oxidant Keap1/Nrf2 pathway modulates efficacy of dihydroartemisinin-based monotherapy and combinatory therapy with ionizing radiation', *Free Radical Biology and Medicine*, 168, pp. 44–54. doi: 10.1016/j.freeradbiomed.2021.03.024.

Baidoo, K. E., Yong, K. and Brechbiel, M. W. (2013) 'Molecular Pathways: Targeted α-Particle Radiation Therapy', *Clinical Cancer Research*, 19(3), pp. 530–537. doi: 10.1158/1078-0432.CCR-12-0298.

Baldo, B. A. and Pham, N. H. (2013) 'Adverse reactions to targeted and non-targeted chemotherapeutic drugs with emphasis on hypersensitivity responses and the invasive metastatic switch', *Cancer and Metastasis Reviews*, 32(3–4), pp. 723–761. doi: 10.1007/s10555-013-9447-3.

Bao, L. *et al.* (2011) 'Increased Expression of P-Glycoprotein Is Associated with Doxorubicin Chemoresistance in the Metastatic 4T1 Breast Cancer Model', *The American Journal of Pathology*, 178(2), pp. 838–852. doi: 10.1016/j.ajpath.2010.10.029.

Barroso-Sousa, R. and Metzger-Filho, O. (2016) 'Differences between invasive lobular and invasive ductal carcinoma of the breast: results and therapeutic implications', *Therapeutic Advances in Medical Oncology*, 8(4), pp. 261–266. doi: 10.1177/1758834016644156.

Baskar, R. *et al.* (2012) 'Cancer and Radiation Therapy: Current Advances and Future Directions', *International Journal of Medical Sciences*, 9(3), pp. 193–199. doi: 10.7150/ijms.3635.

Belpomme, D. *et al.* (2007) 'The multitude and diversity of environmental carcinogens', *Environmental Research*, 105(3), pp. 414–429. doi: 10.1016/j.envres.2007.07.002.

Beretta, G. L. and Zaffaroni, N. (2023) 'Radiotherapy-induced ferroptosis for cancer treatment', *Frontiers in Molecular Biosciences*, 10. doi: 10.3389/fmolb.2023.1216733.

Beslija, S. *et al.* (2007) 'Second consensus on medical treatment of metastatic breast cancer', *Annals of Oncology*, 18(2), pp. 215–225. doi: 10.1093/annonc/mdl155.

Bhat, V. *et al.* (2022) 'Radiotherapy and radiosensitization in breast cancer: Molecular targets and clinical applications', *Critical Reviews in Oncology/Hematology*, 169, p. 103566. doi: 10.1016/j.critrevonc.2021.103566.

Birch, J. and Gil, J. (2020) 'Senescence and the SASP: many therapeutic avenues', *Genes & Development*, 34(23–24), pp. 1565–1576. doi: 10.1101/gad.343129.120.

Blamey, R. W. *et al.* (2013) 'Radiotherapy or tamoxifen after conserving surgery for breast cancers of excellent prognosis: British Association of Surgical Oncology (BASO) II trial', *European Journal of Cancer*, 49(10), pp. 2294–2302. doi: 10.1016/j.ejca.2013.02.031.

Blücher, C. and Stadler, S. C. (2017) 'Obesity and Breast Cancer: Current Insights on the Role of Fatty Acids and Lipid Metabolism in Promoting Breast Cancer Growth and Progression', *Frontiers in Endocrinology*, 8. doi: 10.3389/fendo.2017.00293.

Bonadonna, G. *et al.* (1995) 'Adjuvant Cyclophosphamide, Methotrexate, and Fluorouracil in Node-Positive Breast Cancer — The Results of 20 Years of Follow-up', *New England Journal of Medicine*, 332(14), pp. 901–906. doi: 10.1056/NEJM199504063321401.

Borst, P. *et al.* (2000) 'A Family of Drug Transporters: the Multidrug Resistance-Associated Proteins', *JNCI Journal of the National Cancer Institute*, 92(16), pp. 1295–1302. doi: 10.1093/jnci/92.16.1295.

De Brabander, M. *et al.* (1981) 'Taxol induces the assembly of free microtubules in living cells and blocks the organizing capacity of the centrosomes and kinetochores.', *Proceedings of the National Academy of Sciences*, 78(9), pp. 5608–5612. doi: 10.1073/pnas.78.9.5608.

Bray, F. *et al.* (2018) 'Global cancer statistics 2018: GLOBOCAN estimates of incidence and mortality worldwide for 36 cancers in 185 countries', *CA: A Cancer Journal for Clinicians*, 68(6), pp. 394–424. doi: 10.3322/caac.21492.

Brenton, J. D. *et al.* (2005) 'Molecular Classification and Molecular Forecasting of Breast Cancer: Ready for Clinical Application?', *Journal of Clinical Oncology*, 23(29), pp. 7350–7360. doi: 10.1200/JCO.2005.03.3845.

Brierley, JD, Godspodarowicz, MK, Wittekind, C. (2016) *TNM atlas 8th Ed*. Wiley-Blackwell. doi: ISB:978-1-119-26357-9.

Brown, J. M., Carlson, D. J. and Brenner, D. J. (2014) 'The tumor radiobiology of SRS and SBRT: are more than the 5 Rs involved?', *International journal of radiation oncology, biology, physics*, 88(2), pp. 254–62. doi: 10.1016/j.ijrobp.2013.07.022.

Brozovic, A., Ambriović-Ristov, A. and Osmak, M. (2010) 'The relationship between cisplatin-induced reactive oxygen species, glutathione, and BCL-2 and resistance to cisplatin', *Critical Reviews in Toxicology*, 40(4), pp. 347–359. doi:

10.3109/10408441003601836.

Bull, F. C. *et al.* (2020) 'World Health Organization 2020 guidelines on physical activity and sedentary behaviour', *British Journal of Sports Medicine*, 54(24), pp. 1451–1462. doi: 10.1136/bjsports-2020-102955.

Bunz, F. (2001) 'Cell death and cancer therapy', *Current Opinion in Pharmacology*, 1(4), pp. 337–341. doi: 10.1016/S1471-4892(01)00059-5.

Burgess, C. *et al.* (2005) 'Depression and anxiety in women with early breast cancer: five year observational cohort study', *BMJ*, 330(7493), p. 702. doi: 10.1136/bmj.38343.670868.D3.

Cailleau, R. *et al.* (1974) 'Breast Tumor Cell Lines From Pleural Effusions2', *JNCI: Journal of the National Cancer Institute*, 53(3), pp. 661–674. doi: 10.1093/jnci/53.3.661.

Campbell, E. J. *et al.* (2016) 'The combined endocrine receptor in breast cancer, a novel approach to traditional hormone receptor interpretation and a better discriminator of outcome than ER and PR alone', *British Journal of Cancer*, 115(8), pp. 967–973. doi: 10.1038/bjc.2016.206.

Cao, J. Y. and Dixon, S. J. (2016) 'Mechanisms of ferroptosis', *Cellular and Molecular Life Sciences*, 73(11–12), pp. 2195–2209. doi: 10.1007/s00018-016-2194-1.

Cardoso, F. *et al.* (2017) '3rd ESO–ESMO International Consensus Guidelines for Advanced Breast Cancer (ABC 3)', *Annals of Oncology*, 28(1), pp. 16–33. doi: 10.1093/annonc/mdw544.

Carey, L. A. *et al.* (2006) 'Race, Breast Cancer Subtypes, and Survival in the Carolina Breast Cancer Study', *JAMA*, 295(21), p. 2492. doi: 10.1001/jama.295.21.2492.

Carmeliet, P. and Jain, R. K. (2000) 'Angiogenesis in cancer and other diseases', *Nature*, 407(6801), pp. 249–257. doi: 10.1038/35025220.

Carter, S. K. (1972) 'Single and combination nonhormonal chemotherapy in breast cancer', *Cancer*, 30(6), pp. 1543–1555. doi: 10.1002/1097-0142(197212)30:6<1543::AID-CNCR2820300621>3.0.CO;2-V.

Castle, K. D. and Kirsch, D. G. (2019) 'Establishing the Impact of Vascular Damage on Tumor Response to High-Dose Radiation Therapy', *Cancer Research*, 79(22), pp. 5685–5692. doi: 10.1158/0008-5472.CAN-19-1323.

Chang, A. E. *et al.* (2018) 'Phase I/II Trial of Combined Pegylated Liposomal Doxorubicin and Cyclophosphamide in Metastatic Breast Cancer', *Clinical Breast Cancer*, 18(1), pp. e143–e149. doi: 10.1016/j.clbc.2017.10.005.

Chen, C., Wang, S. and Liu, P. (2019) 'Deferoxamine Enhanced Mitochondrial Iron Accumulation and Promoted Cell Migration in Triple-Negative MDA-MB-231 Breast

Cancer Cells Via a ROS-Dependent Mechanism', *International Journal of Molecular Sciences*, 20(19), p. 4952. doi: 10.3390/ijms20194952.

Chen, M.-S. *et al.* (2017) 'CHAC1 degradation of glutathione enhances cystine-starvation-induced necroptosis and ferroptosis in human triple negative breast cancer cells via the GCN2-eIF2α-ATF4 pathway', *Oncotarget*, 8(70), pp. 114588–114602. doi: 10.18632/oncotarget.23055.

Chen, X. *et al.* (2020) 'Ferroptosis: machinery and regulation', *Autophagy*, pp. 1–28. doi: 10.1080/15548627.2020.1810918.

Chen, Y. *et al.* (2023) 'Oxidative stress induces mitochondrial iron overload and ferroptotic cell death', *Scientific Reports*, 13(1), p. 15515. doi: 10.1038/s41598-023-42760-4.

Chen, Z. *et al.* (2023) 'Ferroptosis as a potential target for cancer therapy', *Cell Death & Disease*, 14(7), p. 460. doi: 10.1038/s41419-023-05930-w.

Chiang, S. P. H., Cabrera, R. M. and Segall, J. E. (2016) 'Tumor cell intravasation', *American Journal of Physiology-Cell Physiology*, 311(1), pp. C1–C14. doi: 10.1152/ajpcell.00238.2015.

Choi, E.-J. and Jeon, S.-M. (2020) 'NRF2-driven redox metabolism takes center stage in cancer metabolism from an outside-in perspective', *Archives of Pharmacal Research*, 43(3), pp. 321–336. doi: 10.1007/s12272-020-01224-3.

Chowdhury, N. *et al.* (2006) 'Interobserver variation in breast cancer grading: a statistical modeling approach.', *Analytical and quantitative cytology and histology*, 28(4), pp. 213–8. Available at: http://www.ncbi.nlm.nih.gov/pubmed/16927641.

Christidi, E. and Brunham, L. R. (2021) 'Regulated cell death pathways in doxorubicin-induced cardiotoxicity', *Cell Death & Disease*, 12(4), p. 339. doi: 10.1038/s41419-021-03614-x.

Cianfrocca, M. and Goldstein, L. J. (2004) 'Prognostic and Predictive Factors in Early-Stage Breast Cancer', *The Oncologist*, 9(6), pp. 606–616. doi: 10.1634/theoncologist.9-6-606.

Cobler, L. *et al.* (2018) 'xCT inhibition sensitizes tumors to γ-radiation via glutathione reduction', *Oncotarget*, 9(64), pp. 32280–32297. doi: 10.18632/oncotarget.25794.

Codogno, P. and Meijer, A. J. (2005) 'Autophagy and signaling: their role in cell survival and cell death', *Cell Death & Differentiation*, 12(S2), pp. 1509–1518. doi: 10.1038/sj.cdd.4401751.

Cohen, S. M. *et al.* (2011) 'Subcutaneous delivery of nanoconjugated doxorubicin and cisplatin for locally advanced breast cancer demonstrates improved efficacy and decreased toxicity at lower doses than standard systemic combination therapy in vivo',

The American Journal of Surgery, 202(6), pp. 646–653. doi: 10.1016/j.amjsurg.2011.06.027.

Colles, S. M. and Chisolm, G. M. (2000) 'Lysophosphatidylcholine-induced cellular injury in cultured fibroblasts involves oxidative events.', *Journal of lipid research*, 41(8), pp. 1188–98. Available at: http://www.ncbi.nlm.nih.gov/pubmed/10946005.

Colotta, F. *et al.* (2009) 'Cancer-related inflammation, the seventh hallmark of cancer: links to genetic instability', *Carcinogenesis*, 30(7), pp. 1073–1081. doi: 10.1093/carcin/bgp127.

Cosialls, E. *et al.* (2021) 'Ferroptosis: Cancer Stem Cells Rely on Iron until "to Die for" It', *Cells*, 10(11), p. 2981. doi: 10.3390/cells10112981.

Costa, P. M. da S. *et al.* (2023) 'Epigenetic reprogramming in cancer: From diagnosis to treatment', *Frontiers in Cell and Developmental Biology*, 11. doi: 10.3389/fcell.2023.1116805.

Cotto-Rios, X. M. and Gavathiotis, E. (2016) 'Unraveling cell death mysteries', *Nature Chemical Biology*, 12(7), pp. 470–471. doi: 10.1038/nchembio.2110.

Creative Bioarray (2023) *Cell Proliferation Assay Services*, *Creative Bioarray*. Available at: https://www.creative-bioarray.com/Services/cell-proliferation-assay-services.htm.

Cross, N. A. *et al.* (2008a) 'Phenotypic variations of TRAIL sensitivity in cloned populations of prostate cancer cells', *Journal of Cellular Biochemistry*, 104(4), pp. 1452–1464. doi: 10.1002/jcb.21721.

Cross, N. A. *et al.* (2008b) 'Phenotypic variations of TRAIL sensitivity in cloned populations of prostate cancer cells', *Journal of Cellular Biochemistry*, 104(4), pp. 1452–1464. doi: 10.1002/jcb.21721.

Cuzick, J. *et al.* (2011) 'Prognostic value of a combined estrogen receptor, progesterone receptor, Ki-67, and human epidermal growth factor receptor 2 immunohistochemical score and comparison with the Genomic Health recurrence score in early breast cancer.', *Journal of clinical oncology : official journal of the American Society of Clinical Oncology*, 29(32), pp. 4273–8. doi: 10.1200/JCO.2010.31.2835.

D'Arcy, M. S. (2019) 'Cell death: a review of the major forms of apoptosis, necrosis and autophagy', *Cell Biology International*, 43(6), pp. 582–592. doi: 10.1002/cbin.11137.

Daher, B. *et al.* (2019) 'Genetic Ablation of the Cystine Transporter xCT in PDAC Cells Inhibits mTORC1, Growth, Survival, and Tumor Formation via Nutrient and Oxidative Stresses', *Cancer Research*, 79(15), pp. 3877–3890. doi: 10.1158/0008-5472.CAN-18-3855.

Dammermann, A., Desai, A. and Oegema, K. (2003) 'The minus end in sight', *Current Biology*, 13(15), pp. R614–R624. doi: 10.1016/S0960-9822(03)00530-X.

DelNero, P. *et al.* (2015) '3D culture broadly regulates tumor cell hypoxia response and angiogenesis via pro-inflammatory pathways', *Biomaterials*, 55, pp. 110–118. doi: 10.1016/j.biomaterials.2015.03.035.

Demetriadou, C., Koufaris, C. and Kirmizis, A. (2020) 'Histone N-alpha terminal modifications: genome regulation at the tip of the tail', *Epigenetics & Chromatin*, 13(1), p. 29. doi: 10.1186/s13072-020-00352-w.

Demuynck, R. *et al.* (2020) 'A 3D Cell Death Assay to Quantitatively Determine Ferroptosis in Spheroids', *Cells*, 9(3), p. 703. doi: 10.3390/cells9030703.

DeNardo, D. G., Andreu, P. and Coussens, L. M. (2010) 'Interactions between lymphocytes and myeloid cells regulate pro- versus anti-tumor immunity', *Cancer and Metastasis Reviews*, 29(2), pp. 309–316. doi: 10.1007/s10555-010-9223-6.

DeSantis, C. *et al.* (2011) 'Breast cancer statistics, 2011', *CA: A Cancer Journal for Clinicians*, 61(6), pp. 408–418. doi: 10.3322/caac.20134.

DeSantis, C. E. *et al.* (2017) 'Breast cancer statistics, 2017, racial disparity in mortality by state', *CA: A Cancer Journal for Clinicians*, 67(6), pp. 439–448. doi: 10.3322/caac.21412.

Diaz-Moralli, S. *et al.* (2013) 'Targeting cell cycle regulation in cancer therapy', *Pharmacology & Therapeutics*, 138(2), pp. 255–271. doi: 10.1016/j.pharmthera.2013.01.011.

Dilshara, M. G. *et al.* (2017) 'Glutamine deprivation sensitizes human breast cancer MDA-MB-231 cells to TRIAL-mediated apoptosis', *Biochemical and Biophysical Research Communications*, 485(2), pp. 440–445. doi: 10.1016/j.bbrc.2017.02.059.

Dixon, S. J. *et al.* (2012) 'Ferroptosis: An Iron-Dependent Form of Nonapoptotic Cell Death', *Cell*, 149(5), pp. 1060–1072. doi: 10.1016/j.cell.2012.03.042.

Dixon, S. J. *et al.* (2014) 'Pharmacological inhibition of cystine–glutamate exchange induces endoplasmic reticulum stress and ferroptosis', *eLife*, 3. doi: 10.7554/eLife.02523.

Dixon, S. J. *et al.* (2015) 'Human Haploid Cell Genetics Reveals Roles for Lipid Metabolism Genes in Nonapoptotic Cell Death', *ACS Chemical Biology*, 10(7), pp. 1604–1609. doi: 10.1021/acschembio.5b00245.

Dixon, S. J. (2017) 'Ferroptosis: bug or feature?', *Immunological Reviews*, 277(1), pp. 150–157. doi: 10.1111/imr.12533.

Dixon, S. J. and Stockwell, B. R. (2014) 'The role of iron and reactive oxygen species in cell death', *Nature Chemical Biology*, 10(1), pp. 9–17. doi: 10.1038/nchembio.1416.

Dmitriev, O. Y. (2011) 'Mechanism of tumor resistance to cisplatin mediated by the copper transporter ATP7BThis paper is one of a selection of papers published in a Special

Issue entitled CSBMCB 53rd Annual Meeting — Membrane Proteins in Health and Disease, and has undergone the', *Biochemistry and Cell Biology*, 89(2), pp. 138–147. doi: 10.1139/O10-150.

Dodson, M., Castro-Portuguez, R. and Zhang, D. D. (2019) 'NRF2 plays a critical role in mitigating lipid peroxidation and ferroptosis', *Redox Biology*, 23, p. 101107. doi: 10.1016/j.redox.2019.101107.

Dojindo (2023) *Mito-FerroGreen Technical Manual*. Available at: https://www.dojindo.com/products/manual/M489e.pdf.

Doll, S., Proneth, B., Tyurina, Yulia Y., *et al.* (2017) 'ACSL4 dictates ferroptosis sensitivity by shaping cellular lipid composition', *Nature Chemical Biology*, 13(1), pp. 91–98. doi: 10.1038/nchembio.2239.

Doll, S., Proneth, B., Tyurina, Yulia Y, *et al.* (2017) 'ACSL4 dictates ferroptosis sensitivity by shaping cellular lipid composition', *Nature Chemical Biology*, 13(1), pp. 91–98. doi: 10.1038/nchembio.2239.

Dolma, S. *et al.* (2003) 'Identification of genotype-selective antitumor agents using synthetic lethal chemical screening in engineered human tumor cells', *Cancer Cell*, 3(3), pp. 285–296. doi: 10.1016/S1535-6108(03)00050-3.

Dong, Z. *et al.* (2014) 'Paclitaxel: new uses for an old drug', *Drug Design, Development and Therapy*, p. 279. doi: 10.2147/DDDT.S56801.

Dubey, A. K., Gupta, U. and Jain, S. (2015) 'Breast Cancer Statistics and Prediction Methodology: A Systematic Review and Analysis', *Asian Pacific Journal of Cancer Prevention*, 16(10), pp. 4237–4245. doi: 10.7314/APJCP.2015.16.10.4237.

Duggan, C. *et al.* (2021) 'National health system characteristics, breast cancer stage at diagnosis, and breast cancer mortality: a population-based analysis', *The Lancet Oncology*, 22(11), pp. 1632–1642. doi: 10.1016/S1470-2045(21)00462-9.

Dunn, T. A. *et al.* (1997) 'Comparative cytotoxicity of oxaliplatin and cisplatin in non-seminomatous germ cell cancer cell lines.', *Investigational new drugs*, 15(2), pp. 109–14. doi: 10.1023/a:1005800520747.

EBCTCG (Early Breast Cancer Trialists' Collaborative Group) (2014) 'Effect of radiotherapy after mastectomy and axillary surgery on 10-year recurrence and 20-year breast cancer mortality: meta-analysis of individual patient data for 8135 women in 22 randomised trials', *The Lancet*, 383(9935), pp. 2127–2135. doi: 10.1016/S0140-6736(14)60488-8.

Faget, D. V., Ren, Q. and Stewart, S. A. (2019) 'Unmasking senescence: context-dependent effects of SASP in cancer', *Nature Reviews Cancer*, 19(8), pp. 439–453. doi: 10.1038/s41568-019-0156-2.

Fang, D. and Maldonado, E. N. (2018) 'VDAC Regulation: A Mitochondrial Target to Stop Cell Proliferation', in, pp. 41–69. doi: 10.1016/bs.acr.2018.02.002.

Fang, Y. *et al.* (2017) 'Transcriptome sequencing reveals key pathways and genes associated with cisplatin resistance in lung adenocarcinoma A549 cells', *PLoS ONE*. Edited by A. Ahmad, 12(1), p. e0170609. doi: 10.1371/journal.pone.0170609.

Feng, Y. *et al.* (2018) 'Breast cancer development and progression: Risk factors, cancer stem cells, signaling pathways, genomics, and molecular pathogenesis', *Genes and Diseases*, 5(2), pp. 77–106. doi: 10.1016/j.gendis.2018.05.001.

Feng, Y. *et al.* (2019) 'Liproxstatin-1 protects the mouse myocardium against ischemia/reperfusion injury by decreasing VDAC1 levels and restoring GPX4 levels', *Biochemical and Biophysical Research Communications*, 520(3), pp. 606–611. doi: 10.1016/j.bbrc.2019.10.006.

Fernald, K. and Kurokawa, M. (2013) 'Evading apoptosis in cancer', *Trends in Cell Biology*, 23(12), pp. 620–633. doi: 10.1016/j.tcb.2013.07.006.

Fischbach, C. *et al.* (2007) 'Engineering tumors with 3D scaffolds', *Nature Methods*, 4(10), pp. 855–860. doi: 10.1038/nmeth1085.

Fisher, B. (1971) 'Status of adjuvant therapy. Results of the national surgical adjuvant breast project studies on oophorectomy, postoperative radiation therapy, and chemotherapy.Other comments concerning clinical trials', *Cancer*, 28(6), pp. 1654–1658. doi: 10.1002/1097-0142(197112)28:6<1654::AID-CNCR2820280648>3.0.CO;2-D.

Fisher, B. *et al.* (1975) 'L-Phenylalanine Mustard (L-PAM) in the Management of Primary Breast Cancer', *New England Journal of Medicine*, 292(3), pp. 117–122. doi: 10.1056/NEJM197501162920301.

Flint, Lucy E *et al.* (2020) 'Characterization of an Aggregated Three-Dimensional Cell Culture Model by Multimodal Mass Spectrometry Imaging.', *Analytical chemistry*, 92(18), pp. 12538–12547. doi: 10.1021/acs.analchem.0c02389.

Flint, Lucy E. *et al.* (2020) 'Characterization of an Aggregated Three-Dimensional Cell Culture Model by Multimodal Mass Spectrometry Imaging', *Analytical Chemistry*, 92(18), pp. 12538–12547. doi: 10.1021/acs.analchem.0c02389.

Flint, L. E. *et al.* (2021) 'Comparison of Osteosarcoma Aggregated Tumour Models with Human Tissue by Multimodal Mass Spectrometry Imaging.', *Metabolites*, 11(8). doi: 10.3390/metabo11080506.

Flusberg, D. A. *et al.* (2013) 'Cells surviving fractional killing by TRAIL exhibit transient but sustainable resistance and inflammatory phenotypes', *Molecular Biology of the Cell*. Edited by D. D. Newmeyer, 24(14), pp. 2186–2200. doi: 10.1091/mbc.e12-10-0737.

Formenti, S. C. and Demaria, S. (2009) 'Systemic effects of local radiotherapy', *The*

Lancet Oncology, 10(7), pp. 718–726. doi: 10.1016/S1470-2045(09)70082-8.

Friedrich, J. *et al.* (2009) 'Spheroid-based drug screen: considerations and practical approach', *Nature Protocols*, 4(3), pp. 309–324. doi: 10.1038/nprot.2008.226.

Fu, D. *et al.* (2021) 'Induction of ferroptosis by ATF3 elevation alleviates cisplatin resistance in gastric cancer by restraining Nrf2/Keap1/xCT signaling', *Cellular & Molecular Biology Letters*, 26(1), p. 26. doi: 10.1186/s11658-021-00271-y.

Gadducci, A. *et al.* (2005) 'Polycystic ovary syndrome and gynecological cancers: Is there a link?', *Gynecological Endocrinology*, 20(4), pp. 200–208. doi: 10.1080/09513590400021201.

Gajria, D. and Chandarlapaty, S. (2011) 'HER2-amplified breast cancer: mechanisms of trastuzumab resistance and novel targeted therapies', *Expert Review of Anticancer Therapy*, 11(2), pp. 263–275. doi: 10.1586/era.10.226.

Gao, M. *et al.* (2015) 'Glutaminolysis and Transferrin Regulate Ferroptosis', *Molecular Cell*, 59(2), pp. 298–308. doi: 10.1016/j.molcel.2015.06.011.

Gao, M. *et al.* (2016) 'Ferroptosis is an autophagic cell death process', *Cell Research*, 26(9), pp. 1021–1032. doi: 10.1038/cr.2016.95.

van Geldermalsen, M. *et al.* (2016) 'ASCT2/SLC1A5 controls glutamine uptake and tumour growth in triple-negative basal-like breast cancer.', *Oncogene*, 35(24), pp. 3201–8. doi: 10.1038/onc.2015.381.

Geoffrey M Cooper (2000) *The cell : a molecular approach*. 2 nd, *ASM Press*. 2 nd. Washington, D.C.: Sinauer Associates.

Ghoochani, A. *et al.* (2021) 'Ferroptosis Inducers Are a Novel Therapeutic Approach for Advanced Prostate Cancer', *Cancer Research*, 81(6), pp. 1583–1594. doi: 10.1158/0008-5472.CAN-20-3477.

Glicklis, R. *et al.* (2000) 'Hepatocyte behavior within three-dimensional porous alginate scaffolds', *Biotechnology and Bioengineering*, 67(3), pp. 344–353. doi: 10.1002/(SICI)1097-0290(20000205)67:3<344::AID-BIT11>3.0.CO;2-2.

Go, R. S. and Adjei, A. A. (1999) 'Review of the comparative pharmacology and clinical activity of cisplatin and carboplatin', *Journal of Clinical Oncology*, 17(1), pp. 409–422. doi: 10.1200/jco.1999.17.1.409.

Gonzalez-Angulo, A. M., Morales-Vasquez, F. and Hortobagyi, G. N. (2007) 'Overview of Resistance to Systemic Therapy in Patients with Breast Cancer', in, pp. 1–22. doi: 10.1007/978-0-387-74039-3_1.

Gorgoulis, V. *et al.* (2019) 'Cellular Senescence: Defining a Path Forward', *Cell*, 179(4), pp. 813–827. doi: 10.1016/j.cell.2019.10.005.

Gratas-Delamarche, A. *et al.* (2014) 'Physical inactivity, insulin resistance, and the oxidative-inflammatory loop', *Free Radical Research*, 48(1), pp. 93–108. doi: 10.3109/10715762.2013.847528.

Grivennikov, S. I., Greten, F. R. and Karin, M. (2010) 'Immunity, Inflammation, and Cancer', *Cell*, 140(6), pp. 883–899. doi: 10.1016/j.cell.2010.01.025.

Gudipaty, S. A. *et al.* (2018) 'Unconventional Ways to Live and Die: Cell Death and Survival in Development, Homeostasis, and Disease', *Annual Review of Cell and Developmental Biology*, 34(1), pp. 311–332. doi: 10.1146/annurev-cellbio-100616-060748.

Guo, J. *et al.* (2018) 'Ferroptosis: A Novel Anti-tumor Action for Cisplatin', *Cancer Research and Treatment*, 50(2), pp. 445–460. doi: 10.4143/crt.2016.572.

Gupta, P. *et al.* (2022) 'A Systematic Comparative Assessment of the Response of Ovarian Cancer Cells to the Chemotherapeutic Cisplatin in 3D Models of Various Structural and Biochemical Configurations—Does One Model Type Fit All?', *Cancers*, 14(5), p. 1274. doi: 10.3390/cancers14051274.

Gupta, S. C. *et al.* (2012) 'Upsides and Downsides of Reactive Oxygen Species for Cancer: The Roles of Reactive Oxygen Species in Tumorigenesis, Prevention, and Therapy', *Antioxidants & Redox Signaling*, 16(11), pp. 1295–1322. doi: 10.1089/ars.2011.4414.

Habib, E. *et al.* (2015) 'Expression of xCT and activity of system xc– are regulated by NRF2 in human breast cancer cells in response to oxidative stress', *Redox Biology*, 5, pp. 33–42. doi: 10.1016/j.redox.2015.03.003.

Hamadneh, L. *et al.* (2021) 'Doxorubicin–paclitaxel sequential treatment: insights of DNA methylation and gene expression changes of luminal A and triple negative breast cancer cell lines', *Molecular and Cellular Biochemistry*, 476(10), pp. 3647–3654. doi: 10.1007/s11010-021-04191-5.

Hamanishi, J. *et al.* (2016) 'PD-1/PD-L1 blockade in cancer treatment: perspectives and issues', *International Journal of Clinical Oncology*, 21(3), pp. 462–473. doi: 10.1007/s10147-016-0959-z.

Hamburger, A. and Salmon, S. (1977) 'Primary bioassay of human tumor stem cells', *Science*, 197(4302), pp. 461–463. doi: 10.1126/science.560061.

Hanahan, D. (2022) 'Hallmarks of Cancer: New Dimensions', *Cancer Discovery*, 12(1), pp. 31–46. doi: 10.1158/2159-8290.CD-21-1059.

Hanahan, D. and Weinberg, R. A. (2000) 'The Hallmarks of Cancer', *Cell*, 100(1), pp. 57–70. doi: 10.1016/S0092-8674(00)81683-9.

Hanahan, D. and Weinberg, R. A. (2011) 'Hallmarks of Cancer: The Next Generation', *Cell*, 144(5), pp. 646–674. doi: 10.1016/j.cell.2011.02.013.

Hannon, G. J. and Beach, D. (1994) 'pl5INK4B is a potentia| effector of TGF-β-induced cell cycle arrest', *Nature*, 371(6494), pp. 257–261. doi: 10.1038/371257a0.

Hartmann, S. *et al.* (2018) 'MAGE-A11 expression contributes to cisplatin resistance in head and neck cancer', *Clinical Oral Investigations*, 22(3), pp. 1477–1486. doi: 10.1007/s00784-017-2242-8.

Hassannia, B., Vandenabeele, P. and Vanden Berghe, T. (2019) 'Targeting Ferroptosis to Iron Out Cancer', *Cancer Cell*, 35(6), pp. 830–849. doi: 10.1016/j.ccell.2019.04.002.

Hassanpour, S. H. and Dehghani, M. (2017) 'Review of cancer from perspective of molecular', *Journal of Cancer Research and Practice*, 4(4), pp. 127–129. doi: 10.1016/j.jcrpr.2017.07.001.

He, S. and Sharpless, N. E. (2017) 'Senescence in Health and Disease', *Cell*, 169(6), pp. 1000–1011. doi: 10.1016/j.cell.2017.05.015.

Holen, I. *et al.* (2002) 'Osteoprotegerin (OPG) is a survival factor for human prostate cancer cells.', *Cancer research*, 62(6), pp. 1619–23. Available at: http://www.ncbi.nlm.nih.gov/pubmed/11912131.

Horman, S. R. (2016) 'Complex High-Content Phenotypic Screening', in *Special Topics in Drug Discovery*. InTech. doi: 10.5772/65387.

Huang, C. *et al.* (2013) 'Shikonin Kills Glioma Cells through Necroptosis Mediated by RIP-1', *PLoS ONE*, 8(6), pp. 1–10. doi: 10.1371/journal.pone.0066326.

Huang, R.-X. and Zhou, P.-K. (2020) 'DNA damage response signaling pathways and targets for radiotherapy sensitization in cancer', *Signal Transduction and Targeted Therapy*, 5(1), p. 60. doi: 10.1038/s41392-020-0150-x.

IMAMURA, Y. *et al.* (2015) 'Comparison of 2D- and 3D-culture models as drug-testing platforms in breast cancer', *Oncology Reports*, 33(4), pp. 1837–1843. doi: 10.3892/or.2015.3767.

Irigaray, P. *et al.* (2007) 'Lifestyle-related factors and environmental agents causing cancer: An overview', *Biomedicine & Pharmacotherapy*, 61(10), pp. 640–658. doi: 10.1016/j.biopha.2007.10.006.

Ivascu, A. and Kubbies, M. (2006) 'Rapid Generation of Single-Tumor Spheroids for High-Throughput Cell Function and Toxicity Analysis', *SLAS Discovery*, 11(8), pp. 922–932. doi: 10.1177/1087057106292763.

Jaffray, D. A. (2012) 'Image-guided radiotherapy: from current concept to future perspectives', *Nature Reviews Clinical Oncology*, 9(12), pp. 688–699. doi: 10.1038/nrclinonc.2012.194.

Jemal, A. *et al.* (2011) 'Global cancer statistics', *CA: A Cancer Journal for Clinicians*, 61(2),

pp. 69–90. doi: 10.3322/caac.20107.

Ji, Q. *et al.* (2022) 'ACSL4 is essential for radiation-induced intestinal injury by initiating ferroptosis', *Cell Death Discovery*, 8(1), p. 332. doi: 10.1038/s41420-022-01127-w.

Jiang, L. *et al.* (2015) 'Ferroptosis as a p53-mediated activity during tumour suppression', *Nature*, 520(7545), pp. 57–62. doi: 10.1038/nature14344.

Jones, A. (2003) 'Combining trastuzumab (Herceptin®) with hormonal therapy in breast cancer: what can be expected and why?', *Annals of Oncology*, 14(12), pp. 1697–1704. doi: 10.1093/annonc/mdg483.

Jones, S. E. (2008) 'Metastatic Breast Cancer: The Treatment Challenge', *Clinical Breast Cancer*, 8(3), pp. 224–233. doi: 10.3816/CBC.2008.n.025.

Jordan, M. A. *et al.* (1993) 'Mechanism of mitotic block and inhibition of cell proliferation by taxol at low concentrations.', *Proceedings of the National Academy of Sciences*, 90(20), pp. 9552–9556. doi: 10.1073/pnas.90.20.9552.

Jordan, M. A. and Wilson, L. (1998) 'Microtubules and actin filaments: dynamic targets for cancer chemotherapy', *Current Opinion in Cell Biology*, 10(1), pp. 123–130. doi: 10.1016/S0955-0674(98)80095-1.

Jose, M. J. G. R. J. T. D. X. P. C. R. K. G. S. R. K. D. P. I. G. R. B. (1998) 'Long-term expression of differentiated functions in hepatocytes cultured in three-dimensional collagen matrix', *Journal of Cellular Physiology*, 177(4), pp. 553–562. doi: 10.1002/(SICI)1097-4652(199812)177:4<553::AID-JCP6>3.0.CO;2-F.

Joshi, S. C. *et al.* (2007) 'Role of radiotherapy in early breast cancer: an overview.', *International journal of health sciences*, 1(2), pp. 259–64. Available at: http://www.ncbi.nlm.nih.gov/pubmed/21475437.

Justice, B. A., Badr, N. A. and Felder, R. A. (2009) '3D cell culture opens new dimensions in cell-based assays', *Drug Discovery Today*, 14(1–2), pp. 102–107. doi: 10.1016/j.drudis.2008.11.006.

Kalkavan, H. and Green, D. R. (2018) 'MOMP, cell suicide as a BCL-2 family business', *Cell Death & Differentiation*, 25(1), pp. 46–55. doi: 10.1038/cdd.2017.179.

Kamińska, M. *et al.* (2015) 'Breast cancer risk factors', *Menopausal Review*, 3, pp. 196–202. doi: 10.5114/pm.2015.54346.

Kapałczyńska, M. *et al.* (2016) '2D and 3D cell cultures – a comparison of different types of cancer cell cultures', *Archives of Medical Science*. doi: 10.5114/aoms.2016.63743.

Karachaliou, N. *et al.* (2012) 'A multicenter phase II trial of docetaxel and capecitabine as salvage treatment in anthracycline- and taxane-pretreated patients with metastatic breast cancer', *Cancer Chemotherapy and Pharmacology*, 70(1), pp. 169–176. doi:

10.1007/s00280-012-1901-3.

Karnoub, A. E. and Weinberg, R. A. (2007) 'Chemokine Networks and Breast Cancer Metastasis', *Breast Disease*. Edited by L. Wakefield and K. Hunter, 26(1), pp. 75–85. doi: 10.3233/BD-2007-26107.

Kartalou, M. and Essigmann, J. M. (2001) 'Mechanisms of resistance to cisplatin', *Mutation Research/Fundamental and Molecular Mechanisms of Mutagenesis*, 478(1–2), pp. 23–43. doi: 10.1016/S0027-5107(01)00141-5.

Katano, K. *et al.* (2002) 'Acquisition of resistance to cisplatin is accompanied by changes in the cellular pharmacology of copper.', *Cancer research*, 62(22), pp. 6559–65. Available at: http://www.ncbi.nlm.nih.gov/pubmed/12438251.

Katayama, Y. *et al.* (2019) 'Tumor Neovascularization and Developments in Therapeutics', *Cancers*, 11(3), p. 316. doi: 10.3390/cancers11030316.

Kelm, J. M. *et al.* (2003) 'Method for generation of homogeneous multicellular tumor spheroids applicable to a wide variety of cell types', *Biotechnology and Bioengineering*, 83(2), pp. 173–180. doi: 10.1002/bit.10655.

Kemp, C. J. (2015) 'Animal Models of Chemical Carcinogenesis: Driving Breakthroughs in Cancer Research for 100 Years', *Cold Spring Harbor Protocols*, 2015(10), p. pdb.top069906. doi: 10.1101/pdb.top069906.

Kennedy, L. *et al.* (2020) 'Role of Glutathione in Cancer: From Mechanisms to Therapies.', *Biomolecules*, 10(10). doi: 10.3390/biom10101429.

Kim *et al.* (2019) 'Cellular Stress Responses in Radiotherapy', *Cells*, 8(9), p. 1105. doi: 10.3390/cells8091105.

Kim, J. W. *et al.* (2023) 'FSP1 confers ferroptosis resistance in KEAP1 mutant non-small cell lung carcinoma in NRF2-dependent and -independent manner', *Cell Death & Disease*, 14(8), p. 567. doi: 10.1038/s41419-023-06070-x.

Kipp, A. P. *et al.* (2017) 'Time- and cell-resolved dynamics of redox-sensitive Nrf2, HIF and NF-κB activities in 3D spheroids enriched for cancer stem cells', *Redox Biology*, 12, pp. 403–409. doi: 10.1016/j.redox.2017.03.013.

Köberle, B. *et al.* (2010) 'Cisplatin resistance: Preclinical findings and clinical implications', *Biochimica et Biophysica Acta - Reviews on Cancer*, 1806(2), pp. 172–182. doi: 10.1016/j.bbcan.2010.07.004.

Kong, P. *et al.* (2023) 'Ferroptosis triggered by STAT1- IRF1-ACSL4 pathway was involved in radiation-induced intestinal injury', *Redox Biology*, 66, p. 102857. doi: 10.1016/j.redox.2023.102857.

Koppula, P. *et al.* (2018) 'Amino acid transporter SLC7A11/xCT at the crossroads of

regulating redox homeostasis and nutrient dependency of cancer', *Cancer Communications*, 38(1), p. 12. doi: 10.1186/s40880-018-0288-x.

Koppula, P., Zhuang, L. and Gan, B. (2021) 'Cystine transporter SLC7A11/xCT in cancer: ferroptosis, nutrient dependency, and cancer therapy', *Protein & Cell*, 12(8), pp. 599–620. doi: 10.1007/s13238-020-00789-5.

Kose, T. *et al.* (2019) 'Curcumin and (−)- Epigallocatechin-3-Gallate Protect Murine MIN6 Pancreatic Beta-Cells Against Iron Toxicity and Erastin-Induced Ferroptosis', *Pharmaceuticals*, 12(1), p. 26. doi: 10.3390/ph12010026.

Kunitski, M. *et al.* (2019) 'Double-slit photoelectron interference in strong-field ionization of the neon dimer', *Nature Communications*, 10(1), p. 1. doi: 10.1038/s41467-018-07882-8.

Kwon, Y.-S. *et al.* (2021) 'Acyl-CoA synthetase-4 mediates radioresistance of breast cancer cells by regulating FOXM1', *Biochemical Pharmacology*, 192, p. 114718. doi: 10.1016/j.bcp.2021.114718.

Kyndi, M. *et al.* (2008) 'Estrogen Receptor, Progesterone Receptor, HER-2, and Response to Postmastectomy Radiotherapy in High-Risk Breast Cancer: The Danish Breast Cancer Cooperative Group', *Journal of Clinical Oncology*, 26(9), pp. 1419–1426. doi: 10.1200/JCO.2007.14.5565.

Lang, X. *et al.* (2019) 'Radiotherapy and Immunotherapy Promote Tumoral Lipid Oxidation and Ferroptosis via Synergistic Repression of SLC7A11', *Cancer Discovery*, 9(12), pp. 1673–1685. doi: 10.1158/2159-8290.CD-19-0338.

Lawen, A. (2003) 'Apoptosis?an introduction', *BioEssays*, 25(9), pp. 888–896. doi: 10.1002/bies.10329.

LAWRENCE, C. L. (2012) *The impact of chemotherapy for breast cancer on managing daily tasks: a longitudinal study of cognitive, psychosocial and safety outcomes in the home and workplace.* Loughborough University. doi: http://creativecommons.org/licenses/by-nc-nd/2.5/.

Lee, S. and Schmitt, C. A. (2019) 'The dynamic nature of senescence in cancer', *Nature Cell Biology*, 21(1), pp. 94–101. doi: 10.1038/s41556-018-0249-2.

Lei, G. *et al.* (2020a) 'The role of ferroptosis in ionizing radiation-induced cell death and tumor suppression', *Cell Research*, 30(2), pp. 146–162. doi: 10.1038/s41422-019-0263-3.

Lei, G. *et al.* (2020b) 'The role of ferroptosis in ionizing radiation-induced cell death and tumor suppression', *Cell Research*, 30(2), pp. 146–162. doi: 10.1038/s41422-019-0263-3.

Lei, G., Mao, C., *et al.* (2021) 'Ferroptosis, radiotherapy, and combination therapeutic

strategies', *Protein & Cell*, 12(11), pp. 836–857. doi: 10.1007/s13238-021-00841-y.

Lei, G., Zhang, Y., *et al.* (2021) 'Ferroptosis as a mechanism to mediate p53 function in tumor radiosensitivity', *Oncogene*, 40(20), pp. 3533–3547. doi: 10.1038/s41388-021-01790-w.

Li, J. *et al.* (2020) 'Ferroptosis: past, present and future', *Cell Death and Disease*, 11(2). doi: 10.1038/s41419-020-2298-2.

Li, M. *et al.* (2021) 'RSL3 enhances the antitumor effect of cisplatin on prostate cancer cells via causing glycolysis dysfunction', *Biochemical Pharmacology*, 192, p. 114741. doi: 10.1016/j.bcp.2021.114741.

Li, Q. *et al.* (2011) '3D Models of Epithelial-Mesenchymal Transition in Breast Cancer Metastasis: High-Throughput Screening Assay Development, Validation, and Pilot Screen', *SLAS Discovery*, 16(2), pp. 141–154. doi: 10.1177/1087057110392995.

LI, Q. *et al.* (2016) 'Downregulation of microRNA-196a enhances the sensitivity of non-small cell lung cancer cells to cisplatin treatment', *International Journal of Molecular Medicine*, 37(4), pp. 1067–1074. doi: 10.3892/ijmm.2016.2513.

Li, X. *et al.* (2019) 'Ferroptosis inhibitor alleviates Radiation-induced lung fibrosis (RILF) via down-regulation of TGF-β1', *Journal of Inflammation*, 16(1), p. 11. doi: 10.1186/s12950-019-0216-0.

Li, X. *et al.* (2020) 'Clinical development and potential of photothermal and photodynamic therapies for cancer', *Nature Reviews Clinical Oncology*, 17(11), pp. 657–674. doi: 10.1038/s41571-020-0410-2.

Li, X., Zhuang, X. and Qiao, T. (2019) 'Role of ferroptosis in the process of acute radiation-induced lung injury in mice', *Biochemical and Biophysical Research Communications*, 519(2), pp. 240–245. doi: 10.1016/j.bbrc.2019.08.165.

Li, Y. *et al.* (2019) 'Erastin/sorafenib induces cisplatin-resistant non-small cell lung cancer cell ferroptosis through inhibition of the Nrf2/xCT pathway', *Oncology Letters*. doi: 10.3892/ol.2019.11066.

Li, Y., Qian, L. and Yuan, J. (2017) 'Small molecule probes for cellular death machines', *Current Opinion in Chemical Biology*, 39, pp. 74–82. doi: 10.1016/j.cbpa.2017.05.007.

Liang, C. *et al.* (2019) 'Recent Progress in Ferroptosis Inducers for Cancer Therapy', *Advanced Materials*, 31(51), p. 1904197. doi: 10.1002/adma.201904197.

Lin, R.-Z. and Chang, H.-Y. (2008) 'Recent advances in three-dimensional multicellular spheroid culture for biomedical research', *Biotechnology Journal*, 3(9–10), pp. 1172–1184. doi: 10.1002/biot.200700228.

Lin, W. *et al.* (2022) 'Metabolic heterogeneity protects metastatic mucosal melanomas

cells from ferroptosis', *International Journal of Molecular Medicine*, 50(4), p. 124. doi: 10.3892/ijmm.2022.5180.

Liu, C. *et al.* (2015) 'Potential effect of matrix stiffness on the enrichment of tumor initiating cells under three-dimensional culture conditions', *Experimental Cell Research*, 330(1), pp. 123–134. doi: 10.1016/j.yexcr.2014.07.036.

Liu, L. *et al.* (2022) 'ESR1 inhibits ionizing radiation-induced ferroptosis in breast cancer cells via the NEDD4L/CD71 pathway', *Archives of Biochemistry and Biophysics*, 725, p. 109299. doi: 10.1016/j.abb.2022.109299.

Liu, P. *et al.* (2016) 'Deferoxamine-induced increase in the intracellular iron levels in highly aggressive breast cancer cells leads to increased cell migration by enhancing TNF-α-dependent NF-κB signaling and TGF-β signaling', *Journal of Inorganic Biochemistry*, 160, pp. 40–48. doi: 10.1016/j.jinorgbio.2016.04.014.

Liu, Q. and Wang, K. (2019) 'The induction of ferroptosis by impairing STAT3/Nrf2/GPx4 signaling enhances the sensitivity of osteosarcoma cells to cisplatin', *Cell Biology International*, 43(11), pp. 1245–1256. doi: 10.1002/cbin.11121.

Liu, R. *et al.* (2022) 'Molecular pathways associated with oxidative stress and their potential applications in radiotherapy (Review)', *International Journal of Molecular Medicine*, 49(5), p. 65. doi: 10.3892/ijmm.2022.5121.

Liu, S. *et al.* (2023) 'Tubastatin A potently inhibits GPX4 activity to potentiate cancer radiotherapy through boosting ferroptosis', *Redox Biology*, 62, p. 102677. doi: 10.1016/j.redox.2023.102677.

Liu, X. *et al.* (2023) 'Targeting NRF2 uncovered an intrinsic susceptibility of acute myeloid leukemia cells to ferroptosis', *Experimental Hematology & Oncology*, 12(1), p. 47. doi: 10.1186/s40164-023-00411-4.

Liu, Y. *et al.* (2014) 'Deferoxamine Promotes MDA-MB-231 Cell Migration and Invasion through Increased ROS-Dependent HIF-1a Accumulation', *Cellular Physiology and Biochemistry*, 33(4), pp. 1036–1046. doi: 10.1159/000358674.

Loap, P. *et al.* (2021) 'Combination of Olaparib and Radiation Therapy for Triple Negative Breast Cancer: Preliminary Results of the RADIOPARP Phase 1 Trial', *International Journal of Radiation Oncology*Biology*Physics*, 109(2), pp. 436–440. doi: 10.1016/j.ijrobp.2020.09.032.

Long, B. H. and Fairchild, C. R. (1994) 'Paclitaxel inhibits progression of mitotic cells to G1 phase by interference with spindle formation without affecting other microtubule functions during anaphase and telephase.', *Cancer research*, 54(16), pp. 4355–61. Available at: http://www.ncbi.nlm.nih.gov/pubmed/7913875.

Lu, B. *et al.* (2018) 'The Role of Ferroptosis in Cancer Development and Treatment Response', *Frontiers in Pharmacology*, 8. doi: 10.3389/fphar.2017.00992.

Lu, Z. *et al.* (2023) 'The potential of ferroptosis combined with radiotherapy in cancer treatment', *Frontiers in Oncology*, 13. doi: 10.3389/fonc.2023.1085581.

Luke, J. J. *et al.* (2018) 'Safety and Clinical Activity of Pembrolizumab and Multisite Stereotactic Body Radiotherapy in Patients With Advanced Solid Tumors', *Journal of Clinical Oncology*, 36(16), pp. 1611–1618. doi: 10.1200/JCO.2017.76.2229.

Lyons, K. E. *et al.* (2020) 'Breast Milk, a Source of Beneficial Microbes and Associated Benefits for Infant Health', *Nutrients*, 12(4), p. 1039. doi: 10.3390/nu12041039.

Mai, T. T. *et al.* (2017) 'Salinomycin kills cancer stem cells by sequestering iron in lysosomes', *Nature Chemistry*, 9(10), pp. 1025–1033. doi: 10.1038/nchem.2778.

Mansouri, A. *et al.* (2022) 'Antioxidant Effects of Statins by Modulating Nrf2 and Nrf2/HO-1 Signaling in Different Diseases', *Journal of Clinical Medicine*, 11(5), p. 1313. doi: 10.3390/jcm11051313.

Manual, T. (2020) 'Mito-FerroGreen', pp. 5–7.

Maria, R. M. *et al.* (2015) 'Characterization of metabolic profile of intact non-tumor and tumor breast cells by high-resolution magic angle spinning nuclear magnetic resonance spectroscopy', *Analytical Biochemistry*, 488, pp. 14–18. doi: 10.1016/j.ab.2015.07.015.

Marinello, J., Delcuratolo, M. and Capranico, G. (2018) 'Anthracyclines as Topoisomerase II Poisons: From Early Studies to New Perspectives.', *International journal of molecular sciences*, 19(11). doi: 10.3390/ijms19113480.

Masrour-Roudsari, J. and Ebrahimpour, S. (2017) 'Causal role of infectious agents in cancer: An overview.', *Caspian journal of internal medicine*, 8(3), pp. 153–158. doi: 10.22088/cjim.8.3.153.

Matos, C. F. De *et al.* (2023) 'gold Nanoparticle-mediated enhancement of radiation responses in 2d and 3d cell culture', in *CRUK-ARR Radiation Research Conference, Glasgow.*

Maughan, Karen L, Lutterbie, M. A. and Ham, P. S. (2010) 'Treatment of breast cancer.', *American family physician*, 81(11), pp. 1339–46. Available at: http://www.ncbi.nlm.nih.gov/pubmed/20521754.

Maughan, Karen L., Lutterbie, M. A. and Ham, P. S. (2010) 'Treatment of breast cancer', *American Family Physician*, 81(11), pp. 1339–1346. doi: 10.1056/nejm199810013391407.

McPherson, K. (2000) 'ABC of breast diseases: Breast cancer---epidemiology, risk factors, and genetics', *BMJ*, 321(7261), pp. 624–628. doi: 10.1136/bmj.321.7261.624.

Mei, H. *et al.* (2020a) 'Inhibition of ferroptosis protects House Ear Institute-Organ of Corti 1 cells and cochlear hair cells from cisplatin-induced ototoxicity.', *Journal of cellular*

and molecular medicine, 24(20), pp. 12065–12081. doi: 10.1111/jcmm.15839.

Mei, H. *et al.* (2020b) 'Inhibition of ferroptosis protects House Ear Institute-Organ of Corti 1 cells and cochlear hair cells from cisplatin-induced ototoxicity', *Journal of Cellular and Molecular Medicine*, 24(20), pp. 12065–12081. doi: 10.1111/jcmm.15839.

Micha, J. P. *et al.* (2022) 'Hormone Therapy and Risk of Breast Cancer: Where Are We Now?', *Journal of Menopausal Medicine*, 28(2), p. 47. doi: 10.6118/jmm.21035.

Mike Richards, Ruth Thorlby, R. F. and Catherine Turton (2018) *Unfinished business: An assessment of the national approach to improving cancer services in England 1995–2015*.

Muguruma, M. *et al.* (2020) 'Differences in drug sensitivity between two-dimensional and three-dimensional culture systems in triple-negative breast cancer cell lines', *Biochemical and Biophysical Research Communications*, 533(3), pp. 268–274. doi: 10.1016/j.bbrc.2020.08.075.

Nagane, M. *et al.* (2018) 'Sulfasalazine, an inhibitor of the cystine-glutamate antiporter, reduces DNA damage repair and enhances radiosensitivity in murine B16F10 melanoma', *PLOS ONE*. Edited by A. Ahmad, 13(4), p. e0195151. doi: 10.1371/journal.pone.0195151.

Napoletano, F. *et al.* (2019) 'Intersections between Regulated Cell Death and Autophagy', *Trends in Cell Biology*, 29(4), pp. 323–338. doi: 10.1016/j.tcb.2018.12.007.

Negrini, S., Gorgoulis, V. G. and Halazonetis, T. D. (2010) 'Genomic instability — an evolving hallmark of cancer', *Nature Reviews Molecular Cell Biology*, 11(3), pp. 220–228. doi: 10.1038/nrm2858.

Neville-Webbe, H. L. *et al.* (2004) 'Osteoprotegerin (OPG) Produced by Bone Marrow Stromal Cells Protects Breast Cancer Cells from TRAIL-Induced Apoptosis', *Breast Cancer Research and Treatment*, 86(3), pp. 271–282. doi: 10.1023/B:BREA.0000036900.48763.b3.

Nguyen, A. T., Shiao, S. L. and McArthur, H. L. (2021) 'Advances in Combining Radiation and Immunotherapy in Breast Cancer', *Clinical Breast Cancer*, 21(2), pp. 143–152. doi: 10.1016/j.clbc.2021.03.007.

Niero, E. L. *et al.* (2014) 'The multiple facets of drug resistance: one history, different approaches', *Journal of Experimental & Clinical Cancer Research*, 33(1), p. 37. doi: 10.1186/1756-9966-33-37.

Nikounezhad, N., Nakhjavani, M. and Shirazi, F. H. (2017) 'Cellular glutathione level does not predict ovarian cancer cells' resistance after initial or repeated exposure to cisplatin.', *Journal of experimental therapeutics & oncology*, 12(1), pp. 1–7. Available at: http://www.ncbi.nlm.nih.gov/pubmed/28472558.

No, J. H., Kim, Y.-B. and Song, Y. S. (2014) 'Targeting Nrf2 Signaling to Combat Chemoresistance', *Journal of Cancer Prevention*, 19(2), pp. 111–117. doi: 10.15430/JCP.2014.19.2.111.

Nowacka, M. *et al.* (2021) 'Drug resistance evaluation in novel 3D in vitro model', *Biomedicine & Pharmacotherapy*, 138, p. 111536. doi: 10.1016/j.biopha.2021.111536.

Ogston, K. N. *et al.* (2003) 'A new histological grading system to assess response of breast cancers to primary chemotherapy: prognostic significance and survival', *The Breast*, 12(5), pp. 320–327. doi: 10.1016/S0960-9776(03)00106-1.

Okada, K. *et al.* (2005) 'Expression of hypoxia-inducible factor (HIF-1alpha), VEGF-C and VEGF-D in non-invasive and invasive breast ductal carcinomas.', *Anticancer research*, 25(4), pp. 3003–9. Available at: http://www.ncbi.nlm.nih.gov/pubmed/16080559.

Olynik, B. M. and Rastegar, M. (2012) 'The Genetic and Epigenetic Journey of Embryonic Stem Cells into Mature Neural Cells', *Frontiers in Genetics*, 3. doi: 10.3389/fgene.2012.00081.

Ono, K. *et al.* (2022a) 'Reproduction of the Antitumor Effect of Cisplatin and Cetuximab Using a Three-dimensional Spheroid Model in Oral Cancer.', *International journal of medical sciences*, 19(8), pp. 1320–1333. doi: 10.7150/ijms.74109.

Ono, K. *et al.* (2022b) 'Reproduction of the Antitumor Effect of Cisplatin and Cetuximab Using a Three-dimensional Spheroid Model in Oral Cancer', *International Journal of Medical Sciences*, 19(8), pp. 1320–1333. doi: 10.7150/ijms.74109.

Osborne, G., Rudel, R. and Schwarzman, M. (2015) 'Evaluating chemical effects on mammary gland development: A critical need in disease prevention', *Reproductive Toxicology*, 54, pp. 148–155. doi: 10.1016/j.reprotox.2014.07.077.

Overgaard, M. *et al.* (1987) 'The value of the NSD formula in equation of acute and late radiation complications in normal tissue following 2 and 5 fractions per week in breast cancer patients treated with postmastectomy irradiation', *Radiotherapy and Oncology*, 9(1), pp. 1–11. doi: 10.1016/S0167-8140(87)80213-X.

Owada, S. *et al.* (2021) 'Evaluation of Erastin as a Therapeutic Agent Under Hypoxic Conditions in Pancreatic Cancer Cells', *Anticancer Research*, 41(12), pp. 6051–6059. doi: 10.21873/anticanres.15424.

Ozoren, N. *et al.* (2000) 'The caspase 9 inhibitor Z-LEHD-FMK protects human liver cells while permitting death of cancer cells exposed to tumor necrosis factor-related apoptosis-inducing ligand.', *Cancer research*, 60(22), pp. 6259–65. Available at: http://www.ncbi.nlm.nih.gov/pubmed/11103780.

Palubeckaite, I. (2018) *Analysis of three dimensional cell cultures using mass spectrometry imaging*. Sheffield Hallam University. doi: 10.7190/shu-thesis-00179.

Palubeckaitė, I. *et al.* (2020) 'Mass spectrometry imaging of endogenous metabolites in response to doxorubicin in a novel 3D osteosarcoma cell culture model', *Journal of Mass Spectrometry*, 55(4), p. e4461. doi: 10.1002/jms.4461.

Panzilius, E. *et al.* (2019) 'Cell density-dependent ferroptosis in breast cancer is induced by accumulation of polyunsaturated fatty acid-enriched triacylglycerides', *bioRxiv*, p. 417949. Available at: https://doi.org/10.1101/417949%0Ahttps://www.biorxiv.org/content/10.1101/417949 v2%0Ahttps://www.biorxiv.org/content/10.1101/417949v2.abstract.

Parise, C. A. *et al.* (2009) 'Breast Cancer Subtypes as Defined by the Estrogen Receptor (ER), Progesterone Receptor (PR), and the Human Epidermal Growth Factor Receptor 2 (HER2) among Women with Invasive Breast Cancer in California, 1999-2004', *The Breast Journal*, 15(6), pp. 593–602. doi: 10.1111/j.1524-4741.2009.00822.x.

Park, S. Y. *et al.* (2023) 'Irreversible HER2 inhibitors overcome resistance to the RSL3 ferroptosis inducer in non-HER2 amplified luminal breast cancer', *Cell Death & Disease*, 14(8), p. 532. doi: 10.1038/s41419-023-06042-1.

Parness, J. and Horwitz, S. (1981) 'Taxol binds to polymerized tubulin in vitro', *Journal of Cell Biology*, 91(2), pp. 479–487. doi: 10.1083/jcb.91.2.479.

Patel, A. (2020) 'Benign vs Malignant Tumors', *JAMA Oncology*, 6(9), p. 1488. doi: 10.1001/jamaoncol.2020.2592.

Pathania, S. *et al.* (2018) 'Drug metabolizing enzymes and their inhibitors' role in cancer resistance', *Biomedicine & Pharmacotherapy*, 105, pp. 53–65. doi: 10.1016/j.biopha.2018.05.117.

Pati, S. *et al.* (2023) 'Obesity and Cancer: A Current Overview of Epidemiology, Pathogenesis, Outcomes, and Management', *Cancers*, 15(2), p. 485. doi: 10.3390/cancers15020485.

Paul, B. T. *et al.* (2017) 'Mitochondria and Iron: current questions', *Expert Review of Hematology*, 10(1), pp. 65–79. doi: 10.1080/17474086.2016.1268047.

Perou, C. M. *et al.* (2000) 'Molecular portraits of human breast tumours', *Nature*, 406(6797), pp. 747–752. doi: 10.1038/35021093.

Polyak, K. (2007) 'Breast cancer: origins and evolution', *Journal of Clinical Investigation*, 117(11), pp. 3155–3163. doi: 10.1172/JCI33295.

Promega*, C. (2011) 'GSH/GSSG-Glo™ Assay: Instructions for use of products V6611 and V6612.', pp. 1–20.

Promega (2002) 'CellTiter-Glo ® Luminescent Cell Viability Assay Cell Viability Assay', pp. 8–10.

Provenzano, E. *et al.* (2015) 'Standardization of pathologic evaluation and reporting of postneoadjuvant specimens in clinical trials of breast cancer: recommendations from an international working group', *Modern Pathology*, 28(9), pp. 1185–1201. doi: 10.1038/modpathol.2015.74.

Pucci, B., Kasten, M. and Giordano, A. (2000) 'Cell Cycle and Apoptosis', *Neoplasia*, 2(4), pp. 291–299. doi: 10.1038/sj.neo.7900101.

Puck, T. T. and Marcus, P. I. (1956) 'ACTION OF X-RAYS ON MAMMALIAN CELLS', *Journal of Experimental Medicine*, 103(5), pp. 653–666. doi: 10.1084/jem.103.5.653.

Qian, B.-Z. and Pollard, J. W. (2010) 'Macrophage Diversity Enhances Tumor Progression and Metastasis', *Cell*, 141(1), pp. 39–51. doi: 10.1016/j.cell.2010.03.014.

Rak, J. *et al.* (1995) 'Oncogenes as inducers of tumor angiogenesis', *Cancer and Metastasis Reviews*, 14(4), pp. 263–277. doi: 10.1007/BF00690598.

Rakha, E. A. *et al.* (2010) 'Breast cancer prognostic classification in the molecular era: the role of histological grade', *Breast Cancer Research*, 12(4), p. 207. doi: 10.1186/bcr2607.

Rao, S. *et al.* (1995) 'Characterization of the Taxol Binding Site on the Microtubule', *Journal of Biological Chemistry*, 270(35), pp. 20235–20238. doi: 10.1074/jbc.270.35.20235.

Reynolds, D. S. *et al.* (2017) 'Breast Cancer Spheroids Reveal a Differential Cancer Stem Cell Response to Chemotherapeutic Treatment.', *Scientific reports*, 7(1), p. 10382. doi: 10.1038/s41598-017-10863-4.

Robbins, P. *et al.* (1995) 'Histological grading of breast carcinomas: A study of interobserver agreement', *Human Pathology*, 26(8), pp. 873–879. doi: 10.1016/0046-8177(95)90010-1.

Roh, J.-L. *et al.* (2017) 'Nrf2 inhibition reverses the resistance of cisplatin-resistant head and neck cancer cells to artesunate-induced ferroptosis', *Redox Biology*, 11, pp. 254–262. doi: 10.1016/j.redox.2016.12.010.

Roos, Wynand P.Roos, W. P. and Kaina, B. (2013) 'DNA damage-induced cell death: From specific DNA lesions to the DNA damage response and apoptosis', Cancer Letters, 332(2), pp. 237–248. doi: 10. 1016/j. canlet. 2012. 01. 007. and Kaina, B. (2013) 'DNA damage-induced cell death: From specific DNA lesions to the DNA damage response and apoptosis', *Cancer Letters*, 332(2), pp. 237–248. doi: 10.1016/j.canlet.2012.01.007.

Roubalová, E. *et al.* (2010) 'The effect of cellular environment and p53 status on the mode of action of the platinum derivative LA-12', *Investigational New Drugs*, 28(4), pp. 445–453. doi: 10.1007/s10637-009-9270-4.

Rowinsky, E. K. and Donehower, R. C. (1995) 'Paclitaxel (Taxol)', *New England Journal of*

Medicine. Edited by A. J. J. Wood, 332(15), pp. 1004–1014. doi: 10.1056/NEJM199504133321507.

Rubinsztein, D. C. *et al.* (2007) 'Potential therapeutic applications of autophagy', *Nature Reviews Drug Discovery*, 6(4), pp. 304–312. doi: 10.1038/nrd2272.

Rutqvist, L. E., Rose, C. and Cavallin-ståhl, E. (2003) 'A Systematic Overview of Radiation Therapy Effects in Breast Cancer', *Acta Oncologica*, 42(5–6), pp. 532–545. doi: 10.1080/02841860310014444.

Ruzza, P. *et al.* (2009) 'Glutathione Transferases as Targets for Cancer Therapy', *Anti-Cancer Agents in Medicinal Chemistry*, 9(7), pp. 763–777. doi: 10.2174/187152009789056895.

S Darby, P McGale, C Correa, C Taylor, R Arriagada, M Clarke, D Cutter, C Davies, M Ewertz, J Godwin, R Gray, L Pierce, T Whelan, Y. W. (2011) 'Effect of radiotherapy after breast-conserving surgery on 10-year recurrence and 15-year breast cancer death: meta-analysis of individual patient data for 10 801 women in 17 randomised trials', *The Lancet*, 378(9804), pp. 1707–1716. doi: 10.1016/S0140-6736(11)61629-2.

Sackett, D. and Fojo, T. (1997) 'Taxanes.', *Cancer chemotherapy and biological response modifiers*, 17, pp. 59–79. Available at: http://www.ncbi.nlm.nih.gov/pubmed/9551209.

Sahebkar, A. *et al.* (2023) 'Ferroptosis, a new pathogenetic mechanism in cardiometabolic diseases and cancer: Is there a role for statin therapy?', *Metabolism*, 146, p. 155659. doi: 10.1016/j.metabol.2023.155659.

Salk, J. J., Fox, E. J. and Loeb, L. A. (2010) 'Mutational Heterogeneity in Human Cancers: Origin and Consequences', *Annual Review of Pathology: Mechanisms of Disease*, 5(1), pp. 51–75. doi: 10.1146/annurev-pathol-121808-102113.

Sang, M. *et al.* (2019) 'Mitochondrial membrane anchored photosensitive nano-device for lipid hydroperoxides burst and inducing ferroptosis to surmount therapy-resistant cancer', *Theranostics*, 9(21), pp. 6209–6223. doi: 10.7150/thno.36283.

Sargazi, Z. *et al.* (2023) 'NFR2/ABC transporter axis in drug resistance of breast cancer cells', *Molecular Biology Reports*, 50(6), pp. 5407–5414. doi: 10.1007/s11033-023-08384-7.

Sarin, N. *et al.* (2018) 'Key Players of Cisplatin Resistance: Towards a Systems Pharmacology Approach', *International Journal of Molecular Sciences*, 19(3), p. 767. doi: 10.3390/ijms19030767.

Sarkar, S. *et al.* (2013) 'Cancer Development, Progression, and Therapy: An Epigenetic Overview', *International Journal of Molecular Sciences*, 14(10), pp. 21087–21113. doi: 10.3390/ijms141021087.

Sato, M. *et al.* (2018) 'The ferroptosis inducer erastin irreversibly inhibits system xc− and

synergizes with cisplatin to increase cisplatin's cytotoxicity in cancer cells', *Scientific Reports*, 8(1), p. 968. doi: 10.1038/s41598-018-19213-4.

Satoh, T., McKercher, S. R. and Lipton, S. A. (2013) 'Nrf2/ARE-mediated antioxidant actions of pro-electrophilic drugs', *Free Radical Biology and Medicine*, 65, pp. 645–657. doi: 10.1016/j.freeradbiomed.2013.07.022.

Scagliotti, G. V. (2005) 'Pemetrexed: a new cytotoxic agent in the development for first-line non-small-cell lung cancer', *Lung Cancer*, 50, pp. S18–S19. doi: 10.1016/S0169-5002(05)81555-7.

SCHIFF, P. B., FANT, J. and HORWITZ, S. B. (1979) 'Promotion of microtubule assembly in vitro by taxol', *Nature*, 277(5698), pp. 665–667. doi: 10.1038/277665a0.

Schnekenburger, M., Karius, T. and Diederich, M. (2014) 'Regulation of epigenetic traits of the glutathione S-transferase P1 gene: from detoxification toward cancer prevention and diagnosis', *Frontiers in Pharmacology*, 5. doi: 10.3389/fphar.2014.00170.

Schwarz, M. *et al.* (2019) 'Crosstalk of Nrf2 with the Trace Elements Selenium, Iron, Zinc, and Copper', *Nutrients*, 11(9), p. 2112. doi: 10.3390/nu11092112.

Segeritz, C.-P. and Vallier, L. (2017) 'Cell Culture', in *Basic Science Methods for Clinical Researchers*. Elsevier, pp. 151–172. doi: 10.1016/B978-0-12-803077-6.00009-6.

Seyfried, T. N. and Huysentruyt, L. C. (2013) 'On the Origin of Cancer Metastasis', *Critical Reviews⬛ in Oncogenesis*, 18(1–2), pp. 43–73. doi: 10.1615/CritRevOncog.v18.i1-2.40.

Shadyro, O. I., Yurkova, I. L. and Kisel, M. A. (2002) 'Radiation-induced peroxidation and fragmentation of lipids in a model membrane', *International Journal of Radiation Biology*, 78(3), pp. 211–217. doi: 10.1080/09553000110104065.

Shafei, A. *et al.* (2017) 'A review on the efficacy and toxicity of different doxorubicin nanoparticles for targeted therapy in metastatic breast cancer', *Biomedicine & Pharmacotherapy*, 95, pp. 1209–1218. doi: 10.1016/j.biopha.2017.09.059.

Sharma, G. N. *et al.* (2010) 'Various types and management of breast cancer: an overview.', *Journal of advanced pharmaceutical technology & research*, 1(2), pp. 109–26. Available at: http://www.ncbi.nlm.nih.gov/pubmed/22247839.

Sharma, P. *et al.* (2019) 'Emerging trends in the novel drug delivery approaches for the treatment of lung cancer', *Chemico-Biological Interactions*, 309, p. 108720. doi: 10.1016/j.cbi.2019.06.033.

Sheibani, N. *et al.* (2000) 'Thrombospondin-1, a Natural Inhibitor of Angiogenesis, Is Present in Vitreous and Aqueous Humor and Is Modulated by Hyperglycemia', *Biochemical and Biophysical Research Communications*, 267(1), pp. 257–261. doi: 10.1006/bbrc.1999.1903.

Sheikh, M. and Fornace, A. (2000) 'Death and decoy receptors and p53-mediated apoptosis', *Leukemia*, 14(8), pp. 1509–1513. doi: 10.1038/sj.leu.2401865.

Shimada, K. *et al.* (2016) 'Global survey of cell death mechanisms reveals metabolic regulation of ferroptosis', *Nature Chemical Biology*, 12(7), pp. 497–503. doi: 10.1038/nchembio.2079.

Shin, D. *et al.* (2018) 'Nrf2 inhibition reverses resistance to GPX4 inhibitor-induced ferroptosis in head and neck cancer', *Free Radical Biology and Medicine*, 129, pp. 454–462. doi: 10.1016/j.freeradbiomed.2018.10.426.

Shoval, H. *et al.* (2017) 'Tumor cells and their crosstalk with endothelial cells in 3D spheroids', *Scientific Reports*, 7(1), p. 10428. doi: 10.1038/s41598-017-10699-y.

Simpson, C. D., Anyiwe, K. and Schimmer, A. D. (2008) 'Anoikis resistance and tumor metastasis', *Cancer Letters*, 272(2), pp. 177–185. doi: 10.1016/j.canlet.2008.05.029.

Singh, A. *et al.* (2016) 'Small Molecule Inhibitor of NRF2 Selectively Intervenes Therapeutic Resistance in KEAP1-Deficient NSCLC Tumors', *ACS Chemical Biology*, 11(11), pp. 3214–3225. doi: 10.1021/acschembio.6b00651.

Singh, B. *et al.* (2020) 'Oxidative stress associated metabolic adaptations regulate radioresistance in human lung cancer cells', *Journal of Photochemistry and Photobiology B: Biology*, 213, p. 112080. doi: 10.1016/j.jphotobiol.2020.112080.

Singhal, R. *et al.* (2021) 'HIF-2α activation potentiates oxidative cell death in colorectal cancers by increasing cellular iron', *Journal of Clinical Investigation*, 131(12). doi: 10.1172/JCI143691.

Sinha, B. K. *et al.* (2023) 'Ferroptosis-Mediated Cell Death Induced by NCX4040, The Non-Steroidal Nitric Oxide Donor, in Human Colorectal Cancer Cells: Implications in Therapy', *Cells*, 12(12), p. 1626. doi: 10.3390/cells12121626.

Skinner, M. K. (2011) 'Role of epigenetics in developmental biology and transgenerational inheritance', *Birth Defects Research Part C: Embryo Today: Reviews*, 93(1), pp. 51–55. doi: 10.1002/bdrc.20199.

Smith, L. *et al.* (2009) 'Proteomic Identification of Putative Biomarkers of Radiotherapy Resistance: A Possible Role for the 26S Proteasome?', *Neoplasia*, 11(11), pp. 1194–1207. doi: 10.1593/neo.09902.

Smoot, B., Wampler, M. and Topp, K. S. (2009) 'Breast Cancer Treatments and Complications: Implications for Rehabilitation', *Rehabilitation Oncology*, 27(3), pp. 16–26. doi: 10.1097/01893697-200927030-00004.

Sopik, V., Sun, P. and Narod, S. A. (2017) 'The prognostic effect of estrogen receptor status differs for younger versus older breast cancer patients', *Breast Cancer Research and Treatment*, 165(2), pp. 391–402. doi: 10.1007/s10549-017-4333-2.

Sørlie, T. *et al.* (2001) 'Gene expression patterns of breast carcinomas distinguish tumor subclasses with clinical implications', *Proceedings of the National Academy of Sciences*, 98(19), pp. 10869–10874. doi: 10.1073/pnas.191367098.

Sørlie, T. *et al.* (2003) 'Repeated observation of breast tumor subtypes in independent gene expression data sets', *Proceedings of the National Academy of Sciences*, 100(14), pp. 8418–8423. doi: 10.1073/pnas.0932692100.

Sotiriou, C. *et al.* (2003) 'Breast cancer classification and prognosis based on gene expression profiles from a population-based study', *Proceedings of the National Academy of Sciences*, 100(18), pp. 10393–10398. doi: 10.1073/pnas.1732912100.

Soule, H. D. *et al.* (1973) 'A Human Cell Line From a Pleural Effusion Derived From a Breast Carcinoma 2', *JNCI: Journal of the National Cancer Institute*, 51(5), pp. 1409–1416. doi: 10.1093/jnci/51.5.1409.

Sourla, A., Doillon, C. and Koutsilieris, M. (1996) 'Three-dimensional type I collagen gel system containing MG-63 osteoblasts-like cells as a model for studying local bone reaction caused by metastatic cancer cells.', *Anticancer research*, 16(5A), pp. 2773–80. Available at: http://www.ncbi.nlm.nih.gov/pubmed/8917385.

Sparano, J. A. *et al.* (2018) 'Adjuvant Chemotherapy Guided by a 21-Gene Expression Assay in Breast Cancer', *New England Journal of Medicine*, 379(2), pp. 111–121. doi: 10.1056/NEJMoa1804710.

Spencer, Sabrina L *et al.* (2009) 'Non-genetic origins of cell-to-cell variability in TRAIL-induced apoptosis.', *Nature*, 459(7245), pp. 428–32. doi: 10.1038/nature08012.

Spencer, Sabrina L. *et al.* (2009) 'Non-genetic origins of cell-to-cell variability in TRAIL-induced apoptosis', *Nature*, 459(7245), pp. 428–432. doi: 10.1038/nature08012.

Spiotto, M., Fu, Y.-X. and Weichselbaum, R. R. (2016) 'The intersection of radiotherapy and immunotherapy: Mechanisms and clinical implications', *Science Immunology*, 1(3). doi: 10.1126/sciimmunol.aag1266.

Srinivas, U. S. *et al.* (2019) 'ROS and the DNA damage response in cancer', *Redox Biology*, 25, p. 101084. doi: 10.1016/j.redox.2018.101084.

Stetler-Stevenson, W. G. (1999) 'Matrix metalloproteinases in angiogenesis: a moving target for therapeutic intervention', *Journal of Clinical Investigation*, 103(9), pp. 1237–1241. doi: 10.1172/JCI6870.

Stockwell, B. R. *et al.* (2017) 'Ferroptosis: A Regulated Cell Death Nexus Linking Metabolism, Redox Biology, and Disease', *Cell*, 171(2), pp. 273–285. doi: 10.1016/j.cell.2017.09.021.

Su, X. *et al.* (2022) 'HIF-α activation by the prolyl hydroxylase inhibitor roxadustat suppresses chemoresistant glioblastoma growth by inducing ferroptosis', *Cell Death &*

Disease, 13(10), p. 861. doi: 10.1038/s41419-022-05304-8.

Sun, Y. *et al.* (2021) 'Fin56-induced ferroptosis is supported by autophagy-mediated GPX4 degradation and functions synergistically with mTOR inhibition to kill bladder cancer cells', *Cell Death & Disease*, 12(11), p. 1028. doi: 10.1038/s41419-021-04306-2.

Sun, Y. and Peng, Z.-L. (2009) 'Programmed cell death and cancer', *Postgraduate Medical Journal*, 85(1001), pp. 134–140. doi: 10.1136/pgmj.2008.072629.

Sung, H. *et al.* (2021) 'Global Cancer Statistics 2020: GLOBOCAN Estimates of Incidence and Mortality Worldwide for 36 Cancers in 185 Countries', *CA: A Cancer Journal for Clinicians*, 71(3), pp. 209–249. doi: 10.3322/caac.21660.

Syu, J.-P., Chi, J.-T. and Kung, H.-N. (2016) 'Nrf2 is the key to chemotherapy resistance in MCF7 breast cancer cells under hypoxia.', *Oncotarget*, 7(12), pp. 14659–72. doi: 10.18632/oncotarget.7406.

T. Sayers, N. C. (2014) 'Triggering death receptors as a means of inducing tumoricidal activity', in *Tumour Immunology and Immunotherapy*. Oxford University Press, p. Chapter 8.

Taddei, M. *et al.* (2012) 'Anoikis: an emerging hallmark in health and diseases', *The Journal of Pathology*, 226(2), pp. 380–393. doi: 10.1002/path.3000.

Takahashi, N. *et al.* (2020) '3D Culture Models with CRISPR Screens Reveal Hyperactive NRF2 as a Prerequisite for Spheroid Formation via Regulation of Proliferation and Ferroptosis', *Molecular Cell*, 80(5), pp. 828-844.e6. doi: 10.1016/j.molcel.2020.10.010.

Tan, X. *et al.* (2022) 'Targeting GSTP1-dependent ferroptosis in lung cancer radiotherapy: Existing evidence and future directions', *Frontiers in Molecular Biosciences*, 9. doi: 10.3389/fmolb.2022.1102158.

Tanenbaum, L. M. *et al.* (2017) 'Ovarian cancer spheroid shrinkage following continuous exposure to cisplatin is a function of spheroid diameter', *Gynecologic Oncology*, 146(1), pp. 161–169. doi: 10.1016/j.ygyno.2017.04.014.

Taufani, I. P. *et al.* (2023) 'Mitochondrial ROS induced by ML385, an Nrf2 inhibitor aggravates the ferroptosis induced by RSL3 in human lung epithelial BEAS-2B cells', *Human & Experimental Toxicology*, 42, p. 096032712211496. doi: 10.1177/09603271221149663.

Teng, M. W. L. *et al.* (2015) 'From mice to humans: developments in cancer immunoediting', *Journal of Clinical Investigation*, 125(9), pp. 3338–3346. doi: 10.1172/JCI80004.

Thomas, E. and Berner, G. (2000) 'Prognostic and predictive implications of HER2 status for breast cancer patients', *European Journal of Oncology Nursing*, 4, pp. 10–17. doi: 10.1054/ejon.2000.0073.

Thomson, C. A. (2012) 'Diet and Breast Cancer', *Nutrition in Clinical Practice*, 27(5), pp. 636–650. doi: 10.1177/0884533612454302.

Thorn, C. F. *et al.* (2011) 'Doxorubicin pathways', *Pharmacogenetics and Genomics*, 21(7), pp. 440–446. doi: 10.1097/FPC.0b013e32833ffb56.

Trujillo-Alonso, V. *et al.* (2019) 'FDA-approved ferumoxytol displays anti-leukaemia efficacy against cells with low ferroportin levels', *Nature Nanotechnology*, 14(6), pp. 616–622. doi: 10.1038/s41565-019-0406-1.

Urrutia, P. J., Mena, N. P. and NúÃ±ez, M. T. (2014) 'The interplay between iron accumulation, mitochondrial dysfunction, and inflammation during the execution step of neurodegenerative disorders', *Frontiers in Pharmacology*, 5. doi: 10.3389/fphar.2014.00038.

Valashedi, M. R. *et al.* (2022) 'CRISPR/Cas9-mediated knockout of Lcn2 in human breast cancer cell line MDA-MB-231 ameliorates erastin-mediated ferroptosis and increases cisplatin vulnerability', *Life Sciences*, 304, p. 120704. doi: 10.1016/j.lfs.2022.120704.

Vandiver, A. R. *et al.* (2015) 'DNA methylation is stable during replication and cell cycle arrest', *Scientific Reports*, 5(1), p. 17911. doi: 10.1038/srep17911.

Veikkola, T. and Alitalo, K. (1999) 'VEGFs, receptors and angiogenesis', *Seminars in Cancer Biology*, 9(3), pp. 211–220. doi: 10.1006/scbi.1998.0091.

Vinh-Hung, V. and Verschraegen, C. (2004) 'Breast-Conserving Surgery With or Without Radiotherapy: Pooled-Analysis for Risks of Ipsilateral Breast Tumor Recurrence and Mortality', *JNCI Journal of the National Cancer Institute*, 96(2), pp. 115–121. doi: 10.1093/jnci/djh013.

Vogel, C. L. *et al.* (2001) 'First-Line Herceptin® Monotherapy in Metastatic Breast Cancer', *Oncology*, 61(Suppl. 2), pp. 37–42. doi: 10.1159/000055400.

Vogg, A. T. J. *et al.* (2018) 'Modulation of glutathione promotes apoptosis in triple-negative breast cancer cells', *The FASEB Journal*, 32(5), pp. 2803–2813. doi: 10.1096/fj.201701157R.

Wang, B., Kohli, J. and Demaria, M. (2020) 'Senescent Cells in Cancer Therapy: Friends or Foes?', *Trends in Cancer*, 6(10), pp. 838–857. doi: 10.1016/j.trecan.2020.05.004.

Wang, C. *et al.* (2023) 'CircRNF10 triggers a positive feedback loop to facilitate progression of glioblastoma via redeploying the ferroptosis defense in GSCs', *Journal of Experimental & Clinical Cancer Research*, 42(1), p. 242. doi: 10.1186/s13046-023-02816-9.

Wang, H. *et al.* (2018) 'Cancer Radiosensitizers', *Trends in Pharmacological Sciences*, 39(1), pp. 24–48. doi: 10.1016/j.tips.2017.11.003.

Wang, H. *et al.* (2019) 'Hypoxic Radioresistance: Can ROS Be the Key to Overcome It?', *Cancers*, 11(1), p. 112. doi: 10.3390/cancers11010112.

Wang, L. *et al.* (2020) 'ATF3 promotes erastin-induced ferroptosis by suppressing system Xc–', *Cell Death & Differentiation*, 27(2), pp. 662–675. doi: 10.1038/s41418-019-0380-z.

Wang, X. *et al.* (2023) 'Ferrostatin-1 mitigates ionizing radiation-induced intestinal injuries by inhibiting apoptosis and ferroptosis: an in vitro and in vivo study', *International Journal of Radiation Biology*, 99(10), pp. 1607–1618. doi: 10.1080/09553002.2023.2194399.

Wang, Y. *et al.* (2011) 'A retrospective study of breast cancer subtypes: the risk of relapse and the relations with treatments', *Breast Cancer Research and Treatment*, 130(2), pp. 489–498. doi: 10.1007/s10549-011-1709-6.

Weaver, B. A. (2014) 'How Taxol/paclitaxel kills cancer cells', *Molecular Biology of the Cell*. Edited by W. Bement, 25(18), pp. 2677–2681. doi: 10.1091/mbc.e14-04-0916.

Weinberg, R. A. (2013) *The Biology of Cancer*. W.W. Norton & Company. doi: 10.1201/9780429258794.

White-Gilbertson, S., Rubinchik, S. and Voelkel-Johnson, C. (2008) 'Transformation, translation and TRAIL: An unexpected intersection', *Cytokine & Growth Factor Reviews*, 19(2), pp. 167–172. doi: 10.1016/j.cytogfr.2008.01.007.

Whitnall, M. *et al.* (2006) 'A class of iron chelators with a wide spectrum of potent antitumor activity that overcomes resistance to chemotherapeutics', *Proceedings of the National Academy of Sciences*, 103(40), pp. 14901–14906. doi: 10.1073/pnas.0604979103.

Wu, M. *et al.* (2022) 'Cancer stem cell regulated phenotypic plasticity protects metastasized cancer cells from ferroptosis', *Nature Communications*, 13(1), p. 1371. doi: 10.1038/s41467-022-29018-9.

Wu, Y. *et al.* (2020) 'ACSL4 dictates ferroptosis sensitivity by shaping cellular lipid composition', *Frontiers in Oncology*, 10(September). doi: 10.3389/fonc.2020.571127.

Xie, L.-W. *et al.* (2020) 'Green tea derivative (−)-epigallocatechin-3-gallate (EGCG) confers protection against ionizing radiation-induced intestinal epithelial cell death both in vitro and in vivo', *Free Radical Biology and Medicine*, 161, pp. 175–186. doi: 10.1016/j.freeradbiomed.2020.10.012.

Xie, L. *et al.* (2011) 'Solute carrier protein family may involve in radiation-induced radioresistance of non-small cell lung cancer', *Journal of Cancer Research and Clinical Oncology*, 137(12), pp. 1739–1747. doi: 10.1007/s00432-011-1050-9.

Xu, T. *et al.* (2019) 'Molecular mechanisms of ferroptosis and its role in cancer therapy', *Journal of Cellular and Molecular Medicine*, 23(8), pp. 4900–4912. doi:

10.1111/jcmm.14511.

Yagoda, N. *et al.* (2007) 'RAS–RAF–MEK-dependent oxidative cell death involving voltage-dependent anion channels', *Nature*, 447(7146), pp. 865–869. doi: 10.1038/nature05859.

Yang, F. *et al.* (2014) 'Doxorubicin, DNA torsion, and chromatin dynamics', *Biochimica et Biophysica Acta (BBA) - Reviews on Cancer*, 1845(1), pp. 84–89. doi: 10.1016/j.bbcan.2013.12.002.

Yang, F. *et al.* (2023) 'Ferroptosis heterogeneity in triple-negative breast cancer reveals an innovative immunotherapy combination strategy', *Cell Metabolism*, 35(1), pp. 84-100.e8. doi: 10.1016/j.cmet.2022.09.021.

Yang, W. S. *et al.* (2014) 'Regulation of ferroptotic cancer cell death by GPX4', *Cell*, 156(1–2), pp. 317–331. doi: 10.1016/j.cell.2013.12.010.

Yang, W. S. *et al.* (2016) 'Peroxidation of polyunsaturated fatty acids by lipoxygenases drives ferroptosis', *Proceedings of the National Academy of Sciences*, 113(34). doi: 10.1073/pnas.1603244113.

Yang, W. S. and Stockwell, B. R. (2008) 'Synthetic Lethal Screening Identifies Compounds Activating Iron-Dependent, Nonapoptotic Cell Death in Oncogenic-RAS-Harboring Cancer Cells', *Chemistry & Biology*, 15(3), pp. 234–245. doi: 10.1016/j.chembiol.2008.02.010.

Ye, L. F. *et al.* (2020) 'Radiation-Induced Lipid Peroxidation Triggers Ferroptosis and Synergizes with Ferroptosis Inducers', *ACS Chemical Biology*, 15(2), pp. 469–484. doi: 10.1021/acschembio.9b00939.

Ye, Z. *et al.* (2020) 'Abrogation of ARF6 promotes RSL3-induced ferroptosis and mitigates gemcitabine resistance in pancreatic cancer cells.', *American journal of cancer research*, 10(4), pp. 1182–1193. Available at: http://www.ncbi.nlm.nih.gov/pubmed/32368394.

You, J. H., Lee, J. and Roh, J.-L. (2021) 'PGRMC1-dependent lipophagy promotes ferroptosis in paclitaxel-tolerant persister cancer cells', *Journal of Experimental & Clinical Cancer Research*, 40(1), p. 350. doi: 10.1186/s13046-021-02168-2.

Yu, H. *et al.* (2019) 'Sulfasalazine-induced ferroptosis in breast cancer cells is reduced by the inhibitory effect of estrogen receptor on the transferrin receptor', *Oncology Reports*. doi: 10.3892/or.2019.7189.

Yu, Y. *et al.* (2015) 'The ferroptosis inducer erastin enhances sensitivity of acute myeloid leukemia cells to chemotherapeutic agents', *Molecular & Cellular Oncology*, 2(4), p. e1054549. doi: 10.1080/23723556.2015.1054549.

Yuan, H. *et al.* (2016) 'CISD1 inhibits ferroptosis by protection against mitochondrial lipid peroxidation', *Biochemical and Biophysical Research Communications*, 478(2), pp. 838–

844. doi: 10.1016/j.bbrc.2016.08.034.

Yuan, S., Norgard, R. J. and Stanger, B. Z. (2019) 'Cellular Plasticity in Cancer', *Cancer Discovery*, 9(7), pp. 837–851. doi: 10.1158/2159-8290.CD-19-0015.

Yun, C. and Lee, S. (2018) 'The Roles of Autophagy in Cancer', *International Journal of Molecular Sciences*, 19(11), p. 3466. doi: 10.3390/ijms19113466.

Zaza, M. *et al.* (2023) 'PRIMA-1 synergizes olaparib-induced cell death in p53 mutant triple negative human breast cancer cell line via restoring p53 function, arresting cell cycle, and inducing apoptosis', *Canadian Journal of Physiology and Pharmacology*. doi: 10.1139/cjpp-2023-0031.

Zhang, P. *et al.* (2022) 'Mitochondria-Related Ferroptosis Drives Cognitive Deficits in Neonatal Mice Following Sevoflurane Administration', *Frontiers in Medicine*, 9. doi: 10.3389/fmed.2022.887062.

ZHANG, W. *et al.* (2014) 'Deferoxamine enhances cell migration and invasion through promotion of HIF-1α expression and epithelial-mesenchymal transition in colorectal cancer', *Oncology Reports*, 31(1), pp. 111–116. doi: 10.3892/or.2013.2828.

Zhang, X. *et al.* (2020) 'Inhibition of tumor propellant glutathione peroxidase 4 induces ferroptosis in cancer cells and enhances anticancer effect of cisplatin', *Journal of Cellular Physiology*, 235(4), pp. 3425–3437. doi: 10.1002/jcp.29232.

Zhang, Y. *et al.* (2018) 'BAP1 links metabolic regulation of ferroptosis to tumour suppression', *Nature Cell Biology*, 20(10), pp. 1181–1192. doi: 10.1038/s41556-018-0178-0.

Zhang, Y. *et al.* (2019) 'Imidazole Ketone Erastin Induces Ferroptosis and Slows Tumor Growth in a Mouse Lymphoma Model', *Cell Chemical Biology*, 26(5), pp. 623-633.e9. doi: 10.1016/j.chembiol.2019.01.008.

Zhang, Y. *et al.* (2020) 'Computational repositioning of dimethyl fumarate for treating alcoholic liver disease', *Cell Death & Disease*, 11(8), p. 641. doi: 10.1038/s41419-020-02890-3.

Zhang, Z. *et al.* (2021) 'Holo-lactoferrin: the link between ferroptosis and radiotherapy in triple-negative breast cancer', *Theranostics*, 11(7), pp. 3167–3182. doi: 10.7150/thno.52028.

Zhang, Z. *et al.* (2022) 'Inhibition of the PIN1-NRF2/GPX4 axis imparts sensitivity to cisplatin in cervical cancer cells', *Acta Biochimica et Biophysica Sinica*. doi: 10.3724/abbs.2022109.

Zhao, Y. *et al.* (2020) 'The Role of Erastin in Ferroptosis and Its Prospects in Cancer Therapy', *OncoTargets and Therapy*, Volume 13, pp. 5429–5441. doi: 10.2147/OTT.S254995.

Zheng, J. (2012) 'Energy metabolism of cancer: Glycolysis versus oxidative phosphorylation (Review)', *Oncology Letters*, 4(6), pp. 1151–1157. doi: 10.3892/ol.2012.928.

Zheng, X., Liang, Y. and Zhang, C. (2023) 'Ferroptosis Regulated by Hypoxia in Cells', *Cells*, 12(7), p. 1050. doi: 10.3390/cells12071050.

Zheng, Y., Fang, Y. and Li, J. (2019) 'PD-L1 expression levels on tumor cells affect their immunosuppressive activity', *Oncology Letters*. doi: 10.3892/ol.2019.10903.

Zheng, Z. *et al.* (2020) 'Liproxstatin-1 Protects Hair Cell-Like HEI-OC1 Cells and Cochlear Hair Cells against Neomycin Ototoxicity', *Oxidative Medicine and Cellular Longevity*. Edited by D. Muntean, 2020, pp. 1–15. doi: 10.1155/2020/1782659.

Zhou, C. *et al.* (2004) 'Caspase Inhibitors Prevent Endothelial Apoptosis and Cerebral Vasospasm in Dog Model of Experimental Subarachnoid Hemorrhage', *Journal of Cerebral Blood Flow & Metabolism*, 24(4), pp. 419–431. doi: 10.1097/00004647-200404000-00007.

Zhou, Z.-R. *et al.* (2020) 'Building radiation-resistant model in triple-negative breast cancer to screen radioresistance-related molecular markers', *Annals of Translational Medicine*, 8(4), pp. 108–108. doi: 10.21037/atm.2019.12.114.

Zhu, X. *et al.* (2019) 'Triazole Bridged Flavonoid Dimers as Potent, Nontoxic, and Highly Selective Breast Cancer Resistance Protein (BCRP/ABCG2) Inhibitors', *Journal of Medicinal Chemistry*, 62(18), pp. 8578–8608. doi: 10.1021/acs.jmedchem.9b00963.

Zou, Y. *et al.* (2019) 'A GPX4-dependent cancer cell state underlies the clear-cell morphology and confers sensitivity to ferroptosis', *Nature Communications*, 10(1), p. 1617. doi: 10.1038/s41467-019-09277-9.

Zou, Y. and Schreiber, S. L. (2020) 'Progress in Understanding Ferroptosis and Challenges in Its Targeting for Therapeutic Benefit', *Cell Chemical Biology*, 27(4), pp. 463–471. doi: 10.1016/j.chembiol.2020.03.015.

8. Appendices

Appendix 1a: Colony formation assay of RSL3 or ML385 in combination with RTx in MDA-MB-231 cells
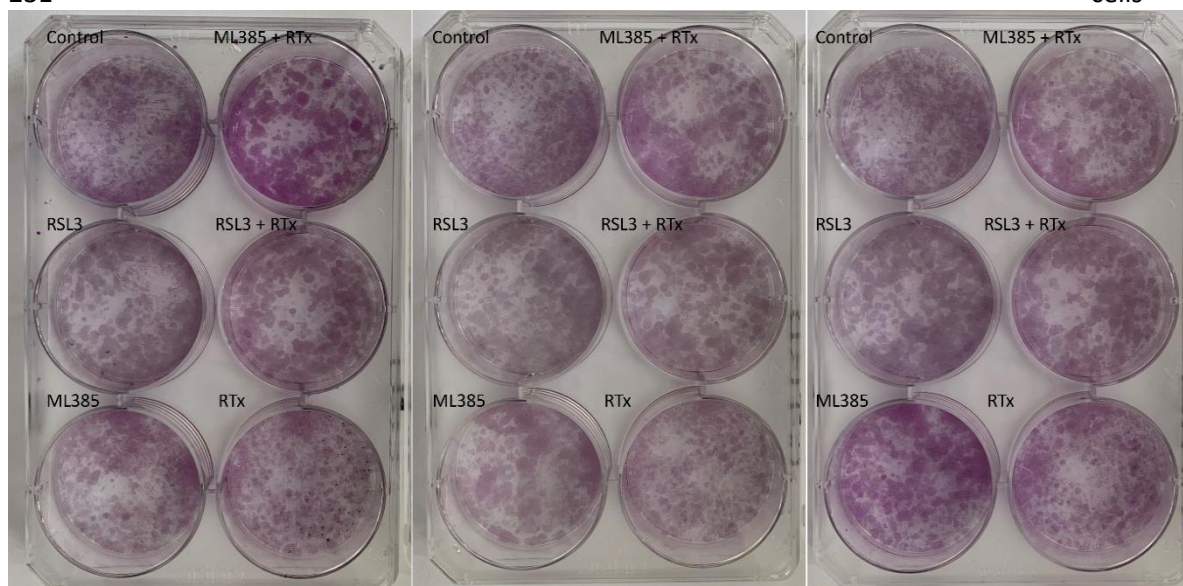
Appendix 1b: Colony formation assay of RSL3 or ML385 in combination with RTx in MCF-7 cells
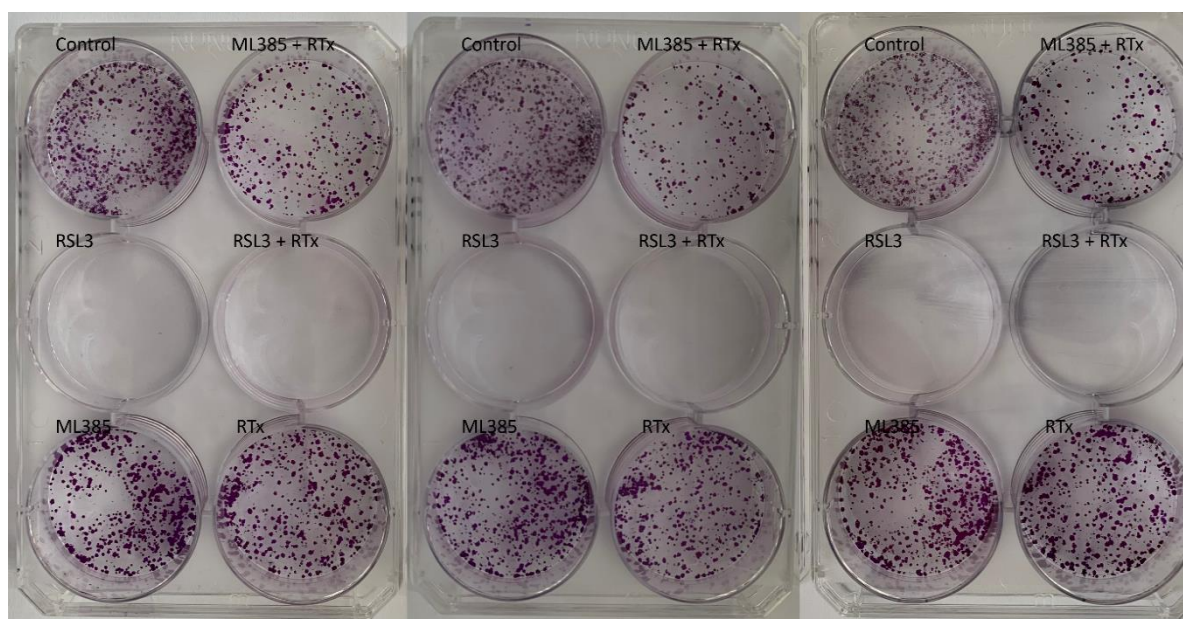
Appendix 1: Colony formation assay of a) MDA-MB-231 and b) MCF-7 cells treated with RSL3 at concentration of 0.0375 µM and 10 µM respectively, ML385 (10 µM) and RTx (1.25 Gy). Plates were stained with Crystal violet. MDA-MB-231 colonies show excessive growth for reliable counting. MCF-7 cells show excessive death in RSL3 treated wells. A modest reduction in colony number is seen for MCF-7 with ML385 + RTx, but likely no effect seen for MDA-MB-231.